ISSN 2410-2547
DOI: 10.32347/2410-2547.2020.105

МІНІСТЕРСТВО ОСВІТИ І НАУКИ УКРАЇНИ

КИЇВСЬКИЙ НАЦІОНАЛЬНИЙ УНІВЕРСИТЕТ
БУДІВНИЦТВА І АРХІТЕКТУРИ

KYIV NATIONAL UNIVERSITY OF CONSTRUCTION AND
ARCHITECTURE

ОПІР МАТЕРІАЛІВ І ТЕОРІЯ СПОРУД

STRENGTH OF MATERIALS AND THEORY OF STRUCTURES

Науково-технічний збірник
Scientific-and-technical collected articles

Випуск
Issue **105**

Заснований у 1965 р.
Founded in 1965

КИЇВ 2020

УДК 539.3/6
ББК 30.121+38.112
О-61

Рекомендовано до випуску Вченою радою Київського національного університету будівництва і архітектури 30 листопада 2020 р. (протокол № 45).

Опір матеріалів і теорія споруд: Науково-технічний збірник. – Вип. 105 / Голов. ред. В.А. Баженов. –К.: КНУБА, 2020. – 312 с. – Укр. та англ. мовами.

У збірнику наведено статті з результатами досліджень у галузі опору матеріалів, будівельної механіки, теорії пружності і пластичності. Особливу увагу приділено розробці й розвитку методів розрахунку міцності, стійкості, динаміки просторових конструкцій з урахуванням геометричної нелінійності, пластичних властивостей руйнування матеріалів; питанням чисельної реалізації рішень; дослідженню напружено-деформованого стану тіл складної структури при сталих і змінних у часі навантаженнях, включаючи випадкові впливи.

Призначений для наукових працівників, викладачів, виробничників, докторантів, аспірантів та студентів.

http://opir.knuba.edu.ua/
Адреса редакційної колегії:
КНУБА, Повітрофлотський пр., 31.
м. Київ, 03037
Тел.: (044) 248-3040
E-mail: omtc@knuba.edu.ua

УДК 539.3/6
ББК 30.121+38.112
О-61

UDC 539.3, 624.02

GENERAL CLASSIFICATION OF SEISMIC PROTECTION SYSTEMS OF BUILDINGS AND STRUCTURES

V.A. Bazhenov,
Doctor of Technical Science

Yu.D. Heraimovych,
Candidate of Science (Engineering)

Kyiv National University of Construction and Architecture
31, Povitroflotsky ave., Kyiv, Ukraine, 03037

DOI: 10.32347/2410-2547.2020.105.3-12

This work complements the general classification of seismic protection systems of buildings and structures. The principles of ensuring a seismic resistance of each of the considered seismic protection systems are briefly characterized.

Keywords:seismic action, seismic protection systems of buildings and structures, classification of seismic protection systems.

Introduction

The issues of ensuring the seismic resistance of buildings and structures hold a leading position despite significant achievements in this area. This is confirmed by the significant loss of human life and destructioncaused by strong earthquakesin Indonesia (December 26, 2004;March 28, 2005;August2, 2019), China (May 12, 2008), Haiti (January 12, 2010), Chile (February 27, 2010), Mexico (April 4, 2010), Japan (March 11, 2011; November 22, 2016), Italy (August 24, 2016; October 30, 2016), Iran (November 8, 2019).

In contrast to commonly applied measures, mainly related to increasing the bearing capacity of structures,any seismic protection system associated with a significant decrease in the level of inertial forces is called active seismic protection measures [1] (1989). And it still raises some misconceptions [2] – [4]. Although in 1993 Professor A.M. Uzdin proposed a seismic protection classification scheme [5]. Then he supplemented this classification in 2012 [6]. But it is also incomplete.Since then, not only a lot of time has passed, but new methods of external reduction of seismic effects and protective devices (screen) have appeared, including insensitive structures, trenches, spatial foundation platforms [7], [8].

According to the principle of operation (properties of ensuring seismic resistance), all seismic protection systems can be conditionally divided into three groups (see fig. 1).

Let us consider each of the groups in more detail.

Traditional methods of seismic protection of buildings and structures are mainly associated with reducing the mass of structures, increasing their strength and stiffness characteristics, as well as with the choice of rational planning and design solutions (fig. 2).

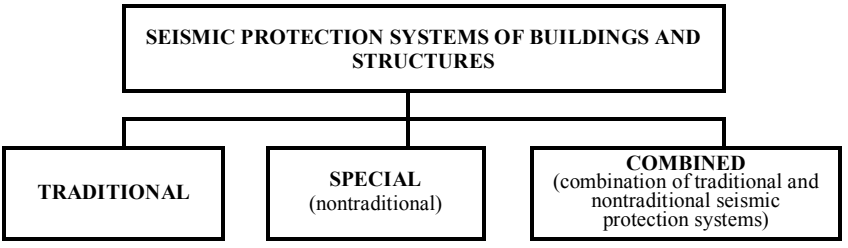

Fig. 1. General classificationof seismic protection systems

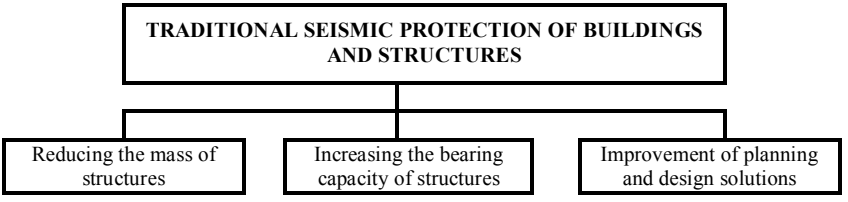

Fig. 2. Classification of traditional seismic protection

Reducing the mass of structures, with the same stiffness characteristics, leads to a decrease in inertial forces, calculated according to the linear-spectral theory laid down in the vast majority of building normsin seismic regions.

An increase in the bearing capacity of structures should guarantee the seismic resistance of structures, but the main disadvantages of this method of seismic protection are the growth of material consumption of structures, increase in cross-sections and mass of elements, which, of course, can be avoided by using materials with increased strength characteristics.

Improvements in planning and design solutions, as a rule, boil down to the fact that earthquake-resistant buildings should have simple and regular shapes both in plan and in height. If the plan has a complex form, then this can be realized by dividing the building with seismic seams into dynamically independent blocks.

To this we can add that during the construction of buildings and structures, the guaranteed quality of construction and installation work must be ensured.

The second group of seismic protection includes approaches associated with reducing the intensity of seismic loads on buildings and structures (fig. 3). Special seismic protection today is one of the most promising areas in the field of earthquake-resistant construction.

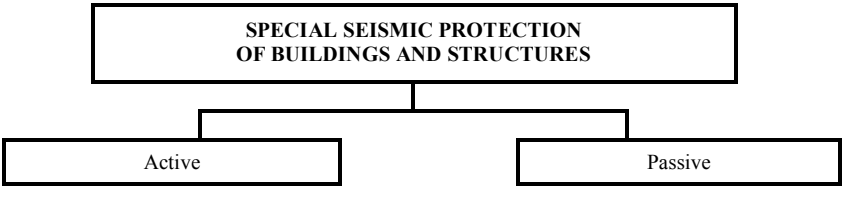

Fig. 3. Classification of specialseismic protection

Activeseismic protection uses additional energy sources and devicesthat regulate the operation of these sources,however, its implementation requires significant costs for arrangement and operation (fig. 4). This excludes the possibility of widespread use of active seismic protection for earthquake-resistant construction. The advantage of this system is that it becomes possible to control the oscillatory process not only from seismic, but also from wind effects.

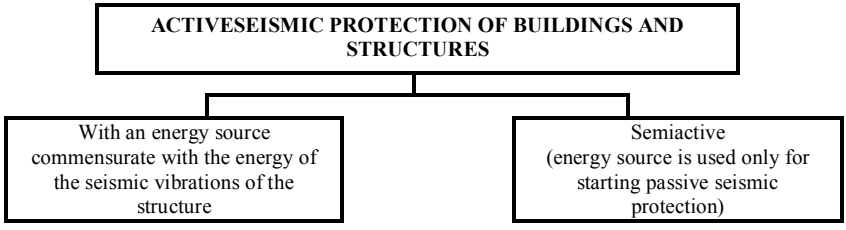

Fig. 4. Classification of active seismic protection

Passiveseismic protectionis the most numerous seismic protection groupaimed at changing the dynamic scheme of a building or structure,which is divided into seismic isolation and seismic suppression.

In seismic isolation, stationary and adaptive seismic isolation systems are distinguished. In stationary seismic isolation systems, dynamic characteristics are retained during an earthquake. And in adaptive systems, the dynamic characteristics of a building or structure change irreversibly during anearthquake, “adapting” to seismic impact. In seismic isolation systems, it's

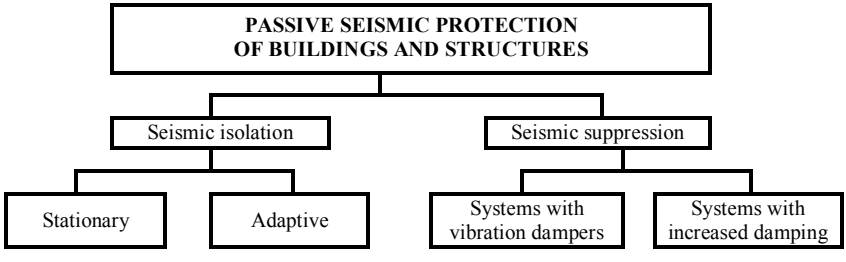

Fig. 5. Classification of passiveseismic protection

provided the reduction of mechanical energy received by a building or structurefrom the subgrade by tuning out the natural frequencies of vibrations from the prevailing frequencies of the seismic impact.

In seismic damping, systems with vibration dampers and systems with increased damping are distinguished.In thesystems with increased damping, reduction of mechanical energy is provided by the transition of mechanical energy to other types of energy. In the systems with vibration dampers, the mechanical energy of the vibrating building is converted into mechanical energy of the damper vibration.The significant disadvantages of systems with

vibration dampers include the impossibility of using in industrial construction due to the need to adjust the damper in each individual case, as well as the relative complexity of vibration dampers.

Stationary seismic isolation of buildings and structures, in turn, is divided into internal and external. External seismic isolationaims to reduce seismic impacts through the use of design solutions that minimize the transfer of energy of seismic vibrations to the building "as a whole".

Geotechnical barriers are trenches or wells, filled with vibration-absorbing material. The advantage of geotechnical barriers is that they are invariant with respect to the frequency composition of the earthquake.

Spatial foundation platforms on a sliding layer, due to their high rigidity, have a large distribution capacity and exert little pressure on the base.

Internal seismic isolation is divided into two groups — with and without restoring force.

An example of internal seismic isolation that does not provide restoring forceisa foundationwith seismic-isolating sliding belt (seismic belt).

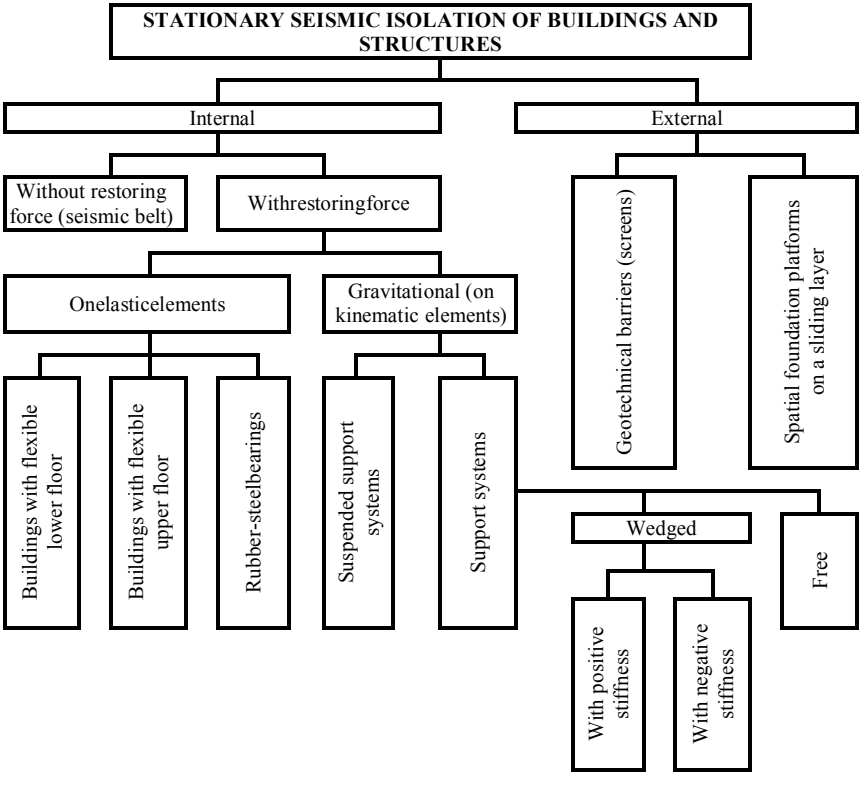

Fig. 6. Classification of stationary seismic isolation

In turn, systems of internal seismic isolation with a restoring force are subdivided into elastic (elastic force) and gravitational (force of gravity).

Seismic-isolating foundations on elastic supports include buildings with a flexible lower floor, buildings with a flexible upper floor, as well as buildings with rubber-steelbearings.

Gravitational seismic-isolatingfoundations can be divided into suspended support systems and support systems.

In suspended support systems, the building is installed on an upper foundation slabwhich is suspended on rods from the frame structure, rigidly connected to the bottom foundation slab.

In support systems, the upper foundation slab rests on kinematic supports. According to the behavior of the supports near the rest position, the kinematic supports are subdivided into free and wedged.

Free supports react to any horizontal load on a building or structure, that is not always desirable.

Kinematic supports which include platforms or recesses in the central part of the rolling surface are called wedged. Platforms or recesses prevent the support from rolling out at low loads, and this design change led to fundamental differences in the operation of free and wedged supports.

Wedged supports can have both positive and negative stiffness.

Adaptiveseismicisolationsystemsaresystemswithswitched on and switched off connections. The features of these systems were studied in KucherenkoTs NIISK under the leadership of Ya.M. Aisenberg [9, 10].

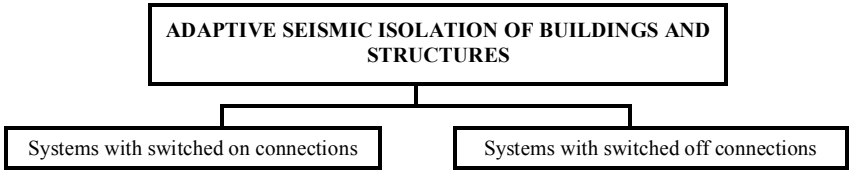

Fig. 7. Classification of adaptiveseismic isolation

Systemswithswitched on connections belong to the class of nonlinear dynamic systems with a rigid characteristic. In systemswithswitched on connections, there is no destruction of links and it is not required to restore them after an earthquake.

Systems with switched off connections belong to the class of nonstationary dynamical systems.Changes in the dynamic characteristics of such systems occur due to the destruction of switched off connections when a certain level of amplitudes is reached. After the destruction of the switched off connections during an earthquake, their immediate restoration is necessary.

Systems with vibration dampers by the nature of interaction with the protected structure are divided into dynamic and shock. Dynamic vibration dampers are divided into three groups depending on the design of the elastic connection: spring, pendularandcombineddampers [1]. The shock vibration damper is based on a massive body colliding with a special element of the protected

structure. Floating dampers during one period of vibration of the protected structure make two successive impacts on each limiter. Spring and pendulum shock dampers differ in type of suspension and one impact per one period of vibration of the protected structure.

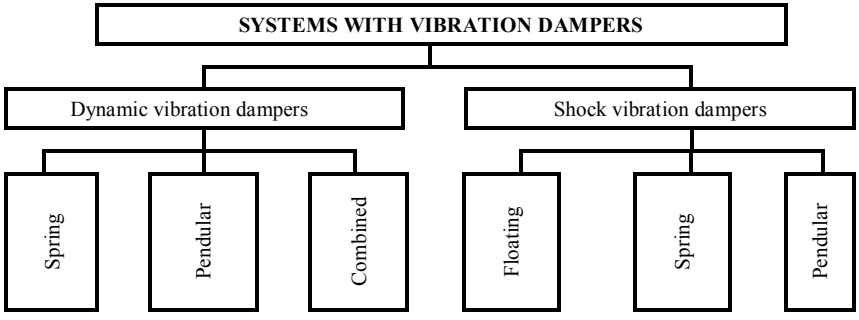

Fig. 8. Seismic suppressionsystems with vibration dampers

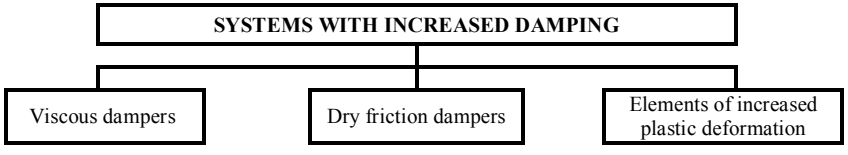

Fig. 9. Seismic suppressionsystems with increased damping

Damping devices used in the practice of earthquake-resistant construction can be conditionally divided into three groups: viscous dampers, dry friction dampers,andelements of increased plastic deformation.

Energy dissipation in viscous dampers occurs due to viscous resistance forcesthat prevent fluid flowing from one part of the damper to another.Mainly two types of viscous dampers are used: liquid and leaden.

Dry friction dampers use rubbing pairs made of different materials: metal to metal, concrete to concrete, polymer pads of various types to metal or to each other. For dry friction dampers to be effective, either a high dry friction coefficient or significant compression of rubbing pairs must be ensured.

Elements of increased plastic deformation are able to absorb the energy of seismic impactsdue to the development of inelastic deformations in the material of the energy absorber.

The massive use of seismic protection systems by design engineers is constrained by the lack of practical calculation methods. This is due to the fact that most seismic protection systems are characterized by a nonlinear deformation diagram, which does not allow the use of the standard linear-spectral methodology for the calculation.

In the new edition of building codes of Ukraine [11],the section 12 “Design of building seismic isolation systems” appeared,in which passive systems for seismic isolation of buildings are considered and the main provisions for the dynamic analysis of buildings with a seismic isolation system are given. Due

to the norms, the structures of rubber-steel seismic blocks were used for vibration and seismic protection of residential buildingsin Kyiv (10-section 10-storeybuilding onKikvidze Str. and two 27-storey buildings on Obolonsky Avenue, located on the deep and shallow undergroundlines). This made it possible to achieve a decrease in vibration levels in residential premises by 7-12 dB (2-4 times) [12].

Conclusions

This article clarifies the general classification of seismic protection systems of buildings and structures.The use of seismic protection systems during strong earthquakes can significantly reduce the amplitude of vibrations,provide less damage to buildings and structures. Seismic protection systems are one of the most effective ways to increase the level of seismic resistance of buildings and structures, although the share of seismic-protected buildings in construction in relation to traditional ones is still very small.

REFERENCES

1. *Polyakov V.S.* Sovremennyye metody seysmozashchity zdaniy (Modern methods of seismic protection of buildings) / V.S. Polyakov, L.Sh. Kilimnik, A.V. Cherkashin. – M: Stroyizdat, 1989. – 320 s.(in Russian)
2. *Chigrinskaya L.S.* Seysmostoykost' zdaniy i sooruzheniy (Seismic resistance of buildings and structures): ucheb. Posobiye dlya studentov spetsial'nostey 270102 "Promyshlennoye i grazhdanskoye stroitel'stvo" i 270105 "Gorodskoye stroitel'stvo i khozyaystvo" / L.S. Chigrinskaya; Angarsk. gos. tekhn. akad. – Angarsk: Izd-vo AGTA, 2009. – 107 s. (in Russian)
3. *Omarov Kh.M.* Optimal'nyye parametry sistem aktivnoy seysmozashchity sooruzheniy s rezinometallicheskimi oporami (Optimal parameters of active seismic protection systems for structures with rubber-steel bearings) / OmarovKh.M.; Monografiya. – Makhachkala: ALEF, 2018. – 210 s. (in Russian)
4. *Rashidov T.R.* Prikladnyye zadachi seysmodinamiki sooruzheniy (Applied problems of seismodynamics of structures) / T.R. Rashidov, S.V. Kuznetsov, B.M. Mardonov, I. Mirzayev; Kniga 1. Deystviye seysmicheskikh voln na podzemnyy truboprovod i fundamenty sooruzheniy, vzaimodeystvuyushchikh s gruntovoysredoy. – Tashkent.: «Navro'z», 2019. – 268 s. (in Russian)
5. *Uzdin A.M.* Osnovy teorii seysmostoykosti i seysmostoykogo stroitel'stva zdaniy i sooruzheniy (Fundamentals of the theory of seismic resistance and earthquake-resistant construction of buildings and structures) / A.M.Uzdin, T.A.Sandovich, Al'-Naser-Mokhomad Samikh Amin. – S.-Peterburg: Izd-vo VNIIG im. B.Ye. Vedeneyeva, 1993. – 176 s. (in Russian)
6. *Uzdin A.M.* Seysmostoykiye konstruktsii transportnykh zdaniy i sooruzheniy (Earthquake resistant structures of transport buildings and structures): ucheb. posobiye / A.M. Uzdin, S.V. Yelizarov, T.A. Belash. – M.: FGBOU Uchebno-metodicheskiy tsentr po obrazovaniyu na zheleznodorozhnom transporte, 2012. –501 s. (in Russian)
7. *Litvinova E.V.* Innovatsionnyye sistemy seysmozashchity zdaniy i sooruzheniy zarubezhom (Innovative systems for seismic protection of buildings and structures abroad) / E.V. Litvinova, B.A. Litvinov // Resursoekonomnimaterialy, konstruktsiyi, budivli ta sporudy: zb. nauk. pr. – Vyp. 28. – Rivne, 2014. – S.386-397. (in Russian)
8. *Semenov V.S.* Sovremennyye sistemy seysmozashchity zdaniy i sooruzheniy. Klassifikatsiya, osnovnyye konstruktivnyye resheniya (Modern systems of seismic protection of buildings and structures. Classification, basic design solutions) / V.S. Semenov, T.V. Veremenko // Vestnik Kyrgyzsko-Rossiyskogo Slavyanskogo universiteta (KRSU). Tom 12. № 6 – Bishkek, 2012. – S. 65-70. (in Russian)
9. *Ayzenberg Ya.M.* Adaptivnyye sistemy seysmicheskoy zashchity sooruzheniy (Adaptive systems for seismic protection of structures) / Ya.M.Ayzenberg, A.I. Neyman, A.D. Abakarov, M.M. Deglina, T.L. Chachua. – M.: Nauka, 1978. – 246 s. (in Russian)
10. *Ayzenberg Ya.M.* Sooruzheniya s vyklyuchayushchimisya svyazyami dlya seysmicheskikh rayonov (Constructions with switched off connections for seismic regions)/ Ya.M.Ayzenberg. – M: Stroyizdat, 1976. – 229 s. (in Russian)

11. Derzhavni budivelni normy Ukrayiny: DBNV.1.1 – 12:2014 – Budivnytstvo u seysmichnykh rayonakh Ukrayiny. (State Building Codes of Ukraine: DBN V.1.1 – 12:2014 – Construction in seismic regions of Ukraine). – K.: Ministerstvo rehionalnoho rozvytku, budivnytstva ta zhytlovo-komunalnoho hospodarstva Ukrayiny, 2014. – 110 s. (in Ukranian)
12. *Nemchinov Yu.I.* Vibroseysmoizolyatsiya zdaniy s pomoshch'yu sistemy elastomernykh blokov (Vibration seismic isolation of buildings using a system of elastomer blocks) / Yu.I. Nemchinov, N.G. Mar'yenkov, L.A. Zharko, A.N. Mar'yenkov, V.I. Dyrda, N.I. Lisitsa, G.N. Agal'tsov, A.V. Novikova // Budivelni konstruktsiyi. Vyp. 83(2). – Kyiv: DP NDIBK, 2016. – S. 554-566. (in Russian)

Стаття надійшла 20.11.2020

Баженов В. А., Гераймович Ю. Д.

ЗАГАЛЬНА КЛАСИФІКАЦІЯ СИСТЕМ СЕЙСМОЗАХИСТУ БУДІВЕЛЬ І СПОРУД

Питання забезпечення сейсмостійкості будівель і споруд займають провідне місце, незважаючи на значні досягнення в цій галузі. Підтвердженням цього є чисельні людські жертви та значні пошкодження і руйнування, що мають місце після сильних землетрусів.

За принципом роботи (властивостями забезпечення сейсмостійкості) всі системи сейсмозахисту можна умовно розділити на три групи: традиційна, спеціальна і комбінована.

Традиційні методи сейсмозахисту будівель і споруд в основному пов'язані зі зменшенням маси конструкцій, підвищенням їх міцності і характеристик жорсткості, а також з вибором раціональних планувальних і конструктивних рішень.

До другої групи сейсмозахисту відносяться підходи, пов'язані зі зниженням інтенсивності сейсмічних навантажень на будівлі і споруди. Спеціальнийсейсмозахист на сьогоднішній день є одним з найбільш перспективних напрямків в галузі сейсмостійкого будівництва. Найчисленніша підгрупа цьогосейсмозахисту - це пасивнийсейсмозахист, спрямований на зміну динамічної схеми роботи будівлі або споруди, який, в свою чергу, ділиться на сейсмоізоляцію і сейсмогасіння.

Комбінована система має на увазі поєднання традиційної і нетрадиційної систем сейсмозахисту.

Масове застосування систем сейсмозахисту інженерами-проектувальниками стримується відсутністю практичних методик розрахунку. Це пов'язано з тим, що більшість систем сейсмозахисту характеризуються нелінійною діаграмою деформування, що не дозволяє використовувати для розрахунку нормативну лінійно-спектральну методику.

У статті уточнена загальна класифікації систем сейсмозахисту будівель і споруд. Застосування систем сейсмозахиступри сильних землетрусах здатне значно зменшити амплітуду коливань, забезпечити меншу пошкоджуваність будівель і споруд. Системи сейсмозахисту є одним з ефективних способів підвищення рівня сейсмостійкості будівель і споруд, хоча частка в будівництві сейсмозащіщенних будівель по відношенню до традиційних ще дуже мала.

Ключові слова: сейсмічні впливи, системи сейсмозахисту будівель і споруд, класифікація систем сейсмозахисту.

Bazhenov V. A.,Heraimovych Yu. D.

GENERAL CLASSIFICATION OF SEISMIC PROTECTION SYSTEMS OF BUILDINGS AND STRUCTURES

The issues of ensuring the seismic resistance of buildings and structures hold a leading position despite significant achievements in this area. This is confirmed by the significant loss of human life and destruction caused by strong earthquakes.

According to the principle of operation (properties of ensuring seismic resistance), all seismic protection systems can be conditionally divided into three groups: traditional, special and combined.

Traditional methods of seismic protection of buildings and structures are mainly associated with reducing the mass of structures, increasing their strength and stiffness characteristics, as well as with the choice of rational planning and design solutions.

The second group of seismic protection includes approaches associated with reducing the intensity of seismic loads on buildings and structures. Special seismic protection today is one of

the most promising areas in the field of earthquake-resistant construction. The largest subgroup of this seismic protection – this is a passive seismic protection aimed at changing the dynamic scheme of a buildings or structures, which, in turn, is divided into seismic isolation and seismic suppression.

The combined system implies a combination of traditional and nontraditional seismic protection systems.

The massive use of seismic protection systems by design engineers is constrained by the lack of practical calculation methods. This is due to the fact that most seismic protection systems are characterized by a nonlinear deformation diagram, which does not allow the use of the standard linear-spectral methodology for the calculation.

This article clarifies the general classification of seismic protection systems of buildings and structures. The use of seismic protection systems during strong earthquakes can significantly reduce the amplitude of vibrations, provide less damage to buildings and structures. Seismic protection systems are one of the most effective ways to increase the level of seismic resistance of buildings and structures, although the share of seismic-protected buildings in construction in relation to traditional ones is still very small.

Keywords: seismic action, seismic protection systems of buildings and structures, classification of seismic protection systems.

Баженов В. А., Гераймович Ю. Д.

ОБЩАЯ КЛАССИФИКАЦИЯ СИСТЕМ СЕЙСМОЗАЩИТЫ ЗДАНИЙ И СООРУЖЕНИЙ

В работе дополнена общая классификация систем сейсмозащиты зданий и сооружений. Коротко охарактеризованы принципы обеспечения сейсмостойкости каждой из рассмотренных систем сейсмозащиты.

Ключевые слова: сейсмические воздействия, системы сейсмозащиты зданий и сооружений, классификация систем сейсмозащиты.

УДК 539.3, 624.02

Баженов В. А., Гераймович Ю. Д. **Загальна класифікація систем сейсмозахисту будівель і споруд**// Опір матеріалів і теорія споруд: наук.-тех. збірн. – Київ: КНУБА, 2020. – Вип. 105. – С. 3-12.–Engl.

В роботі доповнена загальна класифікація систем сейсмозахисту будівель і споруд. Коротко охарактеризовані принципи забезпечення сейсмостійкості кожної з розглянутих систем сейсмозахисту.

Табл. 0. Іл. 9. Бібліогр. 12 назв.

UDC 539.3, 624.02

Bazhenov V.A., Heraimovych Yu.D. **General classification of seismic protection systems of buildings and structures** // Strength of Materials and Theory of Structures: Scientific-and-technical collected articles. – K.: KNUBA, 2020. – Issue 105. – P. 3-12.

This work complements the general classification of seismic protection systems of buildings and structures. The principles of ensuring a seismic resistance of each of the considered seismic protection systems are briefly characterized.

Tabl. 0. Fig. 9. Ref. 12.

УДК 539.3, 624.02

Баженов В. А., Гераймович Ю. Д. **Общая классификация систем сейсмозащиты зданий и сооружений** // Опірматеріалів і теоріяспоруд: наук.-тех. збірн. – Київ: КНУБА, 2020. – Вип. 105. – С. – 3-12.

В работе дополнена общая классификация систем сейсмозащиты зданий и сооружений. Коротко охарактеризованы принципы обеспечения сейсмостойкости каждой из рассмотренных систем сейсмозащиты.

Табл. 0. Ил. 9. Библиогр. 12 назв.

Автор (вчена ступень, вчене звання, посада): *доктор технічних наук, професор, академік Національної академії педагогічних наук України, завідувач кафедри будівельної механіки Київського національного університету будівництва і архітектури, директор НДІ будівельної механіки БАЖЕНОВ Віктор Андрійович*
Адреса робоча: *03680 Україна, м. Київ, Повітрофлотський проспект 31, Київський національний університет будівництва і архітектури.*
Робочий тел.: *+38(044) 245-48-29.*
мобільний тел.: *+38(067)111-22-33*
E-mail: bazhenov.va@knuba.edu.ua
ORCID ID: http//orcid/org/0000-0002-5802-9848

Автор (науковий ступінь, вчене звання, посада): *кандидат технічних наук, докторант Київського національного університету будівництва і архітектури ГЕРАЙМОВИЧ Юрій Дмитрович*
Адреса робоча: *03037 Україна, м. Київ, Повітрофлотський проспект 31, Київський національний університет будівництва і архітектури, відділ докторантури та аспірантури, ГЕРАЙМОВИЧУ Юрію Дмитровичу*
Робочий тел.:*+38(044) 246-16-20;*
Мобільний тел.:*+38(067) 238-73-19;*
E-mail: yury_geraimovich@ukr.net
ORCID ID: http://orcid.org/0000-0002-5605-5276

UDC 539.3

INVESTIGATION OF A STRESS-STRAINED STATE OF A SCREW-SHAPE TUBE OF HEAT EXCHANGER

S.O. Pyskunov,
Doctor of Technical Science,

S.I. Trubachev,
Candidate of Technical Science (Engineering),

O.V. Baranyuk,
Candidate of Technical Science (Engineering),

Igor Sikorsky National Technical University of Ukraine «Kyiv Polytechnic Institute»
Peremogy ave., 37, Kyiv, 03056

DOI: 10.32347/2410-2547.2020.105.13-23

Based on the results of the study of the parameters of the air flow inside of the brass screw-shaped tube of the heat exchanger, the determination of their optimal geometric characteristics and further modeling of the stress-strain state was performed. Verification of simulation results is carried out on the basis of comparison with the test problem.

Keywords: heat transfer, screw-shaped tube, evenly developed surface, forced convection, elastic deformation, stress-strain state.

1. Introduction

One of the ways to increase the efficiency of the gas transmission system is the use of air heaters (regenerators) to utilize the heat of the exhaust gases in the turbine. The creation of new highly efficient and reliable gas transmission units (GTU), as well as the modernization of existing ones, is impossible without the use of reliable and efficient elements of heat exchange in their designs. Screw-shaped pipes with an evenly developed surface meet such requirements

The proposed screw-shaped heat exchange tubes with an evenly developed surface have been comprehensively studied by the authors of publications [1-3]. Their design allows us to increase significantly (in 1.15-1.4 times) both external and internal heat transfer surface. Due to the screw-shaped protrusions-depressions with a given height-depth, which alternate sequentially with a some step, they provide additional turbulence of the air's boundary layer [3]. Due to the twisting of internal and external flows and a sharp change in flow rate when washing the surface there is a simultaneous increase in the intensity of internal and external heat transfer by 1.5-2.5 and 1.1-1.3 times, respectively, depending on the geometric characteristics of the tubes and the steps between them. Due to this, the heat transfer coefficient increases by 25-70% compared to smooth cylindrical tubes.

The technology of obtaining of screw-shaped profiles of tubes, based on the joint use of three-roller and single-roller running heads, was developed at the Mechanical Engineering Institute of Igor Sikorsky KPI [4].

The screw-shaped tubes, studied by the authors [1-3], had an outer diameter of 36 mm and small steps between depressions and protrusions (8-12 mm) at the heights of depressions or protrusions of a 4-5 mm. Increasing the use of screw-shaped tubes with a uniform surface in the industry requires expanding the range of their geometric characteristics. It is possible due to a new technology [5], which allows to obtain brass tubes with a diameter of 16 mm.

Fig. 1. Long dimensional screw-shaped tube (diameter 16 mm, step 8 mm), made in one pass

It is necessary to conduct studies of air flow and to determine on this basis a stress-strain state of these tubes under the influence of the appropriate internal pressure for further wide use of it. This will contribute to the expansion of the use of a new technologies for mass production of screw-shaped profile tubes with an uniform surface, which is currently absent in Ukraine.

The goal of the work is to determine the optimal geometric characteristics of screw-shaped tubes, the surface of which is created on a single-west helical line, and to determine their stress-strain state under non-isothermal conditions. The main geometric parameters that affect the configuration of the outer surface of the tube are the pitch and the height of the protrusions-depressions of the helix. The analysis was performed at a variable pitch values, which was taken of 8, 12 and 20 mm. The height of the protrusions-depressions of the helical line remained unchanged and was 2.5 mm for all three studied pitch value. The values of the parameters, taken for analysis, are determined by technological difficulties associated with the capabilities of the three-roller rolling technology, which is used in the manufacture of tubes. Therefore, determining of the optimal geometric characteristics of screw-shaped tubes is reduced to finding the optimal pitch of the helical line, which is determined by the achievement of the maximum thermal power that can be dissipated by the screw-shaped tube under all other conditions.

The following tasks were solved to achieve of this goal:

- development of CFD-model of screw-shaped tube with uniform surface;
- carrying out of test calculations and calculation of thermoaerodynamic characteristics of the investigated screw-shaped tubes;
- implementation of stress-strain state analysis of screw-shaped tubes.

2. Methods for studying of the flow structure inside the screw-shaped tubes

The following analysis was performed using the developed finite-element CFD-models of screw-shaped tubes using of the software package ANSYS-Fluent. The problem was solved in a stationary setting in compliance with the requirement to achieve no dependence of the solution from the calculation

mesh density (convergence of results). During modeling, the following boundary conditions were chosen to be constant for all tube sizes:

- flow temperature at the entrance to the screw-shaped tube $t_{ent} = 26°C$;
- temperature of tube wall $t_w = 100°C$;
- air flow through the tube, which was chosen equal to $9 \cdot 10^{-4}$, $9 \cdot 10^{-3}$, $3 \cdot 10^{-2}$ kg/s.

The appearance of the fragment of finite-element mesh of the investigated tube of standard sizes is given in Fig. 2.

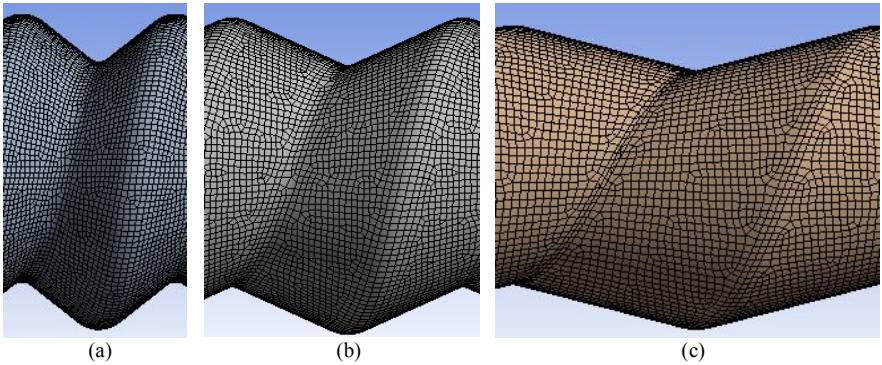

(a) (b) (c)

Fig. 2. Finite element mesh of a screw-shaped tube model with a pitch of a helix of 8 mm (a), 12 mm (b) and 20 mm (c)

The equations system for describing the processes of momentum and heat transfer inside the studied tube includes the equations of continuity, motion and energy in the Reynolds form of the following view:

$$\frac{\partial \overline{U}_j}{\partial x_j} = 0\,, \tag{1}$$

$$\frac{\partial \overline{U}_i}{\partial \tau} + \overline{U}_j \frac{\partial \overline{U}_i}{\partial x_j} = -\frac{1}{\rho}\frac{\partial \overline{P}}{\partial x_i} + \frac{\partial}{\partial x_j}\left[\left(\nu + \nu_{\text{т}}\right)\left(\frac{\partial \overline{U}_i}{\partial x_j} + \frac{\partial \overline{U}_j}{\partial x_i}\right) - \frac{2}{3}\delta_{ij}E\right], \tag{2}$$

$$\frac{\partial \bar{t}}{\partial \tau} + \overline{U}_j \frac{\partial \bar{t}}{\partial x_j} = \frac{\partial}{\partial x_j}\left[\left(\frac{\nu}{\text{Pr}} + \frac{\nu_{\text{т}}}{\text{Pr}_{\text{т}}}\right)\frac{\partial \bar{t}}{\partial x_j}\right]. \tag{3}$$

Assuming the complex nature of the flow in this object, which combines features characteristic of both near-wall and free shear flows, in order to close the basic system of equations (1) - (3) RSM model of Reynolds' stresses was used. The turbulent Prandtl's number for the considered conditions was assumed to be equal to 0.9.

The numerical solution of the system of basic and model equations was based on an implicit ordinary-volume approach using the COUPED pressure correction procedure. The calculation area was covered with a non regular tetrahedral mesh, which was thickened to the walls of the channel. The minimum size of the mesh step was chosen according to the recommendations

[6], the maximum number of finite elements, required for the calculation area sampling was about 4 million. For all system equations the criterion of accuracy of the solution was 10^{-5}.

3. The results of study of the flow structure inside the screw-shaped tube

3.1 Verification of the CFD model was provided using of the CFD-model of a smooth cylindrical tube with an inner diameter and length (16 mm and 500 mm, respectively), which coincide with the studied models of the screw-shaped tube. The study was conducted under the boundary conditions, using of turbulence model and at the same density of finite element mesh, which was were specified in section 2.

To compare the obtained results of numerical simulation - the heat transfer intensity and aerodynamic resistance in the turbulent flow regime a calculated dependences, given in [7, 8], were used:

$$\mathrm{Nu}_{\mathrm{liq}} = 0.021\,\mathrm{Re}_{\mathrm{liq}}^{0,8}\,\mathrm{Pr}_{\mathrm{liq}}^{0,43}\left(\mathrm{Pr}_{\mathrm{liq}}/\mathrm{Pr}_{\mathrm{wl}}\right)^{0,25}\varepsilon_l\,, \tag{4}$$

$$\Delta p = \xi\,\frac{l}{d}\,\frac{\rho w^2}{2}\,, \tag{5}$$

where

$$\xi = \frac{0,31464}{\mathrm{Re}_d^{0,25}}. \tag{6}$$

The correction for the initial section Δ_l, was chosen according to the recommendations [7].

According to the estimates being made using of the above dependences, the calculated data error of heat transfer parameter is 1.2%, and the aerodynamic resistance − 5.8%. Thus, we can conclude that the developed CFD model can be used to calculate heat transfer and hydrodynamics of screw-shaped tubes.

Thermal power is determined by means of ANSYS-Fluent (Fig. 2) by determining the enthalpy of flow at the inlet-outlet of the tube. Based on the obtained data, dimensionless characteristics of heat transfer intensity and aerodynamic resistance for different pitch value *t* of the helical line of the tube were calculated (Figs. 3, 4).

Analysis of Fig. 3 shows that when the air flow in the studied tubes both turbulent and transient flow regime was observed, as evidenced by the characteristic break of the curves at $\mathrm{Re}_d = (8-12)\cdot 10^3$. In its turn this confirms the increase in the intensity of heat transfer in turbulent flow. These results also show that in the case of the use of screw-shaped tubes, the intensity of heat transfer increases by almost 50% compared to a smooth cylindrical one of the same length and outer diameter. It can also be stated that among the studied standard sizes of screw-shaped tubes, the largest heat flux (19 W) can be dissipated by a tube with a helical line pitch of 8 mm. This tube is also characterized by a larger heat transfer surface (3%) than all other ones.

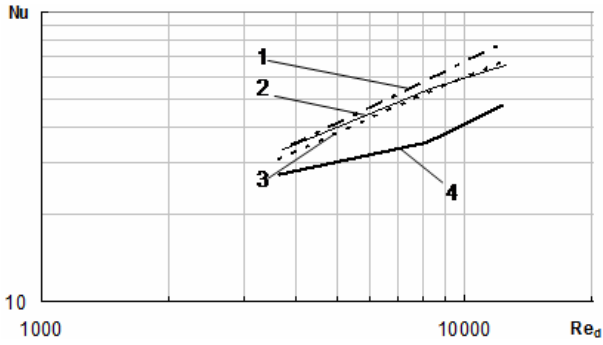

Fig. 3. Analysis of the thermal characteristics of screw-shaped tube (1 - t = 8 mm, 2 - t = 12 mm; 3 - t = 20 mm, 4 - smooth cylindrical tube)

The increase of heat transfer intensity is inextricably linked with the increase in aerodynamic resistance. Thus, for a screw-shaped tube with a pitch of 8 mm, the increase in heat transfer intensity by 50% is accompanied by an increase in aerodynamic resistance by 9...10 times. It should be noted that the screw-shaped tubes of helical line pitch of 20 mm, is able to increase the intensity of heat transfer by 30% while increasing the aerodynamic resistance in 5 ... 6 times.

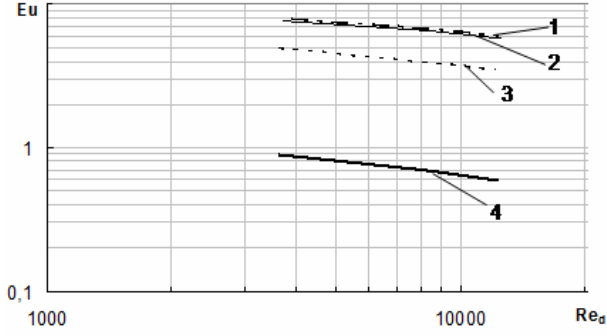

Fig. 4. Aerodynamic resistance of screw-shaped tubes: (1 - t = 8 mm, 2 - t = 12 mm; 3 - t = 20 mm, 4 - smooth cylindrical tube)

This value of aerodynamic resistance is due to an increase in local resistances, i.e. more helix turns at a given length. Therefore, the depth of the protrusions-depressions of 2.5 mm on the helical surface is too large, it would be desirable to reduce it to 1 ... 1.5 mm, as recommended by the authors [9].

The results of the flow structure analysis in the middle of the screw-shaped tubes are shown below. The set of velocities distribution, temperatures, vectors of average and tangential velocity, as well as current lines in the middle of the studied helical pipes are given. This analysis allowed us to investigate more fully the picture of hydrodynamic flow in the investigated screw-shaped tubes and will allow explaining which the processes lead to an increase of heat transfer.

When constructing the shape of screw-shaped tubes, the assumption was applied that the heat transfer intensity will increase due to vortex formation in the protrusions-depressions of the tube surface. So that the results of numerical study of the flow structure obtained for a fixed Reynolds number $\mathrm{Re}_d = 3{,}5 \cdot 10^3$ which corresponds to the average flow velocity of 4 m/s, represented in the plane that intersects the generating coil (Fig. 5).

As it shown in Fig. 5, the temperature field is quite homogeneous − there are no significant areas of low temperature that would occur due to the formed stagnant zones. The flow current lines are twisted together to create a geometric shape like a spiral. In the protrusions-depressions of the helical tube, the interaction of the vortex harness and the non-twisted core of the flow lead to the creation of a three-dimensional vortex, which rotates counterclockwise and moves along the axis of the tube. The local flow rates near the wall of the tube are large, which promote the access of the cold coolant to the heated wall of the heat exchange surface than to increase the heat transfer characteristics of the screw-shape tube as a whole.

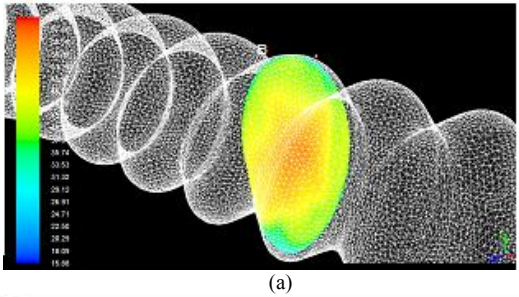

(a)

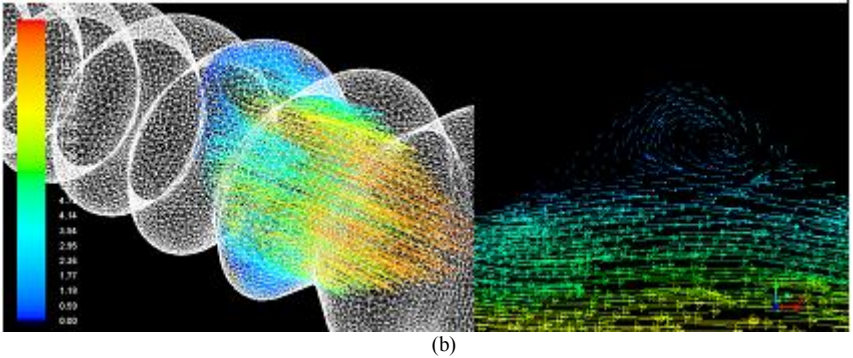

(b)

Fig. 5 Distribution of temperatures (a) and average velocities (b) in the central cross section of the screw-shape tube, and vectors of average speed in the corners of the protrusions-depressions of the tube with a pitch of the helical line t = 8 mm

The above conclusions about the flow development in the volume of a screw-shape tube (pitch of the helical line t = 8 mm) are valid for tubes of helical pitch is 12 and 20 mm (Fig. 6 and 7) also. The differences begin in the

scale and location of the vortex harness in the protrusions-depressions of the helical surface of the tube. Thus, in a case of line pitch t = 12 mm, the vortex formed in the depressions-protrusions is shifted to their top and has a scale close to the radius of curvature at the top of the protrusion-depression of the helical surface. The flow enters freely to the space of the depression and comes into contact with the heated wall. For a screw-shape tube with a pitch of the helical line t = 20 mm, the vortex in question is not formed, and the increase in heat transfer intensity (compared to a cylindrical tube) is associated with the creation of process, preventing to the development and future closure of developing boundary layers on the walls of the screw-shape tube. This reduces the thermal resistance of heat transfer and improves the tube thermal characteristics as a whole.

The above circumstance, regarding the transformation of the flow structure due to the increase in the helical line pitch, which forms the shape of the tube, indicates a decrease in aerodynamic resistance. Indeed, for screw-shape tube with helix steps of 8, 12 and 20 mm to achieve a speed of 4 m/s it is necessary to provide a pressure drop of 124, 78 and 54 Pa respectively. Looking ahead, it must be stated that a smooth cylindrical tube with the same inner diameter has an aerodynamic resistance of 14 Pa.

The resulting situation is quite ambiguous: on the one hand, screw-shape tubes are able to dissipate significantly more heat than smooth cylindrical ones, on the other hand they have high aerodynamic resistance. This result has a simple explanation - the flow in such pipes of the specified length of 500 mm is typical for the initial section. According to the known literature data for a cylindrical tube, the length of the hydrodynamic stabilization section is determined from the condition $L = 50d$, where d is the inner diameter of the tube. In the case of the cylindrical tube studied in this work, we have a stabilized flow, which explains the value of its aerodynamic resistance.

Summarizing the above, it can be stated that the shape of the screw-shape tube allows to organize the movement of the coolant along the helical line, while mixing both the wall layers and the flow core, which generally leads to a significant increase in heat transfer intensity compared to a smooth cylindrical tube of the same diameter. Screw-shape tubes are able to dissipate almost twice the heat flow than a smooth ones, but have aerodynamic resistance in 6… 10 times greater. In this case, the increase in the intensity of heat transfer is affected only by the possibility of organizing the movement along the helical line, and the change of pitch does not cause a significant increase in heat dissipation.

4. Stress-strain state analysis

Using the determined characteristics of heat flow and temperature distribution the stress-strain state of screw-shape tube under the action of internal pressure and the temperature load of the flow on their walls was modeled. The results of calculating of the stress and strain distribution of the model of a screw-shape tube with a helical line pitch of 12 mm are presented in Fig. 6. The values of deformation intensity (Total deformation) and stresses

intensity factor (Equivalent von-Mises stress) were chosen for the analysis. For all other studied forms of the surface of screw-shape tube (the helical line pitch of 8 and 20 mm) the level of stresses and strains is almost the same.

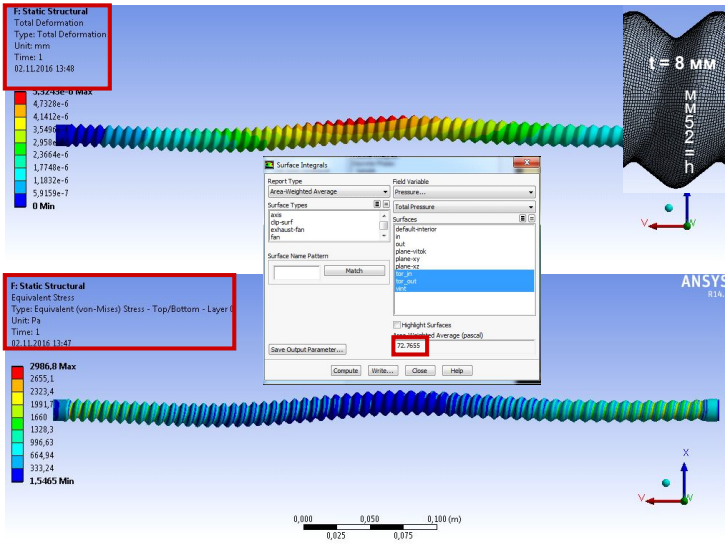

Fig. 6. Distribution of stresses and strains of the screw-shape tube (t = 12 mm)

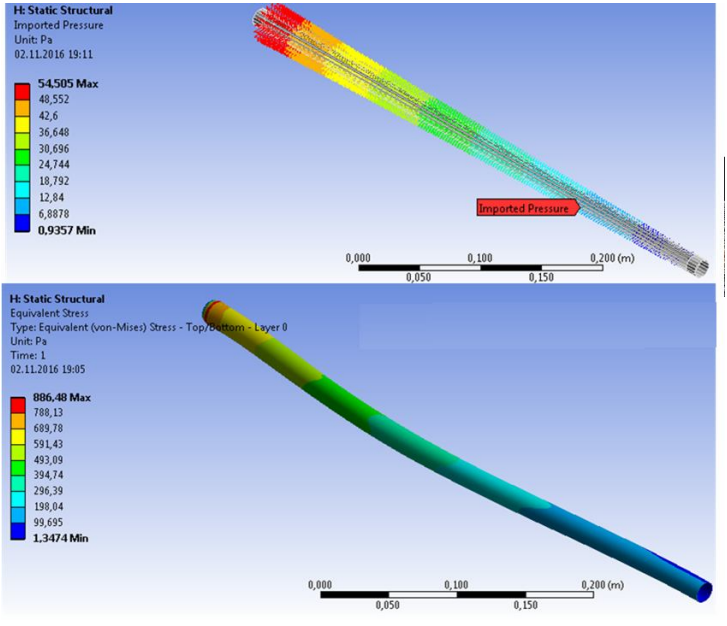

Fig. 7. Distribution of stresses and strains of a smooth cylindrical tube
(inlet temperature 333.15 K = 60°C)

Analysis of this results indicates that for a pressure drop of 74 Pa at an average wall temperature of 48 ° C, the largest displacement values of the tube walls are $5 \cdot 10^{-6}$ mm. This corresponds to a stress intensity of 1300 Pa. It should be note that the stress due to the excess internal pressure in a smooth cylindrical tube (Fig. 7) is 480 Pa.

5. Conclusions

1. Under conditions of ensuring a constant flow rate, the optimal helical line pitch is 8 mm. In this case, while maintaining other constant parameters, the screw-shape tube is able to dissipate almost twice much of heat.

2. For the investigated standard sizes of screw-shape tube (helical line pitch of 8 and 12 mm) growth of heat exchange intensity on 44 ... 50% is followed by growth of aerodynamic resistance in 9 ... 10 times, and for a pitch value of 20 mm heat exchange intensity increases by 30% at simultaneous increase in aerodynamic resistance in 5 ... 6 times.

3. Based on numerical simulation data, it is shown that the largest values of displacements are $5 \cdot 10^{-6}$ мм. In screw-shape tube, this corresponds to a stress of 1300 Pa, which is 2.5 times more than for a cylindrical tube.

It should be noted that obtained results are approximate, as they do not take into account heat transfer from the outer surface and do not reveal all the possibilities of using a uniformly helical surface as an industrial element of heat exchangers, but their efficiency compared to cylindrical tubes is obvious. Study the industrial use of screw-shape tube with a uniform surface needs additional experiments. In addition, due to the complexity of the helical surface configuration, the stress state of such tubes is significantly heterogeneous, and the stress values significantly exceed those that occur under the same conditions in cylindrical tubes. Therefore, the solution of the question of safe operation of the proposed tubes with a helical surface requires numerical analysis of the stress-strained state at different modes of heat load.

REFERENCES

1. *Bystrov Yu.A.* Chislennoe modelirovanie vihrevoj intensifikacii teploobmena v paketah trub [Numerical simulation of heat transfer enhancement in the vortex bags pipes (in Ukrainian)] / Yu.A. Bystrov, S.A. Isaev, N.A. Kudryavcev, A.I. Leontev. – S-Pb.: Sudostroenie, 2005. – 392 p.
2. *Isachenko V.P.* Teploperedacha [Heat transfer (in Ukrainian)] / V.P. Isachenko, V.A. Osipova, A.S. Sukomel - Moskva: Energiya, 1975. - 199 p.
3. *Kalinin E.K.* Effektivnye poverhnosti teploobmena [Efficient heat exchange surface (in Ukrainian)] / E.K. Kalinin, G.A. Drejcer, I.Z. Kopp, A.S. Myakochin. – Moskva.: Energoatomizdat, 1998. – 131 p.
4. *Makovej V.O.* Osoblivosti profilyuvannya odno- ta trohzahidnih gvintopodibnih trub [Features of profiling of one- and three-pass screw-shape tubes (in Ukrainian)] / Makovej V.O., Procenko P.Yu.// Vestnik Nacionalnogo tehnicheskogo universiteta “HPI”. – 2013. - №43(1016). – PP.153-162.
5. Patent 102107 UA, МПК B 21 D 15/04. Sposib profilyuvannya gvintopodibnih trub [The method of profiling screw-shape tubes (in Ukrainian)] / M.I. Bobir, V.O. Makovej, V.S. Melnik, P.Yu. Procenko (UA) - № U201505016; stated. 22.05.2015; publ. 12.10.2015, Bul. №19.
6. *Pismennij Ye.M.* Teploobmin puchkiv trub z rivnorozvinenoyu poverhneyu [Heat exchange of bundles of pipes with an evenly developed surface (in Ukrainian)] / E.N. Pis’mennyi, VA Rogachev, OM Terekh, V.I. Konshin, D.S. Omelchuk // Eastern European Journal of advanced technologies. - 2013. - №1 / 8 (61). - PP. 29 -33.

7. *Reva S.A.* Teploobmin maloryadnih puchkiv gvintopodibnih tryb [Heat exchange of low-row bundles of helical pipes (in Ukrainian)] / S.A. Reva, V.A. Rogachev, O.M. Terekhov, O.V. Alforova // Eastern European Journal of advanced technologies. - 2013. - №3 / 8 (63). PP. 54-56.
8. *Chugayev R.R.* Gidravlika Гидравлика [Hydraulics (in Ukrainian)] / R.R. Chugayev – L.: Energy, 1970. – 552 p.
9. *Pis'mennyi E.N.* Ways for Improving the Tubular Heaters Used in Gas Turbine Units / E.N. Pis'mennyi. // Thermal Engineering. – 2012. – Vol. 59. №6. – P. 485-490.

Стаття надійшла до редакції 20.11.2020 р.

Пискунов С.О., Трубачев С.І., Баранюк О.В.

ДОСЛІДЖЕННЯ НАПРУЖЕНО-ДЕФОРМОВАНОГО СТАНУ ГВИНТОПОДІБНИХ ТРУБ ТЕПЛООБМІННИХ АПАРАТІВ

На основі результатів дослідження параметрів течії повітряного потоку всередині латунної гвинтоподібної труби теплообмінного апарату проведено визначення їх оптимальних геометричних характеристик і подальше моделювання напружено-деформованого стану. Верифікація результатів моделювання здійснена на основі зіставлення з тестовою задачею.

Ключові слова: теплообмін, гвинтоподібна труба, равноразвітая поверхню, вимушена конвекція, пружне деформування, напружено-деформований стан.

Pyskunov S., Trubachev S., Baranyuk O.

INVESTIGATION OF A STRESS-STRAINED STATE OF A SCREW-SHAPE TUBE OF HEAT EXCHANGER

Based on the results of the study of the parameters of the air flow inside of the brass screw-shape tube of the heat exchanger, the determination of their optimal geometric characteristics and further modeling of the stress-strain state was performed. Verification of simulation results is carried out on the basis of comparison with the test task.

Keywords: heat transfer, helical tube, evenly developed surface, forced convection, elastic deformation, stress-strain state.

Пискунов С.О., Трубачев С.И., Баранюк А.В.

ИССЛЕДОВАНИЕ НАПРЯЖЕННО-ДЕФОРМИРОВАННОГО СОСТОЯНИЯ ВИНТООБРАЗНЫХ ТРУБ ТЕПЛООБМЕННЫХ АППАРАТОВ

На основе результатов исследования параметров течения воздушного потока внутри латунной винтообразной трубы теплообменного аппарата проведено определение их оптимальных геометрических характеристик и дальнейшее моделирование напряженно-деформированного состояния. Верификация результатов моделирования осуществлена на основе сопоставления с тестовой задачей.

Ключевые слова: теплообмен, винтообразная труба, равноразвитая поверхность, вынужденная конвекция, упругое деформирование, напряженно-деформированное состояние.

УДК 539.3
Пискунов С.О., Трубачев С.І., Баранюк О.В. **Дослідження напруженого стану гвинтоподібних труб теплообмінних апаратів** // Опір матеріалів і теорія споруд: наук.-тех. збірн. – Київ: КНУБА, 2020. – Вип. 105. – С. 13-23.–Engl.

На основі результатів аналізу параметрів течії повітряного потоку визначено оптимальні геометричні характеристики гвинтоподібних труб та подальше моделювання їх напружено-деформованого стану.

Табл. 0. Іл. 7. Бібліогр. 9 назв.

UDC 539.3
Pyskunov S., Trubachev S., Baranyuk O.
Investigation of a stress-strained state of a screw-shape tubes of heat exchangers // Strength of Materials and Theory of Structures: Scientific-and-technical collected articles. – K.: KNUBA, 2020. – Issue 105. – P. 13-23.

Based on the results of the analysis of the parameters of the air flow, the optimal geometric characteristics of the helical pipes and further modeling of their stress-strain state are determined..

Table 0. Fig. 7. Ref. 9

УДК 539.3
Пискунов С.О., Трубачев С.И., Баранюк А.В..
Исследование напряжено-деформированного состояния винтоподобных труб теплообменных аппаратов // Опір матеріалів і теорія споруд: наук.-тех. збірн. – Київ: КНУБА, 2020. – Вип. 105. – С. 13-23.–Engl.

На основе результатов анализа параметров течения воздушного потока определены оптимальные геометрические характеристики винтовых труб и дальнейшее моделирование их напряженно-деформированного состояния.

Табл. 0. Рис. 7. Библиогр. 9 назв.

Автор (вчений ступінь, вчене звання, посада)*: доктор технічних наук, професор, завідувач кафедрою динаміки і міцності машин та опору матеріалів НТУУ «КПІ ім. Ігоря Сікорського» Пискунов Сергій Олегович.*
Адреса: *03056 Україна, м. Київ, просп. Перемоги 37, Національний технічний університет України "Київський політехнічний інститут імені Ігоря Сікорського", кафедра динаміки і міцності машин та опору матеріалів*
Робочий тел.: *+38(044) 204-95-35*
Мобільний тел.: *+38(050) 962-66-14*
E-mail: s_piskunov@ua.fm
ORCID ID: https://orcid.org/0000-0003-3987-0583

Автор (вчена ступінь, вчене звання, посада)*: доцент, кандидат технічних наук, доцент кафедри динаміки і міцності машин та опору матеріалів Трубачев Сергій Іванович*
Адреса робоча: *03056, Україна, м. Київ, просп. Перемоги, 37, Національний технічний університет України «Київський політехнічний інститут імені Ігоря Сікорського» ТРУБАЧЕВУ Сергію Івановичу*
Робочий тел.: *+38(044) 204-97-87*
E-mail: strubachev@i.ua

Автор (вчена ступінь, вчене звання, посада)*: доцент, кандидат технічних наук, доцент кафедри атомних електростанцій і інженерної теплофізики Баранюк Олександр Володимирович*
Адреса робоча: *03056, Україна, м. Київ, просп. Перемоги, 37, Національний технічний університет України «Київський політехнічний інститут імені Ігоря Сікорського» БАНАНЮКУ Олександру Володимировичу*
Робочий тел.: *+38(044) 204-97-87*
E-mail: aleksandrW@i.ua

UDC 539.375

SEMI-ANALYTICAL METHOD OF FINISHED ELEMENTS IN ELASTIC AND ELASTIC-PLASTIC POSITION FOR CURVILINE PRISMATIC OBJECTS

V.A. Bazhenov,
Doctor of Technical Science

A.A Shkril',
Doctor of Technical Science

Yu.V Maksimyuk,
Doctor of Technical Science

I.Yu. Martyniuk,
Candidate of Technical Science

O.V. Maksimyuk

Kyiv National University of Construction and Architecture

Povitroflotsky Ave., 31, Kyiv, 03037

DOI: 10.32347/2410-2547.2020.105.24-32

In [4,5,6], the solving relations and the algorithm of the method of block iterations of solving linear and nonlinear equations by the semivanalytic finite element method for curvilinear inhomogeneous prismatic bodies are realized. This paper presents the results of the effectiveness of the semi-analytical finite element method for the consideration of curvilinear prismatic objects in elastic and elastic-plastic formulation in comparison with the classical finite element method.

Keywords: finite element method, semi-analytical finite element method, block iteration method, linear and nonlinear equations, elastic and elastic-plastic deformation, Michlin polynomials, curvilinear prismatic bodies.

Introduction. The choice of the optimal in terms of machine time and speed of convergence of the iterative process algorithm for solving systems of linear and nonlinear equations by semi-analytical finite element method [1, 2, 3] is an important factor influencing the efficiency of the method as a whole. Numerous studies have shown that the use of the block iteration method to solve systems of equations of the semi-analytical finite element method for prismatic bodies with variable parameters has a number of important advantages over the solution of systems of the traditional version of the finite element method.

The organization of the computational process and its software implementation takes into account the basic requirements for software for calculating strength on modern software packages. The modular structure of the developed system of programs provides its non-closedness concerning new classes of tasks.

The purpose of this work is to show the effectiveness of the finite element method semianalitic consideration curvilinear prismatic objects in elastic and elastic-plastic formulation compared to the classical method of finite elements.

Effectiveness of SAFEM application to the consideration of curvilinear prismatic objects in elastic and elastic-plastic formulation.

A rational choice of the system of coordinate functions φ^l significantly affects on the main criteria for the effectiveness of the semi-analytical method, such as the convergence of the iterative process of solving systems of equations and the accuracy of the solutions depending on the number of retained members of the schedule.

The easiest way to model various variants of fastenings is allowed by systems of basic functions that take zero values at the butt-end and are supplemented by Lagrange polynomials of zero and first order. It is proposed to use Michlin polynomials as such a system. There are other types of expansions that provide for the equation to zero displacements at the butt-end of the body, such as decomposition in a series along the sines.

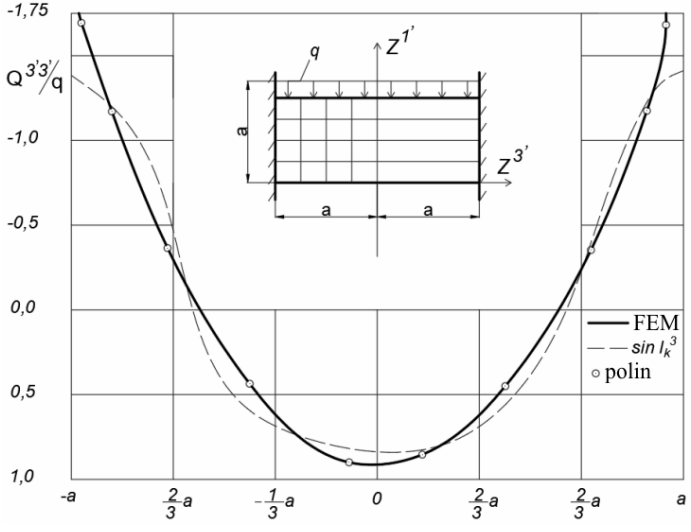

Fig. 1. Calculation of a prismatic beam considered in a flat statement

Let us compare these functions on the example of a prismatic beam rigidly fixed at the ends, which is considered in a flat formulation (Fig. 1), the reference solution of which is obtained by the finite element method. In solving of SAFEM task for both φ^l the 5 members of the row were abstain. The calculations take the unit values of the modulus of elasticity of the material and the intensity of the uniformly distributed surface of the load body.

Analysis of stress distribution $\sigma^{3'3'}$ along $Z^{3'}$, obtained on the basis of both systems of coordinate functions showed, that Michlin polynomials provide a more accurate approximation of the parameters of the stress-strain state along the entire length of the body.

A comparison of the rate of convergence of the iterative process also shows, that using of Michlin polynomials is more acceptable than sinuses, as

to obtain solutions with the same accuracy in the first case required 4 iterations, in the second - 5.

Evaluation of the effectiveness of SAFEM when calculating objects with variables $Z^{3'}$ physical and geometric parameters will be carried out by comparison with the traditional version of FEM.

The various modifications of the Gauss method are most widely used to solve systems of equations of the finite element method. At a constant width of the tape matrix of the system allowing the equations, the estimation of the volume of the required calculations can be conducted by comparing the required number of arithmetic operations to solve systems of linear equations of FEM and SAFEM.

The models with a regular structure of the grid area are considered. Assuming that in all coordinates the dimensions of the grid area are the same and equal to n, determine that the row width of FEM matrix tape is equal to $N_p^{\text{FEM}} = (n^2 + n + 2) \cdot 3$ and SAFEM - $N_p^{\text{SAFEM}} = (n + 2) \cdot 3$, the total number of unknowns for both methods is equal to n^3 .

For a system M of equations with a tape width of the matrix N performing a direct course of the Gauss method requires $M{\cdot}N{\cdot}(N\text{-}1)$ multiplication and $M{\cdot}N$ addition. When performing reverse required M·N multiplication and $M{\cdot}N$ subtraction. It is assumed that the operations of addition and subtraction take the same amount of time. Since the ratio of the width of the row of the matrix of FEM and SAFEM:

$$\frac{N_p^{\text{FEM}}}{N_p^{\text{SAFEM}}} \approx n \qquad (1)$$

to perform the direct course of the Gauss method requires n^2 more multiplication and addition operations than for the SAFEM matrix, and to reverse n times more multiplications and additions. Using the method of block iterations the convergence of the solution of the systems of linear equations of SAFEM is achieved, on average, by n iterations (at ω close to ω_{op}). Considering, that the time of formation of the right part with equal parameters of the grid area the same for SAFEM and FEM, then numerical solution of the system of equations SAFEM using the algorithm investigated, requires 2 operations less than the solution of FEM equations by the Gauss method.

The efficiency of solving systems of equations by the method of block iterations is determined by several factors, such as convergence of the iterative process, determination of the optimal value of the relaxation parameter ω_{op} at the minimum computational costs and the effect of increasing the number of unknowns on the convergence rate.

A quantitative research is carried out on an example of elastic and elastic-plastic deformation of an infinite strip with a rectangular cutout considered in the conditions of plane deformation (Fig. 2). At the butt-end of the boundary conditions are adopted, appropriate reliance on absolutely rigid in the cross-sectional plane and the flexible diaphragm from it:

$$U^{1'}\big/_{Z^{3'}=\pm 1} = \sigma^{3'3'}\big/_{Z^{3'}=\pm 1} = 0. \qquad (2)$$

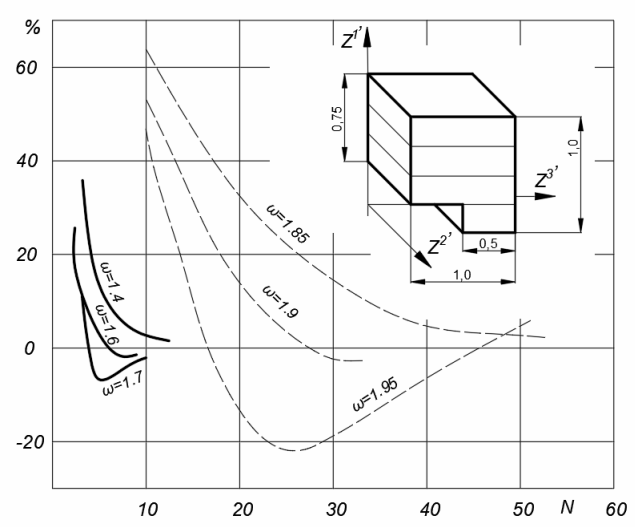

Fig. 2. Elastic and elastic-plastic deformation of an infinite strip with a rectangular cutout

On the upper surface of the body is applied uniformly distributed load intensity of which gradually increases from $0,3\tau_s$ (elastic task) till $0,5\tau_s$. The modulus of elasticity of the material is taken equal to 1, the Poisson's ratio 0,3.

A necessary condition for the correctness of the results of SAFEM and FEM ratio is the same number of unknowns and the number of blocks in the matrices of systems of permitting equations. The calculations took the number of nodes of the grid region in the direction Z^3 at a finite element approximation equal to 9, respectively, kept the first 9 members of the decomposition. Along $Z^{1'}$ in both cases 13 nodes of the grid area were used.

The results of the study of the convergence rate of the block iterations method on the elastic deformation task at different values of the parameter ω for FEM and SAFEM are presented in Fig. 2. The allowable inaccuracy in calculating the maximum relative displacements was calculated as a percentage of the reference result obtained by the FEM using 289 grid nodes. The optimal values of the relaxation parameter were determined in accordance for FEM - $\omega_{op}=1,9$, for SAFEM - $\omega_{op}=1,6$.

Analysis of the curves shows that the rate of convergence of the iterative process in solving systems of linear equations of SAFEM s 5 times higher than for FEM.

Determine ω_{op} is a time-consuming process and to carry it out rationally on the basis of a more liquid finite element grid, so as not to repeatedly solve the problem with a large number of finite elements. In this regard, studies of the change in the rate of convergence of the iterative process with increasing

number of blocks in the matrix at a fixed value of ω on the example of elastic deformation of the strip with a cutout.

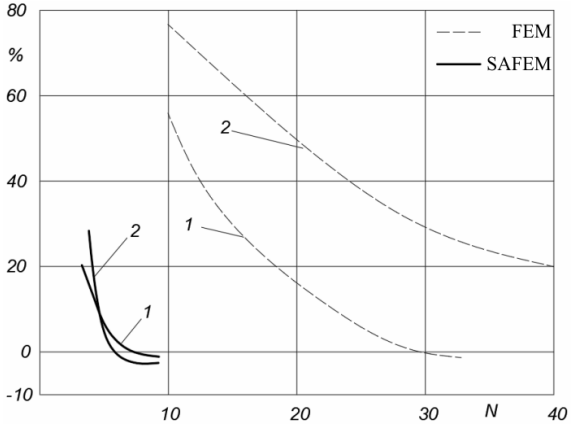

Fig 3. Permissible inaccuracy in determining the maximum displacements from the number of iterations

At optimal values of ω, the convergence of the block iteration method was studied for the given grid area with an increase of 1,5 times respectively the number of finite elements along Z^3 or retained basis functions. The results are shown in Fig. 3 in the form of graphs that show the permissible inaccuracy in determining the maximum displacements from the number of iterations. The number 1 indicates the graphs obtained for the reference grid area, 2 - for the specified. The figure shows that the increase in the number of blocks in a matrix SAFEM does not affect the rate of convergence of the iterative process. The figure shows that the increase in the number of blocks in a matrix SAFEM does not affect the rate of convergence of the iterative process, while for FEM matrix it leads to a significant (2,2 times) increase in the number of iterations.

The curves characterizing the dependence of the number of iterations on the value of the relaxation parameter for the elastic-plastic calculation are shown in Fig. 4. Analysis of the data indicates a significant advantage of SAFEM for a class of the tasks considered. Thus, at the maximum level of development of plastic deformations, the iterative process for SAFEM converges 5 times faster than for FEM. However, the actual reduction in the amount of calculations is much greater due to a significant reduction in additional research to determine the optimal value of the relaxation parameter ω_{op}.

Analysis of the nature of the graphs for the finite element method shows that the relaxation parameter should be chosen from the narrow neighborhood ω_{op}, because failure the condition $\omega=\omega_{op}$ leads to a significant deterioration in the convergence of the computational process. With increasing level of plastic deformation there is a shift of the optimal value of ω in the direction of increase, but the convergence of the iterative process in solving the problem of

plasticity by semi-analytical method at ω_{op}=1,70 - determined at the last step load is only 5% better than at ω_{op}=1,6, found in the first step of the load, while for FEM the use of the value of ω_{op}=1,9, the optimal at $\varepsilon_p^{max} = 0\%$ gives an increase in the number of iterations by 40% compared to ω_{op}=1,95, determined in the last step of the load.

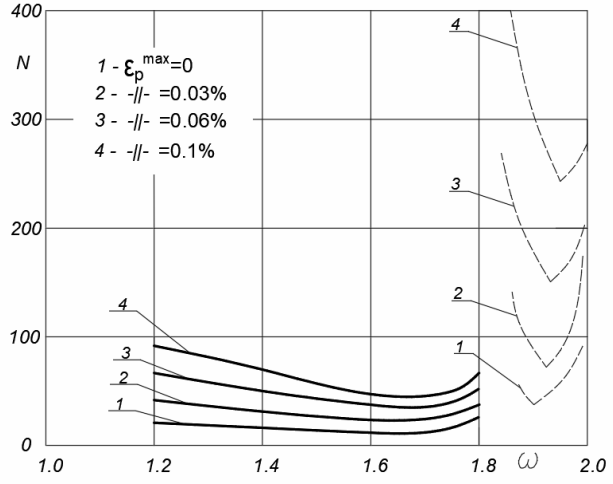

Fig. 4. The dependence of the number of iterations on the value of the relaxation parameter for the elastic-plastic calculation

Consequently, solving the FEM problem requires more time-consuming preliminary studies at maximum levels of plastic deformation to determine the optimal value of the relaxation parameter which is not required when using the semi-analytical variant, because ω_{op}, which was found in the first load step, provides good convergence and next steps.

Conclusion. On this basis, it is advisable to determine the optimal value of the relaxation parameter for the semi-analytical method on a liquid grid and in the elastic stress region, because the same value is optimal on dense grids, and the shift in plasticity problems does not lead to a significant reduction in computational volume with the required costs at the relaxation parameter optimal for the elastic problem. Using the finite element method to search for ω_{op}, it is necessary to repeatedly solve a physically nonlinear problem without reducing the size of the grid area, which requires significant quantitative research.

Using block of iterations to solving systems of nonlinear equations SAFEM about an order of magnitude performance dominates the traditional finite element method.

REFERENCES

1. *Bazhenov V.A.* Neliniine deformuvannia ta stiikist pruzhnykh obolonok neodnoridnoi struktury (Nonlinear deformation and stability of elastic shells of inhomogeneous structure) / V.A. Bazhenov, O.P. Kryvenko, M.O. Solovei – K. : ZAT «Vipol», 2010. – 315 p.
1. *Bazhenov V.A.* Chyselne modeliuvannia protsesiv neliniinoho deformuvannia til z urakhuvanniam velykykh plastychnykh deformatsii (Numerical modeling of nonlinear deformation processes of bodies taking into account large plastic deformations) / V.A. Bazhenov, Yu.V. Maksymiuk, I.I. Solodei, R.L. Stryhun – Kyiv: "Karavela", 2019. – 223 p.
2. *Bazhenov V. A.* Napivanalitychnyi metod skinchennykh elementiv v zadachakh ruinuvannia prostorovykh til : Monohrafiia (Semi-analytical method of finite elements in problems of destruction of spatial bodies: Monograph) / V. A. Bazhenov, O. I. Huliar, S. O. Pyskunov, O. S. Sakharov – K. : KNUBA, 2005. – 298 p.
3. *Huliar O.I.* Universalnyi pryzmatychnyi skinchenyi element zahalnoho typu dlia fizychno i heometrychno neliniinykh zadach deformuvannia pryzmatychnykh til (Universal prismatic finite element of general type for physically and geometrically nonlinear problems of deformation of prismatic bodies) / O.I. Huliar, Yu.V. Maksymiuk, A.A. Kozak, O.V. Maksymiuk // Budivelni konstruktsii teoriia i praktyka – 2020. – Issue 6. – P. 72–84.
4. *Maksymiuk Yu.V.* Alhorytm rozviazannia systemy liniinykh ta neliniinykh rivnian napivanalitychnym metodom skinchenykh elementiv dlia kryvoliniinykh neodnoridnykh pryzmatychnykh til (Algorithm for solving a system of linear and nonlinear equations by the semivanalytic finite element method for curvilinear inhomogeneous prismatic bodies) / Yu.V. Maksymiuk, M.V. Honcharenko, I.Iu. Martyniuk, O.V. Maksymiuk // Budivelni konstruktsii teoriia i praktyka – 2020. – Issue 7. – P. 101–108.
5. *Maksimyuk Yu.V.* Basic relations for physically and geometrically nonlinear problems of deformation of prismatic bodies (Основні співвідношення для фізично і геометрично нелінійних задач деформування призматичних тіл) / Yu.V. Maksimyuk, S.O. Pyskunov, A.A. Shkril, O.V. Maksimyuk // Opir materialiv i teoriia sporud. – 2020. – Issue 104. – P. 255–264.

Стаття надійшла до редакції 03.09.2020

Баженов В.А., Шкриль А.А., Максимюк Ю.В., Мартинюк І.Ю., Максимюк О.В.

НАПІВАНАЛІТИЧНОГО МЕТОД СКІНЧЕННИХ ЕЛЕМЕНТІВ У ПРУЖНІЙ І ПРУЖНОПЛАСТИЧНЫЙ ПОСТАНОВЦІ ДЛЯ КРИВОЛІНІЙНИХ ПРИЗМАТИЧНИХ ОБ'ЄКТІВ

В статті наведені результати ефективності застосування напіваналітичного методу скінчених елементів до розгляду криволінійних призматичних об'єктів у пружній та пружно-пластичній постановці в порівнянні з класичним методом скінчених елементів.

Ключові слова: метод скінченних елементів (МСЕ), напіваналітичного метод кінцевих елементів (ПМКЕУ), метод блокових ітерацій (МБІ), лінійні і нелінійні рівняння, пружне і пружно-пластичне деформування, поліноми Михлина, криволінійні призматичні тіла.

Bazhenov V.A., Shkril' A.A.,Maksimyuk Yu.V., Martyniuk I.Yu., Maksimyuk O.V.

SEMI-ANALYTICAL METHOD OF FINISHED ELEMENTS IN ELASTIC AND ELASTIC-PLASTIC POSITION FOR CURVILINE PRISMATIC OBJECTS

In [4, 5, 6] the algorithm of the method of block iterations of solving linear and nonlinear equations by the semivanalytic finite element method for curvilinear inhomogeneous prismatic bodies is realized. This paper presents the results of the effectiveness of the semi-analytical finite element method for the consideration of curvilinear prismatic objects in elastic and elastic-plastic formulation.

The choice of the optimal in terms of machine time and speed of convergence of the iterative process algorithm for solving systems of linear and nonlinear equations by the semivanalytic finite element method [1, 2, 3] is an important factor influencing the efficiency of the method as a whole. Numerous studies have shown that using the block iteration method to solve systems of

equations of the semivanalytic finite element method for prismatic bodies with variable parameters has a number of important advantages over solving systems of the traditional variant of the finite element method.

The organization of the computational process and its software implementation takes into account the basic requirements for software for calculating strength on modern software packages. The modular structure of the developed system of programs provides its non-closedness concerning new classes of tasks.

The use of the block iteration method to solve systems of nonlinear equations of SAFEM is approximately an order of magnitude superior to the traditional finite element method.

Keywords: finite element method, semi-analytical finite element method, block iteration method, linear and nonlinear equations, elastic and elastic-plastic deformation, Michlin polynomials, curvilinear prismatic bodies.

Баженов В.А., Шкрыль А.А., Максимюк Ю.В.,Мартинюк И.Ю., Максимюк О.В.
ПОЛУАНАЛИТИЧЕСКИЙ МЕТОД КОНЕЧНЫХ ЭЛЕМЕНТОВ В УПРУГОЙ И УПРУГОПЛАСТИЧЕСКОЙ ПОСТАНОВКЕ ДЛЯ КРИВОЛИНЕЙНЫХ ПРИЗМАТИЧЕСКИХ ОБЪЕКТОВ

В данной работе приведены результаты эффективности применения полуаналитического метода конечных элементов к рассмотрению криволинейных призматических объектов в упругой и упруго-пластической постановке по сравнению с классическим методом конечных элементов.

Ключевые слова: метод конечных элементов (МКЭ), полуаналитического метод конечных элементов (ПМКЭ), метод блочных итераций (МБИ), линейные и нелинейные уравнения, упругое и упруго-пластическое деформирование, полиномы Михлина, криволинейные призматические тела.

УДК 539.375
Баженов В.А., Шкриль О.О., Максим'юк Ю.В., Мартинюк І.Ю., Максим'юк О.В. **Напіваналітичний метод скінчених елементів у пружній та пружно-пластичній постановці для криволінійних призматичних об'єктів** // Опір матеріалів і теорія споруд: наук.-тех. збірн. – Київ: КНУБА, 2020. – Вип. 105. – С. 24-32.

В статті наведені результати ефективності застосування напіваналітичного методу скінчених елементів до розгляду криволінійних призматичних об'єктів у пружній та пружно-пластичній постановці в порівнянні з класичним методом скінчених елементів.
Табл. 0. Іл. 4. Бібліогр. 6 назв.

UDC 539.375
Bazhenov V.A., Shkril' A.A.,Maksimyuk Yu.V., Martyniuk I.Yu., Maksimyuk O.V. **Semi-analytical method of finished elements in elastic and elastic-plastic position for curviline prismatic objects** // Strength of Materials and Theory of Structures: Scientific-&-Technical collected articles – Kyiv: KNUBA, 2020. – Issue 105. – P. 24-32.

This paper presents the results of the effectiveness of the semi-analytical finite element method for the consideration of curvilinear prismatic objects in elastic and elastic-plastic formulation in comparison with the classical finite element method.
Tabl. 0. Fig. 4. Ref. 6.

УДК 539.375
Баженов В.А., Шкриль О.О., Максим'юк Ю.В., Мартинюк І.Ю., Максим'юк О.В. **Полуаналитический метод конечных элементов в упругой и упругопластической постановке для криволинейных призматических объектов** // Сопротивление материалов и теория сооружений: науч.-тех. сборн. – К.: КНУСА, 2020. – Вып. 105. – С. 24-32.

В статье приведены результаты эффективности применения полуаналитического метода конечных элементов к рассмотрению криволинейных призматических объектов в упругой и упруго-пластической постановке по сравнению с классическим методом конечных элементов.
Табл. 0. Ил. 4. Библиогр. 6 назв.

Автор (вчена ступень, вчене звання, посада): *доктор технічних наук, професор, академік Національної академії педагогічних наук України, завідувач кафедри будівельної механіки Київського національного університету будівництва і архітектури, директор НДІ будівельної механіки БАЖЕНОВ Віктор Андрійович*
Адреса робоча: *03037 Україна, м. Київ, Повітрофлотський проспект 31, Київський національний університет будівництва і архітектури.*
Робочий тел.: *+38(044) 245-48-29.*
мобільний тел.: *+38(067)111-22-33*
E-mail: bazhenov.va@knuba.edu.ua
ORCID ID: https://orcid/org/0000-0002-5802-9848

Author (degree, academic rank, position): *doctor of technical sciences, professor, academician Of the National Academy of Pedagogical Sciences of Ukraine, Director of the Research Institute of Structural Mechanics Bazhenov Viktor Andriyovych.*

Автор (вчена ступень, вчене звання, посада)*: професор, доктор технічних наук, професор кафедри будівельної механіки КНУБА Шкриль Олексій Олександрович.*
Author (degree, academic rank, position): *Associate Professor, Doctor of Technical Sciences, Professor of the Department of Structural Mechanics of KNUBA Shkryl Oleksii Oleksandrovych.*
Адреса:*03680 Україна, м. Київ, Повітрофлотський проспект 31, Київський національний університет будівництва і архітектури, кафедра будівельної механіки.*
Мобільний тел.: *+38(050) 307-61-49.*
E-mail: alexniism@ukr.net
ORCID ID: http://orcid.org/0000-0003-0851-4754

Автор (вчена ступень, вчене звання, посада)*: професор, доктор технічних наук, професор кафедри будівельної механіки КНУБА Максим'юк Юрій Всеволодович.*
Author (degree, academic rank, position): *Associate Professor, Doctor of Science (Engineering), Professor at the KNUCA Department of Structural Mechanics Maksymiuk Yurii Vsevolodovych.*
Адреса: *03680 Україна, м. Київ, Повітрофлотський проспект 31, Київський національний університет будівництва і архітектури, кафедра будівельної механіки.*
Робочий тел.: *+38(044) 241-55-38.*
Мобільний тел.: *+38(067) 230-94-72.*
E-mail: maximyuk@ukr.net
ORCID ID: http://orcid.org/0000-0002-5814-6227

Автор (вчена ступень, вчене звання, посада)*: кандидат технічних наук, докторант кафедри будівельної механіки КНУБА Мартинюк Іван Юрійович.*
Author (academic degree, academic rank, position): *candidate of technical sciences, doctoral student of the KNUCA department of structural mechanics Martyniuk Ivan Yuriyovych.*
Адреса: *03680 Україна, м. Київ, Повітрофлотський проспект 31, Київський національний університет будівництва і архітектури, кафедра будівельної механіки.*
Мобільний тел.: *+38(096) 068-00-29*
E-mail: ivan.martinyuk@gmail.com
ORCID ID: http://orcid.org/0000-0001-7957-2068

Автор (вчена ступень, вчене звання, посада): *аспірант Київського національного університету будівництва і архітектури Максим'юк Олександр Всеволодович.*
Author (Academic Degree, Academic Title, Position): *Maksymiuk Oleksandr Vsevolodovych, graduate student of Kyiv National University of Construction and Architecture.*
Адреса: *03680 Україна, м. Київ, Повітрофлотський проспект 31, Київський національний університет будівництва і архітектури, кафедра будівельної механіки.*
Мобільний тел.: +38(067) 306-17-81.
E-mail: sashamaksymiuk@gmail.com
ORCID ID: https://orcid.org/0000-0002-2367-3086

UDC 539.3

ESTABLISHING THE CORRELATION OF THE VERTICAL AND HORIZONTAL PASSIVE FAILURE PRESSURE IN FRONT OF CONSTRUCTED TBM TUNNELS FACE

Nguyen Anh Tuan,
PhD

Tran Van Dung,
M.Eng.

Hochiminh City University of Transport,
No. 2, Vo Oanh St., Ward 25, Binh Thanh Dist., Hochiminh City, Vietnam

DOI: 10.32347/2410-2547.2020.105.33-47

The paper aims to investigate the relationship between factors which have the impacts on the tunnel and the ground and establish formulas to calculate the correlation of the passive failure pressure in front of tunnel face in the vertical and horizontal directions by using the Finite Element Method (FEM).

Keywords: TBM tunnel, FEM, passive failure pressure, tunnel face, sand.

1. Introduction

The Finite Element Method (FEM) was formed from the 40s of the twentieth century and is widely used up to now to find solutions to the problem of elasticity, elasticity - plasticity, ductility - plasticity. Its advantage is taking into account the discontinuity and heterogeneity of stratigraphic structures, which can solve complex boundary problems and calculate the values of stresses - their deformation and distribution. Thanks to these distribution rules, it helps analyze the mechanism of underground construction.

At the beginning of development, numerical analysis was known as a design tool, which was strongly criticized. However, the development of information technology has made a revolution in the field of underground construction. Tunnel construction are calculated with full numerical analysis.

Currently, numerical analysis methods have been simplified and tunnel design is mainly based on experience, intuition and solutions. The underdevelopment of information technology makes the great amount of data be difficult to input and analyze. The difficulty now is solved by powerful computers, user-friendly interface. It also saves time to analyze data from weekly to daily or even hours.

The convenience of numerical analysis methods has been proven. Both the behavior of the materials and boundary conditions have been included in the calculations, and the study of parameters to improve the design of tunnel construction can be done more easily.

2. Literature review

In order to avoid ground loss which can trigger collapse of tunnel face due to instability of surrounding soil, EPB-TBM machine is designed with a closed

boring chamber creating an effective surface stabilization, this makes pressure balance of soils between inside and outside boring machine. Working principle of EPB-TBM is that the excavated soils will be mixed with water, clayey slurry or additives such as foam or polymer. This mixture will form a layer pasting on the boring chamber and creates a balancing pressure versus overburden pressure of ground, and this mixture shall be removed out through conveyors upon completion of construction.

This face pressure shall be kept stably during tunneling process. It is, however that, due to the overburden and water pressures increase from the top to bottom of the tunnel face so the supporting pressure at the bottom must be higher to ensure the balancing condition.

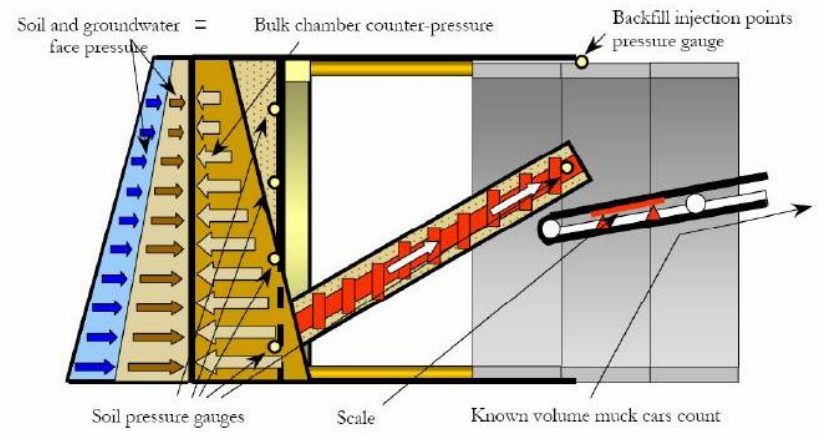

Fig. 1. Schematic representation of the tunnel face pressure control [11]

Broms & Bennermark (1967) evaluated tunnel face stability by using the ratio N which is defined as: [4]

$$N = \frac{\sigma_{ob} - \sigma_T}{S_u} = \frac{\sigma_S - \sigma_T + \gamma(C + \frac{D}{2})}{S_u}. \quad (1)$$

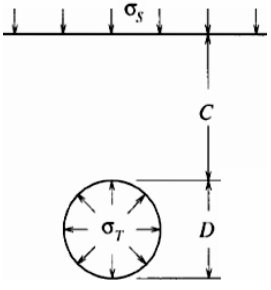

Fig. 2. Cross section of shield tunnelling [7]

Where σ_{ob} is the overburden pressure. And σ_S, σ_T, C, D are defined as Fig. 2.

In the undrained case, all parameters in Equation (1) shall be assumed to be constant, excepting for face pressure σ_T. Hence, N value depends on σ_T. If this supporting pressure reach ultimate value σ_{ob} then tunnel face is completely stable which corresponds to value of $N = 0$.

Davis et. al. (1980) has found four upper bound failure modes which are dependent on tunnel structure as indicated in Fig. 3. [7]

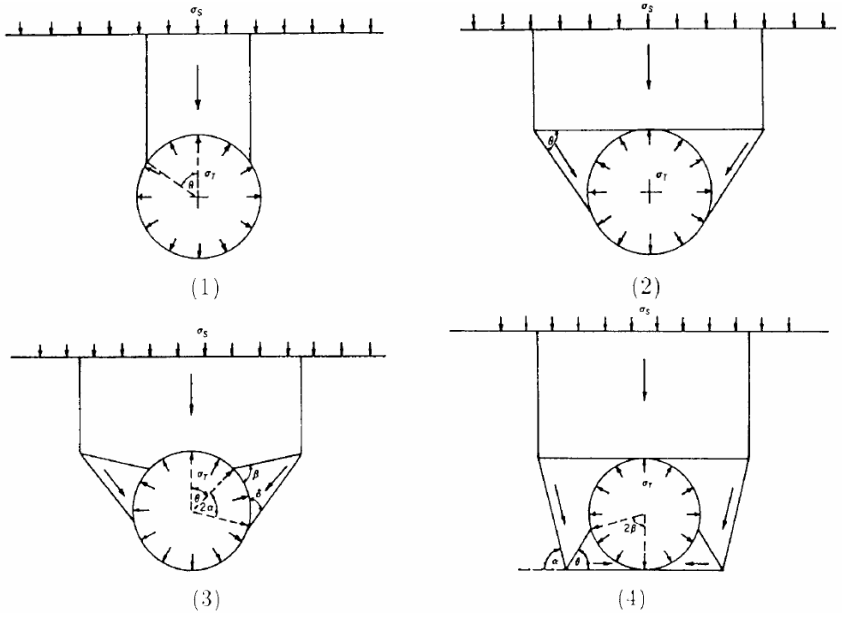

Fig.3. Upper bound failure mechanism [7]

Failure modes (1) and (2) are simple mechanisms, “tunnel roof” and “roof effect and two sides”. Mode (3) is a particular case, covering both (1) and (2). Type (4) is a mechanism with 03 variable angles, saying “tunnel roof side and bottom”.

And lower bound and upper bound stability coefficients with respect to circular tunnel in plane strain condition shall be determined following Fig. 4.

In case of layered soils or soil properties changing over depth, stability coefficient is followed underneath formula:

$$N=\frac{\sigma_S-\sigma_T+\gamma(C+(D/2))}{c_{u0}\left[1+\rho(C+(D/2))\right]}. \quad (2)$$

If assuming stress closed to tunnel crown to be larger than calculated value, then stability coefficient will be:

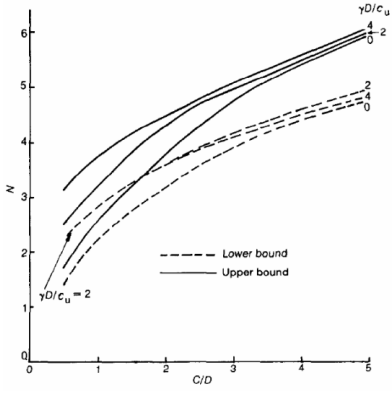

Fig. 4. Upper and lower bound limitation [20]

$$N_{\text{ground}}=\frac{\gamma(C+(D/2))}{c_{u0}\left[1+\rho(C+(D/2))\right]}. \quad (3)$$

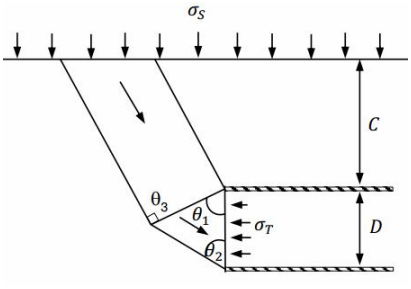

Fig. 5. Upper bound failure mechanism by Davis and partners (1980) [7]

According to Davis et al. (1984), with C/D = 1.5, lower bound and upper bound limits of N vary from 2.9 to 3.4, while $N_{\text{ground}} = 1.67$.

These authors also proposed a upper bound failure mechanism of ground in front of tunnel face based on angles as θ_1, θ_2 and θ_3.

Where:

$$\tan\theta_1 = \tan\theta_2 = 2\sqrt{C/D + 1/4}\,, \quad (4)$$

$$\theta_3 = \pi/2. \quad (5)$$

Table 1

Summary of tunnel face supporting pressure [9]

Tunnel diameter, m	Soil type	Applicable supporting pressure
Earth Pressure Balance (EPB)		
7.45	Soft mud	Earth pressure
8.21	Sand, cohesive soil	Earth pressure + water pressure + 20kPa
5.54	Fine sand	Earth pressure + water pressure + surplus pressure
4.93	Sand, cohesive soil	Earth pressure + 30 to 50 kPa
2.48	Gravel, bed rock, cohesive soil	Earth pressure + water pressure
7.78	Gravel, Cohesive soil, soft soil/mud	Passive earth pressure + water pressure
7.35	Soft soil/mud	Earth pressure +10kPa
5.86	Soft cohesive soil	Earth pressure +20kPa
Slurry Pressure Balance		
6.63	Gravel	Water pressure + 10 to 20kPa
7.04	Cohesive soil	Earth pressure
6.84	Soft cohesive soil, sandy diluvium soil	Passive earth pressure + water pressure +20kPa
7.45	Sandy soil, cohesive soil, gravel	Water pressure +30kPa
10.00	Sandy soil, cohesive soil, gravel	Water pressure +40 to 80kPa
7.45	Sandy soil	Pressure of lost soil + water pressure + surplus pressure
10.58	Sandy soil, cohesive soil	Passive earth pressure + water pressure +20kPa
7.25	Sand, gravel, soft soil	Water pressure + 30kPa

Kanayasu (1995) [9] has summarized many tunneling projects using various methods of creating different supporting pressure of tunnel face. When

EPB shield is used, supporting pressure of tunnel face will depend on geological condition, water pressure and surplus pressure. Mortar EPB shield will be controlled by water pressure to act on active earth pressure and excess pressure. This additional pressure is to prevent unfavorable change of pressure during tunneling works. From Table 1, it can be seen that this additional pressure will be 20 kPa.

Mair (1981) [12] has presented and defined Load Factor (LF) as a ratio of stability coefficient in working condition (service state) over failure state. This factor essentially correlates to stability coefficient against failure:

$$LF = \frac{(\sigma_{V0} - \sigma_i)}{(\sigma_{V0} - \sigma_{ic})}. \quad (6)$$

In which σ_{ic} is value of σ_i at failure moment.

Using this coefficient *LF* is convenient to define safety level of tunnel face [18].

Pavlos Vardoulakis et al. (2009) [24] also implemented scaled-down models to investigate failure mechanism of front soil mass. There were 9 experiments with respect to *C/D* ratios of 0.5; 1 and 2 in dry sand. These experiments models a half of circular-shaped tunnel which is originally 7 m diameter. During experiment process, piston moves backward with constant speed and failure mechanism of ground in front of tunnel face is illustrated in Fig. 6. All failure modes have cylindrical-shaped and runs up to ground surface.

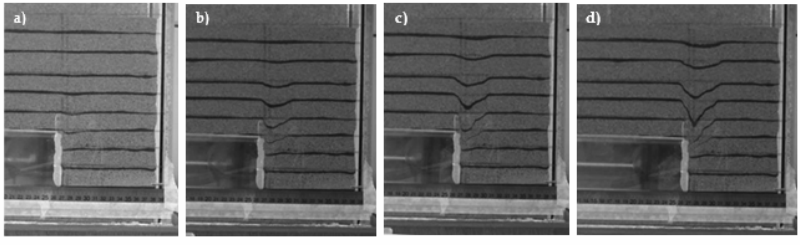

Fig. 6. Test result of *C/D* = 2 [24]

Chambon and Corte (1994) [6] studied failure mechanism and failure active pressure for tunnels embedded at various depth ratio *C/D* ranging from 0.5 - 4.0 by centrifuge tests. Tested dry unit weight of sand was 15.3-16.1 kN/m3, equivalent to void ratios of 0.65-0.92. Prototype diameter of tunnel corresponding to 5m, 10m and 13m were modeled by changing spinning speed of centrifuge machine. Fig. 7. shows the active failure mechanism of tunnels with C/D ratios of 0.5; 1.0 and 2.0. With respect to *C/D* of 0.5, failure mechanism climbs up to ground surface. Fig. 8. shows failure mechanism of 13m-diameter tunnel with *C/D* of 4.0. The observed internal collapse actually caused ground subsidence. It was found that tunnel diameter has a close relationship with failure pressure.

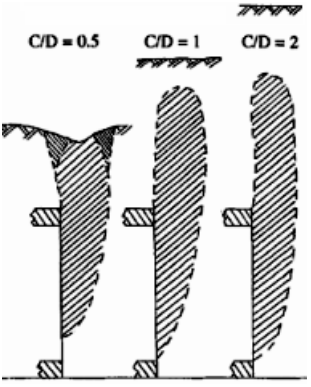

Fig. 7. Failure mechanisms of tunnel *C/D* = 0.5; 1.0 and 2.0 [6]

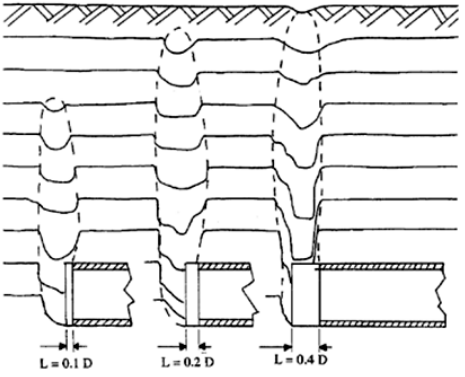

Fig. 8. Failure mechanisms of tunnel face with *D*=13m at *C/D* =4.0, various length of tunnel face [6]

However, surveys on soil around the tunnel are limited. Their disadvantages are not to focus on the soil failure pressure in front of the tunnel face and provide the relationship between factors which have the impacts on the tunnel and the ground. Therefore, the paper helps establish formulas to calculate the correlation of the passive failure pressure in front of tunnel face in the vertical and horizontal directions.

2. Numerical simulation

2.1. Material parameters

Soil parameters for sand and clay and TBM is shown as Table 2.

Table 2

Geological parameters

Soil parameters	Sand	Clay
Saturated unit weight, γ_{sat} (kN/m^3)	20.3	21.1
Unsaturated unit weight, γ_{unsat} (kN/m^3)	19.5	20
Cohesion intercept, c'(kPa)	1.0	300
Angle of friction, φ' (degree)	30^0	1
Angle of dilation, ψ (degree)	0	0
Young modulus, E_{50} (MPa)	27	100
Unloading and reloading modulus, E_{ur} MPa)	81	300
Oedometer modulus, E_{eod} (MPa)	27	100
Poisson's ratio, υ	0.3	0.3
m	0.5	1.0
R_f	0.9	

2.2. Analysis

The tunnel with the 5m diameter is stimulated for cases with *C/D* ratio of 1.5; 2.0; 2.5; 3.3 and 4.0 respectively by using PLAXIS 3D TUNNEL software.

Due to symmetry, only a half of the tunnel was stimulated in this model. The model extended 20m in the z-direction, with the width and depth of 30m and 50.5m respectively. This model is large enough to allow any collapse mechanism to evolve and avoid significantly influence on the boundary of the model.

The interaction between the TBM and soil is defined by the boundary. During excavation, the tunnel pressure is put in the z-direction.

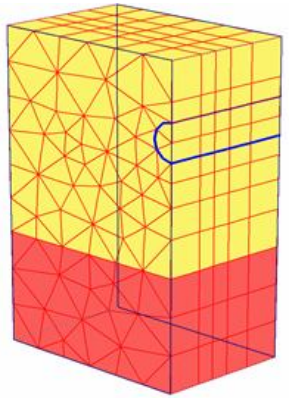

Fig. 9. Finite element mesh adopted for three-dimensional numerical modelling

2.3. Establishing the correlation of passive failure pressure between vertical and horizontal stress in front of the tunnel face

The calculated figures are shown in Table 2.

Table 2

σ_{zz}/σ_{yy} ratio

***C/D*=1.5**		***C/D*=2**		***C/D*=2.5**		***C/D*=3.3**		***C/D*=4**	
σ_{yy}	σ_{zz}	σ_{yy}	σ_{zz}	σ_{yy}	σ_{zz}	σ_{yy}	σ_{zz}	σ_{yy}	σ_{zz}
14.7	11.0	45.5	33.1	51.8	37.1	33.4	22.6	30.7	19.1
71.0	49.0	34.6	22.8	31.4	20.9	66.1	43.7	69.5	41.5
60.2	41.5	92.4	62.2	99.0	67.5	98.3	65.4	117.3	71.0
65.3	44.4	94.8	63.0	120.8	82.5	153.4	102.4	213.6	129.5
153.3	105.6	158.2	107.9	169.2	117.1	208.3	142.3	296.7	175.7
152.6	108.5	185.4	128.3	218.6	150.0	278.1	183.0	338.2	198.6
σ_{zz}/σ_{yy}		σ_{zz}/σ_{yy}		σ_{zz}/σ_{yy}		σ_{zz}/σ_{yy}		σ_{zz}/σ_{yy}	
0.749006		0.728074		0.717220		0.675334		0.622753	
0.690680		0.660592		0.664892		0.661056		0.597708	
0.688416		0.672616		0.681638		0.665371		0.605556	
0.679980		0.664796		0.683047		0.667535		0.606562	
0.689154		0.682144		0.692097		0.683163		0.592043	
0.711103		0.691804		0.686197		0.658096		0.587409	

Let K be a variable depending on the depth of tunnel C and diameter of tunnel D, the relationship of stresses in two directions is shown through K as follows:

$$\sigma_T = K.\sigma_z. \quad (7)$$

To determine the relationship between K and C/D, K_1, K_2, K_3, K_4, K_5 and K_6 is seen as the sections at 8.38406 m, 9.97974 m, 11.38978m 13.64642m, 15.64052 m, 18.83188 m respectively in front of the tunnel face in Z axis.

Based on the data in Table 3, the charts between the parameters are shown in Fig. (10-15).

Table 3

Coefficients K_1, K_2, K_3, K_4, K_5 and K_6

C/D	K_1	K_2	K_3	K_4	K_5	K_6
4	0.622753	0.597708	0.605556	0.606562	0.592043	0.587409
3.3	0.675334	0.661056	0.665371	0.667535	0.683163	0.658096
2.5	0.71722	0.664892	0.681638	0.683047	0.692097	0.686197
2	0.728074	0.660592	0.672616	0.664796	0.682144	0.691804
1.5	0.749006	0.69068	0.688416	0.67998	0.689154	0.711103

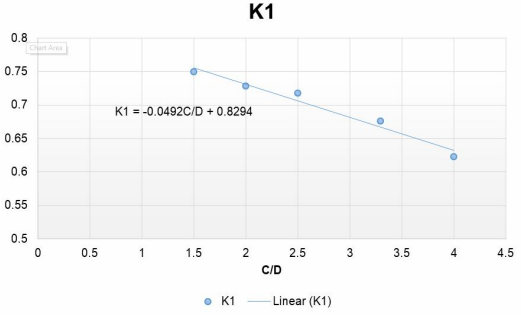

Fig. 10. Relationship chart between K_1 and *C/D*

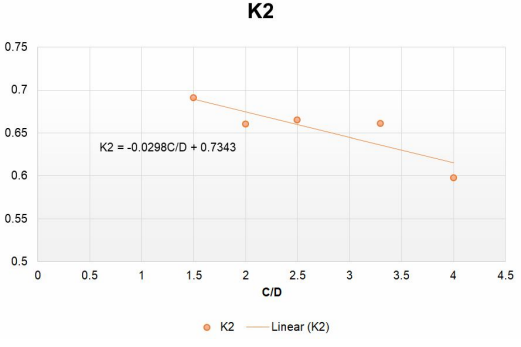

Fig. 11. Relationship chart between K_2 and *C/D*

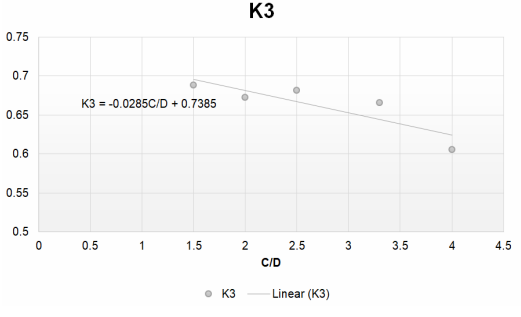

Fig. 12. Relationship chart between K_3 and *C/D*

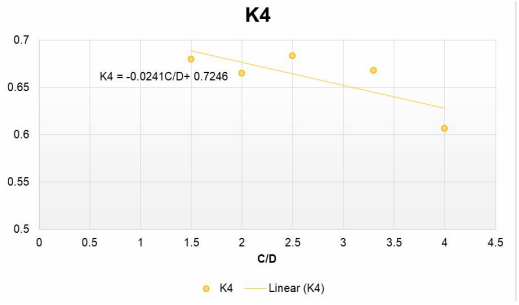

Fig. 13. Relationship chart between K_4 and C/D

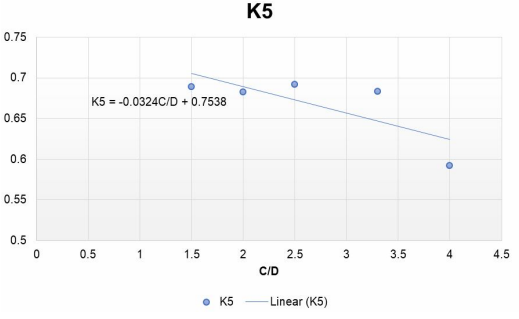

Fig. 14. Relationship chart between K_5 and C/D

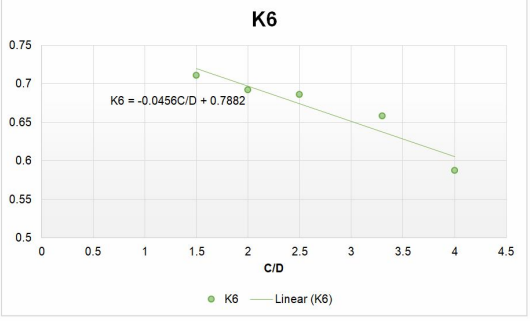

Fig.15. Relationship chart between K_6 and C/D

Let the general formula K be:

$$K = A_1.\frac{C}{D} + A_2. \tag{8}$$

K will change with each cross-sectional area in front of the tunnel face with the coefficients A and B in the graphs in Fig. 10 to Fig. 15, we sum them up into Table 4.

Table 4

Coefficients A_1, A_2 and K_1-K_6

Coefficient	A_1	A_2	z, m
K_1	-0.0492	0.8294	8.38406
K_2	-0.0298	0.7343	9.97974
K_3	-0.0285	0.7385	11.38978
K_4	-0.0241	0.7246	13.64642
K_5	-0.0324	0.7538	15.64052
K_6	-0.0456	0.7882	18.83188

Based on the data in Table 4, we use the chart to show the relationship between the coefficient A_1, A_2 and the sections in front of the tunnel face. The charts are shown in Fig. 16 and Fig. 17.

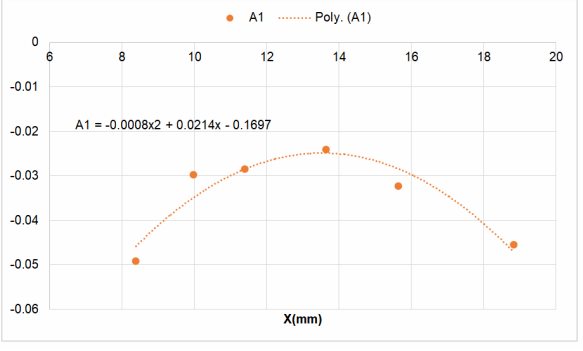

Fig. 16. Chart of A_1 along the vertical axis

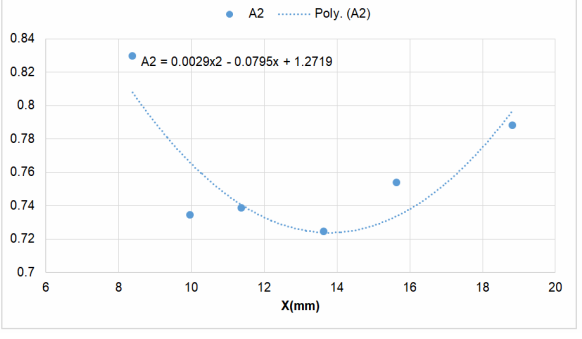

Fig. 17. Chart of A_2 along the vertical axis

The relationship beween K and C/D:

$$K=(-0.0008x^2+0.0214x-0.1697)\frac{C}{D}+0.0029x^2-0.0795x+1.2719. \quad (9)$$

After changing the numbers, we have a table of K coefficient corresponding to the different depths of tunnels as in Table 5.

Table 5

Coefficients $K_{1.5}$, K_2, $K_{2.5}$, $K_{3.3}$ and K_4

Z, m	$K_{1.5}$	K_2	$K_{2.5}$	$K_{3.3}$	K_4
8.38406	0.739443	0.716185	0.692928	0.655716	0.623155
9.97974	0.713622	0.695717	0.677812	0.649165	0.624098
11.38978	0.69801	0.68314	0.66827	0.644478	0.62366
13.64642	0.687092	0.673769	0.660445	0.639128	0.620476
15.64052	0.691853	0.676507	0.66116	0.636605	0.615119
18.83188	0.727606	0.702402	0.677197	0.636869	0.601583

The formula shows the relationship of stress in vertical and horizontal directions:

$$\sigma_z = [(-0.0008x^2 + 0.0214x - 0.1697)\frac{C}{D} + 0.0029x^2 - 0.0795x + 1.2719]\sigma_y. \quad (10)$$

Table 6

Values σ_y in FEM

z, m	σ_y kN/m^2				
	***C/D*=1.5**	***C/D*=2**	***C/D*=2.5**	***C/D*=3.3**	***C/D*=4**
8.38406	14.70697	45.48453	51.75698	33.42773	30.72395
9.97974	70.99307	34.55252	31.36562	66.1367	69.47639
11.38978	60.24304	92.43649	99.00351	98.25886	117.2908
13.64642	65.28522	94.81899	120.7609	153.3606	213.5641
15.64052	153.2471	158.2327	169.1545	208.3287	296.7107
18.83188	152.6218	185.3962	218.5622	278.1142	338.1551

Based on Table 6 and combined with Equation (10), we find σ_z as Table 7.

Table 7

Stress in horizontal direction σ_z calculated by Equation (10)

z, m	σ_y kN/m^2				
	***C/D*=1.5**	***C/D*=2**	***C/D*=2.5**	***C/D*=3.3**	***C/D*=4**
8.38406	10.87496	32.57535	35.86385	21.91909	19.14578
9.97974	50.66223	24.03879	21.26	42.93361	43.36007
11.38978	42.05027	63.14709	66.16108	63.32565	73.14954
13.64642	44.85694	63.88606	79.75595	98.01708	132.5113
15.64052	106.0245	107.0455	111.8382	132.6231	182.5125
18.83188	111.0486	130.2226	148.0096	177.1224	203.4282

After having results from Equation (10), we compare the figures with the results from FEM. The comparison are shown in Fig. 18 to Fig. 22.

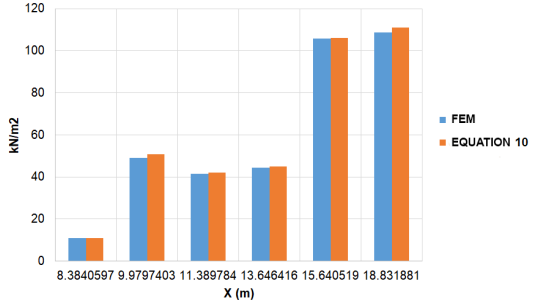

Fig. 18. Deviation σ_z by FEM and Equation (10) at *C/D*=1.5

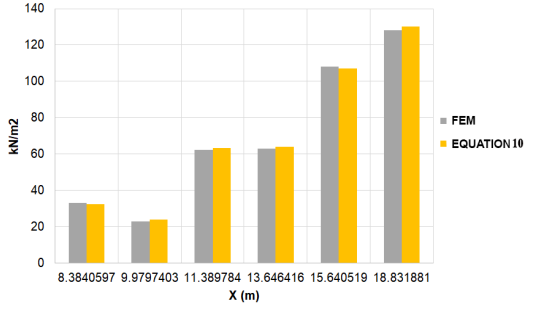

Fig. 19. Deviation σ_z by FEM and Equation (10) at *C/D*=2.0

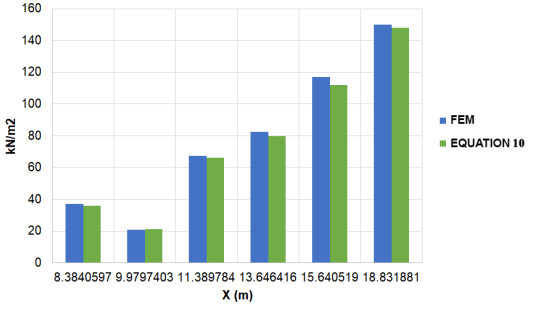

Fig. 20. Deviation σ_z by FEM and Equation (10) at *C/D*=2.5

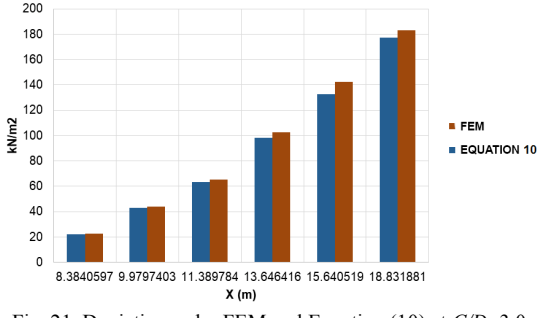

Fig. 21. Deviation σ_z by FEM and Equation (10) at *C/D*=3.0

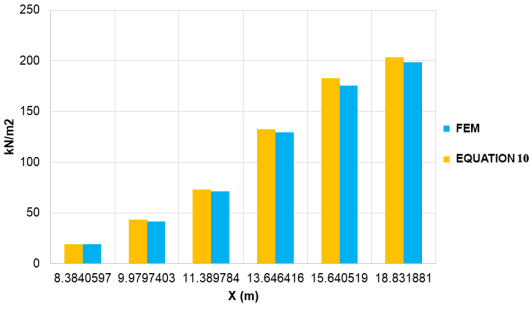

Fig. 22. Deviation σ_z by FEM and Equation (10) at C/D=4.0

It can be seen that the calculated results of stress in vertical and horizontal direction in front of tunnel face from Formula (10) and results from FEM are approximately the same. Thus, under similar geological conditions, we can use the proposed formula by the author to calculate the passive failure pressures in front of the tunnel face.

3. Conclusion

From the results of the calculation, the following conclusions can be drawn:

- It is important to determine the tunnel pressure during the construction process, the greater the depth of tunnel is, the greater the stress in front of tunnel face is. Therefore, it is necessary to calculate the minimum amount of bentonite to avoid the instability of tunnel face.

- For the small errors, it can refer to the given formula to determine the stress in front of tunnel face in the vertical and horizontal directions. However, it is also necessary to refer to results from other methods to obtain the most accurate data because this study only consider a certain geological form, which can result in some mistakes. In addition, the paper has not mentioned changes in groundwater level, rainfall and the existing load on the ground.

REFERENCES

1. Anagnostou, G., & Kovari, K. (1994), The face stability of slurry-shield-driven tunnels.Tunnelling and Underground Space Technology incorporating Trenchless, 9(2), 165-174.
2. Anagnostou, G., & Kovari, K. (1996), Face Stability Conditions with Earth-PressureBalanced Shields. Tunnelling and Underground Space Technology, 11(2), 165-173.
3. Atkinson, J. H., Brown, E. T. and Potts, D. M. (1975), Collapse of shallow unlined tunnels in dense sand. Tunnels and Tunnelling, Vol. 3, pp. 81-87.
4. Broms, B. B. and Bennermark, H. (1967), Stability of clay at vertical openings. ASCE Journal of Soil Mechanics and Foundation Engineering Division SM1, Vol. 93, pp. 71-94.
5. Brinkgreve R. B. J. and Vermeer P. A. (2001), PLAXIS Finite Element Code for Soil and Rock Analyses. A. A. Balkema, Rotterdam.
6. Chambon, P., Corte, J. F. (1994), Shallow tunnels in cohesionless soil: stability of tunnel face. Journal of Geotechnical Engineering - ASCE, 120(7), pp.1148-1165.
7. Davis, E. H., Gunn, M. J., Mair, R. J., Seneviratne, H. N. (1980), The stability of shallow tunnels and underground openings in cohesive material. Geotechnique, 30(4), pp. 397- 416.

8. Dias, D., Janin, J. P., Soubra, A. H., & Kastner, R. (2008), Three-dimensional face stability analysis of circular tunnels by numerical simulations. In Geotechnical Special Publication, (eds), pp. 886-893.
9. Kanayasu S, Kubota I, Shikibu N (1995), Stability of face during shield tunneling-A survey of Japanese shield tunneling. In: Fujita K, Kusakabe O (eds) Proceedings Underground Construction in Soft Ground. New Delhi, pp 337-343.
10. Leca, E., & Dormieux, L. (1990), Upper and lower bound solutions for the face stability of shallow circular tunnels in frictional material. Geotechnique, 40(4), 581-606.
11. Luca Borio (2008), Characterization of soil conditioning for mechanized tunnelling. UNITRACC.
12. Mair, R. J., Gunn, M. J. and O'Reilly, M. P. (1981), Centrifugal testing of model tunnels in soft clay. Presented at the 10th International Conference on Soil Mechanics and Foundation Engineering, Vol.1, pp. 323-328.
13. Mollon, G., Dias, D., Soubra, A. H., (2010), Face Stability Analysis of Circular Tunnels Driven by a Pressurized Shield. Journal of Geotechnical and GeoEnvironmental Engineering, 136(1), 215-229.
14. O'Reilly, M. P. and New, B. M. (1982), Settlements above tunnels in the United Kingdom - their magnitude and prediction. Tunnelling '82, Papers Presented at the 3 International Symposium, Institute of Mining and Metallurgy, London, England, pp. 173-181.
15. 15. O'Reilly, M. and New, B. (1998), Evaluating and predicting ground settlements caused by tunneling in London clay. Proceedings of Tunneling Symposium.
16. Oblozinsky, P., & Kuwano, J. (2004), Centrifuge experiments on stability of tunnel face. Slovak Journal of Civil Engineering (3), 23-29.
17. Sagaseta. C. (1987), Analysis of undrained soil deformation due to ground loss. Géotechnique, Vol.37, No.3, pp. 301-320.
18. Sang-Hwan Kim (1996), Model testing and analysis of interactions between tunnels in clay. DPhil Thesis, Oxford University.
19. Sang-Hwan Kim (1996), Evaluation of Shield Tunnel Face Stability in Soft Ground. International Symposium on Underground Excavation and Tunnelling, pp 213-220.
20. Shirlaw, J. N., (1995), Observed and calculated pore pressures and deformation induced by an earth balace shield: Discussion. Canada Geotech, J. 32, pp. 181-189.
21. Soubra, A. H. (2002), Kinematical approach to the face stability analysis of shallow circular tunnels. Proceedings of the Eight International Symposium on Plasticity, 443-445.
22. Soubra, A. H., Dias, D., Emeriault, F., & Kastner, R. (2008), Three-dimensional face stability analysis of circular tunnels by a kinematical approach. Geotechnical Special Publication, 894-901.
23. Talebinejad, A. et al (2011), Numerical and empirical analysis of face pressure effect on surface subsidence at a tunnel excavated by EPB method. First Asian and 9th Iranian Tunnelling Symposium.
24. Vardoulakis, P., Maria Stavropoulou, George Exadaktylos (2009), Sandbox modeling of the shallow tunnel face collapse. Rivista Italiana Di Geotenica 1/2009, pp. 9-22.
25. Vermeer, P. A., Nico Ruse and Thomas Marcher (2002), Tunnel Heading Stability in Drained Ground. FELSBAU 20, pp. 8-18.
26. Verruijt, A. and Booker, J. R. (1996), Surface settlements due to deformation of a tunnel in an elastic half plane. Géotechnique, Vol. 46, No. 4, pp. 753-756.
27. WONG Kwong Soon (2012), Passive failure and deformation mechanisms due to tunnelling in sand and clay. PhD. Thesis, The Hong Kong University of Science and Technology.

Стаття надійшла до редакції 03.05.2020

Нгуен Ань Туан, Чан Ван Зунг

ВИЗНАЧЕННЯ СПІВВІДНОШЕННЯ ВЕРТИКАЛЬНОГО І ГОРИЗОНТАЛЬНОГО ПАСИВНИХ ТИСКІВ ДЕФОРМОВАНОСТІ ГРУНТІВ ПРИ СПОРУДЖЕННІ ТБМ ТУНЕЛЮ

Метою статті є дослідження взаємозв'язку факторів, що впливають на тунель та основу, та визначити формули для розрахунку кореляції тиску пасивного руйнування перед торцем тунелю у вертикальному та горизонтальному напрямках за допомогою методу кінцевих елементів (МСЕ).

Ключові слова: ТБМ тунель, МСЕ, пасивний тиск руйнування, грань тунелю, пісок.

Nguyen Anh Tuan, Tran Van Dung

ESTABLISHING THE CORRELATION OF THE VERTICAL AND HORIZONTAL PASSIVE FAILURE PRESSURE IN FRONT OF CONSTRUCTED TBM TUNNELS FACE IN SAND

The paper aims to investigate the relationship between factors which have the impacts on the tunnel and the ground and establish formulas to calculate the correlation of the passive failure pressure in front of tunnel face in the vertical and horizontal directions by using the Finite Element Method (FEM).

Keywords: TBM tunnel, FEM, passive failure pressure, tunnel face, sand.

УДК 539.3
Нгуен Ань Туан, Чан Ван Зунг. **Визначення співвідношення вертикального і горизонтального пасивних тисків деформованості грунтів при спорудженні ТБМ тунелю**// Опір матеріалів і теорія споруд: наук.-тех. збірн. – К.: КНУБА, 2020. – Вип. 105. – С. 33-47.
Іл. 22. Бібліогр. 27 назв.

UDC 539.3
Nguyen Anh Tuan, Tran Van Dung. **Establishing the correlation of the vertical and horizontal passive failure pressure in front of constructed tbm tunnels face in sand** // Strength of Materials and Theory of Structures: Scientific-and-technical collected articles. – K.: KNUBA, 2020. – Issue 105. – P. 33-47.
Fig. 22. Ref. 27.

Автор (вчена ступень, вчене звання, посада)*: PhD, Lecturer, Faculty of Transportation Engineering, Hochiminh City University of Transport, Nguyen Anh Tuan*
Адреса: *No. 2, D3 St., Ward 25, Binh Thanh Dist., Hochiminh City, Vietnam.*
Тел.: *(+84) 917.863.898.*
E-mail: *tuankct@hcmutrans.edu.vn*

Автор (вчена ступень, вчене звання, посада)*: MEng, Faculty of Transportation Engineering, Hochiminh City University of Transport, Tran Van Dung*
Адреса: *No. 2, D3 St., Ward 25, Binh Thanh Dist., Hochiminh City, Vietnam.*
Тел.: *(+84) 917.863.898.*
E-mail: *tuankct@hcmutrans.edu.vn*

UDC 539.3

NONLINEAR PROBLEM OF STRUCTURAL DEFORMATION IN INTERACTION WITH ELASTOPLASTIC MEDIUM

I.I. Solodei,
DSc, Department of Structural mechanics

E.Yu. Petrenko,
PhD, Department of Geotechnics

Gh.A. Zatyliuk,
Postgraduate student, Department of Structural mechanics

Kyiv National University of Construction and Architecture

DOI: 10.32347/2410-2547.2020.105.48-63

On the basis of modern numerical implementations of the finite element method the article presents the theoretical foundations of the analysis of deformation processes of machines and structures in their contact interaction with the elastic-plastic nonlinear soil medium within the three-dimensional spatial problem taking into account the previous stress state and load history. The methodology of construction of computational models of joint deformation and mutual influence of rigid structures and essentially plastic external medium is developed, new special heterogeneous finite elements of SAFEM of general form with variable geometrical and physical-mechanical parameters and arbitrary boundary conditions for approximation of arrays of hardly connected reinforced soils are developed.

Keywords: elastic-plastic medium, reinforced soils model, semi-analytical finite element method, moment scheme of finite element.

Introduction. Development of new and improvement of existing production technologies, application of new materials, effective constructive schemes is explained by constant complication of operating conditions. Acute shortage of territories, especially in large cities with dense buildings and limited land space, solving the transport collapse problem due to underground transport, laying pipelines and construction of ground and underground tanks for storage of fuel, water, chemical and food industries components, underground protective structures for military purposes - a small list of challenges that practicing engineers and scientists face today and encourage the continuous improvement of tools for comprehensive analysis of the model behavior that describe the interaction of structures with the environment.

The use of numerical methods in the calculation of machines and structures, taking into account their interaction with the elastic-plastic medium is largely determined by the complexity or even impossibility of analytical calculation due to the complexity of structural schemes, heterogeneity of material features, uneven soil layers, implementation of step-by-step work execution technologies and so on. The development of computer technologies has opened wide opportunities and encouraged researchers to use more complex models, the construction of which is accompanied by various issues: the choice of boundary conditions, load schemes, soil base models, taking into account the history of

the structure final state. Therefore, the development on the basis of modern numerical implementations of the finite element method of new effective methods of computational mechanics for the analysis of nonlinear processes of deformation of structures and buildings in their contact with the elastic-plastic medium is certainly an actual problem of structural mechanics.

Compatible calculations of structures and nonlinear basis, which are described by modern mechanical and soil models in one problem is a significant technical problem. And neither the existing "problem-oriented" software packages, nor the "universal" ones - do not fully contain such models. In designing practice, the simplest Mohr-Coulomb Soil Model is often used for engineering calculations. The model is a logical continuation of the linear-elastic model and is based on the Hooke's Law and the Coulomb's strength condition. Despite the model defects (ignoring the nonlinear dependences between deformations and stresses, constant modulus of deformation), it has a number of significant advantages (traditional parameters, the definition of which is clearly regulated by the norms) and continues to interest domestic and foreign scientists, researches on its improvement continue [31, 1]. The achievements of modern soil mechanics are a large number of mathematical soil models: Hardening Soil Model and its derivatives (Hardening Soil Small-strain), Soft Soil and its derivatives, Cam-Clay etc. Noteworthy are the works that compare different models [11, 4], outline the possible limits of their use [12] and describe the application experience [21]. The Hardening Soil model is attracting more and more attention, which takes into account the soil hardening upon increasing stress levels. The biggest problems when using the model arise due to the large number of parameters, the definition of which is not regulated by the norms. Early publications contained a number of inaccuracies and errors, although they made an invaluable contribution to the model expansion, and recent publications have clarified a number of problematic issues [12]. Research on improving the model continues [20, 8].

The tasks solution is possible only within the framework of numerical methods, the most common of which is the finite element method (FEM) [24]. The construction of the calculated finite element model raises many complex questions that require additional detailed study. In addition, the compliance with the state building norms and regulations is an important factor for further practical use.

The combination of the latest achievements in the field of structural mechanics and soil mechanics is a promising direction for the development of effective approaches for building discrete models of spatial systems "structure-nonlinear base" for solving applied problems.

1. Problem statement. Let's consider in some arbitrary coordinate system $Z^{i'}$ spatial rotation bodies or prismatic bodies formed by the motion of some generating surface along a closed or open arbitrary guide without breaks and which are under the action of nonstationary load, in the time interval $T \in [t_0, t_1]$.

The coordinate system $Z^{i'}$ will be further called basic and used to describe the geometric and mechanical characteristics, initial and ultimate kinematic conditions, external loads. To represent the stress-strain state of the body, we introduce the local curvilinear coordinate system x^i, which is related to the body geometry. The coordinate lines x^1 and x^2 are placed in the generating surface area, and x^3 is oriented along the guide.

It is considered that at any point of the body there is a clear relationship between the basic and local coordinate systems, which is determined by the forward and inverse tensors of the coordinate transformation:

$$z^{i'}_{,j} = \frac{\partial Z^{i'}}{\partial x^j}, \; x^i_{,j'} = \frac{\partial x^i}{\partial Z^{j'}}. \tag{1}$$

Hereinafter, the indices denoted by Latin letters take the values 1, 2, 3, and by Greek - 1, 2, comma before the index shows the operation of differentiation.

The covariant components of the metric tensor of the local coordinate system can be represented through the covariant components of the basic system:

$$g_{ij} = z^{m'}_{,i} z^{n'}_{,j} g_{m'n'}. \tag{2}$$

The contravariant components are located under known covariants:

$$g^{ij} = \frac{\mathrm{A}(g_{ij})}{g}, \tag{3}$$

where $\mathrm{A}(g_{ij})$ is the algebraic addition to the element g_{ij}, $g = \det\left[g_{ij}\right]$ is the matrix determinant.

Geometric Cauchy relationships in curvilinear coordinate systems. In the general case, the strain tensor components in the local coordinate system are determined by the ratio:

$$\varepsilon_{ij} = \frac{1}{2}\left(u_{i,j} + u_{j,i}\right) - u_k \Gamma^k_{ij}, \tag{4}$$

where $u_{i,j} = \frac{\partial u_i}{\partial x^j}$, Γ^k_{ij} are the Christoffel symbols of the second kind, u_i is the movement in the local coordinate system.

For convenience, let's present the movements and the Christoffel symbols by their values in the basic coordinate system:

$$u_k = z^{m'}_{,k} u_{m'}, \tag{5}$$

$$\Gamma^k_{ij} = x^k_{r'} z^{m'}_{,i} \left(z^{n'}_{,j} \Gamma^{r'}_{m'n'} + \frac{\partial z^{r'}_{,j}}{\partial z^{m'}} \right), \tag{6}$$

where $z^{s'}_{,k} x^k_{,r'} = \delta^{s'}_{r'}$ (7).

After substitution (5) – (7) in (4) we obtain the formula for representing the strain tensor components in the local coordinate system through the movements components in the basic [6]:

$$\varepsilon_{ij} = \frac{1}{2}\left(u_{k',i}z^{k'}_{,j} + u_{k',j}z^{k'}_{,i}\right) - u_{k'}z^{m'}_{,i}z^{n'}_{,j}\Gamma^{k'}_{m'n'}. \quad (8)$$

Geometric Cauchy relationships in the Cartesian and the orthogonal cylindrical coordinate systems. The description of prismatic bodies and rotation bodies with variable geometrical and physical-mechanical parameters is most naturally carried out in the orthogonal cylindrical:

$$g_{1'1'} = g_{2'2'} = 1,\ g_{3'3'} = \left(Z^{2'}\right)^2,\ \Gamma^{2'}_{3'3'} = -Z^{2'},\ \Gamma^{3'}_{3'2'} = \Gamma^{3'}_{2'3'} = \frac{1}{Z^{2'}} \quad (9)$$

and the Cartesian coordinate systems:

$$g_{1'1'} = g_{2'2'} = g_{3'3'} = 1,\ \Gamma^{k'}_{l'm'} = 0. \quad (10)$$

In this case, the metric tensor components in the local coordinate system are presented through the components in the basic by the formula:

$$g_{ij} = z^{1'}_{,i}z^{1'}_{,j} + z^{2'}_{,i}z^{2'}_{,j} + z^{3'}_{,i}z^{3'}_{,j}g_{3'3'}. \quad (11)$$

The relationship between movements and deformations (8) can be written as:

$$\varepsilon_{ij} = \frac{1}{2}\left(u_{k',i}z^{k'}_{,j} + u_{k',j}z^{k'}_{,i}\right) - u_{2'}z^{3'}_{,i}z^{3'}_{,j}\Gamma^{2'}_{3'3'} - u_{3'}z^{2'}_{,i}z^{3'}_{,j}\Gamma^{3'}_{2'3'} - u_{3'}z^{3'}_{,i}z^{2'}_{,j}\Gamma^{3'}_{3'2'}. \quad (12)$$

Geometric Cauchy relationships for rotation bodies and rectilinear prismatic bodies. An important partial case of independent practical significance are objects with a canonical guide, for which the geometric equations (12) are greatly simplified. These are primarily heterogeneous circular rotation bodies and prismatic rectilinear bodies with a variable cross-sectional area.

Due to the convergence x^3 and $Z^{3'}$, and their orthogonality to the cross-sectional area in the cylindrical coordinate system ($0 \le x^3 \le 2\pi$):

$$z^{3'}_{,\alpha} = z^{\alpha'}_{,3} = 0,\quad z^{3'}_{,3} = 1 \quad (13)$$

in the Cartesian ($0 \le x^3 \le 2$):

$$z^{3'}_{,\alpha} = z^{\alpha'}_{,3} = 0,\quad z^{3'}_{,3} = a, \quad (14)$$

where a is a half the body length.

Taking into account (13) and (14), the correlations (12) take the form in the orthogonal cylindrical coordinate system:

$$\varepsilon_{\alpha\beta} = \frac{1}{2}\left(z^{\gamma'}_{,\alpha}u_{\gamma',\beta} + z^{\gamma'}_{,\beta}u_{\gamma',\alpha}\right),$$

$$\varepsilon_{\alpha 3} = \frac{1}{2}\left(u_{3',\alpha} + z^{\gamma'}_{,\alpha}u_{\gamma',3} - \frac{2z^{2'}_{,\alpha}u_{3'}}{Z^{2'}}\right),$$

$$\varepsilon_{33} = u_{3',3} + Z^{2'}u_{2'} \quad (15)$$

in the Cartesian:

$$\varepsilon_{\alpha\beta} = \frac{1}{2}\left(z^{\gamma'}_{,\alpha}u_{\gamma',\beta} + z^{\gamma'}_{,\beta}u_{\gamma',\alpha}\right),$$

$$\varepsilon_{\alpha 3} = \frac{1}{2}\left(au_{3',\alpha} + z^{\gamma'}_{,\alpha}u_{\gamma',3}\right),$$

$$\varepsilon_{33} = au_{3',3}. \tag{16}$$

The stress tensor components in the local coordinate system are expressed through the strain tensor components based on the generalized Hooke's Law [6]:

$$\sigma^{ij} = d^{ijkl}\varepsilon_{kl}. \tag{17}$$

In isotropic body, the elastic constant tensor components d^{ijkl} are related to the Lame coefficients λ and μ ratios [23]:

$$d^{ijkl} = \lambda g^{ij}g^{kl} + \mu\left(g^{jl}g^{ik} + g^{il}g^{jk}\right), \tag{18}$$

where $\lambda = \dfrac{E\nu}{(1-2\nu)(1+\nu)}$, $\mu = \dfrac{E}{2(1+\nu)}$, $E = E\left(Z^{i'}\right)$, $\nu = \nu\left(Z^{i'}\right)$ is the value of the elastic modulus and the Poisson's ratio at the body point under consideration.

Within the framework of the accepted dilatancy model for the soil in the boundary state, the deformation increment consists of two parts:

$$d\varepsilon = d\varepsilon^e + d\varepsilon^p. \tag{19}$$

The upper indexes e and p in the values notation indicate their elastic and plastic nature, respectively. The stress increment $d\sigma$ is associated with the elastic deformation increment by the ratio:

$$d\sigma = C \cdot d\varepsilon^e, \tag{20}$$

where C is the elastic constant tensor, the components of which are determined by the formula:

$$C^{ijkl} = \frac{E}{1+\nu}\left[\frac{\nu}{1-\nu}q^{ij}q^{kl} + 0.5\left(q^{ik}q^{jl} + q^{il}q^{jk}\right)\right]. \tag{21}$$

The parameters E and ν denote, respectively, the medium elasticity modulus and the Poisson's ratio, and q^{ij} are the metric tensor components.

The plastic deformation increment $d\varepsilon^p$ is determined based on the unassociated law of plastic flow:

$$d\varepsilon^p = d\lambda\frac{\partial F}{\partial\sigma}, \tag{22}$$

where F is the plastic potential function, $d\lambda$ is the small scalar factor that determines the absolute value $d\varepsilon^p$.

With it:

$$F \neq f, \tag{23}$$

where f is the function that determines the plasticity condition ($f = 0$).

The modified Mises-Schleicher-Botkin condition is used as the boundary state criterion:

$$\begin{cases} f = T + \sigma_m \operatorname{tg}\psi - \tau_s & \text{if} \quad \sigma_m \le p_o, \\ f = T + p_o \operatorname{tg}\psi - \tau_s & \text{if} \quad \sigma_m > p_o, \end{cases} \tag{24}$$

σ_m is the average (hydrostatic) pressure:

$$\sigma_m = \frac{1}{3}\sigma^{ij} q_{ij}\,, \tag{25}$$

T is the intensity of tangent stresses (the second invariant of the stress deviator):

$$T = \sqrt{\frac{1}{2} S^{ij} S_{ij}}\,,\ S_{ij} = \sigma_{ij} - \frac{1}{3}\sigma_m q_{ij}\,, \tag{26}$$

ψ - the friction angle on the octahedral site, $H_R = \dfrac{\tau_s}{\operatorname{tg}\psi}$ is the ultimate resistance to uniform tension, p_o is the soil medium parameter. The condition (24) in the space of principal stresses corresponds to the combined boundary surface, which is a combination of a cone and a cylinder (Fig. 1).

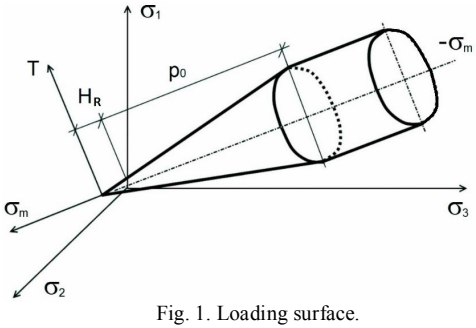

Fig. 1. Loading surface.
General view in space of principal stresses

The need to accept the condition (24) is due to the fact that with a large all-round compression, soils behave like solid bodies, in which it is not possible to achieve loosening even with significant shearings, i.e. there is no dilatancy, and in addition, the ultimate shear load is no longer dependent on the compression level. This corresponds to the acceptance of the conditions for the medium plastic incompressibility and the independence of the limiting shear load from the uniform pressure level – the cylindrical part of the modified condition (24). The value of the parameter p_o of the conical part transition (24) to the cylindrical one was taken equal to $p_o = -2,0$ MPa in accordance with the experimental data of Sidorov and Sipidin [26].

The modified criterion (24) has another distinctive feature. The Mises-Schleicher-Botkin condition in it is consistent with the Coulomb-Mohr condition in such a way that for all kinds of stress states the discrepancy (in the limiting value *T*) is minimal. In addition, the expressions τ_s and $\operatorname{tg}\psi$ were obtained as functions of the norming parameters c (adhesion) and φ (angle of internal friction).

$$\tau_s = \frac{6\sqrt{3} C\cos\varphi}{9 - \sin^2\varphi},\ \operatorname{tg}\psi = \frac{6\sqrt{3}\sin\varphi}{9 - \sin^2\varphi}\,. \tag{27}$$

The procedure for obtaining (27) is described in detail in the work [7].

It can be shown that upon the direct differentiation of the plastic potential function, the expression $\dfrac{dF}{d\sigma^{ij}}$ is similar to that obtained by A.K. Bugrov [9]:

$$F = T + \sigma_m \lambda(x) + \text{const}. \quad (28)$$

It should be noted that the need to accept the potential in the form (28) was pointed out by A.S. Stroganov [30], but all his constructions were made within the framework of the deformation theory of soil plasticity. A.S. Stroganov emphasized [30] that the actual value of the dilatancy coefficient λ is always less than the value $\text{tg}\psi$, i.e. the condition of association $\lambda = \text{tg}\psi$ is not met. A similar form of the potential surface was proposed in the works [32].

V.N. Nikolaevskiy [15] showed that the nature of the plastic potential function corresponding to the dilatancy model depends on the sign of the dilatancy coefficient λ and is represented by the expression:

$$F = T^2 - \lambda \text{tg}\psi\left(\sigma_m + H_R\right)^2. \quad (29)$$

For $\lambda < 0$, the surface corresponding to the function F has the form of an ellipse arc, for $\lambda = 0$, a straight line segment, and for $\lambda > 0$, a hyperbola arc.

In the closing correlations $\lambda = \lambda\left(x\right)$ in the works of V.N. Nikolaevskiy, the volumetric plastic deformation [16] and the density [14] are used as the hardening parameter. In the work [14], the following formula is proposed to determine the dilatancy coefficient:

$$\lambda = -\sqrt{1-\left(\frac{\rho}{\rho^{\text{cr}}}\right)^2} \text{ for } \rho < \rho^{\text{cr}}, \ \lambda = \sqrt{1-\left(\frac{\rho^{\text{cr}}}{\rho}\right)^2} \text{ for } \rho > \rho^{\text{cr}}, \quad (30)$$

where ρ is the current density, ρ^{cr} is the critical density at a given hydrostatic pressure $\rho^{\text{cr}} = \rho^{\text{cr}}(\sigma_m)$. The angle of internal friction is also variable.

$$\varphi = \varphi_0 + \arcsin\lambda, \quad (31)$$

where φ_0 is the angle of internal friction of the soil when it reaches the critical density.

The variable value of the angle of internal friction φ determines the nature of the dilatancy elastic-plastic model hardening, and the loading surfaces represent a family of straight lines on the plane (Fig. 2).

In the formula (30), the density ρ is taken as the hardening parameter. In this case, the following conditions are satisfied, which follow directly from the initial preconditions of the model:

$$\begin{cases} \lambda > 0 \text{ if } \rho > \rho^{\text{cr}}; \\ \lambda < 0 \text{ if } \rho < \rho^{\text{cr}}; \\ \lambda = 0 \text{ if } \rho = \rho^{\text{cr}}. \end{cases} \quad (32)$$

The expressions for the angle (coefficient) of internal friction (31) contain two components, and when the soil reaches the critical density (porosity), one of the components becomes equal to zero. The need to separate the strength of sandy soil was noted as early as 1950 by A. Skempton and A. Bishop [27],

who proposed to consider separately the strength due to friction and due to dilatancy. In 1958 B. Hansen introduced the concept of dilatancy angle. The variable nature of the angle of internal friction of the soil was emphasized by K. Roscoe [5, 2] and A. Bishop [5]. The strength division into two components in the expression of the yield function is also used by V.N. Shirokov [25].

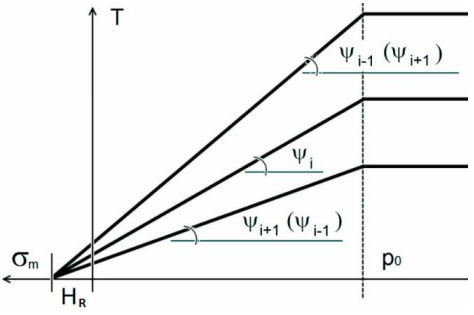

Fig. 2. Loading surfaces. Meridional sections

Of the two components of the angle of internal friction, one (namely, the dilatancy angle), as indicated, is a variable value tending to zero at the critical density, and the other component is a constant value over a wide pressure range and does not depend on the initial density.

In describing the concept of critical density (porosity), it was pointed out the need to take into account its dependence on the hydrostatic pressure level. At low pressures, a significant change in the critical density does not occur, however, when it reaches σ_m about 1.0-2.0 MPa, it can significantly increase, and at $\sigma_m > 2.0$ MPa, the dilatancy loosening is practically impossible to achieve. To describe this phenomenon, the dependence of the critical density on the hydrostatic pressure was introduced in [5] in the form:

$$\begin{cases} \rho_{\text{cr}} = \rho_{\text{cr}}^{o}, & \text{if } \sigma_m > 0, \\ \rho_{\text{cr}} = -\dfrac{2\rho_{\text{cr}}^{m} - \rho_{\text{cr}}^{o}}{P_o^3}\sigma_m^3 + \dfrac{3(\rho_{\text{cr}}^{m} - \rho_{\text{cr}}^{o})}{P_o^2} + \rho_{\text{cr}}^{o}, & \text{if } \rho_o \le \sigma_m \le 0, \\ \rho_{\text{cr}} = \rho_{\text{cr}}^{m}, & \text{if } \sigma_m < \rho_o, \end{cases} \qquad (33)$$

where ρ_{cr}^{o} is the critical density in the absence of hydrostatic pressure, ρ_{cr}^{m} is the maximum density of the given soil, the soil medium parameter, taken $P_o = -2,0$ MPa. The dependence diagram (33) is shown on Fig. 3.

One of the most common issues in modeling the "structure-soil massif" system is the choice of the calculation area boundaries. The issue of choosing the model lower boundary is especially acute if the object of study is subsidence. In this case, the calculation model sizes should be chosen so that the influence of boundary conditions on the forces

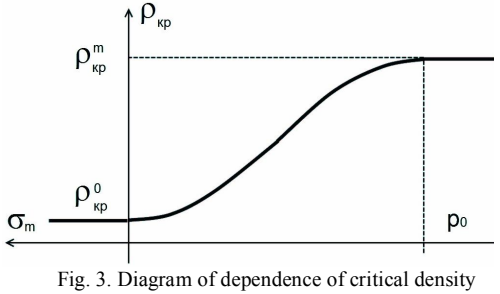

Fig. 3. Diagram of dependence of critical density on hydrostatic pressure

distribution was minimal [18]. This approach is implemented in the works of Berezhnyi D.V., Sagdatullin M.K., Sultanov L.U., Petrov D.N., Demenkov P.O., Potiomkin D.O. [3, 18]. On the other hand, while reducing the impact on the forces distribution, this leads to an unjustified increase in subsidence deformations. In this case, it is recommended to limit the calculation scheme to the compressible zone depth [17, 10].

However, often, due to the peculiarities of the studied objects, it is impossible to use the recommendation to limit the calculation scheme to the compressible zone depth. Therefore, the issue of developing such approaches to modeling the "structure-soil massif" system is relevant, for which the subsidence values in the calculation were identical regardless of the selected lower limit of the calculation model. In order to overcome these problems in the works [28, 29] the detailed description of the accepted correlations, as well as the step-by-step algorithm for the correction of the elasticity mole of the reinforced elastic-plastic medium are presented:

$$E_{inc} = \frac{E^{ref} m}{\frac{c \cdot \mathrm{ctg}\varphi}{\gamma \cdot K_0} + z_{ref}}. \qquad (34)$$

The above ratios make it possible to model the stress-strain state of the soil medium, to determine the pressure distribution in the soil under its own weight and various external influences, taking into account the medium heterogeneity, changes in the relief and physical and mechanical characteristics in the deformation process.

2. Finite element method model. Known analytical methods for determining the structure deformation parameters are usually based on idealized schemes, which significantly narrows the scope of their use. There is a large layer of experimental methods, which are traditionally considered the most reliable basis for obtaining real data. But in practice, we often face more complex geometric shapes and mechanical processes. In this case, numerical methods are brought to the forefront, the most common of which is the finite element method (FEM). FEM has become very widely used in world engineering practice. Almost all known computational complexes rest on its scientific basis. However, there are a number of issues within the task scope, the effectiveness of solution of which requires further development of existing approaches. Structure design standards require considering joint work of structures and bases. It is known that soils show significant nonlinearity, the nature of which varies depending on the load type: deviator or isotropic. The dependence of the deformation characteristics on the stress state in the base, the process development over time, etc. adds to the difficulties.

The solution of the problems of elastic-plastic deformation of spatial bodies is based on the use of the semi-analytic finite element method (SAFEM) and the moment scheme of finite element (MSFE) [2, 19]. The underlying hypotheses allow us to describe arbitrary circular and prismatic geometric configurations with a variable cross-sectional area and heterogeneous material features under arbitrary boundary conditions (Fig. 4).

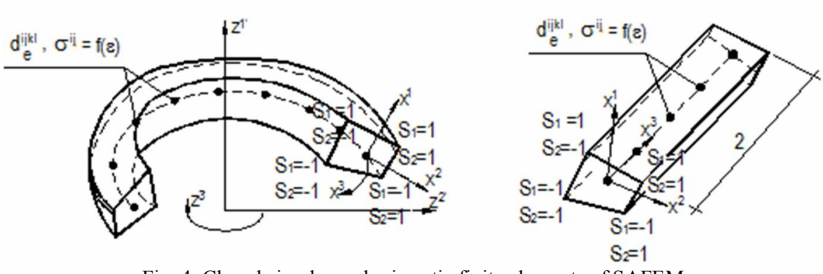

Fig. 4. Closed circular and prismatic finite elements of SAFEM

Based on the basic circular and prismatic finite elements of SAFEM, a new special finite element (FE) has been developed for modeling a nonlinear elastic-plastic soil base. The feature of the accepted FE is the stress tensor correction obtained at the next stage under the load parameter under the assumption of the soil linear operation on the deformation increment. For soil that is in the borderline state, the stress differential has the form:

$$d\sigma^{ij} = C^{ijkl} d\varepsilon_{kl}^{e} = C^{ijkl}\left(d\varepsilon_{kl} - d\varepsilon_{kl}^{p}\right) = d\sigma_{e}^{ij} - d\lambda C^{ijkl}\frac{\partial F}{\partial \sigma^{kl}}. \qquad (35)$$

where C^{ijkl} is the deformation constant tensor; $d\varepsilon_{kl}, d\varepsilon_{kl}^{e}, d\varepsilon_{kl}^{p}$ are the differentials of complete, elastic and plastic deformations, respectively; $d\sigma_{e}^{ij}$ is the stress increment provided that $d\varepsilon_{kl}^{p} = 0$.

Within one step it is considered tt the material does not strengthen and for it the condition of a borderline state is fulfilled:

$$\frac{\partial f}{\partial \sigma^{ij}} d\sigma^{ij} = 0. \qquad (36)$$

Solving together (35) and (36) we get the expression for $d\lambda$. :

$$d\lambda = \frac{\dfrac{\partial f}{\partial \sigma^{mn}} C^{mnlk} d\varepsilon_{kl}}{\dfrac{\partial f}{\partial \sigma^{uv}} C^{uvst} \dfrac{\partial F}{\partial \sigma^{st}}} \qquad (37)$$

and substituting this in (35) we get:

$$d\sigma^{ij} = d\sigma_{e}^{ij} - C^{ijgr}\frac{\partial F}{\partial \sigma^{gr}} \frac{\dfrac{\partial f}{\partial \sigma^{mn}} C^{mnlk} d\varepsilon_{kl}}{\dfrac{\partial f}{\partial \sigma^{uv}} C^{uvst} \dfrac{\partial F}{\partial \sigma^{st}}}. \qquad (38)$$

Dilatancy ratios are analogous to the use of the plastic potential function in the form of:

$$F = T + \sigma_m \Lambda + \text{const}. \qquad (39)$$

After differentiation we get:

$$\frac{\partial F}{\partial \sigma^{ij}} = \frac{S_{ij}}{2T} + \frac{\Lambda \sigma_{ij\text{ш}}}{3\sigma_m}, \tag{40}$$

where S_{ij} and $\sigma_{ij\text{ш}}$ are the components of the deviator and layer part of the stress tensor, respectively.

Expression $\frac{\partial f}{\partial \sigma^{ij}}$, where f is the yield function according to (24) is written similarly:

$$\frac{\partial f}{\partial \sigma^{ij}} = \frac{S_{ij}}{2T} + \frac{\mathrm{tg}\psi \sigma_{ij\text{ш}}}{3\sigma_m}. \tag{41}$$

Taking into account the expressions (40) and (41) for (38) we get:

$$d\sigma^{ij} = d\sigma_e^{ij} - \left(\frac{\mathrm{G}}{T} S^{ij} + \frac{\mathrm{K}\Lambda}{\sigma_m} \sigma_{ij\text{ш}} \right) dL, \tag{42}$$

where K and G are the volumetric and shear elasticity modulus, respectively, related to the traditional parameters E and ν ratios:

$$K = \frac{E}{3(1-2\upsilon)}; G = \frac{E}{2(1+\upsilon)}, \tag{43}$$

dL is the small scalar multiplier:

$$dL = \frac{1}{A} \left(\frac{G}{T} S^{kl} + \frac{K\mathrm{tg}\psi}{\sigma_m} \sigma_{\text{ш}}^{kl} \right) d\varepsilon_{kl} \tag{44}$$

A is the constant, which is determined:

$$A = G + K\Lambda \mathrm{tg}\psi. \tag{45}$$

The integration of the expression (42) allows determining the stress tensor component increment $\Delta\sigma^{ij}$ at this step. The following method is more efficient for calculating the equations discrepancies.

In the transition in (42) from the differentials to increments in the assumption that $\Delta\sigma^{ij}$ and $\Delta\sigma_e^{ij}$ are determined from the same stress state σ^{ij}, determined in the previous step by the load parameter then:

$$S^{ij} = \left(1 - \frac{\mathrm{G}\Delta L}{T + \mathrm{G}\Delta L} \right) S_e^{ij}, \tag{46}$$

$$\sigma_{\text{ш}}^{ij} = \left(1 - \frac{\mathrm{K}\Lambda\Delta L}{\sigma_m + \mathrm{K}\Lambda\Delta L} \right) \sigma_{\text{ш}e}^{ij}. \tag{47}$$

Therefore, it is seen that for the soil which is in the boundary state, the deviator S^{ij} and the layer $\sigma_{\text{ш}}^{ij}$ components of the stress tensor σ^{ij} are proportional to the respective components S_e^{ij} and $\sigma_{\text{ш}e}^{ij}$ of the stress tensor σ_e^{ij}, determined in the assumption that on the next deformation increment $\Delta\varepsilon_{kl}$ the soil operates linearly:

$$S^{ij} = q_1 S_e^{ij}, \quad \sigma_{uu}^{ij} = q_2 \sigma_{uu\,e}^{ij} \tag{48}$$

By substituting (48) in (46) and (47) we get:

$$q_1 = \frac{1}{T_e} \frac{-\mathrm{tg}\psi\left(\sigma_{me} - T_e \frac{K\Lambda}{G}\right) + \tau_s}{-\mathrm{tg}\psi \frac{K\Lambda}{G} + 1}, \tag{49}$$

$$q_2 = \frac{1}{\sigma_{me}} \frac{\left(\sigma_{me} - T_e \frac{K\Lambda}{G}\right) + \tau_s \frac{K\Lambda}{G}}{\mathrm{tg}\psi \frac{K\Lambda}{G} + 1}. \tag{50}$$

The correlations for q_1 and q_2 can also be obtained from the geometric constructions by considering the meridional cross section of the plasticity surface at a given step of the load parameter in the axes (T, σ_m) in Fig. 5. The correction process consists in drawing a straight line at the angle α to the axis σ_m through the point A to the intersection with the straight section of the plasticity surface. The cross-point C (T, σ_m) will be the desired stress state. It can be seen from the constructions that $\mathrm{tg}\alpha = \frac{AB}{BD}$, where AB and BD are the invariants of the fictitious stress tensor determined in the assumed elastic work of the soil outside the plasticity surface.

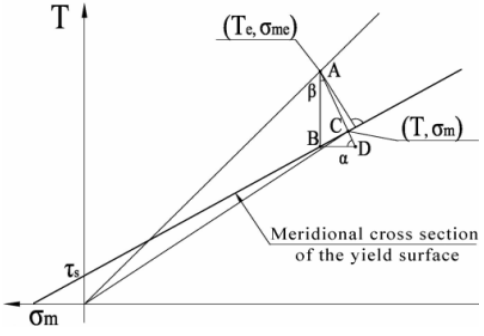

Fig. 5. Geometric interpretation of ratios of the stress tensor correction

Therefore:

$$\mathrm{tg}\alpha = \frac{AB}{BD} = \frac{Gd\gamma^p}{Kd\varepsilon_m^p} = \frac{Gd\gamma^p}{K\Lambda d\varepsilon_m^p} = \frac{G}{K\Lambda}. \tag{51}$$

The equation of the straight line AC takes the form:

$$T - T_e = \frac{G}{K\Lambda}\left(\sigma_m - \sigma_{m\,e}\right). \tag{52}$$

To find T and σ_m it is necessary to solve the system of two equations:

$$\begin{cases} T = \frac{G}{K\Lambda}(\sigma_m - \sigma_{m\,e}) + T_e, \\ T = -\sigma_m \mathrm{tg}\psi + \tau_s. \end{cases} \tag{53}$$

By denoting $T = q_1 T_e$ and $\sigma_m = q_2 \sigma_{me}$ from the system of equations we find the values of the coefficients q_1 and q_2, which are analogous to (49) and (50), which proves the correctness of these coefficients definition.

Conclusions. Therefore, on the basis of modern numerical implementations of the finite element method, the theoretical foundations of the analysis of nonlinear deformation processes of machines and structures in their contact interaction with the elastic-plastic medium within the three-dimensional spatial problem taking into account the previous stress state and load history are presented. The methodology of construction of computational models of joint deformation and mutual influence of rigid structures and essentially plastic external medium is developed, new special heterogeneous finite elements of SAFEM of general form with variable geometrical and physical-mechanical parameters and arbitrary boundary conditions for approximation of arrays of hardly connected reinforced soils are developed.

REFERENCES

1. *Alexanderov A.S.* Modification of the criterion of Kulon-Mora for raschet constructive roads on the resistance of the sdvyh. Part 1. Enter the third parameter of the motherhood / *A.S. Alexanderov, G.V. Dolgikh* // Mezhdunarodnyi nauchno-issledovatelskii zhurnal. – 2016. – №. 6-2 (48).
2. *Bazhenov V.A.* Formulation and calculation ratios of the problem of destruction mechanics for spatial bodies under the action of dynamic loads within the semi-analytical method of finite elements / *V.A. Bazhenov, I.I Солодей, M.O Вабіщевич, O.O Чепурна* // Opir materialiv i teoriia sporud. – 2017. – №. 99. – P. 58-70.
3. *Berezhnoy D.V.* Choosing a soil model for numerical simulation of the influence of deep excavation on the existing building. / *D.V. Berezhnoy, M.K. Sagdatullin, L.U. Sultanov* // Bulletin of Kazan Technological University. – 2013. – № 9. – P. 250-255.
4. *Bhutto A.H.* Mohr-Coulomb and hardening soil model comparison of the settlement of an embankment dam / *A.H. Bhutto et al.* //Engineering, Technology & Applied Science Research. – 2019. – T. 9. – №. 5. – P. 4654-4658.
5. *Bishop A.U.* Strength parameters when undisturbed and crumpled soil samples shift / *A.U. Bishop* // Opredeliaiushchie zakony mehaniki gruntov. - M.: Mir, 1975. P. 7-75.
6. *Blokh V.I.* Theory of resilience / *V.I. Blokh* - Harkov: Izd-vo Hark. un-ta.- 1964. –483 p.
7. Boiko *I.P.* The method of numerical modeling of the development of limit-state zones in the ground of the bases under the ICE / *I.P. Boiko, A.E. Delnik, A.S. Saharov* – K.: Inzh.-stroit. in-t., 1983. - 46 p.
8. *Bower T.A., Jefferson A.D., Cleall P.J.* A reformulated hardening soil model / *T.A. Bower, A.D. Jefferson, P.J. Cleall* //Proceedings of the Institution of Civil Engineers-Engineering and Computational Mechanics. – 2020. – T. 173. – №. 1. – P. 11-29.
9. *Bugrov A.K.* On solving the mixed problem of the theory of elasticity and the theory of plasticity of primes / *A.K. Bugrov* // Osnovaniia, fundamenty i mehanika gruntov. – 1974. - №36. - P. 20-23.
10. *Horodetskii A.S.* Kompiuternye modeli konstruktsii (Computer models of constructions) / *A. S. Horodetskii, I. D. Evzerov.* – Kiev: Fakt, 2005. – 344 p.
11. *Kudasheva M.I.* Comparison of the Mor-Coulomb model and the hardening ground model in the Plaxis software complex / *M.I. Kudasheva, C.V. Kaloshina* // Stroitelstvo i arhitektura. Opyt i sovremennye tekhnologii. – 2017. – Resource Access Mode: http://sbornikstf.pstu.ru/council/?n=9
12. *Melnikov R.V.* Calibrating the Hardening Soil parameters based on laboratory tests in the program Soiltest / *R.V. Melnikov, R.K. Sagitova.* // Akademicheskii vestneyk UralNIIproekt RAASN. – 2016. – № 3. – P. 79-83.

13. *Mirnyi A.Iu.* Areas of use of modern mechanical models of soils / *A.Iu. Mirnyi, A.Z. Ter-Martirosian.* // Geotekhnika. – 2017. – № 1. – P. 20-26.
14. *Nicolaevskii V.N.* Determining equations of plastic deformation of the loose environment / V.N. Nicolaevskii // PMM. – 1971. - т. 35, № 6. - P. 1070-1082.
15. *Nicolaevskii V.N.* Dilatansia and the laws of irreversible deformation of soils / *V.N. Nicolaevskii* // Osnovaniia, fundamenty i mehanika gruntov. – 1979. - № 5. - P. 29-32.
16. *Nicolaevskii V.N.* Dynamics of elastic-plastic dilating environments / *V.N. Nicolaevskii, N.M. Syrnikov, G.M. Shchefter* // V kn.: Uspehi mehaniki deformiruemykh sred. - M.: Nauka, 1975. - P. 397-413.
17. *Perelmuter A.V.* Raschetnye modeli sooruzhenij i vozmozhnost ikh analiza (Design models of structures and the possibility of their analysis) / *A.V. Perelmuter, V.I. Slivker.* – Moscow: SKAD SOFT, 2011. 736 p.
18. *Petrov, D.N., Demenkov, P.A., Potemkin, D.A.* Numerical modeling of the stress state in the lining of columnar stations without side platforms. / *D.N. Petrov, P.A Demenkov., D.A. Potemkin //* Notes of the Mining Institute. – 2010. – 185. – P. 166-170.
19. *Piskunov S. O.*.Features of the use of the torque scheme of finite elements (ISSE) in linear calculations of shells and plates. / *S.O. Piskunov, I.I. Solodei, Iu.V.Maksimiuk, & A.D. Solodenko* // Opir materialiv ta teoriia sporud, (91), P. 62-78.
20. *Pramthawee P.* Integration of creep into a modified hardening soil model for time-dependent analysis of a high rockfill dam / *P.Pramthawee, P.Jongpradist, R.Sukkarak* // Computers and Geotechnics. – 2017. – T. 91. – P. 104-116.
21. *Riabkov S.V.* Experience of the Plaxis 3D software complex by the tunnel construction design department / *C.V. Riabkov, H.A. Solovev.* // Metro i tonneli. – 2016. – №9. – P. 53–55.
22. *Rosko K.* The value of deformations in soil mechanics / *K. Rosko* // V kn.: Mehanika. - M.: Mir, 1971. - № 3 (127). - P. 91-145.
23. *Saharov A.S.* End-of-life method in solid mechanics / *A.S. Saharov, V.N. Kislookii, V.V. Kirichevskii i dr.* - Kiev: Vishcha shkola, 1982.- 479p.
24. *Schweiger H.F.* Examples of successful numerical modelling of complex geotechnical problems / *H.F. Schweiger et al.* // Innovative Infrastructure Solutions. – 2019. – T. 4. – №. 1. – P. 2.
25. *Shirokov V. N.* Model of sandy soil / *V.N. Shirokov* // V kn.: Sovremennye problemy nelineinoi mehaniki gruntov, Cheliabinsk, ChPI. – 1985. - P. 27-28.
26. *Sidorov N.I., Spidin V.P.* Modern methods of determining the characteristics of mechanical properties of soils / *N.I. Sidorov, V.P. Spidin.* – L.: Stroiizdat, 1972. – 136 p.
27. *Skocsylas K.* Analiza statecznosci skaroy nawodnionej / *K. Skocsylas, E. Stilger-Szyd Lo* // Prace Naukowe Insc Geotech. Politech. Wroclawskij. - 1987. - K 52. - P. 317-322.
28. *Solodei I.* Implementation of the linear elastic structure half-space in the Plaxis in the study of settlements / *I. Solodei I., Gh. Zatyliuk* // Proceedings of Odessa Polytechnic University. – 2019. – № 1 (57). – P. 22-28.
29. *Solodei I.* Mohr-coulomb model with corrected parameters in the study of base settlements / *I. Solodei, Gh. Zatyliuk* // The Austrian Journal of Technical and Natural Sciences, Premier Publishing s.r.o. Vienna. 2020.– 9-10 – P.36-39.
30. *Stroganov A.S.* Analysis of flat plastic deformation of the ground / *A.S. Stroganov* // Inzhenernyi zhernal. – 1965. - tom 5, vyp. 4. - P. 734-742.
31. *Xiang X.* Numerical implementation of a modified Mohr–Coulomb model and its application in slope stability analysis / *X. Xiang, D. Zi-Hang* //Journal of Modern Transportation. – 2017. – T. 25. – №. 1. – P. 40-51.
32. *Zienkiewicz O.C.* Non-linear seismic response and liquefaction / *O.C. Zienkiewicz, C.T. Chang, E. Hinton* // Intern. J. Numer. and Anal. Meth. Geomech. - 1978. - Vol. 2. – N4. - P. 381-404.

Стаття надійшла до редакції 03.09.2020

Солодей І.І., Петренко Е.Ю., Затилюк Г.А.

НЕЛІНІЙНА ЗАДАЧА ДЕФОРМУВАННЯ КОНСТРУКЦІЙ ПРИ ВЗАЄМОДІЇ ІЗ ПРУЖНОПЛАСТИЧНИМ СЕРЕДОВИЩЕМ

У статті на базі сучасних чисельних реалізацій метода скінченних елементів представлені теоретичні основи аналізу процесів деформування конструкцій машин і споруд при їх контактній взаємодії із пружнопластичним нелінійним грунтовим середовищем в рамках тривимірної просторової задачі з урахуванням попереднього напруженого стану та історії навантаження. Створена методика побудови розрахункових моделей сумісного деформування і взаємного впливу жорстких конструкцій і суттєво пластичного зовнішнього середовища, розроблені нові спеціальні неоднорідні скінченні елементи НМСЕ загального вигляду із змінними геометричними і фізико-механічними параметрами та довільними граничними умовами для апроксимації масивів малозв'язних зміцнюваних грунтів.

Ключові слова: пружнопластичне середовище, модель зміцнюваних грунтів, напіваналітичний метод скінченних елементів, моментна схема скінченного елемента.

Solodei I.I., Petrenko E.Yu., Zatyliuk Gh.A.

NONLINEAR PROBLEM OF STRUCTURAL DEFORMATION IN INTERACTION WITH ELASTOPLASTIC MEDIUM

The use of numerical methods in the calculation of machines and structures, taking into account their interaction with the elastic-plastic medium is largely determined by the complexity or even impossibility of analytical calculation due to the complexity of structural schemes, heterogeneity of material features, uneven soil layers, implementation of step-by-step work execution technologies and so on.

Compatible calculations of structures and nonlinear basis, which are described by modern mechanical and soil models in one problem is a significant technical problem. And neither the existing "problem-oriented" software packages, nor the "universal" ones - do not fully contain such models.

The tasks solution is possible only within the framework of numerical methods, the most common of which is the finite element method (FEM). The construction of the calculated finite element model raises many complex questions that require additional detailed study. In addition, the compliance with the state building norms and regulations is an important factor for further practical use.

The combination of the latest achievements in the field of structural mechanics and soil mechanics is a promising direction for the development of effective approaches for building discrete models of spatial systems "structure-nonlinear base" for solving applied problems.

On the basis of modern numerical implementations of the finite element method the article presents the theoretical foundations of the analysis of deformation processes of machines and structures in their contact interaction with the elastic-plastic nonlinear soil medium within the three-dimensional spatial problem taking into account the previous stress state and load history. The methodology of construction of computational models of joint deformation and mutual influence of rigid structures and essentially plastic external medium is developed, new special heterogeneous finite elements of SAFEM of general form with variable geometrical and physical-mechanical parameters and arbitrary boundary conditions for approximation of arrays of hardly connected reinforced soils are developed.

Keywords: elastic-plastic medium, reinforced soils model, semi-analytical finite element method, moment scheme of finite element.

Солодей И.И., Петренко Э.Ю., Затылюк Г.А.

НЕЛИНЕЙНАЯ ЗАДАЧА ДЕФОРМИРОВАНИЯ КОНСТРУКЦИЙ ПРИ ВЗАИМОДЕЙСТВИИ С УПРУГОПЛАСТИЧЕСКОЙ СРЕДОЙ

В статье на базе современных численных реализаций метода конечных элементов представлены теоретические основы анализа процессов деформирования конструкций машин и сооружений при их контактном взаимодействии с упругопластической нелинейной грунтовой средой в рамках трехмерной пространственной задачи с учетом предыдущего напряженного состояния и истории нагрузки. Создана методика построения расчетных моделей совместного деформирования и взаимного влияния жестких конструкций и существенно пластической внешней среды, разработаны новые специальные неоднородные конечные элементы НМСЕ общего вида с переменными геометрическими и физико-механическими параметрами и произвольными граничными условиями для аппроксимации массивов малосвязных упрочняющихся грунтов.

Ключевые слова: упругопластическая среда, модель упрочняющихся грунтов, полуаналитический метод конечных элементов, моментная схема конечного элемента.

УДК 539.3
Солодей І.І., Петренко Е.Ю., Затилюк Г.А. **Нелінійна задача деформування конструкцій при взаємодії із пружнопластичним середовищем** // Опір матеріалів і теорія споруд: наук.-тех. збірн. – К.: КНУБА, 2020. – Вип. 105. – С. 48-63.

Розглянуто метод розв'язання задач деформування конструкцій машин і споруд при їх контактній взаємодії із пружнопластичним нелінійним грунтовим середовищем.
Іл. 5. Бібліогр. 32 назв.

UDC 539.3
Solodei I.I., Petrenko E.Yu., Zatyliuk Gh.A. **Nonlinear problem of structural deformation in interaction with elastoplastic medium** // Strength of Materials and Theory of Structures: Scientific-and-technical collected articles. – K.: KNUBA, 2020. – Issue 105. – P. 48-63.

The method of solving the nonlinear deformation problems of structures during their contact interaction with the elastic-plastic medium is considered.
Fig. 5. Ref. 32.

УДК 539.3
Солодей И.И., Петренко Э.Ю., Затылюк Г.А. **Нелинейная задача деформирования конструкций при взаимодействии с упругопластической средой** // Сопротивление материалов и теория сооружений. – 2020. – Вып. 105. – С. 48-63.

Рассмотрен метод решения задач деформирования конструкций машин и сооружений при их контактном взамодействии с упругопластической нелинейной грунтовой средой.
Ил. 5. Библиогр. 32 назв.

Автор: *доктор технічних наук, професор, професор кафедри будівельної механіки СОЛОДЕЙ Іван Іванович*
Адреса: *03037 Україна, м. Київ, Повітрофлотський проспект 31, Київський національний університет будівництва і архітектури*
Робочий тел.: *+38 (044) 241-55-55*
Мобільний тел.: *+38 (050)357-44-90*
E-mail: *solodei.ii@knuba.edu.ua*
ORCID ID: *http://orcid.org/0000-0001-7638-3085*

Автор: *кандидат технічних наук, доцент, доцент кафедри геотехніки ПЕТРЕНКО Едуард Юрійович*
Адреса: *03037 Україна, м. Київ, Повітрофлотський проспект 31, Київський національний університет будівництва і архітектури*
Email: *petrenko.ey@knuba.edu.ua*
ORCID ID: *http://orcid.org/0000-0002-9792-4757*

Автор: *аспірант, асистент кафедри будівельної механіки ЗАТИЛЮК Герман Анатолійович*
Адреса: *03037 Україна, м. Київ, Повітрофлотський проспект 31, Київський національний університет будівництва і архітектури*
Мобільний тел.: *+38 (099) 11-00-564*
Email: *zatyliuk.ha@knuba.edu.ua*
ORCID ID: *http://orcid.org/0000-0003-0392-2214*

UDC 531.66

MODEL OF HIGH-SPEED SHOCK INTERACTION WITH COMPATIBLE TYPE

A.V. Kovtun,
Candidate of Technical Science, Associate Professor[1]

V.O. Tabunenko,
Candidate of Technical Science, Associate Professor[2]

S.I. Nesterenko,
Candidate of Technical Science, Associate Professor[3]

[1]*National Academy of the National Guard of Ukraine, Kharkiv, Square Zakhysnykiv Ukrayiny3, Kharkiv, 61001*
[2]*National Air Force UniversityIvan Kozhedub, Kharkiv, Sumska Street 77/79, Kharkiv, 61023*
[3]*National Aerospace University – Kharkiv Aviation Institute, Kharkiv, Chkalova Street 17, Kharkiv, 61070*

DOI: 10.32347/2410-2547.2020.105.64-72

This research aims to the process of interaction of a bullet (fragment) with protective barriers, which are formed by a set of hollow cylinders of a compatible type. Models for determining the depth of penetration of the drummer into an obstacle in the form of a set of hollow cylinders of compatible type are proposed. The results of calculations of the value of the depth of penetration of the bullet into the protective barrier in the form of a set of compatible cylinders. Further research is related to the improvement of the armor protection designs by developing new technical solutions using the latest technologies.

Keywords: model, compatible cylinders, high-speed drummer, bullet, protective obstacle, deformation, hollow cylinder.

Formulation of the problem. In connection with the ongoing hostilities in eastern Ukraine, the issue of developing the protection of servicemen from bullets and shrapnel remains relevant. Modern research on the interaction of bullets and fragments with protective barriers is based on the search for new types of structures and protective materials. The main focus is on the development of protective structures that would increase the level of protection of servicemen, according to NATO standards, using inexpensive available materials with minimal costs for their production and intended use.

Despite some progress in the investigation of collisions of solids, the known results of theoretical and experimental research do not describe a holistic picture of the interaction of the element of damage and interference. Therefore, in the development of protective structures take into account only certain aspects of impact interaction, which are based on the absorption of kinetic energy of the element of damage [1].

The scientific and technical task remains important study of the process of interaction of bullets (fragments) with protective barriers, at the stages of penetration, breaking and their departure, which will develop new models of

protection design for servicemen, which are relevant for the Armed Forces of Ukraine.

Analysis of recent research and publications. The issues of interaction of bullets (fragments) with protective obstacles have long been dealt with and various methods and approaches to calculating the depth of penetration of obstacles have been known. Fundamental results of the study of the phenomenon of impact and determination of the conditions for breaking through obstacles by drummers (bullets, fragments) were obtained in the works of Euler, Jacob de Mar, Noble, J. Reinhart and J. Pearson, Berzin K.A. and others [1].

In modern research, methods and ways to increase the security of personnel of military bases and units, combat vehicles and fortifications are given considerable attention [1-7].

In [1] the parameters of the multilayer protective structure of combat vehicles based on nonlinear mathematical models are substantiated. In [2] the method of research of complex systems of military purpose is resulted. In [3-6] the modeling of the dynamics of the reaction of the protective structure to the action of the shock-wave load at the impact of a bullet or a fragment of a projectile is considered. In [7] materials for local and individual armoring are investigated. A study of the use of non-traditional methods of interaction of bullets (fragments) with protective barriers is given in research [8].

The main method of studying the process of impact and punching an obstacle with a bullet (fragment) is a combination of analytical and experimental researches. Analytical research methods are based on mathematical modeling of the stages of interaction of bullets (fragments) with the elements of the protective barrier, followed by appropriate mathematical calculations [1]. Experimental research methods are based on determining the level of protection of protected objects and require complex research in laboratory and landfill conditions. The combination of the results of analytical and experimental research allows us to more fully consider the level of protection of protected objects.

However, studies of the interaction of bullets (fragments) with protective obstacles have not been completed, the processes occurring when hitting bullets (fragments) on the obstacle are not fully studied, and the applied models and methods do not fully take into account the design parameters of protective obstacles.

The purpose of the article is to investigate the process of interaction of a bullets with a protective obstacle in the form of a set of compatible cylinders.

The main material. The use of single cylinders and bonded structures are only two of the possible means of increasing the strength of protective structures [8]. Another possible way to increase the strength of protective structures is a method that consists not of a nozzle of structures in the hot state with tension, but by the formation between the component structures (cylinders) of the gap into which the liquid (gas) is injected under pressure. By placing the cylinders in each other and adjusting the pressure of the liquid (gas) in the free zones between the cylinders, it can be achieved that at the

same thickness in the cylinder walls, the pressure in the inner cylinder can be greater than in a single cylinder [9].

For a single cylinder, the ultimate pressure in it can reach half the strength limit of the material. For bonded and compatible cylinders, the maximum pressure is twice as high as for a single cylinder. For compatible cylinders, the limit pressure can be increased by another 25%. If autofretted cylinders are used for compatible cylinders, the limiting pressure in the inner cylinder can be four times higher than for a single cylinder [9].

The prop that occurs in compatible cylinders and in bonded cylinders is not the same thing. The prop in the bonded cylinders, brought to a certain limit, then remains constant for the entire period of operation of the bonded cylinders. Prop in compatible cylinders can be variable.

Consider a structure consisting of two cylinders – the outer (2) and inner (1), with the outer diameter of the inner cylinder, in contrast to the bonded cylinders, is smaller than the inner diameter of the outer cylinder. Fluid is injected under pressure into the gap between the outer and inner cylinders (Fig. 1).

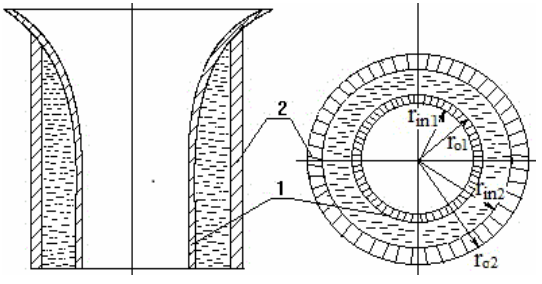

Fig. 1. Scheme of a compatible cylinder

Using the known formula for calculating normal stresses in the tangential direction [9,10]:

$$\sigma_\theta = \frac{p_{in} \cdot r_{in}^2 - p_{ex} \cdot r_o^2}{r_o^2 - r_{in}^2} + \frac{(p_{in} - p_{ex}) \cdot r_o^2 \cdot r_{in}^2}{r^2 \cdot (r_o^2 - r_{in}^2)}, \quad (1)$$

where p_{in} – is the internal pressure in the cylinder, Pa; p_{ex} – is external pressure on the cylinder, Pa; r_{in} – is the internal radius of the cylinder, m; r_o – is the external radius of the cylinder, m; r – is the current radius of the cylinder, m.

For compatible cylinders, the following expressions can be written [9]:
when $r = r_{in}$

$$\sigma_\theta = p_{in} \cdot \frac{1 + k_r^2 \cdot (1 - k_p)}{k_r^2 - 1}, \quad (2)$$

when $r = r_o$

$$\sigma_\theta = p_{in} \cdot \frac{2 - k_p^2 \cdot (1 + k_r^2)}{k_r^2 - 1}, \quad (3)$$

where

$$k_r = \frac{r_o}{r_{in}}, k_p = \frac{p_{ex}}{p_{in}}. \quad (4)$$

Pressure in the radial direction [9]:

on the inner surface

$$\sigma_r = p_{in} \cdot \frac{2 \cdot k_r^2 \cdot (1 - k_p)}{k_r^2 - 1}, \tag{5}$$

on the outer surface

$$\sigma_r = p_{in} \cdot \frac{2 \cdot (1 - k_p)}{k_r^2 - 1}. \tag{6}$$

Equating the values of stresses to the allowable stress for the cylinder material $[\sigma]$, to determine the expression σ_θ when $r = r_{in}$ we obtain the formula for determining the maximum allowable internal pressure [9]:

$$p_i = [\sigma] \cdot \frac{k^2{}_r - 1}{2 \cdot k^2{}_r \cdot (1 - k_p)}. \tag{7}$$

If the protective structure consists of two cylinders (outer and one inner), then for the outer cylinder:

$$k_{p2} = \frac{p_{ex2}}{p_{in2}} = 0, \tag{8}$$

the maximum allowable pressure will be:

$$p_{in2} = [\sigma] \cdot \frac{k^2{}_{r2} - 1}{2 \cdot k^2{}_{r2}}. \tag{9}$$

For any intermediate cylinder (if the protective structure consists of several cylinders: external and several (i) internal), the maximum allowable internal pressure can be written as:

$$p_{ini} = [\sigma_i] \cdot \frac{k^2{}_{ri} - 1}{2 \cdot k^2{}_{ri} (1 - k_{pi})}. \tag{10}$$

Maximum allowable internal pressure in the inner cylinder with n cylinders [9]:

$$p_{in} = [\sigma] \cdot \frac{k^2{}_{rn} - 1}{2 \cdot k^2{}_{rn}} + \sum_{2}^{n-1} [\sigma_i] \cdot \frac{k^2{}_{ri} - 1}{2 \cdot k^2{}_{ri}} + [\sigma] \cdot \frac{k^2{}_{r1} - 1}{2 \cdot k^2{}_{r1}}. \tag{11}$$

For a compatible design consisting of two cylinders, the value of the internal pressure in the outer cylinder is determined by the equation:

$$p_{i2} = [\sigma] \cdot \frac{k^2{}_{r2} - 1}{2 \cdot k^2{}_{r2}}. \tag{12}$$

The value of the internal pressure in the inner cylinder is determined by the equation:

$$p_{i1} = [\sigma] \cdot \frac{k^2{}_{r1} - 1}{2 \cdot k^2{}_{r1}} + [\sigma] \cdot \frac{k_{r2}^2 - 1}{2 \cdot k_{r2}^2}. \tag{13}$$

The contact pressure that occurs when passing a bullet in the middle of a cylinder of smaller diameter (than the diameter of the bullet) is determined by the expression [10]:

$$p_c = \frac{\delta \cdot E}{4 \cdot r_b^3} \cdot \frac{r_b^2 \cdot (r_{co}^2 - r_b^2)}{r_{co}^2},$$

where p_c – the contact pressure between the bullet and the cylinder, Pa; r_{co} – outer radius of the cylinder, m; r_b – radius of the bullet, m; δ – tension between the bullet and the cylinder, m; E – is the modulus of elasticity of the cylinder material, Pa.

To determine the parameters of the process of interaction of the ball with a protective barrier in the form of compatible cylinders, we equate $p_i = p_c$.

Algorithm for solving the problem. Determine the depth of penetration of the bullet from the AK-74 into the protective barrier in the form of compatible cylinders. Output data: r_{bullet}=0,00273 m; r_{ic1}=0,0025 m; r_{oc1}=0,0035 m; r_{ic2}=0,0036 m; r_{oc2}=0,0057 m; f = 0,9; $E = 2{,}1 \cdot 10^5$ МПа; $l = 0{,}012$ m; $[\sigma] = 3 \cdot 10^3$ MPa (Fig. 2).

The force under which the bullet will move along the inner surface of the cylinder, determine the formula based on the equation given in [8,10]:

$$P = f_1 \cdot p_c \cdot \pi \cdot D \cdot k \cdot l, \qquad (14)$$

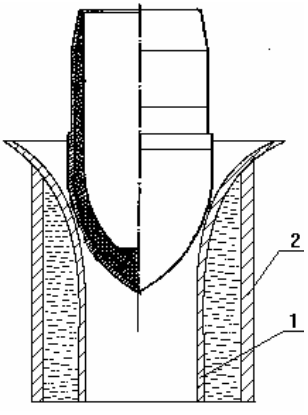

Fig. 2. The scheme of movement of a bullet along the compatible cylinder

where f_1 – effective coefficient of friction between the bullet and the inner surface of the cylinder, $f_1 = 2 \cdot m \cdot f$ [11]; m – the number of pairs of contact surfaces of the bullet with the inner surface of the cylinder; p_c – contact pressure, Pa; D – bullet caliber, m; l – length of the bullet, m; k – the proportion of the bullet that entered in the cylinder, $0 \le k \le 1$.

The depth of penetration of the bullet into the cylinder h is determined by the formula:

$$h = \frac{E_\Sigma}{P}, \qquad (15)$$

where P – the force under which the bullet moves along the inner surface of the cylinder, H; E_Σ – kinetic energy of a bullet, J ($E_\Sigma = 2019\,J$).

Define value $k_r = \frac{r_{ex}}{r_{in}}$ for outer 2 and inner 1 cylinders:

$$k_{r2} = \frac{r_{o2}}{r_{in2}} = \frac{0{,}0057}{0{,}0036} = 1{,}58\,; \; k_{r1} = \frac{r_{01}}{r_{in1}} = \frac{0{,}0035}{0{,}0025} = 1{,}4\,.$$

The value of the internal pressure in the outer cylinder is determined by the formula (12):

$$p_{i2} = 3 \cdot 10^9 \cdot \frac{(1,58^2 - 1)}{2 \cdot 1,58^2} = 0,9 \cdot 10^9 \, Pa.$$

The value of the internal pressure in the inner cylinder is determined by the formula (13):

$$p_{i1} = 3 \cdot 10^9 \cdot \frac{(1,4^2 - 1)}{2 \cdot 1,4^2} + 3 \cdot 10^9 \cdot \frac{(1,58^2 - 1)}{2 \cdot 1,58^2} = 1,65 \cdot 10^9 \, Pa.$$

We equate the value of the internal pressure in the inner cylinder and the value of the contact pressure that occurs when the bullet passes in the middle of the inner cylinder:

$$p_{i1} = p_c \, ,$$

and determine the magnitude of the force under which the bullet will move along the inner surface of the cylinder (14):

$$P = f_1 \cdot p_c \cdot \pi \cdot D \cdot k \cdot l = 0,9 \cdot 1,65 \cdot 10^9 \cdot 3,14 \cdot 0,00545 \cdot 0,012 = 305108 \;\; H \, .$$

The depth of penetration of the bullet into the cylinder h is determined by the formula:

$$h = \frac{2019}{305108} = 0,0066 \, m.$$

Thus, the obtained value of the depth of penetration of the bullet into the compatible cylinder is less than the depth of penetration of the bullet into the bonded cylinder, which is given in research [8].

Conclusions

1. The process of interaction of a bullet with a protective obstacle in the form of a set of hollow cylinders of compatible type is investigated.

2. A model for determining the depth of penetration of a high-velocity bullet into a hollow cylinder of a compatible type is proposed.

3. Calculations performed of the depth of penetration of the bullet from a Kalashnikov rifle (AK-74) into steel hollow cylinders of compatible type.

4. Further improvement of armor protection structures can be achieved by developing new technical solutions using the latest technologies.

REFERENCES

1. *Petruchenko O.S.* Obgruntuvannia parametriv bahatosharovoi zakhysnoi konstruktsii boiovykh mashyn na osnovi neliniinykh matematychnykh modelei. (Substantiation of parameters of multilayer protective construction of combat vehicles based on nonlinear mathematical models) - Manuscript. Dissertation for the degree of Doctor of Philosophy (Candidate of Technical Sciences) in the specialty 05.02.09 - Dynamics and Strength of Machines / O.C. Petruchenko - Lviv, 2018. – 160 p.
2. *Lapitsky S.V.* Metodologiya issledovaniya slozhnykh sistem voyennogo naznacheniya (Methodology for the study of complex military systems)/ S.V. Lapitsky, A.V. Kuchinsky, A.I. Sbitnev [and others]; ed .: S.V. Lapitsky. - K.: 2013. – 477 p.
3. *Bruhl S.T.* K voprosu modelirovaniya reaktsii korpusov legkobronirovannykh mashin na deystviye udarno- impul'snykh zagruzok (On the issue of modeling the reaction of lightly armored vehicle bodies to shock-pulse loading)// Bulletin of NTU "KPI". Coll. of sciences. wash. Series: New Solutions in Modern Technologies. - Kharkiv: NTU "KPI", 2013. - № 43 (1016). - P. 46-50.

4. *Vasilyev A.Yu.* Chislennoye modelirovaniye reaktsii bronekorpusov legkobronirovanikh mashin na deystviye udarno-volnovoy zagruzki (Numerical simulation of the response of lightly armored vehicles to the effect of shock wave loading) // Mechanics and Mechanical Engineering. - KPI .: - Kharkiv, 2010. - №2. – P. 73-97.
5. *Velichko L.D.* Dynamika zakhysnoi konstruktsii pry udari kuli abo oskolka snariada (Dynamics of the protective structure when struck by a bullet or a projectile fragment) // Military Technical Collection / Academy of Land Forces. - № 13. - Lviv: ACB, 2015. - P. 13-19.
6. *Gerasimov A.V.* Teoreticheskiye i eksperimental'nyye issledovaniya vysokoskorostnogo vzaimodeystviya tel (Theoretical and experimental studies of high-speed interaction of bodies) / Ed. A.V. Gerasimova. - Tomsk: Publisher Tom. Univ., 2007 - 572 p.
7. *Grigoryan V.A.* Materialy i zashchitnyye struktury dlya lokal'nogo i individual'nogo bronirovaniya Materials and security structures for local and individual booking (Materials and protective structures for local and individual reservations) / VA Grigoryan, IF Kobylkin, V.M. Marinin, E.N. Chistyakov - M.: Izd. RadioSoft. 2008. - 406 p.
8. *Kovtun A.V.* Modeli vzaiemodii vysokoshvydkisnoho udarnyka z zakhysnymy pereshkodamy (Models of interaction of high-speed striker with protective obstacles) / A.V. Kovtun, V.O. Tabunenko, S.I. Nesterenko. // Strength of Materials and Theory of Structures / Strength of Materials and Theory of Structures. 2019. Issue 102, –P. 207-211.
9. *Zayarny V.I.* Osnovy teorii sovmeshchennykh sosudov (Fundamentals of the theory of combined vessels)/ V.I. Zayarny. – Lviv: Publishing House of the Lviv State. University, 1972. - 124 p.
10. Prakticheskiye raschety na prochnost' konstruktivnykh elementov. Ch. I. (Practical strength calculations of structural elements) / A. G. Dibir, O. V. Makarov, N. I. Pekelny, G. I. Yudin, M. N. Grebennikov. - Study. allowance. ─ Kharkov: Nat. aerospace. Universities «Kharkov aviation. Institute », 2007. - 102 p.
11. *Kovtun A.V.* Dinamika slozhnykh mekhanicheskikh sistem so svyazyami sukhogo treniya (Dynamics of Complex Mechanical Systems with Dry Friction Bonds). // Kovtun, V.F. Grekov, VA Procopius. - Kharkov: MO, 1996. - 116 p.

Стаття надійшла 12.05.2020

Ковтун А.В., Табуненко В.О., Нестеренко С.І.

МОДЕЛЬ ВЗАЄМОДІЇ ВИСОКОШВИДКІСНОГО УДАРНИКА З ЗАХИСНОЮ ПЕРЕШКОДОЮ СУМІСНОГО ТИПУ

В даній роботі розглянуто процес взаємодії кулі (осколку) з захисними перешкодами, які утворені набором пустотілих циліндрів сумісного типу. Запропоновані моделі визначення глибини проникнення ударника в перешкоду у вигляді набору пустотілих циліндрів сумісного типу. Наведені результати розрахунків величини глибини проникнення кулі в захисну перешкоду у вигляді набору сумісних циліндрів. Подальші дослідження пов'язані з вдосконаленням конструкцій бронезахисту шляхом розробки нових технічних рішень з використанням новітніх технологій.

Ключові слова: модель, високошвидкісний ударник, куля, захисна перешкода, деформация, порожнистий циліндр.

Anatoly Kovtun, Volodimir Tabunenko, Sergey Nesterenko

MODEL OF HIGH-SPEED SHOCK INTERACTION WITH COMPATIBLE TYPE

In connection with military operations, the issue of developing protection for military personnel against bullets and splinters remains an issue. Modern studies of the interaction of bullets and fragments with protective obstacles are based on the search for new types of structures and materials of protection. The focus is on the development of NATO-compliant protective structures to increase the level of protection for military personnel using low-cost, affordable materials with minimal production and intended use.

Despite some advances in the study of solid-body impact, the known results of theoretical and experimental studies do not describe the overall picture of the interaction of the element of damage and interference. When designing protective structures, only certain aspects of the shock interaction are considered, based on the absorption of the kinetic energy of the element of damage. Therefore, it remains important for the scientific and technical task - to continue the study of the process of interaction of bullets (fragments) with protective obstacles, at the stages of penetration, penetration and their departure, which will allow to develop new models of protection structure of military personnel that are relevant for military use.

The main method of studying the process of striking and punching an obstacle with a bullet (fragment) is a combination of analytical and experimental studies. Analytical methods of research are based on mathematical modeling of stages of interaction of bullets (fragments) with elements of a protective obstacle with the subsequent carrying out of corresponding mathematical calculations. Experimental research methods are based on determining the level of security and require complex research in laboratory and polygonal conditions. The combination of analytical and experimental research results makes it possible to consider the level of security more fully.

In this work the process of interaction of a ball (fragment) with the protective obstacles formed by a set of hollow cylinders of compatible type is considered. Models for determining the depth of penetration of the impactor into the obstacle in the form of a set of hollow cylinders of compatible type are proposed. The results of calculations of the depth of penetration of the ball from Kalashnikov (AK-74) in steel hollow cylinders of compatible type are presented. Further research is concerned with improving the design of armor by developing new technical solutions using the latest technologies.

Keywords: model, high-speed impactor, ball, protective obstacle, deformation, hollow cylinder.

УДК 531.66
Ковтун А.В., Табуненко В.О., Нестеренко С.І. **Модель взаємодії високошвидкісного ударника з захисною перешкодою сумісного типу** // Опір матеріалів і теорія споруд: наук.-тех. збірник. – К.: КНУБА, 2020. – Вип. 105. – С. 64-72.

В даній роботі розглянуто процес взаємодії кулі (осколку) з захисними перешкодами, які утворені набором пустотілих циліндрів сумісного типу. Запропоновані моделі визначення глибини проникнення ударника в перешкоду у вигляді набору пустотілих циліндрів сумісного типу. Наведені результати розрахунків величини глибини проникнення кулі в захисну перешкоду у вигляді набору сумісних циліндрів. Подальші дослідження пов'язані з вдосконаленням конструкцій бронезахисту шляхом розробки нових технічних рішень з використанням новітніх технологій.
Ил. 2. Бібліогр. 11 назв.

UDC 531.66
Kovtun A.V., Tabunenko V.A., Nesterenko S.I. **Model of high-speed shock interaction with compatible type** // Strength of Materials and Theory of Structures: Scientific-and-technical collected articles – Kyiv: KNUBA, 2020. – Issue 100. – P. 64-72.

In this work the process of interaction of a ball (fragment) with the protective obstacles formed by a set of hollow cylinders of compatible type is considered. Models for determining the depth of penetration of the impactor into the obstacle in the form of a set of hollow cylinders of compatible type are proposed. The results of calculations of the depth of penetration of the ball into the protective obstacle in the form of a set of compatible cylinders are presented. Further research is concerned with improving the design of armor by developing new technical solutions using the latest technologies.
Fig. 2. Ref. 11.

УДК 531.66
Ковтун А.В., Табуненко В.А., Нестеренко С.И. **Модель взаимодействия высокоскоростного ударника с защитной преградой совместного типа** // Сопротивление материалов и теория сооружений. – К.: КНУБА, 2020. – Вып. 105. – С. 64-72.

В данной работе рассмотрен процесс взаимодействия пули (осколка) с защитными препятствиями, которые образованы набором пустотелых цилиндров совместного типа. Предложены модели определения глубины проникновения ударника в препятствие в виде набора пустотелых цилиндров совместного типа. Приведены результаты расчетов величины глубины проникновения пули в защитную преграду в виде набора совместимых цилиндров. Дальнейшие исследования связаны с совершенствованием конструкций бронезащиты путем разработки новых технических решений с использованием новейших технологий.
Ил. 2. Библиогр. 11 назв.

Автор (науковий ступінь, вчене звання, посада): *кандидат технічних наук, доцент, доцент кафедри бойового та логістичного забезпечення Національної академії Національної гвардії України КОВТУН Анатолій Васильович.*
Адреса робоча: *61001 Україна, м. Харків, майдан Захисників України 3, НАНГУ, кафедра бойового та логістичного забезпечення, Ковтун А.В.*
Мобільний тел.: *+38(097) 708-04-41;*
E-mail: kav-60@ukr.net
ORCID ID: http://orcid.org/0000-0002-8427-1005

Автор (науковий ступінь, вчене звання, посада)*: кандидат технічних наук, доцент, професор кафедри електротехнічних систем комплексів озброєння військової техніки Харківського національного університету Повітряних Сил ім. Івана Кожедуба, ТАБУНЕНКО Володимир Олександрович.*
Адреса робоча: *61023 Україна, м. Харків, вулиця Сумська 77/79, ХНУПС, кафедра електротехнічних систем комплексів озброєння військової техніки, Табуненко В.О.*
Мобільний тел.: *+38(097) 225-62-60;*
E-mail: tabunenko55@ukr.net
ORCID ID: http://orcid.org/0000-0003-1347-5390

Автор (науковий ступінь, вчене звання, посада): *кандидат технічних наук, доцент, доцент кафедри автомобілів та транспортної інфраструктури Національного аерокосмічного університету ім. М.Є. Жуковского «Харківський авіаційний інститут», НЕСТЕРЕНКО Сергій Іванович.*
Адреса робоча: *61070 Україна, м. Харків, вул. Чкалова, 17, НАУ «ХАІ», доцент кафедри автомобілів та транспортної інфраструктури Національного аерокосмічного університету ім. М.Є. Жуковского «Харківський авіаційний інститут», НЕСТЕРЕНКО С.І.*
Мобільний тел.: *+38(096) 965-59-33;*
E-mail: nesterenko.geo@gmail.com
ORCID ID: http://orcid.org/0000-0003-3119-9887

UDC 519.853, 624.04, 624.014.2

SIZE OPTIMIZATION OF SINGLE EDGE FOLDS FOR COLD-FORMED STRUCTURAL MEMBERS

S.I. Bilyk,
Doctor of Technical Science, Professor

V.V. Yurchenko,
Doctor of Technical Science, Professor

Kyiv National University of Construction and Architecture
Povitroflotskyj av., 31, Kyiv, 030370

DOI: 10.32347/2410-2547.2020.105.73-86

Optimization problem for single edge fold size in cold-formed structural members has been considered by the paper. Linear convolution of criteria, namely minimization criterion of design area of stiffener cross-section and maximization criterion effective area of stiffener cross-section which defines it reduced load-bearing capacity due to distortional buckling has been used as optimization criterion.

Results of performed study can be served as design recommendations for companies-manufacturers of cold-formed profiles as well as recommendations in scope of elaboration national standard – assortments of effective cold-formed profiles. It will promote wider implementation of cold-formed building structures in building practice.

Key words: load-bearing capacity, cold-formed profile, optimization problem, single edge fold, stiffener, distortional buckling, linear convolution of criteria.

Introduction. Previously, the use of cold-formed thin-walled profiles was limited to cases where reducing the weight of the structure was a priority, such as in the aviation or automotive industries. However, due to the development of production technology, corrosion protection, product availability as well as implementation of the design code the use of thin-walled structural elements, including cold-formed profiles is gradually expanding.

Today, various structural systems made from thin-walled cold-formed profiles, which are widely used in the construction industry, are actively imported to the Ukrainian market of steel structures. Implementation of steel structures made from thin-walled cold-formed profiles in building practice is relevant and economically reasonable. There are specific fields of application where their efficiency is the highest [9]. However, the widespread application of the structures made from thin-walled cold-formed profiles of the domestic production is delayed due to the lack of domestic experience in economic and reliable design of such structures.

Design and verification of thin-walled structural members made of cold-formed profiles is fully reflected in the European design standards implemented in Ukraine [1, 2]. The design code considers not only local and overall buckling due to flexural, flexural-torsional or lateral-torsional buckling of the cold-formed structural member, but also *distortional buckling*. The latter is a mode of buckling in which the lip stiffener is insufficient to retard the

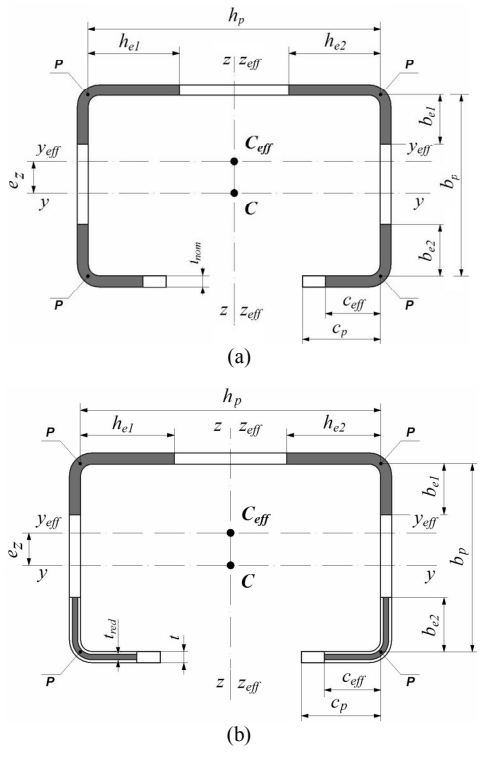

Fig. 1. Construction of the "effective" C-profile cross-section of the cold-formed structural members according to the design code: (a) – at the first stage; (b) – at the second stage

compressed flange and attached web from becoming unstable. In other words, distortional buckling occurs in cases when flange end stiffeners (single edge folds or double edge folds) or intermediate stiffeners are not able to resist the local displacement of the cross-section plane elements conjugation nodes.

Calculation the load-bearing capacity of the cold-formed structural members includes two stages according to the design code. At the first stage calculation of the "effective" (reduced) widths of the compressed cross-section plane elements is performed taking into account local buckling effects in these elements (Fig. 1a). At the second stage calculation of the "effective" (reduced) thicknesses of the compressed cross-section plane elements is performed taking into account distortional buckling effects (see Fig. 1b). Then calculation the load-bearing capacity of the cold-formed structural members is performed using the geometrical properties calculated based on the constructed "effective" (reduced) cross-sections.

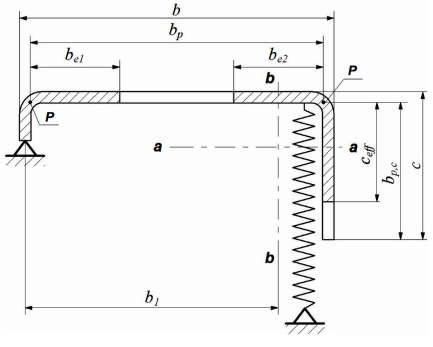

Fig. 2. Plane section element (flange) stiffened by the single edge fold (flange width b should not exceed $60t$, t is profile thickness)

Optimization problem formulation. Let consider a searching problem for optimum sizes of single edge folds which stiffens the flanges in steel structural members made from cold-formed profiles subjected to central compression (Fig. 2).

Initial data for optimization presented as follow: cross-

sectional sizes of C-profile – web height h, flange width b, profile thickness t, internal radius for section plane elements conjunction $r = 1,5t$; steel basic yield strength f_{yb}, MPa; E – steel elastic modulus, MPa.

Let consider single edge fold size c as *design variable* (see Fig. 3). Plane element's design widths for C- and Z- cold-formed profiles which are considered *as state variables* of the optimization problem should be calculated depending on the profile overall dimensions h and b, internal radius $r = 1,5t$ and profile thickness t as follow:

– web plane element design width of the profile:

$$h_p = h - 2,5t;$$

– flange plane element design width of the profile:

$$b_p = b - 2,5t;$$

– single edge fold plane element design width of the profile:

$$c_p = c - 1,25t.$$

Slenderness of the profile flange with design width b_p, which is stiffened by single edge fold, is calculated according to [1, 2] as presented below:

$$\bar{\lambda}_{pb} = \frac{b_p}{28,4t\sqrt{k_{\sigma 1,jkm}}}\sqrt{\frac{f_{yb}}{235}} = \frac{b_{pb}}{56,8t}\sqrt{\frac{f_{yb}}{235}}.$$

Profile flange with slenderness $\bar{\lambda}_{pb}$ is subjected to local buckling effects (post-buckling behavior) in case when $\bar{\lambda}_{pb} > 0,673$ or

$$\frac{b_p}{56,8t}\sqrt{\frac{f_{yb}}{235}} > 0,673$$

or

$$b_p > 38,2264t\sqrt{\frac{235}{f_{yb}}}.$$

At the same time "effective" flange width b_{eff} is calculated according to [1, 2] as follow:

$$b_{eff} = \frac{b_p}{\bar{\lambda}_{pb}}\left(1 - \frac{0,22}{\bar{\lambda}_{pb}}\right) = 56,8t\sqrt{\frac{235}{f_{yb}}}\left(1 - \frac{12,496t}{b_p}\sqrt{\frac{235}{f_{yb}}}\right).$$

The combined action of the single edge fold and a part of the "effective" (reduced) flange is considered when calculating the flexural buckling verification of the stiffener. The part of the "effective" flange with width b_{e2} (see Fig. 2) is included to the stiffener design section and is calculated according to [1, 2] as presented below:

$$b_{e2} = 0,5b_{p,eff} = \frac{b_p}{2\bar{\lambda}_{pb}}\left(1-\frac{0,22}{\bar{\lambda}_{pb}}\right) = 28,4t\sqrt{\frac{235}{f_{yb}}}\left(1-\frac{12,496t}{b_p}\sqrt{\frac{235}{f_{yb}}}\right). \quad (1)$$

In case when the local buckling of the flange stiffened by the single edge fold does not occur, i. e. when $\bar{\lambda}_{pb} \le 0,673$ or

$$b_p \le 38,2264t\sqrt{\frac{235}{f_{yb}}}.$$

Then the combined action of the single edge fold and the half of the design flange width b_p is considered when calculating the flexural buckling verification of the stiffener:

$$b_{e2} = 0.5b_p.$$

Plane element slenderness with design width c_p of the single edge fold stiffened the flange is calculated according to [1, 2] as presented below:

– for short single edge folds (when $c_p \le 0,35b_p$):

$$\bar{\lambda}_{pc} = \frac{c_p}{28,4t\sqrt{0,5}}\sqrt{\frac{f_{yb}}{235}} = 0,0498\frac{c_p}{t}\sqrt{\frac{f_{yb}}{235}};$$

– for long single edge folds (when $0,35b_p < c_p \le 0,6b_p$):

$$\bar{\lambda}_{pc} = \frac{c_p}{28,4t\sqrt{0,5+0,83\left((c_p/b_p)-0,35\right)^{2/3}}}\sqrt{\frac{f_{yb}}{235}}.$$

For single edge fold with design width c_p local buckling occurs when $\bar{\lambda}_{pc} > 0,748$ or

– for short single edge folds (when $c_p \le 0,35b_p$):

$$\bar{\lambda}_{pc} = \frac{c_p}{28,4t\sqrt{0,5}}\sqrt{\frac{f_{yb}}{235}} = 0,0498\frac{c_p}{t}\sqrt{\frac{f_{yb}}{235}} > 0,748;$$

whence it follows:

$$c_p > 15,02121t\sqrt{\frac{235}{f_{yb}}};$$

– for long single edge folds (when $0,35b_p < c_p \le 0,6b_p$):

$$\bar{\lambda}_{pc} = \frac{c_p}{28,4t\sqrt{0,5+0,83\left((c_p/b_p)-0,35\right)^{2/3}}}\sqrt{\frac{f_{yb}}{235}} > 0,748;$$

whence it follows:

$$c_p > 21,2432t\sqrt{\frac{235}{f_{yb}}}\sqrt{0,5+0,83\left((c_p/b_p)-0,35\right)^{2/3}}\ .$$

For single edge fold with post-buckling behavior (local buckling occurs in plane element of the stiffener), "effective" width c_{eff} should be calculated according to [1, 2] as presented below:

– if $\overline{\lambda}_{pc} > 0,748$ and $c_p \le 0,35b_p$:

$$c_{eff} = \frac{t}{0,0498}\sqrt{\frac{235}{f_{yb}}}\left(1-3,7754\frac{t}{c_p}\sqrt{\frac{235}{f_{yb}}}\right); \tag{2}$$

– if $\overline{\lambda}_{pc} > 0,748$ and $0,35b_p < c_p \le 0,6b_p$:

$$c_{eff} = 28,4t\sqrt{\frac{235}{f_{yb}}}\sqrt{0,5+0,83\left(\frac{c_p}{b_p}-0,35\right)^{2/3}} \times$$
$$\times\left(1-5,3392\frac{t}{c_p}\sqrt{\frac{235}{f_{yb}}}\sqrt{0,5+0,83\left(\frac{c_p}{b_p}-0,35\right)^{2/3}}\right). \tag{3}$$

In case when the local buckling of the single edge fold plane element is not occurred, that is when $\overline{\lambda}_{pc} \le 0,748$, or

– for short single edge folds (when $c_p \le 0,35b_p$):

$$c_p \le 15,02121t\sqrt{\frac{235}{f_{yb}}};$$

– for long single edge folds (when $0,35b_p < c_p \le 0,6b_p$):

$$c_p \le 21,2432t\sqrt{\frac{235}{f_{yb}}}\sqrt{0,5+0,83\left(\frac{c_p}{b_p}-0,35\right)^{2/3}};$$

"effective" width of the single edge fold plane element c_{eff} should be equal to the design width:

$$c_{eff} = c_p\ .$$

Slenderness of the single edge fold corresponded to the flexural buckling of the stiffener is calculated according to [1, 2] as follow:

$$\overline{\lambda}_d = \sqrt{\frac{f_{yb}A_s}{2\sqrt{KEI_s}}} = \sqrt{\frac{f_{yb}t\left(c_{eff}+b_{e2}\right)}{\sqrt{KEtc_{eff}^3\left(\frac{1}{3}+\frac{b_{e2}}{c_{eff}+b_{e2}}\right)}}}\ , \tag{4}$$

where A_s and I_s – geometrical properties of the single edge fold design section; K – stiffness of the linear spring (using the spring partial restraint of

the plane section element (flange) by the single edge fold is simulated) calculated according to [1, 2] as for cold-formed central compressed cross-sections symmetrical relating to the main axes of inertia which is perpendicular to the web plane with flange stiffened by the single edge folds as presented below:

$$K = \frac{E}{3,64} \cdot \frac{t^3}{\left(b_p - \frac{0,5(b_{e2})^2}{c_{eff} + b_{e2}}\right)^2 \left(1,5h_p + b_p - \frac{0,5(b_{e2})^2}{c_{eff} + b_{e2}}\right)}.$$

The reduction factor corresponded to the flexural buckling of the stiffener (or distortional buckling factor) should be calculated depending on slenderness $\overline{\lambda}_d$ of the stiffener as presented below:

$$\chi_d = \Xi\left(\overline{\lambda}_d\right);$$

where Ξ – is the functional dependence described in [1, 2] as follow:

$$\Xi\left(\overline{\lambda}_d\right) = \begin{cases} 1,0 & \text{if } \overline{\lambda}_d \le 0,65; \\ 1,47 - 0,723\overline{\lambda}_d & \text{if } 0,65 < \overline{\lambda}_d \le 1,38; \\ 0,66\overline{\lambda}_d^{-1} & \text{if } \overline{\lambda}_d > 1,38. \end{cases} \quad (5)$$

It should be noted, that when $\overline{\lambda}_d \le 0,65$ distortional buckling of the section does not occur.

The reduced area of the stiffener (single edge fold) design section determined the reduced load-bearing capacity of the stiffener due to flexural buckling is calculated depending on distortional buckling factor χ_d as follow:

$$A_{s,red} = \chi_d A_s . \quad (6)$$

The reduced load-bearing capacity of the stiffener due to flexural buckling is taken into account by reduction of the thickness for the stiffener design section as presented below:

$$t_{red} = t\frac{A_{s,red}}{A_s}.$$

In the paper [6] load-bearing capacity region in “axial force – bending moment” coordinates for a doubly symmetrical cross-section of the thin-walled cold-formed structural members has been constructed according to the requirements of the design code [1, 2]. Performed analysis of the constructed load-bearing capacity region has shown the non-convexity and abrupt changing of the region boundaries occurred in cases where the section goes to the post-buckling stage, which is characterized by the phenomenon of local buckling of the plane section elements and/or distortional buckling of the section. In addition, this analysis also showed an increase the load-bearing capacity with increasing axial tensile internal force due to the increase of the “effective” (reduced) design section.

Presented arguments lead to consider as a purpose function in cross-

sectional sizes optimization problems formulated for cold-formed structural members the following criterion of minimum difference between initial cross-section area and "effective" (reduced) cross-section area:

$$\mathbf{FES}_A = A_s - A_{s,red} \to \min$$

or taking into account (1.6):

$$\mathbf{FES}_A = A_s - A_{s,red} = A_s - \chi_d A_s = A_s\left(1-\chi_d\right) \to \min$$

or

$$\mathbf{FES}_A\left(c\right) = t\left(c_{eff} + b_{e2}\right)\left(1-\chi_d\left(\overline{\lambda}_d\right)\right) \to \min, \qquad (7)$$

where c_{eff}, b_{e2} and $\overline{\lambda}_d$ are calculated according to (2) or (3), (1) and (4) respectively depending on overall profile dimensions h, b, t and variable size of the single edge fold c, and functional dependency $\chi_d(\overline{\lambda}_d)$ is defined according to (5).

Proposed optimization criterion (7) for size optimization of the single edge fold stiffened the flanges in cold-formed structural members in fact is a linear convolution (with the same weight factors) of the following two criteria:

1) minimization of the design cross-section area of the stiffener A_s, which provides minimum material consumption;

2) maximization of the "effective" (reduced) cross-sectional area of the singe edge fold $A_{s,red}$ determined the reduced load-bearing capacity of the stiffener taking into account flexural buckling effects, or in other words, load-bearing capacity maximization of the single edge fold.

Thus, cross-section size optimization problem for cold-formed structural members has been formulated as searching problem for optimum single edge fold size c with minimization of the determined purpose function (7) taking into account state variables calculated according to (1) – (6). The parametric optimization problem stated by (1) – (7) has been solved using the method of objective function gradient projection onto the active constraints surface with simultaneous correction of the constraints violations [3, 4]. In order to realize the formulated optimization problem, software OptCAD intended to solve parametric optimization problems for steel structural systems has been used [5, 6].

Results and discussion. Optimization results of the single edge folds for the cold-formed C-profiles manufactured by «Blachy Pruszyński» [8] company are presented in Table 1, for the cold-formed C-profiles manufactured by «BF FACTORY» company – in Table 2, for the cold-formed C-profiles manufactured by «STEELCO» company – in Table 3.

Table 1

Optimization results obtained for C-profiles manufactured by «Blachy Pruszyński» company

Profile sizes, mm	Initial design				Optimum solution by the criterion				
					$A_s - A_{s,red} \to \min$				$A_{s,red} \to \max$
	c, mm	χ_d	t_{red}, mm	$A_{s,red}$, mm	$c_{\min}^{opt}$, mm	χ_d	t_{red}, mm	$A_{s,red}$, mm	$c_{\max}^{opt}$, mm
100×48×1,5	**18**	0,968	1,452	87,66	**20,5**	1,0	1,5	94,31	**28,4**
100×48×2,0	**18**	1,0	2,0	117,0	**15,7**	1,0	2,0	112,40	**28,3**
100×48×2,5	**18**	1,0	2,5	141,56	**13,3**	1,0	2,5	129,81	**28,1**
100×48×3,0	**18**	1,0	3,0	164,25	**12,0**	1,0	3,0	146,25	**28,0**
150×48×1,5	**18**	0,921	1,381	83,36	**24,5**	1,0	1,5	100,31	**28,5**
150×48×2,0	**18**	0,996	1,993	116,56	**18,3**	1,0	2,0	117,6	**28,3**
150×48×2,5	**18**	1,0	2,5	141,56	**15,2**	1,0	2,5	134,56	**28,2**
150×48×3,0	**18**	1,0	3,0	164,25	**13,5**	1,0	3,0	150,75	**28,1**
200×48×1,5	**18**	0,883	1,324	79,95	**28,3**	1,0	1,5	106,01	**28,5**
200×48×2,0	**18**	0,964	1,927	112,73	**20,7**	1,0	2,0	122,4	**28,3**
200×48×2,5	**18**	1,0	2,5	141,56	**16,9**	1,0	2,5	138,81	**28,2**
200×48×3,0	**18**	1,0	3,0	164,25	**14,8**	1,0	3,0	154,65	**28,1**
250×48×1,5	**19**	0,869	1,304	80,02	**28,5**	0,976	1,464	103,66	**28,5**
250×48×2,0	**19**	0,952	1,904	113,30	**22,9**	1,0	2,0	126,80	**28,3**
250×48×2,5	**19**	1,0	2,5	144,06	**18,4**	1,0	2,5	142,5625	**28,2**
250×48×3,0	**19**	1,0	3,0	167,25	**15,9**	1,0	3,0	157,95	**28,1**
280×48×1,5	**19**	0,853	1,279	78,51	**28,5**	0,963	1,444	102,25	**28,5**
280×48×2,0	**19**	0,938	1,876	111,62	**24,1**	1,0	2,0	129,2	**28,3**
280×48×2,5	**19**	0,996	2,491	143,52	**19,3**	1,0	2,5	144,8125	**28,2**
280×48×3,0	**19**	1,0	3,0	167,25	**16,6**	1,0	3,0	160,05	**28,1**
300×49×1,5	**18**	0,813	1,220	74,84	**29,1**	0,951	1,427	103,32	**29,1**
300×49×2,0	**18**	0,903	1,805	107,40	**25,8**	1,0	2,0	134,60	**28,9**
300×49×2,5	**18**	0,964	2,409	138,83	**20,5**	1,0	2,5	150,31	**28,8**
300×49×3,0	**18**	1,0	3,0	167,25	**17,5**	1,0	3,0	165,75	**28,7**
100×60×1,5	**19**	0,880	1,321	96,90	**30,0**	1,0	1,5	125,77	**35,7**
100×60×2,0	**19**	0,960	1,921	137,33	**21,9**	1,0	2,0	148,80	**35,5**
100×60×2,5	**19**	1,0	2,5	174,06	**18,1**	1,0	2,5	171,81	**35,4**
100×60×3,0	**19**	1,0	3,0	203,25	**15,9**	1,0	3,0	193,95	**35,3**
150×60×1,5	**19**	0,827	1,240	90,97	**35,7**	0,979	1,469	127,27	**35,7**
150×60×2,0	**19**	0,913	1,826	130,58	**25,9**	1,0	2,0	156,80	**35,5**
150×60×2,5	**19**	0,972	2,430	169,20	**21,0**	1,0	2,5	179,06	**35,4**
150×60×3.0	**19**	1,0	3,0	203,25	**18,1**	1,0	3,0	200,55	**35,3**
200×60×1,5	**22**	0,837	1,256	95,92	**35,7**	0,947	1,420	123,06	**35,7**
200×60×2,0	**22**	0,924	1,848	137,64	**29,4**	1,0	2,0	163,8	**35,5**
200×60×2,5	**22**	0,983	2,457	178,46	**23,5**	1,0	2,5	185,31	**35,4**
200×60×3,0	**22**	1,0	3,0	212,25	**20,1**	1,0	3,0	206,55	**35,3**
250×60×1,5	**22**	0,804	1,206	92,11	**35,7**	0,919	1,379	119,51	**35,7**
250×60×2,0	**22**	0,895	1,790	133,33	**32,8**	1,0	2,0	170,6	**35,5**
250×60×2,5	**22**	0,957	2,392	173,74	**25,8**	1,0	2,5	191,0625	**35,4**
250×60×3,0	**22**	1,0	3,0	212,25	**21,8**	1,0	3,0	211,65	**35,3**
280×60×1,5	**22**	0,786	1,179	90,07	**35,7**	0,905	1,357	117,61	**35,7**
280×60×2,0	**22**	0,879	1,759	131,03	**34,8**	1,0	2,0	174,60	**35,5**
280×60×2,5	**22**	0,943	2,358	171,22	**27,2**	1,0	2,5	194,56	**35,4**

Profile sizes, mm	Initial design				Optimum solution by the criterion				
					$A_s - A_{s,red} \to \min$				$A_{s,red} \to \max$
	c, mm	χ_d	t_{red}, mm	$A_{s,red}$, mm	$c_{\min}^{opt}$, mm	χ_d	t_{red}, mm	$A_{s,red}$, mm	$c_{\max}^{opt}$, mm
280×60×3,0	**22**	0,990	2,970	210,14	**22,8**	1,0	3,0	214,65	**35,3**
300×60×1,5	**21**	0,757	1,136	85,62	**35,7**	0,896	1,34	116,42	**35,7**
300×60×2.0	**21**	0,854	1,708	125,50	**35,5**	0,997	1,99	175,51	**35,5**
300×60×2.5	**21**	0,920	2,299	164,66	**28,0**	1,0	2,5	196,56	**35,4**
300×60×3.0	**21**	0,968	2,904	202,58	**23,4**	1,0	3,0	216,75	**35,3**
350×60×1,5	**23**	0,766	1,150	88,94	**35,7**	0,874	1,312	113,67	**35,7**
350×60×2,0	**23**	0,863	1,725	130,24	**35,5**	0,980	1,96	172,43	**35,5**
350×60×2,5	**23**	0,928	2,321	170,86	**30,2**	1,0	2,5	202,06	**35,4**
350×60×3,0	**23**	0,977	2,931	210,29	**25,1**	1,0	3,0	221,55	**35,3**
400×60×1,5	**22**	0,726	1,089	83,19	**35,7**	0,855	1,283	111,19	**35,7**
400×60×2,0	**22**	0,827	1,655	123,26	**35,5**	0,964	1,928	169,66	**35,5**
400×60×2,5	**22**	0,896	2,241	162,73	**32,2**	1,0	2,5	207,06	**35,4**
400×60×3,0	**22**	0,947	2,842	201,06	**26,6**	1,0	3,0	226,05	**35,3**
280×75×1,5	**24**	0,728	1,092	58,43	**44,7**	0,835	1,253	79,625	**44,7**
280×75×2,0	**24**	0,792	1,584	144,94	**44,5**	0,962	1,923	211,06	**44,5**
280×75×2,5	**24**	0,864	2,159	193,50	**38,8**	1,0	2,5	261,06	**44,4**
280×75×3,0	**24**	0,916	2,749	241,22	**32,0**	1,0	3,0	287,25	**44,3**
350×75×1,5	**20**	0,615	0,923	45,68	**44,7**	0,803	1,204	76,54	**44,7**
350×75×2,0	**20**	0,674	1,347	117,86	**44,5**	0,935	1,870	205,18	**44,5**
350×75×2,5	**20**	0,754	1,886	161,50	**43,4**	1,0	2,5	272,56	**44,4**
350×75×3,0	**20**	0,814	2,441	204,41	**35,4**	1,0	3,0	297,45	**44,3**
400×75×1.5	**20**	0,589	0,883	43,72	**44,7**	0,782	1,173	74,59	**44,7**
400×75×2.0	**20**	0,648	1,296	113,40	**44,5**	0,918	1,836	201,46	**44,5**
400×75×2.5	**20**	0,732	1,829	156,58	**44,4**	0,990	2,475	272,25	**44,4**
400×75×3.0	**20**	0,792	2,377	199,10	**37,7**	1,0	3,0	304,35	**44,3**

Table 2

Optimization results obtained for C-profiles manufactured by «BF FACTORY» company

Profile sizes, mm	Initial design				Optimum solution by the criterion				
					$A_s - A_{s,red} \to \min$				$A_{s,red} \to \max$
	c, mm	χ_d	t_{red}, mm	$A_{s,red}$, mm	$c_{\min}^{opt}$, mm	χ_d	t_{red}, mm	$A_{s,red}$, mm	$c_{\max}^{opt}$, mm
100×48×2,0	**20**	1,0	2,0	121,0	**15,7**	1,0	2,0	112,40	**28,3**
150×48×2,0	**20**	1,0	2,0	121,0	**18,3**	1,0	2,0	117,6	**28,3**
100×60×2,0	**20**	0,975	1,951	141,44	**21,9**	1,0	2,0	148,80	**35,5**
150×60×2,0	**20**	0,930	1,859	134,80	**25,9**	1,0	2,0	156,80	**35,5**
150×60×2,5	**20**	0,988	2,469	174,35	**21,0**	1,0	2,5	179,06	**35,4**
200×60×2.0	**20**	0,893	1,787	129,52	**29,4**	1,0	2,0	163,8	**35,5**
200×60×2,5	**20**	0,955	2,387	168,56	**23,5**	1,0	2,5	185,31	**35,4**
200×60×3,0	**20**	1,0	3,0	206,22	**20,1**	1,0	3,0	206,55	**35,3**
200×65×1.5	–	–	–	–	**38,7**	0,926	1,390	84,30	**38,7**

200×65×2,0	–	–	–	–	**33,5**	1,0	2,0	182,0	**38,5**
200×65×2,5	**20**	0,917	2,292	173,35	**26,5**	1,0	2,5	205,31	**38,4**
200×65×3,0	–	–	–	–	**22,5**	1,0	3,0	228,75	**38,3**
250×60×2,0	**20**	0,863	1,725	125,09	**32,8**	1,0	2,0	170,6	**35,5**
250×60×2,5	**20**	0,927	2,318	163,69	**25,8**	1,0	2,5	191,06	**35,4**
250×60×3,0	**20**	0,975	2,924	201,00	**21,8**	1,0	3,0	211,65	**35,3**
250×65×1,5	–	–	–	–	**38,7**	0,899	1,349	81,83	**38,7**
250×65×2,0	**20**	0,820	1,639	127,03	**37,5**	1,0	2,0	190,0	**38,5**
250×65×2,5	–	–	–	–	**29,3**	1,0	2,5	212,31	**38,4**
250×65×3,0	–	–	–	–	**24,6**	1,0	3,0	235,05	**38,3**
250×70×1,5	–	–	–	–	**41,7**	0,875	1,312	81,64	**41,7**
250×70×2,0	–	–	–	–	**41,5**	0,995	1,989	206,55	**41,5**
250×70×2,5	**20**	0,848	2,120	170,93	**32,9**	1,0	2,5	233,81	**41,4**
250×70×3,0	**20**	0,901	2,701	212,73	**27,5**	1,0	3,0	258,75	**41,3**
300×60×3,0	**20**	0,953	2,858	196,47	**23,4**	1,0	3,0	216,75	**35,3**
300×70×1,5	–	–	–	–	**41,7**	0,850	1,275	79,35	**41,7**
300×70×2,0	–	–	–	–	**41,5**	0,974	1,949	202,34	**41,5**
300×70×2,5	**20**	0,821	2,052	165,48	**35,9**	1,0	2,5	241,31	**41,4**
300×70×3,0	**20**	0,876	2,627	206,85	**29,7**	1,0	3,0	265,35	**41,3**

Table 3

Optimization results obtained for C-profiles manufactured by «STEELCO» company

Profile sizes, mm	Initial design				Optimum solution by the criterion				
					$A_s - A_{s,red} \to \min$				$A_{s,red} \to \max$
	c, mm	χ_d	t_{red}, mm	$A_{s,red}$, mm^2	$c_{\min}^{opt}$, mm	χ_d	t_{red}, mm	$A_{s,red}$, mm^2	$c_{\max}^{opt}$, mm
60×60×0,8	**20**	0,695	0,556	17,98	**35,8**	0,790	0,632	23,51	**35,8**
60×60×1,0	**20**	0,819	0,916	31,34	**35,8**	0,902	0,902	40,08	**35,8**
60×60×1,2	**20**	0,904	1,085	47,00	**35,7**	0,979	1,175	59,77	**35,7**
60×60×1,4	**20**	0,946	1,325	60,54	**25,3**	1,0	1,4	71,40	**35,7**
80×40×0,8	**20**	0,894	0,715	23,20	**23,8**	0,913	0,730	24,77	**23,8**
80×40×1,0	**20**	0,982	0,982	54,89	**23,4**	1,0	1,0	57,61	**23,8**
80×40×1,2	**20**	1,0	1,2	66,6	**17,5**	1,0	1,2	63,60	**23,7**
80×40×1,4	**20**	1,0	1,4	76,65	**15,0**	1,0	1,4	69,65	**23,7**
100×40×0,8	**20**	0,867	0,693	22,51	**23,8**	0,887	0,710	24,06	**23,8**
100×40×1,0	**20**	0,958	0,958	53,55	**23,8**	0,979	0,979	56,57	**23,8**
100×40×1,2	**20**	1,0	1,2	66,6	**19,3**	1,0	1,2	65,76	**23,7**
100×40×1,4	**20**	1,0	1,4	76,65	**16,4**	1,0	1,4	71,61	**23,7**
150×50×0,8	**20**	0,683	0,547	17,81	**29,7**	0,747	0,597	21,41	**29,8**
150×50×1,0	**20**	0,808	0,808	30,79	**29,8**	0,864	0,864	36,63	**29,8**
150×50×1,2	**20**	0,883	1,059	44,17	**29,7**	0,946	1,135	54,28	**29,7**
150×50×1,4	**20**	0,913	1,279	82,79	**28,4**	1,0	1,4	102,41	**29,7**
150×50×1,5	–	–	–	–	**26,2**	1,0	1,5	105,86	**29,7**
150×50×2,0	**20**	1,0	2,0	125,0	**19,5**	1,0	2,0	124,0	**29,5**
150×50×2,5	–	–	–	–	**16,1**	1,0	2,5	141,81	**29,4**
150×50×3,0	–	–	–	–	**14,2**	1,0	3,0	158,85	**29,3**
200×50×0,8	**20**	0,633	0,506	16,50	**29,8**	0,701	0,560	20,11	**29,8**
200×50×1,0	**20**	0,765	0,765	29,16	**29,8**	0,825	0,825	34,98	**29,8**

Profile sizes, mm	Initial design				Optimum solution by the criterion				
					$A_s - A_{s,red} \to \min$				$A_{s,red} \to \max$
	c, mm	χ_d	t_{red}, mm	$A_{s,red}$, mm^2	$c_{\min}^{opt}$, mm	χ_d	t_{red}, mm	$A_{s,red}$, mm^2	$c_{\max}^{opt}$, mm
200×50×1,2	**20**	0,844	1,013	42,25	**29,7**	0,912	1,094	52,33	**29,7**
200×50×1,4	**20**	0,876	1,226	79,37	**29,7**	0,974	1,364	100,74	**29,7**
200×50×1,5	–	–	–	–	**29,7**	0,995	1,493	110,49	**29,7**
200×50×2,0	**20**	0,976	1,952	121,97	**22,0**	1,0	2,0	129	**29,5**
200×50×2,5	**20**	1,0	2,5	151,56	**17,9**	1,0	2,5	146,31	**29,4**
200×50×3,0	**20**	1,0	3,0	176,25	**15,6**	1,0	3,0	163,05	**29,3**
250×50×1,4	**20**	0,844	1,181	76,49	**29,7**	0,948	1,327	98,02	**29,7**
250×50×1,5	–	–	–	–	**29,6**	0,970	1,455	107,64	**29,6**
250×50×2,0	**20**	0,949	1,898	118,64	**24,4**	1,0	2,0	133,8	**29,5**
250×50×2,5	**20**	1,0	2,5	151,56	**19,6**	1,0	2,5	150,57	**29,4**
250×50×3,0	**20**	1,0	3,0	176,25	**16,9**	1,0	3,0	166,95	**29,3**
300×87×1,5	–	–	–	–	**51,9**	0,768	1,152	76,19	**51,9**
300×87×2,0	**18**	0,595	1,190	65,42	**51,7**	0,911	1,822	147,59	**51,7**
300×87×2,5	**19**	0,653	1,633	157,75	**51,5**	1,0	2,5	322,81	**51,6**
300×87×3,0	**21**	0,769	2,306	223,12	**41,8**	1,0	3,0	352,65	**51,5**
350×67×2,0	**13**	0,507	1,013	73,47	**39,7**	0,964	1,928	191,21	**39,7**
350×67×2,5	**14**	0,642	1,604	114,86	**36,0**	1,0	2,5	234,06	**39,6**
350×67×3,0	**15**	0,742	2,227	157,52	**29,7**	1,0	3,0	256,35	**39,5**
350×67×4,0	**18**	0,911	3,644	255,09	**23,0**	1,0	4,0	300,0	**39,2**
400×90×1,5	–	–	–	–	**53,7**	0,707	1,061	70,74	**53,7**
400×90×2,0	**16**	0,462	0,925	49,57	**53,5**	0,863	1,726	141,43	**53,5**
400×90×2,5	**17**	0,494	1,236	120,67	**53,4**	0,959	2,396	318,13	**53,4**
400×90×3,0	**19**	0,639	1,918	187,46	**50,8**	1,0	3,0	388,65	**53,3**
400×90×4,0	**23**	0,833	3,334	326,68	**37,4**	1,0	4,0	449,61	**53,0**

Conclusion. Size optimization problem for single edge folds stiffened flanges in cold-formed structural members has been formulated and solved in the paper. The linear convolution of the following two criteria has been considered, namely minimization criterion for design cross-section area of the stiffener providing minimum material consumption as well as maximization criterion for the "effective" (reduced) cross-section area of the single edge fold determined the reduced load-bearing capacity of the stiffener due to flexural buckling or, in other words, maximization criterion for the load-bearing capacity of the stiffener.

The results of the performed investigation can be used as recommendations for companies-manufacturers of the cold-formed profiles, as well as a guide for creation the national assortment base of the effective cold-formed profiles promoting wider implementation of cold-formed steel structures in building practice.

REFERENCES

1. *DSTU-N B EN 1993-1-3:2012* EuroCode 3. Design of steel structures. Part 1-3: General rules – Supplementary rules for cold-formed members and sheeting (EN 1993-1-3:2006, IDT). – Kyiv, Minregionbud of Ukraine, 2012. (ukr)
2. *DSTU-N B EN 1993-1-5:2012* EuroCode 3: Design of steel structures. Part 1-5: General rules – Plated structural elements (EN 1993-1-5:2005, IDT). – Kyiv, Minregionbud of Ukraine, 2012. (ukr)
3. *Guljaev V. I., Bazhenov V. A., Koshkin V. L.* Metodyi optimizatsii v stroitelnoy mehanike (Optimisation methods in structural mechanic). – Kyiv, 1988. – 192 p. (rus)
4. *Peleshko I., Yurchenko V.* An optimum structural computer-aided design using update gradient method // Proceedings of the 8th International Conference "Modern Building Materials, Structures and Techniques" (Lithuania, Vilnius, May 19-21, 2004), Faculty of Civil Engineering, Vilnius Gediminas Technical University. – p. 860-865.
5. *Peleshko I. D., Yurchenko V. V., Beliaev N. A.* Computer-aided design and optimization of steel structural systems // Zeszyty naukowe Politechniki Rzeszowskiej "Budownictwo i inżynieria środowiska". – No. 52(264). – 2009. – p. 145-154.
6. *Perelmuter A. V., Yurchenko V. V.* Doslidzhennia oblasti nesuchoi zdatnosti tonkostinnykh sterzhnevykh elementiv iz kholodnohnutykh profiliv (Load-bearing capacity region analysis of thin-walled structural members from cold-formed profiles) // Science and construction. – № 3 (21), 2019. – p. 42 – 48. https://doi.org/10.33644/scienceandconstruction.v21i3.110 (ukr)
7. *Permyakov V. O., Yurchenko V. V., Peleshko I. D.* An optimum structural computer-aided design using hybrid genetic algorithm // Proceeding of the International Conference "Progress in Steel, Composite and Aluminium Structures" / Gizejowski, Kozlowski, Sleczka & Ziolko (eds.) / Taylor & Francis Group, London, 2006. – p. 819-826.
8. *Assortment ranges of the cold-formed profiles* for light gauge steel structures of the Ukrainian manufacturers. UCSC-014-16, 2016. 32 p. (ukr)
9. *Yurchenko V.* Searching for shear forces flows in arbitrary cross-sections of thin-walled bars: numerical algorithm and software implementation // Strength of Materials and Theory of Structures: Scientific-and-technical collected articles. – Kyiv: KNUBA, 2019. – Issue 103. – p. 82 – 111. https://doi.org/10.32347/2410-2547.2019.103.82-111.

Стаття надійшла 23.08.2020

Білик С. І., Юрченко В. В.

ОПТИМІЗАЦІЯ РОЗМІРІВ ВІДГИНІВ, ЩО ПІДКРІПЛЮЮТЬ ПОЛИЦІ, В СТЕРЖНЕВИХ ЕЛЕМЕНТАХ КОНСТРУКЦІЙ ІЗ ХОЛОДНОГНУТИХ ПРОФІЛІВ

У статті розглядається задача оптимізації розміру одинарного відгину, який підкріплює полиці, в стержневих елементах конструкцій із холодногнутих профілів. Як критерій оптимальності використано лінійна згортка критерію мінімізації площі розрахункового перерізу відгину та критерію максимізації «ефективної» (редукованої) площі відгину, що визначає його понижену несучу здатність за рахунок втрати стійкості при згинальному випучуванні.

Результати виконаних досліджень можуть слугувати рекомендаціями для компаній-виробників холодногнутих профілів, а також рекомендаціями для створення національного сортаменту ефективних холодногнутих профілів, що сприятиме ширшому впровадженню досліджуваного класу конструкцій у практику будівництва.

Ключові слова: несуча здатність, холодногнутий профіль, задача оптимізації, одинарний відгин, елемент жорсткості, втрата стійкості форми перерізу, лінійна згортка критеріїв.

Bilyk S. I., Yurchenko V. V.

SIZE OPTIMIZATION OF SINGLE EDGE FOLDS FOR COLD-FORMED STRUCTURAL MEMBERS

Parametric optimization problem for single edge fold size in cold-formed structural members subjected to central compression has been considered by the paper. Determination the load-bearing

capacity of the cold-formed structural members has been performed using the geometrical properties calculated based on the constructed “effective” (reduced) cross-sections taking into account local buckling effects in the section as well as distortional buckling effects.

Single edge fold size in cold-formed C-profile has been considered as design variable. Linear convolution of criteria, namely minimization criterion of design area of stiffener cross-section and maximization criterion effective area of stiffener cross-section which defines it reduced load-bearing capacity due to flexural buckling has been used as optimization criterion. The parametric optimization problem has been solved using the method of objective function gradient projection onto the active constraints surface with simultaneous correction of the constraints violations. In order to realize the formulated optimization problem, software OptCAD intended to solve parametric optimization problems for steel structural systems has been used.

Optimization results of the single edge folds for the cold-formed C-profiles manufactured by «Blachy Pruszyński» company, «BF FACTORY» company as well as «STEELCO» company have been presented by the paper. The results of the performed investigation can be used as recommendations for companies-manufacturers of the cold-formed profiles, as well as a guide for creation the national assortment base of the effective cold-formed profiles promoting wider implementation of cold-formed steel structures in building practice.

Key words: load-bearing capacity, cold-formed profile, optimization problem, single edge fold, stiffener, distortional buckling, linear convolution of criteria.

УДК 519.853, 624.04, 624.014.2

Билык С. И., Юрченко В. В.

ОПТИМИЗАЦИЯ РАЗМЕРОВ ОТГИБОВ, ПОДКРЕПЛЯЮЩИХ ПОЛКИ, В СТЕРЖНЕВЫХ ЭЛЕМЕНТАХ КОНСТРУКЦИЙ ИЗ ХОЛОДНОГНУТЫХ ПРОФИЛЕЙ

В статье рассматривается задача оптимизации размера одинарного отгиба, подкрепляющего полки, в стержневых элементах конструкций из холодногнутых профилей. В качестве критерия оптимальности использована линейная свертка критерия минимизации расчетной площади отгиба и критерия максимизации редуцированной площади отгиба, определяющей его пониженную (за счет потери устойчивости при изгибном выпучивании) несущую способность.

Результаты выполненных исследований служат рекомендациями для компаний-изготовителей холодногнутых профилей, а также рекомендациями для создания национального сортамента эффективных холодногнутых профилей, что будет способствовать более широкому внедрению исследуемого класса конструкций в практику строительства.

Ключевые слова: несущая способность, холодногнутый профиль, задача оптимизации, одинарный отгиб, элемент жесткости, потеря устойчивости формы сечения, линейная свертка критериев.

УДК 519.853, 624.04, 624.014.2

Білик С. І., Юрченко В. В. **Оптимізація розміру відгину, що підкріплює полиці, у стержневих елементах конструкцій із холодногнутих профілів** // Опір матеріалів і теорія споруд: наук.-тех. збірн. – К.: КНУБА, 2020. – Вип. 105. – С. 73-86.

У статті розглядається задача оптимізації розміру одинарного відгину, що підкріплює полички, в стержневих елементах конструкцій із холодногнутих профілів. Як критерій оптимальності використана лінійна згортка критерію мінімізації площі розрахункового перерізу відгину та критерію максимізації «ефективної» (редукованої) площі відгину, що визначає його понижену несучу здатність за рахунок втрати стійкості при згинальному випучуванні. Результати виконаних досліджень можуть слугувати рекомендаціями для компаній-виробників холодногнутих профілів, а також рекомендаціями для створення національного сортаменту ефективних холодногнутих профілів.

Іл. 2. Табл. 3. Бібліог. 9 назв.

UDC 519.853, 624.04, 624.014.2
Bilyk S. I., Yurchenko V. V. **Size optimization of single edge folds for cold-formed structural members** // Strength of Materials and Theory of Structures: Scientific-and-technical collected articles – Kyiv: KNUBA, 2020. – Issue 104. – P. 73-86.

The paper considers an optimization problem for single edge fold size in the cold-formed structural members. Linear convolution of criteria, namely minimization criterion of design area of stiffener cross-section and maximization criterion effective area of stiffener cross-section which defines it reduced load-bearing capacity due to distortional buckling has been used as optimization criterion. Results of the performed study can be served as design recommendations for companies-manufacturers of the cold-formed profiles as well as recommendations in scope of elaboration national standard – assortments of the effective cold-formed profiles.
Figs. 2. Tabs. 3. Refs. 9.

УДК 519.853, 624.04, 624.014.2
Билык С. И., Юрченко В. В. **Оптимизация размеров отгибов, подкрепляющих полки, в стержневых элементах конструкций из холодногнутых профилей** // Сопротивление материалов и теория сооружений: науч.- тех. сборн. – К.: КНУСА, 2020. – Вып. 105. – С. 73-86.

В статье рассматривается задача оптимизации размера одинарного отгиба, подкрепляющего полки, в стержневых элементах конструкций из холодногнутых профилей. В качестве критерия оптимальности использована линейная свертка критерия минимизации площади расчетного сечения отгиба и критерия максимизации редуцированной площади отгиба, определяющей его пониженную несущую способность за счет потери устойчивости при изгибном выпучивании. Результаты выполненных исследований могут послужить рекомендациями для компаний-изготовителей холодногнутых профилей, а также рекомендациями для создания национального сортамента эффективных холодногнутых профилей.
Ил. 2. Табл. 3. Библиог. 9 назв.

Автор: *доктор технічних наук, професор кафедри металевих та дерев'яних конструкцій Білик Сергій Іванович*
Адреса робоча: *03680 Україна, м. Київ, Повітрофлотський пр. 31, Київський національний університет будівництва і архітектури*
Робочий тел.: *+38 (044) 241-54-89*
Мобільний тел..: *+38(098)044-82-88*
E-mail: *vartist@ukr.net*
SCOPUS ID: 25636796400
ORCID ID: http://orcid.org/0000-0001-8783-5892

Автор: *доктор технічних наук, професор кафедри металевих та дерев'яних конструкцій Юрченко Віталіна Віталіївна*
Адреса робоча: *03680 Україна, м. Київ, Повітрофлотський пр. 31, Київський національний університет будівництва і архітектури*
Робочий тел.: *+38(044)249-71-91*
Мобільний тел..: *+38(063)89-26-491*
E-mail: *vitalina@scadsoft.com*
SCOPUS ID: 25637856200
ORCID ID: http://orcid.org/0000-0003-4513-809X

UDK 69.001.5

FEATURES OF APPLICATION OF SMART TECHNOLOGIES IN CONSTRUCTION

Yurii Khlaponin[1],
Doctor of Technical Science, professor

Oleksandr Selyukov[1],
Doctor of Technical Science

Dmytro Khlaponin[2],
associate professor

Sergei Palchik[1],
engineer

[1]*Kyiv National University of Construction and Architecture,*
31, Povitroflotsky ave., Kyiv, Ukraine, 03037

[2]*State University of Telecommunications,*
7 Solomyanska Street, Kyiv, Ukraine, 03110

DOI: 10.32347/2410-2547.2020.105.87-98

A study of aspects of the use of smart technologies in construction. This technology originated in the IT industry with the advent of digital devices. Until now, this technology has been invested primarily in the concept of "smart home" with digital control technologies. Then smart technologies spread to the technology of energy-efficient housing and its maintenance. Today, this technology also includes technologies of ecological and energy-saving construction, i.e. smart technologies for the construction of, first of all, modular. Thus, smart technology in construction in any sense means the organization of "smart", i.e. healthy, economical, safe and comfortable human housing at all stages of its life cycle. The surge in interest in "smart" homes and technology is a consequence of the global "digitalization" of human life. In 2017, Ukraine adopted the Law “On Energy Efficiency of Buildings”, which defines the legal, socio-economic and organizational principles of activities in the field of energy efficiency of buildings and aims to reduce energy consumption in buildings. This law defines the basic principles of state policy of Ukraine in this area, namely: ensuring the appropriate level of energy efficiency of buildings in accordance with technical regulations, national standards, norms and rules; stimulating the reduction of energy consumption in buildings; ensuring the reduction of greenhouse gas emissions into the atmosphere; creating conditions for attracting investments in order to implement measures to ensure increase the energy efficiency of buildings; ensuring thermal modernization of buildings, stimulating the use of renewable energy sources; development and implementation of a national plan to increase the number of buildings with close to zero energy consumption. The article considers five areas of implementation of these requirements - energy independence, environmental friendliness, comfort, economy and safety.

Most effectively, in terms of minimizing the components of the technological process, and the cost-effectiveness of the implemented project, these principles can be implemented using materials and technologies that can integrate these requirements in one complex. When implementing the requirements laid down in the above four areas when using smart technologies in construction as a material that combines these areas, it is possible to provide products based on basalt fiber-rigid and semi-rigid thermal insulation boards, mats, harnesses and other materials. These materials can be used in the development of part of the requirements of the fifth direction - security. They are implemented in the development of environmental safety of housing, fire resistance of the building, biological safety of the material, indoor air quality and other aspects of smart technologies.

Keywords: smart technologies, smart home, energy efficiency, ecology, safety, alternative energy sources.

Introduction. The word "smart" is by definition "clever". This technology originated in the IT industry with the advent of digital devices. Until now, this technology has been invested primarily in the concept of "smart home" with digital technologies for its management, which at this time was transformed into a component of smart technology: the concept of "Internet of Things" (IoT). Then smart technologies spread to the technology of energy-efficient housing and its maintenance. Today, this technology also includes technologies of ecological and energy-saving construction, i.e. smart technologies for the construction of, first of all, modular. Reason such a strong difference in the interpretation of the concept of smart technology - the information vacuum in the construction and equipment of "smart" homes [1]. But the researchers are united in one thing: smart technology is an innovative solution. Thus, smart technology in construction in any sense means the organization of "smart", i.e. healthy, economical, safe and comfortable human housing at all stages of its life cycle. The surge in interest in "smart" homes and technology is a consequence of the global "digitalization" of human life. What seemed strange and incomprehensible yesterday is now a faithful helper to millions of people around the world. Even familiar objects, in particular, windows and furniture, acquire new properties.

Results and discussion

But what should a house be like to be considered "smart"? Currently, there are several areas of technology development in construction.

The first direction, which was called "Construction of energy efficient buildings" [2]. In 2017, Ukraine adopted the Law “On Energy Efficiency of Buildings”, which defines the legal, socio-economic and organizational principles of activities in the field of energy efficiency of buildings and aims to reduce energy consumption in buildings. This law defines the basic principles of state policy of Ukraine in this area, namely: ensuring the appropriate level of energy efficiency of buildings in accordance with technical regulations, national standards, norms and rules; stimulating the reduction of energy consumption in buildings; ensuring the reduction of greenhouse gas emissions into the atmosphere; creating conditions for attracting investments in order to implement measures to ensure (increase) the energy efficiency of buildings; ensuring thermal modernization of buildings, stimulating the use of renewable energy sources; development and implementation of a national plan to increase the number of buildings with close to zero energy consumption.

According to DBN B.2.6-31: 2016 "Thermal insulation of buildings" under the energy efficiency of the building means the property of the building, its structural elements and engineering equipment to provide during the expected life cycle of the building household needs and optimal microclimatic conditions for its stay and / or living in premises of such a building at the normatively permissible (optimal) level of energy resources for heating, lighting, ventilation, air conditioning, hot water supply, taking into account local climatic conditions.

Of course, everyone wants to live in a house, where you do not need to insulate the walls of your apartment, get tired of the heat in summer and pay huge sums for heating in winter. The ideal option is to create a building where the need for external energy is close to zero (Fig. 1). The EU has decided that this should be all buildings built after 2019. Such a house is an independent facility, which actively uses alternative energy sources, such as solar, as well as energy produced by electrical appliances and the residents themselves. The main goal of the energy-saving concept is the rational use of resources, care for the environment and the creation of a comfortable building for living. Achieve maximum energy efficiency of the house is possible only with a comprehensive approach to all subsystems - insulation, carefully thought-out ventilation, lighting, heating and cooling, special windows, doors and roof, use of only ecological energy saving devices, etc. Control of home systems, namely: temperature, lighting, alarm - is through an application on a smartphone.

Fig. 1. The first serial energy efficient house in Ukraine

The second direction is environmental friendliness. The main purpose of the green direction in construction is to reduce the burden on the environment, while striving to improve the quality of buildings and ensure the most comfortable environment in the premises. The purpose of this area is the environmental safety of housing and indoor air quality. It is the principles of "external" ecology in construction that will help humanity to preserve the basics of our children's lives, will make it possible to leave them our Earth in a clean and pleasant form. While the "internal" ecology of each building will allow us to raise healthy offspring who will be able to fully enjoy their lives on a clean planet, in the absence of environmental, climatic and energy disasters. To achieve this goal, a separate direction in the industry of building environmentally friendly materials, such as building blocks of sea salt and wooden buildings. It is clear that the most environmentally friendly is engineering equipment that works on the basis of renewable energy sources. Ideally, an environmentally friendly building should use equipment that does not burn raw materials (getting very high temperatures, while in the building we only need some 30-50 degrees), but would work by producing only the really necessary "temperature delta" in the middle of the building. Such equipment includes, for example, heat pumps and solar collectors. By producing thermal energy, they do not burn electricity or other raw materials, but simply select the temperature delta we need to operate the buildings from the environment.

The third direction is comfort. This concept includes both comfortable housing and comfortable management of its operation. This direction is formed first of all from Internet things: the smartphone, the smart socket, the smart TV, the smart watch, the robot vacuum cleaner, etc., but has development and

further: hotel halls are equipped with terminals for independent electronic registration, hotel guests can adjust lighting, climate regulation, control of multimedia equipment and blinds [3]. With the help of a smart system it is possible to make changes in the light regime, you can quickly change both the interior lighting from intimate to the front, and the mode of use of the building (security mode, operating mode, presence simulation, etc.). No less important is the automation of switching on / off lighting fixtures, which allows you to save on utility bills.

The fourth direction is efficiency. Reducing the use of expensive gas and switching to renewable solar energy, energy-saving integrated construction technologies, including passive energy saving, passive cold, reducing water consumption through rainwater collection and aeration. The next step in the development of technologies for the construction of energy-efficient homes should be the creation of energy-efficient homes, that is, homes that produce more energy than they consume.

Most effectively, in terms of minimizing the components of the technological process, and the cost-effectiveness of the implemented project, these principles can be implemented using materials and technologies that can integrate these requirements in one complex. In the implementation of the requirements laid down in the above four areas in the application of smart technologies in construction as a material that allows you to combine these areas, it is possible to cite products based on basalt fiber-rigid and semi-rigid thermal insulation boards, mats, harnesses and other materials. These materials can be used in the development of part of the requirements of the fifth direction - security. They are implemented in the development of environmental safety of housing, fire resistance of the building, biological safety of the material, indoor air quality and other aspects of smart technologies.

Basalts and their structural analogues (diabases, amphiboles, etc.) are used for their production - mountain volcanic ecologically pure raw materials, the reserves of which in the world are practically inexhaustible. Structural and heat-insulating materials based on basalt fiber meet the above conditions. In addition to high technical properties should take into account their lower cost, compared with similar materials based on any other mineral, and even more organic, fibers. The strength of basalt reaches 18000-25000 kg/cm², basalt-containing materials can withstand much greater elastic deformations, because in the basalt fiber there are no plastic deformations in tension, and the elasticity is superior to steel.

The main difference between materials based on basalt fibers is their high strength at all types of stress and the ability to withstand large deformations. The relative deformation of materials based on basalt fibers, without the formation of cracks can reach 0.7 .... 0.9%, which is much higher than for conventional materials. In accordance with the provisions of DBN B.2.6-31: 2016 "Thermal insulation of buildings" requirements of regulations on thermal protection of buildings and structures have led to a growing trend to create new materials that ensure sustainable operation of structures and equipment in the face of intense

destructive external influences. Such materials are subject to a set of (sometimes mutually exclusive) requirements that must combine: physical and mechanical, chemical, hygienic, thermophysical, decorative and other properties of materials. In this regard, there is a need to create materials that at low average density, high strength can withstand significant temperature loads, the impact of extreme natural and operational factors. One such material is mineral fibers based on erupted rocks. The raw materials for their production are non-deficient, widespread in Ukraine main rocks of magmatic origin - basalts and their structural analogues - diabases, amphiboles and others. The relatively low melting point allows the use of these rocks for the production of mineral fibers in a simplified scheme, directly with the loading of rock into the smelting unit, which provides high efficiency of the product, stability of process parameters and no harmful load on the environment. In this case, the melting of raw materials is a one-step principle, the materials obtained on these drags are not only not inferior to traditional glass and mineral fibers, but in a number of properties far outweigh them. Table 1 shows a comparative description of the main technical characteristics of the fiber obtained from different raw materials.

Table 1

The main technical characteristics of mineral fiber-based various materials

#	Fiber material	Density, kg/m3	Tensile strength, MPa 103	Modul Jung, MPa 103	Elongation at tension, MPa 103
1	Steel fiber	7.8	0.8…2.15	200	3…4
2	Asbestos	2.6	0.91…3.1	68	0.6
3	Fiberglass	2.6	1.05…3.85	70… 80	1.5…3.5
4	Carbon	2.0	2.0	245	1.0
5	Basalt	1.1… 1.6	4.0…12.0	184…210	1.2…1.8

It is shown that obtaining structural and heat and sound insulation materials based on basalt fibers with high thermophysical and acoustic properties is possible when creating a porous system in the material with a predetermined textural characteristic of pores of different class, purpose and combination.

It should also be noted that basalt fibers and materials based on them have high thermal and insulating properties, as well as structural properties. In terms of temperature resistance, basalt fibers and products based on them significantly outperform similar indicators of heat and sound insulation products based on glass and mineral fibers. But the requirements of modern regulations on improving the heat and sound performance of buildings and structures raise questions about further improving the performance of thermal insulation materials.

As can be seen from the data given in table 2 heat-insulating products (TZIV), for the production of which basalt fibers were used have an unconditional advantage over other types of TZIV based on mineral fibers and, moreover, based on fibers made of polymeric materials. But at the same time

as meeting the growing needs of industry in the production of thermal insulation materials come to the fore requirements to improve their performance, including such as operating temperature, thermal conductivity, density and others. It should be noted that basalt fibers and materials based on them have high thermal and sound insulation and structural properties. In terms of temperature resistance, basalt fibers and products based on them significantly outperform similar indicators of heat and sound insulation products based on glass and mineral fibers.

Table 2

Comparative characteristics of the main technical indicators of thermal insulation materials based on mineral fibers

#	Indicators	BTSH (10mm)	HSP (20mm)	BTSH (30mm)	SHAON (15mm)	SHAON (15mm)
1	Operating temperature, ^{0}C	700	700	1150	400	400
2	Thermal conductivity, VT/mK	0.055	0.055	0.055	-	-
3	Linear density, tex	25	60	100	56-79	200-240
4	Sorption hydration	2	2	16	-	-
5	Density, kg/m3	450	200	190	-	-

Analyzing the structure, mineral and chemical composition of the fibers, it is possible to conclude that there are common features in all thermal and sound insulation materials, which impose certain restrictions on improving their performance. Thus, a common feature of all thermal and sound insulation materials is the use for their production of fibers of dense structure with mineralogical and chemical composition, which is similar to the raw material, which predetermines the marginal performance. Therefore, one of the ways to increase the performance of products based on inorganic mineral fibers is to modify the structure of the fiber, as well as adjust its chemical and mineralogical composition in the direction of increasing the operating temperature and thermal insulation properties of the fibers.

The fifth direction is security. First, it is the environmental safety of housing, for example, fire protection of wood and provides a high level of fire resistance of the building, the quality of indoor air largely determines the quality of human health. Secondly, it is the safety of the person who lives in it. Of course, smart technologies have many different security and video surveillance systems that allow a person to feel protected. Thus, in the event of unauthorized intrusion into the house of strangers, the smart system will automatically notify the security service and the owners of the intrusion and may not include sound and light alarms, lighting, thereby assisting in apprehending criminals, and, conversely, turn on audible alarms and lighting to warnthe owners and scare the intruders. With the help of the emergency warning system, an emergency rescue service

will be automatically called, and in addition, the water will be cut off, the power supply will be turned off autonomously and the fire extinguishing system will be turned on. In the absence of the hosts, the smart system will notify you that someone has come, and thanks to the Internet, you can see who it is and through the Internet or SMS you can open the door and let the guest. You can always view the image broadcast from video cameras on a personal mobile gadget, portable (wall) displays or TVs online. For example, a smart system by displaying an image will let you know that a child has woken up in a child's room or a car has approached the gate. the power supply will be switched off autonomously and the fire extinguishing system will be switched on. In the absence of the hosts, the smart system will notify you that someone has come, and thanks to the Internet, you can see who it is and through the Internet or SMS you can open the door and let the guest. You can always view the image broadcast from video cameras on a personal mobile gadget, portable (wall) displays or TVs online. For example, a smart system by displaying an image will let you know that a child has woken up in a child's room or a car has approached the gate. The power supply will be switched off autonomously and the fire extinguishing system will be switched on. In the absence of the hosts, the smart system will notify you that someone has come, and thanks to the Internet, you can see who it is and through the Internet or SMS you can open the door and let the guest. You can always view the image broadcast from video cameras on a personal mobile gadget, portable (wall) displays or TVs online. For example, a smart system by displaying an image will let you know that a child has woken up in a child's room or a car has approached the gate. You can always view the image broadcast from video cameras on a personal mobile gadget, portable (wall) displays or TVs online. For example, a smart system by displaying an image will let you know that a child has woken up in a child's room or a car has approached the gate. You can always view the image broadcast from video cameras on a personal mobile gadget, portable (wall) displays or TVs online. For example, a smart system by displaying an image will let you know that a child has woken up in a child's room or a car has approached the gate.

Materials and methods

These areas have formed the composition of smart technologies in construction.

1. Modular assembly (Fig. 2) of buildings of any type: residential buildings, commercial, administrative and even industrial buildings. First of all, the demand for modular buildings is determined by the possibility of quick installation and relatively low price.

Fig. 2. Modular house (photo from http://ukrdream.in.ua)

The modular construction technology allows to erect the building with any necessary

sizes, planning, level of comfort in the minimum terms. Modular construction is developing rapidly in the construction of buildings and, in particular, hotels [4].

2. Technology in the interior: concept Smart House -these are robot vacuum cleaners, sockets (Fig. 3) with a Wi-Fi module and light bulbs, which can be controlled using a smartphone. Even familiar objects, in particular windows and furniture, acquire new properties, for example, touch furniture facades are compatible with the concept of "smart" houses: connecting furniture with the surrounding space, smart management, adaptation to different life situations and people's daily routine. Modern smart TVs are a combination of rich functionality and stylish appearance. For example, Samsung's The Frame has a "chip" in the form of interchangeable frames in six colors. With this design, it is difficult to immediately understand whether you have a TV or a picture. Complements such sensations and a special mode "Picture", which turns off the TV automatically: instead of a boring black screen, the device displays works of art, turning the room into a personal gallery. In the built-in Art Store application you can choose from more than 1,200 works by famous artists and photographers from the largest galleries and museums in the world. Smart technology has touched almost furniture. "Smart" furniture is characterized, first of all, by the compactness and comfort (Fig. 4), extreme ergonomics coupled with convenient functionality. That is why it is so popular with pragmatic, "advanced" interior designers. Especially when it comes to the so-called Smart-apartments, ranging from 9 to extreme ergonomics coupled with convenient functionality. That is why it is so popular with pragmatic, "advanced" interior designers. Especially when it comes to the so-called Smart-apartments, ranging from 9 to 30 m^2. Although smart furniture is becoming increasingly popular with young families who have a little more, but still not very many square meters.

Fig. 3. Smart socket HS110 (photo from https://www.wildberries

Fig. 4. Smart furniture (photo from https://mebshop.kiev.ua)

3. A house built and equipped with smart technologies does not become "smart".

To make it so, you need something more, namely an IT platform that will integrate all communications into a common network and allow you to connect them to cloud services. In addition, the classic concept of Smart House provides for the presence in the building of such qualities as energy efficiency, as well as a high level of comfort and safety of residents. In addition to automatically controlling the entire complex of electronics in the house, the smart system can transmit a failure signal to the owners, service personnel, emergency services via voice message to a mobile phone, SMS or Internet message.

The system is controlled via a global computer network or mobile phone, thus providing the ability to choose heating modes, optimal climate in the right rooms, adjust the water temperature, the usual or special lighting design, background music and news of interest.

To do this, simply send an SMS to the smart system. Despite the variety of data transmission technologies used in "smart homes", the composition of smart systems and the scheme of operation are not fundamentally different. Components of any smartsystems: IT platform (controller, processor), actuators (actuators, regulators, etc.), controls (windows, doors, heaters, air conditioners, home theater, etc.), communication lines (wireless, in the environment Wi-Fi or using Z-Wave wireless technology).

Conclusions

1. The house of the future of each of us will be built on smart technologies.

2. In the long run, not only houses will become "smart", but also cities and even (some) states [5]: every resident will be provided with free Internet access, the city will develop a computer program to combat street crime, on the wheels of cars special sensors will be installed, which collect information about each pothole on the road and send data to the utility server, the program of introduction of electric vehicles will be implemented, garbage in the city will be collected by cleaning robbers, mail will be delivered by postmen. The authorities of any city can set an ambitious goal: to bring the level of emissions of harmful gases to absolute zero by 2025.

3. The main disadvantage of these systems is the dependence on the availability of the Internet and mobile communications. Without these types of communication, all of the above ceases to exist.

REFERENCES

1. What is smart technology. // [Electronic resource] - Access mode: https://techsad.com/aksessuary/chto-takoe -smart-tehnologiya / (access date: 14.05.2020).
2. Energy efficient house: rules for building energy-efficient cottages. - [Electronic resource]. - Access mode: https://www.maximuscentr.com.ua/enerhoefektyvnyi-budynok (access date: 14.05.2020).
3. *Canestri I.* Hotel Citizen: affordable luxury / I. Canestri // Lifestyle. - 2013. - № 9. - P. 47-51.
4. *Korobkin A.* Hotel-konstruktor: nove slovo v hotelnomu budivnytstvi Hotel-constructor: a new word in hotel building / A. Korobkin // Suchasnyi hotel. - 2015. - № 6. - P. 56-58.
5. Rating of smart cities in the world for 2019. - [Electronic resource]. - Access mode: https://spilno.org/article/reitynh-rozumnykh-mist-svitu (access date: 14.05.2020).
6. *Iler R.K.* Kolloidnaya himiya kremnezema i silikatov (Colloidal chemistry of silica and silicates). - Moskva: Gosstroyizdat, 1959. - 288 s.

7. *Mitsyuk G.M.* Povedinka kremnezemu v hidrotermalnykh umovakh (Behavior of silica in hydrothermal conditions). – K.: Naukova dumka, 1971.
8. *Abrahamyan A.V.* Izuchenie protsessa vyischelachivaniya steklovidnyih bazaltov (Study of the process of leaching of vitreous basalts). - Steklo i keramika, 1963. - № 7.
9. *Dmitrov M.V.* Application of smart-technologies in the educational process.
10. Methods of application of SMART Board technology in the educational process: a textbook / G.F. Bonch-Bruevich, VO Abramov, TI Kosenko. - K .: KMPU named after B.D. Grinchenko, 2007. - 102 p.
11. *Semenikhina O.V.* New paradigms in the field of education in the transition to SMART-society [Electronic resource] Access mode:http: // irbis-nbuv.gov.ua
12. *Yakubov S.* Rozumni tekhnolohii ta navchalni materialy (SMART technologies and educational materials) / S. Yakubov, J. Yakinin // Hi-Tech at school. - 2011. - № 3 - 4.
13. Smart-technologies in Ukraine and the world [Electronic resource]. - Access mode: http://molodi.in.ua/smart-tehnolohiji/
14. *Kodenska M., Sokolyuk K.* Prospects and problems of smart-technologies development in Ukraine.
15. "Smart-technologies in energy and electronics - 2020". V International Scientific and Technical Conference.
16. *Zakharova M.V. Ponomar A.B.* Dosvid budivnytstva budivel ta sporud za modulnoiu tekhnolohiieiu (Experience in construction of buildings and structures using modular technology). – Budivnytstvo. Aarkhitektura.
17. *Lisnyak S.M.* «Smart technologies in education ».
18. *Tverdokhlib I.A.* Rozumni tekhnolohii yak osnova formuvannia suchasnykh tendentsii v osviti (Smart technologies as a basis for the formation of modern trends in education)». - Pedahohichni nauky. 2017 № 1 (13).
19. *Kim K.* Ubiquitous Learning Supporting System for Future Classroom in Korea / K. Kim // Proc. Soc. for Information Technology and Teacher Education Int'l Conf., K.McFerrin et al., eds. - 2008, Mar. - R. 2648–2657.
20. Smart technologies in Ukraine and the world [Electronic resource] - Access mode: http // molodi.in.ua/smart-tehnolohiji/
21. Smart technologies will change the education system [Electronic resource] - Access mode: http://trainings.ru/library/education_experience/?id=14024

Стаття надійшла 28.04.2020

Хлапонін Ю.І., Селюков О.В., Хлапонін Д.Ю., Пальчик С.П.

ОСОБЛИВОСТІ ВИКОРИСТАННЯ РОЗУМНИХ ТЕХНОЛОГІЙ В БУДІВНИЦТВІ

Дослідження аспектів використання смарт-технологій в будівництві. Ця технологія виникла в IT-галузі з появою цифрових пристроїв. До цього часу ця технологія вкладалася головним чином у концепцію «розумного будинку» з цифровими технологіями управління. Потім розумні технології поширились на технологію енергоефективного житла та його обслуговування. Сьогодні ця технологія також включає технології екологічного та енергозберігаючого будівництва, тобто розумні технології для будівництва, насамперед, модульні. Таким чином, розумна технологія в будівництві в будь-якому сенсі означає організацію «розумного», тобто здорового, економічного, безпечного та комфортного житла людини на всіх етапах його життєвого циклу. Сплеск інтересу до "розумних" будинків та технологій є наслідком глобальної "цифровізації" людського життя. У 2017 році Україна прийняла Закон «Про енергоефективність будівель», який визначає правові, соціально-економічні та організаційні принципи діяльності у сфері енергоефективності будівель та спрямований на зменшення споживання енергії в будинках. Цей закон визначає основні принципи державної політики України у цій галузі, а саме: забезпечення належного рівня енергоефективності будівель відповідно до технічних регламентів, національних стандартів, норм та правил; стимулювання зменшення споживання енергії в будівлях; забезпечення зменшення викидів парникових газів в атмосферу; створення умов для залучення інвестицій з

метою здійснення заходів щодо підвищення енергоефективності будівель; забезпечення теплової модернізації будівель, стимулювання використання відновлюваних джерел енергії; розробка та реалізація національного плану збільшення кількості будівель з майже нульовим споживанням енергії. У статті розглянуто п'ять областей реалізації цих вимог - енергетична незалежність, екологічність, комфорт, економія та безпека.

Найефективніше, з точки зору мінімізації компонентів технологічного процесу та економічної ефективності реалізованого проекту, ці принципи можуть бути реалізовані з використанням матеріалів та технологій, які можуть інтегрувати ці вимоги в один комплекс. При реалізації вимог, викладених у вищезазначених чотирьох областях, при використанні інтелектуальних технологій у будівництві як матеріалу, що поєднує ці сфери, можна пропонувати вироби на основі базальтових волоконних та напівжорстких теплоізоляційних плит, матів, джгутів та інших матеріалів. Ці матеріали можуть бути використані при розробці частини вимог п'ятого напрямку - безпеки. Вони впроваджені в розробку екологічної безпеки житла, вогнестійкості будівлі, біологічної безпеки матеріалу, якості повітря в приміщеннях та інших аспектів розумних технологій.

Ключові слова: розумні технології, розумний дім, енергоефективність, екологія, безпека, альтернативні джерела енергії.

Хлапонин Ю.И., Селюков О.В., Хлапонин Д.Ю., Пальчик С.П.

ОСОБЕННОСТИ ПРИМЕНЕНИЯ УМНЫХ ТЕХНОЛОГИЙ В СТРОИТЕЛЬСТВЕ

Исследование аспектов использования умных технологий в строительстве. Эта технология зародилась в ИТ-индустрии с появлением цифровых устройств. До сих пор эта технология вкладывалась в основном в концепцию «умного дома» с технологиями цифрового управления. Затем умные технологии распространились на технологии энергоэффективного жилья и его обслуживания. Сегодня в эту технологию входят также технологии экологического и энергосберегающего строительства, то есть интеллектуальные технологии для строительства, в первую очередь, модульные. Таким образом, интеллектуальные технологии в строительстве в любом смысле означают организацию «умного», т.е. здорового, экономичного, безопасного и комфортного жилья человека на всех этапах его жизненного цикла. Всплеск интереса к «умным» домам и технологиям - следствие глобальной «цифровизации» человеческой жизни. В 2017 году Украина приняла Закон «Об энергоэффективности зданий», который определяет правовые, социально-экономические и организационные принципы деятельности в области энергоэффективности зданий и направлен на снижение потребления энергии в зданиях. Этот закон определяет основные принципы государственной политики Украины в этой сфере, а именно: обеспечение надлежащего уровня энергоэффективности зданий в соответствии с техническими регламентами, национальными стандартами, нормами и правилами; стимулирование снижения потребления энергии в зданиях; обеспечение снижения выбросов парниковых газов в атмосферу; создание условий для привлечения инвестиций с целью реализации мероприятий по повышению энергоэффективности зданий; обеспечение тепловой модернизации зданий, стимулирование использования возобновляемых источников энергии; разработка и реализация национального плана по увеличению количества зданий с почти нулевым потреблением энергии. В статье рассматриваются пять направлений реализации этих требований - энергонезависимость, экологичность, комфорт, экономичность и безопасность.

Наиболее эффективно, с точки зрения минимизации составляющих технологического процесса и рентабельности реализуемого проекта, эти принципы могут быть реализованы с использованием материалов и технологий, позволяющих объединить эти требования в один комплекс. При реализации требований, изложенных в вышеуказанных четырех областях, при использовании интеллектуальных технологий в строительстве в качестве материала, объединяющего эти области, можно предоставлять изделия на основе жестких и полужестких теплоизоляционных плит из базальтового волокна, матов, жгутов и других материалов. материалы. Эти материалы могут быть использованы при разработке части требований пятого направления - безопасности. Они реализованы в разработке экологической безопасности жилья, огнестойкости здания, биологической безопасности материала, качества воздуха в помещениях и других аспектов интеллектуальных технологий.

Ключевые слова: умные технологии, умный дом, энергоэффективность, экология, безопасность, альтернативные источники энергии.

УДК 519.853, 624.04, 624.014.2
Хлапонін Ю.І., Селюков О.В., Хлапонін Д.Ю., Пальчик С.П. **Особливості використання розумних технологій в будівництві** // Опір матеріалів і теорія споруд: наук.-тех. збірн. – К.: КНУБА, 2020. – Вип. 105. – С. 87-98.
Іл. 4. Табл. 2. Бібліог. 21 назв.

УДК 519.853, 624.04, 624.014.2
Khlaponin Yu., Selyukov O., Khlaponin D., Palchik S. **Features of application of smart technologies in construction** // Strength of Materials and Theory of Structures: Scientific-and-technical collected articles – Kyiv: KNUBA, 2020. – Issue 105. – P. 87-98.
Figs. 4. Tabs. 2. Refs. 21.

УДК 519.853, 624.04, 624.014.2
Хлапонин Ю.И., Селюков О.В., Хлапонин Д.Ю., Пальчик С.П. **Особенности применения умных технологий в строительстве //** Сопротивление материалов и теория сооружений: науч.- тех. сборн. – К.: КНУСА, 2020. – Вып. 105. – С. 87-98.
Ил. 4. Табл. 2. Библиог. 21 назв.

Автор (науковий ступінь, вчене звання, посада)*: доктор технічних наук, професор, завідувач кафедри кібербезпеки та комп'ютерної інженерії КНУБА Хлапонін Юрій Іванович.*
Адреса: *03680, Україна, м. Київ, Повітрофлотський проспект 31, КНУБА, кафедра кібербезпеки та комп'ютерної інженерії.*
Робочий тел.: *+38 (044) 244-96-45;*
Мобільний тел.: *+38(050) 311-03-73;*
E-mail: *y.khlaponin@gmail.com*
ORCID: https://orcid.org/0000-0002-9287-0817

Автор (науковий ступінь, вчене звання, посада)*: доктор технічних наук, ст.науковий співробітник, професор кафедри кібербезпеки та комп'ютерної інженерії КНУБА Сєлюков Олександр Володимирович.*
Адреса: *03680, Україна, м. Київ, Повітрофлотський проспект 31, КНУБА, кафедра кібербезпеки та комп'ютерної інженерії.*
Мобільний тел.: *+38 (067) 874-83-76;*
E-mail*: selukov@3g.ua*
ORCID ID: https://orcid.org/0000-0001-7979-3434

Автор (науковий ступінь, вчене звання, посада)*: кандидат наук з державного управління, доцент кафедри публічного управління та адміністрування Державного університету телекомунікацій Хлапонін Дмитро Юрійович*
Адреса: *03110, Україна, м. Київ, вул Солом'янська, 7, Державний університет телекомунікацій, кафедра публічного управління та адміністрування*
Мобільний тел.: *+38 (050) 334-68-10;*
E-mail*: kmld85@gmail.com*
ORCID: https://orcid.org/0000-0002-7797-4319

Автор (науковий ступінь, вчене звання, посада)*: інженер кафедри кібербезпеки та комп'ютерної інженерії КНУБА Пальчик Сергій Петрович*
Адреса: *03680, Україна, м. Київ, Повітрофлотський проспект 31, КНУБА, кафедра кібербезпеки та комп'ютерної інженерії.*
Мобільний тел.: *+38(066) 511-43-24;*
E-mail*: orfav@ukr.net*
ORCID: https://orcid.org/0000-0003-1823-676X

UDC 539.3

ALGORITHM FOR COMPUTATIONAL COSTS REDUCING IN PROBLEMS OF CALCULATION OF ASYMMETRICALLY LOADED SHELLS OF ROTATION

A.P. Dzyuba,
Doctor of Technical Science

I.A. Safronova,

L.D. Levitina

Oles Honchar Dnipro National University,
72, Gagarina Av, Dnipro, Ukraine, 49010

DOI: 10.32347/2410-2547.2020.105.99-113

The problem of calculating shells of rotation of a variable along the stiffness meridian under asymmetric loading is reduced to a set of systems of one-dimensional boundary value problems with respect to the amplitudes of the expansion of the desired functions in trigonometric Fourier series. An approach to reduce the required number of solutions such one-dimensional problems is proposed. The approach is based on predicting the values of variables along the meridian of expansion coefficients. This allows reducing the computational steps for finding a solution. The results of calculating the stress-strain state of a steel ring plate under asymmetric transverse loading are given as an example.

Keywords: rotation shells**,** variable stiffness, asymmetric loading, coefficient prediction in the Fourier method, reduction in computing costs.

Introduction

Shell structures are used in the creation of structures of modern engineering, in the oil and gas, chemical and other industries widely. By this way requires not only weight indicators, but also various characteristics that lead to the need to build more reliable models and methods for calculating shell structures with inhomogeneous (in particular, with variable stiffness) parameters. [1 – 6].

In problems of determining the optimal distribution of material [7] or calculating the durability of shells, taking into account the degradation of their surface in an aggressive environment [8], the stiffness parameters change at each step of successive approximations. This leads to difficulties in rebuilding the grid with using well-known finite element analysis packages [9, 10] for each step of the iterative computational (search) algorithm.

A fairly common approach to studying the behavior of such structural elements is to directly solve boundary value problems for systems of partial differential equations describing their state, where the components of the stress-strain state are unknown [1, 5, 11].

In the case of shells of rotation with a variable wall thickness along the meridian, the method of separation of variables is used using decompositions of the components of the stress-strain state and load in trigonometric Fourier series in a circular coordinate [1, 2, 5, 11 – 14]. As a result, the problem of solving a system of partial differential equations is reduced in the general case

to solving $n + 1$ systems of ordinary differential equations to find n harmonics of the expansion of the desired functions in Fourier series. Here, the inhomogeneity parameters (changing the shell wall thickness) are taken into account quite simply, since they turn out to be components of the coefficients of these systems. Further, the main computational steps of this approach are mainly associated with the need to solve a large number of such one-dimensional boundary value problems only. Therefore, reducing the computational cost of finding their solution is quite important.

1. Mathematical model description

The equations of the moment theory of shells under asymmetric loading are accepted under the assumption that shells of revolution (with a generally arbitrary shape of the meridian), round (ring) plates in particular, are isotropic, elastic and thin-walled. The validity of Kirchhoff hypotheses, small deformations and rotation angles in comparison with unity is accepted. The shell wall thickness is taken variable along the meridian $h = h(s)$. It should be noted that the change in the thickness $h(s)$ of the shells of rotation should be sufficiently smooth dh/ds much less, then one [1, 2, 15]. Otherwise, the accepted initial hypotheses will be violated, and the results obtained in the calculations may turn out to be unreliable.

In this case, the equations of moment theory for thin elastic shells of rotation of variable stiffness under asymmetric loading can be, as is known [1, 2, 5, 11], reduced to a system of eight partial differential equations. For power factors, generally accepted designations are introduced $N_1, N_2, S, M_1, M_2, M, Q_1, Q_2$; for appropriate movements and rotation angles – $u, v, w, \vartheta_1, \vartheta_2, \vartheta$, and for the meridional, circumferential and normal components of the external loading intensity – q_1, q_2, q_3.

These well-known equations of the theory of shells, in order to reduce the bulkiness of the presentation, are not given in the article, and in the future, for the sake of definiteness, the statements are taken in the form [1], where four variables that characterize the displacements are taken as the main variables u, v, w, ϑ_1 and four corresponding force factors N_1, S^*, Q_1^*, M_1, where $S^* = S + \dfrac{2M}{R_2}$; $Q_1^* = Q_1 + \dfrac{1}{r}\dfrac{\partial M}{\partial \varphi}$ – reduced efforts.

We will further use the decompositions of the load, displacements, and forces acting in the shell into Fourier series [16] along the circumferential coordinate φ in the form:

$$f = \sum_{k=0}^{\infty} f_k^c \cos k\varphi + \sum_{k=1}^{\infty} f_k^t \sin k\varphi; \quad \psi = \sum_{k=1}^{\infty} \psi_k^c \sin k\varphi - \sum_{k=0}^{\infty} \psi_k^t \cos k\varphi, \qquad (1)$$

where the functions f in the common notation [1] mean functions $u, w, \varepsilon_1, \varepsilon_2, \vartheta_1, \chi_1, \chi_2, N_1, N_2, Q_1, M_1, M_2, q_1, q_3$; functions ψ – functions v, γ_{12},

ϑ_2, χ_{12}, S, Q_2, M, q_2, and f^c_k, f^t_k, ψ^c_k, ψ^t_k – coefficients of their expansion in trigonometric series.

With this choice of functions, the expansion coefficients with the superscript "*t*", which correspond to a skew-symmetric deformation of the shell meridian, are determined by exactly the same system of equations as the coefficients with the index "*c*", which correspond to the symmetric deformation. Therefore, the results of further transformations for these coefficients coincide, which allows them to be carried out only for functions with index "*c*", omitting this sign.

Moreover, the displacements and forces that correspond to the "*k*"-th term of the expansion are determined by the formulas [1]:

$$\begin{aligned}
&u = u_k \cos k\varphi, && v = v_k \sin k\varphi, && w = w_k \cos k\varphi,\\
&\vartheta_1 = \vartheta_{1k} \cos k\varphi, && \vartheta_2 = \vartheta_{2k} \sin k\varphi, && N_1 = N_{1k} \cos k\varphi,\\
&S^* = S^*_k \sin k\varphi, && Q^*_1 = Q^*_{1k} \cos k\varphi, && N_2 = N_{2k} \cos k\varphi,\\
&M_1 = M_{1k} \cos k\varphi, && M_2 = M_{2k} \cos k\varphi, && M = M_k \sin k\varphi.
\end{aligned} \qquad (2)$$

The use of the Fourier method (this is possible in the case when the shell wall thickness in the circumferential direction is constant, but changes only in the meridional $h = h(s)$ allows reducing the adopted system of partial differential equations of state of the shell to a system of ordinary differential equations with respect to the expansion coefficients of the corresponding functions in trigonometric series in the form:

$$\frac{du_k}{ds} = -\mu\frac{\cos\theta}{r}u_k - \mu\frac{k}{r}v_k - \left(\frac{1}{R_1} + \mu\frac{\sin\theta}{r}\right)w_k + \frac{1-\mu^2}{Ehr}(N_{1k}r),$$

$$\frac{dv_k}{ds} = \frac{k}{r}u_k + \frac{\cos\theta}{r}v_k + \frac{2(1+\mu)}{Ehr}(S^*_k r),$$

$$\frac{dw_k}{ds} = \frac{1}{R_1}u_k - \vartheta_{1k},$$

$$\frac{d\vartheta_{1k}}{ds} = -\mu\frac{k}{r^2}\sin\theta v_k - \mu\frac{k^2}{r^2}w_k - \mu\frac{\cos\theta}{r}\vartheta_{1k} + \frac{12(1-\mu^2)}{Eh^3 r}(M_{1k}r),$$

$$\frac{d(N_{1k}r)}{ds} = -\frac{Eh}{r}\left[\cos^2\theta + \frac{k^2h^2\sin^2\theta}{6(1+\mu)r^2}\right]u_k + k\frac{Eh}{r}\cos\theta v_k +$$

$$+\frac{Eh}{r}\sin\theta\cos\theta\left[1 - \frac{k^2h^2}{6(1+\mu)r^2}\right]w_k - \frac{k^2Eh^3}{6(1+\mu)r^2}\sin\theta\cdot\vartheta_{1k} +$$

$$+\frac{\mu}{r}\cos\theta(N_{1k}r) - \frac{k}{r}(S^*_k r) - \frac{1}{R_1}(Q^*_{1k}r) - q_{1k}r,$$

$$\frac{d\left(S_k^* r\right)}{ds}=\frac{Eh}{r}k\cos\theta u_k+\frac{Eh}{r}k^2 v_k+\frac{Eh}{r}k\sin\theta\left(1+\frac{k^2h^2}{12r^2}\right)w_k+$$

$$+\frac{Eh^3}{12r^2}k\sin\theta\cos\theta\cdot\vartheta_{1k}+\mu\frac{k}{r}(N_{1k}r)-\frac{\cos\theta}{r}(S_k^* r)+\mu\frac{k}{r^2}\sin\theta(M_{1k}r)-q_{2k}r,$$

$$\frac{d\left(Q_{1k}^* r\right)}{ds}=\frac{Eh}{r}\sin\theta\cos\theta\left[1-\frac{k^2h^2}{6(1+\mu)r^2}\right]u_k+\frac{Eh}{r}k\sin\theta\left(1+\frac{k^2h^2}{12r^2}\right)v_k+$$

$$+\frac{Eh}{r}\left[\sin^2\theta+\frac{k^4h^2}{12r^2}+\frac{k^2h^2\cos^2\theta}{6(1+\mu)r^2}\right]w_k+\frac{3+\mu}{1+\mu}\cdot\frac{Eh^3}{12r^2}k^2\cos\theta\cdot\vartheta_{1k}+$$

$$+\left(\frac{1}{R_1}+\mu\frac{\sin\theta}{r}\right)(N_{1k}r)+\mu\frac{k^2}{r^2}(M_{1k}r)-q_{3k}r,$$

$$\frac{d(M_{1k}\cdot r)}{ds}=-\frac{k^2Eh^3}{6(1+\mu)r^2}\sin\theta\cdot u_k+\frac{Eh^3}{12r^2}k\sin\theta\cos\theta\cdot v_k+\frac{3+\mu}{1+\mu}\frac{Eh^3}{12r^2}k^2\cos\theta\cdot w_k+$$

$$+\frac{Eh^3}{12r}\left(\cos^2\theta+\frac{12k^2}{1+\mu}\right)\vartheta_{1k}+(Q_{1k}^* r)+\mu\frac{\cos\theta}{r}(M_{1k}\cdot r). \qquad (3)$$

Here, the components of the vector of the main variables of the stress-strain state are the expansion coefficients of displacements $u_k, v_k, w_k, \vartheta_{1k}$. As for the coefficients of decomposition of force factors, it is convenient to take their product by the radius r of the parallel circle as the main unknowns $N_{1k}r$, $S_k^* r$, $Q_{1k}^* r$, $M_{1k}r$.

The coefficients of decomposition of displacements and forces, which are not the main variables, using the relations of the theory of elasticity and the dependencies between displacements and deformations are expressed in terms of the main variables as follows:

$$\vartheta_{2k}=\left(\frac{\sin\theta}{r}v_k+\frac{k}{r}w_k\right)\sin k\varphi,$$

$$N_{2k}=\left[\mu N_{1k}+Eh\left(\frac{k}{r}v_k+\frac{\cos\theta}{r}u_k+\frac{\sin\theta}{r}w_k\right)\right]\cos k\varphi,$$

$$M_{2k}=\left[\mu M_{1k}+\frac{Eh^3}{12}\left(\frac{\cos\theta}{r}\vartheta_{1k}+\frac{k}{r^2}\sin\theta v_k+\frac{k^2}{r^2}w_k\right)\right]\cos k\varphi,$$

$$M_k=D\left(-\frac{k}{r}\vartheta_{1k}-\frac{k\cos\theta}{r^2}w_k+\frac{k\sin\theta}{r^2}u_k\right)\sin k\varphi. \qquad (4)$$

Here k – is the harmonic number of the decomposition; $R_1, R_2, r(s)$ – the radii of curvature of the shell surface and the parallel circle; $\theta(s)$ – angle

between normal and axis of rotation shell; $D = Eh^3 / (12(1-\mu^2))$ – cylindrical stiffness; E, μ – elastic modulus and Poisson's ratio, respectively.

A disadvantage of the system of equations (3) is that the forces and displacements are related to the local coordinate system associated with the normal and tangent to the meridian of the shell. Therefore, the coefficients of the system have discontinuities when the meridian of the shell consists of several sections with corner points between them. In this case, it is necessary to draw up the compatibility equation for different sections.

According to [1], these difficulties can be circumvented if we pass to global coordinates. For this, forces and displacements are projected not on the tangent and normal to the meridian, but on the normal to the axis of symmetry of the shell and to the axis itself. In this case, instead of displacements u, w, displacements ξ, ζ are introduced, and instead of forces N_1, Q_1^*, forces X, Z are introduced as follows:

$$\xi = u\cos\theta + w\sin\theta \qquad \zeta = u\sin\theta - w\cos\theta,$$
$$X = N_1\cos\theta + Q_1^*\sin\theta \qquad Z = N_1\sin\theta - Q_1^*\cos\theta. \tag{5}$$

The same dependencies are related to each other and the coefficients of the expansion in the Fourier series of the corresponding functions. Substituting $u_k, w_k, N_{1k}, Q_{1k}^*$ and their derivatives through ξ_k, ζ_k, X_k, Z_k into system (3) brings it to the form:

$$\frac{d\xi_k}{ds} = -\mu\frac{\cos\theta}{r}\xi_k - \mu\frac{k\cos\theta}{r}v_k - \sin\theta\cdot\vartheta_{1k} + \frac{1-\mu^2}{Eh}\frac{\cos^2\theta}{r}\left(X_k r\right) + \\ + \frac{1-\mu^2}{Eh}\frac{\sin\theta\cos\theta}{r}\left(Z_k r\right),$$

$$\frac{d\zeta_k}{ds} = -\mu\frac{\sin\theta}{r}\xi_k - \mu\frac{k\sin\theta}{r}v_k + \cos\theta\cdot\vartheta_{1k} + \\ + \frac{1-\mu^2}{Eh}\frac{\sin\theta\cdot\cos\theta}{r}\left(X_k r\right) + \frac{1-\mu^2}{Eh}\frac{\sin^2\theta}{r}\left(Z_k r\right),$$

$$\frac{dv_k}{ds} = k\frac{\cos\theta}{r}\xi_k + k\frac{\sin\theta}{r}\zeta_k + \frac{\cos\theta}{r}v_k + \frac{2(1+\mu)}{Ehr}\left(S_k^*\cdot r\right),$$

$$\frac{d\vartheta_{1k}}{ds} = -\mu k^2\frac{\sin\theta}{r^2}\xi_k + \mu k^2\frac{\cos\theta}{r^2}\zeta_k - \mu k\frac{\sin\theta}{r^2}v_k - \mu\frac{\cos\theta}{r}\vartheta_{1k} + \\ + \frac{12(1-\mu^2)}{Eh^3 r}\left(M_{1k}\cdot r\right),$$

$$\frac{d\left(X_k\cdot r\right)}{ds} = \frac{Eh}{r}\left(1 + \frac{h^2k^4}{12r^2}\sin^2\theta\right)\xi_k - \frac{Eh^3}{12}\cdot\frac{k^4\sin\theta\cdot\cos\theta}{r^3}\zeta_k +$$

$$+\frac{Ehk}{r}\left(1+\frac{h^2k^2}{12r^2}\sin^2\theta\right)v_k+\frac{Eh^3k^2}{12}\cdot\frac{\sin\theta\cdot\cos\theta}{r^2}\vartheta_{1k}+\mu\frac{\cos\theta}{r}\left(X_k\cdot r\right)+$$

$$+\mu\frac{\sin\theta}{r}\left(Z_k\cdot r\right)-k\frac{\cos\theta}{r}\left(S_k^*\cdot r\right)+\mu k^2\frac{\sin\theta}{r^2}\left(M_{1k}\cdot r\right)-rq_{xk},$$

$$\frac{d\left(Z_k\cdot r\right)}{ds}=-k^4\frac{Eh^3}{12}\cdot\frac{\sin\theta\cdot\cos\theta}{r^3}\xi_k+\frac{Eh^3}{12r^3}\left(\frac{2k^2}{1+\mu}+k^4\cos^2\theta\right)\zeta_k-$$

$$-\frac{Eh^3k^3}{12}\cdot\frac{\sin\theta\cdot\cos\theta}{r^3}v_k-\frac{Eh^3k^2}{12}\cdot\frac{2+(1+\mu)\cos^2\theta}{(1+\mu)r^2}\vartheta_{1k}-k\frac{\sin\theta}{r}\left(S_k^*\cdot r\right)-$$

$$-\mu k^2\frac{\cos\theta}{r^2}\left(M_{1k}\cdot r\right)-rq_{zk},$$

$$\frac{d\left(S_k^*\cdot r\right)}{ds}=\frac{Ehk}{r}\left(1+\frac{h^2k^2}{12r^2}\sin^2\theta\right)\xi_k-\frac{Eh^3k^3}{12}\cdot\frac{\sin\theta\cdot\cos\theta}{r^3}\zeta_k+$$

$$+\frac{Ehk^2}{r}v_k+\frac{Eh^3k}{12r^2}\cdot\sin\theta\cdot\cos\theta\cdot\vartheta_{1k}+\mu k\frac{\cos\theta}{r}\left(X_k r\right)+$$

$$+\mu\frac{k\sin\theta}{r}(Z_k\cdot r)-\frac{\cos\theta}{r}\left(S_k\cdot r\right)+\mu\frac{k\sin\theta}{r^2}\left(M_{1k}\cdot r\right)-rq_{2k},$$

$$\frac{d\left(M_{1k}\cdot r\right)}{ds}=\frac{Eh^3k^2}{12}\cdot\frac{\sin\theta\cdot\cos\theta}{r^2}\xi_k-\frac{Eh^3k^2}{12}\frac{2+(1+\mu)\cos^2\theta}{(1+\mu)r^2}\zeta_k+$$

$$+\frac{Eh^3k}{12}\cdot\frac{\sin\theta\cdot\cos\theta}{r^2}v_k+\frac{Eh^3}{12r}\left(\cos^2\theta+\frac{2k^2}{1+\mu}\right)\vartheta_{1k}+ \qquad (6)$$

$$+\sin\theta\left(X_k r\right)-\cos\theta\left(Z_k r\right)-\mu\frac{\cos\theta}{r}\left(M_{1k}\cdot r\right).$$

where for the radial and axial components of the loading such designations are introduced:

$$q_{xk}=q_{1k}\cos\theta+q_{3k}\sin\theta;\qquad q_{zk}=q_{1k}\sin\theta-q_{3k}\cos\theta. \qquad (7)$$

Since the coefficients of the obtained system of equations do not contain the curvature of the meridian $1/R_1$, they remain continuous even for a shell whose curvature is discontinuous. As a result, the main unknowns assigned to the fixed coordinate system remain continuous with an arbitrary meridian shape, including for composite shells, which allows us not to compose docking equations for such cases. As for power unknowns, $X_k r, Z_k r, S_k^* r, M_{1k} r$ experience discontinuities of a previously known magnitude only where concentrated efforts are applied to the shells on a specific parallel of the load.

For arbitrary k, the system of equations (6) is of the eighth order. For $k=0$ the system breaks down into two: a system that describes axisymmetric

torsion, and a system that describes axisymmetric bending of the shell. System order can also be reduced in case of wind load ($k=1$). For the case $\theta=0$ (6) also splits into two systems of four equations, which describe, respectively, asymmetric transverse bending and tensile tension in its plane of an annular plate along the radius of thickness.

It is convenient to represent the resulting closed-loop system (6) of linear differential equations in matrix form:

$$\frac{d\overline{Y}_k}{ds}=\overline{A}_k\overline{Y}_k+\overline{B}_k, \tag{8}$$

where the components of the state vector $\overline{Y}_k=\{y_{ik}\}$ for the shells are quantities ξ_k, ζ_k, v_k, ϑ_{1k}, $X_k r$, $Z_k r$, $S_k^* r$, $M_{1k} r$, and matrix elements $\overline{A}_k$ and column vector loads $\overline{B}_k$ – corresponding variable system coefficients (6).

When solving specific problems, the system of equations of state (6) is supplemented by an appropriate number of boundary conditions characterizing the method of fixing the shell contour at the start s_0 and end s_L points:

$$\overline{F}\left(\overline{Y}(s_p)\right)=0, \quad (s_p=s_0\vee s_L). \tag{9}$$

Expanding the elements of matrix $\overline{F}$ (9) in Fourier series, we can obtain the corresponding boundary conditions for all harmonics. For asymmetric loading of shells, system (6) consists of $8k$ equations, and for round (ring) plates, it consists of $4k$ equations. The solution of problems (8), (9) is carried out by the sweep method with orthogonalization according to S. K. Godunov [17].

Thus, the problem of calculating shells of rotation of a variable along the stiffness meridian under asymmetric loading reduces to solving a set of boundary value problems for systems of ordinary differential equations (8) $(k=1, 2, ..., \infty)$ with respect to variables along the meridian of the coefficients of expansion of the main variables in Fourier series with boundary conditions (9).

2. An algorithm for predicting the values of expansion coefficients in trigonometric Fourier series

In this section, we propose a technique for reducing the number of one-dimensional boundary value problems (8), (9) necessary to achieve the given accuracy of solving the problem in the form (1) to determine the stress-strain state of shells of rotation of a variable along the meridian of the wall thickness.

It is known [16] that the approximation of a certain function $g(z)$, $z\in[-\pi,\pi]$ can be represented in the form of a trigonometric Fourier series:

$$g(z)\approx a_0/2+\sum_{k=1}^{m}\left(a_k\cos(kz)+b_k\sin(kz)\right), \tag{10}$$

where the coefficients a_0, a_k, b_k (the sequence of values of which converge with increasing harmonic numbers, not necessarily monotonously, to zero) are determined by the well-known Euler – Fourier formulas:

$$a_0 = \frac{1}{\pi}\int_{-\pi}^{\pi} g(z)dz, \quad a_k = \frac{1}{\pi}\int_{-\pi}^{\pi} g(z)\cos(kz)dz,$$

$$b_k = \frac{1}{\pi}\int_{-\pi}^{\pi} g(z)\sin(kz)dz, \quad k = 1,2,...,\infty. \qquad (11)$$

The idea of the proposed approach is to reduce the number of calculations of coefficients a_k, b_k in accordance with (11) by periodically extrapolating their values using the results of calculations of the previous coefficients of this series, thus replacing them with some forecast values calculated using simple formulas.

To construct such forecast values in optimization problems in [18], the simulation forecasting algorithm was used, one of the difficulties of its application was the need to determine the weight coefficients of the forecast formula using the results of a special numerical experiment, and interpolation with cubic splines when solving shell calculation problems in [19].

In this paper, to solve this problem, we propose the joint use of the Aitken – Steffensen extrapolation dependences [20] and in the form of an increment of the Adams method [7], which is quite effective in solving the Cauchy problem for systems of ordinary differential equations and is based on extrapolation dependences -compasses of Lagrange and Newton.

Let, as a result of three successive calculations of the coefficients of the Fourier series a_k, b_k (hereinafter, denoted $c_k = a_k \vee b_k$), we obtain the values c_{k-2}, c_{k-1}, c_k.

In this case, the following cases of sequences of changes in the coefficient values c_k depending on the number are possible k (Fig. 1).

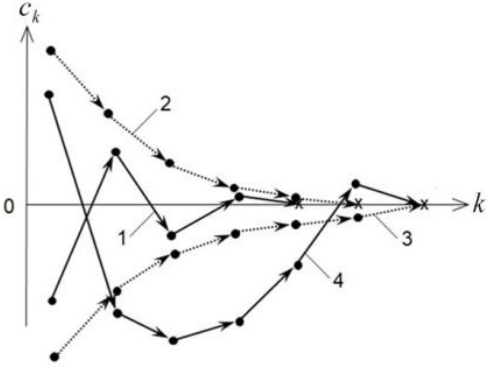

Fig. 1. Possible trajectories of changes in values Fourier series coefficients depending on the harmonic number

Here, line 1 corresponds to the case of a nonmonotonic sequence:

$$(c_{k-1}-c_{k-2})(c_k-c_{k-1})<0 \quad (12)$$

lines 2, 3 – respectively, monotonically decreasing and increasing sequences:

$$(c_{k-1}-c_{k-2})(c_k-c_{k-1})\geq 0 \quad (13)$$

line 4 – mixed.

The predicted values of the next member c_{k+1} of the sequence of these coefficients are determined by the results of the values of the three previous members of this series c_{k-2}, c_{k-1}, c_k, calculated using (11) depending on the type of iterative process. In the case

when the sequence c_k is nonmonotonic (12), the forecast is proposed to be carried out according to the Aitken – Steffensen formula [20]:

$$c_{k+1} = \frac{c_k c_{k-2} - (c_{k-1})^2}{c_{k-2} - 2c_{k-1} + c_k}, \quad k \geq 2, \tag{14}$$

and in the case of a monotonic process (13) – in the form of an increment in the second order Adams formula:

$$c_{k+1} = \frac{23c_k - 16c_{k-1} + 5c_{k-2}}{12}, \quad k \geq 2, \tag{15}$$

Further, using coefficients (11), c_{k+2}, c_{k+3} are calculated and the process of forecasting the next value c_{k+4} is continued taking into account three new points, starting from the forecast point.

Thus, this approach avoids the need to calculate the coefficients of the Fourier series at every third step.

3. Numerical results

The developed approach was tested for the case of acceleration of convergence of the iterative algorithm for solving physically nonlinear problems of the mechanics of shells of rotation in [7].

Here, the reliability of the proposed approach was verified using the results of a system numerical experiment by predicting the values of the expansion coefficients of Fourier series of known functions, typical sequences of which are shown in Fig. 1.

As an example in Fig. 2(a), a sequence of values of coefficients (11) for $k = \overline{0,20}$ is shown where «•» is the predicted values (14), (15) of the coefficients a_k of the function:

$$f(z) = \begin{cases} 1, & 0 \leq z \leq d, \quad d = \pi/10, \\ 0, & d < z \leq \pi, \end{cases}$$

the coefficients of the expansion of which in a Fourier series in cosines are: $a_0 = 2d/\pi$; $a_k = 2\sin(kd)/(k\pi)$; $k = \overline{1,\infty}$.

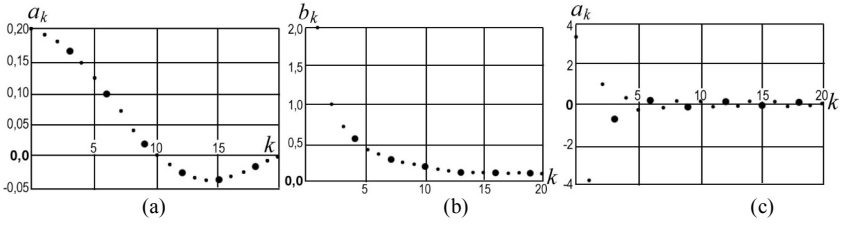

Fig. 2. The calculated (·) and forecast (•) values
the coefficients Fourier expansion of given functions

Fig. 2(b) shows a graph of the monotonically decreasing values of the calculated and predicted expansion coefficients in the Fourier series with

respect to the sines of the function $f(z)=\pi-z,\ \ z\in[0,2\pi]$, which have the form $b_k=2/k,\ \ k=\overline{1,\infty}$.

Changing the expansion coefficients in the Fourier series with respect to the cosines of a function $f(z)=z,\ z\in[-\pi,\pi]$, for which $a_0=\pi^2/3$; $a_k=(-1)^k\ 4/k^2,\ k=\overline{1,\infty}$ are given in Fig. 2(c).

The relative error in the calculation, for example, of the value of the function $f(z)=1$ (for $z=0$) (Fig. 2(a)) when using the first 20 harmonics of decomposition, of which 7 are determined by the forecast results, was 1,4%, and when using the exact values of the coefficients – 0,3%.

It should be noted that for higher harmonics, the relative error in the predictive determination of the values of the coefficients of the Fourier series can increase. However, taking into account that with increasing k the coefficients of the Fourier series decrease to zero, their contribution to the final value of the function decreases, which, on the whole, practically does not affect the accuracy of the solution to the problem. From the analysis of the results shown in Fig. 2, it follows that, if necessary, some of the Fourier coefficients can be determined approximately, that is, not by the usual way of calculating the integrals (11), but as a result of interpolation at some reference points.

It should be noted that the examples of forecasting the Fourier coefficients considered above to illustrate the main idea of the proposed approach do not have independent practical value, since the process of interpolating the coefficients for the considered functions of one variable requires no less computational costs than the usual method of obtaining the coefficients in the form (10), (11).

At the same time, this approach is very effective in problems of calculating asymmetrically loaded shells of revolution with a variable along the meridian thickness, when the Fourier coefficients (1) are functions of the longitudinal coordinate, and are calculated as a result of solving the boundary value problem (8), (9). In this case, the systems of differential equations (6) with respect to the amplitudes of expansion into trigonometric series are solved only for individual "reference" harmonics, and the amplitudes for each third harmonic are calculated as a result of interpolation of their values $(s_0\le s^*\le s_L)$ for all nodal integration points (8), (9). This can significantly reduce the computational cost of obtaining a solution as a whole.

The effectiveness of the approach is illustrated in Fig. 3(a) by the calculation of a thin elastic steel ring plate under the action of an asymmetric load:

$$q(r,\varphi)=\begin{cases} q(r), & -\pi/5\le\varphi\le\pi/5,\\ 0, & \varphi\notin[-\pi/5;\pi/5].\end{cases}$$

represented by its expansion in Fourier series in cosines:

$$q(r,\varphi) = q_0(r)/2 + \sum_{k=1}^{N} q_k(r)\cos(k\varphi), \qquad -\pi \le \varphi \le \pi .$$

The solution of the arising systems of ordinary differential equations (8), (9) with respect to the expansion coefficients was carried out by the method of sweeping with orthogonalization according to Godunov for various values of geometric parameters and options for fixing the contour. The dependence on the number k of the coefficients of the expansion of the radial deflection parameter $w_k E / q_k$ at the point $r = r_2$ in the Fourier series in cosines is shown in Fig. 3(b), and in Fig. 3(c) is the parameter $M_{1(k)}^{(k)} / q_k$ of the longitudinal moment at the point $r = r_1$ for the case of an annular plate (Fig. 3(a)) with a thickness $h = 0,05\,\text{m}$ with a clamped internal $r_1 = 0,2\,\text{m}$ and free external contour $r_2 = 1\,\text{m}$; $E = 200\,\text{GPa}$; $\mu = 0,3$.

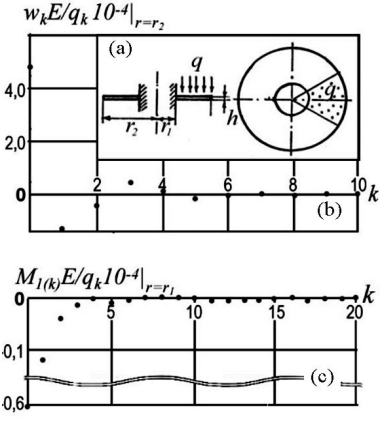

Fig. 3. The values of the expansion coefficients in the Fourier series of the deflection (b) and longitudinal moment (c) for the annular plate (a)

In this case, to compute the terms of the Fourier series $w_k(s)$, $M_{1k}(s)$, $(k = \overline{0,20})$, 14 solutions of the boundary value problems (8), (9) were needed without a noticeable loss of accuracy (about 0,07%) compared to using the Fourier coefficients obtained as a result of solving 21 such boundary value problems.

The computational efficiency of the proposed approach is most clearly manifested when it is used in problems of optimal design of structures [7], since multi-step iterative optimization algorithms provide for the solution of direct problems of calculating the stress-strain state of a structure at each search step, which leads to rather large computational costs.

Conclusions

Thus, the presented article proposes a fairly general and effective way to reduce the computational costs arising in the problems of calculating asymmetrically loaded elements of shell structures using the Fourier method by reducing the number of solutions to the corresponding one-dimensional boundary value problems. Such an approach can be useful in solving a fairly wide range of problems in the mechanics of shells, as well as the mechanics of liquid, gas, and plasma, and in other fields.

REFERENCES

1. *Biderman V. L.* Mechanics of thin-walled structures / V. L. Biderman. – Mashinostroenie. – Mosscow, 1977. – 488 p. (in Russian).
2. *Grigorenko Ya. M.* Methods for calculating shells. Theory of shells of variable rigidity. Vol. 4 / Ya. M. Grigorenko, A. T. Vasilenko. – Naukova Dunka, Kiev, 1981. – 544 p. (in Russian).
3. *Grigorenko A. Ya*. Stress-strain state of shallow rectangular shells of variable thickness under various boundary conditions / A. Ya Grigorenko, N. P Yaremchenko., C. N. Yaremchenko // Bul. of NAS Ukraine. – Vol. 6. – 2016. – P. 31-37 (in Ukrainian).
4. *Dzyuba A. P.* Calculation algorithm on the basis of a discrete-continuous approach for cylindrical shell of variable rigidity in circular direction / A. P. Dzyuba, I. A. Safronova, L. D. Levitina // Problems of computational mechanics and strength of structures, Collection of scientific articles. –Vol. 30. – 2019. – P. 53-67 (in Ukrainian).
5. *Myachenkov V. I.* Calculation of composite shell structures on a computer: Reference / V. I. Myachenkov I. V. Grigoryev. – Mashinostroenie. – Moscow, 1981. – 212 p. (in Russian).
6. *Sineva N. F.* Calculation of a cylindrical shell of variable stiffness interacting with a nonlinear elastic base / N. F. Sineva, F. S. Selivanov, D. V. Nikityuk // Bull. Saratov State Techn. Un-ty. Ser.: Construction and architecture. – Vol. 4(60). – Iss 2. – 2011. – P. 15-21 (in Russian).
7. Models and algorithms for optimization of elements of nonuniform shell structures, in N. V. Polyakov (Eds.) / A. P. Dzyuba, V. N. Sirenko, A. A. Dzyuba and I. A. Safronova // Actual problems of mechanics: Monograph, Lira, Dnipro, 2018. – P. 225-243 (in Ukrainian).
8. *Ovchinnikov I. G.* Thin-walled structures under conditions of corrosion wear: Calculation and optimization / I. G. Ovchinnikov, Yu. M. Pochtman. – DNU. – Dnepropetrovsk, 1995. – 190 p. (in Russian).
9. *Dashchenko A. F.* ANSYS in the problems of mechanical engineering: monograph. second ed. / A. F. Dashchenko, D. V. Lazareva, N. G. Suryaninov. – BURUN and K^0. – Kharkiv, 2011. – 504 p. (in Russian).
10. *Alyamovsky A. A.* SolidWorks/COSMOSWorks. Finite Element Engineering Analysis. / A. A. Alyamovsky. – DMK Press. – Moscow, 2004. 432 p. (in Russian).
11. *Grigorenko Ya. M.* Solving the problems of shell theory on a computer / Ya. M. Grigorenko, A. P. Mukoed. – High School. – Kiev, 1979. – 280 p. (in Russian).
12. *Mossakovsky V. I.* Contact Interactions of Elements of Shell Structures / V. I. Mossakovsky, V. S. Hudramovich, E. M. Makeev. – Naukova Dunka. – Kiev, 1988. – 288 p. (in Russian).
13. *Emel'yanov I. G.* Application of discrete Fourier series to the stress analysis of shell structures / I. G. Emel'yanov // Computational Continuum Mechanics. – Vol 8(3). – 2015. – P. 245-253. (in Russian).
14. *Hudramovich V. S.* Contact interaction and optimization of locally loaded shell structures / V. S. Hudramovich, A. P. Dzyuba // Journal of mathematical Science - Springer Science + Business media. – 2009. – P. 231-245.
15. Strength. Sustainability. Fluctuations: Handbook, vol.1. / (Eds.) I. A. Birger, Ya. G. Panovko. – Mashinostroenie. – Moscow, 1968. – 821 p. (in Russian).
16. *Tolstov G. P.* Fourier Series / G. P. Tolstov. – Fizmatgiz. – Moscow, 1960. – 392 p. (in Russian).
17. *Godunov S. K.* On the numerical solution of boundary value problems for systems of linear ordinary differential equations / S. K. Godunov // Advances in Mathematical Sciences. – Vol. 16. – Iss.3 (99). –1961. – P. 171-174 (in Russian).
18. *Bulakajev P. I.* An algorithm for the prediction of search trajectory in nonlinear programming problems optimum design / P. I. Bulakajev, A. P. Dzjuba // Structural Optimization: Research Journal of Intern. Society of Struct. and Multidisciplinary Optimiz. – Springer – Verlag. –Vol. 13(2, 3). – 1997. –P. 199-202.
19. *Dzyuba A. P.* An algorithm for reducing the computational cost of using the Fourier method in the problems of shell structural mechanics / A. P. Dzyuba, O. O. Bobilev, P. I. Bulakaev // Bull. of Dnepropetrovsk state university. Vol. 2(2). – 1999. – P. 47-57 (in Russian).
20. *Shamansky V. E.* Methods of numerical solution of boundary value problems on a computer / V. E. Shamansky. – Academia Science USSR. – Kiev. – Part. 1, 1963. – 196 p. – Part. 2, 1966. – 242 p. (in Russian).

Стаття надійшла 23.07.2020

Дзюба А.П., Сафронова І.А., Левитіна Л.Д.

АЛГОРИТМ ЗМЕНШЕННЯ ОБЧИСЛЮВАЛЬНИХ ВИТРАТ В ЗАДАЧАХ РОЗРАХУНКУ НЕСИМЕТРИЧНО НАВАНТАЖЕНИХ ОБОЛОНОК ОБЕРТАННЯ

Задача розрахунку оболонок обертання змінної уздовж меридіана жорсткості при несиметричному навантаженні зводиться до сукупності систем одновимірних крайових задач щодо амплітуд розкладання шуканих функцій в тригонометричні ряди Фур'є.

Пропонується методика зменшення кількості одновимірних крайових задач, необхідних для досягнення заданої точності визначення напружено-деформованого стану оболонок обертання зі змінною уздовж меридіана товщиною стінки при несиметричному навантаженні. Ідея запропонованого підходу полягає в застосуванні періодичного екстраполювання (прогнозування) значень коефіцієнтів розкладання шуканих функцій з використанням результатів обчислень попередніх коефіцієнтів відповідного тригонометричного ряду, замінюючи їх, таким чином, деякими прогноз-значеннями, обчисленими за простими формулами.

Для вирішення цієї задачі пропонується сумісне використання екстраполяційних залежностей Ейткена – Стеффенса і в формі складової приросту в методі Адамса, який є досить ефективним при розв’язанні задачі Коші для систем звичайних диференціальних рівнянь і базується на екстраполяційних залежностях Лагранжа і Ньютона.

Перевірка достовірності запропонованого підходу здійснювалася за результатами системного числового експерименту шляхом прогнозування значень коефіцієнтів розкладень в ряди Фур'є відомих функцій однієї змінної.

Підхід виявляється досить ефективним в задачах розрахунку несиметрично навантажених оболонок обертання зі змінною вздовж меридіана товщиною, коли коефіцієнти розкладання шуканих функцій в ряди Фур'є є функціями поздовжньої координати і обчислюються в результаті розв’язання відповідної крайової задачі. В цьому випадку підхід дозволяє вирішувати системи диференціальних рівнянь щодо амплітуд розкладання в тригонометричні ряди тільки для окремих «опорних» гармонік, а амплітуди для кожної третьої гармоніки можуть бути обчислені в результаті інтерполяції їх значень для всіх вузлових точок інтегрування відповідної крайової задачі. Це дозволяє істотно скоротити обчислювальні витрати на отримання розв’язку в цілому.

Як приклад наведено результати розрахунку напружено-деформованого стану сталевої кільцевої пластини при несиметричному поперечному навантаженні.

Ключові слова: оболонки обертання, змінна жорсткість; несиметричне навантаження, прогнозування коефіцієнтів в методі Фур'є; зниження обчислювальних витрат.

Dzyuba A. P.,Safronova I. A., Levitina L. D.

ALGORITHM FOR REDUCING THE CALCULATIONAL COSTS IN THE PROBLEM OF CALCULATION ASYMMETRIC LOADING ROTATION SHELLS

The problem of calculating the shells of rotation of a variable along the meridian of rigidity under asymmetric loading is reduced o a set of systems of one-dimensional boundary value problems with respect to the amplitudes of decomposition of the required functions into trigonometric Fourier series.

A method for reducing the number of one-dimensional boundary value problems required to achieve a given accuracy in determining the stress-strain state of the shells of rotation with a variable along the meridian wall thickness under asymmetric load. The idea of the proposed approach is to apply periodic extrapolation (prediction) of the values of the decomposition coefficients of the required functions using the results of calculations of previous coefficients of the corresponding trigonometric series, thus replacing them with some prediction values calculated by simple formulas.

To solve this problem, we propose the joint use of Aitken-Steffens extrapolation dependences and Adams method in the form of incremental component, which is quite effective in solving the Cauchy problem for systems of ordinary differential equations and is based on Lagrange and Newton extrapolation dependences.

The validity of the proposed approach was verified b the results of a systematic numerical experiment by predicting the values of the expansion coefficients in the Fourier series of known functions of one variable.

The approach is quite effective in the calculation of asymmetrically loaded shells of rotation with variable along the meridian thickness, when the coefficients of decomposition of the required functions into Fourier series are functions of the longitudina lcoordinate and are calculated by solving the corresponding boundary value problem. In this case, the approach allows solving

solutions of differential equations for the amplitudes of decompositionin to trigonometric series only for individual "reference" harmonics, and the amplitudes for every third harmonic can be calculated by interpolating their values for all node integration points of the corresponding boundary value problem. This significantly reduces the computational cost of obtaining the solution as a whole.

As an example, the results of the calculation of the stress-strain state of a steel annular plate under asymmetric transverse loading are given.

Keywords: rotation shells**,** variable stiffness, asymmetric loading, coefficient prediction in the Fourier method, reduction in computing costs.

Дзюба А.П., Сафронова И.А., Левитина Л.Д.

АЛГОРИТМ СНИЖЕНИЯ ВЫЧИСЛИТЕЛЬНЫХ ЗАТРАТ В ЗАДАЧАХ РАСЧЕТА НЕСИММЕТРИЧНО НАГРУЖЕННЫХ ОБОЛОЧЕК ВРАЩЕНИЯ

Задача расчета оболочек вращения переменной вдоль меридиана жесткости при несимметричном нагружении сводится к совокупности систем одномерных краевых задач относительно амплитуд разложения искомых функций в тригонометрические ряды Фурье. Предложен подход, основанный на прогнозировании значений переменных вдоль меридиана коэффициентов разложений для сокращения необходимого количества решений таких одномерных задач. Это позволяет снизить вычислительные затраты на поиск решения. В качестве примера приведены результаты расчёта напряженно-деформированного состояния стальной кольцевой пластины при несимметричном поперечном нагружении.

Ключевые слова: оболочки вращения, переменная жесткость, несимметричное нагружение, прогнозирования коэффициентов в методе Фурье; снижение вычислительных затрат.

УДК 539.3
Дзюба А.П., Сафронова І.А., Левитіна Л.Д. **Алгоритм зменшення обчислювальних витрат в задачах розрахунку несиметрично навантажених оболонок обертання** // Опір матеріалів і теорія споруд: наук.-тех. збірн. – К.: КНУБА, 2020. – Вип. 105. – С. 99-113. – Англ.

Запропоновано алгоритм прогнозування значень змінних уздовж меридіана коефіцієнтів розкладання в ряди Фур'є для зниження обчислювальних витрат в задачах розрахунку несиметрично навантажених оболонок обертання змінної жорсткості.
Іл. 3. Бібліогр. 20 назв.

UDC 539.3
Dzyuba A. P., Safronova I. A., Levitina L. D. **Algorithm for reducing computational costs in problems of calculation of asymmetrically loaded shells of rotation** // Strength of Materials and Theory of Structures: Scientific-and-technical collected articles. – K.: KNUBA, 2020. – Issue 105. – P. 99-113.

An algorithm for predicting the values of variables along the meridian of decomposition coefficients into Fourier series to reduce computational costs in the calculation of asymmetrically loaded shells of rotation of variable stiffness is proposed.
Figs. 3. Refs. 20.

УДК 539.3
Дзюба А.П., Сафронова И.А., Левитина Л.Д. **Алгоритм снижения вычислительных затрат в задачах расчета несимметрично нагруженных оболочек вращения** // Сопротивление материалов и теория сооружений: науч.-техн. сборник. – К.: КНУБА, 2020. – Вып. 105. – С. 99-113. – Англ.

Предложен алгоритм прогнозирования значений переменных вдоль меридиана коэффициентов разложения в ряды Фурье для снижения вычислительных затрат в задачах расчета несимметрично нагруженных оболочек вращения переменной жесткости.
Ил. 3. Библиогр. 20 назв.

Автор (вчена ступень, вчене звання, посада): доктор технічних наук, професор, професор кафедри теоретичної та комп'ютерної механіки ДЗЮБА Анатолій Петрович
Адреса робоча: 49010 Україна, м. Дніпро, проспект Гагаріна, 72, Дніпровський Національний університет імені Олеся Гончара.
Робочий тел.: +38(056) 745-00-85.
мобільний тел.: +38(095)349-38-78
Імейл: dzb@ua.fm
ORCID ID: http://orcid.org/0000-0001-6331-7783

Автор (вчена ступень, вчене звання, посада): старший викладач кафедри комп'ютерних технологій САФРОНОВА Інга Анатоліївна
Адреса робоча: 49010 Україна, м. Дніпро, проспект Гагаріна 72, Дніпровський Національний університет імені Олеся Гончара.
Робочий тел.: +38(0562) 46-10-47.
мобільний тел.: +38(067)695-95-95
Імейл: safronovainga12@gmail.com
ORCID ID: http://orcid.org/0000-0003-0242-3798

Автор (вчена ступень, вчене звання, посада): завідувач навчальної лабораторії обчислювальної механіки і міцності конструкцій кафедри теоретичної та комп'ютерної механіки ЛЕВИТІНА Лариса Данилівна
Адреса робоча: 49010 Україна, м. Дніпро, проспект Гагаріна 72, Дніпровський Національний університет імені Олеся Гончара.
Робочий тел.: +38(056) 745-00-85.
мобільний тел.: +38(097)553-13-54
Імейл: ldlora@i.ua

UDK 624.014

TALL VON-MISES TRUSSES' SKEW-SYMMETRIC DEFORMATION

S.I. Bilyk,
Doctor of Technical Science, Professor

H.M. Tonkacheiev,
Doctor of Technical Science, Professor

A.S. Bilyk,
Candidate of Engineering Science, Associate Professor

V.H. Tonkacheiev,
Candidate of Engineering Science, Associate Professor

Kyiv National University of Construction and Architecture
Povitroflotskyj av., 31, Kyiv, 030370

DOI: 10.32347/2410-2547.2020.105.114-126

The work's aim is to investigate the tall two-rods three-hinged von-Mises trusses' deformation regularities at the sloped load that applied to the ridge joint.The horizontal elastic support influence in the ridge joint when changing the force's inclination angle in a wide range is also investigated Particular attention is paid to the tall two-rod trusses' skew-symmetric stability loss possibility. The possibility of the skew-symmetric shape of a loss of stability of high trusses with at a very small angle of inclination of the force from the vertical axis was confirmed. The horizontal elastic support's influence on increasing the stability against skew-symmetric deformation was shown.It was found that skew-symmetry deformation is essentially non-linear, but under certain conditions it is not catastrophic.It is also noticed that asymmetric deformation depends on vertical deformation.Scientific novelty lies in a detailed study of the tall two-rod three-hinged trusses' deformation, and the establishment of the tendency of such structures to skew-symmetric buckling.The tall von-Mises trusses' new detailed deformation regularities character at skew-symmetric deformation at small inclination angles of force that applied in the ridge joint has been established. Also, the two-rod structures' new deformation regularities has been revealed with a wide inclination angles range of the concentrated force applied in the ridge joint. It is shown that on increasing the loading's inclination angles, which coincide with the rod's inclination angles , the stability loss of the individual rods is possible, since there is a significant increase in the truss' carrying capacity. The research results can be used in the structure design of large general dimensions, modeling of which gives the real structure work under various loads.

Keywords: buckling; skew-symmetric deformation; tall von-Mises truss; horizontl elastic supports; sloped load; three-hinged truss; ridge joint.

1. Introduction. Topicality. Simple structural systems, which contain two three or four tall support legs, are in use in special metal constructions. The structures with two legs additionally could be fixed by the cable-stayed system. There are not enough researches, which consists to the deformation patterns of such systems in the literature. The behavior of such systems on reach maximum carrying capacity could be non-linear by the character. It is important because the support legs' dimensions could reach 10-50 m for such structures as Ferris wheels and other attractions, bridge and overpass supports

[1]. The design scheme of such systems is hinge-connected: support legs are hinged to the base and hinge-connected in the ridge. (Fig. 1).

Thus, there are a number of tasks of the tall elastic three-hinged systems stress-strain state.

Historically, the elastic shallow von-Mises trusses' stability loss of has captured the researchers attention primarily by nonlinear snapping-through collapsing processes [25, 26]. Subsequently, such effects as snapping-through and nonlinear deformation were found as a thin-walled shells' stability loss characteristic sign [1, 2, 3, 4, 20], various structural systems' nonlinear deformation's aspects, including the stability loss, are described in [5, 11, 14, 22, 23]. The efficiency of using spatial rod systems is due to construction volume approximation's possibility to the functional one on well-known criterion [6]. Therefore, the stability problems study of rod spatial domes and shells, frame systems with constant and variable cross-section is aimed at creating economic structural systems [7, 8, 9, 10, 11, 22]. The revealed aspects of calopstic nonlinear deformation of systems found a new direction for complex systems under the influence of destructive loads [12].

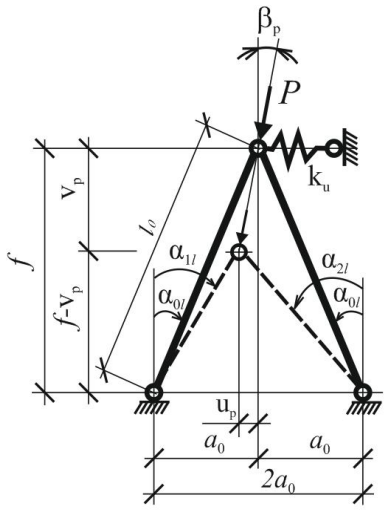

Fig. 1. The tall three-hinged system's design scheme

In general, the three-hinged systems, which type is shown at Fig. 1, could be assigned name the tall von-Mises trusses (Mises R. (Richard Edler von Mises) [10, 15, 25, 26].

In recent years, interesting new studies [10, 13, 15, 16-19, 21, 22, 24] have been devoted to the rod systems' like von-Mises trusses nonlinear deformation study. But the tall trusses' systems at a sloped loading demand additional research. Particular attention should be paid to the tall two-rod systems' tendency to skew-symmetric deformation and stability loss with skew-symmetric shape [10, 13, 15, 16-19, 21, 22, 27]. In specified works, the von-Mises shallow trusses studies' overview under various conditions of fixing and loading is provided.

In studies [17, 19, 27], it is shown that tall three-hinged trusses have a nonlinear deformation character under asymmetric load, and, accordingly, are subject to the skew-symmetric buckling. But more detailed von-Mises trusses' studies on the tendency to manifest skew-symmetric stability loss have not been carried out enough.

2. The work aim is to investigate the influence of the horizontal elastic support and inclined loading in the truss ridge joint to the tall von-Mises trusses deformational state.

3. Research. The tall three-hinged truss deformational scheme was reviewed (Fig. 1) under applying the loading force P with an angle β_P in the ridge joint. To investigate the tall three-hinged truss deformational state the classic, static and energetic approaches used [3, 6]. In these researches, the structure stress-strain is determining through the trusses deformational calculations taking into account the rods reduction and potential energy change.

The three-hinged tall truss, which consists of two rods with a length l_0 was considered (Fig. 1). The truss has a span $2*a_0$ and height of structure f. The support's leg inclination angle out of the vertical axis is α_{0l}. The horizontal support rigidity characteristic marked as k_u.

After loading the considered system by force P inclined with an angle β_P at the structure's top joint there will be rods compression with their length reduction: $\Delta l_{01} = l_0 - l_1$; $\Delta l_{02} = l_0 - l_2$. At the deformation state, the rods length will have the values l_1 and l_2. The relative deformations of each inclined rack will be:

$$\varepsilon_1 = \Delta l_{01} / l_0 = 1 - l_1 / l_0, \quad (1.a)$$

$$\varepsilon_2 = \Delta l_{02} / l_0 = 1 - l_2 / l_0. \quad (1.b)$$

The forces in the rods due to force balance in the joint:

$$P\sin\beta_P - u_P k_u = N_1 \sin(\alpha_{1l}) - N_2 \sin(\alpha_{2l}),$$
$$P\cos\beta_P = N_1 \cos(\alpha_{1l}) + N_2 \cos(\alpha_{2l}). \quad (2)$$

The relations between the three-hinged truss' dimensions and the topjoint's displacements could be written as:

$$\begin{gathered} \mathrm{tg}\alpha_{0l} = \frac{a_0}{f} \to f = \frac{a_0}{tg\alpha_{0l}}; u_p = v_p \mathrm{tg}\beta_P, \\ a_0 - u_P = a_0\left(1 - \frac{u_P}{a_0}\right); a_0 - u_P = a_0\left(1 - \frac{v_P}{a_0}\mathrm{tg}\beta_P\right), \\ a_0 + u_P = a_0\left(1 + \frac{u_P}{a_0}\right); a_0 + u_P = a_0\left(1 + \frac{v_P}{a_0}\mathrm{tg}\beta_P\right), \\ (f - v_P) = \left(\frac{a_0}{\mathrm{tg}\alpha_{0l}} - v_P\right) = a_0\left(\frac{1}{\mathrm{tg}\alpha_{0l}} - \frac{v_P}{a_0}\right). \end{gathered} \quad (3)$$

Geometrically the relation through the top-joint's displacements and structure's initial dimensions to the deformations links the rod's angles trigonometric functions after the deformations each to other.

$$\sin(\alpha_{1l}) = \frac{a_0 - u_P}{\sqrt{(a_0 - u_P)^2 + (f - v_P)^2}},$$
$$\cos(\alpha_{1l}) = \frac{f - v_P}{\sqrt{(a_0 - u_P)^2 + (f - v_P)^2}}, \quad (4)$$

$$\cos(\alpha_{2l}) = \frac{f - v_P}{\sqrt{(a_0 + u_P)^2 + (f - v_P)^2}},$$
$$\sin(\alpha_{2l}) = \frac{a_0 + u_P}{\sqrt{(a_0 + u_P)^2 + (f - v_P)^2}}. \quad (5)$$

From the equations (3…5) the truss deformational state consists of the deformations continuity equation trough the equal vertical displacements at the top joint with the inclined loading.

$$f - v_P = l_{1l}\cos(\alpha_{1l}) = l_{2l}\cos(\alpha_{2l});$$
$$2a_0 = l_{1l}\sin(\alpha_{1l}) + l_{2l}\sin(\alpha_{2l}). \quad (6)$$

The rod's relative deformations is (Fig. 1):

$$\boldsymbol{\varepsilon_1 = 1 - \left(1 - \frac{v_P}{a_0}\mathrm{tg}\beta_p\right)\frac{\sin(\alpha_{0l})}{\sin(\alpha_{1l})}},$$
$$\varepsilon_2 = 1 - \left(1 + \frac{v_P}{a_0}\mathrm{tg}\beta_P\right)\frac{\sin(\alpha_{0l})}{\sin(\alpha_{2l})}. \quad (7)$$

The rod's compressive internal forces at the deformational state with the inclined loading is:

$$\boldsymbol{N_1 = \varepsilon_1 EA_{cal}; \rightarrow N_1 = \left[1 - \left(1 - \frac{v_P}{a_0}\mathrm{tg}\beta_P\right)\frac{\sin(\alpha_{0l})}{\sin(\alpha_{1l})}\right] EA_{cal}},$$
$$N_2 = \varepsilon_2 EA_{cal}; \rightarrow N_2 = \left[1 - \left(1 + \frac{v_P}{a_0}\mathrm{tg}\beta_P\right)\frac{\sin(\alpha_{0l})}{\sin(\alpha_{2l})}\right] EA_{cal}. \quad (8)$$

The external forces balance with the elastic support's internal forces ($r_u = -u_p k_u$) gives an equation:

$$P\sin\beta_P - u_P k_u = N_1\sin(\alpha_{1l}) - N_2\sin(\alpha_{2l}),$$
$$P\cos\beta_P = N_1\cos(\alpha_{1l}) + N_2\cos(\alpha_{2l}). \quad (9)$$

Combining the ratios (3 ... 8) with equation 9 gives the criterion for von-Mises truss' operation at an inclined load and the horizontal elastic support in the top joint.

$$\frac{P\cos\beta_P}{EA_{cal}} =$$
$$= \frac{\frac{1}{\mathrm{tg}\alpha_{0l}} - \frac{v_P}{a_0}}{\sqrt{\left(1 - \frac{v_P}{a_0}\mathrm{tg}\beta_P\right)^2 + \left(\frac{1}{\mathrm{tg}\alpha_{0l}} - \frac{v_P}{a_0}\right)^2}} + \frac{\frac{1}{\mathrm{tg}\alpha_{0l}} - \frac{v_P}{a_0}}{\sqrt{\left(1 + \frac{v_P}{a_0}\mathrm{tg}\beta_P\right)^2 + \left(\frac{1}{\mathrm{tg}\alpha_{0l}} - \frac{v_P}{a_0}\right)^2}} -$$
$$- 2\sin(\alpha_{0l}),$$

$$\frac{P\sin\beta_P}{EA_{cal}} - \frac{u_P}{a_0}\frac{k_u a_0}{EA_{cal}} =$$
$$= \frac{1 - \frac{v_P}{a_0}\mathrm{tg}\beta_P}{\sqrt{\left(1 - \frac{v_P}{a_0}\mathrm{tg}\beta_P\right)^2 + \left(\frac{1}{\mathrm{tg}\alpha_{0l}} - \frac{v_P}{a_0}\right)^2}} - \frac{1 + \frac{v_P}{a_0}\mathrm{tg}\beta_P}{\sqrt{\left(1 + \frac{v_P}{a_0}\mathrm{tg}\beta_P\right)^2 + \left(\frac{1}{\mathrm{tg}\alpha_{0l}} - \frac{v_P}{a_0}\right)^2}} +$$
$$+ 2\frac{v_P}{a_0}\mathrm{tg}\beta_P\sin(\alpha_{0l}).$$

Finally:

$$\frac{P\cos\beta_P}{EA_{cal}} = \\ = \frac{1}{\sqrt{1+\frac{\left(1-\frac{v_P}{a_0}\mathrm{tg}\beta_P\right)^2}{\left(\frac{1}{\mathrm{tg}\alpha_{0l}}-\frac{v_P}{a_0}\right)^2}}} + \frac{1}{\sqrt{1+\frac{\left(1+\frac{v_P}{a_0}\mathrm{tg}\beta_P\right)^2}{\left(\frac{1}{\mathrm{tg}\alpha_{0l}}-\frac{v_P}{a_0}\right)^2}}} - 2\sin(\alpha_{0l}), \quad (10.a)$$

$$\frac{\boldsymbol{P\sin\beta_P - u_P k_u}}{\boldsymbol{EA_{cal}}} = \\ = \frac{\boldsymbol{1}}{\sqrt{\boldsymbol{1+\frac{\left(\frac{1}{\mathrm{tg}\alpha_{0l}}-\frac{v_P}{a_0}\right)^2}{\left(1-\frac{v_P}{a_0}\mathrm{tg}\beta_P\right)}}}} - \frac{\boldsymbol{1}}{\sqrt{\boldsymbol{1+\frac{\left(\frac{1}{\mathrm{tg}\alpha_{0l}}-\frac{v_P}{a_0}\right)^2}{\left(1+\frac{v_P}{a_0}\mathrm{tg}\beta_P\right)^2}}}} + \quad (10.b)$$

$$+ \boldsymbol{2\frac{v_P}{a_0}\mathrm{tg}\beta_P \sin(\alpha_{0l})}.$$

The equation (10.a) is a regularity that describes the truss' deformation in the vertical direction. Equation (10.a) is similar to the von-Mises truss' level of stability, which was obtained in [10]. The equation (10.b) is a regularity that describes the truss' deformation in the horizontal direction with the inclined loading taking into account the elastic support's horizontal reaction.

Equation (10.a) was well studied for sloped von-Mises trusses with the support racks' angle to the vertical axis $\alpha_{0l} \geq 70°$earlier at the scientific researches [10, 15].

Equation (10.a) will became to the well-known equation [] when force's angle is absent $\beta_P = 0$, $\cos\beta_P = 1$ (formula 11).

$$\frac{P}{EA_{cal}} = 2\left(\frac{1}{\mathrm{tg}\alpha_{0l}}-\frac{v_P}{a_0}\right)\left[\frac{1}{\sqrt{1+\left(\frac{1}{\mathrm{tg}\alpha_{0l}}-\frac{v_P}{a_0}\right)^2}} - \sin(\alpha_{0l})\right]. \quad (11)$$

4. The numerical studies results. The deformed state numerical researches of the tall three-hinged trusses with sloped load. The tall two-rod trusses' numerical studies with an inclined loading have done with support's rack sloping angle values from the vertical axis $15^o \leq \alpha_{0l} \geq 70^o$. The research aim is the tall von-Mises trusses tendency influence to nonlinear deformation under inclined load.

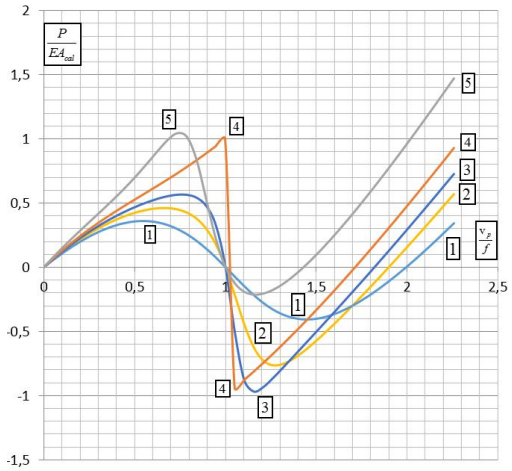

Fig. 2. The von-Mises trusses deformations numerical studies using an equation (10.a) with the relative vertical displacements v_P/f with $\alpha_{0l} = 35°$. Where: 1 - β_P=10°; 2 - β_P=25°; 3 - β_P=30°; 4 - β_P=35°; 5 - β_P=45°

The tall three-hinged truss structure' deformations (Fig. 2) corresponds to the low structures' deformation regularities at the angles of inclination of the support racks $\alpha_{0l} \geq 70°$. However, such deformation is possible only with significant deformations and absolutely elastic material. The maximum critical loading was determined with a top joint's serial vertical displacements. It is shown that an increasing the force P inclination angle β_P increases the critical loading value. But the deformation's character significantly changes if an angle value β_P is equals or bigger than support rack's angle from vertical $\beta_P \geq 35^o$.

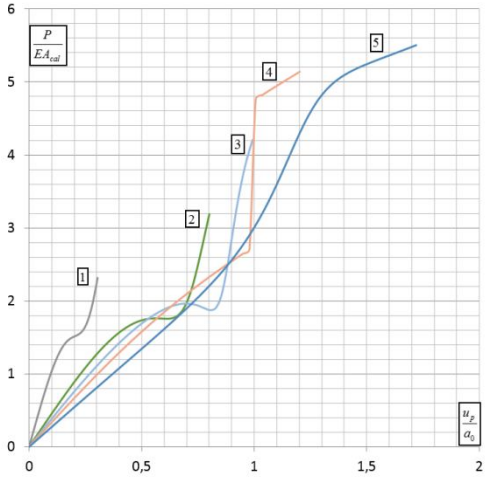

Fig. 3. The von-Mises truss numerical studies results using the equation (10.b) with the relative horizontal displacements v_P/f with $\alpha_{0l} = 35°$ (k_u =0). Where: 1 - β_P = 10°; 2 - β_P = 25°; 3 - β_P = 30°; 4 - β_P = 35°; 5 - β_P = 45°

The von-Mises truss deformation analysis using an equation (10.b) with the relative horizontal displacements v_P/f and $\alpha_{0l} = 35^{\circ}$ reveals the nonlinear local effects with big loading values, which are relative to reaching a structure a critical loading obtained with the equation (10.a).

1. Elastic horizontal support's impact to the structure deformation with an inclined loading. The Numerical studies of the horizontal elastic support's effect on the tall trusses' deformation were carried out (Fig. 4).

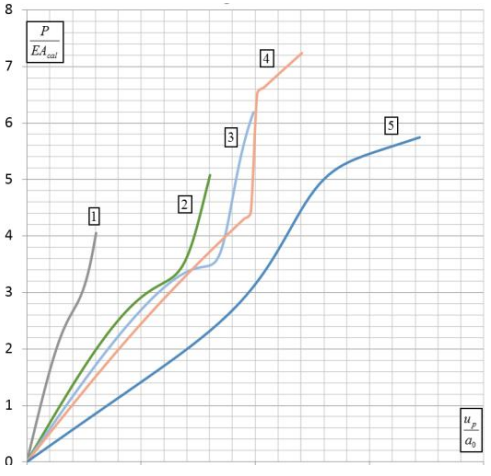

Fig. 4. The von-Mises truss' numerical studies results by equation (10.b) with the relative horizontal displacements v_P/f and α_{0l}=35°, and with relative horizontal elastic support's stiffness($(k_u a_0)/(EA_{cal})$=1,0). Where: 1 - β_P=10°; 2 - β_P=25°; 3 - β_P=30°; 4 - β_P=35°; 5 - β_P=45°

The tall trusses' strain-state analysis and comparison using an equation (10.b) without horizontal elastic support (Fig. 3, k_u =0 and with horizontal elastic support shows that horizontal elastic support (Fig. 4, ($k_u a_0$ =1,0)) ($k_u a_0$ - an elastic horizontal support relative stiffness) reduces the nonlinear effects influence and increases the structure's carrying capacity. The structure's deformation nature along the axis u_P/a_0 is determined by the structure's riged joint deformation along the axis, depending on the values (v_P/f).

It is noticed that the influence of the elastic horizontal support increases at $\beta_P \geq \alpha_{0l}$, comparison of graph 5 to graphs 2, 3, 4 in Fig. 3 and in Fig. 4.

2. An asymmetrical shape stability loss' possibility analysis under symmetrical load.

The skew-symmetric shape buckling possibility for the tall von-Mises trusses were investigated in works [10]. The tall von-Mises trusses' deformation with small vertical force's angles (Fig. 5) which is applied at the ridge joint by equation (10.b) and β_P=0,01° and with horizontal elastic support absense: k_u=0 is showing (Fig. 5). Based on the numerical studies results has built the dependencies' diagrams of the ridged force's projection on the

horizontal axis ($P\sin\beta_P$ with β_P=0,01°) to the relative horizontal displacements(u_P/a_0) with the angles' range from the vertical axis α_{0l}=15°… 33°. It has been confirmed that, at angle α_{0l}<22,637 °, the tall trusses are subject to a skew-symmetric stability loss (Fig. 5, diagrams 1, 2, 3). This effect manifests itself at the very beginning of loading and is not catastrophic, and is associated with deformation with the symmetrical load.

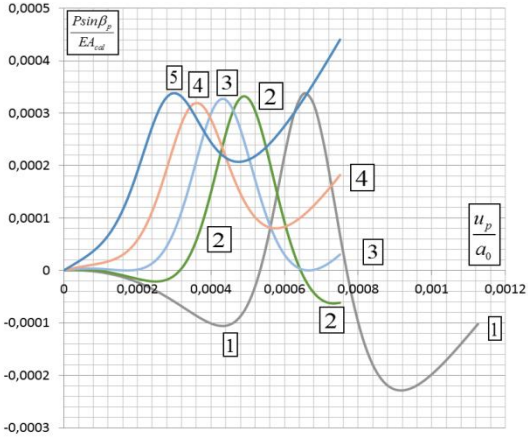

Fig. 5. The von-Mises truss' deformation numerical studies results by equation (10.b) with the relative horizontal displacements u_P/a_0 with β_P=0,01°, and with the relative horizontal elastic support's stiffnes (k_u=0).Where: 1 – α_{0l}=15°; 2- α_{0l}=20°; 3 - α_{0l}=22,637°; 4 - α_{0l}=27°; 5- α_{0l}=33°

An Influence of the horizontal elastic support that placed at the ridge joint to the skew-symmetric stability loss tendency was investigated (Fig. 6, 7, 8).

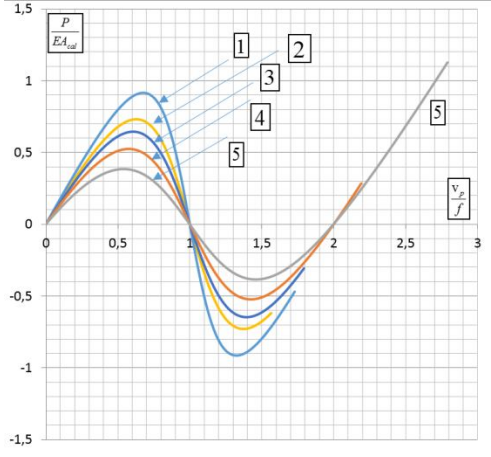

Fig. 6. The von-Mises truss' deformations numerical studies by the equation (10.a) with the vertical relative displacements v_P/f and with $((k_u a_0)/(EA_{cal})$=0,25), β_P=0,01°. Where:1 - α_{0l}=15 °; 2 - α_{0l} =20°; 3 - α_{0l}=22,637 °; 4 - α_{0l}=27°; 5- α_{0l}=33 °.

It has been confirmed that the horizontal elastic support has no effect on the truss' stability in the vertical direction (Fig. 1, Fig. 6). The skew-symmetric buckling study was carried out at a small load angle β_P =0,01° (β_P =0,00017) applied in the ridge joint. The results of such studies are presented in (Fig. 7, 8).

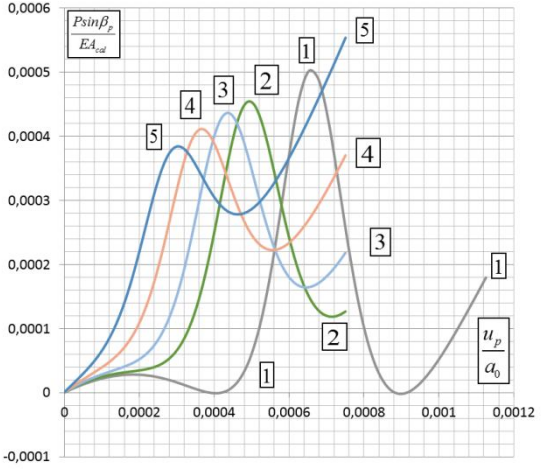

Fig. 7. The force's projection altereations numerical studies results $(P\sin\beta_P)/(EA_{cal})$ by the equation (10.b) with the horizontal relative displacements u_P/a_0 and β_P =0,01° and with the horizontal support's relative stiffnes $((k_u a_0)/(EA_{cal}) = 0{,}25)$. Where: 1 - α_{0l}=15°; 2 - α_{0l}=20°; 3 - α_{0l}=22,637°; 4 - α_{0l}=27°; 5- α_{0l}=33°

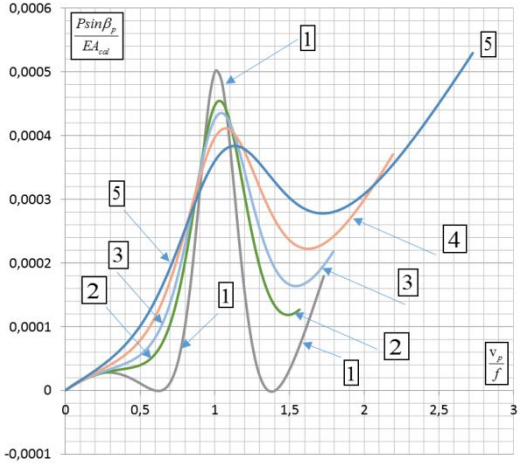

Fig. 8. The force's projection altereations numerical studies results $(P\sin\beta_P)/(EA_{cal})$ by the equation (10.b) with the vertical relative displacements v_P/f and β_P =0,01° and with the horizontal support's relative stiffnes $((k_u a_0)/(EA_{cal}) = 0{,}25)$. Where: 1 - α_{0l}=15°; 2 - α_{0l}=20°; 3 - α_{0l}=22,637°; 4 - α_{0l}=27°; 5 - α_{0l}=33°

Studies have confirmed (Fig. 5, 7, 8) that at small inclination angles the two-rod trusses could be subjected to a buckling with a skew-symmetric shape α_{0l}<22,637°, but with a horizontal elastic support the value of the critical angle from the vertical decreases. This behavior is observed at $\frac{k_u a_0}{EA_{cal}}$ =0.25 and with the angle values α_{0l}<15,0°.

5. Conclusions. Scientific novelty and practical significance. It is shown that for tall trusses a load inclination angles dohave avalue. Increasing an inclination angle the trusses' load capacity also increasing but it changes the deformation pattern. With force's inclination angle, approaching to racks angle ($\boldsymbol{\beta_P \rightarrow \alpha_{0l}}$) the stability loss will occur faster since reaching the critical loading (Fig. 2). It was shown that with an increasing the load's inclination angles, which coincide with the rods' inclination angles, the individual rods stability loss is possiblesince there is a significant increasing the truss carrying capacity (Fig. 2, 3, 4, diagrams 4, 5).

It was confirmed three-hinged trusses' deformation nonlinear nature. The horizontal support's stiffness reduces the skew-symmetric effects (Fig. 4, 6, 7, 8). The initial imperfections' influence on the tall trusses' nonlinear skew-symmetric deformations (Fig. 5, 7, 8) happens with the rod's angles from the vertical axis α_{0l}< 22,637°. However, it was shown that the horizontal elastic support's influence on increasing the stability from skew-symmetric deformations and corresponds to decreasing the truss' rod critical angle values from the vertical axis (Fig. 7, 8). It was found that skew-symmetric deformation has essentially nonlinear, but under certain conditions, it is not catastrophic.

It found that asymmetric deformations essentially depend on vertical deformations. The scientific novelty is laying on the tall two-rod three-hinged truss' detailed investigation and on such structures' skew-symmetric buckling tendency determination. The study resultsused for designing the large general dimensions structures which modeling gives us the structures real work under the different loads.

It is important to investigate refined models and the structures' buckling tendency when designing various structures with large overall dimensions in which testing cannot be fully performed but when their initial imperfections affect the structures' operation as a whole.

REFERENCES

1. *Bazhenov V.A.* Budivelna mekhanika i teoriia sporud. Narysy z istorii / *V.A.Bazhenov, Yu.V.Vorona, A.V.Perelmuter.* – K.: Karavela, 2016. – 428 s.
2. *Bazhenov V. A., Krivenko O. P., Solovei N. A.* Nonlinear Deformation and Buckling of Elastic Shells with Inhomogeneous Structure [in Ukrainian] – ZAT «Vipol», (Kyiv), 2010. – 316 p.
3. *Bazhenov V. A., Krivenko O.P., Solovei N. A.* Nonlinear Deformation and Buckling of Elastic Shells with Inhomogeneous Structure: Models, Methods, Algorithms, Poorly Studied and New Problems [in Russian]. – Book House "LIBRIKOM" (Moscow), 2013. – 336 p.
4. *Bazhenov V.A., Solovei N.A., Krivenko O.P.* Modeling of Nonlinear Deformation and Buckling of Elastic Inhomogeneous Shells // Strength of Materials and Theory of Structures:

Scientificand-technical collected articles – Kyiv: KNUBS. – Issue 92, pp. 121-147 (2014), [in Ukrainian]. http://opir.knuba.edu.ua/

5. *Ba˘zant Z.P., Cedolin L.* (2010) Stability of structures: Elastic, inelastic, fracture and damage theories World Scientific Publishing, Co. 1040 p. https://doi.org/10.1142/7828https://www.scholars.northwestern.edu/en/publications/stability-of-structures-elastic-inelastic-fracture-and-damage-the-4/
6. *Bilyk S. I.* Optimal form of the geometrical circuitry of the frame carcase with incline elements around functional cubature / Bilyk S. I. // Applied geometry and engineering graphics: Collection of scientific papers/ KNUBA. –K., 2004. – V. 74. – P. 228–235.
7. *Bilyk S. I.* Stability analysis of bisymmetrical tapered I-beams / S. I. Bilyk // Progress in Steel, Composite and Aluminium Structures Proceeding of the XI international conference on metal structures (ICMS–2006): Pzeszow, Poland, 21–23 June 2006-p. – Pzeszow, 2006. – C.254–255.
8. *Bilyk S.* Determination of critical load of elastic steel column based on experimental data // Pidvodni tekhnolohii. Promyslova ta tsyvilna inzheneriia. mizhnar. nauk.-vyrob. zhurn. K., KNUBA, Vyp.04/2016, S.89-96.http://repositary.knuba.edu.ua/handle/987654321/821
9. *Bilyk S.I., BilykA.S., Nilova T.O., Shpynda V.Z., Tsyupyn E.I.* Buckling of the steel frames with the I-shaped cross-section columns of variable web height // Strength of Materials and Theory of Structures: Scientific-and-technical collected articles – Kyiv: KNUBA, 2018. – Issue 100. – P. 140-154. library.knuba.edu.ua/books/zbirniki/12/201604.pdf.
10. *Bilyk Sergiy, Tonkacheiev Vitaliy*, Determining sloped-load limits inside von Mises truss with elastic support. Materiali in tehnologije., Ljubljana, Slovenija 52 (2018), 105-109, doi:10.17222/mit.2016.083 http://mit.imt.si/Revija/izvodi/mit182/bilyk.pdf .
11. *Błażejewski P., Marcinowski J., Rotter M.*Buckling of externally pressurised spherical shells. Experimental results compared with recent design recommendations/ EUROSTEEL 2017, September 13–15, 2017, Copenhagen, Denmark, Ernst & Sohn Verlag für Architektur und technische Wissenschaften GmbH & Co. KG, Berlin · ce/papers 1 (2017), No. 2 & 3, p.1010-1018. https://doi.org/10.1002/cepa.141
12. *Daurov M.K., Bilyk A.S.* Providing of the vitality of steel frames of high-rise buildings under action of fire // Strength of Materials and Theory of Structures: Scientific-and-technical collected articles – Kyiv: KNUBA, 2019. – Issue 102. – P. 62-68.
13. *Frantık P.* Simulation of the stability loss of the von Mises truss in an unsymmetrical stress state/ Engineering MECHANICS, Vol. 14, 2007, No. 1, p. 155–161 http://www.engineeringmechanics. cz/pdf/14_3_155.pdf
14. *Galambos V.,* Stability Design Criteria for Metal Structures. John Wiley and Sons, Ltd., 1998, p. 911.
15. *Greco Marcelo, Carlos Eduardo Rodrigues Vicente*, Analytical solutions for geometrically nonlinear trusses, Revista Escola de Minas, 62 (2009) 2, 205-214, doi:10.1590/S0370-44672009000200012
16. *Kala Z. Kalina M.* Static equilibrium states of von Mises trusses. INTERNATIONAL JOURNAL OF MECHANICS, volume 10, 2016, p. 294-298. https://www.researchgate.net/publication/305175165Kala, Zdenek & Kalina, Martin. (2016).
17. *Kala Z.* Stability of von-Misses truss with initial random imperfections.Modern Building Materials, Structures and Techniques, MBMST 2016. Procedia Engineering 172 (2017) p.473 – 480. https://pdf.sciencedirectassets.com/278653/
18. *Kalina, M.* "Static Task of von Mises Planar Truss Analyzed using Potential Energy," AIP Conference Proceedings, vol. 1558, 2013, pp. 2107-2110,.
19. *Kalina, M.* Stability Problems of Pyramidal von Mises Planar Trusses with Geometrical Imperfection. International Journal of Theoretical and Applied Mechanics, volume 1, 2016 p.118-123. https://www.iaras.org/iaras/filedownloads/ijtam/2016/009-0018.pdf
20. *Kaplan, A. & Fung, Y. C.* A nonlinear theory of bending and buckling of thin elastic shallow spherical shells. U.S. N.A.C.A. Technical Note 3112, 1954.
21. *Ligarò S.S., Valvo P.S.* Large Displacement Analysis of Elastic Pyramidal Trusses. International Journal of Solids and Structures, Vol.43, No.16, 2006, pp. 206-212. 43, pp. 4867-4887. https://www.researchgate.net/profile/Paolo_Valvo/publication/229292690.
22. *Marcinowski J.* Statecznosc konstrukcji sprezystych? Wroclaw, DWE, 2017, 278
23. *Makhinko A.V., Makhinko N.O.* Some aspects of vertical cylindrical shells' calculation at the

unsymmetrical load // Strength of materials and theory of structures: scientific-and-technical collected articles. – Kyiv: KNUBA, 2019. – Issue 102. – P. 46-52.
24. *Mikhlin Y. V.*: Nonlinear normal vibration modes and their applications, Proceedings of the 9th Brazilian Conference on Dynamics Control and their Applications Serra Negra, (**2010**), 151-171, http://www.sbmac.org.br/dincon/trabalhos/PDF/invited/68092.pdf, 23.11.2016
25. *R. V. Mises*, Über die Stabilitätsprobleme der Elastizitätstheorie, Z. angew. Math. Mech., 3 (1923), 406–422, doi:10.1002/zamm.19230030602 https://onlinelibrary.wiley.com/doi/abs/10.1002/zamm.19230030602.
26. *R. von Mises, J. Ratzersdorfer*, "Die Knicksicherheit von Fachwerken ZAMM 5, pp. 218-235, 1925/https://doi.org/10.1002/zamm.19250050305
27. *Feodosiev V.*, Theory of strength of materials chosen problems and questions, Moskow, Nauka, 1967, 376.

Стаття надійшла 19.07.2020

Білик С.І., Тонкачеєв Г.М., Білик А.С., Тонкачеєв В.Г.

КОСОСИМЕТРИЧНА ДЕФОРМАЦІЯ ВИСОКИХ ФЕРМ МИЗЕСА

Мета роботи - дослідити закономірності деформації високих двоштангових три шарнірних ферм фон-Мізеса при навантаженні з нахилом, що прикладається до конькового з'єднання. Також досліджується вплив горизонтальної пружної опори на конькове з'єднання при зміні кута нахилу сили в широкому діапазоні. Особливу увагу приділено можливості втрати симметричної стійкості високих дво ступінчастих ферм. Підтверджено можливість кососиметричної форми втрати стійкості високих ферм при дуже малому куті нахилу сили від вертикальної осі. Показано вплив горизонтальної пружної опори на підвищення стійкості проти кососиметричної деформації, встановлено, що кососиметртчна деформація по суті є нелінійною, але за певних умов вона не катастрофічна. Також зазначається, що асиметрична деформація залежить від вертикальної деформації. Наукова новизна полягає в детальному вивченні деформації високих двоштангових три шарнірних ферм та встановленні схильності таких конструкцій до кососиметричного вигину. Встановлено нові деталізовані закономірності деформації високих ферм фон Мізеса при кососиметричній деформації при малих кутах нахилу сили, що застосовується в коньковому з'єднанні. Також виявлено нові закономірності деформації двострижневих конструкцій із широким діапазоном кутів нахилу концентрованої сили, прикладеної в коньковому з'єднанні. Показано, що при збільшенні кутів нахилу навантаження, які збігаються з кутами нахилу стрижня, можлива втрата стійкості окремих стрижнів, оскільки відбувається значне збільшення несучої здатності ферми. Результати досліджень можуть бути використані при проектуванні конструкцій великих загальних розмірів, моделювання яких дає реальну роботу конструкції під різними навантаженнями.

Ключові слова: згин; кососиметрична деформація; висока ферма Мізеса; горизонтальна пружна опора; навантаження з нахилом; три шарнірна ферма; конькове з'єднання.

Bilyk S.I., Tonkacheiev H.M., Bilyk A.S., Tonkacheiev V.H.

TALL VON-MISES TRUSSES' SKEW-SYMMETRIC DEFORMATION

The work's aim is to investigate the tall two-rods three-hinged von-Mises trusses' deformation regularities at the sloped load that applied to the ridge joint.The horizontal elastic support influence in the ridge joint when changing the force's inclination angle in a wide range is also investigated Particular attention is paid to the tall two-rod trusses' skew-symmetric stability loss possibility. The possibility of the skew-symmetric shape of a loss of stability of high trusses with at a very small angle of inclination of the force from the vertical axis was confirmed. The horizontal elastic support's influence on increasing the stability against skew-symmetric deformation was shown.It was found that skew-symmetry deformation is essentially non-linear, but under certain conditions it is not catastrophic.It is also noticed that asymmetric deformation depends on vertical deformation.Scientific novelty lies in a detailed study of the tall two-rod three-hinged trusses' deformation, and the establishment of the tendency of such structures to skew-symmetric buckling.The tall von-Mises trusses' new detailed deformation regularities character at skew-symmetric deformation at small inclination angles of force that applied in the ridge joint has

been established. Also, the two-rod structures' new deformation regularities has been revealed with a wide inclination angles range of the concentrated force applied in the ridge joint. It is shown that on increasing the loading's inclination angles, which coincide with the rod's inclination angles, the stability loss of the individual rods is possible, since there is a significant increase in the truss' carrying capacity. The research results can be used in the structure design of large general dimensions, modeling of which gives the real structure work under various loads.

Keywords: buckling; skew-symmetric deformation; tall von-Mises truss; horizontl elastic supports; sloped load; three-hinged truss; ridge joint.

УДК 539.3
Білик С.І., Тонкачеєв Г.М., Білик А.С., Тонкачеєв В.Г. **Кососиметрична деформація високих ферм Мізеса** // Опір матеріалів і теорія споруд: наук.-тех. збірн. – К.: КНУБА, 2020. – Вип. 105. – С. 114-126. – Англ.
Іл. 8. Бібліогр. 27 назв.

UDC 539.3
Bilyk S.I., Tonkacheiev H.M., Bilyk A.S., Tonkacheiev V.H. **Tall von-Mises trusses' skew-symmetric deformation** // Strength of Materials and Theory of Structures: Scientific-and-technical collected articles. – K.: KNUBA, 2020. – Issue 105. – P. 114-126.
Fig. 8. Ref. 27.

Автор (науковий ступінь, вчене звання, посада): доктор технічних наук професор, професор кафедри металевих та дерев'яних конструкцій, завідувач кафедри металевих та дерев'яних конструкцій КНУБА Білик Сергій Іванович.
Адреса робоча: 03680 Україна, м. Київ, Повітрофлотський проспект 31, Київський національний університет будівництва і архітектури.
Робочий тел.: +38(044) 241-55-56.
Мобільний тел.: +38(067) 098-044-82 88;
E-mail: vartist@ukr.net

Автор (науковий ступінь, вчене звання, посада): кандидат технічних наук, доцент, доцент кафедри металевих та дерев'яних конструкцій КНУБА Білик Артем Сергійович.
Адреса робоча: 03680 Україна, м. Київ, Повітрофлотський проспект 31, Київський національний університет будівництва і архітектури.
Робочий тел.: +38(044) 241-55-56.
Мобільний тел.: +38(067) 588-8-295;
E-mail: vartist@ukr.net

Автор (науковий ступінь, вчене звання, посада): доктор технічних наук, професор кафедри будівельних технологій, проректор КНУБА з навчально-методичної роботи Тонкачеєв Геннадій Миколайович
Адреса робоча: 03680 Україна, м. Київ, Повітрофлотський проспект 31, Київський національний університет будівництва і архітектури.
Мобільний тел.: +38(050) 922-84-13;
E-mail: tonkacheiev.gm@knuba.edu.ua

Автор (науковий ступінь, вчене звання, посада): кандидат технічних наук, доцент кафедри металевих та дерев'яних конструкцій Тонкачеєв Віталій Геннадійович
Адреса робоча: 03680 Україна, м. Київ, Повітрофлотський проспект 31, Київський національний університет будівництва і архітектури.
Мобільний тел.: +38(063) 322-40-50;
E-mail: tonkacheiev.vg@knuba.edu.ua

UDC 539.3

OSCILLATIONS OF CLOZED CONICAL SHELLS AT COMPLEX ROTATION

P.P. Lizunov,
Doctor of Technical Science

E.Z. Kriksunov,
Candidate of Technical Science

O.M. Fesan,
Candidate of Technical Science

Kyiv national university of construction and architecture,
Kyiv, Povitroflotsky ave., 31, Kyiv. 03037

DOI: 10.32347/2410-2547.2020.105.127-132

This paper presents the relations that determine the oscillations of a system of two closed conical shells connected by a central rigid insert, which rotate at a constant angular velocity around the axis of symmetry of the system, the center of mass of which moves in the central force field.

Key words: oscillations, closed conical shell, rotational motion, forms of oscillations, central force field.

Introduction. When studying the oscillations of rotating mechanical systems, there are situations when the axis of rotation of the system can rotate, which leads to not only portable and relative, but also Coriolis forces of inertia, which change periodically over time. The gyroscopic interaction between the rotational portable motion of the system and the relative elastic oscillations of the elements is a source of excitation of precession oscillations, which can be resonant or unstable. Occurring when changing the axis of orientation of the system gyroscopic moment causes the appearance of alternating stresses, which significantly affect the strength and reliability of structural elements.

Such tasks arise in construction machinery, mechanical engineering, aircraft construction, space engineering and other sectors of the national economy. The main load acting on the elements of such systems are significant centrifugal forces of inertia, which significantly affect the strength characteristics of structures.

The stress-strain state and oscillations of membranes, plates and shells that perform complex motion in the central force field were researched in the works [1 - 10]. In this work, a mathematical modeling of the oscillations of a system of two folded conical shells with a central rigid insert during complex rotation is performed.

1. Consider a system of two closed conical shells connected by a central rigid insert rotating in opposite directions in the central force field with a constant angular velocity ω around the axis of symmetry of the system [4, 6, 10]. The shell element is subjected to a load consisting of gravitational and

inertial forces, but at large values of the angular velocity of the system, the gravitational loads can be neglected. Then the intensity of the inertial load on the shell element is determined by the formula:

$$\vec{q}^{\,I} = -\rho h(\vec{a}^{\,e} + \vec{a}^{\,r} + \vec{a}^{\,c}), \tag{1.1}$$

where ρ - is the density of the shell material; h - its thickness; $\vec{a}^{\,e}, \vec{a}^{\,r}, \vec{a}^{\,c}$ - vectors of portable, relative and Coriolis accelerations of the shell element.

The components of the vector of portable acceleration of the shell element in the direction of the coordinate lines x_1, x_2, x_3 of the curvilinear coordinate system associated with the shell element have the form [10]:

$$\begin{aligned}
a^e_{x_1} &= \omega^2 (R - x_1\cos\alpha)\cos\alpha + 2\omega\omega_0 (R - x_1\cos\alpha)\sin\alpha\sin\tau + \\
&+ \omega_0^2[(R - x_1\cos\alpha)\cos\alpha\cos^2\tau - x_1\sin^2\alpha]; \\
a^e_{x_2} &= \omega_0^2 (R - x_1\cos\alpha)\sin\tau\cos\tau; \\
a^e_{x_3} &= \omega^2 (R - x_1\cos\alpha)\sin\alpha - 2\omega\omega_0 (R - x_1\cos\alpha)\sin\alpha\sin\tau + \\
&+ \omega_0^2\sin\alpha[(R - x_1\cos\alpha)\cos^2\tau + x_1\cos\alpha],
\end{aligned} \tag{1.2}$$

where ω_0 - angular velocity of rotation of the center of mass of the system; $\tau = \omega t + x_2$ - phase coordinate.

The components of the relative acceleration vector $\vec{a}^{\,r}$ in the direction of the coordinate lines x_1, x_2, x_3 are equal, respectively

$$a^r_{x_1} = \ddot{u};\ a^r_{x_2} = \ddot{v};\ a^r_{x_3} = \ddot{w}, \tag{1.3}$$

where u, v, w - is the movement of the shell element in the direction of the coordinate lines x_1, x_2, x_3 . The components of the Coriolis acceleration vector in the direction of the coordinate lines x_1, x_2, x_3 have the form: where u, v, w - moving the shell element in the direction of the coordinate lines $x_1 x_2 x_3$. The components of the Coriolis acceleration vector $\vec{a}^{\,c}$ in the direction of the coordinate lines x_1, x_2, x_3 have the form:

$$\begin{aligned}
a^c_{x_1} &= 2[\dot{w}\omega_0\cos\tau + \dot{v}(\omega\cos\alpha + \omega_0\sin\alpha\sin\tau)]; \\
a^c_{x_2} &= -2[\dot{w}(\omega\sin\alpha - \omega_0\cos\alpha\sin\tau) + \dot{u}(\omega\cos\alpha + \omega_0\sin\alpha\sin\tau)]; \\
a^c_{x_3} &= 2[\dot{v}(\omega\sin\alpha - \omega_0\cos\alpha\sin\tau) - \dot{u}\omega_0\cos\tau].
\end{aligned} \tag{1.4}$$

Adding expressions (1.2), (1.3) and (1.4), we obtain the components of the vector of absolute acceleration in the coordinate system $x_1 x_2 x_3$:

$$\begin{aligned}
a_{x_1} &= \omega^2 (R - x_1\cos\alpha)\cos\alpha + 2\omega\omega_0 (R - x_1\cos\alpha)\sin\alpha\sin\tau + \\
&+ \omega_0^2[(R - x_1\cos\alpha)\cos\alpha\cos^2\tau - x_1\sin^2\alpha] + \ddot{u} + 2[\dot{w}\omega_0\cos\tau + \dot{v}(\omega\cos\alpha + \omega_0\sin\alpha\sin\tau)],
\end{aligned}$$

$$a_{x_2}=\omega_0^2(R-x_1\cos\alpha)\sin\tau\cos\tau+\ddot{v}-2[\dot{w}(\omega\sin\alpha-\omega_0\cos\alpha\sin\tau)+$$
$$+\dot{u}(\omega\cos\alpha+\omega_0\sin\alpha\sin\tau)],$$
$$a_{x_3}=\omega^2(R-x_1\cos\alpha)\sin\alpha-2\omega\omega_0(R-x_1\cos\alpha)\cos\alpha\sin\tau+$$
$$+\omega_0^2\sin\alpha[(R-x_1\cos\alpha)\cos^2\alpha)\cos^2\tau+x_1\cos\alpha]+\ddot{w}+$$
$$+2[\dot{v}(\omega\sin\alpha-\omega_0\cos\alpha\sin\tau)-\dot{u}\omega_0\cos\tau]. \quad (1.5)$$

In the case where the angular velocity of the shell is much greater than the angular velocity of the center of mass of the system $(\omega>>\omega_0)$, the expressions for the projections of the inertial load acting on the conical shell on the axis of the coordinate system $x_1x_2x_3$, associated with the shell element, will look like:

$$q_{x_1}=-\rho h\{\omega^2(R-x_1\cos\alpha)\cos\alpha+2\omega\omega_0(R-x_1\cos\alpha)\sin\alpha\sin\tau+$$
$$+\ddot{u}+2[\dot{w}\omega_0\cos\tau+\dot{v}(\omega\cos\alpha+\omega_0\sin\alpha\sin\tau)]\},$$
$$q_{x_2}=-\rho h\{\ddot{v}-2[w(\omega\sin\alpha-\omega_0\cos\alpha\sin\tau)+\dot{u}(\omega\cos\alpha+\omega_0\sin\alpha\sin\tau)]\},$$
$$q_{x_3}=-\rho h\{\omega^2(R-x_1\cos\alpha)\sin\tau-2\omega\omega_0(R-x_1\cos\alpha)\cos\alpha\sin\tau+$$
$$+\ddot{w}+2[\dot{v}(\omega\sin\alpha-\omega_0\cos\alpha\sin\tau)-\dot{u}\omega_0\cos\tau]\}. \quad (1.6)$$

2. Consider the problem of oscillations of a composite conical shell with a central rigid insert rotating at a constant angular velocity ω relative to the axis of natural rotation, making a plane rotation with a constant angular velocity ω_0. In this case, the equations describing the stress-strain state of the shell have the form [4]

$$\frac{E}{1-\nu^2}\left\{\frac{\partial^2u}{\partial x_1^2}+\frac{1}{x_1}\left[\frac{\partial u}{\partial x_1}-\frac{1}{x_1}(u-w\operatorname{tg}\alpha)-\nu\frac{\partial w}{\partial x_1}\operatorname{tg}\alpha\right]\right\}+\rho\omega^2x_1\cos^2\alpha=0,$$
$$\frac{E}{1-\nu^2}\left\{\frac{\partial u}{\partial x_1}\left[\frac{\partial^2w}{\partial x_1^2}+\frac{\nu}{x_1}\left(\operatorname{tg}\alpha-\frac{\partial w}{\partial x_1}\right)\right]+\frac{1}{x_1}(u-w\operatorname{tg}\alpha)\left[\nu\frac{\partial^2w}{\partial x_1^2}+\frac{1}{x_1}(\operatorname{tg}\alpha-\frac{\partial w}{\partial x_1})\right]\right\}-$$
$$-\rho\omega^2x_1\sin\alpha\cos\alpha=0, \quad (2.1)$$

where E - is the modulus of elasticity of the shell material; ν - Poisson's ratio.

The equations of oscillations of the shell with respect to the state of elastic equilibrium described by relations (2.1), taking into account expressions (1.6), have the form:

$$\frac{E}{1-\nu^2}\left\{\frac{\partial^2\Delta u}{\partial x_1^2}+\frac{1}{x_1}\left[\frac{\partial\Delta u}{\partial x_1}-\frac{1}{x_1}(\Delta u+\frac{3-\nu}{2\cos\alpha}\frac{\partial\Delta v}{\partial x_2}-\Delta w\operatorname{tg}\alpha)\right]+\right.$$
$$\left.+\frac{1}{x_1}\left(\frac{1+\nu}{2\cos\alpha}\frac{\partial^2\Delta v}{\partial x_1\partial x_2}-\nu\operatorname{tg}\alpha\frac{\partial\Delta w}{\partial x_1}\right)+\frac{1-\nu}{2x_1^2\cos^2\alpha}\frac{\partial^2\Delta u}{\partial x_2^2}\right\}-$$

$$-\rho\left\{2\omega\omega_0 x_1\sin\alpha\cos\alpha\sin\tau+\Delta\ddot{u}+2\left[\Delta\dot{w}\omega_0\cos\tau-\Delta\dot{v}\left(\omega\cos\alpha-\omega_0\sin\alpha\sin\tau\right)\right]\right\}=0,$$

$$\frac{E}{1-\nu^2}\left\{\frac{1-\nu}{2}\frac{\partial^2\Delta v}{\partial x_1^2}+\frac{1}{x_1}\left[\frac{1+\nu}{2\cos\alpha}\frac{\partial^2\Delta u}{\partial x_1\partial x_2}+\frac{1-\nu}{2}\frac{\partial\Delta v}{\partial x_1}-\frac{1-\nu}{2x_1}\Delta v+\right.\right.$$

$$\left.\left.+\frac{1}{x_1\cos\alpha}\left(\frac{3-\nu}{2}\frac{\partial\Delta u}{\partial x_2}+\frac{1}{\cos\alpha}\frac{\partial^2\Delta v}{\partial x_2^2}-\operatorname{tg}\alpha\frac{\partial\Delta w}{\partial x_2}\right)\right]\right\}-$$

$$-\rho\left\{\Delta\ddot{v}-2\left[\Delta w\left(\omega_0\cos\alpha\sin\tau+\omega\sin\alpha\right)-\Delta\dot{u}\left(\omega\cos\alpha-\omega_0\sin\alpha\sin\tau\right)\right]\right\}=0, \quad (2.2)$$

$$N_{11}^*\frac{\partial^2\Delta w}{\partial x_1^2}+\frac{N_{22}^*}{x_1}\left(\frac{1}{x_1\cos^2\alpha}\frac{\partial^2\Delta w}{\partial x_2^2}-\frac{\partial\Delta w}{\partial x_1}-\frac{\operatorname{tg}\alpha}{x_1 c\cos\alpha}\frac{\partial\Delta v}{\partial x_2}\right)+$$

$$+\frac{Eh}{1-\nu^2}\frac{\operatorname{tg}\alpha}{x_1}\left[\frac{1}{x_1}\left(\frac{1}{\cos\alpha}\frac{\partial\Delta v}{\partial x_2}+\Delta u-\Delta w tg\alpha\right)+\nu\frac{\partial\Delta u}{\partial x_1}\right]-$$

$$-\rho h\left\{2\omega\omega_0 x_1\cos^2\alpha\sin\tau+2\left[\Delta\dot{v}\left(\omega_0\cos\alpha\sin\tau+\omega\sin\alpha\right)-\Delta\dot{u}\omega_0\cos\tau\right]+\Delta\ddot{w}\right\}=0,$$

where $\Delta u,\Delta v,\Delta w$ - the movement of the shell in the direction of the coordinate lines x_1,x_2,x_3 ; N_{11}^*,N_{22}^* - radial and circumferential forces due to the rotation of the shell relative to the axis of symmetry.

Considering the periodicity of the right-hand side and the coefficients of the system of resolving equations (2.2), using the projection method, we can reduce equations (2.2) to a system of ordinary differential equations with an independent variable x_1, that approximately replaces the original one.

Conclusions. Differential equations (2.2) describe the oscillations of a system of two closed conical shells connected by a central rigid insert, which rotate at a constant angular velocity around the axis of symmetry of the system, the center of mass of which moves in the central force field.

The solution of the obtained system of equations allows one to determine the forms of vibrations and forces in a composite conical shell for various parameters of the shell and the ratios of the velocities of the shell's own rotation and the rotation of its center of mass.

REFERENCES

1. *Bazhenov V.A.* Oscillations of a rotating membrane disk with a central rigid insert / V.A. Bazhenov, V.I. Gulyaev, S.G. Kravchenko, P.P. Lizunov // Strength problems. - 1986. - No. 6. - P. 108-113.
2. *Gulyaev V.I.* Oscillations of a rotating circular membrane in the field of inertial and gravitational forces / V.I. Gulyaev, S.G. Kravchenko, P.P. Lizunov // Applied Mechanics. - 1986. - 22, No. 11. - P. 112-117.
3. *Lizunov P.P.* Oscillations of a compound conical shell during complex rotation / P.P. Lizunov // Strength of Materials and Theory of Structures. - 1988. - V. 52. - S. 22-27.
4. *Gulyaev V.I.* Oscillations of systems of rigid and deformable bodies during complex motion / V.I. Gulyaev, P.P. Lizunov. - K .: Vyshcha shkola, 1989 .-- 160 p.
5. *Kravchenko S.G.* Nonlinear oscillations of a system of two membranes with a central rigid insert / S.G. Kravchenko, P.P. Lizunov // Strength of Materials and Theory of Structures. -

1986. - V. 49.- P. 11-14.
6. *Grom A.A.* Processional oscillations of plates and shells during complex motion / A.A. Grom, P.P. Lizunov, N. A. Snezhko // Applied Mechanics. - 1997. - 33, No. 7. - P. 652-56.
7. *Lizunov P.P.* Oscillations of the membrane surface of the space reflector / P.P. Lizunov, A.A. Grom // Strength of Materials and Theory of Structures. - 2002. - V.71.-P.146-152.
8. *Lizunov P.P.* Elastic equilibrium of a spherical shell in the central force field / P.P. Lizunov // Strength of Materials and Theory of Structures. - 2013. - V. 91. - P.84-87.
9. *Lizunov P.P.* Oscillations of a spherical shell in the central force field / P.P. Lizunov // Strength of Materials and Theory of Structures. - 2014. - V. 93. - P. 37-42.
10. *Lizunov P.P.* Stress-deformed state of closed conical shells during complex rotation / P.P. Lizunov, E.Z. Kriksunov, O.M. Fesan // Strength of Materials and Theory of Structures. - 2019. - V. 102. - P. 191-198.

Стаття надійшла 29.09.2020

Лізунов П.П., Криксунов Е.З., Фесан О.М.

КОЛИВАННЯ ЗАМКНЕНИХ КОНІЧНИХ ОБОЛОНОК ПРИ СКЛАДНОМУ ОБЕРТАННІ

В даній роботі розглядається система двох замкнених конічних оболонок, з'єднаних центральною жорсткою вставкою, що обертаються в протилежних напрямах в центральному силовому полі з постійною кутовою швидкістю навколо осі симетрії системи. На елемент оболонки діє навантаження, що складається з гравітаційних та інерційних сил, але при великих значеннях кутової швидкості власного обертання системи гравітаційними навантаженнями можна знехтувати. Гіроскопічна взаємодія між обертальним переносним рухом системи і відносними пружними коливаннями елементів є джерелом збудження прецесійних коливань, які можуть носити резонансний або нестійкий характер. Виникаючий при зміні осі орієнтації системи гіроскопічний момент викликає появу знакозмінних напружень, які істотно впливають на міцність та надійність оболонок. Такі задачі виникають в будівельній техніці, машинобудуванні, авіабудуванні, космічній техніці та інших галузях народного господарства. Основним навантаженням, яке діє на елементи таких систем, є значні відцентрові сили інерції, які істотно впливають на міцнісні характеристики конструкцій. Враховуючи періодичність правої частини і коефіцієнтів системи розв'язувальних рівнянь, за допомогою проекційного методу можна звести розв'язувальні рівняння до системи звичайних диференціальних рівнянь, які наближено замінюють вихідну. Розв'язок отриманої системи рівнянь дозволяє визначати форми коливань і зусилля в складеній конічної оболонці при різних параметрах оболонки і співвідношеннях швидкостей власного обертання оболонки і обертання її центру мас.

Ключові слова: коливання, замкнені конічні оболонки, обертальний рух, форми коливань, центральне силове поле.

Lizunov P.P., Kriksunov E.Z., Fesan O.M.

OSCILLATIONS OF CLOSED CONICAL SHELLS WITH COMPLEX ROTATION

The paper consider a system of two closed conical shells connected by a central rigid insert rotating in opposite directions in a central force field with a constant angular velocity around the axis of symmetry of the system. The shell element is subjected to a load consisting of gravitational and inertial forces, but at large values of the angular velocity of the system, the gravitational loads can be neglected. The gyroscopic interaction between the rotational portable motion of the system and the relative elastic oscillations of the elements is a source of excitation of precession oscillations, which may be resonant or unstable. Occurring when changing the axis of orientation of the system gyroscopic moment causes the appearance of alternating stresses, which significantly affect the strength and reliability of the shells. Such problems arise in construction engineering, mechanical engineering, aircraft construction, space engineering and other sectors of the economy. The main load acting on the elements of such systems are significant centrifugal forces of inertia, which significantly affect the strength characteristics of structures. Taking into account the periodicity of the right-hand side and the coefficients of the system of resolving equations, with the help of the projection method it is possible to reduce the resolving equations to the system of ordinary differential equations, which approximately replaces the original one. The solution of the obtained system of equations makes it possible to determine the forms of oscillations and forces in a composite conical shell at various

parameters of the shell and the ratios of the velocities of the shell's own rotation and the rotation of its center of mass.

Key words: oscillations, closed conical shell, rotational motion, forms of oscillations, central force field.

УДК 539.3
Лізунов П.П., Криксунов Е.З., Фесан О.М. **Коливання замкнених конічних оболонок при складному обертанні** // Опір матеріалів і теорія споруд: наук.-тех. збірн. – К.: КНУБА, 2020. – Вип. 105. – С. 127-132. – Англ.

Наведені співвідношення, що визначають коливання системи двох замкнених конічних оболонок, з'єднаних центральною жорсткою вставкою, які обертаються з постійною кутовою швидкістю навколо осі симетрії системи, центр мас якої здійснює рух в центральному силовому полі.
Бібліогр. 10 назв.

UDC 539.3
Lizunov P.P., Kriksunov E.Z., Fesan O.M. **Oscillations of closed conical shells with complex rotation** // Strength of Materials and Theory of Structures: Scientific-and-technical collected articles. – K.: KNUBA, 2020. – Issue 105. – P. 127-132.

This paper presents the relations that determine the oscillations of a system of two closed conical shells connected by a central rigid insert, which rotate at a constant angular velocity around the axis of symmetry of the system, the center of mass of which moves in the central force field.
Ref. 10.

УДК 539.3
Лизунов П.П., Криксунов Э.З., Фесан А.Н. Колебания **замкнутых конических оболочек при сложном вращении //** Сопротивление материалов и теория сооружений: научно-тех. сборник. - К .: КНУБА, 2020. - Вып. 105. - С. 127-132.

Приведены соотношения, определяющие колебания системы двух замкнутых конических оболочек, соединенных центральной жесткой вставкой, которые вращаются с постоянной угловой скоростью вокруг оси симметрии системы, центр масс которой осуществляет движение в центральном силовом поле.
Библиогр. 10 назв.

Автор (науковий ступінь, вчене звання, посада)*: доктор технічних наук, професор, завідувач кафедри основ інформатики КНУБА ЛІЗУНОВ Петро Петрович.*
Адреса робоча: *03037 Україна, м. Київ, Повітрофлотський проспект 31, КНУБА, кафедра основ інформатики, ЛІЗУНОВ Петро Петрович.*
Адреса домашня: *Україна, м. Київ, вул. Кавказька, 12, кв. 48.*
Мобільний тел.: *+38(067) 921-70-05;*
E-mail*: lizunov@knuba.edu.ua*
ORCID ID: http://orcid.org/0000-0003-2924-3025

Автор (науковий ступінь, вчене звання, посада)*: кандидат технічних наук, провідний науковий співробітник КНУБА КРИКСУНОВ Едуард Зиновійович.*
Адреса робоча: *03037 Україна, м. Київ, Повітрофлотський проспект 31, КНУБА, НДІ будівельної механіки, КРИКСУНОВ Едуард Зиновійович.*
E-mail*: edk@scadsoft.com*
ORCID ID: http://orcid.org/0000-0002-3357-7020

Автор (науковий ступінь, вчене звання, посада)*: кандидат технічних наук, провідний науковий співробітник КНУБА ФЕСАН Олександр Миколайович.*
Адреса робоча: *03037 Україна, м. Київ, Повітрофлотський проспект 31, КНУБА, НДІ будівельної механіки, ФЕСАН Олександр Миколайович.*
E-mail: *lizunov@knuba.edu.ua*

UDC 623.1/.7:007.52 (477)

INFLUENCE OF AIR SHOCK WAVE ON SHELTER

V.I. Kotsyuruba,
Doctor of Technical Science, Professor, Honored Inventor of Ukraine

I.P. Datsenko,
Candidate of Technical Sciences

V.O. Dachkovsky,
Candidate of Technical Science

R.M. Cherevko,

V.M. Polyulyak,

O.A. Ivashchuk,

I.I. Furman,
Doctor of Historical Science, Docent

National Defense University of Ukraine named after Ivan Chernyakhovsky
28, Povitroflotskiy avenu, Kyiv, Ukraine

DOI: 10.32347/2410-2547.2020.105.133-144

In modern conditions, sheltering people in protective structures, as a way of protection from dangers, in combination with evacuation from the affected areas (pollution) and the use of personal protective equipment, increases the reliability of public protection. In conditions when evacuation measures from cities can be complicated in a short time, protection of the population in shelters becomes the only possible and effective. Therefore, an important task is to study the impact of loads caused by the explosion of various munitions, substantiate recommendations for improving the protective properties of the shelter and the choice of their location.

The most common issues are considered in the article that arise during the arrangement of shelter in buildings and outside them. Based on experimental studies, Taylor's formula and the system of non-stationary Navier-Stokes equations for gas, it's conducted an analysis of the influence of external and internal factors on the possible nature of the dynamic load from the shock wave on buildings, structures and structural elements in which shelters are located.

The results of studies of the parameters of dynamic loads showed that if the storage facilities are located in the basements of buildings, their stability is characterized by three parameters: maximum pressure, time to increase the load to maximum and effective time. The parameters of the loads and the law of their change over the time depend on the location of the structure relative to the surface of the earth and the building, the force of the explosion and the distance to the center of the explosion.

Key words: dynamic load, shock wave, breakthrough wave, shock wave pressure, load rise time, load action time, technical basement, separate shelters.

Introduction. In recent years, issues of civil protection have come to the fore and become one of the most actual problems of the modern world. This applies to all countries in the world, regardless of economic and political status: the ever-increasing threat of terrorist acts, man-made and natural disasters, the modern conditions of urbanization of society and the high probability of military conflicts, such as hostilities in eastern Ukraine

supported by the Russian Federation. During armed conflicts, the most part of hostilities takes place near or directly in settlements, and settlements are shelled by illegal armed groups, necessitating the protection of not only military formations but also civilians. As a result, there is a need to study and determine the optimal location of shelter equipment and materials for their equipment.

The analysis of works devoted to the study of the action of dynamic loads and properties of structures used in the construction of shelters indicates the aggravation of the need to study the impact of loads caused by explosions of different nature [1-5].

Currently, one of the main materials for construction is reinforced concrete, which is an integral part of most modern buildings. In accordance to the building codes and rules, the construction of shelters are calculated on the totality of all loads that may affect the structure [6-9].

The above-indicated causes the necessity of the more deeper study of the impact of the results of the explosion process, the calculation of the stability of shelter structures and the choice of their locations. Therefore, the aim of the article is to research the effect of dynamic loads from the shock wave on the shelter.

The main material of the article. Dynamic loads from the shock wave in practical calculations are reduced to equivalent static loads that cause the same deformations in the structure as dynamic.

If we take into account the displacement of the structure and the deformation of the structural elements, the equivalent loads are determined in two stages. At the first stage, the dynamic loads on the structural elements of the structure are determined, and at the second stage, the static loads are determined directly. Dynamic loads caused by an explosion are usually characterized by three parameters: maximum pressure $P_{\max}$, the time of increase of the load to the maximum t_{nar} and the time of action τ_e . The parameters of the load and the law of its change in time depend on the location of the structure relative to the surface of the earth and the building, the force of the explosion and the distance to the center of the explosion [7].

In the practice of design, different storage options can be reduced to four calculation cases:

1) shelters are placed on the ground floor of the building;

2) shelters are erected in the basement or basement of the building;

3) shelters are placed under the technical basement (TB) (technical underground);

4) shelters are located separately, completely or partially sunk into the ground.

The results of the study on 3 and 4 options are revealed in the article. In particular, the influence of dynamic loads from the shock wave on the elements of reinforced concrete structures, the study of which was carried out using experimental data, the finite element method, Taylor's formula, the

system of nonstationary Navier-Stokes equations for gas and their approximation [10-12].

1. Determination of dynamic loads on the shelter are placed under the technical basement. In the case when the shelter is placed under the TB, when exposed to an air shock wave on the building, the wave first flows into the premises of the first floor, and then into the premises of the TB through the holes formed by the destruction of the floor (Fig. 1).

When determining the characteristics of the wave flowing into the TB, the following prerequisites are accepted: the time of pressure build-up in all rooms of the first floor and the estimated margin of safety are not taken into account; floor slabs under load work for the scheme of the hinged beam, the destruction of which occurs in the hinge of plasticity; the wave flows through the responses, which are simultaneously created by rotating the convenient structures relative to the supports; the walls of the TB are not destroyed.

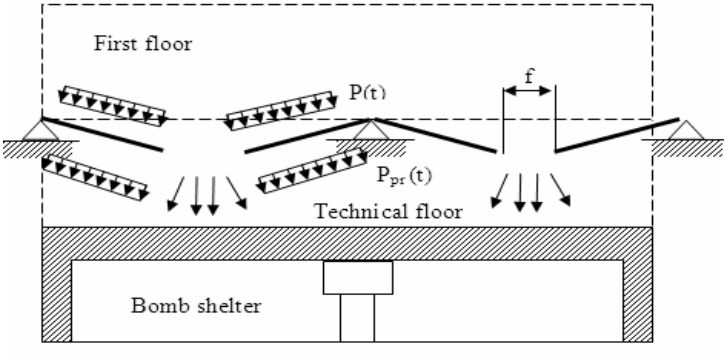

Fig. 1. Calculation scheme for determining the parameters of the penetration wave in the technical floor

The destruction of the NB floor slabs occurs under the action of load. After the destruction of the plastic hinge on the inside of the floor, back pressure begins to act, which is taken equal to the pressure of the breakthrough wave $\Delta P_F = [\varphi(t), t]$. After the failure of the hinge, the load depends on the movement of the floor halves, the size of the gap and the process of flow of the wave into a closed volume, that's there is a relationship. The solution of the equations of motion of the floor slabs is carried out together with the equations of gas dynamics on the flow of the wave into closed volumes.

The maximum pressure in the flow wave is taken equal to the pressure at the moment of equalization of pressures before the break and inside the TB. The results of calculations of corresponding types of overlap (Table 2) are shown in Table 1.

Table 1

The parameters of the flow wave in the TB at the pressure on their overlap, 10^5 Pa

Type of overlapping	0,5		3	
	ΔP_{zat}^{max},10^5 Pa	t_{nar} , m/sec	ΔP_{zat}^{max},10^5 Pa	t_{nar} , m/sec
1	0,43	124	2,36	57
2	0,43	137	2,31	64
3	0,44	129	2,39	58
4	0,48	143	2,33	65
5	0,44	130	2,39	63
6	0,43	146	2,32	70
7	0,42	150	2,25	70
8	0,42	142	2,30	70

Table 2

Characteristics of overlapping by types

Type of overlapping	Weight per unit area, kg/m2	Characteristics of overlapping
1	240	1. Overlapping from plates of continuous section. Material - heavy concrete. 2. Overlapping from monolithic reinforced concrete
2	330	1. Overlapping from plates of continuous section. Material - heavy concrete. 2. Overlapping from monolithic reinforced concrete
3	260	Precast reinforced concrete, hollow decking
4	350	Precast reinforced concrete, hollow decking. Floors: 1 - light concrete 50 mm, cement-sand screed 25 mm, cold mastic 1 mm, linoleum 4 mm; 2 - plank floor on logs.
5	260	Precast concrete, ribbed slab.
6	350	Precast concrete, ribbed slab, linoleum floor, 90 kg/m2.
7	420	1. Overlapping from plates of continuous section. Material - heavy concrete. 2. Overlapping from monolithic reinforced concrete. The weight of the floor per unit area is 90 kg/m2.
8	330	1. Overlapping from plates of continuous section. Material - heavy concrete. 2. Overlapping from monolithic reinforced concrete. The weight of the floor per unit area is 90 kg/m2.

Calculations have shown that the destruction of the floor of the TB, made of the most common in the practice of building slabs, reduces the pressure of the inflow wave by 14% at a pressure of $0{,}5 \cdot 10^5$ Pa and by 22% at a pressure of $3 \cdot 10^5$ Pa. The time of increase of pressure during the destruction of these plates makes: at pressure $0.5 \cdot 10^5$ Pa - 130 ms; at a pressure of $3 \cdot 10^5$ Pa - 60 ms.

The dependence of the time of increase t_{nar} of the penetration wave and the coefficient of the shielding effect C_n from the pressure P_F at the destruction of the floor of different densities is shown in Fig. 2.

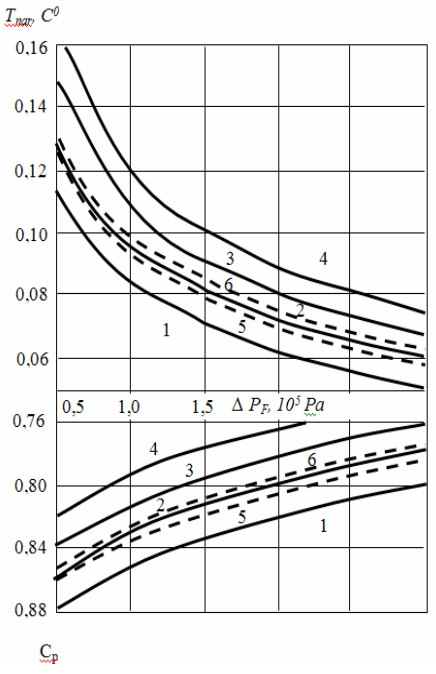

Fig. 2. The dependence of t_{nar} and c_p from the pressure P_F at the destruction of the floor: 1 – at the weight of overlapping of 200 kg/m^2; 2 - the same, 300 kg/m^2; 3 - the same, 400 kg/m^2; 4 - the same, 500 kg/m^2; 5 - overlapping of multilayer empty flooring (PK8-58-16); 6 - overlapping of ribbed plates (NC-5-1)

Analysis of the established dependences (Fig. 2) showed that the dynamic load on the floors of shelters located under the TB, as well as on the walls of shelters adjacent to the basement, not protected from shock waves, gradually increases to a maximum, which is determined by the formula:

$$P_{\max} = \Delta P_F C_{cp} C_p \ , \qquad (1)$$

where C_p – coefficient that takes into account the shielding effect of the overlap, taken according to the graphs (Fig. 2); C_{cp} – the coefficient taking into account the shielding effect of the enclosing structures of shelters, which is accepted for buildings with a capacity of less than 10% in accordance with Table 3, and for buildings with a capacity of 10% or more is equal to 1.

2. Determination of dynamic loads on separately located shelters. The presence of a soil layer above the floor of separately located storage facilities leads to the fact that the structure is not affected by an air shock wave, but by a compression wave in the soil. The dynamic load on the floor is determined taking into account the reflection of the compression wave from the structure, which is displaced on the ground. The unloading wave, propagating from the free surface, is added to the compression wave, which reduces the load on the

floor. As a result, the effect of the reflection pressure will be short-lived. If the thickness h of the soil layer above the floor is less than 1 m, the effect of reflection on the bearing capacity of structural elements is insignificant and can be neglected.

Table 3

The value of the coefficient c_{cp}

Characteristics of wall materials	Wall thickness, cm	Coefficient c_{cp}
Panels of lightweight concrete with density p = 700 - 1200 kg/m^3	10 20-30	0,95 0,90
Brick masonry of ordinary brick, p= 1800 kg/m^3	25; 38 64	0,90 0,85
Lightweight concrete blocks p = 700 - 1200 kg/m^3	40-50	0,85

The dynamic load on the solid slabs of the foundation and walls at $h \leq 1$ m is determined in the same way as for shelters built into the building with a capacity of more than 50%. However, when calculating the loads on the floor and the foundation at 1 m take into account the effect of reflection of the compression wave. The equation of motion of the shelter is written in the form:

$$Mu'' = \left[\sigma_m f(t) k^*_{otr} - A_p u'\right] F_p - A_F u' F_F, \qquad (2)$$

where M, F_p, F_F – the mass of the structure, the area of its floor and foundation; σ_m – maximum of stress in the soil at the level of the floor; k^*_{otr} – reflection coefficient from a solid obstacle; A_p, A_F – acoustic resistance of loose soil and base; u' – moving storage with specific weight m; $f(t)$ – load function.

The expression $A_p u' F_p$ takes into account the reduction of load due to the displacement of the structure.

Equation (2) at $m = \frac{M}{F_p}$, $P^n_{\max} = \sigma_m k^*_{otr}$, take to the following form:

$$mu'' = P^n_{\max} f(t) - \overline{A}_F u' . \qquad (3)$$

where $P^n_{\max}$ is the maximum pressure on the floor; $\overline{A}_F$ is acoustic resistance of compacted soil.

For practical calculations the load on the floor is determined by the formulas:

$$P^n_{\max} = \Delta P_F k_{zat} k_{otr}, \qquad (4)$$

$$k_{otr}=k_{otr}^{*}\left[1-\frac{1}{k_2}+\frac{1}{k_2}\left(1-\exp(-\frac{1}{k_1})\right)\right]; \quad (5)$$

$$k_1=\frac{m}{A_p k_2 t_{nar}}, \quad k_2=1+a_1 A_F A_p \ , \quad a_1=\frac{F_F}{F_p} \ ,$$

where k_{zat} is the attenuation coefficient of the wave; k_{otr}^{*} determined by the formula:

$$k_{otr}^{*}=2-(1-\frac{a_1}{a_0})\frac{\sigma_s}{\sigma_m}(X), \quad (6)$$

If in the calculations k_{otr} is less than one, then $k_{otr}=1$ is accepted.

The load on the foundation (at $a_1=1$, $R=(A_F+\frac{A_p}{m})$) is determined by the formula

$$P_{\max}^{n}=\Delta P_F k_{zat} k_F \ , \quad (8)$$

where k_F is the strength factor of the foundation material.

For built-in storage, the time of action of the load on the floor, including the increase to the maximum and decrease to zero, is taken equal to the effective time of the shock wave τ_e . For separately located shelters with a scattering of more than 1 m, the time τ_e is equal only to the time of reduction of the load on the floor.

3. Determination of dynamic loads on the elements of the entrances to the shelter. Loads on the elements of the entrances (walls, protective and airtight doors, etc.) mainly depend on their design solutions, air shock wave pressure and shielding effect of enclosing structures.

The calculation of dynamic loads is performed according to the formula

$$P_{\max}^{B}=\Delta P_F k_B \ , \quad (9)$$

in which the value of the coefficient k_B is taken from Table 4. Data k_B (Table 4) are obtained by solving problems about the interaction of shock waves with the structures of the entrance and the propagation of waves inside buildings, taking into account their destruction.

Formula (9) determines the maximum value of the dynamic load on the areas of the outer walls of the shelter at the entrances and on the first (outer) protective or protective-airtight doors. The values k_B given in Table 4 take into account almost all calculated cases.

It is established that if the entrances are located in unprotected basements, then take into account the consumption energy of the wave to destroy their floors. In this case, the coefficient k_B is taken equal to the value C_p according to the schedule (Fig. 2). The coefficient k_B for all types of entrances located in buildings with a capacity of less than 10%, should be multiplied by a

factor C_{cp} that takes into account the shielding effect of the building (Table 3).

The temporal characteristics of the laws of change of the input load are determined by the same dependencies that are used in determining similar values for the enclosing structures of storage.

The rise time t_{nar} for the inputs in Table 4 is determined by the schedule (Fig. 2).

Table 4

The value of the coefficient k_B depending on the type of entrance to the shelter

№ in order	Entrance		k_B at P_F,10^5		
			1	2	3
1	From basements, not protected from shock waves		0,8	0,8	0,8
2	Through with a covered area against the entrance		1	1,1	1,2
3	From the premises of the first floor with the area of holes 10-50%	a) below ground level	1	1	1
		b) above ground level	1,7	1,5	1,3
4	From stairwells with an area of holes 10-50% at the entrance to the stairwell from the street	a) below ground level	2,5	2,2	
		b) above ground level			
5	From the premises of the first floor and stairwells with an area of holes > 60%	a) below ground level	2,7	2,5	2,2
		b) above ground level	3	2,7	2,3
6	Dead end without an area or with a light (collapsible) pavilion		2,7	2,5	2,2
7	Those that rise above the surface in the walls, as well as the entrance from the apron		3	2,7	2,3

Dynamic loads on the inner walls, floor, ceilings and the second protective and airtight door of the vestibule-gateway are determined from the condition of possible flow of the shock wave through the open first protective-airtight door at the time of filling the vestibule-gateway. In this case, the dynamic load is approximately equal to the dynamic load on the outer walls of the shelter at the location of the entrance, multiplied by a factor of 0.8.

The dynamic load on the outer walls of the shelter at the location of the first protective and airtight door is determined by Table 4. The load from the

inflow wave is taken linearly increasing to a maximum over time t_{nar} with a subsequent decline to zero over time $t_{nar} = \tau_e - t_{nar}$.

It is proposed to determine the dynamic load on the inner walls of the vestibules and airtight doors under the conditions of the shock wave flow through possible leaks along the perimeter of the external door to the door frame. Such leaks can be due to hidden defects when installing embedded parts and elements of external doors.

At $\Delta P_F = 0{,}2...0{,}3$ MPa dynamic loading on the specified designs is accepted equal 0,025 MPa, and at $\Delta P_F = 0{,}1 - 0{,}015$ MPa.

Dynamic loads from the shock wave of leakage on the structure of the emergency exit (walls, ceilings and floor), designed in the form of a protected head with a mine and tunnel, as well as on the part of the wall at the junction of the exit are taken equal to the pressure ΔP_F multiplied by 1.6. It is also established that if the emergency exit is designed in the form of an inclined descent and a tunnel, the dynamic loads on its structural elements are taken equal to the pressure ΔP_F multiplied by the factor k_B .

These dynamic loads on the structures of the inputs and outputs are given for internal loads. Along with this load, the enclosing structures will experience external loads. These loads are determined in the same way as for coverings, walls and foundations of shelters.

Conclusion. Thus, the results of studies of the parameters of dynamic loads showed that at the location of storage facilities in the basements of buildings, their stability is characterized by three parameters: maximum pressure $R_{\max}$, time to increase t_{nar} the load to maximum and effective action time τ_e . The parameters of the loads and the law of their change in time depend on the location of the structure relative to the surface of the earth and the building, the force of the explosion and the distance to the center of the explosion.

Calculations have shown that the destruction of the floor of the TB, made of the most common in the practice of building slabs, reduces the pressure of the inflow wave by 14% at a pressure of $0{,}5 \cdot 10^5$ Pa and by 22% at a pressure of $3 \cdot 10^5$ Pa. The time of increase of pressure at destruction of plates makes: at pressure $0{,}5 \cdot 10^5$ Pa - 130 m/sec; at a pressure of $3 \cdot 10^5$ Pa - 60 m/sec.

It is established that due to the dynamic loads of separately located shelters, the presence of a soil layer over the floor of separately located storage facilities leads to the fact that the structure is not affected by an air shock wave, but a compression wave in the soil.

For built-in storage, the time of action of the load on the floor, including the increase to the maximum and decrease to zero, is taken equal to the effective time of the shock wave τ_e . For separately located shelters with scattering of more than 1 m, the time τ_e is equal only to the time of load drop on the layer of scattering.

Calculations of dynamic loads on the elements of the entrances to the shelter have showed that their dependence on the inflow wave is linearly increasing to a

maximum over time t_{nar} with a subsequent decline to zero over time $t_{nar} = \tau_e - t_{nar}$. At $\Delta P_F = 0{,}2–0{,}3$ MPa dynamic loading on the specified designs is accepted equal 0,025 MPa, and at $\Delta P_F = 0{,}1$ Mpa - 0,015 MPa.

As a direction of further researches is to establish the characteristics of the resistance of building elements to the dynamic impact of fragmentary elements.

REFERENCES

1. *Mykhaylovska O.V.* Zakriplennya stinok zakhysnykh sporud iz zastosuvannyam gruntotsementnykh elementiv (Fixing the walls of protective structures with the use of soil-cementing elements)/ O.V. Mykhaylovska, O.B.Oleksiyenko // Visnyk Odeskoyi derzhavnoyi akademiyi budivnytstva ta arkhitektury, 2019. – № 75. – S. 44-52. (in Ukrainian)
2. *Birbrayer A.N.* Raschet konstruktsii na seysmostoykost (Structural analysis for seismic resistance)/ A.N. Birbrayer. – S.-Pb.: Nauka, 1998. – 255 s. (in Ukrainian)
3. *Remez N.S.* Dynamichna vzayemodiya hruntovykh osnov ta budivel pid chas diyi seysmovybukhovoho navantazhennya (Dynamic interaction of soil foundations and buildings during seismic and explosive loads) / N.S. Remez, I.A. Ivanova // Visnyk NTUU «KPI». – 2015 r. – №29. – S. 24-30. (in Ukrainian)
4. Mkrtychev O.V. Raschet konstruktsiy zhelezobetonnogo zdaniya na vzryvnyye nagruzki v nelineynoy dinamicheskoy postanovke (Analysis of structures of a reinforced concrete building for explosive loads in a nonlinear dynamic setting) / O.V. Mkrtychev, V.B. Dorozhinskiy, O.V. Lazarev // Vestnik MGSU. – 2011. – №4. – S. 243–247. (in Russian)
5. *Nabiullin M. I.* Matematicheskaya model rascheta amplitudy izbytochnogo davleniya na fronte vozdushnoy udarnoy volny (Mathematical model for calculating the amplitude of excess pressure at the front of an air shock wave)/ M. I. Nabiullin, A. V. Guseva, D. YU. Verin, S. A. Vilokhin // Vestnik tekhnologicheskogo universiteta. 2017. T.20, №3 – S. 141-144. (in Russian)
6. *Tuzikov S.A.* Analiz vymoh do zakhysnykh sporud tsyvilnoho zakhystu i metodolohichni pidkhody do yikh klasyfikatsiyi (Analysis of requirements for protective structures of civil defense and methodological approaches to their classification) / S.A. Tuzikov, S.O. Kovzhoha, YE.V. Karmannyy, A.F. Lazutskyy, A.V. Pysaryev // Zbirnyk naukovykh prats KHUPS. – 2013. – №1(34). – S. 186-189. (in Ukrainian)
7. *Vasylchenko O.V.* Budivelni konstruktsiyi ta yikh povedinka v umovakh nadzvychaynykh sytuatsiy: Navchalnyy posibnyk (Building structures and their behavior in emergency situations: A textbook) / O.V. Vasylchenko, YU.V. Kvitkovskyy, O.V. Myrhorod, O.A. Stelmakh. – Kharkiv: KHNADU, 2015. – 488s. (in Ukrainian)
8. *Kobylkin I.F.* Udarnyye i detonatsionnyye volny: Metody issledovaniya (Shock and Detonation Waves: Research Methods) / [I.F. Kobylkin, V.V. Selivanov, V.S. Solov'yev, N.N. Sysoyev].–M.: Fizmatlit, 2004. – 375s. (in Russian)
9. *Kvitkovskyy Yu.V.* Vyznachennya parametriv udarnoyi khvyli, shcho utvoryuyetsya pid chas vybukhu hazopovitryanoyi sumishi (Determination of the parameters of the shock wave formed during the explosion of the gas-air mixture) / Kvitkovskyy YU.V, Prokhach E.YU.// Zbirka naukovykh prats UTSZU. - №4, 2006. – S.120-124. (in Ukrainian)
10. *Ovcharenko V.A.* Osnovy metodu kintsevykh elementiv i yoho zastosuvannya v inzhenernykh rozrakhunkakh: nachalnyy posibnyk. (Fundamentals of the finite element method and its application in engineering calculations: a textbook)/ Ovcharenko V.A., Podlyesnyy S.V., Zinchenko S.M. – Kramatorsk: DDMA, 2008. – 380 s. (in Ukrainian)
11. *Ivanova S.V.* Formula Teylora i yeye prilozheniya k vychesleniyu predelov funktsiy: Uchebno-metodicheskoye posobiye (Taylor's formula and its application to calculating the limits of functions: Educational-methodical manual). - M.: MFTI, 2011. – 66 s. (in Russian)
12. *Kalion V.A.* Obchyslyuvalna hidromekhanika. Rivnyannya Navye-Stoksa: navch. posib. (Computational hydromechanics. Navier-Stokes equation: textbook.)/ V.A. Kalion. – K.: VPTS “ Kyyiv□kyy universytet”, 2016. – 221 s. (in Ukrainian)

Стаття надійшла 15.09.2020

Коцюруба В.І., Даценко І.П., Дачковський В.О., Черевко Р.М., Полюляк В.М., Іващук О.А., Фурман І.І.

ВПЛИВ ПОВІТРЯНОЇ УДАРНОЇ ХВИЛІ НА УКРИТТЯ

У протистоянні народу України агресивній політиці Російської Федерації є актуальним питання вивчення досвіду бойових дійна сході нашої держави. Аналіз втрат, яких зазнали Збройні Сили України та мирне населення, за час ведення операції Об'єднаних сил (антитерористичної операції) на території Донецької та Луганської областей чітко вказують на необхідність вивчення питання впливу навантажень, викликаних вибухом різних за спорядженням боєприпасів, обгрунтування рекомендацій щодо підвищення захисних властивостей укрить та вибору місць їх розташування.

Конструкції таких споруд розраховують на особливі сполучення навантажень, що складаються з постійних, тимчасових, тривалих навантажень і навантажень, створюваних ударною хвилею.

В статті розглянуто найбільш поширені питання, що виникають на етапі улаштування укрить в будівлях та поза ними. На основі експериментальних досліджень, формули Тейлора та системи нестаціонарних рівнянь Нав'є-Стокса для газу проведено аналіз впливу зовнішніх та внутрішніх факторів на можливий характер динамічного навантаження від ударної хвилі на будівлі споруди та елементи конструкцій, у яких розташовуються укриття.

Метою статті є дослідження впливу динамічних навантажень від ударної хвилі на укриття які розміщені під технічним підвальним приміщенням, що окремо розташовані та елементи входів в укриття.

Результати досліджень параметрів динамічних навантажень показали, що при розташуванні сховищ у підвальних приміщеннях будівель їх стійкість характеризується трьома параметрами: максимальним тиском, часом наростання навантаження до максимуму і ефективним часом дії. Параметри навантажень і закон їх зміни в часі залежать від розміщення споруди відносно поверхні землі і будівлі, сили вибуху і відстані до центру вибуху.

Ключові слова: динамічне навантаження, ударна хвиля, хвиля прориву, тиск ударної хвилі, час наростання навантаження, час дії навантаження, технічне підвальне приміщення, окремо розташовані укриття.

УДК 623.1/.7:007.52 (477)
Коцюруба В.І., Даценко І.П., Дачковський В.О., Черевко Р.М., Полюляк В.М., Іващук О.А., Фурман І.І. **Вплив повітряної ударної хвилі на укриття** // Опір матеріалів і теорія споруд: наук.-тех. збірн. – К.: КНУБА, 2020. – Вип. 105. – С. 133-144.

Розглянуто питання, що виникають на етапі улаштування укрить в будівлях та поза ними. На основі експериментальних досліджень, формули Тейлора та системи нестаціонарних рівнянь Нав'є-Стокса для газу проведено аналіз впливу зовнішніх та внутрішніх факторів на можливий характер динамічного навантаження від ударної хвилі на будівлі споруди та елементи конструкцій, у яких розташовуються укриття.
Табл. 4. Іл. 2. Бібліограф. 12 назв.

UDC 623.1/.7:007.52 (477)
Kotsiuruba V.I., Datsenko I.P., Dachkovsky V.O., Cherevko R.M., Polyulyak V.M, Ivashchuk O.A., Furman I.I. **Influence of air shock wave on shelter** // Strength of Materials and Theory of Structures: Scientific-and-technical collected articles – Kyiv: KNUBA, 2020. – Issue 105. – P. 133-144.

The most common issues are considered in the article that arise during the arrangement of shelter in buildings and outside them. Based on experimental studies, Taylor's formula and the system of non-stationary Navier-Stokes equations for gas, it's conducted an analysis of the influence of external and internal factors on the possible nature of the dynamic load from the shock wave on buildings, structures and structural elements in which shelters are located.
Tabl. 4. Fig. 2. Ref. 12.

Автор (вчена ступень, вчене звання, посада): доктор технічних наук, професор кафедри оперативного та бойового забезпечення Національного університету оборони України імені Івана Черняховського, КОЦЮРУБА Володимир Іванович
Адреса робоча: 03049, м. Київ, Повітрофлотський пр., 28, Національний університет оборони України ім. Івана Черняховського.
Робочий тел.: +38 044 271-08-68, факс +38 044 271-06-97 03680
Мобільний тел.: +38(050) 833-31-90,

E-mail: kotcuru@ukr.net
ORCID ID: http://orcid.org/0000-0001-6565-9576

Автор (вчена ступень, вчене звання, посада): кандидат технічних наук, докторант Національного університету оборони України імені Івана Черняховського, ДАЦЕНКО Іван Петрович
Адреса робоча: 03049, м. Київ, Повітрофлотський проспект, 28, Національний університет оборони України імені Івана Черняховського
Робочий тел.: +38 044 271-08-68, факс +38 044 271-06-97 03680
Мобільний тел.: +38(093) 475-31-67
E-mail: docik_ivan@i.ua
ORCID ID: https://orcid.org/0000-0002-0047-413X

Автор (вчена ступень, вчене звання, посада): кандидат технічних наук, доцент, доцент кафедри технічного забезпечення Національного університету оборони України імені Івана Черняховського, ДАЧКОВСЬКИЙ Володимир Олександрович
Адреса робоча: 03049, м. Київ, Повітрофлотський проспект, 28, Національний університет оборони України імені Івана Черняховського.
Робочий тел.: +38 044 271-06-97, факс +38 044 271-06-97 03680
Мобільний тел.: +38(067) 422-21-75,
E-mail: 1903vova@ukr.net
ORCID ID: http://orcid.org/0000-0003-1480-5021

Автор (вчена ступень, вчене звання, посада): ад'юнкт кафедри оперативного та бойового забезпечення Національного університету оборони України імені Івана Черняховського, ЧЕРЕВКО Руслан Михайлович
Адреса робоча: 03049, м. Київ, Повітрофлотський проспект, 28, Національний університет оборони України імені Івана Черняховського
Робочий тел.: +38 044 271-08-68, факс +38 044 271-06-97 03680
Мобільний тел.: +38(067) 841-04-44
E-mail: cherepruslan2017@gmail.com
ORCID ID: http://orcid.org/0000-0003-0414-0695

Автор (вчена ступень, вчене звання, посада): старший викладач кафедри оперативного та бойового забезпечення Національного університету оборони України імені Івана Черняховського, ПОЛЮЛЯК Василь Миколайович
Адреса робоча: 03049, м. Київ, Повітрофлотський проспект, 28, Національний університет оборони України імені Івана Черняховського
Робочий тел.: +38 044 271-08-68, факс +38 044 271-06-97 03680
Мобільний тел.: +38(097) 933-93-24
E-mail: polulyak1978@gmail.com
ORCID ID: http://orcid.org/0000-0002-6536-5612

Автор (вчена ступень, вчене звання, посада): ад'юнкт кафедри оперативного та бойового забезпечення Національного університету оборони України імені Івана Черняховського, ІВАЩУК Олександр Анатолійович
Адреса робоча: 03049, м. Київ, Повітрофлотський проспект, 28, Національний університет оборони України імені Івана Черняховського
Робочий тел.: +38 044 271-08-68, факс +38 044 271-06-97 03680
Мобільний тел.: +38(097) 584-61-63
E-mail: sashik-ivashchuk84@ukr.net
ORCID ID: http://orcid.org/0000-0002-8189-6472

Автор (вчена ступень, вчене звання, посада): доктор історичних наук, доцент, начальник кафедри історії війн і воєнного мистецтва Національного університету оборони України імені Івана Черняховського, ФУРМАН Ігор Іванович
Адреса робоча:03049, м. Київ, Повітрофлотський проспект, 28, Національний університет оборони України імені Івана Черняховського.
Робочий тел.: +38 044 271-08-68, факс +38 044 271-06-97 03680
Мобільний тел.: +38(096) 364-62-26,
E-mail:fi.2005@ukr.net
ORCID ID: http://orcid.org/0000-0002-3594-5499

UDC 539.3; 624.073.4

STRESS - STRAIN STATE OF A THREE-LAYER CYLINDRICAL SHELL UNDER INTERNAL AXISYMMETRIC PULSE LOAD

V.V. Gaidaichuk,
Doctor in Engineering Science

K.E. Kotenko,
Ph.D. in Engineering Science

Kyiv National University of Construction and Architecture,
31 Povitroflotskyi ave., Kyiv 03680

DOI: 10.32347/2410-2547.2020.105.145-151

The article presents the assessment results of the stress-strain state of a three-layer cylindrical shell with regard to its structural feature, the interrelation of the sheathing thicknesses and physical and mechanical characteristics of the solid polymer filler. Optimization of the structural concept is recommended.

Key words: three-layer cylindrical shell, polymer filler, axisymmetric pulse load, stress-strain state, finite element model.

Introduction. Problem statement

Over the last years, the amount of the layered shells used in different engineering and production areas has considerably increased. Characteristic aspects of the related design solutions were extended. The reliability control of that kind of structures became topical.

Based on the analysis performed, the solution methods for this issue is basically focused on ensuring such conditions at which the maximal stress-strain state values of the shell would not exceed the specified admissible values.

The restricted regulatory and methodological bases, as well as a relatively limited operating experience regarding the layered structures do not allow ensuring their reliability in full. Additional efforts facilitating the optimization of the structures' design and engineering solutions are required: determination of the rational balance of the structural elements' thicknesses, the appropriate selection of the related structural materials etc.

Efficiency effect of these efforts has been tested on the three-layer cylindrical shell under the conditions of rigid clamping of the shell ends. Three types of shells and the different polymer filler's physical and mechanical characteristics have been considered. Fig. 1 shows the shell's flowchart, which was analyzed. The shell's stress-strain state indexes have been investigated provided the following proportions of the shell's inner and outer sheathing thicknesses: $h_1/h_3= 1$, $h_1/h_3= 2$, $h_3/h_1= 2$ (Table 1) and the ratios of physical and mechanical characteristics of the inner base layer and the integral filling material $E_1/E_2 = 500$ and $E_1/E_2 = 50$. Values of physical and mechanical characteristics were as follows: $E_1 = E_3 = 70$ MPa, $E_2 = 0.14$ and 1.4 MPa, $\mu_1 = \mu_3 = 0.3$, $\rho_1 = \rho_3 =$

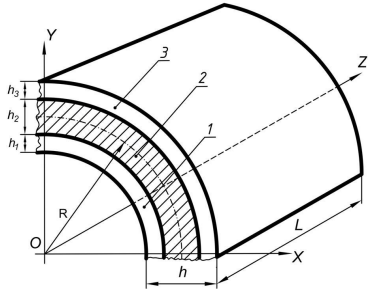

Fig. 1. Design of the three-layer shell: 1 – inner layer; 2 – filling material; 3 – external layer

$2.7*10^{-3}$ kg/m^3. The shell's external diameter was 408 mm and its length L was 250 mm.

Table 1

Geometric parameters of the structural elements of the three-layer shell

h_1, m	h_3, m	h, m	$\frac{R}{h_1}$	$\frac{L}{h_1}$	$\frac{L}{R}$
$1*10^{-3}$	$1*10^{-3}$	$8*10^{-3}$	200	250	1.25
$2*10^{-3}$	$1*10^{-3}$	$9*10^{-3}$	100	125	1.25
$1*10^{-3}$	$2*10^{-3}$	$9*10^{-3}$	200	250	1.25

The shell has been loaded by the axiosymmetrical internal impulse load (Fig. 2). Parameters of the internal load distribution Q were set as follows:

$$Q(t) = A^* \sin\frac{\pi^* t}{T}, \quad (1)$$

where: A – amplitude of the impulsive power load; T – load duration; t – time interval.

The following loading parameters have been accepted: $A = 10^6$ Pa; $T = 50*10^{-6}$ sec.

Provided the preset loading, calculations have been performed for the time interval $0 \le t \le 10T$.

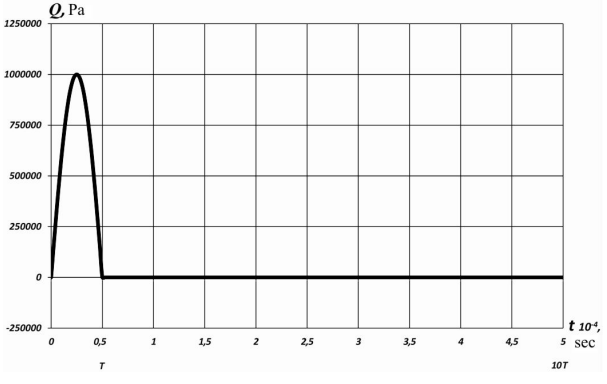

Fig. 2. Distribution of the internal load along the investigated time interval (t)

The stress-strain state indicators were calculated - the values of the displacements and stresses of the shell's bearing layers. Distribution of values of these indicators in the XZ plane has been analyzed at the point of time when the displacement T_y reached its maximal value within the time interval t. Calculations have been performed by the software package Nastran [6]. Values of displacements and stresses have been calculated by applying the direct transient dynamic process algorithm. The time interval was 0.0000025 sec, and

the total number of steps was 200. Choice of the solid finite element type was conditioned by acquiring the more detailed and accurate calculation results. The finite element model (Fig. 3) included 19000 three-dimensional solid finite elements and 20800 nodes.

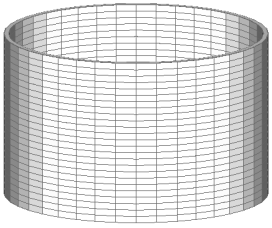

Fig. 3. The finite element model of the three-layer cylindrical shell

Analysis of investigation results

The dependence diagrams of values of the shell T_y maximal displacements in Table 2 (1 – inner layer displacement, 2 – outer layer displacement) demonstrate that the shell with the equal inner and outer sheathing layers' thickness (h_1=h_3) is the most deformation-yieldable.

Table 2

Maximal displacement T_y of the shell sheathings having different layered structure and different physical and mechanical properties of the polymeric filler along the surveyed time interval (t)

Layered structure h_1-h_2-h_3, mm	Correlation between the elasticity modules of the shell inner layer and the polymer filler	
	E_1/E_2 = 500	E_1/E_2 = 50
1-6-1	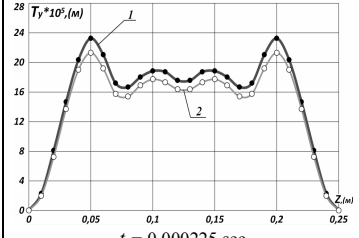 t = 0.000225 sec	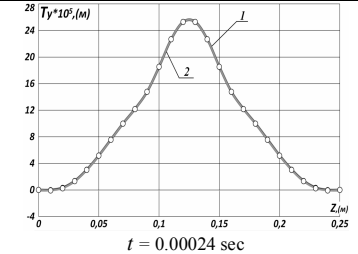 t = 0.00024 sec
2-6-1	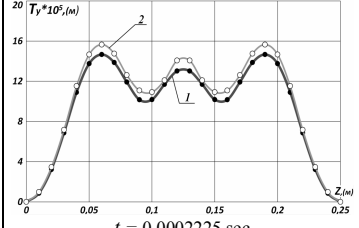 t = 0.0002225 sec	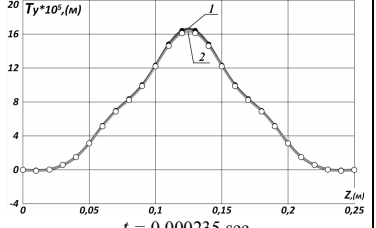 t = 0.000235 sec
1-6-2	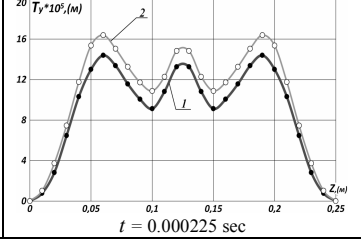 t = 0.000225 sec	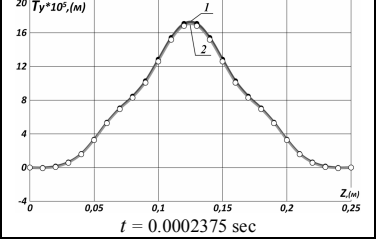 t = 0.0002375 sec

Its displacements (T_y) have the maximal values of 0.000231587 m given E_1/E_2=500 at the moment of time t= 4.5T (0.000225 sec) and T_y = 0.00025297 m given E_1/E_2= 50 at the moment of time t = 4.8T (0.00024 sec). The increased thickness of just a single sheathing increases the aggregate deformational stability of the three-layer shell, whereas the effect can be quite considerable. Thus, in case the internal layer thickness is doubled, the maximal value of displacement T_y decreases by almost 37%. A similar pattern is observed in case of similar thickening of the outer sheathing. This behavior is observed at different ratios of physical and mechanical characteristics of the inner carrying layer and the solid polymer filler E_1/E_2= 500 and E_1/E_2= 50. And the value of the elasticity coefficient of the latter impacts considerably the displacement distribution T_y along the shell length L. Thus, at E_1/E_2= 500 (the polymeric filler elasticity coefficient E_2 = 0.14 MPa) the distribution is quite steady along the entire shell length with the peak values 0.000231587 m at Z_= 0.05 m; Z = 0.2 m. And at E_1/E_2= 50 (E_2 = 1.4 MPa), the displacement distribution T_y decreases considerably and reaches its maximal value of 0.00025297 m in the shell center at Z = 0.125 m and falls dramatically close to its ends. At that, the displacement values of the inner and outer shell sheathings are almost equal.

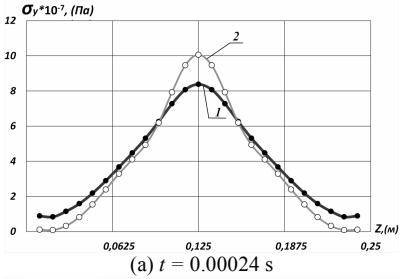

(a) t = 0.00024 s

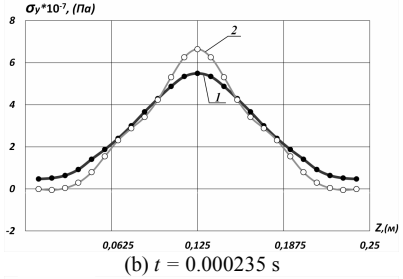

(b) t = 0.000235 s

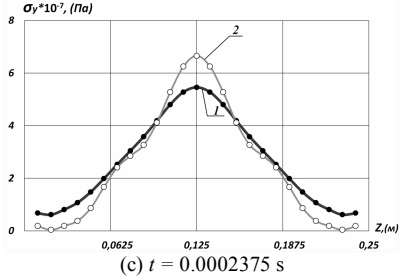

(c) t = 0.0002375 s

Fig. 4. Maximal stress σ_y of the sheathing bearing layers (1 – inner layer, 2 – outer layer) provided the ratio E_1/E_{2m} = 50 and the following layered structure of the sheathing h_1 - h_2 - h_3, mm : (a) 1-6-1; (b) 2-6-1; (c) 1-6-2

Fig. 4 demonstrates the dependency graphs of the stress σ_y maximal values related to the shell bearing layers (provided the correlation E_1/E_2 = 50) over the investigated time interval (t).

As is obvious, the structure with the equal thickness of the shell's layers appeared to be the most strained. The alternate increase of the inner and outer sheathing thicknesses has lowered the maximal strain values by almost 34%.

Comparison of the demonstrated results to the materials of other similar studies and cases [1-5, 7] evidence the integrity of the approach applied and the expediency of its application when defining the stress-strain state of the three-layer

cylindrical sheathings within the time interval $0 \le t \le 10T$, taking into account other predetermined statements.

Conclusions

Consideration was given to the dynamic deformation of the three-layer cylindrical sheathing under the conditions of the time-dependent loads in case of rigid clamping of the shell ends.

Impact of the geometric parameters of the shell's layers with different physical and mechanical properties of the integral filler on the stress-strain state under the axiosymmetrical internal impulse load conditions has been investigated.

Change in proportions between the thickness of the inner and outer sheathings of the shell considerably impacts the shell's stress-strain state and its performance. Increase of the inner sheathing thickness contributes significantly to the increase of the shell's performance.

Numerical results concerning the dynamics of the three-layer structure, which have been obtained by the finite-element method, allow providing the insight into the stress-strain state of the three-layer cylinder-type elastic structure at any point in time within the investigated temporary time interval.

REFERENCES

1. *Lugovoi P.Z., Meish V.F., Meish Yu.A., Orlenko S.P.* Dynamic Design of Compound Shell Structures of Revolution Under Nonstationary Loads //Intern. Appl. Mech. – 2020, 56, № 1 – P. 22–32.
2. *Andreev A.N., Nemirovskii Yu.V.* Mnogosloynye anisotropnye obolochki i plastiny. Izgib, ustoychivost' i kolebaniya (Multilayered anisotropic shells and plates. Bending, stability and vibration). - Novosibirsk, Nauka Publ., 2002. - 288 p. (in Russian).
3. *Bazhenov V.A., Krivenko O.P., Solovei N.A.* Nelineinoe deformirovanie i ustoichivost′ uprugikh obolochek neodnorodnoi struktury: Modeli, metody, algoritmy, maloizuchennye i novye zadachi (Nonlinear deformation and stability of elastic shells of non-uniform structure: Models, methods, algorithms, the insufficiently studied and new problems). - Moskva, Knizhnyi dom «LIBROKOM», 2012. - 336 p.(in Russian).
4. *Golovko, K.G., Lugovoi, P.Z., Meish, V.F.* (2012). Dynamics of inhomogeneous shells under nonstationary loads. Ed. Guz A. N. - Kyiv: Publ. Center. "Kyiv University" (in Russian).
5. *Pikul V.V.* Mekhanika obolochek (Mechanics of shells). - Vladivostok, Dal'nauka, 2009. - 536 p. (in Russian).
6. *Rychkov S.P.* MSC.visualNASTRAN dlia Windows (Modeling of structures in the environment MSC.visual NASTRAN for Windows). - Moscow: NT Press, 2004. - 552 p.
7. *Solomonov Yu.S., Georgievskii V.P., Nedbai A.Ya.,* Prikladnye zadachi mekhaniki kompozitnykh cilindricheskikh obolochek (Applied problems of mechanics of composite cylindrical shells). - Moskva, Fizmatlit, 2014/ - 408 p. (in Russian).

Стаття надійшла 15.09.2020

Гайдайчук В.В., Котенко К.Е.

НАПРУЖЕНО-ДЕФОРМОВАНИЙ СТАН ТРИШАРОВОЇ ЦИЛІНДРИЧНОЇ ОБОЛОНКИ ПРИ ДІЇ ВНУТРІШНЬОГО ОСЕСІМ-МЕТРИЧНИОГО ІМПУЛЬСНОГО НАВАНТАЖЕННЯ

Розглянуто проблему динамічної деформації тришарової циліндричної оболонки при нестаціонарних навантаженнях у разі жорсткого затискання кінців оболонки. У статті представлені результати оцінки напружено-деформованого стану тришарової циліндричної оболонки з урахуванням її структурних особливостей, співвідношення товщини обшивки та

фізико-механічних характеристик цілісного полімерного наповнювача. Розрахунки були проведені програмним комплексом Nastran. Значення переміщень і напружень розраховували за алгоритмом прямого перехідного динамічного процесу. Тривалість кроку інтервалу часу становила 0,0000025 с, а загальна кількість кроків - 200. Вибір типу тривимірного скінченного елемента був обумовлений отриманням більш детальних і точних результатів розрахунку. Модель скінченних елементів включала 19000 тривимірних скінченних елементів і налічувала 20800 вузлів. Досліджено вплив геометричних параметрів шарів оболонки з різними фізико-механічними властивостями цілісного наповнювача на напружено-деформований стан при осесиметричному внутрішньому імпульсному навантаженні. Чисельні результати щодо динаміки тришарової структури, отримані методом скінченних елементів, дозволяють охарактеризувати напружено-деформований стан тришарової пружної структури циліндричного типу в будь-який час досліджуваного інтервалу часу. Рекомендується оптимізація конструкції оболонки. Зміна співвідношення товщини внутрішньої та зовнішньої шарів оболонки суттєво впливає на напружено-деформований стан оболонки та її експлуатаційні характеристики. Збільшення товщини внутрішнього шару оболонки суттєво сприяє збільшенню останньої. Порівняння наведених результатів з матеріалами інших подібних досліджень та позицій, свідчать про об'єктивність зробленого підходу.

Ключові слова: тришарова циліндрична оболонка, полімерний наповнювач, імпульсне осесиметричне навантаження, напружено-деформований стан, скінчено-елементна модель.

Gaidaichuk V. V., Kotenko K. E.

STRESS - STRAIN STATE OF THE THREE-LAYER CYLINDRICAL SHELL UNDER INTERNAL AXISYMMETRIC PULSE LOAD

The problem of dynamic deformation of a three-layer cylindrical shell under non-stationary loads in the case of rigid clamping of the shell ends is considered. The article presents the results of assessing the stress-strain state of a three-layer cylindrical shell, taking into account its structural feature, the ratio of the sheathing thickness and the physical and mechanical characteristics of a one-piece polymer filler. Calculations were performed by software complex Nastran. The values of displacements and stresses were calculated by the algorithm of direct transient dynamic process. The step duration of the time interval was 0.0000025 s, and the total number of steps was 200. The choice of the type of three-dimensional finite element was due to obtaining more detailed and accurate calculation results. The finite element model included 19000 three-dimensional finite elements and numbered 20800 nodes.

The influence of geometrical parameters of shell layers with different physical and mechanical properties of one-piece filler on the stress-strain state under axisymmetric internal impulse load is investigated. Numerical results on the dynamics of the three-layer structure, obtained by the finite element method, allow to characterize the stress-strain state of the three-layer elastic structure of the cylindrical type at any time in the studied time interval. Optimization of the shell design is recommended. Changing the ratio of the thickness of the internal and external shells of the shell significantly affects the stress-strain state of the shell and its performance. Increasing the thickness of the internal layer of the shell significantly contributes to the increase of the latter. Comparison of the given results with materials of other similar researches and positions, testify to objectivity of the made approach.

Key words: three-layer cylindrical shell, polymer filler, pulse axisymmetric load, stress-strain state, finite element model.

Гайдайчук В.В., Котенко К.Э.

НАПРЯЖЕННО-ДЕФОРМИРОВАННОЕ СОСТОЯНИЕ ТРЕХСЛОЙНОЙ ЦИЛИНДРИЧЕСКОЙ ОБОЛОЧКИ ПРИ ДЕЙСТВИИ ВНУТРЕННЕЙ ОСЕСИММЕТРИЧНОЙ ИМПУЛЬСНОЙ НАГРУЗКИ

В статье приведены результаты оценки напряженно-деформированного состояния трехслойной цилиндрической оболочки, учитывающие ее структурную особенность, соотношение толщины обшивки и физико-механические характеристики цельного полимерного наполнителя. Рекомендуется оптимизация конструкционного решения оболочки.

Ключевые слова: трехслойная цилиндрическая оболочка, полимерный наполнитель, импульсная осесимметричная нагрузка, напряженно-деформированное состояние, конечно-элементная модель

УДК 539.3
Гайдайчук В.В., Котенко К.Е. **Напружено-деформований стан тришарової циліндрічної оболонки при внутрішньому осесиметричному імпульсному навантажені //** Опір матеріалів і теорія споруд: наук.-тех. збірн. – К.: КНУБА, 2020. – Вип. 105. – С. 145-151.

У статті наведено результати оцінки напружено-деформованого стану тришарової циліндричної оболонки, враховуючі її структурну особливість, співвідношення товщини обшивки і фізико-механічні характеристики цільного полімерного наповнювача. Рекомендується оптимізація конструкційного рішення оболонки.
Табл. 2. Іл. 4. Бібліогр. 7 назв.

UDC 539.3
Gaidaichuk V.V., Kotenko K.E. **Stress-strain state of a three-layer cylindrical shell under internal axisymmetric pulse load //** Strength of Materials and Theory of Structures: Scientific-and-technical collected articles – Kyiv: KNUBA, 2020. – Issue 105. – P. 145-151.

The article presents the results of assessing the stress-strain state of a three-layer cylindrical shell, taking into account its structural feature, the ratio of the sheathing thickness and the physical and mechanical characteristics of a one-piece polymer filler. Optimization of the shell design is recommended.
Tabl. 2. Fig. 4. Ref. 7.

УДК 539.3
Гайдайчук В.В., Котенко К.Э. **Напряженно-деформированное состояние трехслойной цилиндрической оболочки при действии внутренней осесимметричной импульсной нагрузки //** Сопротивление материалов и теория сооружений. – 2020. – Вып. 105. – С. 145-151.

В статье приведены результаты оценки напряженно-деформированного состояния трехслойной цилиндрической оболочки, учитывающие ее структурную особенность, соотношение толщины обшивки и физико-механические характеристики цельного полимерного наполнителя. Рекомендуется оптимизация конструкционного решения оболочки.
Табл. 2. Ил. 4. Библиогр. 7 назв.

Автор (вчена ступень, вчене звання, посада)*:* доктор технічних наук, професор, завідувач кафедри теоретичної механіки Київського національного університету будівництва і архітектури *ГАЙДАЙЧУК Віктор Васильович*.
Адреса робоча: *03680 Україна, т. Київ, проспект Повітрофлотський, 31, к. 433, Київський національний університет будівництва і архітектури, кафедра теоретичної механіки, ГАЙДАЙЧУКУ Віктору Васильовичу.*
Роб. тел. *+380 (44) 241-55-72*
Моб. тел. *+380 (97) 542-94-27*
E-mail: viktor_gaydaychuk@bigmir.net
ORCID ID: http://orcid.org/0000-0003-2059-7433

Автор (вчена ступень, вчене звання, посада): кандидат технічних наук, доцент кафедри теоретичної механіки Київського національного університету будівництва і архітектури *КОТЕНКО Костянтин Едуардович*.
Адреса робоча: *03680 Україна, т. Київ, проспект Повітрофлотський, 31, к. 433, Київський національний університет будівництва і архітектури, кафедра теоретичної механіки, КОТЕНКУ Костянтину Едуардовичу.*
Роб. тел. *+380 (44) 241-55-72*
Моб. тел. *+380 (94) 855-09-37*
E-mail: 1969box@mail.ru
ORCID ID: https://orcid.org/0000-0002-3181-3819

UDC 624.014

LIMIT STATE THEORETICAL AND EXPERIMENTAL INVESTIGATION OF CORRUGATED SINE-WEB UNDER PATCHLOADING

S.I. Bilyk,
Doctor of Technical Sciences, professor

L.I. Lavrinenko,
Candidate of Technical Sciences, assistant professor

O.O. Nilov,
Candidate of Technical Sciences, professor

T.O. Nilova,
Candidate of Technical Sciences, assistant professor

I.Y. Semchuk,
master

Kyiv National University of Construction and Architecture
Povitroflotskyave., 31, Kyiv, Ukraine 03680

DOI: 10.32347/2410-2547.2020.105.152-164

It's presented results of the behavior and limit state investigation of thin-webbed I-beams with transversal corrugations under patch loading action. Numerical analyses via finite element method (FEM) on physical and mathematical models created according to profiles range of company Zeman and experimental investigations on two physical models with similar to them parameters and steel were executed.

At numerical investigations it was ascertained that the loss of web stability can occur both as the local form of corrugation buckling or the general buckling form for corrugations with the greater height or thickness. As the investigations result it is proved that normal stresses in the beam web under local loading reach ultimate strength of the web steel, while significant plastic strains occur in it and the bearing capacity is lost.

Keywords: corrugated web, web local stability, patch loading, buckling form, effect of patch loading parameters.

Introduction

The concept of beams with thin transverse corrugated webs to improve their stability appeared in the 1930s. Nevertheless, the problem of web-flange conjunction was resolved only in the last years with help of the modern ways of automated fabrication of structures and their welding. Nowadays, such beams are being in demand in Ukraine and through the entire world.

The current paper researches the limit state onset conditions of thin-web I-beams with transversal corrugations under patch loading.

1. Web stability analysis

A numerical analytic method for calculation of local stresses in steel beam corrugated web at the level, where it joins the flange, under patch loading, is presented in [1]. The corrugated beam section stresses σ_{loc} should not be more

than steel yield strength f_y according to [2, 3], that is $\sigma_{loc} \leq f_y$. The condition of non-occurrence plastic stresses was investigated in the papers [4, 5, 6, 7].

We should note, that all previously mentioned articles do not account for flange bending rigidity and shear force between flange and web, length of patch loading distribution also. Therefore, it means that results, obtained via proposed methodic by there, do not have enough scientific justification, and do not match with experimental testing, so they should be refined.

According to Broude B.M. [8], web bearing capacity does not run out reaching steel yield strength and even ultimate strength. At the same time at the level of the web and flange connection the web is crumpled.

Given article considers two types of loading application on top compression beam flange. The first type (fig. 1(a)) – the loading is applied through a purlin, welded to transversally located angles. The second (fig. 1(b)) – the loading is applied through a transversal element in the form of a strip.

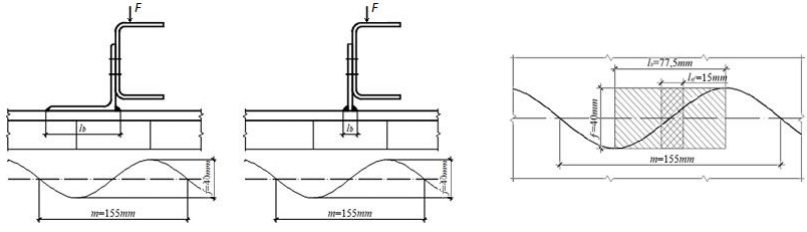

(a) (b) (c)

Fig. 1. The supporting nodes of purlins on the beam with corrugated web:
(a) through angles; (b) through transversal elements; (c) load action regions

The flange width (l_b) usually is less or equal to 75…80 mm. Thus, in this paper is considered to take flange width as half of sine wave-length $\frac{m}{2} = 77.5$ mm (fig. 1(a)), and vertical element thickness as $l_b = 15$ mm (fig. 1(b), (c)).

Below is presented the results of numerical investigations via the finite elements method (FEM) of corrugated beam web limit state due to local stability loss under patch loading, distributed on the region, shown on fig. 1(c).

Local stability analysis was performed on physical and mathematical models (PMM), which had been created according to standard corrugated profiles range of company Zeman. Used profile models WTA, WTB and WTC had such geometrical parameters:

- web thickness $t_w = [2.0; 2.5; 3.0]$ mm respectively;
- web height $h_w = [500; 750; 1000; 1250; 1500]$ mm;
- flange width $b_f = 200$ mm;
- flange thickness $t_f = 8$ mm;
- f – wave amplitude with the projection length m (fig. 1)
- model length $L = 12m = 1860$ mm.

Beams were modeled by finite elements of thin shell. The mark of steel was E335 ($f_y = 305$ MPa).

The stability calculations were performed in three stages. The 1st stage included critical stress calculations with the assumption of steel elastic behavior and geometric linearity of beam models by FEM.

In the 2nd stage, the stability analysis accounted for geometric non-linear behavior of the model and elastic behavior of steel. The results of calculations showed insignificant effect of geometric non-linear behavior account in comparison with results from previous stage (the discrepancy is less than 0.3%).

According to the 1st stage results analysis it was arranged, that critical stresses depends on web thickness,t_w, and loading distribution region length, l_b.So critical stresses increase simultaneously with the web thickness, t_w, and decrease, when l_b rises, and do not depend on the web height (table 1).

In addition, it was found two web buckling forms (fig. 2):

- Local (L) – the buckling locates on the top part of one corrugation.
- General (G) − the buckling distributes through the height of one or more corrugations.

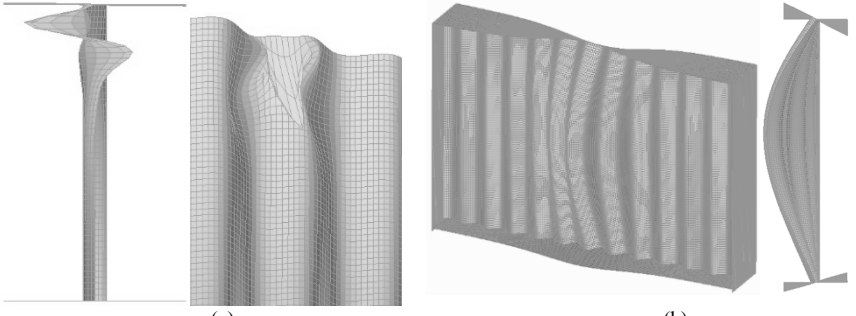

(a) (b)

Fig. 2. (a) local buckling of corrugation; (b) general buckling of corrugation

In the local form of buckling the deformation region does not depend on the web height and thickness and starts directly under the compressed flange. The shape of this region looks crumpled (fig. 2(a)).

The form of buckling (local or general) depends on the web's slenderness ratio$\left(\lambda_w = \frac{h_w}{t_w}\right)$ (table 1) and the degree of its fixation from rotational displacements by flanges. The greater the web's slenderness ratio and less the degree of the web's edges fixation from rotational displacements by flanges the smaller the probability of general buckling form occurrence.

It is reasonable to calculate critical stresses in PMM with an accounting of plastic strains by analytic method basing on the results, got according to the linear theory and FEM.

The main parameters for webs steel is elastic module E, yieldstrengthσ_y, and proportional elastic limit $\sigma_e = 0.8\sigma_y$. Hereinafter let us use such proportion $\tau = \frac{E_t}{E}$, where E_t – tangential module, and write it in the next formula [9]:

$$\tau = \frac{(\sigma_y - \sigma_{cr})\sigma_{cr}}{(\sigma_y - \sigma_e)\sigma_e}. \quad (1)$$

Let us use the formula (1) for critical stresses calculation according to analytic method ${\sigma_{cr}}^a$ with plastic strains accounting [10]:

$${\sigma_{cr}}^a = \frac{D f_y}{1 + D}, \quad (2)$$

where $D = \frac{(\sigma_{cr})^2}{0.16\,\sigma_y^2}$; σ_{cr}– critical stresses, calculated by FEM with accounting elastic strains.

The critical stresses ${\sigma_{cr}}^a$ values got via formula (2) are shown in table 1. As we can see, the results are insignificantly different with steel yield strength value f_y = 305 MPa(tolerance is less than 0.36%). At the same time, the critical stress σ_{cr} obtained via FEM for all models are exactly equal to f_y = 305 MPa.

Table 1

Critical stresses of local buckling in models'webs

Model	h_w, mm	l_b = 15 mm			l_b = 77,5 mm		
		Local buckling form	σ_{cr}, MPa	${\sigma_{cr}}^a$, MPa	Local buckling form	σ_{cr}, MPa	${\sigma_{cr}}^a$, MPa
WTA	500	L	2566.57	304.31	L	2042.87	303.92
	750	L	2561.30	304.31	L	2038.53	303.91
	1000	L	2575.69	304.32	L	2046.19	303.92
	1250	L	2583.86	304.32	L	2053.54	303.93
	1500	L	2588.52	304.32	L	2057.54	303.93
WTB	500	L	3720.48	304.67	L	2889.66	304.34
	750	L	3716.97	304.67	L	2879.52	304.45
	1000	L	3727.51	304.67	L	2886.38	304.46
	1250	L	3735.69	304.67	L	2893.18	304.46
	1500	G+L	3737.06	304.67	G	2485.89	304.27
WTC	500	L	5036.89	304.82	L	3831.51	304.69
	750	L	5029.48	304.83	L	3813.15	304.67
	1000	L	5040.54	304.82	L	3819.13	304.67
	1250	G+L	5034.86	304.82	G	3233.17	304.57
	1500	G	4159.87	304.74	G	2621.63	304.34

According to table results we can make conclusion, that beams with corrugated webs (by profiles range of company Zeman) will be ensured from local buckling, when web stresses by design loads are less than yield strength f_y. Such beams don't demand to install stiffening ribs.

2. Investigation of the corrugated web actual behavior

The web stability calculation by proposed above analytic method is comfortable in use, but does not an opportunity to determine a real boundary

bearing capacity under local loading action. Therefore, it is important to investigate web behavior in case of its stresses significant exceeding the yield strength f_y and nearing to the ultimate strength f_u. In addition, the way of web failure should be researched.

The main purpose of the 3rd stage was investigation of real web behavior under local loading action, cross-section geometric and mechanical properties influence, and loading application schemas. As a result, it were performed numerical (on four models PMM) and experimental analysis (on two beam samples PM).

All beams were designed according to profiles range of company Zeman (table 2) with such geometric characteristics (fig. 3):

- Flange – $b_f \times t_f = 200 \times 8$ mm;
- Span – $L = 1860$ mm.

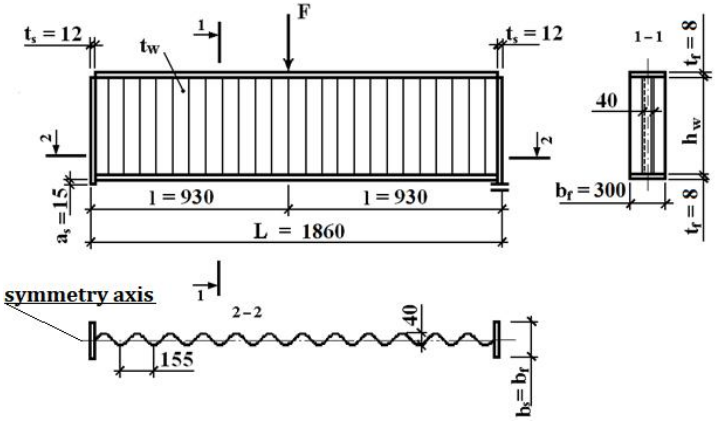

Fig. 3. Analyzed beams models schema

Table 2

	Model			
	PMM-1 / PM-1	PMM-2 / PM-2	PM-3	PM-4
h_w, mm	500	500	1000	1000
t_w, mm	3.0	3.0	2.0	3.0
l_b, mm	15.0	77.5	77.5	77.5
$F_{i,cal}$, t	14.24	20.81	14.54	20.39
$F_{i,exp}$, t	16.0	20.6	–	–

To avoid bending moment influence on bearing capacity all beams were designed with a small span.

All geometric parameters of experimented beam models (PM-1, PM-2) match with suitable analytic physical and mathematical beam models (PMM-1, PMM-2). All beams properties you can find in table 2.

Web flexibility and height influence on bearing capacity were determined via numerical investigations on additional models PMM-3 and PMM-4. Explored models had such properties:

- web thickness $t_w = [2.0; 3.0]$ mm respectively;
- web height $h_w = 1000$ mm.

Both models were loaded across the region with the length $l_b = 77.5$ mm. The research results were used for calculation of theoretical bearing capacity for the models PMM-3 and PMM-4.

The mechanical characteristics of the models' steel were got from standard samples:

- For the web – the yield strength was $\sigma_{yw} = 296.5$ MPa, the ultimate strength $\sigma_{uw} = 441.8$ MPa (sample-1);
- For the flange – the yield strength was $\sigma_{yf} = 293.9$ MPa, the ultimate strength $\sigma_{uf} = 449.2$ MPa (sample-2).

Steel behavior diagram was adopted by experimental probation of the sample-1 (fig. 4). The mechanical characteristics for analytical beam models (PMM) were taken from experimental beam models (PM).

One of the supports had the possibility to move in a horizontal direction (rolling support). Models' top flanges were fastened from horizontal movements. The sections, loaded by vertical loading, were fastened in the same way to ensure beam behavior with flat bending condition.

All PMM's were loaded in the middle of its length (fig. 1, *c*) while numerical investigation. The loading was continuously increasing with the step t (fig. 5) until bearing capacity failure. All maximum bearing capacity values of models $F_{i,cal}$, based on numerical investigations results, are shown on table 2.

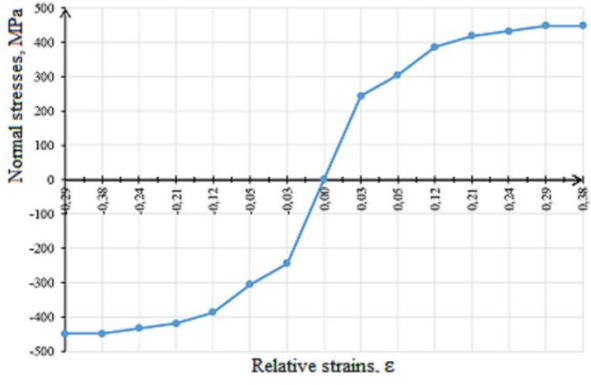

Fig. 4. Experimental diagram of steel behavior

According to normal stress to step-loading dependence diagram (fig. 5) stresses value only depends on loading distribution length l_b (curves 1, 3)and web thickness t_w (curves 2, 4) but do not depends on web height h_w (curves 3, 4).

The dependency of normal local stresses (by the loading action axis at the level of the web and flange connection) to the value of loading is shown in fig. 6(a), (b). The failure did not happen after reaching the ultimate strength f_u according to diagrams. Therefore, the web continued taking increased loading. It can be explained by that fact, that web takes stresses at the level of the web and flange connection alongside region with the length $S = 26$ mm. Moreover, these stresses do not depend on loading distribution length $l_b = 15.5$ mm or 77.5 mm. For both cases, maximum stresses are reached alongside the axis of force F application, and they decrease with deviation from this axis. After having reached the ultimate strength of the web steel σ_{uw} maximum stresses stopped increasing, but stresses, at some distance from the force F action axis, started increasing (fig. 6 (a), (b)). Therefore, the loading force reaches its maximum value.

After supporting length l_b having changed from 77.5 mm to 15 mm $\left(\frac{77.5}{15} \approx 5.17\right)$, the crashing force F decreased from 20.81 t to 14.24 t (in 1.46 times). It means that critical stresses increase when supporting length l_b decreases. That is why it is recommended to select supporting length l_b according to feasibility study.

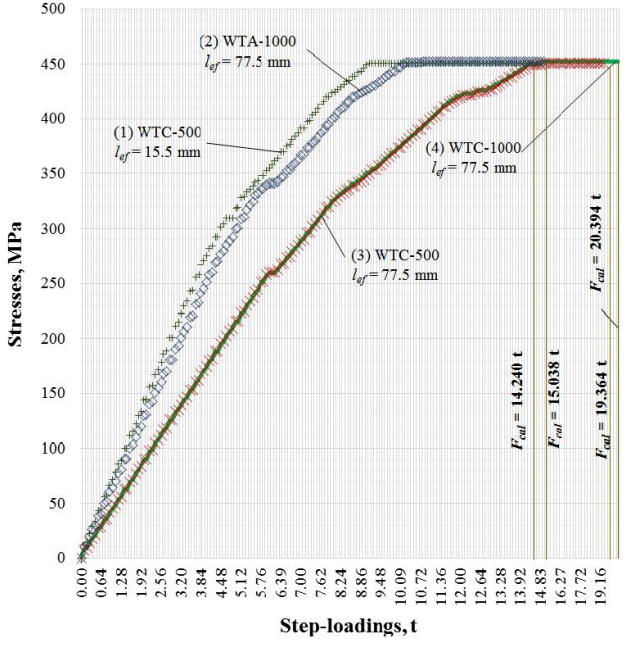

Fig. 5. Stress to step-loading dependency diagram

Figure 7 shows the mosaics that demonstrate the changing of web stress condition under increasing patch loading with values of loading distribution length ($l_b = 77.55$ mm and 15 mm respectively). Besides, it reflects the way of web stress change with different loadings and loading distribution lengths l_b.

Figure 7 (a) shows the stresses distribution in the section with maximum stress 398 MPa, which reached by force ($F = 10.9$ t and 7.2 t respectively). Figures 7, *b* and *c,* show the stresses distribution in the section with almost the same stresses of yield line start and end (453 MPa i 451 MPa respectively), reached by force ($F = 14.8$ t and 20.81 t respectively for *b*, and $F = 9.12$ *t* and 14.24 *t* for *c*).

According to numerical investigation results, bearing capacity (calculated by standard codes [2, 3]) failure, caused by patch loading, always happens earlier than web buckling, regardless of cross-section geometric parameters of corrugated beam.

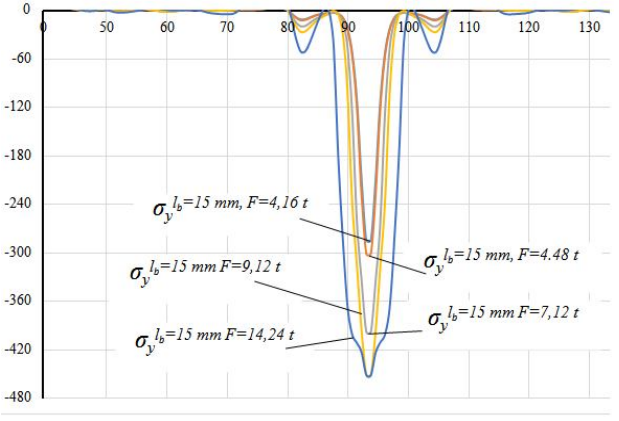

(a) $l_b = 15$ mm

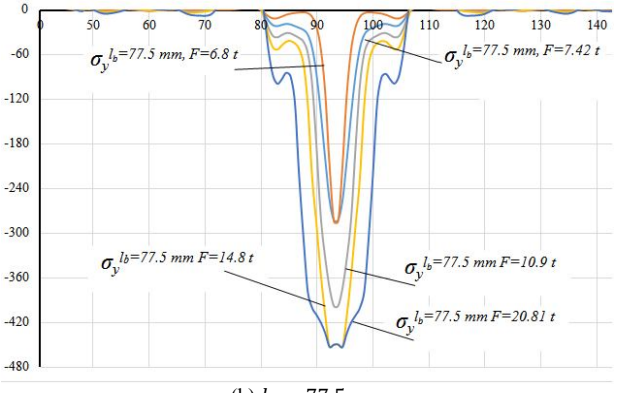

(b) $l_b = 77.5$ mm

Fig. 6. Local stresses distribution diagrams with different loadings

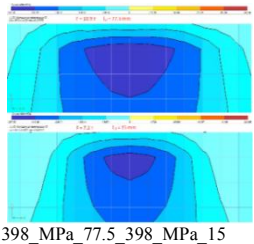
398_MPa_77.5_398_MPa_15

(a)

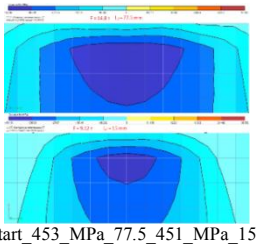
start_453_MPa_77.5_451_MPa_15

(b)

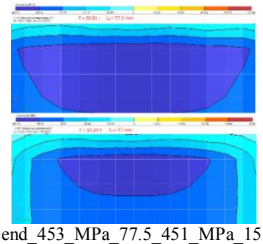
end_453_MPa_77.5_451_MPa_15

(c)

Fig. 7. Stresses change mosaic with different loadings

The PM experimental investigation was performed in the same way to PMM numerical research. The loading was applied in the middle of beam's length by two jack-screws $Q = 2 \times 25\ t$, and was controlled by mechanical dynamometer. Reactions and deflections were noted and matched while the beam was being loaded for accurate beam behavior observing. The beams had been previously loaded until 20 kN and unloaded after some endurance for work control of jack-screws and measurement devices. Beams deflections were controlled by time type deflectometer, because of insignificant beam span value and its ratio to beam height$\left(\frac{L}{H} = \frac{1.68}{0.5} = 3.33\right)$.

The flanges were loaded through the steel filler plate with thickness 15 mm and width 300 mm (the same to flanges). The loading was distributed on the length $l_b = 15$ mm (for PM-1), and$l_b = 77.5$ mm (for PM-2).

(a) $l_b = 15$ mm

(b) $l_b = 77.5$ mm

Fig. 8. The local buckling of corrugations

After having endurance, the loading was the same as in numerical investigation before bearing capacity failure with the same step (fig. 5). The limit loading value was established according to the maximum indicator of the mechanical dynamometer (table 2). The local buckling was occurring at the moment of bearing capacity failure at the level of the web and flange connection on the region, limited by corrugation half-wave length. The shape of this region looks crumpled (fig. 8).

Conclusions

According to theoretical and experimental investigations, the web bearing capacity failure and its crumpling happen, when local critical normal stresses σ_{cr} in the web (at the level of its connection with the flange under patch-loading) reach ultimate strength of the web steel σ_{uw}.

The bearing capacity of I-girders with a transversally corrugated thin web (from Zeman's profile range), under patch loading with every distribution length will be always ensured from failure if normal local stresses in the web do not exceed the steel yield strength f_y.

REFERENCES

1. *Semchuk I.Y., Nilova T.O.* Stress-strain state of beam corrugated web under patch loading // Opir Materialiv I Teoria Sporud - Strength of Materials and Theory of Structures: Scientific-and-technical collected articles – Kyiv: KNUBA, 2019. – Issue 102. – P. 53-61.
2. Eurocode No. 3, Design of Steel Structures. Part 1.5. Plated structural elements (EN 1993-1-5, 2008).
3. DBN V.2.6-198:2015 «Stalevi konstruktsiï. Normi proektuvannya». Kiïv 2015.– 297 s.[State building codes B.2.6-198:2015 «Steel structures. Design standards»Kiïv 2015.– 297 p. In Ukranian]
4. *Siokola W.*, Wellstegträger. Herstellung und Anwendung von Trägernmitprofiliertem Steg // Stahlbau 9/1997. — P. 596 — 605.
5. *Ramberger G*., Gutachtenüber die Berechnung von Geschweissten I-TrägernMitStegenAusGewelltenBlechen // O. Univ., Wien 1989 — not published.
6. *Pasternak H*., *Brańka P*., Tragverhalten von WellstegträgernunterlokalerLasteinleitung // Bauingenieur 5/1999. — P. 219 — 224.
7. *Kuchta K.R*., Nośności Sztywność Blachownic o Falistychśrodnikach // Politechnika Krakowska. — Kraków 2004.
8. *Broude, B.M.,*Raspriedielienie Sosriedotocziennowo Dawlienia W Mietaliczeskich Bałkach // Strojizdat, Moskwa – Leningrad 1950. [Distribution of concentrated stress in metal beams // Strojizdat, Moscow – Leningrad 1950. In Russian]
9. *Bleich F.,* Buckling strength of metal structures // NY, 1952 (v perevode: Bleyh F., Ustoychivost metallicheskih konstruktsiy) — M.: Fizmatgiz, 1959. — 544 p. [In Russian]
10. *Nilova T.O.* Mitsnist i stiykist ramnih elementiv z poperechno-gofrovanoyu sinusoidnoyu stinkoyu. Disertatsiya na zdobuttya naukovogo stupenya kandidata tehnichnih nauk, Kiïv 2013. [Strength and stability of the frame elements with transversely corrugated sinusoidal web // Thesis to obtain the scientific degree of Candidate of Technical Sciences, Kiïv 2013. In Ukrainian]

Стаття надійшла 11.08.2020

Білик С.І., Лавриненко Л.І., Нілов О.О., Нілова Т.О., Семчук І.Ю.

ТЕОРЕТИЧНЕ І ЕКСПЕРИМЕНТАЛЬНЕ ДОСЛІДЖЕННЯ ГРАНИЧНОГО СТАНУ ПОПЕРЕЧНО-ГОФРОВАНОЇ СИНУСОЇДНОЇ СТІНКИПРИ ДІЇ ЛОКАЛЬНОГО НАВАНТАЖЕННЯ

У статті досліджується робота і граничний стан тонкостінних двотаврових балок з поперечними гофрами при локальному навантаженні. Аналіз місцевої стійкості стінки виконувався на моделях балок, які були створені відповідно до сортаменту гофрованих профілів фірми Zeman. Проводилися чисельні дослідження на фізико-математичних і експериментальні на двох фізичних моделях, подібних за параметрами і матеріалом.

Аналіз критичних напружень виконувався за методом скінченних елементів в припущенні пружної роботи сталі з врахуванням як геометричної лінійності роботи моделей, так і їх нелінійності. Розрахунок показав, що при умові пружної роботи сталі врахування геометричної нелінійності практично не впливає на результати.

Встановлено, що втрата стійкості стінки може відбуватися як за місцевою формою випинання, так і за загальною формою при більших товщинах стінки. При збільшенні довжини спирання прогонів на балку величина критичного навантаження збільшувалася, а критичні напруження в стінці зменшувалися. При цьому для всіх моделей величина критичних напружень практично не відрізнялася від межі текучості сталі f_y = 305 МПа (відхилення не більше ніж на 0,36%).

Представлені результати чисельних та експериментальних досліджень роботи гофрованої стінки при локальному навантаженні. Встановлено, що після досягнення теоретичними і експериментальними нормальними напруженнями в стінці величини межі міцності сталі несуча здатність моделі не втрачається, а руйнівне навантаження збільшується на 30-35% внаслідок перерозподілу напружень в стінці по довжині.

Результати розрахунків і експериментів свідчать, що при виконанні вимоги міцності, зазначеної Eurocode No. 3, несуча здатність гофрованої стінки буде завжди забезпеченою.

Ключові слова: гофрована стінка, місцева стійкість стінок, локальне навантаження, форма випинання, вплив параметрів навантаження.

Bilyk S.I., Lavrinenko L.I., Nilov O.O., Nilova T.O., Semchuk I.Y.

STRESS STRAIN STATE THEORETICAL AND EXPERIMENTAL INVESTIGATION OF CORRUGATED SINE-WEB UNDER PATCH LOADING

The article researches the behavior and limit state of thin-web bedI-beams with transversal corrugations under patch loading action. Web local stability analysis was performed on beam models, which had been created according to standard corrugated profiles range of company Zeman. Numerical analyses on physical and mathematical models and experimental investigations on two physical models with similar to them parameters and steel were executed.

The critical stress analyses were carried out via the finite elements method (FEM) with the assumption of steel elastic behavior accounting both geometric linearity and geometric nonlinearity. The calculation shows that taking into account the elastic behavior of steel the geometric nonlinearity has insignificant effect on the results.

Two buckling forms (local and general for thicker webs) were ascertained while investigating the stability loss of web. The critical loading's value increases with increasing of purlin's supporting length, but the web's critical stress decreases. But for all models critical stresses value is almost similar (tolerance is less than 0.36%) to steel yield strength f_y= 305MPa.

The numerical and experimental investigation results of corrugated web behavior under patch loading are presented. Established that model's bearing capacity does not fail after reaching by theoretical and experimental normal stresses the ultimate strength of the web steel, and ultimate loading increases by 35 – 40 % due to the stress's redistribution in the web along the length.

The results of calculations and experiments certificates that when the strength requirement specified by Eurocode No. 3 is met the corrugated web's bearing capacity will be alwaysensured.

Key words: corrugated web, web local stability, patch loading, buckling form, effect of patch loading parameters.

Билык С.И., Лавриненко Л.И., Нилов А.А.,Нилова Т.А.,Семчук И.Ю.

ТЕОРЕТИЧЕСКОЕ И ЭКСПЕРИМЕНТАЛЬНОЕ ИССЛЕДОВАНИЕ ПРЕДЕЛЬНОГО СОСТОЯНИЯ ПОПЕРЕЧНО-ГОФРИРОВАННОЙ СИНУСОИДНОЙ СТЕНКИ ПРИ ДЕЙСТВИИ ЛОКАЛЬНОГО НАГРУЖЕНИЯ

Представлены результаты исследования работы и предельного состояния гофрированной синусоидальной стенки балки при действии локальной нагрузки. Доказано, что при действии локального нагружения нормальные напряжения в стенке балки достигают предела прочности стали стенки, при этом в ней возникают значительные пластические деформации и несущая способность исчерпывается.

Ключевые слова: гофрированная стенка, местная устойчивость стенок, локальное нагружение, форма выпучивания, влияние параметров нагружения.

УДК 624.014

Білик С.І., Лавриненко Л.І., Нілов О.О., Нілова Т.О., Семчук І.Ю. **Теоретичне і експериментальне дослідження граничного стану гофрованої синусоїдної стінки при дії локального навантаження** // Опір матеріалів і еоріяспоруд: наук.-тех. збірн. – К.: КНУБА, 2020. – Вип. 105. – С. 152-164. – Англ.

Наведені результати теоретичного і експериментального дослідження роботи і граничного стану гофрованої синусоидальної стінки при дії локального навантаження. Доведено, що нормальні напруження в стінці балки при локальному навантаженні досягають межі міцності сталі стінки, при цьому в ній виникають значні пластичні деформації і несуча здатність втрачається.

Табл. 2. Іл. 8. Бібліогр. 10 назв.

UDC624.014

Bilyk S.I., Lavrinenko L.I., Nilov O.O., Nilova T.O., Semchuk I.Y. **Limit state theoretical and experimental investigation of corrugated sine-web under patch loading** // Strength of Materials and Theory of Structures: Scientific-and-technical collected articles. – K.: KNUCA, 2020. – Issue 105. – P. 152-164.

Results obtained via limit state theoretical and experimental investigation of corrugated sine-web under patch loading action are presented. It is proved that normal stresses in the beam web under patch loading reach ultimate strength of the web steel, while significant plastic strains occur in it and the bearing capacity is lost.

Table 2. Fig. 8. Ref. 10.

УДК 624.014

Билык С.И., Лавриненко Л.И., Нилов А.А., Нилова Т.А., Семчук И.Ю. **Теоретическое и экспериментальное исследование предельного состояния гофрированной синусоидальной стенки при действии локального нагружения** // Опір матеріалів і теорія споруд: наук.-тех. збірн. – К.: КНУБА, 2020. – Вип. 105. – С. 152-164. – Англ.

Представлены результаты теоретического и экспериментального исследования работы и предельного состояния гофрированной синусоидальной стенки при действии локального нагружения. Доказано, что при действии локального нагружения нормальные напряжения в стенке балки достигают предела прочности стали стенки, при этом в ней возникают значительные пластические деформации и несущая способность исчерпывается.

Табл. 2. Ил. 8. Библиогр. 10 назв.

Автор (науковий ступінь, вчене звання, посада): *доктор технічних наук, професор, завідувач кафедри металевих та дерев'яних конструкцій КНУБА Білик Сергій Іванович.*
Адреса робоча: *03680 Україна, м. Київ, Повітрофлотський проспект 31, Київський національний університет будівництва і архітектури, кафедра металевих і дерев'яних конструкцій.*
Робочий тел.: +38(044) 241-55-56
Мобільний тел.: +38(067) 588-8-295
Імейл: *vartist@ukr.net*
ORCID ID: https://orcid.org/0000-0001-8783-5892

Автор (науковий ступінь, вчене звання, посада): *кандидат технічних наук, доцент кафедри металевих та дерев'яних конструкцій Лавриненко Людмила Іванівна.*
Адреса робоча: *03680 Україна, м. Київ, Повітрофлотський проспект 31, Київський національний університет будівництва і архітектури, кафедра металевих і дерев'яних конструкцій.*
Робочий тел.: +38(044) 241-55-56
Мобільний тел.: +38(067) 777-15-36
Імейл: *ludmila.lavrinenko@gmail.com*
ORCID ID: https://orsid.org/0000-0001-5601-0943

Автор (вчена ступень, вчене звання, посада): *кандидат технічних наук, професор кафедри металевих і дерев'яних конструкцій КНУБА Нілов Олексій Олександрович.*
Адреса робоча: *03680 Україна, м. Київ, Повітрофлотський проспект 31, Київський національний університет будівництва і архітектури, кафедра металевих і дерев'яних конструкцій.*
Робочий тел.Orsid.org/0000-0001-5601-0943
Мобільний тел.:*+38(067) 774-12-72*
Імейл: *onilmk@gmail.com*
ORCIDID: https://orcid.org/0000-0003-3300-1002

Автор (вчена ступень, вчене звання, посада): *кандидат технічних наук, доцент кафедри металевих і дерев'яних конструкцій КНУБА Нілова Тетяна Олексіївна.*
Адреса робоча: *03680 Україна, м. Київ, Повітрофлотський проспект 31, Київський національний університет будівництва і архітектури, кафедра металевих і дерев'яних конструкцій.*
Робочий тел.:*+38(044) 248-31-17*
Мобільний тел.:*+38(068) 128-30-62*
Імейл: *tatic70@gmail.com*
ORCIDID: https://orcid.org/0000-0001-9282-8136

Автор (вчена ступень, вчене звання, посада): *магістр Семчук Ігор Юрійович.*
Адреса робоча: *03680 Україна, м. Київ, Повітрофлотський проспект 31, Київський національний університет будівництва і архітектури, кафедра металевих і дерев'яних конструкцій.*
Робочий тел.:*+38(044) 248-31-17*
Мобільний тел.:*+38(096) 201-57-68*
Імейл: *semchuk7@ukr.net*

UDC 539.3

STRESS-STRAIN STATE OF THICK-WALLED ANISOTROPIC CYLINDRICAL SHELLS UNDER THERMAL POWER LOAD, PROTECTED BY THE FUNCTIONALLY GRADED MATERIAL

M.P. Semenyuk[1],
Dr. Eng.

V.M. Trach[2],
Dr. Eng.

A.V.Podvornyi[2],
PhD (Engineering)

[1]*Institute of Mechanics of the National Academy of Sciences of Ukraine, Kyiv, Petra Nesterova str.,3, 02000*

[2]*National University of Water and Environmental Engineering, Rivne, Soborna str., 11, 33028*

DOI: 10.32347/2410-2547.2020.105.165-178

In the article the stress-strain state of thick-walled structurally anisotropic composite cylindrical shells under thermal power load, which are protected by a functionally graded material, are analysed. Based on the interrelations of the spatial theory of elasticity, a system of inhomogeneous differential equations in three-dimensional formulation, which describes the stress-strain state of thick-walled anisotropic cylindrical shells, was obtained. To reduce the dimensionality of this system, the Bubnov-Galerkin analytical method was used. Thus, the obtained one-dimensional system of twelve equations of normal Cauchy form was implemented using the numerical method of discrete orthogonalization. To represent the possibilities of the proposed approach, there were used stress-strain states of two, four and five-layered anisotropic cylindrical shells of fibrous composites, protected from temperature by a layer of transversely isotropic functionally graded material.

Key words: thick-walled anisotropic cylindrical shell, stress-strain state, three-dimensional formulation, functionally graded material.

1. Introduction

Thin-walled structures made of composite materials are widely used in a variety of elements of up-to-date equipment. For example, the aerospace and rocket industries require the use of shells made of lightweight, high-strength composite materials. Unfortunately, traditional composite materials are not always able to be used in high temperatures, because their load-bearing capacity can be significantly reduced. Heat-resistant ceramics can be used to protect thin-walled composites from temperatures, but it is well known that this material has brittle properties and does not bend and twist.

Relatively recently, a new class of composite materials known as functionally graded materials (FGMs) has emerged [16]. Typical FGMs is an inhomogeneous composite made of different phases of material components (usually ceramics and metal). FGMs ceramic components are able to withstand high-temperature environments due to the better heat resistance characteristics, and metal components provide higher mechanical properties and reduce the

possibility of destruction. Thus, the use of FGMs can help to protect the shell structure from the effects of variable temperature fields, which will allow the structure to absorb the load without reducing its strength, for instance.

At present, a sufficiently detailed analysis of the stress-strain state of thin-walled and thick-walled cylindrical shells of both conventional composites and FGMs in the calculations of two-dimensional systems under the thermal power load [1, 3, 12, 15, 16, 17] is made. In this paper, the change of the characteristics of the stress-strain state in the thickness of the structure is modeled by hypotheses of varying degrees of accuracy. It is generally known that to calculate the stress-strain state of thick-walled cylindrical shells it should be applied an approach [2, 6, 7, 10, 11, 13], based on the use of equations of the spatial theory of elasticity and which allows you to correctly analyze changes of parameters such as stress-strain state of the construction by the thickness.

The authors propose an approach to the establishment of the stress-strain state of a thick layered anisotropic cylindrical shell made of a fibrous composite, which is made at an angle to the generatrix, and a layer of FGMs. It is also necessary to take into account the effect of anisotropy caused by the discrepancy between the directions of reinforcement and the shell axes (Fig. 1) [1, 2, 3, 6, 7, 10, 11, 13, 14], and to assess the impact of temperature on such a combined structure thickness.

In this paper a three-dimensional theory of elasticity is used to solve the problem of the stress-strain state of a thick-walled anisotropic cylindrical shell made of fibrous composites [5]. The obtained solutions can serve as references in the calculations of stress-strain states of thin-walled structures of more complex geometry established, for example, when using the finite element method.

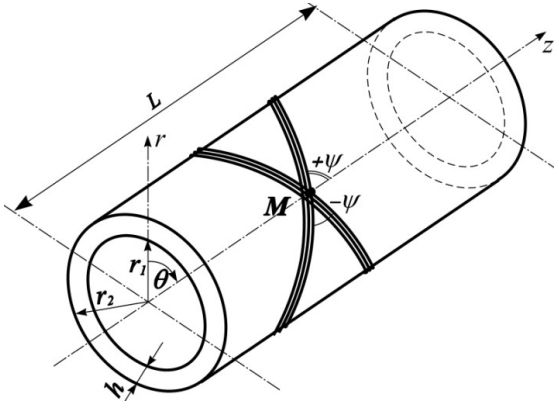

Fig. 1. Cylindrical thick-walled anisotropic shell

2. Formulation of the problem

Linear equilibrium equations in non-axisymmetric stress-strain state for each i-th layer are as follows [5]:

$$\frac{\partial \sigma_{rr}^{i}}{\partial r}=-\frac{1}{r}\left[\sigma_{rr}^{i}+r\frac{\partial}{\partial z}(\tau_{zr}^{i})+\frac{\partial}{\partial \theta}(\tau_{\theta r}^{i})-\sigma_{\theta\theta}^{i}+rF_{r}^{i}\right];$$

$$\frac{\partial \tau_{rz}^i}{\partial r}=-\frac{1}{r}\left[\tau_{rz}^i+r\frac{\partial}{\partial z}(\sigma_{zz}^i)+\frac{\partial}{\partial \theta}(\tau_{\theta z}^i)+rF_z^i\right];$$

$$\frac{\partial \tau_{r\theta}^i}{\partial r}=-\frac{1}{r}\left[\tau_{r\theta}^i+\tau_{\theta r}^i+r\frac{\partial}{\partial z}(\tau_{z\theta}^i)+\frac{\partial}{\partial \theta}(\sigma_{\theta\theta}^i)+rF_\theta^i\right], \quad (1)$$

where r_i (i=1,2) – radius of the cylinder, which does not depend on the coordinates z and θ; σ_{zz}^i, σ_{rr}^i, $\sigma_{\theta\theta}^i$, τ_{rz}^i, $\tau_{r\theta}^i$, $\tau_{z\theta}^i$ – components of the stress tensor, F_r, F_z, F_θ – vector projections of specific volume forces on the directions tangent to the coordinate lines r, z, θ.

The relationship between the components of deformation and displacement will take the form:

$$e_{zz}^i=\frac{\partial u_z^i}{\partial z};\ e_{\theta\theta}^i=\frac{1}{r}\frac{\partial u_\theta^i}{\partial \theta}+\frac{1}{r}u_r^i;\ e_{rr}^i=\frac{\partial u_r^i}{\partial r};$$

$$e_{z\theta}^i=\frac{\partial u_\theta^i}{\partial z}+\frac{1}{r}\frac{\partial u_z^i}{\partial \theta};\ e_{rz}^i=\frac{\partial u_r^i}{\partial z}+\frac{\partial u_z^i}{\partial r};\ e_{r\theta}^i=\frac{\partial u_\theta^i}{\partial r}-\frac{1}{r}u_\theta^i+\frac{1}{r}\frac{\partial u_r^i}{\partial \theta}. \quad (2)$$

And u_z^i, u_θ^i, u_r^i – displacement in the direction of the axes z, θ, r respectively; e_{zz}^i, $e_{\theta\theta}^i$, e_{rr}^i – relative linear deformations in the directions of the coordinate axes z, θ, r; $e_{z\theta}^i$, e_{rz}^i, $e_{r\theta}^i$ – relative tangential displacements at the point to the corresponding coordinate surfaces.

The ratios of the generalized Hooke's law, which connect the components of deformations and stresses, when the axes of orthotropy with the coordinate axes are coincident:

$$e_{zz}^i=a_{11}^{i/}\sigma_{zz}^i+a_{12}^{i/}\sigma_{\theta\theta}^i+a_{13}^{i/}\sigma_{rr}^i;$$
$$e_{\theta\theta}^i=a_{12}^{i/}\sigma_{zz}^i+a_{22}^{i/}\sigma_{\theta\theta}^i+a_{23}^{i/}\sigma_{rr}^i;$$
$$e_{rr}^i=a_{13}^{i/}\sigma_{zz}^i+a_{23}^{i/}\sigma_{\theta\theta}^i+a_{33}^{i/}\sigma_{rr}^i;$$
$$e_{r\theta}^i=a_{44}^{i/}\tau_{r\theta}^i;\ e_{rz}^i=a_{55}^{i/}\tau_{rz}^i;\ e_{z\theta}^i=a_{66}^{i/}\tau_{z\theta}^i. \quad (3)$$

When rotating the axes of orthotropy relative to the z axis, these dependencies take the form:

$$e_{zz}^i=a_{11}^i\sigma_{zz}^i+a_{12}^i\sigma_{\theta\theta}^i+a_{13}^i\sigma_{rr}^i+a_{16}^i\tau_{z\theta}^i;$$
$$e_{\theta\theta}^i=a_{12}^i\sigma_{zz}^i+a_{22}^i\sigma_{\theta\theta}^i+a_{23}^i\sigma_{rr}^i+a_{26}^i\tau_{z\theta}^i;$$
$$e_{rr}^i=a_{13}^i\sigma_{zz}^i+a_{23}^i\sigma_{\theta\theta}^i+a_{33}^i\sigma_{rr}^i+a_{36}^i\tau_{z\theta}^i;$$
$$e_{r\theta}^i=a_{44}^i\tau_{r\theta}^i+a_{45}^i\tau_{rz}^i;\ e_{rz}^i=a_{45}^i\tau_{r\theta}^i+a_{55}^i\tau_{rz}^i;$$
$$e_{z\theta}^i=a_{16}^i\sigma_{zz}^i+a_{26}^i\sigma_{\theta\theta}^i+a_{36}^i\sigma_{rr}^i+a_{66}^i\tau_{z\theta}^i. \quad (4)$$

In the equations (3, 4) $a_{kl}^{i/}$ and a_{kl}^i – are mechanical constants of the i-th layer of orthotropic material and material with one plane of elastic symmetry, the relationship between which is established in [4].

3. Research methodology

The relation of the generalized Hooke's law for a material with one plane of elastic symmetry (4) takes the form [2], which is used in the solution of the system (1):

$$\sigma_{zz}^i = b_{11}^i e_{zz}^i + b_{12}^i e_{\theta\theta}^i + b_{16}^i e_{z\theta}^i + c_1^i \sigma_{rr}^i + \beta_{11}^i T;$$
$$\sigma_{\theta\theta}^i = b_{12}^i e_{zz}^i + b_{22}^i e_{\theta\theta}^i + b_{26}^i e_{z\theta}^i + c_2^i \sigma_{rr}^i + \beta_{22}^i T;$$
$$\tau_{z\theta}^i = b_{16}^i e_{zz}^i + b_{26}^i e_{\theta\theta}^i + b_{66}^i e_{z\theta}^i + c_3^i \sigma_{rr}^i + \beta_{12}^i T;$$
$$e_{rr}^i = -c_1^i e_{zz}^i - c_2^i e_{\theta\theta}^i - c_3^i e_{z\theta}^i + c_4^i \sigma_{rr}^i + \alpha_{33}^i T + a_{13}^i \beta_{11}^i T + a_{23}^i \beta_{22}^i T + a_{36}^i \beta_{12}^i T;$$
$$e_{rz}^i = a_{45}^i \tau_{r\theta}^i + a_{55}^i \tau_{rz}^i + \alpha_{13}^i T;$$
$$e_{r\theta}^i = a_{44}^i \tau_{r\theta}^i + a_{45}^i \tau_{rz}^i + \alpha_{23}^i T, \qquad (5)$$

where b_{kl}^i (k,l=1, 2, 6), c_k^i ($k = 1 \div 4$) – are the characteristics of the i-th layer that are determined by the mechanical constants a_{kl}^i of the shell material; β_{11}^i, β_{22}^i, β_{12}^i – are the components of the stress-strain state of the i-th layer, related with the temperature dependences $T(^0\text{K})$:

$$\beta_{11}^i T = -\left(b_{11}^i \alpha_{11}^i + b_{12}^i \alpha_{22}^i + b_{16}^i \alpha_{12}^i\right) T;$$
$$\beta_{22}^i T = -\left(b_{12}^i \alpha_{11}^i + b_{22}^i \alpha_{22}^i + b_{26}^i \alpha_{12}^i\right) T;$$
$$\beta_{12}^i T = -\left(b_{16}^i \alpha_{11}^i + b_{26}^i \alpha_{22}^i + b_{66}^i \alpha_{12}^i\right) T.$$

In this system of equations and in (5) α_{ij}^i (i,j=1÷3) – are the coefficients of linear thermal expansion of the material of the i-th shell layer.

Replacing in (5) the deformations e_{zz}^i, $e_{\theta\theta}^i$, $e_{z\theta}^i$ by their expressions from (2) and substituting the obtained dependences for σ_{zz}^i, $\sigma_{\theta\theta}^i$, $\tau_{z\theta}^i$ in (1), and for e_{rz}^i, $e_{r\theta}^i$, e_{rr}^i in (2) we obtain for each i-th layer a complete system of differential equations in partial derivatives, in which we take into account that the shell is deformed according to the axial symmetry:

$$\frac{\partial \sigma_{rr}^i}{\partial r} = \frac{c_2^i - 1}{r}\sigma_{rr}^i - \frac{\partial \tau_{rz}^i}{\partial z} + \frac{b_{22}^i}{r^2}u_r + \frac{b_{12}^i}{r}\frac{\partial u_z^i}{\partial z} + \frac{b_{26}^i}{r}\frac{\partial u_\theta^i}{\partial z} - \frac{b_{12}^i}{r}\alpha_{11}^i T - \frac{b_{22}^i}{r}\alpha_{22}^i T -$$
$$- \frac{b_{26}^i}{r}\alpha_{12}^i T;$$
$$\frac{\partial \tau_{rz}^i}{\partial r} = -c_1^i \frac{\partial \sigma_{rr}^i}{\partial z} - \frac{1}{r}\tau_{rz}^i - \frac{b_{12}^i}{r}\frac{\partial u_r^i}{\partial z} - b_{11}^i \frac{\partial^2 u_z^i}{\partial z^2} - b_{16}^i \frac{\partial^2 u_\theta^i}{\partial z^2} + b_{11}^i \alpha_{11}^i \frac{dT}{dz} +$$
$$+ b_{12}^i \alpha_{22}^i \frac{dT}{dz} + b_{16}^i \alpha_{12}^i \frac{dT}{dz};$$

$$\frac{\partial \tau_{r\theta}^i}{\partial r} = -\frac{2}{r}\tau_{r\theta}^i - b_{66}^i \frac{\partial^2 u_\theta^i}{\partial z^2} - c_3^i \frac{\partial \sigma_{rr}^i}{\partial z} - \frac{b_{26}^i}{r}\frac{\partial u_r^i}{\partial z} - b_{16}^i \frac{\partial^2 u_z^i}{\partial z^2} + b_{16}^i \alpha_{11}^i \frac{dT}{dz} +$$
$$+ b_{26}^i \alpha_{22}^i \frac{dT}{dz} + b_{66}^i \alpha_{12}^i \frac{dT}{dz};$$
$$\frac{\partial u_r^i}{\partial r} = c_4^i \sigma_{rr}^i - \frac{c_2^i}{r} u_r^i - c_1^i \frac{\partial u_z^i}{\partial z} - c_3^i \frac{\partial u_\theta^i}{\partial z} + \alpha_{33}^i T - a_{13}^i b_{11}^i \alpha_{11}^i T - a_{13}^i b_{12}^i \alpha_{22}^i T -$$
$$- a_{13}^i b_{16}^i \alpha_{12}^i T - a_{23}^i b_{12}^i \alpha_{11}^i T - a_{23}^i b_{22}^i \alpha_{22}^i T - a_{23}^i b_{26}^i \alpha_{12}^i T - a_{36}^i b_{16}^i \alpha_{11}^i T -$$
$$- a_{36}^i b_{26}^i \alpha_{22}^i T - a_{36}^i b_{66}^i \alpha_{12}^i T;$$
$$\frac{\partial u_z^i}{\partial r} = a_{55}^i \tau_{rz}^i + a_{45}^i \tau_{r\theta}^i - \frac{\partial u_r^i}{\partial z} + \alpha_{13}^i T;$$
$$\frac{\partial u_\theta^i}{\partial r} = a_{45}^i \tau_{rz}^i + a_{44}^i \tau_{r\theta}^i + \frac{1}{r} u_\theta^i + \alpha_{23}^i T. \qquad (6)$$

If the temperature field is constant to the cylinder surface, the system (6) will be rewritten:

$$\frac{\partial \sigma_{rr}^i}{\partial r} = \frac{c_2^i - 1}{r}\sigma_{rr}^i - \frac{\partial \tau_{rz}^i}{\partial z} + \frac{b_{22}^i}{r^2} u_r + \frac{b_{12}^i}{r}\frac{\partial u_z^i}{\partial z} + \frac{b_{26}^i}{r}\frac{\partial u_\theta^i}{\partial z} - \frac{b_{12}^i}{r}\alpha_{11}^i T - \frac{b_{22}^i}{r}\alpha_{22}^i T -$$
$$- \frac{b_{26}^i}{r}\alpha_{12}^i T;$$
$$\frac{\partial \tau_{rz}^i}{\partial r} = -c_1^i \frac{\partial \sigma_{rr}^i}{\partial z} - \frac{1}{r}\tau_{rz}^i - \frac{b_{12}^i}{r}\frac{\partial u_r^i}{\partial z} - b_{11}^i \frac{\partial^2 u_z^i}{\partial z^2} - b_{16}^i \frac{\partial^2 u_\theta^i}{\partial z^2};$$
$$\frac{\partial \tau_{r\theta}^i}{\partial r} = -\frac{2}{r}\tau_{r\theta}^i - b_{66}^i \frac{\partial^2 u_\theta^i}{\partial z^2} - c_3^i \frac{\partial \sigma_{rr}^i}{\partial z} - \frac{b_{26}^i}{r}\frac{\partial u_r^i}{\partial z} - b_{16}^i \frac{\partial^2 u_z^i}{\partial z^2};$$
$$\frac{\partial u_r^i}{\partial r} = c_4^i \sigma_{rr}^i - \frac{c_2^i}{r} u_r^i - c_1^i \frac{\partial u_z^i}{\partial z} - c_3^i \frac{\partial u_\theta^i}{\partial z} + \alpha_{33}^i T - a_{13}^i b_{11}^i \alpha_{11}^i T - a_{13}^i b_{12}^i \alpha_{22}^i T -$$
$$- a_{13}^i b_{16}^i \alpha_{12}^i T - a_{23}^i b_{12}^i \alpha_{11}^i T - a_{23}^i b_{22}^i \alpha_{22}^i T - a_{23}^i b_{26}^i \alpha_{12}^i T - a_{36}^i b_{16}^i \alpha_{11}^i T -$$
$$- a_{36}^i b_{26}^i \alpha_{22}^i T - a_{36}^i b_{66}^i \alpha_{12}^i T;$$
$$\frac{\partial u_z^i}{\partial r} = a_{55}^i \tau_{rz}^i + a_{45}^i \tau_{r\theta}^i - \frac{\partial u_r^i}{\partial z} + \alpha_{13}^i T;$$
$$\frac{\partial u_\theta^i}{\partial r} = a_{45}^i \tau_{rz}^i + a_{44}^i \tau_{r\theta}^i + \frac{1}{r} u_\theta^i + \alpha_{23}^i T. \qquad (7)$$

The solution of the system (7) must correspond to the conditions on the side surfaces at $r = r_1$, $r = r_2$

$$\sigma_{rr}^1(r_1,z) = \pm q_r^1(z); \quad \tau_{rz}^1(r_1,z) = 0; \quad \tau_{r\theta}^1(r_1,z) = 0;$$
$$\sigma_{rr}^2(r_2,z) = \pm q_r^2(z); \quad \tau_{rz}^2(r_2,z) = 0; \quad \tau_{r\theta}^2(r_2,z) = 0, \qquad (8)$$

conditions at the ends are $z = 0$, $z = L$

$$\sigma_{zz}^{i} = u_{r}^{i} = u_{\theta}^{i} = 0 \tag{9}$$

and the conditions of hard contact of the layers:

$$\sigma_{rr}^{i}(r_i)=\sigma_{rr}^{i+1}(r_i);\quad \tau_{rz}^{i}(r_i)=\tau_{rz}^{i+1}(r_i);\quad \tau_{r\theta}^{i}(r_i)=\tau_{r\theta}^{i+1}(r_i);$$
$$u_{r}^{i}(r_i)=u_{r}^{i+1}(r_i);\quad u_{z}^{i}(r_i)=u_{z}^{i+1}(r_i);\quad u_{\theta}^{i}(r_i)=u_{\theta}^{i+1}(r_i). \tag{10}$$

There is a diaphragm, which is absolutely rigid in its plane and flexible, at the edges of the cylinder in conditions (9). In (8) $q_r^1(z)$, $q_r^2(z)$ - an internal and external pressure is distributed on the side surfaces of the shell, respectively.

To solve the three-dimensional problem (7) and (8-9), we use the Bubnov-Galerkin methodology. According to it, we decompose all functions into trigonometric series on the coordinate along the cylinder generatrix z, so that they would satisfy the boundary conditions (9):

$$\sigma_{rr}^{i}(r,z)=\sum_{m=1}^{\infty}\left[y_{1,p}^{i}(r)+y_{1,m}^{i/}(r)\right]\sin l_m z;$$

$$\tau_{rz}^{i}(r,z)=\sum_{m=0}^{\infty}\left[y_{2,p}^{i}(r)+y_{2,m}^{i/}(r)\right]\cos l_m z;$$

$$\tau_{r\theta}^{i}(r,z)=\sum_{m=1}^{\infty}\left[y_{3,p}^{i}(r)+y_{3,m}^{i/}(r)\right]\sin l_m z;$$

$$u_{r}^{i}(r,z)=\sum_{m=1}^{\infty}\left[y_{4,p}^{i}(r)+y_{4,m}^{i/}(r)\right]\sin l_m z;$$

$$u_{z}^{i}(r,z)=\sum_{m=0}^{\infty}\left[y_{5,p}^{i}(r)+y_{5,m}^{i/}(r)\right]\cos l_m z;$$

$$u_{\theta}^{i}(r,z)=\sum_{m=1}^{\infty}\left[y_{6,p}^{i}(r)+y_{6,m}^{i/}(r)\right]\sin l_m z, \tag{11}$$

where $y_{i,pk}$, $y_{i,mk}^{/}$ $(i=\overline{1,6})$ – are the components of expansion into trigonometric Fourier series of components of the stress-strain state of shell, p, m – are the wave numbers in the series.

After some mathematical transformations and separation of variables in equations (7) using the ratios (11), we obtain for each i-th layer a system of differential equations of the twelfth order in the normal Cauchy form

$$\frac{d\overline{y}^{i}}{dr}=T^{i}(r)\overline{y}^{i}+f^{i},\quad T^{i}(r)=t_{nl}^{i}(r),\ n,l=1\div 12, \tag{12}$$

where $\overline{y}^{i}=\left\{y_{1,p}^{i};y_{2,p}^{i};y_{3,p}^{i};y_{4,p}^{i};y_{5,p}^{i};y_{6,p}^{i};y_{1,m}^{i/};y_{2,m}^{i/};y_{3,m}^{i/};y_{4,m}^{i/};y_{5,m}^{i/};y_{6,m}^{i/}\right\}$ – solving vector function. Non-zero elements of which are written in accordance with [6, 11], $t_{nl}^{i}(r)$ - coefficients for unknown systems (7), f^{i} – the components of the stress-strain state related to the temperature in the system (7) and are determined as:

$$f_1^i = f_7^i = -\frac{b_{12}^i}{r}\alpha_{11}^i T - \frac{b_{22}^i}{r}\alpha_{22}^i T - \frac{b_{26}^i}{r}\alpha_{12}^i T \; ; \; f_2^i = f_3^i = f_8^i = f_9^i = 0 \; ;$$

$$f_4^i = f_{10}^i = \alpha_{33}^i T - a_{13}^i b_{11}^i \alpha_{11}^i T - a_{13}^i b_{12}^i \alpha_{22}^i T - a_{13}^i b_{16}^i \alpha_{12}^i T - a_{23}^i b_{12}^i \alpha_{11}^i T -$$

$$- a_{23}^i b_{22}^i \alpha_{22}^i T - a_{23}^i b_{26}^i \alpha_{12}^i T - a_{36}^i b_{16}^i \alpha_{11}^i T - a_{36}^i b_{26}^i \alpha_{22}^i T - a_{36}^i b_{66}^i \alpha_{12}^i T \; ;$$

$$f_5^i = f_{11}^i = \alpha_{13}^i T \; ;$$

$$f_6^i = f_{12}^i = \alpha_{23}^i T \; .$$

Implementation of the obtained one-dimensional problem on the stress-strain state of a thick-walled cylinder was carried out using the numerical method of discrete orthogonalization [3]. After solving the system (12) taking into account the boundary conditions (8), ratios (11) were used for the transition from the obtained functions to the components of the stress-strain state.

4. Results of the numerical calculations and their analysis

The object of the study is a cylindrical shell made of layers of fibrous boroplastic material and a layer of functionally graded material [16] under the distributed external pressure and external constant temperature. Silicone nitride was chosen as the ceramic component of FGMs, and titanium (Ti-6Al-4V) was chosen as the metal component. The temperature distribution along thickness of the cylinder was determined according to [9, 16]. Physical and mechanical properties of the functionally graded component of the cylinder dependent on the temperature were determined in the tables 1– 4 [12] and according to the dependences [18]:

$$\begin{aligned} E &= P_{0E} \cdot \left(P_{-1E} T^{-1} + 1 + P_{1E} T + P_{2E} T^2 + P_{3E} T^3\right); \\ \nu &= P_{0\nu} \cdot \left(P_{-1\nu} T^{-1} + 1 + P_{1\nu} T + P_{2\nu} T^2 + P_{3\nu} T^3\right), \\ \alpha &= P_{0a} \cdot \left(P_{-1a} T^{-1} + 1 + P_{1a} T + P_{2a} T^2 + P_{3a} T^3\right); \\ \kappa &= P_{0\kappa} \cdot \left(P_{-1\kappa} T^{-1} + 1 + P_{1\kappa} T + P_{2\kappa} T^2 + P_{3\kappa} T^3\right), \end{aligned} \qquad (13)$$

where E – the desired modulus of elasticity, ν – Poisson's ratio, α – coefficient of linear thermal expansion and κ – thermal conductivity, the given temperature $T(^0\text{K})$, and P_{0E}, $P_{0\nu}$, P_{0a}, $P_{0\kappa}$ – the desired characteristics of the material, when T=0^{0}K, P_{iE}, $P_{i\nu}$, P_{ia}, $P_{i\kappa}$ – are given in the tables 1–4.

Table 1

Modulus of elasticity of ceramics and metal, Pa

Material	P_{0E}	P_{-1E}	P_{1E}	P_{2E}	P_{3E}
Silicone nitride	348.43*10^9	0	-3.070*10^{-4}	2.160*10^{-7}	-8.946*10^{-11}
Titanium alloy (Ti-6Al-4V)	122.56*10^9	0	-4.586*10^{-4}	0	0

Table 2

Poisson's ratios of ceramics and metal

Material	P_{0v}	P_{-1v}	P_{1v}	P_{2v}	P_{3v}
Silicone nitride	0.24	0	0	0	0
Titanium alloy (Ti-6Al-4V)	0.2884	0	$1.121*10^{-4}$	0	0

Table 3

Coefficient of linear thermal expansion of ceramics and metal, $^0K^{-1}$

Material	P_{0a}	P_{-1a}	P_{1a}	P_{2a}	P_{3a}
Silicone nitride	$5.8723*10^{-6}$	0	$9.095*10^{-4}$	0	0
Titanium alloy (Ti-6Al-4V	$7.5788*10^{-6}$	0	$6.638*10^{-4}$	$-3.147*10^{-6}$	0

Table 4

Thermal conductivity of ceramics and metal, $W/(m^0K)$

Material	$P_{0\kappa}$	$P_{-1\kappa}$	$P_{1\kappa}$	$P_{2\kappa}$	$P_{3\kappa}$
Silicone nitride	13.723	0	$-1.032*10^{-3}$	$5.466*10^{-7}$	$-7.876*10^{-11}$
Titanium alloy (Ti-6Al-4V	1.000	0	$1.704*10^{-2}$	0	0

Boroplastics has the following mechanical characteristics: $E_{11}=28*10^5$ MPa, $E_{22}=E_{33}=3.1*10^5$ MPa, $G_{12}=G_{23}=1.05*10^5$ MPa, $G_{13}=2.12*10^5$ MPa, $v_{21}=0{,}25$, $v_{12}=0{,}0277$.

Common characteristics of the functionally graded materials were determined in accordance with [8]:

$$E(\xi)=(E_c-E_m)(\xi/h)^N+E_m;$$
$$\nu(\xi)=(\nu_c-\nu_m)(\xi/h)^N+\nu_m;$$
$$\alpha(\xi)=(\alpha_c-\alpha_m)(\xi/h)^N+\alpha_m;$$
$$\kappa(\xi)=(\kappa_c-\kappa_m)(\xi/h)^N+\kappa_m, \qquad (14)$$

where $E(\xi),\nu(\xi),\alpha(\xi),\kappa(\xi)$ – physical and mechanical characteristics of the common material by thickness, E_m, ν_m, α_m, κ_m – mechanical characteristics of metal (titanium alloy), E_c, ν_c, α_c, κ_c – mechanical characteristics of ceramics (zirconium), h – the thickness of the functionally graded component of the shell material, ξ – thickness coordinate $\xi = r - r_1$, r – the coordinate of an arbitrary point in the shell general coordinate system, fig. 1, r_1 – the

coordinate of the cylinder inner surface, N – volume fraction of mixed materials [16].

A cylindrical shell with the following geometric parameters was considered (fig. 1): L=1.2 m, r_1=0.57 m, r_2=0.63 cm, h=0.06 m. Three variants of a thick-walled cylindrical shell were calculated. The first one took into the consideration only power load, and then combined power and thermal load. In this case, the temperature field changed only according to the thickness of the layer of functionally graded material.

In the first variant of this structure, it was assumed that the cylinder consists of two layers: the inner r_1=0.57 m, r_{11}=0.6 m – made of boroplastic material with reinforcement angle ψ=70° to the axes z and the external r_{02}=0.6 m, r_2=0.63 m – made of functionally graded material, when N=1 (titanium alloy Ti-6Al-4V(r_{02}) – silicone nitride (r_2)).

In the second variant, the shell was consisted of three layers: two internal cross-enclosed with reinforcement angles $\psi = \pm 70^0$ to the axis z, made of boroplastic material r_1=0.57 m, r_{11}=0.585 m ($\psi = 70^0$) and r_{21}=0.585 m, r_{22}=0.6 m ($\psi = -70^0$) and external layer r_{02}=0.6 m, r_2=0.63 m – made of functionally graded material, when N=1 (titanium alloy Ti-6Al-4V(r_{02}) – silicone nitride (r_2)).

In the third variant, the shell was consisted of five layers: four internal cross-enclosed with reinforcement angles $\psi = \pm 70^0$ to the axis z, made of boroplastic material r_1=0.57 m, r_{11}=0.5775 m ($\psi = 70^0$) and r_{21}=0.5775 m, r_{22}=0.585 m ($\psi = -70^0$), r_{31}=0.585 m, r_{32}=0.5925 m ($\psi = 70^0$) and r_{41}=0.5925 m, r_{42}=0.6 m ($\psi = -70^0$) and the external layer r_{02}=0.6 m, r_2=0.63 m – made of functionally graded material, when N=1 (titanium alloy Ti-6Al-4V(r_{02}) – silicone nitride (r_2)).

All presented variants of shell structures were under pressure load that was distributed on the external surface $q=-q_0\sin(\pi z/l)$, where q_0=100 MPa. In the case of joint power and thermal load, the temperature field changed only by the thickness of the functionally graded component of the material from T=293°K (20°C), when r_{02} = 0.6 m, to T=373°K (100°C), when r_2 =0.63m for all three variants of the cylindrical shell, and distributed by thickness according to the law presented in [9]

Fig. 2-4 show the change of stress-strain components of the shells with one layer of boroplastic, that is curve 1 (solid), with two and four layers, i.e curve 2 (dashed) and curve 3 (dotted), respectively. The calculation results are given by the coordinate r for the cross-section that is on the middle of generatrix, i.e, when z = 0.5L.

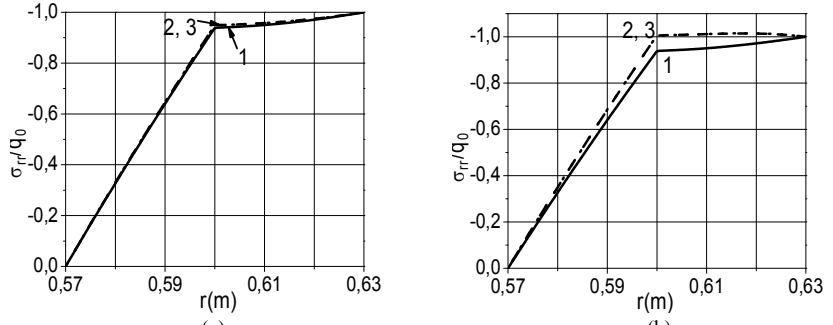

Fig. 2. Stress distribution σ_{rr} by the thickness of the cylindrical shell:
(a) under the power load; (b) under power and thermal load

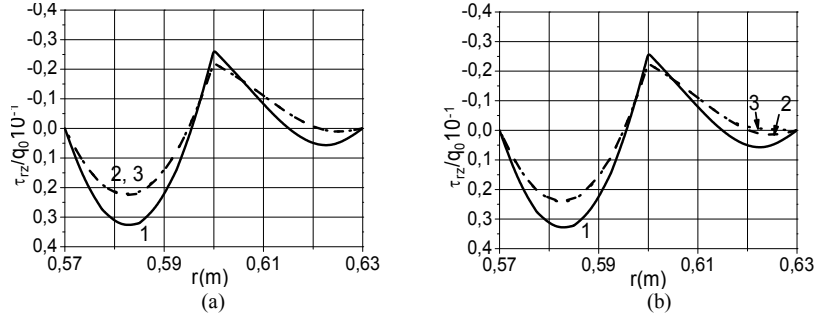

Fig. 3. Stress distribution τ_{rz} by the thickness of the cylindrical shell:
(a) under the power load; (b) under power and thermal load

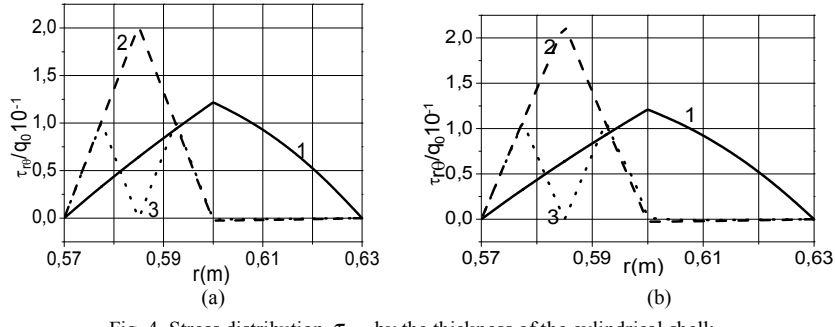

Fig. 4. Stress distribution $\tau_{r\theta}$ by the thickness of the cylindrical shell:
(a) under the power load; (b) under power and thermal load.

The analysis results of calculations in Fig. 2-4 describe the stress-strain state of the layered thick-walled anisotropic composite shells and show that the variable temperature field of the functionally graded component of the shell material within the studied temperatures ranges from T=293^{0}K (20^{0}C), when r=0.6 m to T=373^{0}K (100^{0}C), when r=0.63 m and does not significantly affect

the stress-strain state of a thick-walled anisotropic cylinder. However, it should be noted that variable temperature field and distributed lateral pressure (fig. 2b) effects that the values of normal stresses are slightly, up to 5%, higher compared with those, which are under power load only (fig. 2a).

The graphs presented in figs. 3a and 3b indicate that the cross-laying of fibrous material allows reducing the value of the tangential stresses τ_{rz} compared to one layered of the composite. This is especially evident in the example of the thickness distribution of the tangential stresses $\tau_{r\theta}$ in figs. 4a and 4b, which appear only in anisotropic material. There are anisotropic components of the stress-strain state $\tau_{r\theta}$ for one composite layer in the transversely isotropic FGMs. However, for cross-ply composites having two and four layers the effect is almost absent.

5. Conclusions

In the article the numerical calculations of the stress-strain state of a thick-walled cylindrical anisotropic shell of fibrous composite material that is protected by a functionally graded material under power and thermal load, were conducted based on three-dimensional theory of elasticity. Variants of increasing the number of layers stacked so that their axes of orthotropy of fiber composites do not coincide with the axes of the cylinder coordinate system, creating the effect of a material with one plane of elastic symmetry, are analyzed. It is taken into account that the physical and mechanical properties of FGMs are dependent on temperature. It was found that the stress-strain state of a thick-walled anisotropic cylinder does not change significantly due to the action of high temperature, which is the effect of using FGMs to protect the cylindrical shell.

REFERENCES

1. *Bazhenov V.A., Semeniuk M.P., Trach V.M.* (2010), Nelinijne deformuvannia, stijkist' i zakrytychna povedinka anizotropnykh obolonok (Nonlinear deformation, stability and supercritical behavior of anisotropic shells). - Kyiv, Karavela, 352 p. [in Ukrainian].
2. *Grigorenko Ya.M., Vasilenko A.T., Pankratova N.D.* Zadachi teorii uprugosti neodnorodnyih tel (Problems of the theory of elasticity of inhomogeneous bodies) – Kyiv, Naukova dumka, 1991. - 216 p. [in Russian].
3. *Grigorenko Ya.M., Kryukov N.N.* Chislennyie resheniya zadach statiki gibkih sloistyih obolochek s peremennyimi parametrami (Numerical solutions of problems of statics of flexible layered shells with variable parameters) – Kyiv, Naukova dumka, 1988. - 264 p. [in Russian].
4. *Lekhnitskyi S.G.* Teoriya uprugosti anizotropnogo tela (The theory of elasticity of an anisotropic body). - 2nd ed. - Moscow: Nauka, 1977. - 415 p. [in Russian].
5. *Novozhilov V.V.* Osnovy nelineynoy teorii uprugosti (Fundamentals of the nonlinear theory of elasticity). - L.-M .: OGIZ, 1948. - 211 p. [in Russian].
6. *Trach V.M., Podvorny A.V., Khoruzhiy M.M.* Deformuvannya ta stiykist□ netonkykh anizotropnykh obolonok (Deformation and stability of non-thin anisotropic shells): Monograph. – K.: Karavela, 2019. - 273 p. [in Ukrainian].
7. *Trach V.M., Semenyuk M.P., Podvorny A.V.* Vykorystannia 3D metodyky do rozrakhunku napruzhenoho stanu sharuvatykh anizotropnykh tsylindrychnykh obolonok pid diieiu bokovoho tysku. Resursoekonomni materialy, konstruktsii, budivli ta sporudy (The use of 3D techniques to calculate the stress state of layered anisotropic cylindrical shells under lateral

pressure load). - Resource-saving materials, structures, buildings and constructions: Collection of scientific papers. Issue 37. - NUWEE.- Rivne, 2019.- P.296-306. [in Ukrainian].
8. *Gibson L.J., Ashby M.F., Karam G.N., Wegst U., and Shercliff H.R.* Mechanical properties of natural materials. II. Microstructures for mechanical efficiency, Proceedings of the Royal Society of London Series A, 450, 141–162.
9. *Javaheri R. and Eslami M.R.* Thermal buckling of functionally graded plates. AIAA Journal, 40, 2002, pp. 162–169
10. *Podvornyi A.* The stability of anisotropic cylindrical shells under torsion in spatial position. ActaSci.Pol. Arch. 19 (1) 2020, 103-109.
11. *Podvornyi A.V., Semenyuk N.P., Trach V.M.* Stability of inhomogeneous cylindrical shells under distributed external pressure in a three-dimensional statement // Int. Appl. Mech. – 2017. – 53, N 6. P. 623 – 638.
12. *Reddy J.N. and Chin C.D.* Thermoelastical analysis of functionally graded cylinders and plates, Journal of Thermal Stresses, 21, 593–626
13. *Semenyuk, N.P., Trach, V.M., Podvornyi, A.V.* Spatial Stability of Layered Anisotropic Cylindrical Shells Under Compressive Loads. International Applied Mechanics. №2, 2019.
14. *Semenyuk, N.P., Trach, V.M., Podvornyi, A.V.* Stability of cylindrical anisotropic shells under axial pressure in three-dimensional statement. *Strength of Materials and Theory of Structures*, issue 94, KNUBA (2015), pp. 192–206.
15. *Shahsiah R. And Eslami M.R.* Thermal buckling of functionally graded cylindrical shell, Journal of Thermal Stresses, 26, 2003, 277–294.
16. *Shen, Hui-Shen* Functionally graded materials: nonlinear analysis of plates and shells. - CRC Press Taylor & Francis Group, Boca Raton London New York, 2009, - 266p.
17. *Shen, Hui-Shen* Postbuckling of axially-loaded FGM hybrid cylindrical shells in thermal environments, Composites Science and Technology, 65, 2005, 1675–1690.
18. *Touloukian Y.S.* Thermo physical Properties of High Temperature Solid Materials, McMillan, New York.

Стаття надійшла 13.05.2020

Семенюк М.П., Трач В.М., Подворний А.В.

НАПРУЖЕНИЙ СТАН ТОВСТИХ АНІЗОТРОПНИХ ЦИЛІНДРИЧНИХ ОБОЛОНОК, ЗАХИЩЕНИХ ФУНКЦІОНАЛЬНО-ГРАДІЄНТНИМ МАТЕРІАЛОМ, ПІД ТЕРМОСИЛОВОЮ ДІЄЮ

В роботі приведений напружений стан товстих конструктивно-анізотропних композитних циліндричних оболонок, що захищені функціонально-градієнтним матеріалом, і знаходяться в полі термосилової дії. На основі співвідношень просторової теорії пружності отримана система неоднорідних диференціальних рівнянь в тривимірній постановці, що описує напружений стан товстих анізотропних циліндрів. Для пониження розмірності зазначеної системи, використано аналітичний метод Бубнова-Гальоркіна. Отриману, таким чином, одновимірну систему з дванадцяти рівнянь нормального виду Коші реалізовано за використанням чисельного методу дискретної ортогоналізації. В якості представлення можливостей запропонованого підходу приведені напружені стани дво, чотири і п’яти-шаруватих анізотропних циліндричних оболонок, утворених з волокнистих композитів, що захищені, від дії температури, шаром трансверсально-ізотропного функціонально-градієнтного матеріалу.

Ключові слова: товста анізотропна циліндрична оболонка, напружений стан, тривимірна постановка, функціонально-градієнтний матеріал.

УДК 539.3
Семенюк М.П., Трач В.М., Подворний А.В. **Напружений стан товстих анізотропних циліндричних оболонок, захищених функціонально-градієнтним матеріалом, під термосиловою дією** // Опір матеріалів і теорія споруд: наук.-тех. збірн. – К.: КНУБА, 2020. – Вип. 105. – С. 165-178.

В роботі приведений напружений стан товстих конструктивно-анізотропних композитних циліндричних оболонок, що захищені функціонально-градієнтним матеріалом, і знаходяться в полі термосилової дії. На основі співвідношень просторової теорії пружності отримана система неоднорідних диференціальних рівнянь в тривимірній постановці, що описує напружений стан товстих анізотропних циліндрів. Для пониження розмірності зазначеної системи, використано аналітичний метод Бубнова-Гальоркіна. Отриману, таким чином, одновимірну систему з дванадцяти рівнянь нормального виду Коші реалізовано за використанням чисельного методу дискретної ортогоналізації. В якості представлення можливостей запропонованого підходу приведені напружені стани дво, чотири і п'ятишарових анізотропних циліндричних оболонок, утворених з волокнистих композитів, що захищені, від дії температури, шаром трансверсально-ізотропного функціонально-градієнтного матеріалу.
Табл. 4. Іл. 1. Бібліогр. 18 назв.

UDC 539.3
Semenyuk M.P., Trach V.M., Podvornyi A.V. **Stress-strain state of thick-walled anisotropic cylindrical shells under thermal power load, protected by the functionally graded material**// Strength of Materials and Theory of Structures: Scientific-and-technical collected articles – Kyiv: KNUBA, 2020. – Issue 105. – P. 165-178.

In the article the stress-strain state of thick-walled structurally anisotropic composite cylindrical shells under thermal power load, which are protected by a functionally graded material, are analysed. Based on the interrelations of the spatial theory of elasticity, a system of inhomogeneous differential equations in three-dimensional formulation, which describes the stress-strain state of thick-walled anisotropic cylindrical shells, was obtained. To reduce the dimensionality of this system, the Bubnov-Galerkin analytical method was used. Thus, the obtained one-dimensional system of twelve equations of normal Cauchy form was implemented using the numerical method of discrete orthogonalization. To represent the possibilities of the proposed approach, there were used stress-strain states of two, four and five-layered anisotropic cylindrical shells of fibrous composites, protected from temperature by a layer of transversely isotropic functionally graded material.
Tabl. 4. Fig. 1. Ref. 18.

УДК 539.3
Семенюк М.П., Трач В.М., Подворный А.В. **Напряженное состояние толстых анизотропных цилиндрических оболочек, защищенных функционально-градиентным материалом, под термосиловым действием**// Сопротивление материалов и теория сооружений: науч.-техн. сборн. Вып. 105. - К.: КНУСА, 2020. – С. 165-178.

В работе приведено напряженное состояние толстых конструктивно-анизотропных композитных цилиндрических оболочек, защищенных функционально-градиентным материалом, и находящихся в поле термосилового действия. На основе соотношений пространственной теории упругости получена система неоднородных дифференциальных уравнений в трехмерной постановке, описывающая напряженное состояние толстых анизотропных цилиндров. Для снижения размерности указанной системы, использован аналитический метод Бубнова-Галеркина. Полученная таким образом одномерная система из двенадцати уравнений нормального вида Коши реализована при использовании численного метода дискретной ортогонализации. В качестве представления возможностей предложенного подхода приведены напряженные состояния двух, четырех и пятислойных анизотропных цилиндрических оболочек, образованных из волокнистых композитов, защищеных, от действия температуры, слоем трансверсально-изотропного функционально-градиентного материала.
Табл. 4. Ил. 1. Библиогр. 18 назв.

Автор (науковий ступінь, вчене звання, посада): доктор технічний наук, професор, провідний науковий співробітник СЕМЕНЮК Микола Павлович
Адреса робоча: 02000 Україна, м. Київ, вул. Петра Нестерова, 3, Інститут механіки НАН України, СЕМЕНЮКУ Миколі Павловичу
Контактний тел. +38098-106-06-49
E-mail: mikolasem@ukr.net
ORCID ID: http://orcid.org/0000-0001-5711-4277

Автор (науковий ступінь, вчене звання, посада): доктор технічний наук, професор, завідувач кафедри мостів і тунелів, опору матеріалів і будівельної механіки ТРАЧ Володимир Мирославович
Адреса робоча: 33028 Україна, м. Рівне, вул. Соборна, 11, Національний університет водного господарства та природокористування, ТРАЧУ Володимиру Мирославовичу
Контактний тел. +38097-289-15-80
E-mail: trach-vm@ukr.net
ORCID ID: http://orcid.org/0000-0001-9500-2743

Автор (науковий ступінь, вчене звання, посада): кандидат технічний наук, доцент кафедри мостів і тунелів, опору матеріалів і будівельної механіки ПОДВОРНИЙ Андрій Володимирович
Адреса робоча: 33028 Україна, м. Рівне, вул. Соборна, 11, Національний університет водного господарства та природокористування, ПОДВОРНОМУ Андрію Володимировичу
Контактний тел. +38096-411-12-87
E-mail: andrei_podvornyi@ukr.net
ORCID ID: http://orcid.org/0000-0001-8518-4395

UDC 623.1/.7:007.52 (477)

INFLUENCE OF AIR SHOCK WAVE ON BUILDINGS AND STRUCTURES

M.O. Shyshanov [1],
Doctor of Technical Science, Professor

V.G. Maliuha [2],
Doctor of Technical Sciences, Researcher

V.V. Koval[3],
Candidate of military science, Senior Researcher

V.I. Mirnenko[4],
Doctor of Technical Science, Professor

V.M. Fil[4],
Candidate of Technical Science, Associate Professor

S.O. Hannenko[4],

R.V. Duzhyi[4]

[1]*Central research institute of weapons and military equipment of the Armed Forces of Ukraine, 28, Povitroflotskiy avenu, Kyiv, Ukraine*

[2]*Kharkiv National University of the Air Force. Ivan Kozhedub, Kharkiv*

[3]*Military Scientific Department of the General Staff of the Armed Forces of Ukraine*

[4]*Nationa Defense University of Ukraine named after Ivan Chernyakhovsky, 28, Povitroflotskiy avenu, Kyiv, Ukraine*

DOI: 10.32347/2410-2547.2020.105.179-191

The destruction of buildings and structures takes place as a result of calamities, accidents of various nature, and terrorist attacks which often include explosions. In armed conflicts, the destruction of buildings and constructions happens as a result of munitions completely penetrating structural floors or walls, after which the round explodes inside the construction, followed by the destructive impact of explosion product kinetic energy and the shock wave.

The impact of shock wave on buildings and constructions is characterized by complex pressure: excessive pressure, reflective pressure, dynamic pressure, flowing pressure, seismic wave pressure.

Ensuring the preservation and restoration of buildings and structures includes measures to assess the possible degree of destruction of buildings and structures. Therefore, in modern conditions, the design of buildings, structures and their elements is not possible without taking into account the dynamic effects. When designing and constructing buildings and structures, it is always necessary to take into account the resistance of structural elements to the action of damaging factors, both the explosion in general and the shock wave of the explosion in particular, which will help avoid future possible human losses.

Considering the aforementioned, this article describes the basic characteristics of the air shock wave and building interaction processes, the panel construction rupture time calculation method, and the general characteristics of an explosion's air shock wave that penetrates buildings, constructions that have doors, windows, and openings which appeared due to damage to flooring or wall structures.

Studies show that structural loads depend on the characteristics of the wave that penetrates through openings in constructions and through openings created by wall damage; while comparing calculations with experiment data shows a decent level of similarity between them.

Key words: air shock wave, dynamic load, reflection pressure, breach pressure, developed pressure, cover pressure, rupture time.

Introduction. The current climate change on Earth is followed by techno genic and natural calamities, while international relations are bare terrorist attacks and armed conflicts. Consequently, the need arises to study emerging threats and to predict possible building/construction rupture in order to apply preventive measures that reduce possible material losses and save human lives [1, 2].

Natural disasters, accidents, modern weapon employment often result in explosions. Depending on the type and yield strength of an explosion, as well as distance, design and size of elements of a building, explosion orientation, location of buildings and constructions, the impact of an air shock wave is going to vary. Thus, data characterizing explosions is needed in order to enable decision making on air shock wave protection for buildings and constructions, as well as to ensure explosion protection measures.

The most reliable information about the explosion can be obtained by conducting an experiment. However, this approach cannot always be applied. For that reason the most common calculation methods to determine the values of the parameters that characterize the explosions.

The aforementioned requires a more in-depth study of explosion process result impact and resilience of buildings and constructions calculation.

Analysis of research and publications has shown [1-7] that the study of the impact of the explosion on buildings and structures is given sufficient attention. At the same time, the issues of the impact of the shock wave on the structural elements of buildings and structures need additional study in order to solve the current scientific and practical problem of determining ways to improve the protective properties of reinforced concrete, concrete and brick structural elements of buildings and structures.

An air shock wave is a zone of strong air compression that propagates in all directions from the center of the explosion at high speed [8 -11]. The defeat is primarily caused by the occurrence of high excess pressure, which almost instantly compresses the human body or other object, causing damage and destruction. Along with this, the impact causes high-speed pressure, having a strong metallic ability. In addition to the direct impact of the shock wave, damage can be caused by fragments of elements of buildings, structures or other objects.

Considering everything mentioned above, the purpose of this article will be to determine the parameters of the shock wave of the explosion penetrating the building, structure and the parameters of the dynamic loads on their structures.

The main material of the article. The pressure on the internal structures of buildings depend on the parameters of the wave that flows through the

openings and holes that are formed during the destruction of the walls of the building [3, 9].

The frontal wall is initially affected by the pressure of reflection ΔP_{vid}, at the edges of the wall and its holes there are waves of rarefaction, the outspread of which leads to a decrease in pressure on the structure over time t_{obt} to the value of the flow pressure ΔP_{obt} (Fig. 1).

The time t_{obt}, during which the pressure at the frontal obstacle decreases to the flow pressure is taken depending on the smaller of the two values $S=h$ or $B/2$ by the formula (1)

$$t_{obt}=\frac{3S}{D_F}, \qquad (1)$$

where h – is a distance from the the ground to the window or the height of the building (when the front wall without windows); B – is the width of the building.

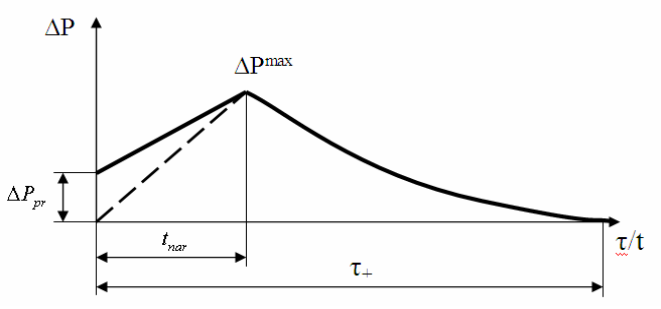

Fig. 1. Estimated pressure graph in the middle of a building with window openings. The dotted line shows the change in pressure inside the room with a smaller capacity 10%

At the same time, the shock wave outspread through holes in the walls of the building. Assume that the measurement of pressure over time inside the building has the form shown in Figure 1.

The leakage pressure ΔP_{pr} corresponds to the excess pressure at the front of the shock wave that passed through the window openings, the second point – the maximum value of the pressure in the flow wave $\Delta P_{zat}^{\max}$. The pressure ΔP_{pr} is determined from the graph (Fig. 2) depending on ΔP_F and the perforation coefficient α equal to the ratio of the area of the holes to the area of the obstacle. The pressure $\Delta P_{zat}^{\max}$ is determined taking into account the conditions that the leakage wave establishes an air flow of leakage, which continues until the pressure inside the building reaches the pressure in front of the hole $\Delta P_{zat}^{\max}=\Delta P t_{nar}$. Practically $\Delta P_{zat}^{\max}\approx\Delta P t_{nar}$.

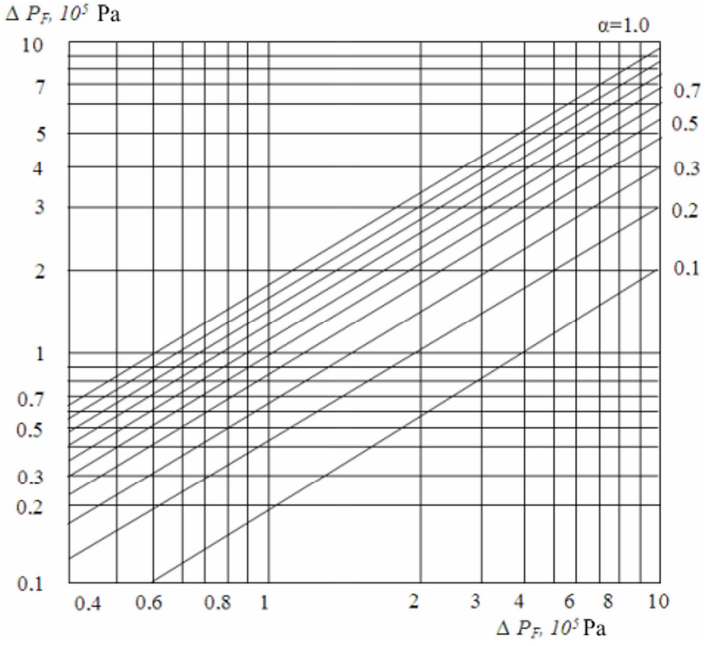

Fig. 2. The pressure depended ΔP_{pr} from parameters α and ΔP_F

To determine the parameters of the wave that flows into the building, taking into account the destruction of the enclosing structures, you can use the following prerequisites: the time of destruction of the building is equal to the time of destruction of its front wall; deformation of the frame of the building during the destruction of the walls is not taken into account, the dynamic load is considered to be normally applied to the surface of the front wall; the load on the front wall (from pressure ΔP_{vid}) and its rear surface (from pressure ΔP_{pr}) act simultaneously.

1. Determining the time of destruction of prefabricated buildings. The change in load $P(t)$ on the front wall width b will be taken as the difference between the loads $P=P_1-P_2$ on the front and rear faces of the wall

$$P_1=\begin{cases} P_{otr}(1-\dfrac{t}{\theta}), & 0<t\le t_{obt} \\ P_{otr}\left[1-\dfrac{(t-t_{obt})}{(\tau_e-t_{obt})}\right], & t_{obt}\le t<\tau_e \end{cases} \tag{2}$$

$$P_2=\begin{cases} P_{pr}\dfrac{(P_{zat}^{\max}-P_{pr})t}{t^{nar}}, & 0<t\le t_{nar} \\ P_{zat}^{\max}\left[1-\dfrac{(t-t_{nar})}{(\tau_e-t_{nar})}\right], & t_{nar}\le t\le \tau_e, \end{cases} \tag{3}$$

where – $P_{otr}=\Delta P^{b}_{otr}, P_{obt}=\Delta P^{b}_{otr}, P_{pr}=\Delta P^{b}_{pr}, \theta=2t_{obt}, \Delta P_{otr}=\frac{\Delta P_{otr}}{2}$.

There may be different relationships between moments of time t_{nar}, t_{obt} and time of destruction t_{raz}. However, regardless of the order of alternation of these moments of time, the load will always have a linear shape, which leads to the same type of formulas in dynamic calculations. You only need to follow the necessary transitional conditions.

Thus, the first segment of the load over time can be represented as

$$P(t)=P_1-P_2=P_*(1-\frac{t}{\tau_*}), \tag{4}$$

where P_*, τ_* easy to express through load parameters P_1, P_2 and

$$0<t\le t_{obt}\le t_{nar} \text{ or } 0<t\le t_{nar}\le t_{obt} \tag{5}$$

At $\alpha\to 1 \Delta P_{pr}\to\Delta P_F$, that is, at values $\alpha>0{,}5$, $\Delta P_{pr}=\Delta P_F$.

Considering also that $P^{\max}_{zat}\approx\Delta P_F$, we get a stationary area of back pressure P_2 at $0<t<t_{nar}$. Since, $\tau_*\gg t_{nar}$, for the function $P(t)$ can accept (4) if

$$\tau_*=\frac{P_*\theta}{\left(P_{otr}-(P_{pr}\theta/t_{nar})\right)}. \tag{6}$$

Schematize the panel with a single-span hinged beam as an elastic-plastic system with one degree of freedom. The termination of the flexible stage marked as t_2 is due to the armature breakdown resulting in rupture. Rupture time is $t_{raz}=t_1+t_2$.

Let us write down the dependencies for a certain time t_{raz} is less or equals $t_{raz}\le t_{obt}$. In the flexible stage, the M resisting moment of spill beam 1 is:

$$M(t)=\frac{1}{8}lP_*T_{(t)}. \tag{7}$$

The dynamic function T from the $T''+\omega^2 f(t)$ equation is

$$T(t)=T_o\cos\omega t+T'_o\omega^{-1}\sin\omega t+\omega\int_o^t f(u)\sin\omega(t-u)du, \tag{8}$$

where – T_o, T'_o are the initial values of T and T'; ω – natural frequency; f – dimentionless load, top dot indicates t derivative.

Linear function $f=1-t/\tau_*$ where $T_o=T'_o=0$ is

$$T(t)=1-\frac{t}{\tau_*}-\cos\omega t+\frac{(\sin\omega t)}{(\omega\tau_*)}. \tag{9}$$

Incorporating (9) into (7) we get $M(t_1)=M_o$ where M_o is the boundary flexible moment, and then find the value of t_1.

Equation of motion panel in the plastic stage in continuation, what $M_o(t)\equiv$const at $t>t_1$, has a pitchfork

$$ml^3\varphi''=3P(t)l^2 24M_o\,, \tag{10}$$

where – P and m – are the load and mass per unit of length; φ – is the angular deflection of the beam as a system of two solid elements held together by a flexible hinge

After we accept the time recording starting at t_1 and introducing $\delta_1=1-t_1/\tau_*$ and integrating (4) into (10), we get

$$\varphi(t)=\frac{3P_*}{ml}\left(\frac{\delta_1 t^2}{2}-\frac{t^3}{6\tau_*}\right)-\frac{12M_o}{ml^3}t^2+\varphi_1 t+\varphi_1\equiv F(t)\,, \tag{11}$$

where – φ is the rotational speed and rotational angle where $t=t^1-0$.

The speed of $\varphi_1(t_1+0)$ is calculated considering the change in the movement form of the beam suggesting constant motion. For the beam in question, the speed at the t moment of time increases by 23%. The φ_1 angle is calculated using the following formula

$$\varphi_1=\frac{51M_0}{(24B)}=\frac{2y_0}{l}\,, \tag{12}$$

where – B is bend firm of the beam's cross; y_o is the flexible deflection.

The moment of time t_{raz} can be derived from (11) via the boundary value of $\varphi(t_2)=\varphi^*_{pr}$, corresponding to beam rupture.

The value of φ^*_{pr} is determined via experiment and can be standardized by the number n of flexible deflections y_o with the help of the ratio (12). Experiments with models building have shown 1:5 that, when loaded more than panels can hold, support mounts rupture after the armature. At the moment of concrete failure to the full height of the compressed zone, the deflection is about $1/15$ he span (the crack opening angle in beams with reinforcement of class A-III $\varphi^*_{pr}=2\varphi^*_{pr}\cong 0,27\,\text{rad}$), and the ratio of the ultimate deflection to elastic.

After integrating φ^*_{pr} or $\frac{2\varphi^*_{pr}}{l}=\frac{28y_0}{l}$ into (11), we can find the t_2 from $F(t_2)=\varphi_{pr}$ or $F(t_2)=\frac{28y_0}{l}=\frac{35M_0 l}{12B}$.

Similarly, we can derive the variable dependencies with other ratios of time variables: t_{raz}, t_{obt}, t_{nar}.

In order to test the calculated dependencies, experiments were conducted involving sir shock wave rupture front and back walls of a building model scale 1:5 with U-sectioned frame and enclosing structures from armored concrete panels size 0,096 m^2. Outside dimensions of the model: height 1,7, width 1,32, length 4 m.

Panels were armored with symmetric welded steel frames class A-III with 8 mm in diameter (relative deformation in case of rupture: ≈ 14%). Armoring coefficient was 0,0027. Concrete class B50. Rupture time 0,2 sec.

Wall rupture time (Table 1) made of armored concrete panels 12 cm thick and 1800 kg/m^3 dense was calculated based on rupture time of wire indicators. The results of experiments and calculations are fairly similar. Figure 3 shows calculation results for the dependency of wall rupture time on pressure ΔP_F and the α coefficient. Works for natural panels with the following specifications: height 6 m, width 1,2 m, thickness 24 cm. Armoring coefficient 0,0015, armature class A-III, pored concrete class B25 density 750 kg/m^3.

Table 1

Experimental and calculated values of wall panel rupture time

ΔP_F , 10^5 Pa	Rupture time, mil sec		Exp / Cal
	experiment	calculation	
0,63	30	28	1,07
1,13	19	25	0,76
1,45	17	19	0,89

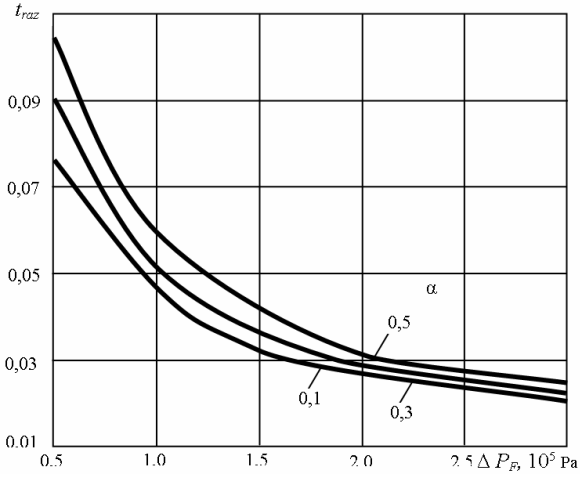

Fig. 3. Dependency of concrete-paneled building wall rupture time on ΔP_F pressure and α coefficient. For 1100 kg/m^3 panels, t_{raz} time should be multiplied by 1,2

Calculation analysis shows that panel rupture time when $\alpha = 0,3$ (penetration 30%), depending on ΔP_F varies between 20 to 100 Msec, while, if pressure increases, the penetration impacts on t_{raz} decreases. Rupture time calculations for panels 1100 kg/m^3 have shown that, if t_{raz} changes in a similar way, its value will increase by approximately 20%.

2. Parameters of the wave flowing into the panel and brick buildings with openings (holes). Estimated loads on the elements of buildings, structures are determined taking into account the change in pressure inside the buildings [4]. To determine the main parameters that characterize the change in pressure inside the building, taking into account the destruction, experiments were conducted on a model of an industrial building on a scale of 1: 5. The walls of the model were obstacles with openings typical of buildings. Under the influence of an air shock wave, the front and rear walls collapsed. The change in pressure inside the model was recorded by membrane sensors. A typical oscillogram of pressures in the flow wave is shown in Figs. 4a, 4b.

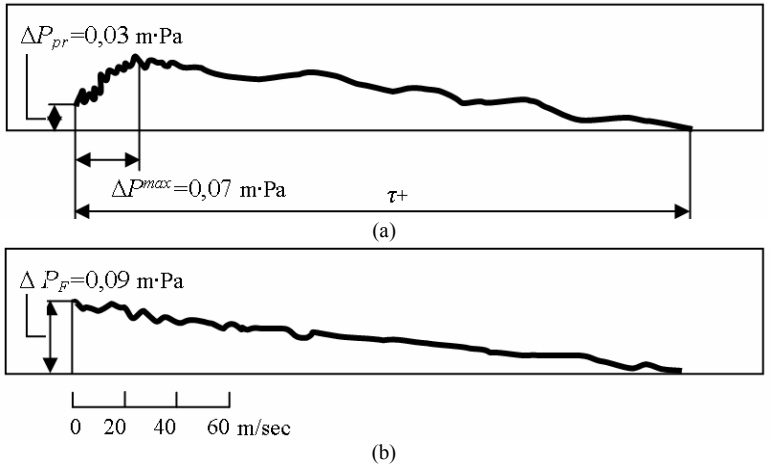

Fig. 4. Pressure change over time inside a building/construction model with openings (a) and outside (b)

Figure 4 shows that at the initial moment the pressure increases by a jump, then to the maximum value the pressure changes smoothly. Some pressure fluctuations near the midline are caused by waves repeatedly reflected from walls and debris. The change in pressure in the flow wave with sufficient accuracy for practice can be approximated in the form of a graph shown in Figure 1. Assume the maximum pressure $\Delta P_{zat}^{\max}$ is approximately equal to the pressure ΔP_F.

It is defined that, if $t_{raz} < t_{zat}$, the time of increase t_{raz} inside equals wall rupture time. If the wave penetration ends by the time the wall collapses, then the time $t_{raz} \approx t_{zat}$.

The t_{zat} is defined via graph shown in Figure 5, calculated based on statistical analysis of wave penetration experiment results for buildings for which the ratio of the area of the openings to the internal volume V more

0,01 m^{-1}. Experiments prove that compression phase for penetrating waves equals τ_* compression phase for shock wave.

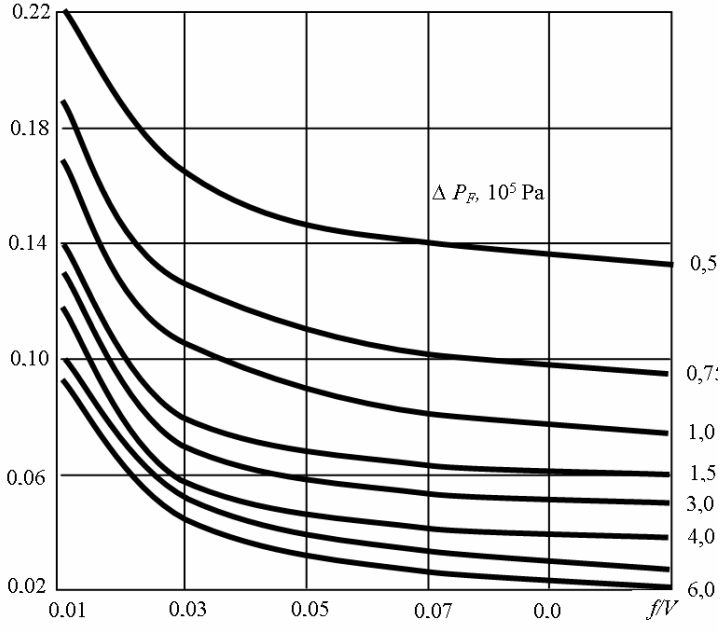

Fig. 5. The dependence of the time of penetration of the wave into the first floors of the building, structure on the ratio and pressure

The results of experiments and their comparison with the calculation are shown in table 2. Comparison of calculated and experimental data indicates their sufficient convergence.

Table 2

The value of the parameters of the wave flowing into the brick buildings

ΔP_F, 10^5Pa	f/V, 1/m	Wall α coefficient		ΔP_{zat}^{max}, 10^5Pa	t_{nar}, m/sec		ΔP_{pr}, 10^5Pa	
		front	rear	Exper.	Exper.	Calc.	Exper.	Calc.
0,60	0,055	0,2	0	0,46	18	21	0,22	0.23
0,93	0,055	0,2	0	0,66	16	15	0,27	0,34
0,74	1,109	0,4	0	0,73	15	17	0,39	0,43
0,90	0,109	0,2	0,2	0,70	16	15,7	0,34	0,33
0,77	0,109	0,4	0,4	0,63	15	14	0,40	0,46
1,06	0,218	0,4	0	0,85	14	14	0,61	0,60

Conclusion. Studying the parameter of an explosion shock wave that penetrates buildings have shown that building-mount construction loads

depend on the parameters of the wave that penetrates openings of a building or construction.

In order to determine the parameters of a wave that penetrates a building, considering that its enclosing structures have been ruptured, we accepted the following pre-conditions: building rupture time equals the rupture time of its front wall; building frame deformation was not considered, dynamic load was considered standardly applied to the front wall surface; front wall load (from ΔP_{otr}) and its rear surface (from ΔP_{pr}) are considered simultaneously applied.

Determination of the time of destruction of panel structures on building models on a scale of 1:5 showed that under loads that are an order of magnitude or more exceeding the load-bearing capacity of the panels, the support fasteners are destroyed after the break of the reinforcement. At the moment of rupture of the concrete, at the full height of the compressed zone, the deflection is about $1/15$ the span, the crack opening angle $\varphi^*_{pr} = 2\varphi^*_{pr} \cong 0,27\text{rad}$. Calculation analysis shows that panel rupture time for $\alpha = 0,3$ (notch 30%), depending on ΔP_F, varies between 20 to 100 Msec, while pressure increase causes opening impact decrease for t_{raz}. Rupture time calculations for 1100 kg/m3 panels have shown that, if the value of t_{raz} changes under similar pattern, its value will increase by approximately 20%.

Under air shock wave impact, the front and rear walls of the construction were ruptured. During the parameter calculation for waves penetrating a building through an opening, experimental and calculated data showed an acceptable level of concordance.

REFERENCES

1. *Vasiychuk V.O.* Osnovy tsyvilnoho zakhystu (Fundamentals of civil protection): Navch. posibnyk / V.O. Vasiychuk, V.Ye Honcharuk, S.I. Kachan, S.M. Mokhnyak - Lviv: Vydavnytstvo Natsionalnoho universytetu "Lvivska politekhnika", 2010.-417s. (in Ukrainian)
2. *Bykova O.V. Boliyev O.V., Derevynskyy D.M., Yeliseyev V.N., Myronets S.M., Osypenko S.I., Piven YU.O.* ta insh. Osnovy tsyvilnoho zakhystu (Fundamentals of civil protection): Navch. posibnyk K: 2008.– 223 s. (in Ukrainian)
3. *Vasylchenko O.V.* Budivelni konstruktsiyi ta yikh povedinka v umovakh nadzvychaynykh sytuatsiy (Building structures and their behavior in emergency situations): Navchalnyy posibnyk / O.V. Vasylchenko, YU.V. Kvitkovskyy, O.V. Myrhorod, O.A. Stelmakh. – Kharkiv: KHNADU, 2015. – 488s. (in Ukrainian)
4. *Mkrtychev O.V.* Raschet konstruktsiy zhelezobetonnogo zdaniya na vzryvnyye nagruzki v nelineynoy dinamicheskoy postanovke (Analysis of structures of a reinforced concrete building for explosive loads in a nonlinear dynamic setting)/ O.V. Mkrtychev, V.B. Dorozhinskiy, O.V. Lazarev // Vestnik MGSU. – 2011. – №4. – S. 243–247. (in Russian)
5. RD 03-409-01. Metodika otsenki posledstviy avariynykh vzryvov toplivno-vozdushnykh smesey (Methodology for assessing the consequences of emergency explosions of fuel-air mixtures). – M.: ZAO NTTS PB, 2014. – 38 s. (in Russian)
6. *Chub I.A.* Prohnozuvannya naslidkiv nadzvychaynoyi sytuatsiyi z vybukhom khmary hazopovitryanoyi sumishi (Forecasting the consequences of an emergency situation with the explosion of a cloud of gas-air mixture) / I.A. Chub, V.V. Matukhno // Problemy nadzvychaynykh sytuatsiy. – 2016. – Vyp. 23. – S.186-191. (in Ukrainian)

7. *Rybakov A.V.* Raschot ustoychivosti konstruktsiy zdaniy k udarno-volnovym nagruzkam (Calculation of the resistance of building structures to shock-wave loads)// Nauchnyye i obrazovatel'nyye problemy grazhdanskoy zashchity, № 4, 2013. S. 23–27. (in Russian)
8. *Kobylkin I.F.* Udarnyye i detonatsionnyye volny: Metody issledovaniya (Shock and Detonation Waves: Research Methods)/ [I.F. Kobylkin, V.V. Selivanov, V.S. Solov'yev, N.N. Sysoyev].– M.: Fizmatlit, 2004. – 375s. (in Russian)
9. *Kvitkovskyy Yu.V.* Vyznachennya parametriv udarnoyi khvyli, shcho utvoryuyetsya pid chas vybukhu hazopovitryanoyi sumishi (Determination of the parameters of the shock wave generated during the explosion of the gas-air mixture)/ Kvitkovskyy YU.V, Prokhach E.YU.// Zbirka naukovykh prats UTSZU. - №4, 2006. – S.120-124. (in Ukrainian)
10. *Mukhin V.I., Rybakov A.V., Vil'danov R.R.* O raschetnoy modeli otsenki porazhayushchego vozdeystviya vozdushnoy udarnoy volny ot obychnikh sredstv porazheniya (On a computational model for assessing the damaging effect of an air shock wave from conventional weapons)// Izvestiya Instituta inzhenernoy fiziki. 2017. №1, s. 58-63. (in Russian)
11. *Nabiullin M.I.* Matematicheskaya model' rascheta amplitudy izbytochnogo davleniya na fronte vozdushnoy udarnoy volny (Mathematical model for calculating the amplitude of excess pressure at the front of an air shock wave) / M.I. Nabiullin, A.V. Guseva, D. Yu. Verin, S.A. Vilokhin // Vestnik tekhnologicheskogo universiteta. 2017. T.20, №3 – S. 141-144. (in Russian)

Стаття надійшла 15.10.2020

Шишанов М.О., Малюга В.Г., Коваль В.В., Мірненко В.І., Філь В.М., Ганненко С.О., Дужий Р.В.

ВПЛИВ ПОВІТРЯНОЇ УДАРНОЇ ХВИЛІ НА БУДІВЛІ І СПОРУДИ

Руйнування будівель та споруд відбувається внаслідок стихійних лих, аварій різного характеру та терористичних актів, що в багатьох випадках супроводжуються вибухами. В ході ведення збройних конфліктів руйнування будівель, споруд відбувається у результаті наскрізного пробивання засобами ураження перекриття або стін з подальшою детонацією боєприпасу всередині споруди, виникненням руйнівної дії кінетичної енергії продуктів вибуху та ударної хвилі.

Дія ударної хвилі на будівлі, споруди характеризується складним комплексом навантажень: надлишковим тиском, тиском відбивання, тиском швидкісного напору, тиском затікання, навантаженням від сейсмічних хвиль.

Забезпечення збереження й відновлення будівель і споруд включає заходи оцінки можливих ступенів руйнування будівель і споруд. Тому у сучасних умовах проектування будівель, споруд та їх елементів не можливе без урахування динамічних впливів. При проектуванні та будуванні будівель, споруд завжди потрібно враховувати стійкість елементів конструкцій до дії вражаючих факторів, як вибуху в цілому так і ударної хвилі вибуху зокрема, що допоможе уникнути майбутніх можливих людських втрат.

Враховуючи це в статті розглянуто загальну характеристику процесів взаємодії повітряної ударної хвилі з будівлею, метод розрахунку часу руйнування панельних споруд та основні параметри повітряної ударної хвилі, яка затікає у результаті вибуху в будівлі, споруди з віконними, дверними прорізами, які виникли в наслідок руйнування конструкцій перекриття або стін.

Дослідження показують, що навантаження на конструкції залежать від параметрів хвилі, яка затікає через прорізи в споруди, які утворюються при руйнуванні стін будівлі, зіставлення розрахункових і експериментальних даних свідчить про їх достатню збіжність.

Ключові слова: повітряна ударна хвиля, динамічне навантаження, тиск відбиття, тиск прориву, тиск наростання, тиск обтікання, час руйнування.

Shyshanov M.O., Maliuha V.G., Koval V.V., Mirnenko V.I., Fil V.M., Hannenko S.O., Duzhyi R.V.
INFLUENCE OF AIR SHOCK WANE ON BUILDINGS AND STRUCTURES

The destruction of buildings and structures occurs as a result of natural disasters, accidents, or terorist attactacts which in many cases are accompanied by explosions.

The action of an air shock wave on a building is characterized by a complex set of loads: excess pressure, reflection pressure, velocity pressure, leakage pressure, load from seismic waves.

Ensuring the preservation and restoration of buildings and structures includes measures to assess the possible degree of destruction of buildings and structures. Therefore, in modern conditions, the design of buildings, structures and their elements is not possible without taking into account the dynamic effects. When designing and constructing buildings and structures, it is always necessary to take into account the resistance of structural elements to the action of damaging factors, both the explosion in general and the shock wave of the explosion in particular, which will help avoid future possible human losses.

Therefore, the article considers the general characteristics of the processes of interaction of the air shock wave with the building, the method of calculating the time of destruction of prefabricated buildings and the main parameters of the air shock wave which flows as a result of an explosion in a building, structure with windows, doorways and openings, which arose as a result of the destruction of floor structures or walls.

Studies have shown that the load on the structure depends on the parameters of the wave that flows through the holes in the buildings and through the holes formed by the destruction of the walls of the building, the comparison of calculated and experimental data indicates their sufficient convergence.

Key words: air shock wave, dynamic loading, reflection pressure, breakthrough pressure, growth pressure, flow pressure, fracture time.

УДК 623.1/.7:007.52 (477)
Шишанов М.О., Малюга В.Г., Коваль В.В., Мірненко В.І., Філь В.М., Ганненко С.О., Дужий Р.В. **Вплив повітряної ударної хвилі на будівлі, споруди** // Опір матеріалів і теорія споруд: наук.-тех. збірн. – К.: КНУБА, 2020. – Вип. 105. – С. 179-191.

В статті розглянуто загальну характеристику процесів взаємодії повітряної ударної хвилі з будівлею, метод розрахунку часу руйнування панельних споруд та основні параметри повітряної ударної хвилі.

Табл. 2. Рис. 5. Бібліогр. 11 назв.

UDC 623.1/.7:007.52 (477)
Shyshanov M.O., Maliuha V.G., Koval V.V., Mirnenko V.I., Fil V.M., Hannenko S.O., Duzhyi R.V.
Influence of air shock wane on buildings and structures // Strength of Materials and Theory of Structures: Scientific-and-technical collected articles – Kyiv: KNUBA, 2020. – Issue 105. – P. 179-191.

Article considers the general characteristics of the processes of interaction of the air shock wave with the building, the method of calculating the time of destruction of prefabricated buildings and the main parameters of the air shock wave.

Tabl. 2. Fig. 5. Ref. 11.

Автор (вчена ступень, вчене звання, посада): доктор технічних наук, професор, провідний науковий співробітник Центрального науково-дослідного інститут озброєння та військової техніки Збройних Сил України, ШИШАНОВ Михайло Олексійович
Адреса робоча: 03049, м. Київ, Повітрофлотський проспект, 28, Центральний науково-дослідний інститут озброєння та військової техніки Збройних Сил України.
Робочий тел.: +38 044 520-12-84.
Мобільний тел.: +38(067) 538-43-18
ORCID ID: http://orcid.org/0000-0002-7121-3666

Автор (вчена ступень, вчене звання, посада): доктор військових наук, старший науковий співробітник, начальник кафедри тактики ЗРВ Харківського національного університету Повітряних Сил імені Івана Кожедуба, МАЛЮГА Володимир Генадійович
Адреса робоча: 61045, м. Харків, вулиця Клочківська, 228, Харківський національний університет Повітряних Сил імені Івана Кожедуба.
Мобільний тел.: +38(099) 770-65-60,
E-mail: maluga_v@i.ua
ORCID ID: http://orcid.org/0000-0001-6227-1269

Автор (вчена ступень, вчене звання, посада): кандидат військових наук, старший науковий співробітник, начальник воєнно-наукового управління Генерального штабу Збройних Сил України, КОВАЛЬ Володимир Валерійович
Адреса робоча: 03049, м. Київ, Повітрофлотський проспект, 28, Воєнно-наукове управління Генерального штабу Збройних Сил України
Робочий тел.: +38 044 234-32-39
Мобільний тел.: +38(096) 103-26-01
E-mail: koval_vol@ukr.net
ORCID ID: http://orcid.org/0000-0002-6209-6779

Автор (вчена ступень, вчене звання, посада): доктор технічних наук, професор, директор департаменту освіти і науки Міністерства оборони України, МІРНЕНКО Володимир Іванович
Адреса робоча: 03049, м. Київ, Повітрофлотський проспект, 28, Департамент освіти і науки Міністерства оборони України.
Робочий тел.: +38 044 271-06-97, факс +38 044 271-06-97 03680.
Мобільний тел.: +38(067) 445-79-60,
ORCID ID: https://orcid.org/0000-0002-7484-1035

Автор (вчена ступень, вчене звання, посада): кандидат технічних наук, доцент, викладач кафедри оперативного та бойового забезпечення Національного університету оборони України імені Івана Черняховського, ФІЛЬ Віктор Миколайович
Адреса робоча: 03049, м. Київ, Повітрофлотський проспект, 28, Національний університет оборони України імені Івана Черняховського.
Робочий тел.: +38 044 271-08-68, факс +38 044 271-06-97 03680.
Мобільний тел.: +38(097) 908-71-78,
E-mail: victorof3@gmail.com
ORCID ID: https://orcid.org/0000-0003-0013-874X

Автор (вчена ступень, вчене звання, посада): старший викладач кафедри зв'язку та автоматизованих систем управління Національного університету оборони України імені Івана Черняховського, ГАННЕНКО Світлана Олександрівна
Адреса робоча: 03049, м. Київ, Повітрофлотський проспект, 28, Національний університет оборони України імені Івана Черняховського
Робочий тел.: +38 044 271-08-68, факс +38 044 271-06-97 03680
Мобільний тел.: +38(067) 769-85-02
E-mail: zima_sveta@ukr.net
ORCID ID: https://orcid.org/0000-0002-8285-1145

Автор (вчена ступень, вчене звання, посада): заступник начальника центру – начальник відділу впровадження інноваційних технологій та технічного супроводження навчального процесу навчально-наукового центру підготовки офіцерів для багатонаціональних штабів Національного університету оборони України імені Івана Черняховського, ДУЖИЙ Роман Володимирович
Адреса робоча:03049, м. Київ, Повітрофлотський проспект, 28, Національний університет оборони України імені Івана Черняховського
Робочий тел.: +38 044 271-09-12, факс +38 044 271-06-97 03680
Мобільний тел.: +38(050) 606-81-66
E-mail: romeojuliet@ukr.net
ORCID ID: https://orcid.org/0000-0002-8064-1312

UDC 624.04, 519.853

PARAMETRIC OPTIMIZATION OF STEEL STRUCTURES BASED ON GRADIENT PROJECTION METHOD

V.V. Yurchenko[1],
Doctor of Technical Science, Associate Professor

I.D. Peleshko[2],
Candidate of Technical Science, Associate Professor

[1]*Kyiv National University of Construction and Architecture*
Povitroflotskyj av., 31, Kyiv, 03680

[2]*Lviv Polytechnic National University*
St. Bandery, 12, Lviv, 79013

DOI: 10.32347/2410-2547.2020.105.192-220

The main research goal is the development of a numerical methodology for solving parametric optimization problems of steel structures with orientation on software implementation in a computer-aided design system. The paper has proposed a new mathematical model for parametric optimization problems of steel structures. The design variable vector includes geometrical parameters of the structure (node coordinates), cross-sectional dimensions of the structural members, as well as initial pre-stressing forces introduced into the specified redundant members of the structure. The system of constraints covers load-carrying capacities constraints formulated for all design sections of structural members of the steel structure subjected to all ultimate load case combinations. The displacements constraints formulated for the specified nodes of the steel structure subjected to all serviceability load case combinations have been also included into the system of constraints. The method of the objective function gradient projection onto the active constraints surface with simultaneous correction of the constraints violations has been used for solving the parametric optimization problem. A numerical algorithm for solving the formulated parametric optimization problems of steel structures has been developed in the paper. The comparison of the optimization results of truss structures presented by the paper confirms the validity of the optimum solutions obtained using the proposed numerical methodology.

Keywords: parametric optimization, steel structures, nonlinear programming, buckling constraints, pre-stressing forces, node coordinates, gradient projection method, finite element analysis, numerical algorithm.

Introduction. Over the past 50 years, numerical optimisation and finite element method have individually made significant advances and have together been developed to make possible the emergence of structural optimisation as a potential design tool. In recent years, great efforts have been also devoted to integrate optimisation procedures into the CAD facilities. With these new developments, lots of computer packages are now able to solve relatively complicated industrial design problems using different structural optimisation techniques.

Applied optimum design problems for the bar structures in some cases are formulated as parametric optimisation problems, namely as searching problems for unknown structural parameters, whose provide an extreme value of the specified purpose function in the feasible region defined by the specified

constraints. In this case structural optimisation performs by variation of the structural parameters when the structural topology, cross-section types and node type connections of the bars, the support conditions of the bar system, as well as loading patterns and load design values are prescribed and constants. Besides, the mathematical model of the parametric optimization problem of the structures includes the set of design variables, the objective function, as well as constraints, whose reflect in general case non-linear interdependences between them [13].

In cases if the purpose function and constraints of the mathematical model are continuously differentiable functions, as well as the search space is smooth, then the parametric optimization problems are successfully solved using gradient-based non-linear methods [14, 16]. The gradient-based methods operate with the first derivatives or gradients only both of the objective function and constraints. The methods are based on the iterative construction such sequence of the approximations of the design variables that provides the convergence to the optimum solution (optimum values of the structural parameters) [5, 6].

Additionally, a sensitivity analysis is a useful optional feature that could be used in scope of the numerical algorithms developed based on the gradients methods [10].

Although many papers are published on the parametric optimization of steel structures, the development of a general computer program for the design and optimization of building structures according to specified design codes remains an actual task. Therefore, the main *research goal* is the development of a methodology for solving parametric optimization problems of steel structures with orientation on software implementation in a computer-aided design system.

In this paper, steel structures are considered as *research object*, which investigated for the searching for optimum parameters of the structural form. The following *research tasks* are formulated: to develop a mathematical model for parametric optimization of steel structures taking into account load-carrying capacities and stiffness constraints; to propose a numerical algorithm for parametric optimization of steel structures based on the gradient projection method; to confirm the validity of the optimum solutions obtained using the proposed methodology based on numerical examples.

1. Problem formulation for parametric optimization of steel structures. Let us consider a parametric optimization problem of a structure consisting of bar members. The problem statement can be performed taking into account the following assumptions widely used in structural mechanic problems: the material of the structure is ideal elastic; the bar structure is deformable linearly; external loadings applied to the structure are quasi-static.

Let us also formulate the following pre-conditions for calculation: cross-section types and dimensions of structural members are constant along member lengths; external loadings are applied to the structural members without eccentricities relating to the center of mass and shear center of its cross-sections; an additional restraining by stiffeners are provided in the design sections where point loads (reactions) applied with the exception of cross-section warping and local buckling of the cross-section elements; load-carrying

capacity of the structural joints, splices and connections are provided by additional structural parameters do not covered by the considered parametric optimization problem.

A parametric optimization problem of the structure can be formulated as presented below: to find optimum values for geometrical parameters of the structure, member's cross-section dimensions and initial pre-stressing forces introduced into the specified redundant members of the bar system, which provide the extreme value of the determined optimality criterion and satisfy all load-carrying capacities and stiffness requirements. We assume, that the structural topology, cross-section types and node type connections of the bars, the support conditions of the bar system, as well as loading and pre-stressing patterns are prescribed and constants.

The formulated parametric optimization problem can be considered integrally using the mathematical model in the form of the non-linear programming task including an objective function, a set of independent design variables and constraints, which reflect generally non-linear dependences between them. The validity of the mathematical model can be estimated by the compliance of its structure with the design code requirements.

The parametric optimization problem of steel structures can be stated in the following mathematical terms: to find unknown structural parameters $\vec{X} = \{X_\iota\}^T$, $\iota = \overline{1, N_X}$, providing the least value of the determined objective function:

$$f^* = f(\vec{X}^*) = \min_{\vec{X} \in \Im} f(\vec{X}), \tag{1.1}$$

in a feasible region (search space) $\Im$ defined by the following system of constraints:

$$\boldsymbol{\psi}(\vec{X}) = \left\{\psi_\kappa(\vec{X}) = 0 \,|\, \kappa = \overline{1, N_{EC}}\right\}, \tag{1.2}$$

$$\boldsymbol{\varphi}(\vec{X}) = \left\{\phi_\eta(\vec{X}) \le 0 \,|\, \eta = \overline{N_{EC}+1, N_{IC}}\right\}, \tag{1.3}$$

where $\vec{X}$ is the vector of the design variables (unknown structural parameters); f, ψ_κ, φ_η are the continuous functions of the the vector argument; $\vec{X}^*$ is the optimum solution or optimum point (the vector of optimum values of the structural parameters); f^* is the optimum value of the optimum criterion (objective function); N_{EC} is the number of constraints-equalities $\psi_\kappa(\vec{X})$, whose define hyperplanes of the feasible solutions; N_{IC} is the number of constraints-inequalities $\varphi_\eta(\vec{X})$, whose define a feasible region in the design space $\Im$.

The vector of the design variables comprises of unknown geometrical parameters of the structure $\vec{X}_G = \{X_{G,\chi}\}^T$, $\chi = \overline{1, N_{X,G}}$, unknown cross-

sectional dimensions of the structural members $\vec{X}_{CS} = \left\{ X_{CS,\alpha} \right\}^T$, $\alpha = \overline{1, N_{X,CS}}$, as well as unknown initial pre-stressing forces $\vec{X}_{PS} = \left\{ X_{PS,\beta} \right\}^T$, $\beta = \overline{1, N_{X,PS}}$, introduced into the specified redundant members of the structure (see Figure 1.1):

$$\vec{X} = \left\{ \vec{X}_G, \vec{X}_{CS}, \vec{X}_{PS} \right\}^T = \left\{ \left\{ X_{G,\chi} \right\}, \left\{ X_{CS,\alpha} \right\}, \left\{ X_{PS,\beta} \right\} \right\}^T, \tag{1.4}$$

where $N_{X,G}$ is the total number of unknown node coordinates of the steel structure; $N_{X,CS}$ is the total number of unknown cross-sectional dimensions of the structural members, $N_{X,PS}$ is the total number of unknown initial pre-stressing forces introduced into the specified redundant members of the bar system, $N_{X,G} + N_{X,CS} + N_{X,PS} = N_X$.

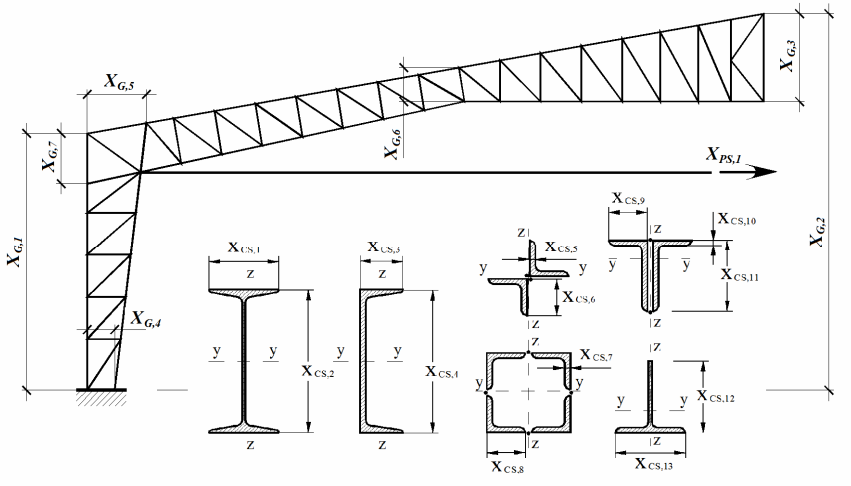

Fig. 1.1. The unknown (variable) parameters of the structure considered as design variables

In cases when vector of the design variables $\vec{X}$ consists of unknown cross-sectional dimensions only:

$$\vec{X} = \vec{X}_{CS} = \left\{ X_{CS,\alpha} \right\}^T; \tag{1.5}$$

then optimum material distribution problem (1.1) – (1.3), (1.5) for the steel structure is under consideration. The vector of the design variables $\vec{X}$ can also consists of unknown initial pre-stressing forces $\vec{X}_{PS} = \left\{ X_{PS,\beta} \right\}^T$, $\beta = \overline{1, N_{X,PS}}$, introduced into the specified redundant members of the structure:

$$\vec{X} = \left\{ \vec{X}_{CS}, \vec{X}_{PS} \right\}^T = \left\{ \left\{ X_{CS,\alpha} \right\}, \left\{ X_{PS,\beta} \right\} \right\}^T, \tag{1.6}$$

where $N_{X,CS} + N_{X,PS} = N_X$. In cases when vector of the design variables $\vec{X}$ consists of unknown cross-sectional dimensions and unknown initial pre-stressing forces, then optimum material and internal forces distribution problem (1.1) – (1.3), (1.6) for the steel structure is under consideration.

The specific technical-and-economic index (material weight, material cost, construction cost etc.) or another determined indicator can be considered as the objective function (1.1) taking into account the ability to formulate its analytical expression as a function of design variables $\vec{X}$.

Load-carrying capacities constraints (strength and stability inequalities) for all design sections of the structural members subjected to all design load combinations at the ultimate limit state as well as displacements constraints (stiffness inequalities) for the specified nodes of the bar system subjected to all design load combinations at the serviceability limit state should be included into the system of constraints (1.2) – (1.3). Additional requirements whose describe structural, technological and serviceability particularities of the considered structure can be included into the system (1.2) – (1.3) as well.

The design internal forces in the structural members used in the strength and stability inequalities of the system (1.2) – (1.3) are considered as state variables depending on design variables $\vec{X}$ and can be calculated from the following linear equations system of the finite element method [7]:

$$\mathbf{K}(\vec{X}_G, \vec{X}_{CS}) \times \vec{z}_{ULS,k} = \vec{p}_{ULS,k}(\vec{X}_G, \vec{X}_{PS}), \; k = \overline{1, N_{LC}^{ULS}}, \tag{1.7}$$

where $\mathbf{K}(\vec{X}_G, \vec{X}_{CS})$ is the stiffness matrix of the finite element model of the bar system, which should be formed depending on the unknown (variable) cross-sectional dimensions of the structural members $\vec{X}_{CS}$, as well as unknown (variable) node coordinates of the structure $\vec{X}_G$; $\vec{p}_{ULS,k}(\vec{X}_G, \vec{X}_{PS})$ is the column-vector of the node's loads for k^{th} design load combination of the ultimate limit state, which should be formed depending on unknown (variable) initial pre-stressing forces $\vec{X}_{PS}$, as well as unknown (variable) node coordinates of the structure $\vec{X}_G$; $\vec{z}_{ULS,k}$ is the result column-vector of the node displacements for k^{th} design load combination of the ultimate limit state, $\vec{z}_{ULS,k} = \mathbf{Z}_{\mathbf{FEM},k}^{ULS}(\vec{X}_G, \vec{X}_{CS}, \vec{X}_{PS}) = \mathbf{Z}_{\mathbf{FEM},k}^{ULS}(\vec{X})$; N_{LC}^{ULS} is the number of the design ultimate load combinations. For each i^{th} design section of j^{th} structural member subjected to k^{th} ultimate design load combination the design internal forces (axial force, bending moments and shear forces) can be calculated depending on node displacement column-vector $\vec{z}_{ULS,k}$.

The node displacement of the bar system used in stiffness inequalities of the system (1.2) – (1.3) are also considered as state variables depending on design variables $\vec{X}$ and can be calculated from the following linear equations

system of the finite element method [7]:

$$\mathbf{K}(\vec{X}_G, \vec{X}_{CS}) \times \vec{z}_{SLS,k} = \vec{p}_{SLS,k}(\vec{X}_G, \vec{X}_{PS}) \,,\; k = \overline{1, N_{LC}^{SLS}} \,, \tag{1.8}$$

where $\vec{p}_{SLS,k}(\vec{X}_{PS})$ is the column-vector of the node's loads for k^{th} design load combination of the serviceability limit state, which should be formed depending on unknown (variable) initial pre-stressing forces $\vec{X}_{PS}$, as well as unknown (variable) node coordinates of the structure $\vec{X}_G$; $\vec{z}_{ULS,k}$ is the result column-vector of the node displacements for k^{th} design load combination of the serviceability limit state, $\vec{z}_{SLS,k} = \mathbf{Z}_{\mathbf{FEM},k}^{SLS}(\vec{X}_G, \vec{X}_{CS}, \vec{X}_{PS}) = \mathbf{Z}_{\mathbf{FEM},k}^{SLS}(\vec{X})$; N_{LC}^{SLS} is the number of the design serviceability load combinations. For each m^{th} node of the finite element model subjected to k^{th} serviceability design load combination the design vertical and horizontal displacements can be calculated depending on node displacement column-vector $\vec{z}_{SLS,k}$.

The system of constraints (1.2) – (1.3) should cover strength and stability constraints formulated for all design sections of all structural members of the considered steel structure subjected to all design load combinations at the ultimate limit state. The following *strength constraints* should be included in the system of constraints (1.2) – (1.3), formulated for all design sections, $\forall i = \overline{1, N_{DS}}$, of all structural members, $\forall j = \overline{1, N_B}$, subjected to all ultimate load case combination, $\forall k = \overline{1, N_{LC}^{ULS}}$, namely:

- normal stresses verifications:

$$\frac{\sigma_{\max,ijk}(\vec{X})}{R_y \gamma_c} - 1 \le 0 \,; \tag{1.9}$$

- shear stresses verifications:

$$\frac{\tau_{\max,ijk}(\vec{X})}{0.58 R_y \gamma_c} - 1 \le 0 \,; \tag{1.10}$$

- as well as equivalent stresses verifications:

$$\frac{\sigma_{eqv,ijk}(\vec{X})}{1.15 R_y \gamma_c} - 1 = \frac{\sqrt{\sigma_{x,ijk}^2(\vec{X}) + 3\tau_{x,ijk}^2(\vec{X})}}{1.15 R_y \gamma_c} - 1 \le 0 \,, \tag{1.11}$$

where $\sigma_{\max,ijk}(\vec{X})$ are $\tau_{\max,ijk}(\vec{X})$ are the maximum value of the normal and shear stresses respectively caused by internal forces (axial force, bending moments and shear forces) acting in i^{th} design section of j^{th} structural member subjected to k^{th} ultimate load case combination calculated from the

linear equations system of the finite element method (1.7); γ_c is the safety factor [4]; R_y is the design strength for steel member subjected to tension, bending and compression; $R_y\gamma_c$, $0.58R_y\gamma_c$ and $1.15R_y\gamma_c$ are allowable values for normal, shear and equivalent stresses respectively [4]; N_{DS} is the number of design sections in structural members; N_B is the number of structural members; $\sigma_{x,ijk}(\vec{X})$, $\tau_{x,ijk}(\vec{X})$ and $\sigma_{eqv,ijk}(\vec{X})$ are normal, shear and equivalent stresses respectively at the specified cross-section point caused by internal forces acting in i^{th} design section of j^{th} structural member subjected to k^{th} ultimate load case combination calculated from the linear equations system of the finite element method (1.7). The maximum value of the normal $\sigma_{\max,ijk}(\vec{X})$ and shear stresses $\tau_{\max,ijk}(\vec{X})$, as well as normal $\sigma_{x,ijk}(\vec{X})$, shear $\tau_{x,ijk}(\vec{X})$ and equivalent $\sigma_{eqv,ijk}(\vec{X})$ stresses at the specified cross-section point should be calculated depending on the variable geometrical parameters of the structure $\vec{X}_G$, variable initial pre-stressing forces $\vec{X}_{PS}$ and variable cross-sectional dimensions of the structural members $\vec{X}_{CS}$.

The following *stability constraints* should be included in the system of constraints (1.2) – (1.3), formulated for all design sections, $\forall i = \overline{1, N_{DS}}$, subjected to all ultimate load case combination, $\forall k = \overline{1, N_{LC}^{ULS}}$, namely:

- flexural buckling verifications for all column structural members, $\forall j = \overline{1, N_{CM}}$:

$$\frac{\sigma_{\max,ijk}(\vec{X})}{\varphi_{y,j}(\vec{X}_G, \vec{X}_{CS})R_y\gamma_c} - 1 \le 0, \tag{1.12}$$

$$\frac{\sigma_{\max,ijk}(\vec{X})}{\varphi_{z,j}(\vec{X}_G, \vec{X}_{CS})R_y\gamma_c} - 1 \le 0; \tag{1.13}$$

- torsional-flexural buckling verifications for all column structural members, $\forall j = \overline{1, N_{CM}}$:

$$\frac{\sigma_{\max,ijk}(\vec{X})}{\varphi_{c,j}(\vec{X}_G, \vec{X}_{CS})R_y\gamma_c} - 1 \le 0; \tag{1.14}$$

- lateral-torsional buckling verifications for all beam structural members, $\forall j = \overline{1, N_{BM}}$:

$$\frac{\sigma_{\max,ijk}(\vec{X})}{\varphi_{b,j}(\vec{X}_G,\vec{X}_{CS})R_y\gamma_c}-1\le 0, \tag{1.15}$$

where $\varphi_{y,j}(\vec{X}_G,\vec{X}_{CS})$ and $\varphi_{z,j}(\vec{X}_G,\vec{X}_{CS})$ are column's stability factors corresponded to flexural buckling relative to main axes of inertia and calculated depending on the design lengths $l_{ef,y,j}$, $l_{ef,z,j}$, cross-section type and cross-section geometrical properties for the j^{th} structural member [4]; $\varphi_{c,j}(\vec{X}_G,\vec{X}_{CS})$ is the column's stability factor corresponded to torsional-flexural buckling and calculated depending on the design lengths $l_{ef,y,j}$, $l_{ef,z,j}$, $l_{ef,T,j}$, cross-section type and cross-section geometrical properties for the j^{th} structural member[4]; N_{CM} is the number of column structural members; $\varphi_{b,j}(\vec{X}_G,\vec{X}_{CS})$ is the beam's stability factor corresponded to lateral-torsional buckling and calculated depending on the design length $l_{ef,b,j}$, cross-section type and cross-section geometrical properties for the j^{th} structural member [4]; N_{BM} is the number of beam structural members. The flexural buckling factors $\varphi_{y,j}(\vec{X}_G,\vec{X}_{CS})$ and $\varphi_{z,j}(\vec{X}_G,\vec{X}_{CS})$, as well as torsional-flexural buckling factor $\varphi_{c,j}(\vec{X}_G,\vec{X}_{CS})$ and the lateral-torsional buckling factor $\varphi_{b,j}(\vec{X}_G,\vec{X}_{CS})$ should be calculated depending on the variable geometrical parameters of the structure $\vec{X}_G$ and variable cross-sectional dimensions of the structural members $\vec{X}_{CS}$.

The following buckling verifications for beam-column structural members should also be included in the system of constraints (1.2) – (1.3), formulated for all design sections, $\forall i=\overline{1,N_{DS}}$, of all beam-column structural members, $\forall j=\overline{1,N_{BCM}}$, subjected to all ultimate load case combination, $\forall k=\overline{1,N_{LC}^{ULS}}$, namely:

$$\frac{\sigma_{\max,ijk}(\vec{X})}{\varphi_{e,ijk}(\vec{X})R_y\gamma_c}-1\le 0, \tag{1.16}$$

$$\frac{\sigma_{\max,ijk}(\vec{X})}{\varphi_{y,j}(\vec{X}_G,\vec{X}_{CS})c_{ijk}(\vec{X})R_y\gamma_c}-1\le 0, \tag{1.17}$$

where $\varphi_{e,ijk}(\vec{X})$ and $c_{ijk}(\vec{X})$ are beam-column's stability factors corresponded to in-plane and out-of-plane buckling and calculated depending on the internal forces (ration of the bending moment to the axial force), as well as depending on the design lengths $l_{ef,y,j}$, $l_{ef,z,j}$, cross-section type and cross-section geometrical properties for the j^{th} structural member [4]; N_{BCM} is the total number of beam-column structural members, $N_{BCM}+N_{CM}+N_{BM}=N_B$. The

beam-column's stability factors $\varphi_{e,ijk}(\vec{X})$ and $c_{ijk}(\vec{X})$ should be calculated depending on variable geometrical parameters of the structure $\vec{X}_G$, variable cross-sectional dimensions of the structural members $\vec{X}_{CS}$ and variable initial pre-stressing forces $\vec{X}_{PS}$.

The following *local buckling constraints* should also be included into the system of constraints:

$$\frac{\overline{\lambda}_{w,j}(\vec{X}_{CS})}{\overline{\lambda}_{uw,j}(\vec{X})}-1\le 0, \tag{1.18}$$

$$\frac{\overline{\lambda}_{f,j}(\vec{X}_{CS})}{\overline{\lambda}_{uf,j}(\vec{X})}-1\le 0, \tag{1.19}$$

where $\overline{\lambda}_{w,j}(\vec{X}_{CS})$ and $\overline{\lambda}_{f,j}(\vec{X}_{CS})$ are the non-dimensional slenderness of the web and flange respectively of the cross-section for j^{th} structural member; $\overline{\lambda}_{uw,j}(\vec{X})$ and $\overline{\lambda}_{uf,j}(\vec{X})$ are the maximum values for corresponded non-dimensional slenderness for column, beam and beam-column structural members calculated depending on the internal forces (ration of the bending moment to the axial force), as well as depending on the design lengths $l_{ef,y,j}$, $l_{ef,z,j}$, cross-section type and cross-section geometrical properties for the j^{th} structural member [4]. The non-dimensional slenderness $\overline{\lambda}_{w,j}(\vec{X}_{CS})$ and $\overline{\lambda}_{f,j}(\vec{X}_{CS})$ should be calculated depending on the variable cross-sectional dimensions of the structural members $\vec{X}_{CS}$ only. At the same time, the maximum values for corresponded non-dimensional slenderness $\overline{\lambda}_{uw,j}(\vec{X})$ and $\overline{\lambda}_{uf,j}(\vec{X})$ should be calculated depending on the variable geometrical parameters of the structure $\vec{X}_G$ and variable cross-sectional dimensions of the structural members $\vec{X}_{CS}$ and variable initial pre-stressing forces $\vec{X}_{PS}$.

The system of constraints (1.2) – (1.3) should also cover the *displacements constraints* (stiffness inequalities) for the specified nodes of the considered steel structure subjected to all design load combinations at the serviceability limit state. The following horizontal and vertical displacements constraints should be included into the system of constraints (1.2) – (1.3), formulated for all nodes, $\forall m=\overline{1,N_N}$, of the steel structure subjected to all serviceability load case combination, $\forall k=\overline{1,N_{LC}^{SLS}}$, namely:

$$\frac{\delta_{x,mk}(\vec{X})}{\delta_{ux,m}}-1\le 0, \tag{1.20}$$

$$\frac{\delta_{z,mk}(\vec{X})}{\delta_{uz,m}} - 1 \le 0, \tag{1.21}$$

where $\delta_{x,mk}(\vec{X})$ and $\delta_{z,lk}(\vec{X})$ are the horizontal and vertical displacements respectively for l^{th} node of the steel structure subjected to k^{th} serviceability load case combination calculated from the linear equations system of the finite element method (1.8); $\delta_{ux,l}$ and $\delta_{uz,l}$ are the allowable horizontal and vertical displacements for l^{th} structural node; N_N is the number of nodes in the considered steel structure.

Additional requirements, whose describe structural, technological and serviceability particularities of the considered structure, as well as constraints on the building functional volume can be also included into the system (1.2) – (1.3). In particular these requirements can be presented in the form of constraints on lower and upper values of the design variables, $\forall \iota = \overline{1, N_X}$:

$$1 - \frac{X_\iota}{X_\iota^L} \le 0, \tag{1.22}$$

$$\frac{X_\iota}{X_\iota^U} - 1 \le 0, \tag{1.23}$$

where X_ι^L and X_ι^U are the lower and upper bounds for the design variable X_ι.

2. An improved gradient projection method for solving the formulated parametric optimisation problem. The parametric optimization problem stated as non-linear programming task by (1.1) – (1.3) can be solved using a gradient projection method. The method of *objective function gradient projection onto the active constraints surface with simultaneous correction of the constraints violations* ensures effective searching for solution of the non-linear programming tasks occurred when optimum designing of the building structures [9, 11].

The gradient projection method operates with the first derivatives or gradients only of both the objective function (1.1) and constraints (1.2) – (1.3). The method is based on the iterative construction of such sequence (2.1) of the approximations of the design variables $\vec{X} = \{X_\iota\}^T$, $\iota = \overline{1, N_X}$, that provides the convergence to the optimum solution (optimum values of the structural parameters):

$$\vec{X}_{\iota+1} = \vec{X}_\iota + \Delta\vec{X}_\iota, \tag{2.1}$$

where $\vec{X}_\iota = \{X_\iota\}^T$, $\iota = \overline{1, N_X}$ is the current approximation to the optimum solution $\vec{X}^*$ that satisfies both constraints-equalities (1.2) and constraints-inequalities (1.3) with the extreme value of the objective function (1.1);

$\Delta\vec{X}_t = \{\Delta X_\iota\}^T$, $\iota = \overline{1, N_X}$, is the increment vector for the current values of the design variables $\vec{X}_t$; t is the iteration's index. The start point of the iterative searching process $\vec{X}_{t=0}$ can be assigned as engineering estimation of the admissible design of the structure.

The active constraints only of constraints system (1.2) – (1.3) should be considered at each iteration. A set of active constraints numbers $\mathbf{A}$ calculated for the current approximation $\vec{X}_t$ to the optimum solution (current design of the structure) is determined as:

$$\mathbf{A} = \boldsymbol{\kappa} \cup \boldsymbol{\eta},\ \boldsymbol{\kappa} = \left\{ \kappa \,\middle|\, \left| \psi_\kappa\left(\vec{X}_t\right) \right| \geq -\varepsilon \right\},\ \boldsymbol{\eta} = \left\{ N_{EC} + \eta \,\middle|\, \phi_\eta\left(\vec{X}_t\right) \geq -\varepsilon \right\}, \qquad (2.2)$$

where ε is a small positive number introduced here in order to diminish the oscillations on movement alongside of the active constraints surface.

The increment vector $\Delta\vec{X}_t$ for the current values of the design variables $\vec{X}_t$ can be determined by the following equation:

$$\Delta\vec{X}_t = \Delta\vec{X}_\perp^t + \Delta\vec{X}_\parallel^t, \qquad (2.3)$$

where $\Delta\vec{X}_\perp^t$ is the vector calculated subject to the condition of elimination the constraint's violations; $\Delta\vec{X}_\parallel^t$ is the vector determined taking into consideration the improvement of the objective function value. Vectors $\Delta\vec{X}_\parallel^t$ and $\Delta\vec{X}_\perp^t$ are directed parallel and perpendicularly accordingly to the subspace with the vectors basis of the linear-independent constraint's gradients, such that:

$$\left(\Delta\vec{X}_\perp^t\right)^T \Delta\vec{X}_\parallel^t = 0. \qquad (2.4)$$

The values of the constraint's violations for the current approximation $\vec{X}_t$ of the design variables are accumulated into the following vector:

$$\mathbf{V} = \left(\psi_\kappa(\vec{X}) \forall \kappa \in \boldsymbol{\kappa};\ \phi_\eta(\vec{X}) \forall \eta \in \boldsymbol{\eta}\right).$$

Let us introduce a set $\mathbf{L}$, $\mathbf{L} \subseteq \mathbf{A}$, of the constraint's numbers, such that the gradients of the constraints at the current approximation $\vec{X}_t$ to the optimum solution are linear-independent.

Component $\Delta\vec{X}_\perp^t$ is calculated from the equation presented below:

$$\Delta\vec{X}_\perp^t = [\nabla\varphi]\vec{\mu}_\perp, \qquad (2.5)$$

where $[\nabla\varphi]$ is the matrix that consists of components $\frac{\partial\psi_\kappa}{\partial X_\iota}$ and $\frac{\partial\phi_\eta}{\partial X_\iota}$, here $\iota=\overline{1,N_X}$, $\kappa\in\mathbf{L}$, $\eta\in\mathbf{L}$; $\vec{\mu}_\perp$ is the column-vector that defines the design variables increment subject to the condition of elimination the constraint's violations. Vector $\vec{\mu}_\perp$ can be calculated as presented below.

In order to correct constraint's violations $\mathbf{V}$, vector $\Delta\vec{X}_\perp^t$ to a first approximation should also satisfy Taylor's theorem for the continuously differentiable multivariable function in the vicinity of point $\vec{X}_t$ for each constraint from set $\mathbf{L}$, namely:

$$-\mathbf{V}=[\nabla\varphi]^T\,\Delta\vec{X}_\perp^t. \tag{2.6}$$

With substitution of (2.5) into (2.6) we obtain the system of equations to determine column-vector $\vec{\mu}_\perp$:

$$[\nabla\varphi]^T[\nabla\varphi]\vec{\mu}_\perp=-\mathbf{V}. \tag{2.7}$$

Component $\Delta\vec{X}_\parallel^t$ is determined using the following equation:

$$\Delta\vec{X}_\parallel^t=\xi\times\vec{p}_{\nabla f}=\xi\left(\nabla\vec{f}-[\nabla\varphi]\vec{\mu}_\parallel\right), \tag{2.8}$$

where $\nabla\vec{f}$ is the vector of the objective function gradient in the current point (current approximation of the design variables) $\vec{X}_t$; $\vec{p}_{\nabla f}$ is the projection of the objective function gradient vector onto the active constraints surface in the current point $\vec{X}_t$; $\vec{\mu}_\parallel$ is the column-vector that defines the design variable's increment subject to the improvement of the objective function value. Column-vector $\vec{\mu}_\parallel$ can be calculated approximately using the least-square method by the following equation:

$$[\nabla\varphi]\vec{\mu}_\parallel\approx\nabla\vec{f}, \tag{2.9}$$

or from the equation presented below:

$$[\nabla\varphi]^T[\nabla\varphi]\vec{\mu}_\parallel=[\nabla\varphi]^T\nabla\vec{f}, \tag{2.10}$$

where ξ is the step parameter, which can be calculated subject to the desired increment Δf of the purpose function on movement along the direction of the purpose function anti-gradient. The increment Δf can be assign as 5...25% from the current value of the objective function $f\left(\vec{X}_t\right)$:

$$\Delta f = \xi \left(\nabla \vec{f}\right)^T \nabla \vec{f}\,,\ \xi = \frac{\Delta f}{\left(\nabla \vec{f}\right)^T \nabla \vec{f}}\,, \tag{2.11}$$

where in case of minimization (1.1) Δf and ξ accordingly have negative values. The parameter ξ can be also calculated using the dependency presented below:

$$\xi = \frac{\Delta f}{\left(\vec{p}_{\nabla f}\right)^T \nabla \vec{f}}\,, \tag{2.12}$$

that follows from the condition of attainment the desired increment of the objective function Δf on the movement along the direction of the objective function anti-gradient projection onto the active constraints surface. Step parameter ξ can be also selected as a result of numerical experiments performed for each type of the structure individually [6, 15].

Using (2.5) and (2.8), (2.3) can be rewritten as presented below:

$$\Delta \vec{X}_t = \left[\nabla \varphi\right] \vec{\mu}_\perp + \xi \left(\nabla \vec{f} - \left[\nabla \varphi\right] \vec{\mu}_\parallel\right) \tag{2.13}$$

or

$$\Delta \vec{X}_t = \xi\ \nabla \vec{f} + \left[\nabla \varphi\right]\left(\vec{\mu}_\perp - \xi\ \vec{\mu}_\parallel\right), \tag{2.14}$$

where column-vectors $\vec{\mu}_\perp$ and $\vec{\mu}_\parallel$ are calculated using (2.7) and (2.9) or (2.10), respectively.

The linear-independent constraints of the system (1.2) – (1.3) should be detected when constructing the matrix of the active constraints gradients $\left[\nabla \varphi\right]$ used by (2.7) and (2.9) or (2.10). Selection of the linear-independent constraints can be performed based on the equivalent transformations of the resolving equations of the gradient projection method using the non-degenerate transformation matrix $\mathbf{H}$, such that the sub-diagonal elements of the matrix $\mathbf{H}\left[\nabla \varphi\right]$ equal to zero. An orthogonal matrix of the elementary mapping (Householder's transformation) [17] has been used to select linear-independent constraints of the system (1.2) – (1.3) as well as to form triangular structure of the nonzero elements of matrix $\mathbf{H}\left[\nabla \varphi\right]$ [12].

Using Householder's transformations described above triangular structure of the nonzero elements of matrix $\mathbf{H}\left[\nabla \varphi\right]$ is formed step-by-step. Besides, (2.7) and (2.9) can be rewritten as follow:

$$\left(\left[\nabla \varphi\right]^T \mathbf{H}^T\right)\left(\mathbf{H}\left[\nabla \varphi\right]\right)\vec{\mu}_\perp = -\mathbf{V}\,, \tag{2.15}$$

$$\mathbf{H}\left[\nabla \varphi\right]\vec{\mu}_\square \approx \mathbf{H}\nabla \vec{f}\,. \tag{2.16}$$

Equivalent Householder transformations of the resolving equations (2.15),

(2.16) have been proposed by the paper [12]. They increase numerical efficiency of the algorithm developed based on the considered method.

In order to calculate column-vectors $\vec{\mu}_{\perp}$ and $\vec{\mu}_{\parallel}$, it is required only to perform forward and backward substitutions in (2.15) and (2.16).

To accelerate the convergence of the minimization algorithm presented above, h^{th} columns should be excluded from matrix $\mathbf{H}[\nabla\varphi]$. These columns correspond to those constraints from (1.3), for whose the following inequality satisfies:

$$\mu_{\perp h} - \xi \times \mu_{\square h} > 0 . \tag{2.17}$$

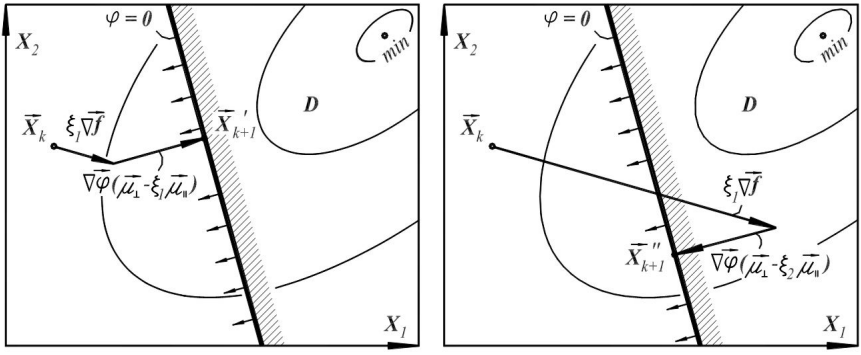

(a) (b)

Fig. 2.1. The selection of the constraints-inequalities:
(a) – $\mu_{\perp h} - \xi_1 \times \mu_{\square h} < 0$; (b) – $\mu_{\perp h} - \xi_2 \times \mu_{\square h} > 0$.

Actually, when $\mu_{\perp h} - \xi \times \mu_{\square h} > 0$, then the return onto the active constraints surface from the feasible region $\Im$ is performed with simultaneous degradation of the objective function value (see Fig. 2.1b). At the same time, in case of $\mu_{\perp h} - \xi \times \mu_{\square h} < 0$, both the improvement of the objective function value and the return from the inadmissible region onto the active constraints surface are performed (see Fig. 2.1a).

When excluding h^{th} columns from matrix $\mathbf{H}[\nabla\varphi]$ corresponded to those constraints for whose (2.17) is satisfied, the matrix $\left(\mathbf{H}[\nabla\varphi]\right)_{red}$ with a broken (non-triangular) structure of the non-zero elements is obtained. The set $\mathbf{L}$ of the linear-independent active constraints numbers transforms into the set $\mathbf{L}_{red}$ respectively. At the same time, the vector of the constraint's violations $\mathbf{V}$ reduced into the vector $\mathbf{V}_{red}$ accordingly. In order to restore the triangular structure of the matrix $\left(\mathbf{H}[\nabla\varphi]\right)_{red}$ with zero sub-diagonal elements, Givens transformations (Givens rotations) [17] can be used.

Considering Givens transformations, (2.15) and (2.16) for column-vectors

$\left(\vec{\mu}_{\perp}\right)_{red}$ and $\left(\vec{\mu}_{\square}\right)_{red}$ can be rewritten as:

$$\left(\left[\nabla\varphi\right]^T \mathbf{H}^T\right)_{red} \mathbf{G}^T\mathbf{G}\left(\mathbf{H}\left[\nabla\varphi\right]\right)_{red}\left(\vec{\mu}_{\perp}\right)_{red} = -\mathbf{V}_{red}, \tag{2.18}$$

$$\mathbf{G}\left(\mathbf{H}\left[\nabla\varphi\right]\right)_{red}\left(\vec{\mu}_{\square}\right)_{red} \approx \mathbf{GH}\nabla\vec{f}\,. \tag{2.19}$$

Equivalent transformations of the resolving equations (2.18), (2.19) using Givens rotations (transformations with matrix $\mathbf{G}$) ensure acceleration of the iterative searching process (2.1) in those cases when (2.17) takes into account due to decreasing the amount of calculations [12].

The main resolving equation of the gradient method (2.13) and (2.14) can be rewritten as presented below:

$$\Delta\vec{X}_t = \left(\mathbf{H}\left[\nabla\varphi\right]\right)_{red}\left(\vec{\mu}_{\perp}\right)_{red} + \xi\left(\nabla\vec{f} - \left(\mathbf{H}\left[\nabla\varphi\right]\right)_{red}\left(\vec{\mu}_{\parallel}\right)_{red}\right) \tag{2.20}$$

or

$$\Delta\vec{X}_t = \xi\ \nabla\vec{f} + \left(\mathbf{H}\left[\nabla\varphi\right]\right)_{red}\left(\left(\vec{\mu}_{\perp}\right)_{red} - \xi\left(\vec{\mu}_{\parallel}\right)_{red}\right). \tag{2.21}$$

It should be noted that the lengths of the gradient vectors for the objective function (1.1), as well as for constraints (1.2) – (1.3), remain as they were in scope of the proposed equivalent transformations ensuring the dependability of the optimization algorithm [12].

The determination the convergence criterion is the final question when using the iterative searching for the optimum point (2.1) described above. Considering the geometrical content of the gradient steepest descent method, we can assume that at the permissible point $\vec{X}_t$ the component of the increment vector $\Delta\vec{X}_{\parallel}^t$ for the design variables should be vanish, $\Delta\vec{X}_{\parallel}^t \to 0$, in case of approximation to the optimum solution of the non-linear programming task presented by (1.1) – (1.5). So, the following convergence criterion of the iterative procedure (2.1) can be assigned:

$$\left\|\Delta\vec{X}_{\parallel}^k\right\| = \sqrt{\sum_{\iota=1}^{N_X}\left(\Delta X_{\parallel,\iota}^k\right)^2} < \varepsilon_1, \tag{2.22}$$

where ε_1 is a small positive number. In the paper [12] the convergence criteria for the iterative procedure (2.1) has been presented in detail.

3. A parametric optimization algorithm based on the gradient projection method. Let us presented the following numerical algorithm to solve the parametric optimization problem for steel structures formulated above.

Step 1. Describing an initial design (a set of design variables) and initial data for structural optimization.

The design variable vector $\vec{X}_k = (\vec{X}_G, \vec{X}_{CS}, \vec{X}_{PS})_k^T$ should be specified, where k is the iteration index, $k = 0$. The structural topology, cross-section types and node type connections of the bars, the support conditions of the bar system, as well as loading and pre-stressing patterns, load case combinations and load design values are prescribed and constants.

Initial data for optimization of the considered steel structure are design strength for steel member R_y, safety factor γ_c, factors to define flexural design lengths $l_{ef,y,j}$, $l_{ef,z,j}$ and flexural-torsional design length $l_{ef,T,j}$ for all column structural members; factor to define lateral-torsional design length $l_{ef,b,j}$ for all beam structural members; allowable values for horizontal and vertical displacements $\delta_{ux,l}$ and $\delta_{uz,l}$ of the specified nodes of the considered steel structure; lower $\vec{X}^L$ and upper $\vec{X}^U$ bounds for the design variables; as well as specified objective function $f(\vec{X}_k)$.

Step 2. Calculation of the geometrical and design lengths for all structural members.

The geometrical lengths l_j of all structural members are calculated based on the node coordinates of the considered steel structure. The latter depend on the unknown (variable) geometrical parameters of the structure $\vec{X}_G$. The design lengths $l_{ef,y,j}$, $l_{ef,z,j}$ and $l_{ef,T,j}$ of all column structural members are calculated using calculated geometrical lengths l_j and initial data relating to the design length factors. Variation of the geometrical lengths l_j and corresponded design lengths $l_{ef,y,j}$, $l_{ef,z,j}$ and $l_{ef,T,j}$ on the further iterations should be performed based on the current values of the variable (unknown) parameters $\vec{X}_G$ of the geometrical scheme.

Step 3. Calculation of the cross-section dimensions and geometrical properties for all design cross-sections.

Geometrical properties of the design cross-sections (areas, moments of inertia, elastic section moments, radiuses of inertia, etc.), as well as non-dimensional slenderness for cross-section elements (webs and flanges) $\bar{\lambda}_{w,j}(\vec{X}_{CS})$ and $\bar{\lambda}_{f,j}(\vec{X}_{CS})$ should be calculated depending on the current values of the unknown (variable) cross-section dimensions $\vec{X}_{CS}$.

Step 4. Linear structural analysis of the considered steel structure.

For each m^{th} node of the finite element model subjected to k^{th} serviceability load case combination the displacements and rotations, as well as the design horizontal $\delta_{x,mk}(\vec{X})$ and vertical $\delta_{z,lk}(\vec{X})$ displacements can be calculated using the linear equations system of the finite element method (1.8).

For each i^{th} design section of j^{th} structural member subjected to k^{th} ultimate load case combination the design internal forces can be calculated

using the linear equations system of the finite element method (1.7).

Step 5. Calculation of the state variables (stresses, buckling factors, allowable non-dimensional slenderness etc.).

The maximum value of the normal $\sigma_{\max,ijk}(\vec{X})$ and shear stresses $\tau_{\max,ijk}(\vec{X})$, as well as normal $\sigma_{x,ijk}(\vec{X})$, shear $\tau_{x,ijk}(\vec{X})$ and equivalent $\sigma_{eqv,ijk}(\vec{X})$ stresses at the specified cross-section point should be calculated depending on the internal forces (axial force, bending moments and shear forces) acting in i^{th} design section of j^{th} structural member subjected to k^{th} ultimate load case combination as presented by the design code.

The flexural buckling factors $\varphi_{y,j}(\vec{X}_G,\vec{X}_{CS})$, $\varphi_{z,j}(\vec{X}_G,\vec{X}_{CS})$, torsional-flexural buckling factor $\varphi_{c,j}(\vec{X}_G,\vec{X}_{CS})$ for column structural members, as well as the lateral-torsional buckling factor $\varphi_{b,j}(\vec{X}_G,\vec{X}_{CS})$ for beam structural members should be calculated depending on the corresponded design lengths, cross-section type and cross-section geometrical properties for the structural members according to the design code [4]. The stability factors $\varphi_{e,ijk}(\vec{X})$ and $c_{ijk}(\vec{X})$ for beam-column structural members should be calculated depending on the ration of the bending moment to the axial force, as well as depending on the corresponded design lengths, cross-section type and cross-section geometrical properties for the structural members according to the design code [4].

The maximum values for corresponded non-dimensional slenderness $\overline{\lambda}_{uw,j}(\vec{X})$ and $\overline{\lambda}_{uf,j}(\vec{X})$ for column, beam and beam-column structural members should be calculated depending on the internal forces (ration of the bending moment to the axial force), as well as depending on the design lengths $l_{ef,y,j}$, $l_{ef,z,j}$, cross-section type and cross-section geometrical properties for the j^{th} structural member [4].

Step 6. Verifications of the constraints and construction the set of active constraints numbers $\mathbf{A}$.

Verification of the constraints (1.9) – (1.17) should be performed for all ultimate load case combinations and all design cross-sections of all structural members. Verification of the constraints (1.20) – (1.21) should be also conducted for all serviceability load case combinations and all design structural nodes. Additional requirements (1.22) – (1.23) in the form of constraints on lower and upper values of the design variables, as well as local buckling constraints (1.18) – (1.19) should also be verified. Set of active constraints numbers $\mathbf{A}$ calculated for the current approximation $\vec{X}_k$ should be constructed according to (2.2).

Step 7. Calculation of the current objective function value $f(\vec{X}_k)$, objective function gradient $\nabla f(\vec{X}_k)$ and determination of the desired

decrement of the objective function value $\Delta f(\vec{X}_k)$.

The objective function gradient $\nabla f(\vec{X}_k)$ can be calculated by the numerical differentiation with respect to the design variables using the finite difference approximation. The desired decrement of the objective function value $\Delta f(\vec{X}_k)$ can be assigned as 5…25% from the current objective function value $f(\vec{X}_k)$.

Step 8. Construction of the constraint's violations vector $\mathbf{V}$ and the matrix of the active constraint's gradients $[\nabla\varphi]$. The vector of the values of the constraint's violations $\mathbf{V}$ and the matrix of the constraint's gradients $[\nabla\varphi]$ are constructed for active constraints only according to the set of active constraints numbers $\mathbf{A}$.

Step 9. Construction the matrix of active linear-independent constraint's gradients with triangular structure. The set of linear-independent constraint's numbers $\mathbf{L}$ and the matrix of active linear-independent constraint's gradients $\mathbf{H}[\nabla\varphi]$ with triangular structure are constructed according to the algorithm presented by the paper [12].

Step 10. Step parameter ξ calculation. Step parameter ξ should be calculated according to (2.10) or (2.11) and can be modified on the further iterations depending on convergence of the iterative process (2.1).

Step 11. Calculation the column-vectors $\vec{\mu}_{\perp}$ and $\vec{\mu}_{\square}$ which define the design variables increment subject to the condition of elimination the constraint's violations and subject to the improvement of the objective function value. The vectors $\vec{\mu}_{\perp}$ and $\vec{\mu}_{\square}$ can be calculated using (2.19) and (2.20) respectively.

If some h^{th} component of the column-vectors $\vec{\mu}_{\perp}$ and $\vec{\mu}_{\square}$ satisfies (2.12), the corresponded constraint gradient $\nabla\varphi_h$ should be excluded from the matrix $[\nabla\varphi]$, and corresponded violations V_h should be excluded from the vector $\mathbf{V}$, as well as the return to step 9 has to be conducted. In contrary case transition to the step 11 should be performed.

Step 12. Calculation the increment vector for the current design variables and determination the improved approximation to the optimum solution. The increment vector $\Delta\vec{X}_k$ for the current design variables values $\vec{X}_k$ should be calculated according to (2.20) or (2.21). The improved approximation $\vec{X}_{k+1}$ to the optimum solution should be determined according to (2.1).

Step 13. Stop criteria verification of iterative searching for the optimum solution. If all constraints (1.9) – (1.23) are satisfied with appropriate accuracy, as well as inequality (2.22) or one of the stop criteria described by the paper [12] is also satisfied, then transition to the step 13 should be performed. In contrary case return to the step 1 should be conducted with $k \leftarrow k+1$.

Step 14. Discretization the optimum solution $\vec{X}_k$ obtained in the continuum space of the design variables.

Step 15. Optimum parameters of the structure is $\vec{X}_k$ with optimum value of the objective function $f(\vec{X}_k)$.

Figure 3.1 presents the flow chart for structural optimization according to the searching technique describing by the gradient projection method considered above.

4. Results and discussion. In order to estimate an efficiency of the new methods or algorithms, a comparison with alternative methods or algorithms presented by other authors using different optimization techniques should be performed. Criteria to implement such comparison are described, e.g. by Haug and Arora [6] and Crowder et al. [3]. Many of these criteria, such as robustness, amount of functions calculations, requirements to the computer memory, numbers of iterations etc. cannot be used due to lack of corresponded information in the technical literature. Therefore, an efficiency estimation of the proposed methodology for solving parametric optimization problems presented above will be based on the comparison of the optimization results obtained using the proposed numerical algorithm, as well as of the results presented by the literature and widely used for testing. The initial data and mathematical models of the parametric optimization problems considered below were assumed as the same as described in the literature.

4.1. Geometry and cross-sectional optimization of a 19-bar cantilever truss. Figure 4.1 shows a 19-bar cantilever truss designed for the vertical loads $P = 10$ kN. Table 4.1 presents initial data for truss optimum design. There were no lower and upper bounds for the cross section areas for all truss members.

Table 4.1

Initial data for optimization of the truss

Unit weight of the truss material ρg	10^4 kg/m^3
Modulus of elasticity E	$2 \cdot 10^4$ kN/cm^2
The allowable normal stresses $\sigma_{\max}$ in tension and compression	300 MPa
The allowable displacement $\delta_{\max}$ in the vertical direction for 11^{th} node	50 mm

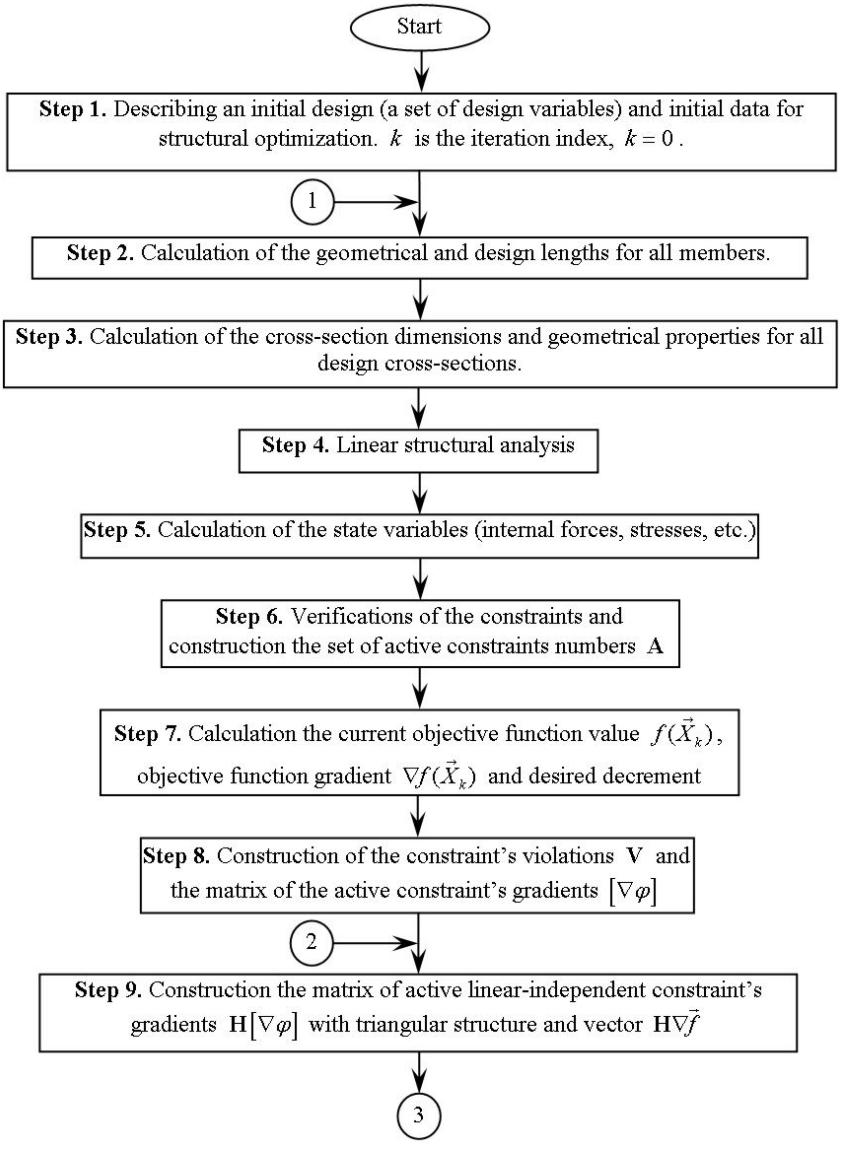

Fig. 3.1. The flow chart for structural optimization
according to the searching technique based on the gradient projection method

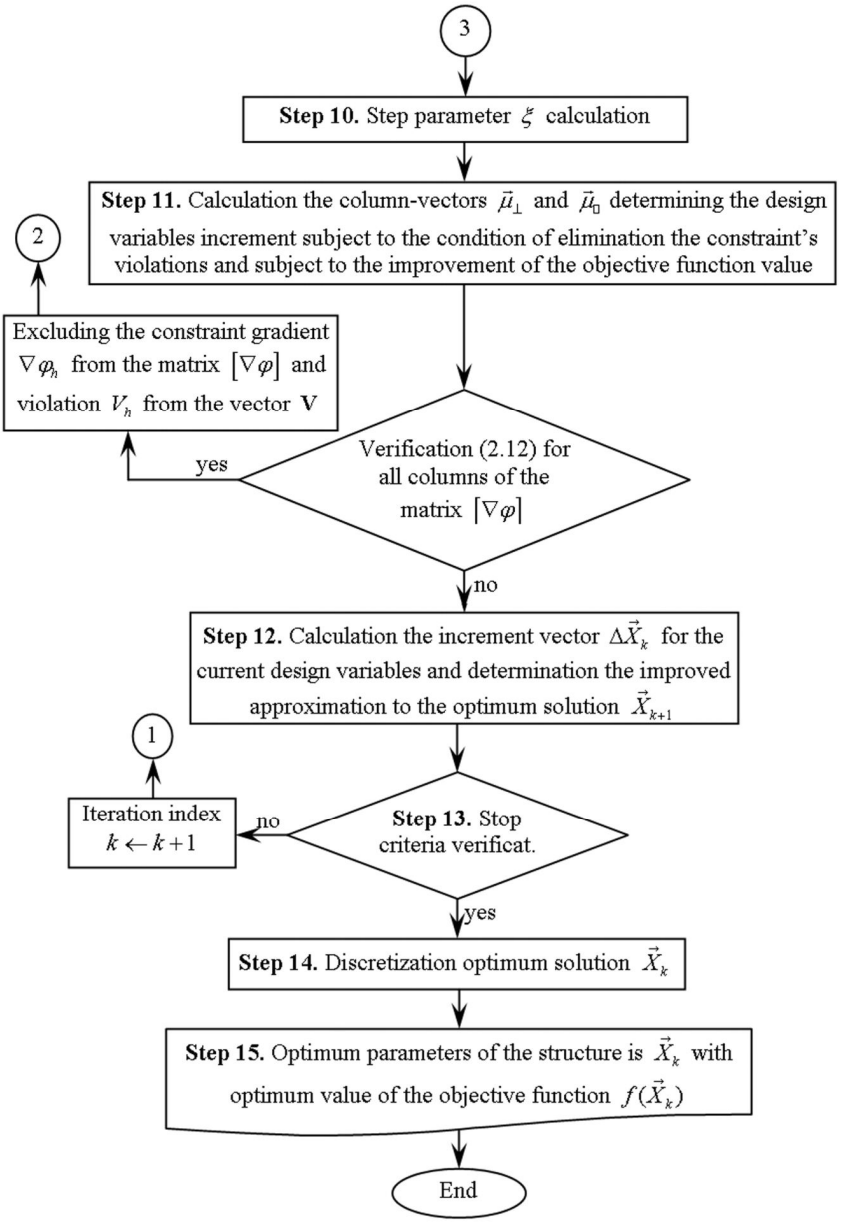

Fig. 3.1 (continuation). The flow chart for structural optimization according to the searching technique based on the gradient projection method

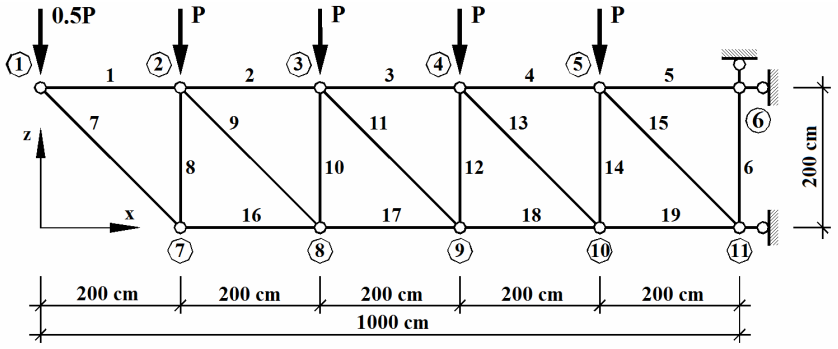

Fig. 4.1. Design scheme of the 19-bar cantilever truss

Truss weight minimization has been considered as the objective function. The geometry and cross-sectional optimization problem has been formulated as searching for optimum values of the vertical coordinates z_i for all nodes of the truss lower chord, as well as for optimum value of the cross sectional area A for all truss members. Variable unknown cross-sectional area A for all truss members as well as unknown vertical coordinates z_i for all truss lower chord nodes, $\vec{X} = (A,\, z_i)^T$, $i = \overline{7,11}$, were considered as design variables. The system of constraints included the normal stress constraints formulated for all truss members depending on axial forces and allowable value of the normal stresses $\sigma_{\max}$. The following displacement constraints have been also formulated for all nodes of the truss lower chord:

$$-1 - \frac{z_i}{z_i^{start} - \delta_{\max}} \le 0\,; \quad \frac{z_i}{z_i^{start} + H - \varepsilon} - 1 \le 0\,; \ \forall\ i = 7...11\,;$$

where H is the height of the truss panel, $H = 200$ cm; ε is the small positive number, $\varepsilon = 10^{-7}$. The considered optimization problem dimensions were 6 design variables and 29 constraints.

Figure 4.2a presents the optimum values for vertical coordinates of the truss lower chord. The optimum cross sectional area for all truss members is $A_{opt} = 4.0626\ \text{cm}^2$. The optimum structural weight for the considered 19-bar cantilever truss is $G_{opt} = 139.634$ kg. There were six active constraints in the optimum point, namely normal stress constraints for the 5th, 6th, 17th, 18th, 19th truss members, as well as displacement constraint for the 11th truss node. The considered geometry and cross-sectional optimization problem for 19-bar cantilever truss has been solved by Czarnecki [1, 2]. He obtained optimal structural weight 187.945 kg.

The next geometry and cross-sectional optimization problem has been formulated as searching for optimum values of the horizontal x_i and vertical coordinates z_i for all nodes of the truss lower chord, as well as for optimum

value of the cross sectional area A for all truss members. Variable unknown cross-sectional area A for all truss members, as well as unknown horizontal x_i and vertical z_i coordinates for all truss lower chord nodes, $\vec{X} = (A,\, x_i,\, z_i)^T,\ i = \overline{7,11}$, were considered as design variables. The system of constraints included the normal stress constraints formulated for all truss members depending on axial forces and allowable value of the normal stresses $\sigma_{\max}$. The following displacement constraints have been also formulated for all nodes of the truss lower chord:

$$-1 - \frac{x_i}{x_i^{start} - L + \varepsilon} \le 0\,;\ \ \frac{z_i}{z_i^{start} + L - \varepsilon} - 1 \le 0\,;\ \forall\ i = 7...10\,;$$

$$-1 - \frac{z_i}{z_i^{start} - \delta_{\max}} \le 0\,;\ \ \frac{z_i}{z_i^{start} + H - \varepsilon} - 1 \le 0\,;\ \forall\ i = 7...11\,;$$

where L is the length of the truss panel, $L = 200$ cm. The considered optimization problem dimensions were 10 design variables and 37 constraints.

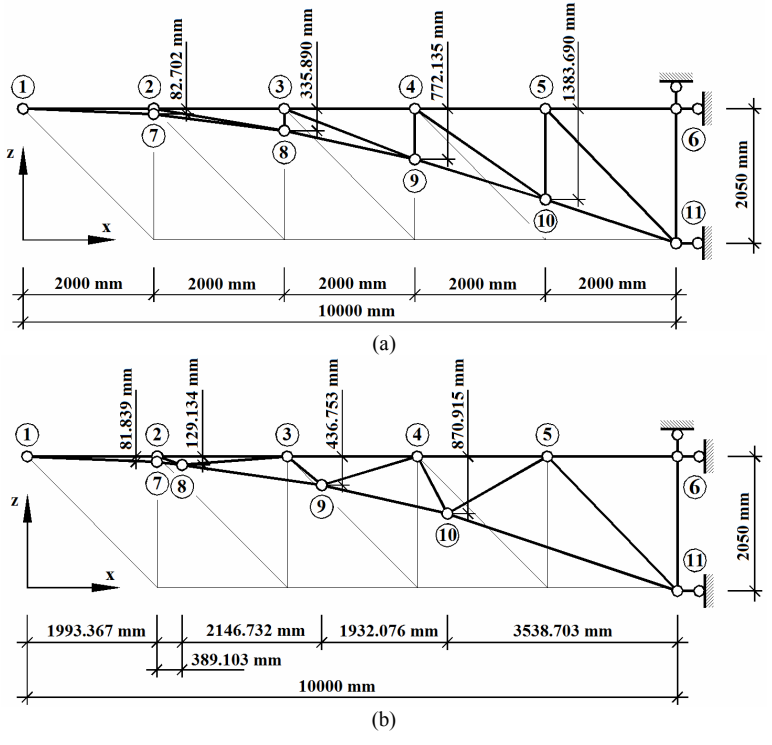

Fig. 4.2. Optimum coordinates values for all nodes of the 19-bar cantilever truss lower chord:
(a) – when vertical coordinates are considered as design variable only;
(b) – when both vertical and horizontal coordinates are considered as design variable

Figure 4.2b presents the optimum design values for vertical and horizontal coordinates of the truss lower chord. The optimum cross sectional area for all truss members is $A_{opt} = 4.0626\ \text{cm}^2$. The optimum structural weight for the considered 19-bar cantilever truss is $G_{opt} = 131.11\ \text{kg}$. There were eight active constraints in the optimum point, namely the normal stresses constraints formulated for the 2nd, 3rd, 4th, 5th, 7th, 16th and 19th truss members, as well as displacement constraint formulated for 11th node. The considered geometry and cross-sectional optimization problems for 19-bar cantilever truss has been solved by Czarnecki [1, 2]. He obtained optimal structural weight 178.842 kg.

The comparison of the optimization results presented by the paper confirms the validity of the optimum solutions obtained using the proposed optimization methodology. For those design cases when the purpose function and constraints of the mathematical model are continuously differentiable functions, as well as the search space is smooth, a gradient projection method provides better optimum results comparing to the genetic algorithms.

4.2. Cross-sectional optimization of a 41-bar roof truss. Figure 4.3 shows a 41-bar roof truss designed for the vertical loads $P = 4\ \text{ton} = 39.24\ \text{kN}$ applied to the upper truss chord and $1.5P = 6\ \text{ton} = 58.86\ \text{kN}$ applied to the lower truss chord. A parametric optimization problem for the roof truss by the criterion of the material volume minimization has been solved by I-Cheng [8] using a genetic algorithm. He obtained the optimum volume $0.121689\ \text{m}^3$ for the considered roof truss.

Initial data (see Table 4.2) and mathematical model of the 41-bar truss optimization problem are assumed as the same as described in the paper [8]. Cross-sectional areas for 21 stiffness types of the roof truss structural members are considered as the design variables, $\vec{X} = (A_i)^T, i = \overline{1,21}$ (see Figure 4.3). Cross-sectional areas of the truss members assumed to be varying discretely starting from $2\ \text{cm}^2$ until and including $64\ \text{cm}^2$ with step $2\ \text{cm}^2$. The system of constraints includes normal stresses verifications for all truss members, as well as vertical displacement constraint for truss node a. Optimization problem dimensions are 21 design variables, 80 constraints.

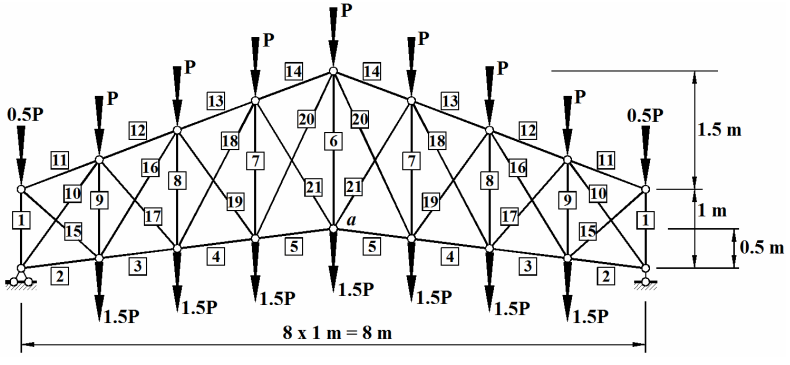

Fig. 4.3. Design scheme of the 41-bar roof truss with stiffness types numbers

Table 4.2

Initial data for optimization of the truss

Modulus of elasticity E	$2.06 \cdot 10^5$ MPa
The allowable normal stresses $\sigma_{\max}$ in tension and compression	1250 kg/cm^2 = 12.2625 kN/cm^2
The allowable value for the vertical displacement of the roof truss node a	6 mm

The parametric optimization problem for optimum cross-section areas of the 41-bar roof truss has been solved in the continuum space of the design variables using the improved gradient projection method described above. Table 4.3 presents the optimization result for the considered 41-bar roof truss. The optimum volume for the optimum truss solution is $V_{opt}^{cont} = 0.109$ m^3. The optimum solution has been validated by the convergence of the optimization algorithm in the same point subjected to the different start approximations to the design variables. The optimum solution for the roof truss obtained in the continuum space of the design variables has been further discretized. The optimum volume for the optimum truss solution in discrete space of the design variables is $V_{opt}^{disc} = 0.119$ m^3 (see Table 4.3).

The comparison of the optimization results presented by the paper confirms the validity of the optimum solutions obtained using the proposed optimization methodology. Start values of the design variables have no influence on the optimum solution of the considered non-linear optimization problem confirming in such way accuracy and validity of the optimum solutions obtained using the proposed numerical algorithm developed based on the presented gradient projection method. For those design cases when the purpose function and constraints of the mathematical model are continuously differentiable functions, as well as the search space is smooth, a gradient projection method provides better optimum results comparing to the genetic algorithms.

Table 4.3

Optimization results for the 41-bar roof truss

Stiffness types numbers	Optimum values for cross-section areas of the truss members [cm^2] depending on space of the design variables	
	in continuum space	in discrete space
1	17.8208	18
2	15.6555	16
3	36.3758	38
4	48.2494	50
5	54.5526	56
6	40.5101	42
7	2.0000	2

8	2.0000	2
9	2.0000	2
10	26.3752	28
11	14.3494	16
12	40.1982	42
13	52.7656	54
14	56.8969	58
15	17.8746	18
16	13.0426	14
17	12.9413	14
18	5.4713	6
19	6.4781	8
20	2.9064	4
21	2.0000	2
Truss volume, cm^3	**0.108997**	**0.118635**

Conslusion. A new mathematical model for parametric optimization problems of steel structures has been proposed by the paper. The design variable vector includes geometrical parameters of the structure (node coordinates), cross-sectional dimensions of the structural members, as well as initial pre-stressing forces introduced into the specified redundant members of the structure has been formulated by the paper. The system of constraints covers load-carrying capacities constraints for all design sections of structural members subjected to all ultimate load case combinations, as well as displacements constraints for the specified nodes of the structure subjected to all serviceability load case combinations.

The method of the objective function gradient projection onto the active constraints surface with simultaneous correction of the constraints violations has been used to solve the formulated parametric optimization problem for steel structures.

A numerical algorithm for solving the formulated parametric optimization problems of steel structures based on the gradient projection method has been developed.

In order to estimate an efficiency of the proposed numerical algorithm, a comparison of the obtained optimization results with the results presented by the literature and widely used for testing has been performed. Good correlation of obtained results with the results of the other authors confirms the validity of the optimum solutions calculated using the proposed numerical algorithm.

It has been shown, that for those design cases when the purpose function and constraints of the mathematical model are continuously differentiable functions, as well as the search space is smooth, a gradient projection method provides better optimum results comparing to the genetic algorithms.

REFERENCES

1. *Czarnecki S.* Optimal structural design using a genetic algorithm // Theoretical Foundations of Civil Engineering. – 1999. – VII. – p. 201–210.
2. *Czarnecki S.* Multithreaded genetic program in truss shape optimization // Theoretical Foundations of Civil Engineering. – 2000. – VIII. – p. 556–560.
3. *Crowder N. P., Denbo R. S., Mulvey J. M.* Reporting computational experiments in mathematical programming // Mathematical Programming. – Vol. 15, 1978. – p. 316–329.
4. *DBN V.2.6-198:2014*. Steel structures. Design codes. – Kyiv: Minregion of Ukraine, 2014. – 199 p. (ukr)
5. *Guljaev V. I., Bazhenov V. A., Koshkin V. L.* Optimization techniques in structural mechanics (Optimization methods in structural mechanic). – Kyiv, 1988. – 192 p. (rus)
6. *Haug E. J., Arora J. S.* Applied optimal design: mechanical and structural systems. – John Wiley & Sons, 1979. – 520 p.
7. *Huebner K. H., Dewhirst D. L., Smith D. E., Byrom T. G.* The finite element method for engineers (4th ed.) – John Wiley & Sons, Inc. 2001. – 744 p.
8. *I-Cheng Y.* Hybrid genetic algorithms for optimization of truss structures // Computer-aided civil and infrastructure engineering. – 1999. – No. 14. – p. 199–206.
9. *Koshkin V. L., Serpak I. O.* Optimal design of flexible rod structural members // Strength of materials. – 1993. – No. 25. – p. 834–840. DOI: 10.1007/BF00780267
10. *Kuci E., Henrotte F., Duysinx P., Geuzaine C.* Design sensitivity analysis for shape optimization based on the Lie derivative // Computer methods in applied mechanics and engineering. – Vol. 317, 2017. – p. 702–722. DOI: 10.1016/j.cma.2016.12.036
11. *Peleshko I., Yurchenko V.* An optimum structural computer-aided design using update gradient method // Proceedings of the 8th International Conference "Modern Building Materials, Structures and Techniques". – Faculty of Civil Engineering, Vilnius Gediminas Technical University, 2004. – p. 860 – 865.
12. *Peleshko I., Yurchenko V.* An improved gradient-based method to solve parametric optimisation problems of the bar structures // Strength of Materials and Theory of Structures: Scientific-and-technical collected articles. – Kyiv: KNUBA, 2020. – Issue 104. (accepted to publication)
13. *Permyakov V. O., Yurchenko V. V., Peleshko I. D.* An optimum structural computer-aided design using hybrid genetic algorithm // Proceeding of the International Conference "Progress in Steel, Composite and Aluminium Structures". – Taylor & Francis Group, London, 2006. – p. 819–826.
14. *Perelmuter A., Yurchenko V.* Parametric optimization of steel shell towers of high-power wind turbines // Procedia Engineering. – No. 57, 2013. – p. 895 – 905. DOI: 10.1016/ j.proeng.2013.04.114.
15. *Reklaitis G. V., Ravindran A., Ragsdell K. M.* Engineering optimization. Methods and applications. – Wiley, 2006. – 688 p.
16. *Yurchenko V., Peleshko I., Beliaev N.* Parametric optimization of steel truss with hollow structural members based on update gradient method // Proceedings of International Conference "Design, Fabrication and Economy of Metal Structures". – Springer Berlin Heidelberg, 2013. – p. 103–109. DOI: 10.1007/978-3-642-36691-8_16
17. *Wilkinson J. H., Reinsch C.* Handbook for Automatic Computation. Volume II: Linear Algebra. – Heidelberg New York Springer-Verlag Berlin, 1971. – 441 p. DOI: 10.1137/1014116.

Стаття надійшла 12.10.2020

Юрченко В. В., Пелешко І. Д.

ПАРАМЕТРИЧНА ОПТИМІЗАЦІЯ МЕТАЛЕВИХ СТЕРЖНЕВИХ КОНСТРУКЦІЙ НА ОСНОВІ МЕТОДУ ПРОЕКЦІЇ ГРАДІЄНТА

Метою дослідження є розробка чисельної методики для розв'язку задачі параметричної оптимізації сталевих стержневих конструкцій при орієнтації на її програмну реалізацію у системі автоматизованого проектування. У статті запропонована нова математична модель для розв'язку задачі параметричної оптимізації металевих стержневих конструкцій. Вектор змінних проектування охоплює параметри геометричної схеми конструкції (координати вузлів), розміри поперечних перерізів несучих елементів конструкції, а також зусилля попереднього напруження, що вводяться у визначені зайві в'язі конструкції. У систему обмежень залучені обмеження несучої здатності, сформульовані для усіх розрахункових перерізів несучих елементів металевої стержневої конструкції, що підлягає дії розрахункових комбінацій навантажень першого граничного стану, а також обмеження переміщень, сформульовані для визначених вузлів стержневої системи, що підлягає дії розрахункових комбінацій навантажень другого граничного стану. Для розв'язку поставленої задачі параметричної оптимізації використаний метод проекції градієнта функції мети на поверхню активних обмежень з одночасною ліквідацією нев'язок в порушених обмеженнях. У статті також запропонований чисельний алгоритм для розв'язку поставленої задачі параметричної оптимізації сталевих конструкцій. Результати оптимізаційних розрахунків стальних ферм, які представлені у статті, підтвердили достовірність оптимальних рішень, отриманих з використанням запропонованої чисельної методики.

Ключові слова: параметрична оптимізація, сталеві стержневі конструкції, нелінійне програмування, обмеження стійкості, зусилля попереднього напруження, координати вузлів, градієнтний метод, метод скінчених елементів, чисельний алгоритм.

Yurchenko V. V., Peleshko I. D.

PARAMETRIC OPTIMIZATION OF STEEL STRUCTURES BASED ON GRADIENT PROJECTION METHOD

The main research goal is the development of a numerical methodology for solving parametric optimization problems of steel structures with orientation on software implementation in a computer-aided design system. The paper has proposed a new mathematical model for parametric optimization problems of steel structures. The design variable vector includes geometrical parameters of the structure (node coordinates), cross-sectional dimensions of the structural members, as well as initial pre-stressing forces introduced into the specified redundant members of the structure. The system of constraints covers load-carrying capacities constraints formulated for all design sections of structural members of the steel structure subjected to all ultimate load case combinations. The displacements constraints formulated for the specified nodes of the steel structure subjected to all serviceability load case combinations have been also included into the system of constraints. The method of the objective function gradient projection onto the active constraints surface with simultaneous correction of the constraints violations has been used for solving the parametric optimization problem. A numerical algorithm for solving the formulated parametric optimization problems of steel structures has been developed in the paper. The comparison of the optimization results of truss structures presented by the paper confirms the validity of the optimum solutions obtained using the proposed numerical methodology.

Keywords: parametric optimization, steel structures, nonlinear programming, buckling constraints, pre-stressing forces, node coordinates, gradient projection method, finite element analysis, numerical algorithm.

Юрченко В. В., Пелешко И. Д.

ПАРАМЕТРИЧЕСКАЯ ОПТИМИЗАЦИЯ МЕТАЛЛИЧЕСКИХ СТЕРЖНЕВЫХ КОНСТРУКЦИЙ НА ОСНОВЕ МЕТОДА ПРОЕКЦИИ ГРАДИЕНТА

Целью исследования является разработка численной методики для решения задач параметрической оптимизации стальных конструкций при ориентации на ее программную реализацию в системе автоматизированного проектирования. В статье предложена новая математическая модель для решения задач параметрической оптимизации стальных конструкций. Вектор переменных проектирования охватывает параметры геометрической схемы конструкции (координаты узлов), размеры поперечных сечений несущих элементов конструкций, а также усилия предварительного натяжения, вводимые в указанные лишние связи конструкции. В систему ограничений включены ограничения несущей способности, сформулированные для всех расчетных сечений несущих элементов стальной стержневой конструкции, подверженной действию расчетных комбинаций нагрузок первого предельного состояния. Ограничения перемещений, сформулированные для определенных узлов стержневой системы, подверженной действию расчетных комбинаций нагрузок второго предельного состояния, также включены в систему ограничений. Для решения поставленной задачи параметрической оптимизации был использован метод проекции градиента функции цели на поверхность активных ограничений с одновременной ликвидацией невязок в ограничениях. В статье также предложен численный алгоритм для решения поставленной задачи параметрической оптимизации стальных конструкций. Результаты оптимизационных расчетов стальных ферм, представленные в статье, подтвердили достоверность оптимальных решений, получаемых с использованием предложенной численной методики.

Ключевые слова: параметрическая оптимизация, стальные стержневые конструкции, нелинейное программирование, ограничения устойчивости, усилия предварительного натяжения, координаты узлов, градиентный метод, метод конечных элементов, численный алгоритм.

УДК 624.04, 519.853

Юрченко В. В., Пелешко І. Д. **Параметрична оптимізація металевих стержневих конструкцій на основі методу проекції градієнта** // Опір матеріалів і теорія споруд: наук.-тех. збірн. – К.: КНУБА, 2020. – Вип. 105. – С. 192-222.

У статті запропонована нова математична модель для розв'язку задачі параметричної оптимізації металевих стержневих конструкцій. Вектор змінних проектування охоплює параметри геометричної схеми конструкції (координати вузлів), розміри поперечних перерізів несучих елементів конструкції, а також зусилля попереднього напруження, що вводяться у визначені зайві в'язі конструкції. У систему обмежень залучені обмеження несучої здатності, сформульовані для усіх розрахункових перерізів несучих елементів металевої стержневої конструкції, що підлягає дії розрахункових комбінацій навантажень першого граничного стану, а також обмеження переміщень, сформульовані для визначених вузлів стержневої системи, що підлягає дії розрахункових комбінацій навантажень другого граничного стану. Для розв'язку поставленої задачі параметричної оптимізації використаний метод проекції градієнта функції мети на поверхню активних обмежень з одночасною ліквідацією нев'язок в порушених обмеженнях. У статті також запропонований чисельний алгоритм для розв'язку поставленої задачі параметричної оптимізації сталевих конструкцій.

Іл. 6. Табл. 3. Бібліог. 17 назв.

УДК 624.04, 519.853
Yurchenko V. V., Peleshko I. D. **Parametric optimization of steel structures based on gradient projection method** // Strength of Materials and Theory of Structures: Scientific-and-technical collected articles – Kyiv: KNUBA, 2020. – Issue 105. – P. 192-222.

The paper has proposed a new mathematical model for parametric optimization problems of steel structures. The design variable vector includes geometrical parameters of the structure (node coordinates), cross-sectional dimensions of the structural members, as well as initial pre-stressing forces introduced into the specified redundant members of the structure. The system of constraints covers load-carrying capacities constraints formulated for all design sections of structural members of the steel structure subjected to all ultimate load case combinations. The displacements constraints formulated for the specified nodes of the steel structure subjected to all serviceability load case combinations have been also included into the system of constraints. The method of the objective function gradient projection onto the active constraints surface with simultaneous correction of the constraints violations has been used for solving the parametric optimization problem. A numerical algorithm for solving the formulated parametric optimization problems of steel structures has been developed in the paper.
Figs. 6. Tabs. 3. Refs. 17.

УДК 624.04, 519.853
Юрченко В. В., Пелешко И. Д. **Параметрическая оптимизация металлических стержневых конструкций на основе метода проекции градиента** // Сопротивление материалов и теория сооружений: науч.- тех. сборн. – К.: КНУСА, 2020. – Вып. 105. – С. 192-222.

В статье предложена новая математическая модель для решения задач параметрической оптимизации стальных конструкций. Вектор переменных проектирования охватывает параметры геометрической схемы конструкции (координаты узлов), размеры поперечных сечений несущих элементов конструкций, а также усилия предварительного натяжения, вводимые в указанные лишние связи конструкции. В систему ограничений включены ограничения несущей способности, сформулированные для всех расчетных сечений несущих элементов стальной стержневой конструкции, подверженной действию расчетных комбинаций нагрузок первого предельного состояния, а также ограничения перемещений, сформулированные для определенных узлов стержневой системы, подверженной действию расчетных комбинаций нагрузок второго предельного состояния. Для решения поставленной задачи параметрической оптимизации использован метод проекции градиента функции цели на поверхность активных ограничений с одновременной ликвидацией невязок в ограничениях. В статье предложен численный алгоритм для решения поставленной задачи параметрической оптимизации стальных конструкций.
Ил. 6. Табл. 3. Библиог. 17 назв.

Автор: *доктор технічних наук, професор кафедри металевих та дерев'яних конструкцій Юрченко Віталіна Віталіївна*
Адреса робоча: *03680 Україна, м. Київ, Повітрофлотський пр. 31, Київський національний університет будівництва і архітектури*
Робочий тел.: *+38(044)249-71-91*
Мобільний тел..: *+38(063)89-26-491*
E-mail: *vitalina@scadsoft.com*
SCOPUS ID: 25637856200
ORCID ID: https://orcid.org/0000-0003-4513-809X

Автор: *кандидат технічних наук, доцент кафедри будівельного виробництва Пелешко Іван Дмитрович*
Адреса робоча: *79013 Україна, м. Львів, вул.. Ст. Бандери 12, Національний університет «Львівська політехніка»*
Робочий тел.: *+38 (032) 258-25-41*
Мобільний тел..: *+38(098)41-57-517*
E-mail: *ipeleshko@polynet.lviv.ua*
SCOPUS ID: 25637832500
ORCID ID: https://orcid.org/0000-0001-7028-9653

UDC 539.3

THE GYROSCOPIC FORCES INFLUENCE ON THE OSCILLATIONS OF THE ROTATING SHAFTS

P.P. Lizunov,
Doctor of Technical Science, Professor

V.O. Nedin,
Assistant of Professor

Kyiv National University of Construction and Architecture,
31, Povitroflotskiy avenue, Kyiv, Ukraine

DOI: 10.32347/2410-2547.2020.105.223-231

The results of numerical investigation of shafts transverse oscillations with account of gyroscopic inertia forces are presented. It is shown what the action and how the gyroscopic forces influence on the transverse oscillations of the shafts during rotation. The study has been done with computer program with a graphical interface that is developed by authors. The process of numerical solution of the differential equations of oscillations of rotating rods using the method of numerical differentiation of rod's bend forms by polynomial spline-functions and the Houbolt time integration method is described. A general block diagram of the algorithm is shown. This algorithm describes the process of repeated (cyclical) solving the system of differential equations of oscillations for every point of mechanical system in order to find the new coordinates of positions of these points in each next point of time $t+\Delta t$. The computer program in which the shown algorithm is realized allows to monitor for the behavior of moving computer model, which demonstrates the process of oscillatory motion in rotation. Moreover, the program draws the graphics of oscillations and changes of angular speeds and accelerations in different coordinate systems. Defines the dynamic stability fields and draw the diagrams of found fields. Using this program, the dynamics of a range of objects which are modeled by long elastic rods have been studied. For some objects is shown that on special rotational speeds of shafts with different lengths, in the rotating with shaft coordinate system, the trajectories of center of the section have an ordered character in the form of n-pointed star in time interval from excitation to the start of established circular oscillation with amplitude that harmoniously changes in time. It is noted that such trajectories are fact of the action of gyroscopic inertia forces that arise in rotation.

Keywords: shafts, transverse oscillations, numerical differentiation, bend forms, gyroscopic forces.

Introduction. The tasks of dynamics of elastic shafts' systems that rotate in fields of inertia forces have actuality while structural elements of machines and devices are designed. The rotating shafts are responsible elements in the constructions of engines, turbines, wind and hydropower plants, other machines. For these objects, in many cases, the cause of oscillations is the periodic changes of the gyroscopic inertia forces of system per time.

When the shaft rotates and begins to bend under the action of external loads, the gyroscopic forces start to transmit energy in direction that is perpendicular to the plane of bending. After it the shaft begins to oscillate in two mutually perpendicular planes of the coordinate system that rotates with it.

The behavior of rotating elastic systems that consist of shafts, rods and rotors is described by complex differential equations systems with partial derivatives with account of gyroscopic inertia forces. Low rigidity, large

length, relatively high values of the excitation intensity parameters, in which the structural elements are used, all of these make the necessary to analysis of oscillatory motion around of critical and overcritical rotational speeds. Also, these make the necessary to search the natural oscillation frequencies range and range of critical rotational speeds with account of gyroscopic forces, and stability analysis in the study of different motion modes.

In recent years, the dynamic tasks of oscillations of shafts and rotating rods were investigated in works of many authors. The task of rotating shaft with influence of axial loads to the propagation characteristics of the elastic waves is studied in paper [14]. The shaft is viewed with non-uniform cross-sections per length. Axial loads considered with constant values.

The paper [8] presents the study of problems with elastic stabilization and long-term strength of the system under cyclically changing external impacts that are appearing because of eccentricities. Task is considered taking into account the gyroscopic loads, in linear statement. The paper [7] presents the results of study of space bending oscillations of horizontal rod that is rotating around its axis. Rod is under the action of periodic harmonic force of self-weight per length. The task is considered with account of the gyroscopic loads, too.

Questions about the transverse oscillations of the rods under the action of axial periodic loads, also the tasks of longitudinal-transverse oscillations under the action of beat loads are considered in papers [5, 6]. But in them the investigated rods don't rotate.

The analysis of presented in scientific literature results shows that the task of investigation of dynamics and strength of rotating elastic systems, with account of gyroscopic forces, is actual. Many authors are paid attention to calculation of critical rotational speeds and natural oscillation frequencies by different system parameters. But the nature of the oscillation process itself and how the certain parameters of the system influence on the development of oscillations almost is not considered. Therefore, it is interesting to study the dynamic behavior of the consider systems and define what kind of effects the gyroscopic forces generate.

Problem statement. In the process of oscillation of rotating shafts or rods with considerable lengths with different physical, geometric and dynamic parameters, the various bend forms that change in time are possible.

As a dynamic model is considered a rod with length l (Fig. 1) that can be exposed by action of an axial load $P(t)$. The rod is rotated on angular speed ω around the rectilinear axis O_1X_1 of the stationary coordinate system $O_1X_1Y_1Z_1$. The rotating coordinate system $OXYZ$ is tied to the rod and rotates with it. The direction of OX axis coincides with

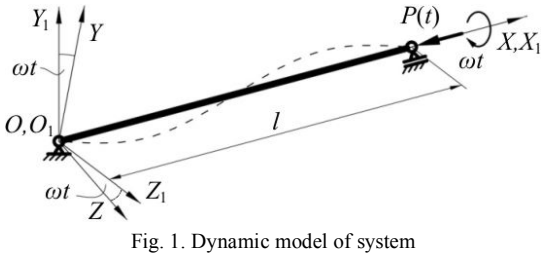

Fig. 1. Dynamic model of system

direction of O_1X_1 axis. Axis of rod in deformed state is coincided with the OX and O_1X_1 axis. The oscillatory motion of the rod in the $OXYZ$ coordinate system is characterized by $y(x,t)$ and $z(x,t)$ displacements of the points, that belong to the axis of rod in the OY and OZ coordinate axes' direction, respectively.

The oscillations of rotating rod in space are described by the corresponding system of differential equations, which taking into account the geometric nonlinearity and the axial force [2, 3] have a form:

$$\begin{cases} \dfrac{d^2}{dx^2}\left(\dfrac{EI_{1(x)}}{\rho_1}\right)-\bar{m}r^2\left(\dfrac{d^4y}{dt^2dx^2}+\omega^2\dfrac{d^2y}{dx^2}\right)-2\omega\bar{m}\dfrac{dz}{dt}-\bar{m}\omega^2y+\bar{m}\dfrac{d^2y}{dt^2}+P(t)\dfrac{d^2y}{dx^2}=0, \\ \dfrac{d^2}{dx^2}\left(\dfrac{EI_{2(x)}}{\rho_2}\right)-\bar{m}r^2\left(\dfrac{d^4z}{dt^2dx^2}+\omega^2\dfrac{d^2z}{dx^2}\right)+2\omega\bar{m}\dfrac{dy}{dt}-\bar{m}\omega^2z+\bar{m}\dfrac{d^2z}{dt^2}+P(t)\dfrac{d^2z}{dx^2}=0, \end{cases} \quad (1)$$

where E – elastic modulus of rod's material; I_1, I_2 – inertia moments of rod section in mutually perpendicular planes; r – radius of gyration; $\bar{m}$ –mass of unit per length; ω – rotational speed of rod around the axis that coincides with the axis of rod in undeformed state; $P(t)$ – periodic axial force; $1/\rho_1$, $1/\rho_2$ – main curvatures of rod's axis in mutually perpendicular planes.

Technique. The solving of differential equations of rotating rods oscillations for searching their geometric position in space in the process of oscillation and analysis of dynamic behavior is carried out using the method of numerical differentiation described in papers [10, 11], and the Houbolt time integration method [13] in form:

$$\ddot{y}_n^{t+\Delta t}=\frac{1}{\Delta t^2}\left[2y_n^{t+\Delta t}-5y_n^t+4y_n^{t-\Delta t}-y_n^{t-2\Delta t}\right],$$

$$\dot{y}_n^{t+\Delta t}=\frac{1}{6\Delta t}\left[11y_n^{t+\Delta t}-18y_n^t+9y_n^{t-\Delta t}-2y_n^{t-2\Delta t}\right],$$

$$\ddot{z}_n^{t+\Delta t}=\frac{1}{\Delta t^2}\left[2z_n^{t+\Delta t}-5z_n^t+4z_n^{t-\Delta t}-z_n^{t-2\Delta t}\right],$$

$$\dot{z}_n^{t+\Delta t}=\frac{1}{6\Delta t}\left[11z_n^{t+\Delta t}-18z_n^t+9z_n^{t-\Delta t}-2z_n^{t-2\Delta t}\right]$$

Such solution executes in order to find the coordinates $y_n^{t+\Delta t}$, $z_n^{t+\Delta t}$ of rod axis for next point of time $t+\Delta t$ (Fig. 2).

To apply the Houbolt method need to know at least the first three points of time integration. To find these points, it is

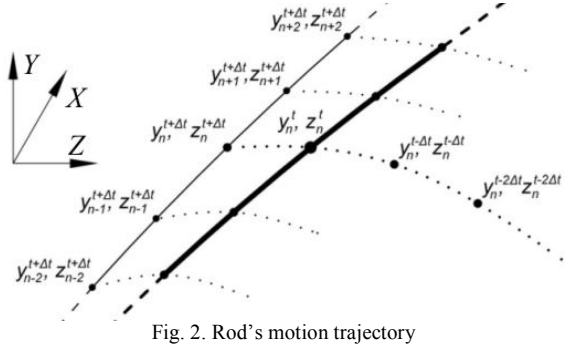

Fig. 2. Rod's motion trajectory

advisable to use the finite differences method with initial conditions, namely, to make the assumption that at time t=0, when the system start out of equilibrium, the initial deviation value for each point of the rod axis is known: $y_n^{t=0} = a_n$, $z_n^{t=0} = 0$, where a_n is random deviation, and values $y_n^{\Delta t} = y_n^{-\Delta t}$, $z_n^{\Delta t} = z_n^{-\Delta t}$.

The solving of the dynamic tasks of the oscillatory motion for rotating shafts and rods, based on described technique, has been done with computer program with a graphical interface. The general block diagram's algorithm of the program is shown in Figure 3.

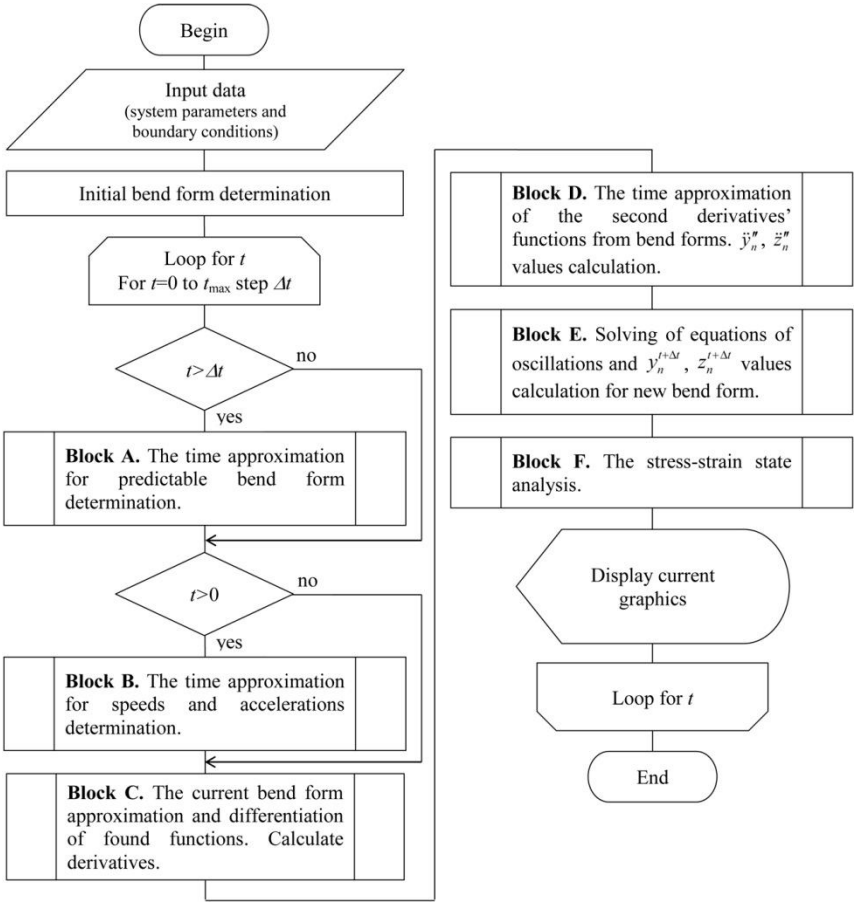

Fig. 3. The general block diagram algorithm of the program

This algorithm describes the process of repeated (cyclical) solving the system of differential equations of oscillations for every point of rod elastic line in order to find the new coordinates for these points in each next point of time $t+\Delta t$. This

is performed with the show of current calculations' results as a moving computer model, which displays the oscillating process of rotating rod in real time.

Results. Using specified program, the dynamics of a range of objects which are modeled by long elastic rods have been studied. For research objects is shown that on special rotational speeds of shafts with different lengths the trajectories of center of the section have an ordered character. For example, for a transmission shaft with outer diameter D=0.1 m, inner diameter d=0.06 m, length l=3 m, on rotational speed ω=31.79 s^{-1} the motion trajectory of center of the section on the middle of shaft, in rotating coordinate system, it will look like a five-pointed star (Fig. 4). On rotational speed ω=52.95 s^{-1} in rotating coordinate system the motion trajectory will look like a tree-pointed star (Fig. 5). On rotational speed ω=79.35 s^{-1} in rotating coordinate system the motion trajectory will look like a four-pointed star (Fig. 6). Herewith, the trajectories of motion in a stationary coordinate system will have a similar character (Fig. 7, 8, 9). The same trajectories of motion are observed for other objects with different parameters, but on other rotational speeds.

The shown below on diagrams trajectories due to the action of gyroscopic inertia forces that are arisen in rotation.

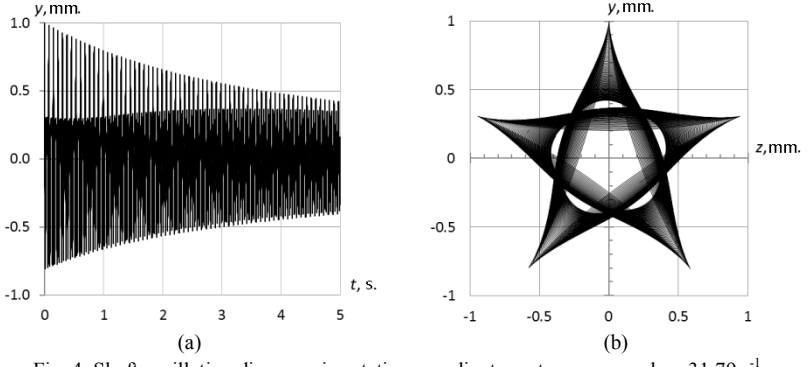

(a) (b)

Fig. 4. Shaft oscillation diagrams in rotating coordinate system, on speed ω=31.79 s^{-1}: (a) oscillation; (b) the motion trajectory

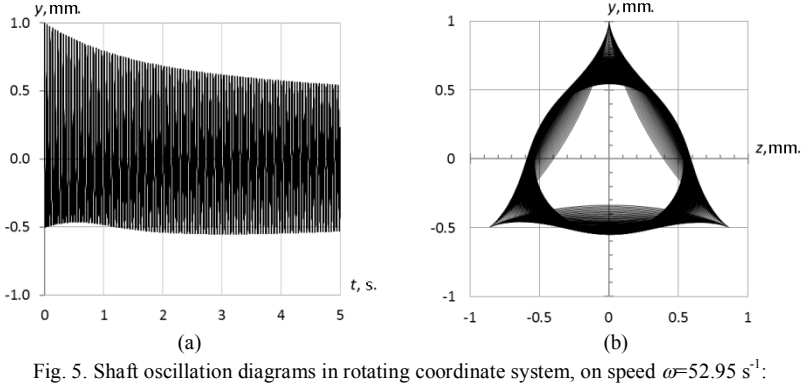

(a) (b)

Fig. 5. Shaft oscillation diagrams in rotating coordinate system, on speed ω=52.95 s^{-1}: (a) oscillation; (b) the motion trajectory

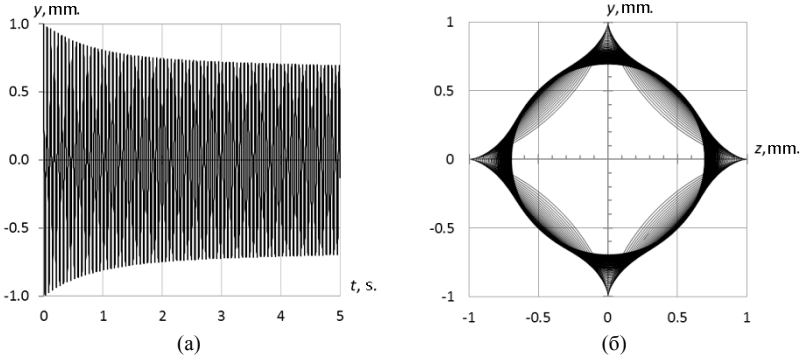

Fig. 6. Shaft oscillation diagrams in rotating coordinate system, on speed ω=79.35 s^{-1}:
(a) oscillation; (b) the motion trajectory

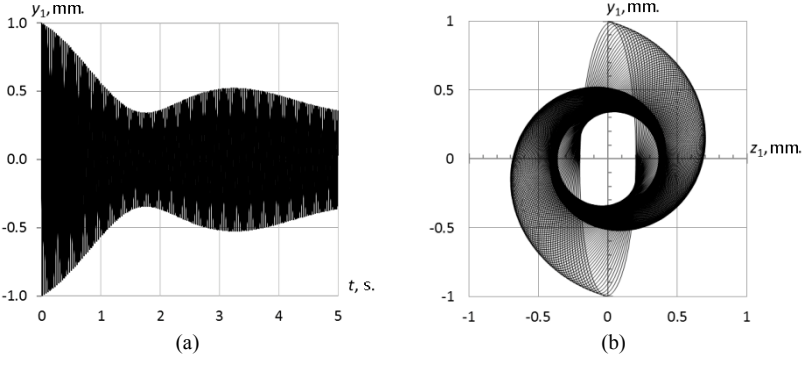

Fig. 7. Shaft oscillation diagrams in stationary coordinate system, on speed ω=31.79 s^{-1}:
(a) oscillation; (b) the motion trajectory

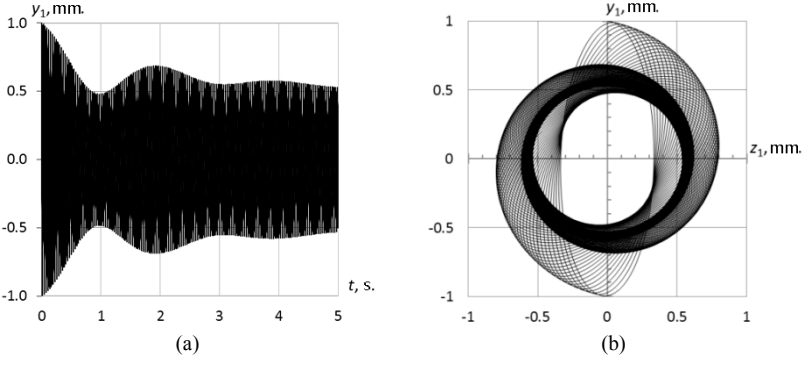

Fig. 8. Shaft oscillation diagrams in stationary coordinate system, on speed ω=52.95 s^{-1}:
(a) oscillation; (b) the motion trajectory

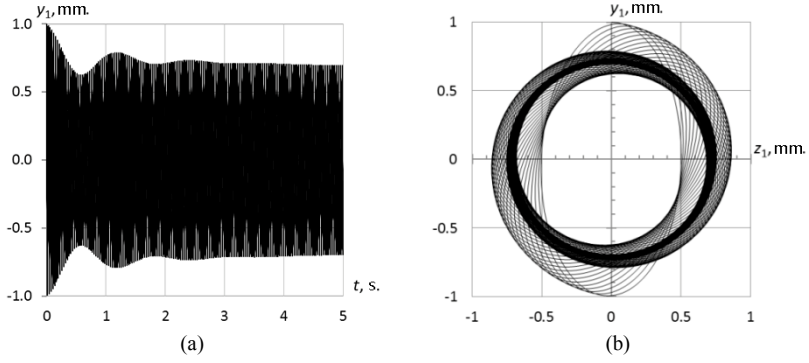

Fig. 9. Shaft oscillation diagrams in stationary coordinate system, on speed ω=79.35 s^{-1}: (a) oscillation; (b) the motion trajectory

Conclusion. Studies of the transverse oscillations of rotating shafts with developed computer program indicate the influence of gyroscopic forces on the nature of oscillatory motion. Depending on the rotational speed the oscillatory motion of the shaft occurs with different trajectories, which at certain speeds have a definite periodicity.

The rotational speeds at which the motion trajectories during transverse shaft oscillations have an ordered character in the form of an *n*-pointed star are found. Such motion happens in the time interval from the moment of excitation to the start of the established circulation with amplitude that harmoniously changes in time.

REFERENCES

1. *Bakhvalov N.S., Judkov N.P., Kobelkov G.M.* Chislennye metody (Numerical methods). M.: BINOM, Laboratoriya znaniy, 2015, 639 pp.
2. *Bolotin V.V*. Dinamicheskaya ustoychivost uprugih system (The dynamic stability of elastic systems). M.: Izdatelstvo tekhniko-teoreticheskoj literatury, 1956, 600 pp.
3. *Dimentberg F.M.* Izgibnyye kolebaniya vrashchayushchikhsya valov (Flexural vibrations of rotating shafts). Moscow: Publishing of AS USSR, 1959, 247.
4. *Karpenko T. N., Muzyka I. N.* Determination of natural frequencies of bending vibrations of rotating shafts. Science and production, 2018, No. 18, 69–78.
5. *Morozov N.F.* Static and Dynamics of a Rod at the Longitudinal Loading / N.F. Morozov, P.E. Tovstik, T.P. Tovstik // Vestnik YUUrGU. Seriya «Matematicheskoye modelirovaniye i programmirovaniye». – 2014. – Vol. 7, No. 1. – S. 76–89.
6. *Morozov N.F.* The rod dynamics under short longitudinal impact / N.F. Morozov, P.E. Tovstik // Vestnik SPbGU. – 2013. – Vup. 3. P.131–141.
7. *Munitsyn A.I.* Prostranstvennyye izgibnyye kolebaniya sterzhnya, vrashchayushchegosya vokrug svoyey osi (Space bending oscillations of a rod rotating around its axis) // Matematicheskoye i komp'yuternoye modelirovaniye mashin i sistem. – 2008. S. 64–67.
8. *Murtazin I.R.* Research of flexural vibrations of rotating shafts with distributed inertial, elastic and eccentricity properties / I.R. Murtazin, A.V. Lukin, I.A. Popov // Scientific and Technical Journal of Information Technologies, Mechanics and Optics. – 2019. – Vol. 19, no. 4, P. 756–766.
9. *Nedin V.O.* Computer modeling of the oscillation's process of rotating elastic rods // Modern methods and problem-oriented complexes for structures calculating and their application in design and educational process. – 2018. – No. 2, 76 – 78.

10. *Nedin V.O.* 2020. The parametric oscillations of rotating rods under action of the axial beat load // Strength of materials and theory of structures. – 2020. – Issue 104, P. 309 – 320.
11. *Nedin V.* Numerical differentiation of complex bend forms of long rotating rods // Management of Development of Complex Systems. – 2020. – No. 43, P. 110–115.
12. *Tondl A.* Dinamika rotorov turbogeneratorov (The rotor dynamics of turbines). L., Energiya, 1971, 297 pp.
13. *Maurice Petyt*. Introduction to Finite Element Vibration Analysis. Cambridge University Press, 1990. – 558 p.
14. *Yimin Wei*. Influence of Axial Loads to Propagation Characteristics of the Elastic Wave in a Non‐Uniform Shaft / Yimin Wei, Zhiwei Zhao, Wenhua Chen and Qi Liu // Chinese Journal of Mechanical Engineering. – 2019 – No. 32:70. P.13.

Стаття надійшла 12.04.2020

Лізунов П.П., Недін В.О.

ВПЛИВ ГІРОСКОПІЧНИХ СИЛ НА КОЛИВАЛЬНИЙ РУХ ВАЛІВ ПРИ ОБЕРТАННІ

Представлено результати чисельного дослідження поперечних коливань валів з урахуванням гіроскопічних сил інерції. Показано, який вплив гіроскопічні сили оказують на поперечні коливання валів при обертанні. Дослідження здійснені за допомогою комп'ютерної програми з графічним інтерфейсом, що розроблена автором. Описано процес чисельного розв'язання рівнянь коливального руху з використанням методики чисельного диференціювання, в якій форми вигину стержнів описуються за допомогою поліноміальних сплайн-функцій, а також метода чисельного інтегрування за часом Хубболта. Наведена загальна блок-схема алгоритму, який описує процес багатократного (циклічного) розв'язку системи рівнянь коливального руху для кожної точки системи з метою пошуку нових координат положення цих точок в кожний наступний момент часу $t+\Delta t$. Комп'ютерна програма, в якій реалізовано наведений алгоритм, дозволяє спостерігати за поведінкою рухомої комп'ютерної моделі, яка демонструє процес коливального руху при обертанні, а також будувати графіки коливального руху, графіки зміни швидкостей та прискорень в різних системах координат, визначати області динамічної стійкості об'єктів, що розглядаються. Використовуючи зазначену програму, здійснено дослідження динаміки ряду об'єктів, робочі органи яких моделюються довгомірними пружними стержнями. Для об'єктів дослідження показано, що при певних швидкостях обертання валів та стержнів різної довжини в системі координат, що обертається разом з валом або стержнем, траєкторія руху центра перерізу вала має упорядкований характер у вигляді n-кінцевої зірки на інтервалі часу від моменту збудження до початку встановленого кругового коливального руху з амплітудою, що гармонійно змінюється за часом. Відмічено, що такі траєкторії руху обумовлені дією гіроскопічних сил інерції, які виникають при обертанні.

Ключові слова: вали, поперечні коливання, чисельне диференціювання, форми вигину, гіроскопічні сили.

Лизунов П.П., Недин В.О.

ВЛИЯНИЕ ГИРОСКОПИЧЕСКИХ СИЛ НА КОЛЕБАТЕЛЬНОЕ ДВИЖЕНИЕ ВРАЩАЮЩИХСЯ ВАЛОВ

Представлены результаты численного исследования поперечных колебаний валов с учётом гироскопических сил. Показано, какое влияние гироскопические силы оказывают на поперечные колебания вращающихся валов. Исследования осуществлены с помощью компьютерной программы с графическим интерфейсом, которая была разработана автором. Описан процесс численного решения уравнений колебательного движения с использованием методики численного дифференцирования, в которой формы изгиба стержней описываются с помощью полиномиальных сплайн-функций, а также метода численного интегрирования по времени Хубболта. Показана общая блок-схема алгоритма программы, который описывает процесс многократного (цикличного) решения системы уравнений колебательного движения для каждой точки системы с целью поиска новых координат положения этих точек в каждый следующий момент времени $t+\Delta t$. Компьютерная программа, в которой реализован представленный алгоритм, позволяет наблюдать за поведением компьютерной модели, демонстрирующей процесс

колебательного движения при вращении, а также строить графики колебательного движения, графики изменения скоростей и ускорений в разных системах координат, определять области динамической неустойчивости рассматриваемых объектов. Используя указанную программу, выполнено исследование динамики рядя объектов, рабочие органы которых моделируются длинными упругими стержнями. Для объектов исследования показано, что при определённых скоростях вращения, в системе координат, вращающейся вместе с валом, траектория движения его центра сечения имеет упорядоченный характер в виде *n*-конечной звезды на интервале времени от момента возбуждения до начала установившегося кругового колебательного движения с гармонически изменяющейся во времени амплитудой. Отмечено, что такие траектории движения обусловлены действием гироскопических сил, которые возникают при вращении.

Ключевые слова: валы, поперечные колебания, численное дифференцирование, формы изгиба, гироскопические силы.

УДК 539.3
Лізунов П.П., Недін В.О. **Вплив гіроскопічних сил на коливальний рух валів при обертанні** // Опір матеріалів і теорія споруд: наук.-тех. збірн. – К.: КНУБА, 2020. – Вип. 105. – С. 223 – 231.
В роботі наведені результати чисельного дослідження поперечних коливань валів з урахуванням гіроскопічних сил інерції. Показано, який вплив гіроскопічні сили оказують на поперечні коливання валів при обертанні.
Табл. 0. Іл. 9. Бібліогр. 14 назв.

UDC 539.3
Lizunov P.P., Nedin V.O. **The gyroscopic forces influence on the oscillations of the rotating shafts** // Strength of Materials and Theory of Structures: Scientific-and-technical collected articles – Kyiv: KNUBA, 2020. – Issue 105. – P. 223 – 231.
The paper presents the results of numerical investigation of shafts transverse oscillations with account of gyroscopic inertia forces. It is shown what the action and how the gyroscopic forces influence on the transverse oscillations of the shafts during rotation.
Tabl. 0. Fig. 9. Ref. 14.

УДК 539.3
Лизунов П.П., Недин В.О. **Влияние гироскопических сил на колебательное движение вращающихся валов** // Сопротивление материалов и теория сооружений: науч.- тех. сборн. – К.: КНУСА, 2020. – Вып. 105. – С. 223 – 231.
В работе представлены результаты численного исследования поперечных колебаний валов с учётом гироскопических сил инерции. Показано, какое влияние гироскопические силы оказывают на поперечные колебания вращающихся валов.
Табл. 0. Ил. 9. Библиогр. 14 назв.

Автор (науковий ступень, вчене звання, посада): *доктор технічних наук, професор, завідувач кафедри основ інформатики КНУБА, ЛІЗУНОВ Петро Петрович.*
Адреса робоча: *03037 Україна, м. Київ, Повітрофлотський проспект 31, КНУБА, кафедра основ інформатики, ЛІЗУНОВ Петро Петрович.*
Адреса домашня: *Україна, м. Київ, вул. Кавказька, 12, кв. 48.*
Мобільний тел.: *+38(067) 921-70-05*
E-mail: *lizunov@knuba.edu.ua*
ORCID ID: http://orcid.org/0000-0003-2924-3025

Автор (науковий ступень, вчене звання, посада): *асистент кафедри основ інформатики НЕДІН Валентин Олегович.*
Адреса робоча: *03037 Україна, м. Київ, Повітрофлотський проспект 31, КНУБА, кафедра основ інформатики, НЕДІН Валентин Олегович.*
Адреса домашня: *04213 Україна, м. Київ, вул. Північна 50, кв. 181.*
Мобільний тел.: *+38(067) 764-95-52*
E-mail: *nedin.vo@knuba.edu.ua*
ORCID ID: http://orcid.org/0000-0003-3138-2892

UDC 621.87

ANALYSIS OF THE START-UP PROCESS OF THE TOWER CRANE SLEWING MECHANISM WITH A STEADY STATE MOTION MODE OF ITS LOAD TROLLEY

V.S. Loveikin[1],

Yu.O. Romasevych[1],

V.P. Kurka[1],

D.I. Mushtyn[1],

K.I. Pochka[2]

[1]*National University of Life and Environmental Sciences of Ukraine*
[2]*Kyiv National University of Construction and Architecture*

DOI: 10.32347/2410-2547.2020.105.232-246

A mathematical model of the tower crane's slew is developed under the condition of constant velocity of the trolley motion along the boom. The model is derived from the second-order Lagrange equations, calculates the tangential and radial load oscillations on a flexible suspension. An analysis of the system motion with the trolley movement to and from the tower has been conducted. A set of estimated figures has been proposed, which made it possible to establish the level of dynamic and energy load of the crane slewing mechanism, as well as to analyze the evolution of the load oscillations on a flexible suspension.

Keywords: mathematical model, slewing, tower crane, load oscillations, analysis, Lagrange equations.

Introduction

Tower cranes are widely used in many sectors of the farming industry. They are especially often used in the construction of civil engineering objects. The tower crane slewing mechanism is one of the main. The effective exploitation of this mechanism is related to the dynamic and energy processes that occur in the transient modes of mechanism motion. It is during the starting and braking of the slewing mechanism in the crane elements (shafts, toothed gears, clutches, etc.), the considerable dynamic loads occur. They have a negative impact on the longevity of the mechanism. In addition, one of the important issues for research is the energy efficiency of the crane slewing drive mechanism. These and others factors cause the need to study the dynamic and energy processes in the crane slewing mechanism. Previous studies have found that they have the greatest impact during transient modes of motion.

Moreover, we specify a factor that has a negative impact on the crane performance - the load oscillations on a flexible suspension. In case of crane's slew, the load oscillations occur in the plane of trolley motion and perpendicular to it. In order to develop methods for their elimination, it is necessary to conduct their study and establish the basic laws of their origin and development.

Analysis of publications

In the paperwork of Vaynson A.A. [1] the calculation of dynamic loads during the operation of the crane slewing mechanism is performed on the basis of a dynamic model with concentrated masses. The integration of the corresponding mathematical model under the condition of starting motion from the quiescent state and with constant driving force allowed to obtain an expression for determining the elastic torque in the crane slewing mechanism. Its analysis allowed the author to make recommendations for reducing dynamic loads in crane elements: it is necessary to increase the inertial features of the drive and to reduce the excess torque (force) of the drive mechanisms. The first method is constructively lies in the insertion of the flywheel to the kinematic chains. This leads to an increase in the start-up time of the mechanisms, which adversely affects its energy indicators. Therefore, the rational way to ensure an acceptable level of dynamic loads at low energy consumption in drive is to control its excessive torque.

In the research of Gaidamaka V.F. [2] the expression of determining the maximum dynamic loads is carried out in the same way: first of all, a dynamic model of the mechanisms is executed, equations of motion of the system reduced masses are recorded, and then the equations are integrated at zero initial conditions and the condition of constancy of the driving factor (torgue or force). The difference in calculations with previous work lies in the moment which is created by the friction forces,the crane tilt and wind. Aside from this, Gaydamaka V.F. did not take into account the effect of centrifugal force in the calculations.

In Scheffler M., Dresig H., Kurt F. [3] the emphasis is on establishing the magnitudes of the deviation of the load from the vertical in radial and tangential directions. This approach is due to the fact that in many calculation methods for the elements of tower cranes it is necessary to know the values of the angles of alteration of the load from the vertical. The authors have shown the results of their own researches and compared them to what is already known.

In general, the approach of determining the dynamic loads at which the driving force is assumed as constant is quite simplistic. It does not reflect the features of the mechanical characteristics of the drive mechanisms, which in many cases are a significant factor in the study of the dynamics of the mechanisms of the crane's slew and changes in load's fly out.

Gohberg M.M. in his work [4] indicated the combinations of load actions that should be used in the calculations of tower crane mechanisms: self-weight, load weight with gripping unit ,inertial loads, tilt forces, forces caused by wind loads, as well as mounting and transport loads. The author points out that in the case of low angular velocity of crane's slew, it is permissible to use expressions related to the dynamics of two-mass systems described in [5, 6]. In this case, the excess effort must be replaced at the appropriate time divided by the magnitude of load's fly out.

One of the important factors that determine the dynamic loads in tower crane elements is the load oscillation on a flexible suspension. Such

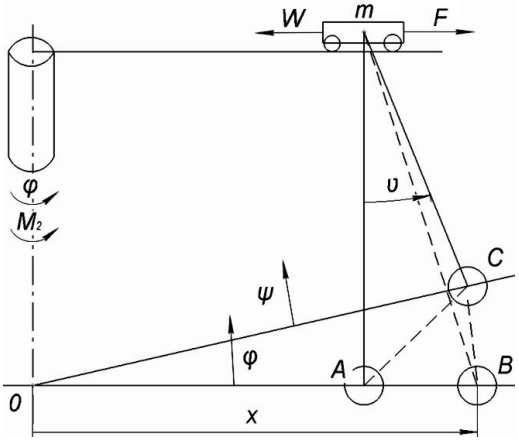

Fig. 1. Dynamic model of the slewing mechanism with steady state mode of the fly out change

oscillations are complex in nature and occur in radial and tangential directions. In addition, they cause difficulty in load positioning . Their elimination is quite a difficult task, which experienced crane operators managed to cope with by constant monitoring of the mechanisms of tower crane's slew and change of load's fly out. In order to establish the main factors that influence their appearance, it is necessary to synthesize mathematical models of the joint masses motion of the tower cranes mechanisms.

In [7, 8], a mathematical model of a crane's boom(jib) system with two degrees of freeness was developed. The authors examined the uniformly and non-uniforly accelerated tilt of the guide link (crane's boom). Nonlinear models have also been used to study oscillations on a flexible suspension [9].

In [10], the dynamics of a tower crane under the condition of pendular load oscillations (they are modeled as linear) was investigated. The construction of the tower crane is described with the finite element method. Dynamic load analysis was performed using an author-developed approach based on numerical method. It is established that the crane metal structure is most responsive to the influences which have the frequencies of the first several harmonics of metal structure oscillations and load oscillations as well. In addition, dynamic loads tend to increase as the angle of pendulum (load) deflection increases too.

In [11], a crane rotation simulation was performed based on the Euler-Lagrange equations. The analysis of the obtained results made it possible to trace the nature of the pendulum oscillations of the load on a flexible suspension and to compare them with the results of experimental studies. To minimize the load oscillatons, authors have come up with a method for controlling the driving torque of the crane slewing mechanism.

In the dissertation work [12] the influence of pendulum load oscillations on mechanical stresses of crane metal structure for different modes of its motion is investigated. On the basis of the analysis the author made a recommendation as to the position of the trolley on the boom in the condition of wind gusts for reducing the risk of emergency crane collapse.

Purpose and research task statement

The purpose of the work is to establish the level of dynamic and energy load of the tower crane slewing mechanism, as well as to study the load oscillations on a flexible suspension. To achieve this goal it is necessary to solve the following problems: 1) to develop a dynamic model of the tower crane slewing mechanism; 2) to synthesize a mathematical model, which is suitable for research, by using a second-order Lagrange equation; 3) to analyze the dynamic and energy load of the tower crane slewing mechanism; 4) to investigate the appearence and evolution of the load oscillations on a flexible suspension and to determine the main factors that affect it.

Research results

The tower crane in the process of starting-up the slewing mechanism in steady-state mode of fly out change will be presented as a holonomic mechanical system (Fig. 1), which consists of absolutely rigid bodies, except for load flexible suspension, which oscillates in the vertical plane of fly out change and when crane is slewing. In the selected dynamic model of the crane we have generalized coordinates, accepted angular coordinates of the crane slew φ and the load ψ, as well as the linear coordinate of the load movement thoughout the plane of fly out change x.

For such a dynamic model, we define the deviation of the load rope from the vertical. In this case, we assume that the deviation of the rope from the vertical, as in the plane of fly out chang, as the crane slew is negligible and does not exceed 12°. Therefore, the arc load movement during its oscillations is replaced by straight lines. As a result we will have next:

$$AB = x - vt, \tag{1}$$

$$BC = x(\varphi - \psi), \tag{2}$$

$$AC = \sqrt{AB^2 + BC^2 - 2AB \cdot BC \cdot \cos \angle ABC}, \tag{3}$$

where t is time; v - steady linear speed of the trolley movement.

For expression (3) we will find $\angle ABC$:

$$\angle ABC = \frac{\pi - (\psi - \varphi)}{2} = \frac{\pi}{2} - \frac{\psi - \varphi}{2}. \tag{4}$$

As a result of substituting dependencies (1), (2) and (4) into expression (3) we will obtain:

$$AC = \sqrt{(x - vt)^2 + x^2(\psi - \varphi)^2 - 2x(x - vt)(\psi - \varphi)\cos\left(\frac{\pi}{2} - \frac{\psi - \varphi}{2}\right)} =$$

$$= \sqrt{(x - vt)^2 + x^2(\psi - \varphi)^2 - 2x(x - vt)(\psi - \varphi)\sin\left(\frac{\psi - \varphi}{2}\right)}.$$

Then the angular coordinate of the deviation of the load rope from the vertical is determined by the dependence:

$$\nu = \frac{AC}{L} = \frac{\sqrt{(x - vt)^2 + x^2(\psi - \varphi)^2 - 2x(x - vt)(\psi - \varphi)\sin\left(\frac{\psi - \varphi}{2}\right)}}{L}. \tag{5}$$

The motion level of the crane's boom system is represented by the dynamic model shown in Fig. 1, we construct on the basis of the Lagrange equations of the second order:

$$\begin{cases} \frac{d}{dt}\frac{\partial T}{\partial \dot{\varphi}}-\frac{\partial T}{\partial \varphi}=Q_{\varphi}-\frac{\partial \Pi}{\partial \varphi}; \\ \frac{d}{dt}\frac{\partial T}{\partial \dot{\psi}}-\frac{\partial T}{\partial \psi}=-\frac{\partial \Pi}{\partial \psi}; \\ \frac{d}{dt}\frac{\partial T}{\partial \dot{x}}-\frac{\partial T}{\partial x}=-\frac{\partial \Pi}{\partial x}, \end{cases} \tag{6}$$

where T, Π is the kinetic and potential energy of the boom system, respectively; $Q\varphi$ is a non-potential component of the generalized force that corresponds to the generalized coordinate φ of the crane's slew.

The potential energy of the boom system looks like:

$$\Pi=m_1gL+mgL(1-\cos\nu), \tag{7}$$

where m_1, m – respectively the weight of the trolley and the load; g - acceleration of free fall. Taking partial derivatives of expression (7) with respect to the dependence (5) of the generalized coordinates φ, ψ and x, we have:

$$\frac{\partial \Pi}{\partial \varphi}=-\frac{mg}{L}xvt(x-\varphi), \tag{8}$$

$$\frac{\partial \Pi}{\partial \psi}=\frac{mg}{L}xvt(x-\varphi), \tag{9}$$

$$\frac{\partial \Pi}{\partial \psi}=\frac{mg}{L}(x-vt(1-\frac{(x-\varphi)^2}{2})). \tag{10}$$

The kinetic energy of the boom system is expressed by next dependency:

$$T=2\frac{I_1}{D^2}v^2+\frac{1}{2}m_1v^2(1+\dot{\varphi}^2t^2)+\frac{1}{2}I_2\dot{\varphi}^2+\frac{1}{2}m(\dot{x}^2+x^2\dot{x}\dot{\psi}^2). \tag{11}$$

Taking the necessary systems (6) derivatives from the expression (11), we obtain:

$$\frac{\partial T}{\partial \varphi}=0,\quad \frac{\partial T}{\partial \psi}=0,\quad \frac{\partial T}{\partial x}=mx\dot{\psi}^2, \tag{12}$$

$$\frac{\partial T}{\partial \dot{\varphi}}=m_1v^2\dot{\varphi}^2t+I_2\dot{\varphi}=(m_1v^2\dot{\varphi}t+I_2)\dot{\varphi}, \tag{13}$$

$$\frac{\partial T}{\partial \dot{\psi}}=mx^2\dot{\psi}, \tag{14}$$

$$\frac{\partial T}{\partial \dot{x}}=m\dot{x}, \tag{15}$$

$$\frac{d}{dt}\frac{\partial T}{\partial \dot{\varphi}}=(m_1v^2t+I_2)\ddot{\varphi}+2m_1v^2t\dot{\varphi}, \tag{16}$$

$$\frac{d}{dt}\frac{\partial T}{\partial \dot{\psi}} = mx^2\ddot{\psi} + 2mx\dot{x}\dot{\psi}, \tag{17}$$

$$\frac{d}{dt}\frac{\partial T}{\partial \dot{x}} = m\ddot{x}. \tag{18}$$

The nonpotential component of the generalized force which corresponds to the generalized coordinate φ is determined by the following dependency:

$$Q_\varphi = \frac{2M_{cr}u\eta(1+as_{cr})}{\frac{s_{cr}}{1-(\dot{\varphi}u/\omega_0)} + \frac{1-(\dot{\varphi}u/\omega_0)}{s_{cr}} + 2as_{cr}} - M_0, \tag{19}$$

where M_{cr} maximum (critical) moment on the electromotor's shaft of the crane slewing mechanism; u and η are respectively the gear ratio and the efficiency coefficient of the crane slewing mechanism; ω_0 synchronous angular velocity of the rotor of the electromotor of the crane slewing mechanism; s_{cr} critical slippage of the engine of the slewing mechanism, which is determined by the following dependency:

$$s_{cr} = (1-\frac{\omega_{nom}}{\omega_0})(\lambda + \sqrt{\lambda^2 - 1}), \tag{20}$$

where $a = R_1 / R_2'$ dimensionless parameter, which is the ratio of the resistance of the stator R_1 to the resistance of the rotor R_2', reduced to the stator windings; ω_{nom} the nominal angular velocity of the motor rotor; $\lambda = M_{cr}/M_{nom}$ is a torque capacity; M_{nom} the nominal moment on the motor shaft.

After substitution of expressions (8)-(19) to a system (6) we obtain a system of differential equations of start-up of the crane slewing mechanism at the steady state mode of the load trolley motion:

$$\begin{cases} (I_2 + m_1v^2t^2)\ddot{\varphi} + 2m_1v^2t\dot{\varphi} = \dfrac{2M_{cr}u\eta(1+as_{cr})}{s_{cr}(1-\frac{\dot{\varphi}u}{\omega_0})^{-1} + (1-\frac{\dot{\varphi}u}{\omega_0})s_{cr}^{-1} + 2as_{cr}} - M_0 + \dfrac{mg}{L}xvt(\psi-\varphi); \\ mx^2\ddot{\psi} + 2mx\dot{x}\dot{\psi} = -\dfrac{mg}{L}xvt(\psi-\varphi); \\ m\ddot{x} + mx\ddot{\psi}^2 = -\dfrac{mg}{L}(x - vt(1-\dfrac{(\psi-\varphi)}{2})). \end{cases} \tag{21}$$

In the following presentation with the model (21), the results of the process of starting-up the tower crane slewing mechanism with the steady state mode of movement of the load trolley were analyzed.

All calculations were made for the parameters of the crane Liebherr 140 hc [13], which are shown in the Table 1.

Table 1

Calculated parameters of the tower crane Liebherr 140 hc

Parameter	Unit of measurement	Value
Trolley weight, m_1	kg	300
Load weight, m	kg	5000
The moment of inertia of the turnable part of the crane relative to its own slewing axis, I_0	kg·m^2	5,5·10^6
The moment of inertia of the rotor of the electromotor of the load fly out change mechanism, I_1	kg·m^2	0,3
The moment of inertia of the rotor of the electromotor of the crane slewing mechanism, I_2	kg·m^2	0,056
The force of static resistance of the trolley movement, W	N	5500
The moment of static resistance of the crane slew, M_0	Nm	50100
The maximum torque on the electromotor shaft of the drive mechanism slewing crane, M_{cr}	Nm	120
The dimensionless parameters of the electromotor of the driving mechanism slewing crane, a_1	-	0,2
The dimensionless parameters of the electromotor of the driving mechanism slewing crane, a_2	-	0,2
Critical slippage of the engine of the crane slewing mechanism s_{cr2}	-	0,37
The gear ratio drive mechanism of the crane slew, U_2	-	1429
The synchronous angular velocity of the engine shaft of the slewing crane mechanism, ω_0	rad	104,7
The drum diameter of the slewing crane mechanism of the trolley movement, D	m	0,3
The length of the load's flexible suspension, L	m	10
Efficiency coefficient of the drive mechanism of the crane slew, η_2	-	0,80

In order to analyze the tower crane slewing mode with the constant velocity of the load trolley motion we have to build following graphical dependencies (Fig. 2).

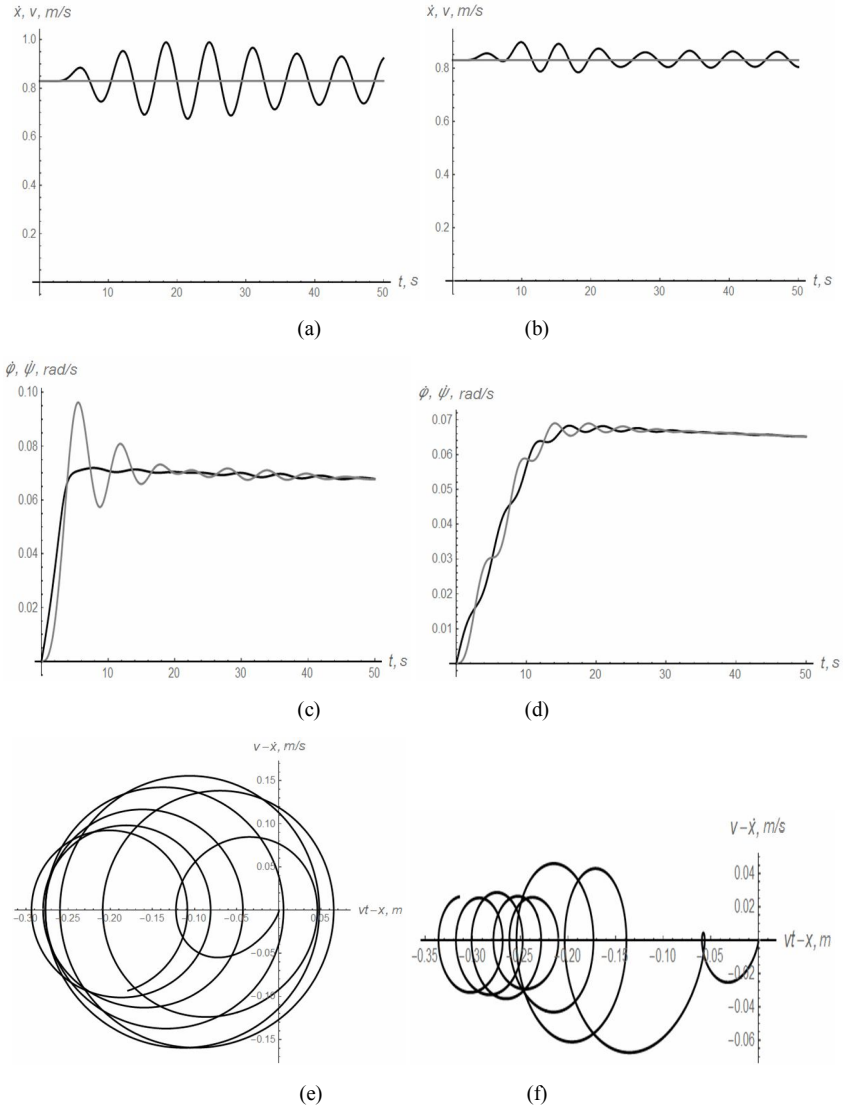

Fig. 2. Graphical dependencies of the crane start-up mode characteristics:
(a) velocity of the trolley (grey line) and the load (black line) in the radial direction at x_0=3 m;
(b) the same at x_0=30 m;
c) angular velocity of the tower (black line) and the load (grey line) in the tangential directionx_0=3 m;
d) the same x_0=30 m;
e) the phase portrait of radial load oscillations at x_0=3 m;
f) the same at x_0=30 m;

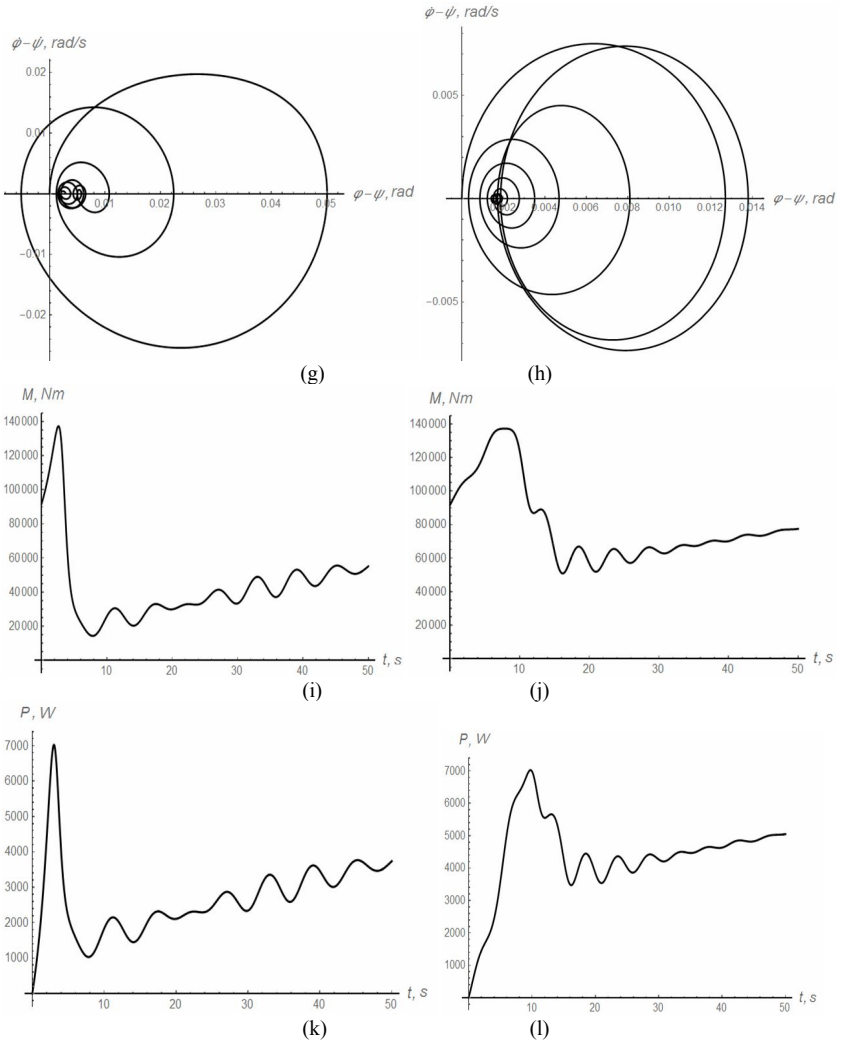

Fig. 2 (continuation). Graphical dependencies of the crane start-up mode characteristics:
g) the phase portrait of the load oscillations in the tangential direction at x_0=3 m;
h) the same at x_0=30 m;
i) the driving torgue of the drive mechanism of the tower at x_0=3 m; j) the same at x_0=30 m;
k) the drive power of the crane slewing mechanism at x_0=3 m;
l) the same at x_0=30 m

Graphical dependencies in Fig. 2 we show as follows: in the left column the graphs correspond to the case x_0=3 m, and in the right - case x_0=30 m.

To establish the quantitative characteristics of the movement of the system, the numerical data that were entered in the Table 2, were calculated.

Table 2

Kinematic, power and energy characteristics of start-up of the tower crane mechanism

Parameter	Unit of measurement	Value at x_0	
		3 m	30 m
Maximum torque value of the drive of the crane's slew	Nm	137253	
The maximum value of the drive power of the crane's slew	W	6993	
The maximum amplitude of the load deviation in the radial direction	m	0,294	0,336
Maximum amplitude of load deviation in tangential direction	rad	0,0501	0,0138
The root-mean-square value of the drive torque of the crane's slew	Nm	112213	111001
The root-mean-square drive power value of the crane's slew	W	4456	4837
The root-mean-square deviation value of the load in the radial direction	m	0,00093	0,10744
The root-mean-square deviation value of the load in the tangetial direction	rad	0,0306	0,0076

Analysis of the graphical dependencies, which are presented in Fig. 2, and the numerical data entered in the Table 2, shows that the maximum torque and power values for the cases x_0=3 m and x_0=30 m are the same. This derives from the overload capability of the crane slewing mechanism. In addition, practically equal root-mean-squere values of these characteristics can be observed.

For the case x_0=30 m, as we can see from Fig. 2 (j) and Fig. 2 (l), the torque and power of the mechanism's slew after the end of transient mode are higher. Thus, the magnitude of the initial load fly out causes the increase of these characteristics. This is due to the fact that with increasing the distance of the trolley relative to the rotational axis, firstly, the moment of system inertia increases, and secondly the angular speed of the crane's slew decreases. To compensate the speed reduction, it is necessary to provide the system with angular acceleration. The product of this acceleration at the increasing moment of inertia caused by the increase in the distance from the trolley to the axis of the crane's slew, causes an increase (compensating) of the engine driving torque. Moreover, the torgue increase causes a slight decrease in the angular speed of the crane's slew (Fig. 2 (c) and (d)).

Inspite of this, a larger value of x_0 causes an increase in the amplitude of the pendulum oscillations of the load in the radial direction. Here, the reason for such an increase is the centrifugal force, which will be as much as value of x_0. Indeed, as can be seen from Fig. 2 (f), the load over the time deviates more radially from the vertical due to the centrifugal force.

On the other hand, the amplitude of the load oscillations in the tangential direction is smaller, which is obviously the reason that, in the case of x_0=30 m, the crane mechanism's starting time is much longer (again, this is caused by an increased moment of the system inertia at a larger value of x_0). Similar tendencies are observed when analyzing the root-mean-square values of the load oscillations in both planes.

Conclusions

1. A dynamic model and an adequate mathematical model for the movement of the crane slewing mechanism with a constant velocity of the trolley movement have been developed. The torgue (force) of the drive is modeled using the Kloss equation.

2. A complex of kinematic, power and energy parameters were proposed, which made it possible to characterize the movement of the cranes lewing mechanism. These metrics reflect maximum and root-mean-square values.

3. The analysis of the modes of joint movement of mechanisms is carried out and it is established that the drive of the mechanism's slew during the transitional mode of movement is overloaded by torque and power. The set power value of the crane slewing mechanism is proportional to the distance from the trolley to the rotational axis. This is the same what refers to the drive torgue.

4. The maximum value of the total power of the mechanisms of the load fly out change and the crane's slew at different x_0 is approximately the same, although the moment of occurrence of the maximum depends on the value x_0.

5. The basic regularities of the load oscillations appearance in the radial and tangential directions, which are in the subsidence of oscillations, which are related to the damping ability of gears, the action of centrifugal force and Coriolis force.

REFERENCES

1. *Vaynson A.A.* Pod'emno-transportnye mashiny (Lifting and transporting machines)/ A.A. Vaynson. – M. Mashinostroenie, 1989. – 536 s.
2. *Gaydamaka V.F.* Gruzopod'emnye mashiny (Hoisting machines)/ V.F. Gaydamaka. – K.: Vishcha shkola, 1989. – 328s.
3. Gruzopod'emnye krany (Hoisting cranes). Kn. 2 / Sheffler M., Dresig Kh., Kurt F.; [transl. s nemeczkogo M.M. Runov, V.N. Fedoseev]; pod red. M.P. Aleksandrova. – M.: Mashinostoenie, 1981. – 287 s.
4. *Gohberg M.M.* Metallicheskie konstrukczii pod`emno-transportnykh mashin (Metal structures of hoisting-and-transport machines) / M.M. Gohberg. – M.: Mashinostroenie, 1969. – 520 s.
5. *Kazak S.A.* Dinamika mostovykh kranov (Dynamics of overhead cranes) / S.A. Kazak. – M.: Mashinostroenie, 1968. – 331 s.
6. *Lobov N.A.* Dinamika gruzopod`emny`kh kranov (The dynamics of cranes) / N.A. Lobov. – M.: Mashinostroenie, 1987. – 160 s.
7. *Priymakov O.G.* Matematichna model` kolivan` vantazhu pri povoroti krana pi`djomno-transportnoyi mashini (Mathematical model of load oscillations when turning the crane of a hoisting machine) / O. G. Priymakov, Yu. O. Gradis`kii // Sil`s`kogospodars`ki mashini. - 2013. - Vip. 25. - S. 111-117.
8. *Kuz`min A.N.* Issledovanie kolebanij gruza na gibkom podvese pri povorote krana (Investigation of vibrations of a load on a flexible suspension when turning a crane) / A.N.

Kuz`min, V.V. Suglobov, V.I. Fedun // Zakhist metalurgi`jnikh mashin vid polomok: zbirnik naukovikh pracz` / PDTU. – Mariupol`, 2011. – Vip. 13. – S. 141-147.
9. *Loveykin V.S.* Nelinijni mayatnikovi kolivannya vantazhu na gnuchkomu pidvsi pri riznikh rezhimakh obertannya (Nonlinear pendulum oscillations of the load on a flexible suspension at different modes of rotation) / V.S. Loveykin, A.V. Boyko, Yu.V. Chovnyuk // Visnik TNTU. – 2010. – Tom 15. – # 3. – S. 41-48.
10. *Bulatov Zh.L.* Sostoyanie voprosa dinamiki bashennykh kranov s uchetom bol`shikh peremeshhenij (The state of the art of tower cranes dynamics, taking into account large movements) / Zh.L. Bulatov, A.V. Sinel`shhikov // Vestnik Astrakhanskogo gosudarstvennogo tekhnicheskogo universiteta. - 2014. - #1 (57). - S. 23-29.
11. *Hamid Nalbandian Abhar*. Dynamic Analysis of the Tower Crane / Dissertation submitted to the faculty of engineering, university of malaya in partial fulfillment of the requirement for the degree of master of mechanical engineering. - P 125.
12. Tower crane Liebherr 140 HC / URL: https://cranemarket.com/specs/liebherr/140-hc (data zvernennya 07.02.2020).

Стаття надійшла 15.08.2020

Ловейкін В.С., Ромасевич Ю.О., Курка В.П., Мушгин Д.І., Почка К.І.

АНАЛІЗ ПРОЦЕСУ ПУСКУ МЕХАНІЗМУ ПОВОРОТУ БАШТОВОГО КРАНА ПРИ УСТАЛЕНОМУ РЕЖИМІ РУХУ ВАНТАЖНОГО ВІЗКА

Розроблено динамічну модель процесу повороту баштового крана з балочною стрілою при умові, що вантажний візок виконує рух із усталеною швидкістю. На основі рівнянь Лагранжа другого роду отримано відповідну математичну модель, яка, крім того, описує коливання вантажу на гнучкому підвісі у тангенціальному та радіальному напрямках. Рушійний момент, прикладений до системи, змодельовано за допомогою рівняння Клосса. Отримана математична модель представляється системою чотирьох нелінійних диференціальних рівнянь другого порядку, тому для її інтегрування використано чисельні методи. Для оцінки рівня динамічних та енергетичних навантажень у елементах системи запропоновано комплекс показників, які відображають максимальні та середньоквадратичні величини. Запропоновано розглядати еволюцію системи для двох випадків: положення візка біля башти (візок рухається від неї) та положення візка біля кінця стріли (візок рухається до башти). Для обох випадків було розраховано значення оціночних показників, які разом із відповідними графічними залежностями дозволили виявити найбільш значимі фактори, що мають вплив на енергетичні, динамічні на кінематичні процеси системи. До них, зокрема, належать: відцентрова сила, сила Коріоліса, демпфуюча здатність асинхронного електроприводу механізму повороту крана. Аналіз коливань вантажу на гнучкому підвісі, який проведений на основі фазових портретів у площині руху візка та перпендикулярно їй, виявив їх залежність від початкового положення візка на стрілі. Крім того, від цього фактора значно залежать споживана потужність приводу, частина якої витрачається на подолання відцентрової сили, що діє на візок і вантаж.

Ключові слова: математична модель, поворот, баштовий кран, коливання вантажу, аналіз, рівняння Лагранжа.

Loveikin V.S., Romasevych Yu.O., Kurka V.P., Mushtyn D.I., Pochka K.I.

ANALYSIS OF THE START-UP PROCESS OF THE TOWER CRANE SLEWING MECHANISM WITH A STEADY STATE MOTION MODE OF ITS LOAD TROLLEY

A dynamic model of the process of a tower crane slew with a saddle jib has been developed, provided that the load trolley moves at a constant velocity. On the basis of the second-order Lagrange equations, a corresponding mathematical model is obtained, which also describes the oscillations of the load on a flexible suspension in tangential and radial directions. The driving torque applied to the system is modeled using the Kloss equation. The obtained mathematical model is represented by a system of four second-order nonlinear differential equations, so numerical methods are used to integrate it. To assess the level of dynamic and energy loads in the system elements, we propose a set of indicators that reflect the maximum and root-mean-square values. It is suggested to consider the evolution of the system in two cases: the position of the

trolley near the tower (the trolley moves from it) and the position of the trolley near the end of the boom (the trolley moves towards the tower). For both cases, the values of the estimation parameters were calculated, which together with the corresponding graphical dependencies allowed to identify the most significant factors that have an impact on the energetic, dynamic and kinematic processes of the system. In particular, these include: centrifugal force, Coriolis force, damping ability of the asynchronous electric drive of the crane slewing mechanism. The analysis of the load oscillation on a flexible suspension, which was carried out on the basis of phase portraits in the plane of the trolley movement and perpendicular to it, revealed their dependence on the initial position of the trolley on the boom. Apart from this, the drive power consumption, a part of which is spent on overcoming the centrifugal force which acts on the trolley and the load, significantly depends on this factor.

Keywords: mathematical model, slewing, tower crane, load oscillations, analysis, Lagrange equations.

Ловейкин В.С., Ромасевич Ю.А., Курка В.П., Муштын Д.И., Почка К.И.

АНАЛИЗ ПРОЦЕССА ПУСКА МЕХАНИЗМА ПОВОРОТА БАШЕННОГО КРАНА ПРИ УСТАНОВИВШЕМСЯ РЕЖИМЕ ДВИЖЕНИЯ ГРУЗОВОЙ ТЕЛЕЖКИ

Разработана динамическая модель процесса поворота башенного крана с балочной стрелой при условии, что грузовая тележка выполняет движение с установившейся скоростью. На основании уравнений Лагранжа второго рода получена соответствующая математическая модель, которая, кроме того, описывает колебания груза на гибком подвесе в тангенциальном и радиальном направлениях. Движущий момент, приложенный к системе, смоделирован с помощью уравнения Клосса. Полученная математическая модель представляется системой четырех нелинейных дифференциальных уравнений второго порядка, поэтому для ее интегрирования использованы численные методы. Для оценки уровня динамических и энергетических нагрузок в элементах системы предложен комплекс показателей, отражающих максимальные и среднеквадратичные величины. Предложено рассматривать эволюцию системы для двух случаев: положение тележки у башни (тележка движется от нее) и положение тележки у конца стрелы (тележка движется к башне). Для обоих случаев было рассчитано значение оценочных показателей, которые вместе с соответствующими графическими зависимостями позволили выявить наиболее значимые факторы, влияющие на энергетические, динамические на кинематические процессы системы. К ним, в частности, относятся: центробежная сила, сила Кориолиса, демпфирующая способность асинхронного электропривода механизма поворота крана. Анализ колебаний груза на гибком подвесе, который проведен на основе фазовых портретов в плоскости движения тележки и перпендикулярно ей, обнаружил их зависимость от начального положения тележки на стреле. Кроме того, от этого фактора значительно зависит потребляемая мощность привода, часть которой расходуется на преодоление центробежной силы, действующей на тележку и груз.

Ключевые слова: математическая модель, изменение вылета, совмещение движений, манипулятор, уравнение Лагранжа второго рода, динамические нагрузки, колебания груза.

УДК 621.87

Ловейкін В.С., Ромасевич Ю.О., Курка В.П., Муштин Д.І., Почка К.І.

Аналіз процесу пуску механізму повороту баштового крана при усталеному режимі руху вантажного візка // Опір матеріалів і теорія споруд: наук.-тех. збірн. – К.: КНУБА, 2020. – Вип. 105. – С. 232-246.

Розроблено математичну модель повороту баштового крана при умові постійної швидкості руху візка по стрілі. Модель, яка отримана на основі рівнянь Лагранжа другого роду, враховує тангенціальні та радіальні коливання вантажу на гнучкому підвісі. Проведено аналіз руху системи при умові переміщення візка до башти та від неї. Запропоновано комплекс оціночних показників, які дали змогу встановити рівень динамічної та енергетичної навантаженості механізму повороту крана, а також проаналізувати еволюцію коливань вантажу на гнучкому підвісі.

Іл. 2. Бібліогр. 13 назв.

UDC 621.87
Loveikin V.S., Romasevych Yu.O., Kurka V.P. Mushtyn D.I., Pochka K.I.
Analysis of the start-up process of the tower crane slewing mechanism with a steady state motion mode of its load trolley// Strength of Materials and Theory of Structures: Scientific-and-technical collected articles – Kyiv: KNUBA, 2020. – Issue 105. – P. 232-246.

A mathematical model of tower crane's slew under the condition of constant velocity of the trolley motion on a boom has been developed. The model, derived from the second-order Lagrange equations, takes into account the tangential and radial load oscillations on a flexible suspension. An analysis of the system motion with the conditions of the trolley movement to and from the tower. A set of estimation indicators, which made it possible to establish the level of dynamic and energy load of the crane slewing mechanism, as well as to analyze the evolution of the load oscillations on a flexible suspension has been proposed.
Fig. 2. Ref. 13.

УДК 621.87
Ловейкин В.С., Ромасевич Ю.А., Курка В.П., Муштын Д.И., Почка К.И.
Анализ процесса пуска механизма поворота башенного крана при установившемся режиме движения грузовой тележки // Сопротивление материалов и теория сооружений: науч.-техн. сборн. Вып. 105. - К.: КНУСА, 2020. – С. 232-246.

Разработана математическая модель поворота башенного крана при условии постоянной скорости движения тележки по стреле. Модель, полученная на основе уравнений Лагранжа второго рода, учитывает тангенциальные и радиальные колебания груза на гибком подвесе. Проведен анализ движения системы при условии перемещения тележки к башне и от нее. Предложенный комплекс оценочных показателей, позволил установить уровень динамической и энергетической нагруженности механизма поворота крана, а также проанализировать эволюцию колебаний груза на гибком подвесе.
Ил. 2. Библиогр. 13 назв.

Автор (вчена ступень, вчене звання, посада)*: доктор технічних наук, професор, завідувач кафедри конструювання машин і обладнання Національного університету біоресурсів і природокористування України ЛОВЕЙКІН Вячеслав Сергійович*
Адреса робоча: *03041, Україна, м. Київ, вул. Героїв Оборони, 12, навчальний корпус № 11, Національний університет біоресурсів і природокористування України, кафедра конструювання машин і обладнання, ЛОВЕЙКІНУ Вячеславу Сергійовичу*
Робочий тел.: *+38(044) 527-87-34;*
Мобільний тел.: *+38(097) 349-14-53;*
E-mail: lovvs@ukr.net
ORCID ID: https://orcid.org/0000-0003-4259-3900

Автор (вчена ступень, вчене звання, посада)*: доктор технічних наук, доцент, професор кафедри конструювання машин і обладнання Національного університету біоресурсів і природокористування України РОМАСЕВИЧ Юрій Олександрович*
Адреса робоча: *03041, Україна, м. Київ, вул. Героїв Оборони, 12, навчальний корпус № 11, Національний університет біоресурсів і природокористування України, кафедра конструювання машин і обладнання, РОМАСЕВИЧУ Юрію Олександровичу*
Робочий тел.: *+38(044) 527-87-34;*
Мобільний тел.: *+38(068) 102-31-64;*
E-mail: romasevichyuriy@ukr.net
ORCID ID: https://orcid.org/0000-0001-5069-5929

Автор (вчена ступень, вчене звання, посада)*: кандидат технічних наук, старший викладач кафедри тракторів, автомобілів та біоенергосистем Національного університету біоресурсів і природокористування України КУРКА Віталій Петрович*
Адреса робоча: *03041, Україна, м. Київ, вул. Героїв Оборони, 12, навчальний корпус № 11, Національний університет біоресурсів і природокористування України, кафедра тракторів, автомобілів та біоенергосистем, КУРЦІ Віталію Петровичу*
Робочий тел.: *+38(044) 527-88-95;*
Мобільний тел.: *+38(097) 72-00-365;*
E-mail: vitaliikurka@gmail.com
ORCID ID: https://orcid.org/0000-0003-1247-6770

Автор (вчена ступень, вчене звання, посада)*: аспірант кафедри конструювання машин і обладнання Національного університету біоресурсів і природокористування України МУШТИН Денис Іванович*
Адреса робоча: *03041, Україна, м. Київ, вул. Героїв Оборони, 12, навчальний корпус № 11, Національний університет біоресурсів і природокористування України, кафедра конструювання машин і обладнання, МУШТИНУ Денису Івановичу*
Робочий тел.: *+38(044) 527-87-34;*
Мобільний тел.: *+38(098) 716-76-85;*
E-mail: denismushtyn@gmail.com
ORCID ID: https://orcid.org/0000-0003-2416-1565

Автор (вчена ступень, вчене звання, посада)*: доктор технічних наук, доцент, завідувач кафедри професійної освіти КНУБА ПОЧКА Костянтин Іванович*
Адреса робоча: *03037, Україна, м. Київ, Повітрофлотський проспект 31, Київський національний університет будівництва і архітектури, кафедра професійної освіти, ПОЧЦІ Костянтину Івановичу*
Робочий тел.: *+38(044) 248-69-25;*
Мобільний тел.: *+38(097) 212-86-29;*
E-mail: shanovniy@ukr.net
ORCID ID: https://orcid.org/0000-0002-0355-002X

UDC 539.3

PECULIARITIES OF WAVE PROPAGATION PROCESSES IN POROELASTIC MEDIA

I.D. Kara,
assistant of structural mechanics department

Kyiv National University of Construction and Architecture
31 Povitroflotskiy Avenue, Kyiv. Ukraine. 03037

DOI: 10.32347/2410-2547.2020.105.247-254

In this paper are presented peculiarities of wave propagation processes in porous media; parameters that determine properties of fluid-saturated materials; basic methods for solution of poroelastic problems, one of which is Boundary Integral Equation Method; boundary integral equations and graphs of fundamental solutions functions versus frequency parameter.

Key words: poroelasticity, porous media, boundary integral equations, fundamental solution.

Introduction. Many natural and unnatural materials have pores structure especially fluid- or gas-saturated soils, rocks and also porous building materials: timbers, sandstones, bricks, fillers for light concretes. That's why investigation of wave propagation processes in porous bodies and media has practical interest. Presence of filler changes the behavior of such materials therefore laws of the theory of elasticity can't be used for studying of wave propagations in saturated materials.

1. Basic methods. In the end of XVIII century seriously problems of dams and dikes building and necessity of understanding of cooperation and common work of water and the solid ware a reason for first description of the porous media. Now in civil construction problems of the soil-water processes are described on the basis of the theory of the porous media that consists of the theory of mixes and the conception of volume factions. The theory of mixes was based on the mechanics of continuous media that is consists of multi-component materials with different physical properties.

Mathematical modeling of the multi-component fluid- or gas-saturated porous media began in thirties of last century. Works by Y.I. Frenkel [2] and M.A. Biot [3, 4] were first works in this direction. In their works was given great attention to models of the porous media dissipation and methods for considering it in the equilibrium equations. Works by M.A. Biot are the linear theory of the effective two phase media and are supposed as the basic and classic theory for solving similar problems. In this works for the porous fluid-saturated media the two phase model that is consists from the porous solid and the fluid that fills up pores was proposed. Also additional parameters for considering cooperation of these phases was introduced such as: the porosity, the fluid viscosity, the permeability, the Biot coefficient of effective stress, the mass densities, the shear modulus and the bulk modulus of the porous material.

Procedures for determining these parameters are presented in works [4, 5]. Also analysis of porous materials properties are elucidated in works [6, 7, 8].

During analyzing of porous structures stress-strain stain is assumed that the pores are disseminate uniformly in the body. The fluid- or gas-saturated porous region when it's considered from the point of view by the mechanics of the continuous media is essentially the two-phase continuous media. The porous solid elements are belonging to the first phase and the elements of pores fluid filler are belong to the second phase. It should be taking into account during studying of the peculiarities of the porous media behavior that are foredoomed by differences of both phase mechanical properties. Breaking of all elements to two classes is also needful because the difference of the one phase elements behavior is less significant than of the different phase elements behavior. The assumption remains that the elementary volume space is full of two continuous media that can interact with each other. Also the fundamental characteristic of the porous media is propagation of three different compression waves: the longitudinal fast wave, the second longitudinal slow wave, and the third transversal slow wave.

In nineties of twentieth century began to appear the science works that are dedicated to studying of poroelastic problems and application of the Boundary Elements Method and the Boundary Integral Equation Method for solving these problems. The two-dimensional poroelastic equations ware represented almost at the same time in works [9] i [10]. The equations [9] were written in terms of the solid displacements and stresses and the fluid pressure when the boundary integral equations in [10] were consists of the dynamic and kinematic parameters.

One of the methods that now are used for solving systems of the differential equations is the integral and numerical Laplace transformation. This method was used to obtain the fundamental solutions for poroelastic systems in [11, 12] where for solving the problems three phase model was used in which porous skeleton is partially saturated by fluid and partially saturated by gas. In [13] were presented the methods for numerical modeling of the three-dimensional poroelastic bodies dynamic and for solving the model problems about wave propagation in such bodies with different boundary conditions. Solving the problem about elastic wave propagation in the porous region that is not full of the fluid is adducing in [14] with presenting of the differential equations for the not saturated space in three-dimensional transform Laplace region. The work [15] presents the fundamental solutions for the singular boundary integral equations of poroelasticity. Some aspects of linear dynamic poroelasticity in the fluid-saturated bodies are in [16-20]. Despite the fact that now are presented a significant number of the singular boundary integral equations variants are only unitary BE-solutions of the poroelastic problems. That's why questions are actual in this direction.

2. Basic Relations. Whereas the components of the different phases in the porous elastic saturated media have the different densities the total density (the

total mass of the fluid-solid aggregate per unit volume) should be considering in calculation. It can be determined by the following expression [3]:

$$\rho=\rho_s+\beta(\rho_f-\rho_s)\,, \tag{1}$$

where β is the porosity of the porous solid, the parameters ρ_s and ρ_f are the mass densities of the solid and fluid, respectively. Should be taking into account the assumption that the relative motion between the solid and the fluid is not exists.

Another peculiarity of the porous fluid-saturated media are, proposed by M.A. Biot [3, 4] and analyzed in [6], the coefficients of the poroelastic material: Q, R, B і M that are expressed from the porosity β, the Biot coefficient of effective stress α and the drained and undrained bulk modules of elasticity K і K_u:

$$Q=\frac{\beta(\alpha-\beta)(K_u-K)}{\alpha^2}\,, \tag{2}$$

$$R=\frac{\beta^2(K_u-K)}{\alpha^2}\,, \tag{3}$$

$$B=\frac{\alpha M}{K+\alpha^2 M}\,, \tag{4}$$

$$M=\frac{R}{\beta^2}\,, \tag{5}$$

where the coefficient α is determined:

$$\alpha=\frac{\beta(Q+R)}{R}\,. \tag{6}$$

The bulk modules of elasticity are determined after three types of the laboratory tests (the drained test, the unjacketed test and the undrained test) [6]:

$$K=\frac{V\cdot\Delta P}{\Delta V}\,, \tag{7}$$

$$K_u=\frac{V_u\cdot\Delta P}{\Delta V_u}\,, \tag{8}$$

where V and V_u are the primary volumes of the drained and undrained rock samples; ΔP is the incremental load in time that is applied on the rock as the pressure; ΔV і ΔV_u are the volume changes of the drained and undrained samples.

The algorithmic bases of the BEM are the boundary analogues of Somiliani's formulas for the solid displacements and the fluid pressure that under zero body conditions can be written [9]:

$$c_{ij}u_i+\int_\Gamma t^*_{ij}u_i d\Gamma+\int_\Gamma \tau^*_j U_i d\Gamma=\int_\Gamma u^*_{ij}t_i d\Gamma+\int_\Gamma \tau U^*_{nj}d\Gamma\,, \tag{9}$$

$$\int_\Gamma t^*_{i3}u_i d\Gamma+\int_\Gamma \tau^*_3 U_n d\Gamma=\int_\Gamma u^*_{i3}t_i d\Gamma+\int_\Gamma \tau\left(U^*_{n3}-JX'^*_i n_i\right)d\Gamma+Jc_{33}\tau\,, \tag{10}$$

where c is the coefficient that is equal 0.5 for points where the boundary is smooth, u_i, U_i, t_i, τ are the displacements and stresses in the solid and fluid

pressure; n is the normal to the boundary; $J=1/(i\omega b-\omega^2\rho_{22})$; u_{ij}^*, t_{ij}^*, τ_j^*, U_{nj}^* are the weighting displacement fields or the fundamental solutions. The first components of the fundamental solution tensors may be written as:

$$u_{11}^*(r,\omega)=\sum_{m=1}^{3}\left[\frac{\delta(m,3)}{2\pi\mu}K_0(i\lambda_m r)+\frac{i\lambda_m a_m}{r}K_1(i\lambda_m r)+\lambda_m^2 a_m (r,_1)^2 K_2(i\lambda_m r)\right], \quad (11)$$

$$u_{12}^*(r,\omega)=u_{21}^*(r,\omega)=\sum_{m=1}^{3}\lambda_m^2 a_m r,_1 r,_2 K_2(i\lambda_m r), \quad (12)$$

$$u_{22}^*(r,\omega)=\sum_{m=1}^{3}\left[\frac{\delta(m,3)}{2\pi\mu}K_0(i\lambda_m r)+\frac{i\lambda_m a_m}{r}K_1(i\lambda_m r)+\lambda_m^2 a_m (r,_2)^2 K_2(i\lambda_m r)\right], \quad (13)$$

where λ_m are the wave numbers that can be obtained as the roots of the characteristic equation; $K_\alpha(i\lambda_m r)$ is the modified Bessel functions;

$$K(\omega)=\frac{R}{b+i\omega\rho_{22}},$$

$$\alpha_1(\omega)=\frac{-(1-i\omega/K\lambda_1^2)}{2\pi(\lambda_2^2-\lambda_1^2)(\lambda+2\mu)},$$

$$\alpha_2(\omega)=\frac{1-i\omega/K\lambda_2^2}{2\pi(\lambda_2^2-\lambda_1^2)(\lambda+2\mu)},$$

$$\alpha_3(\omega)=\frac{-1}{2\pi\rho\omega^2}.$$

When similar fundamental solutions for the elastic region are:

$$U_{11}^*(r,\omega)=\frac{i}{4\mu}\left[H_0(k_2 r)-\frac{1}{k_2 r}\left(H_1(k_2 r)-\frac{C_2^2}{C_1^2}H_1(k_1 r)\right)+\right.$$
$$\left.+r,_1^2\left(H_2(k_2 r)-\frac{C_2^2}{C_1^2}H_2(k_1 r)\right)\right], \quad (14)$$

$$U_{12}^*(r,\omega)=U_{21}^*(r,\omega)=\frac{i}{4\mu}r,_1 r,_2\left(H_2(k_2 r)-\frac{C_2^2}{C_1^2}H_2(k_1 r)\right), \quad (15)$$

$$U_{22}^*(r,\omega)=\frac{i}{4\mu}\left[H_0(k_2 r)-\frac{1}{k_2 r}\left(H_1(k_2 r)-\frac{C_2^2}{C_1^2}H_1(k_1 r)\right)+\right.$$
$$\left.+r,_2^2\left(H_2(k_2 r)-\frac{C_2^2}{C_1^2}H_2(k_1 r)\right)\right], \quad (16)$$

where ρ is the density of the elastic material; $k_\alpha=\frac{\omega}{C_\alpha}$; $C_1=\sqrt{(\lambda+2\mu)/\rho}$, $C_2=\sqrt{\mu/\rho}$ are the velocities of elastic wave propagation.

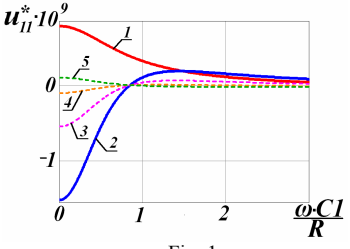

Fig. 1

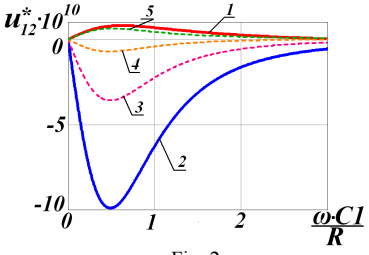

Fig. 2

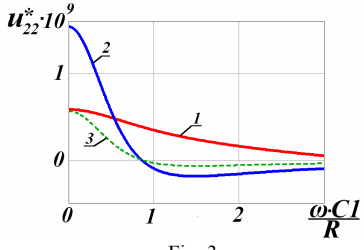

Fig. 3

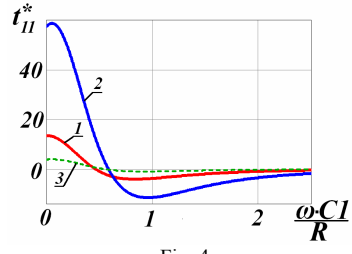

Fig. 4

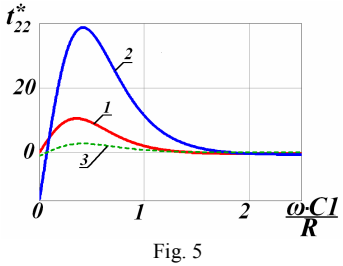

Fig. 5

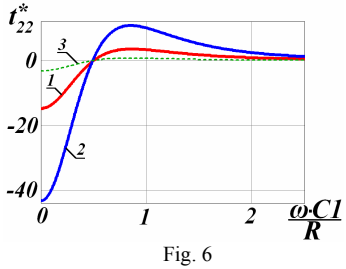

Fig. 6

Figures present the graphs of the fundamental solutions functions: the displacements u_{11}, u_{12}, u_{22} (fig. 1, 2, 3) and the stresses t_{11}, t_{12}, t_{22} (fig. 4, 5, 6) versus frequency parameter $\omega r/C_1$. The curves with designation 1 correspond to the graphs of functions for elastic media and the curves with designation 2 correspond to the graphs of functions for poroelastic fluid-saturated media, respectively.

Conclusion. The graphs of the weighting displacements and stresses fields functions for the elastic and poroelastic regions have different characters and different values depending on the frequency parameter because the body with gas- or fluid-saturated pores is differ from the continuous homogeneous elastic media and it should be modeling with applying of the two phase or the three phase model and the poroelastic equations with additional poroelastic parameters. Figures show that the graphs for the poroelastic region may be gradual approximated to the elastic analogues during changing some parameters. On the graphs in the figures 1-3 was changing of the parameter R namely gradual increase of it for the some order (curves 3, 4, 5). When the graphs of generalized derivatives functions on the figures 4-6 had changing of the parameter Q – one gradual increase for one order was enough (curves 3).

REFERENCES

1. *Ehlers W.* Foundations of multiphasic and porous materials / W.Ehlers, J.Bluh // Porous Media: Theory, Experiments and Numerical Applications, Springer, Berlin. – 2002. – P. 3–8.
2. *Frenkel Ya.I.* K teorii seysmicheskih b seysmoelektricheskih yavleniy vo vlaghnoy pochve / *Ya.I.Frenkel* // Izv. AS USSR. Cer. Geografiya i geophisika. – 1984. – T.8, № 4. – P. 133-150.
3. *Biot M.A.* Theory of propagation of elastic waves in a fluid-saturated porous solid. I. Low-Frequency Range / M.A.Biot // J. Acoust. Soc. Amer. – 1956. – V. 28, № 2. – P.168-178.
4. *Biot M.A.* The elastic coefficients of the theory of consolidation / M.A.Biot, D.G.Willis // J. Appl. Mechanics. – 1957. – P. 594-601.
5. *Yew C.H.* The determination of Biot parameters for sandstone / C.H.Yew, P.N.Jogi // Experimental Mechanics. – 1978. – №.19. – P. 167-177.
6. *Detournay E.* Fundamentals of poroelasticity. Chapter 5 in Comprehensive Rock Engineering: Principles, Practice and Projects / E Detournay., A.H.-D.Cheng // Analysis and Design Method / ed. By C.Fairhurst. // Pergamon Press. – 1993. – V.II. – P. 113-171.
7. *Nikolaevskiy V.N.* Mehanika poristyh i treshchinovatyh sred (Mechanics of porous and fractured media)/ V.N.Nikolaevskiy – M.:Nedra, 1984. – P. 233.
8. *Torraca G.* Porous Building Materials: materials science for architectural conservation / G.Torraca. – Rome: ICCROM, 2005. – P.149.
9. *Dominguez J.* Boundary elements in dynamics / J.Dominguez. – Computational Mechanics Publications. Southampton Boston, 1993. – 689 p.
10. *Cheng A.H.-D.* Integral equations for dynamic poroelasticity in frequency domain with boundary element solution / A.H.-D.Cheng, T. Badmus, D.E. Beskot // J. Eng. Mech., ASCE. – V. 117. – P. 1136-1157.
11. *Schanz M.* Wave propogation in viscoelastic and poroelastic continua / M. Schanz. − Berlin: Springer, 2001. –170 p.
12. *Li P.* Boundary element method for wave propagation in partially saturated poroelastic continua / P.Li. - Verlag der Technischen Universität Graz, 2012. – 143 p.
13. *Igumnov L.A.* Chislenno-analiticheskoe modelirovanie dinamiki tryehmernyh sostavnyh porouprugih tel (Numerical-analytical modeling of dynamic three-dimensional composite poroelastic bodies). [electronic study-methodical manual] / L.A. Igumnov, C.Y. Litvinchuk, A.V. Amenickiy., A.A. Belov. – Nighniy Novgorod: University of Nighniy Novgorod, 2012. – 52 p.
14. Laplace domain 3D dynamic fundamental solutions of unsaturated soils: the 4th International Conference on Geotechnical Engineering and Soil Mechanics, 2-3 November 2010, Tehran, Iran / I.Ashayeri, M.Kamalian, M.K.Jafari. – P. 1-8, № 40.
15. *Manolis G.D.* Integral formulation and fundamental solutions of dynamic poroelasticity and thermoelasticity / G.D.Manolis, D.E.Beskos // Acta Mechanica. − 1989. − № 76. − P. 89-104.
16. *Vorona Yu.V.* Propagation of cylindrical waves in poroelastic media / Yu.V.Vorona, Kara I.D. // Strength of Materials and Theory of Structures. – 2014. – № 93. – P. 146-152.
17. *Kovtun Al.A.* Poverhnosnye volny na granice uprugo-poristoy sredy i gydkosti / Al.A.Rovtun // Voprosy geofiziki (Problems of geophysics). – 2013. – Vol. 46. – P. 14-25.
18. *Bonnet G.* Basic singular solution for a poroelastic medium in the dynamic range / G.Bonnet // J. Acoust. Soc. Amer. – 1987. – V. 82. – P. 1758-1762.
19. *Kara I.D.* Numerical solution of the problem of porous solids vibration // Strength of Materials and Theory of Structures. – 2017. – № 99. – P. 193–202.
20. *Sorokin K.E.* Chislennoe resheniye lineynoy dvumernoy dynamicheskoy zadachi dlya poristyh sred (Numerical solution of a linear two-dimensional dynamic problem for porous media)/ K.E.Sorokin, H.H.Imomnazarov // Journal of Siberian Federal University. Mathematics & Physics. – 2010. – № 3(2). – P. 256-261.

Стаття надійшла 12.11.2020

Кара І.Д.

ОСОБЛИВОСТІ ПРОЦЕСІВ ПОШИРЕННЯ ХВИЛЬ В ПОРОПРУЖНОМУ СЕРЕДОВИЩІ

При дослідженні процесів розповсюдження хвиль в насичених пористих середовищах, на відміну від теорії пружності, має прийматись запропонована М.А.Біо двофазна модель середовища, в якій до першої фази належать тверді часточки пористого каркасу, а до другої відносяться елементи рідини, яка заповнює пори. Іноді для задач використовується трифазна модель середовища, в якій пористий пружний каркас частково заповнений рідиною, частково газом. Для пружного пористого середовища вводяться параметри, зокрема: пористість, в'язкість рідини, проникність, коефіцієнт ефективних напружень Біо, модулі зсуву та об'ємного стиснення, ефективні щільності та узагальнена густина пористого матеріалу. Також фундаментальною властивістю пружно-пористого насиченого середовища є те, що в ньому можуть розповсюджуватись три типи хвиль, а саме: дві поздовжні хвилі: швидка і повільна, а також поперечна повільна хвиля. Одним із методів розв'язання проблем поропружності є метод граничних інтегральних рівнянь. Алгоритмічною основою методу є граничні аналоги формули Соміліани для переміщень в пружному скелеті і тиску в рідині. Граничні інтегральні рівняння та фундаментальні розв'язки, які входять до складу рівнянь поропружності, суттєво відрізняються від аналогічних в теорії пружності, оскільки тіло, в якому містяться заповнені рідиною пори, відрізняється від суцільного однорідного пружного середовища. З рисунків видно, що змінюючи певні параметри, графіки для поропружної області можна поступово наближати до аналогічних для пружної. Найбільший вплив на функції переміщень дає зміна параметра R а саме поступове збільшення його на декілька порядків. В той час як для зміни графіків функцій узагальнених похідних фундаментального розв'язку достатньо одного збільшення на порядок значення параметра модуля Q.

Ключові слова: поропружність, пористе середовище, граничні інтегральні рівняння, фундаментальний розв'язок.

Kara I.D.

PECULIARITIES OF WAVE PROPAGATION PROCESSES IN POROELASTIC MEDIA

During analyzing of wave propagation processes in the fluid-saturated porous media unlike the theory of elasticity should be applied proposed by Biot the two phase model of media in which porous the solid elements are belonging to the first phase and the elements of pores fluid filler are belong to the second phase. Sometimes, for solving problems three phase model are used in which porous skeleton is partially saturated by fluid and partially saturated by gas. For the elastic porous media are introduced parameters such as: the porosity, the fluid viscosity, the permeability, the Biot coefficient of effective stress, the shear modulus and the bulk modulus, the mass densities and the total density of the porous material. Also the fundamental characteristic of the porous media is propagation of three different compression waves: the longitudinal fast wave, the second longitudinal slow wave, and the third transversal slow wave. One of the methods that are used for solving problems of poroelasticity is the Boundary Integral Equation Method. The algorithmic bases of it are the boundary analogues of Somiliani's formulas for the solid displacements and the fluid pressure. The boundary integral equations and the fundamental solutions that are comprised in the poroelastic equations are different from the theory of elasticity analogues because the body with fluid-saturated pores is differ from the continuous homogeneous elastic media. Figures show that the graphs for the poroelastic region may be gradual approximated to the elastic analogues during changing some parameters. The biggest influence for displacements functions has change of the parameter R especially gradual increase of it for the some order. When for changing the functions graphs of the generalized derivatives one gradual increase of the parameter Q for one order is enough.

Key words: poroelasticity, porous media, boundary integral equations, fundamental solution.

УДК 539.3
Кара І.Д. **Особливості процесів поширення хвиль в поропружному середовищі** // Опір матеріалів і теорія споруд: наук.-тех. збірн. – К.: КНУБА, 2020. – Вип. 105. – С. 247 – 254.

Наведені особливості хвильових процесів в пористих середовищах; величини, які визначають властивості насичених пористих матеріалів; основні підходи до розв'язання проблем поропружності, одним із яких є метод граничних інтегральних рівнянь; граничні інтегральні рівняння та графіки залежності фундаментальних розв'язків поропружності від частотного параметра
Табл. 0. Іл. 6. Бібліогр. 19 назв.

UDC 539.3
Kara I.D. **Peculiarities of wave propagation processes in poroelastic media** // Strength of Materials and Theory of Structures: Scientific-and-technical collected articles – Kyiv: KNUBA, 2020. – Issue 105. – P. 247 – 254.

In this paper are presented peculiarities of wave propagation processes in porous media; parameters that determine properties of fluid-saturated materials; basic methods for solution of poroelastic problems, one of which is Boundary Integral Equation Method; boundary integral equations and graphs of fundamental solutions functions versus frequency parameter.
Tabl. 0. Fig. 6. Ref. 20.

УДК 539.3
Кара И.Д. **Особенности процессов распространения волн в пороупругих средах** // Сопротивление материалов и теория сооружений. – К.: КНУБА, 2020. – №. 105. – С. 247 – 254.

Приведены особенности волновых процессов в пористых средах; параметры, которые определяют свойства насыщенных пористых материалов; основные подходы к решению проблем пороупруугости, одним из которых есть метод граничных интегральных уравнений; граничные интегральные уравнения и графики зависимости фундаментальных решений от частотного параметра.
Табл. 0. Ил. 6. Библиогр. 20 назв.

Автор: *асистент кафедри будівельної механіки КАРА Ірина Дмитрівна.*
Адреса робоча*: 03680 Україна, м. Київ, Повітрофлотський пр., 31, Київський національний університет будівництва і архітектури.*
Робочий тел.: *+38(044)2454829*
E-mail*: ikruska007@ukr.net*
ORCID ID: https://orcid.org/0000-0003-4700-997X

UDC 534-21:537.226.86

TRANSIENT RESPONSES IN PIEZOCERAMIC MULTILAYER ACTUATORS TAKING INTO ACCOUNT EXTERNAL VISCOELASTIC LAYERS

L.O. Grigoryeva,
Candidate of Science (Phys.-Math.)

Kyiv National University of Construction and Architecture
31, Povitroflotsky ave., Kyiv, Ukraine, 03680

DOI: 10.32347/2410-2547.2020.105.255-266

The work develops a generalized approach to the study of thickness (radial) vibrations arising in the piezoceramic plates, cylinders, spheres under electrical loads. The state of the problem and the main approaches, used in the problems of studying the oscillations of electroelastic bodies, are described. The use of multilayer elements with electroded interface surfaces and variable direction of polarization of the layers increases the conversion efficiency of electrical energy into mechanical energy, so multilayer piezoceramic plates, cylinders, spheres with changing polarization directions with electroded interfaces are considered. Because of piezoelectric elements are often embedded in the housing and supplemented with matching layers to protect against mechanical damage, it is necessary to study their effect on the oscillations of the element. The proposed approach makes it possible to study the vibrations of plane, cylindrical and spherical bodies with layers made of various electroelastic and elastic materials. Numerical implementation is carried out using finite differences.

Nonstationary oscillations of PZT-4 ceramic elements at zero initial conditions are investigated. Oscillations of multilayer plates, cylinders and spheres with and without an external elastic or viscoelastic reinforcing layer under impulse and harmonic unsteady loads are investigated and compared. There are found own frequencies for 5-layer bodies of different geometry with and without an external layer. The first natural frequency for cylinder and sphere corresponds to the radial mode of oscillations, while the second natural frequency for cylinders and spheres and the first for flat bodies are almost equal and correspond to thickness mode. The transient processes in the elements under impulse loads and the influence of the outer elastic layer (housing or matching layer) are studied, taking into account the Rayleigh attenuation. It is established that for a flat layer the outer layer increases the amplitude and the period of free vibrations after removing the load, and for cylinders and spheres it decreases. The presence of an elastic layer enhances the third and dampens the fourth natural frequency of the transducer, thereby expanding the frequency range of its operation.

Key words: piezoceramic multilayer transducers; non-stationary oscillations; electrical disturbance; piezoelectric actuators; elastic, viscoelastic layers; thickness, radial vibrations.

Piezoelectric transducers are used for exciting (actuators) and receiving (sensors) acoustic (low-frequency) or ultrasonic waves in the environment [1]. They are used in hydroacoustic exploration, medical devices, in the construction and engineering industry in non-destructive testing devices: flaw detectors, concrete scopes, thickness gauges. As their active parts are used piezoelectric elements of plane, cylindrical and spherical shape, usually made of polarized piezoceramic materials [2]. To increase the efficiency of the piezoelectric transducers, varying the frequency range and the type of perturbed waves, several interconnected piezoelectric elements can be used, possibly with different types of polarization. To match the impedances of the piezoceramic and

the controlled object, transition matching layers made of elastic materials are sometimes added. If vibration damping is required, viscoelastic layers are used. To ensure the integrity and the necessary conditions for fixing the working elements of the piezoelectric transducers can be embedded in the housing. Thus, piezoelectric transducers can be a complex object made of materials with different physical and mechanical properties: piezoceramics with different directions of polarization, elastic, viscoelastic, conductive materials, etc.

Piezoceramic spheres, cylinders and flat bodies are often used in acoustoelectric devices to receive and emit an acoustic signal, including non-stationary [3] (Fig. 1). To ensure a more effective acoustic response to electrical perturbation compared with homogeneous bodies, multilayer electro-mechanical transducers are used.

Fig. 1. Piezoceramic actuators of cylindrical, spherical and flat shape

Questions about the oscillations of electromechanical transducers are relatively often raised in the literature due to their widespread use. The principles of operation and scope of piezoceramic transducers are described in [1, 2, 4, 5 etc.]. In [6, 7] the problems of oscillations of homogeneous and non-homogeneous cylinders were solved. Stationary and nonstationary oscillations of piezoceramic bodies with curved surfaces were studied in [8].

The oscillation problems of multilayer transducers are found in single works. The harmonic axisymmetric oscillations of multilayer piezoceramic cylinders without internal electrodes were studied in [9]. Nonstationary oscillations of the piezoceramic sphere without internal electrodes too were considered in [10]. Nonstationary oscillations in cylinders with piezoceramic radially polarized layers were considered in [11]. In [12] plane multilayer element with elastic reinforcing layer taking into account the impact of ideal acoustic medium was investigated.

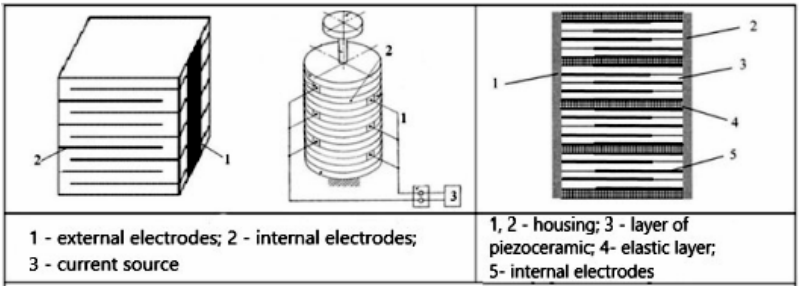

Fig. 2. The structure of the multilayer converter

In resonant modes of operation, energy dissipation in piezoceramic elements is taken into account by introducing complex material constants [1, 5]. In [13] this approach extends to nonstationary modes of operation by excluding the time variable due to the Laplace transform.

An analysis of the literature shows that the study of propagation of perturbations in electroelastic multilayer bodies is indeed an urgent and important task. It arises in the process of designing devices that operate on the basis of the piezoelectric effect. Therefore, it is necessary to study the propagation of electromechanical perturbations in multilayer piezoceramic bodies of different geometries. To model such devices, it is sufficient to use approaches based on direct numerical methods. For studying of the thickness and radial oscillations, that provide the operating frequency of the piezoelectric element, it is convenient to use the finite-difference method. The paper implements a universal approach to the oscillations description of bodies of flat, cylindrical and spherical shape, which follows from the general equations of electroelastic axisymmetric oscillations using the parameter N.

1. Statement of the problem

There are investigated thickness (radial) oscillations of multilayer hollow plates, cylinders and spheres, consisting of n piezoceramic polarized by thickness layers with interface surfaces $R_0 <\ldots< R_k <\ldots< R_n$, where R_n - external, R_0 – internal body surface.

The general equation of motion and the equation for the electrical induction of the k-th layer due to displacement and the electric potential for bodies of different geometries has the form

$$c_{33}{}^k\frac{\partial^2 u^k}{\partial r^2}+\frac{N}{r}c_{33}{}^k\frac{\partial u^k}{\partial r}+\frac{N^2}{r^2}[c_{13}{}^k(1-\frac{1}{N})-c_{11}{}^k+\frac{1}{2}(N-1)(c_{11}{}^k-$$
$$-c_{12}{}^k)]u^k+(e_{33}{}^k-e_{31}{}^k)\frac{N}{r}\frac{\partial\varphi^k}{\partial r}+e_{33}{}^k\frac{\partial^2\varphi^k}{\partial r^2}=\rho\frac{\partial^2 u^k}{\partial t^2}; \quad (1)$$

$$e_{33}{}^k\frac{\partial^2 u^k}{\partial r^2}+\frac{N}{r}(e_{31}{}^k+e_{33}{}^k)\frac{\partial u^k}{\partial r}+N(N-1)e_{31}{}^k\frac{u^k}{r^2}-$$
$$-\varepsilon_{33}{}^k\frac{N}{r}\frac{\partial\varphi^k}{\partial r}-\varepsilon_{33}{}^k\frac{\partial^2\varphi^k}{\partial r^2}=0. \quad (2)$$

Material relations in layers with radial direction of polarization

$$\sigma^k{}_r=c_{33}{}^k\frac{\partial u^k}{\partial r}+Nc_{13}{}^k\frac{u^k}{r}+(-1)^{k+1}e_{33}{}^k\frac{\partial\varphi^k}{\partial r};$$

$$\sigma^k{}_\theta=c_{13}{}^k\frac{\partial u^k}{\partial r}+N[c_{11}-\frac{1}{2}(N-1)(c_{11}-c_{23})]\frac{u^k}{r}+(-1)^{k+1}e_{31}{}^k\frac{\partial\varphi^k}{\partial r};$$

$$D^k{}_r=(-1)^{k+1}(e_{33}{}^k\frac{\partial u^k}{\partial r}+Ne_{31}{}^k\frac{u^k}{r})-\varepsilon_{33}{}^k\frac{\partial\varphi^k}{\partial r},\ k=1...n. \quad (3)$$

In (1)-(3) $u=u_r$ – radial (thickness) displacements, σ_r,σ_θ – radial and circumferential stresses, D_r – electrical induction, φ – electric potential,

$c_{ij}^k = c_{ij}^E$ – modules of elasticity of the material at a constant electric field, e_{ij} – piezoelectric modules, $\varepsilon_{33}^k = \varepsilon_{33}^S$ – dielectric constant at constant deformation, ρ – material density.

In the case of opposite to radial direction of polarization, the sign of the piezoelectric modules changes to the opposite. Previously, in [11] it was established that for maximum amplitude piezoelectric element must have an odd number of layers and layers must be opposite polarized. Going from a single-layer to a multi-layer element, we increase its sensitivity almost in proportion to the number of layers, but in addition we need to control the mechanical and electrical strength of the element [2]. Energy dissipation in piezoelectric transducers is not taken into account. In the future, in non-stationary modes of operation, it can be considered as attenuation by Rayleigh or by the method proposed in [13].

For elastic isotropic layers we have the equation of oscillations

$$\rho \frac{\partial^2 u^k}{\partial t^2} = (\lambda + 2\eta)\left(\frac{d^2 u^k}{dr^2} + \frac{N}{r}\frac{du^k}{dr} - \frac{N}{r^2} u^k \right), \tag{4}$$

where $\lambda = \dfrac{\mu E}{(1+\mu)(1-2\mu)}$, $\eta = \dfrac{E}{2(1+\mu)}$ – Lame parameters. For taking into account the viscoelastic properties of the elastic layer, we introduce oscillation propagation velocity $v_к = \sqrt{\dfrac{\rho}{\lambda + 2\eta}}$ and the Rayleigh attenuation parameter b_k :

$$v_к^2 \frac{\partial^2 u^k}{\partial t^2} + b_k \frac{\partial u^k}{\partial t} = \frac{d^2 u^k}{dr^2} + \frac{N}{r}\frac{du^k}{dr} - \frac{N}{r^2} u^k. \tag{5}$$

The parameter b_k depends on the frequency of perturbation and modal damping of the corresponding forms of natural oscillations, given as a percentage of the critical damping [14].

The initial conditions are superimposed on the displacements and their velocities

$$u(r, t=0) = \overset{0}{f}(r), \quad \frac{\partial u_r}{\partial t}(r, t=0) = \overset{1}{f}(r). \tag{4}$$

Stresses or displacements are set on the outer surfaces

$$u(R_a, t) = U_a(t) \quad \wedge \quad \sigma_r(R_a, t) = p_a(t), \quad a = 0, n. \tag{5}$$

The conditions of full contact between the layers $k = 1...n-1$ are fulfilled

$$u^k(R_k) = u^{k+1}(R_k), \quad \sigma_r^k(R_k) = \sigma_r^{k+1}(R_k), \quad \varphi^k(R_k) = \varphi^{k+1}(R_k). \tag{6}$$

The interface surfaces and the outer surfaces are electroded, the potential difference is set on the electrodes

$$\varphi(R_k) = (-1)^{k+1} V(t), \quad k = 0..n. \tag{7}$$

To make the solution general, we enter dimensionless variables [8, 11, 12]. Dimensionless form of the original equations does not change them.

2. Numerical solution method

We introduce a partition by spatial coordinate:

$$\Omega=\{r_{m(k-1)+i}=R_{k-1}+(i-1)\Delta_k,\ \Delta_k=(R_k-R_{k-1})/m,\ k=1,...,n,\ i=1,...,m+1\}.$$

In the transition to the central differences, equations (1), (2) are transformed into a system of equations $(a_k=c_{13}^k(1-\frac{1}{N})-c_{11}^k+\frac{1}{2}(N-1)(c_{11}^k-c_{12}^k))$:

$$\rho^k\frac{d^2u_{m(k-1)+i}}{dt^2}=(\frac{c_{33}^k}{\Delta r^2}-\frac{Nc_{33}^k}{2\Delta_k r_{m(k-1)+i}})u_{m(k-1)+i-1}+(\frac{N^2a_k}{r_{m(k-1)+i}^2}-2\frac{c_{33}^k}{\Delta r^2})u_{m(k-1)+i}+$$
$$+(\frac{c_{33}^k}{\Delta r^2}+\frac{Nc_{33}^k}{2\Delta r r_{m(k-1)+i}})u_{m(k-1)+i+1}+(\frac{e_{33}^k}{\Delta r^2}+\frac{N(e_{33}^k-e_{31}^k)}{2\Delta_k r_{m(k-1)+i}})\varphi_{m(k-1)+i+1}- \quad (9)$$
$$-2\frac{e_{33}^k}{\Delta r^2}\varphi_{m(k-1)+i}+(\frac{e_{33}^k}{\Delta r^2}-\frac{N(e_{33}^k-e_{31}^k)}{2\Delta r r_{m(k-1)+i}})\varphi_{m(k-1)+i-1};$$

$$(e_{33}^k-\frac{N(e_{31}^k+e_{33}^k)\Delta r}{2r_{m(k-1)+i}})u_{m(k-1)+i-1}+e_{33}^k(\frac{N(N-1)\Delta_k^2}{r_{m(k-1)+i}^2}-2)u_{m(k-1)+i}+$$
$$+(e_{33}^k+\frac{N(e_{31}^k+e_{33}^k)\Delta r}{2r_{m(k-1)+i}})u_{m(k-1)+i+1}-(-\frac{N\varepsilon_{33}^k\Delta r}{2r_{m(k-1)+i}}+\varepsilon_{33}^k)\varphi_{m(k-1)+i-1}+ \quad (10)$$
$$+2\varepsilon_{33}^k\varphi_{m(k-1)+i}-(\frac{N\varepsilon_{33}^k\Delta r}{2r_{m(k-1)+i}}+\varepsilon_{33}^k)\varphi_{m(k-1)+i+1}=0,$$

which in matrix form is written as

$$\rho\frac{d^2U}{dt^2}=AU+B\Phi+F_1,\quad D\Phi=CU+F_2, \quad (11)$$

where $U=\{u_{m(k-1)+i-1}\}$, $\Phi=\{\varphi_{m(k-1)+i-1}\}$, $k=1,\ldots,n$, $i=1,\ldots,m$.

Displacements on external surfaces

$$u_1=(p_0(t)-\frac{c_{33}^1}{2\Delta_1}(4u_2-u_3)-\frac{e_{33}^1}{2\Delta_1}(-3\varphi_1+4\varphi_2-\varphi_3))/(\frac{Nc_{13}^1}{R_0}-3\frac{c_{33}^1}{2\Delta_1});$$
$$u_{nm+1}=(p_n(t)+\frac{c_{33}^n}{2\Delta_n}(4u_{nm}-u_{nm-1})- \quad (12)$$
$$-\frac{e_{33}^n}{2\Delta_n}(3\varphi_{nm+1}-4\varphi_{nm}+\varphi_{nm-1}))/(3\frac{c_{33}^n}{2\Delta_n}+\frac{Nc_{13}^n}{R_n}).$$

Displacements on the section surfaces are found from the conjugation conditions (6)

$$u_{mk+1}=(\frac{c_{33}^{k+1}}{2\Delta_{k+1}}(4u_{mk+2}-u_{mk+3})+\frac{e_{33}^{k+1}}{2\Delta_{k+1}}(-3\varphi_{mk+1}+4\varphi_{mk+2}-\varphi_{mk+3})-$$

$$+\frac{c_{33}^k}{2\Delta_k}(4u_{mk}-u_{mk-1})+\frac{e_{33}^k}{2\Delta_k}(-3\varphi_{mk+1}+4\varphi_{mk}-\varphi_{mk-1}))/c_\kappa, \qquad (13)$$

where $c_\kappa = 3\frac{c_{33}^k}{2\Delta_k}+\frac{Nc_{13}^k}{R_k}+3\frac{c_{33}^{k+1}}{2\Delta_{k+1}}-\frac{Nc_{13}^{k+1}}{R_k}$.

An explicit and implicit difference scheme is used for time integration. When using an implicit difference scheme (Newmark's algorithm))

$$\ddot{u}^{p+1}=\frac{u^{p+1}-u^p}{\xi^2\Delta t^2}-\frac{1}{\xi^2\Delta t}\dot{u}^p-\frac{1-\xi}{\xi}\ddot{u}^p, \qquad (14)$$

where ξ – the parameter of the scheme, equations (11) (12) (13) form a single matrix, from which all unknowns in the internal points and contour points are determined simultaneously. For an explicit scheme on each time layer, the displacements at the internal points are first determined, and then by (12) (13) we find the unknowns on the contour and the boundaries of the section. An important issue in the application of an explicit scheme is the choice of the step of partitioning in spatial and temporal coordinates, as the condition of stability of the explicit scheme must be fulfilled. Practice shows that it is usually enough to take $\Delta_x \geq 10\Delta t$. For an implicit scheme, steps of the same order are taken, ξ=0,5.

3. Obtained results

Nonstationary oscillations of PZT-4 [5, 8, 11, 12] ceramic elements at zero initial conditions are investigated. External radiuses are $R_0=2$cm, $R_n=3$cm. Consider the case n = 5, i.e. piezoelectric elements consist of five layers of oppositely polarized ceramic PZT-4. The thickness of the layers is the same $h_i=(R_n-R_0)/n=2$mm, where n - number of layers. We compare the oscillations of the elements without elastic layers and taking into account the external elastic layer with a thickness of h = 2 mm. For elastic material we take $E=1{,}1\cdot10^{11}$MPa, $\mu=0.25$ (aluminum). The results are given in dimensionless form.

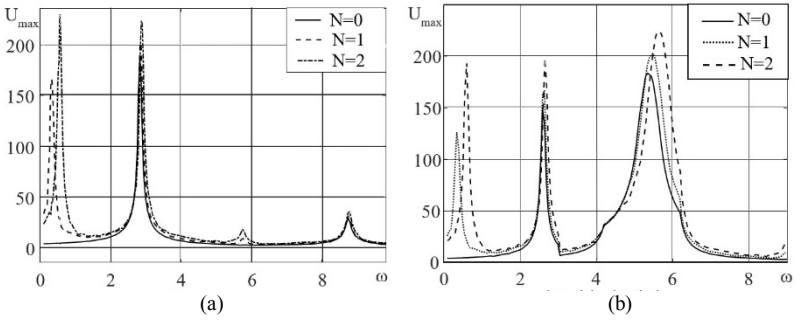

Fig. 3. The value of the maximum displacements in bodies of different geometries depending on the frequency of perturbation: (a) without elastic layer; (b) with elastic layer

An important issue in the design and operation of a piezoelectric element is the determination of its natural (resonant) frequencies. On Fig. 3 the maximum values of displacements for piezoelectric elements without an outer and with an outer elastic layer under non-stationary harmonic loading are compared. The maximum values of displacements occur during loading, the frequency of which coincides with or is close to its own. In cylinders and spheres, the first natural frequency corresponds to radial oscillations of the middle surface, the second frequency is the frequency of thickness oscillations and differs little for bodies of different geometries. The presence of an elastic layer increases the first frequency and lowers the second frequency, as well as enhances the third. Due to this property, such piezoelectric elements become multimode and belong to broadband, i.e. the range of operating frequencies for the element is significantly expanded.

One of the basic operation modes of such elements is a pulse load, which allows you to send a signal to the test medium and receive a response after the attenuation of oscillations in the element. The electric perturbation is given in the form of a half-wave sinusoid

$$V(t)=\begin{cases} V_0 \sin \omega t, \; 0<t<\pi/\omega; \\ 0, \quad 0<t<\pi/\omega. \end{cases}$$

We take ω=1, $V_0 = 2kV$. At such initial data the unit of dimensionless time approximately corresponds to 1 mcs, the unit of dimensionless movement corresponds to 55 mcm. Determining the attenuation parameter b_k is a difficult practical task, as it depends not only on the material, but also on the shape of the structure and the type of perturbation. In practice, the formula $b_k = \dfrac{2\pi\omega_a\omega_b}{(\omega_a+\omega_b)Q_k}$ is used [14], where (ω_a, ω_b) - the frequency range under consideration, Q_k - quality factor (the ratio of the resonant frequency to the width of the resonant curve at 1/2), which is considered constant in the range (ω_a, ω_b). Quality factor is one of the most important characteristics of the oscillator and is determined experimentally.

In connection with the above, we consider cases with arbitrary values b_k, which allows us to establish the dependence of the damping time of oscillations in the element on the value b_k. Note that for the pulse mode rapid attenuation of perturbations is a useful property, so for elastic matching layers materials with pronounced viscoelastic characteristics are selected.

Consider a flat piezoelectric element 1cm thick with free outer surfaces. With such a geometry, oscillations occur only due to the moving of the wave along the thickness of the element. Analyzing the results presented in Fig. 4, we see that the presence of an elastic layer increases the amplitude of natural oscillations, that occur after removal of the external load almost twice (for other loads, the growth is less). The period of oscillations increases from 2.2 mks during the travel of the elastic wave along the thickness of the elastic

layer to 2.4 mks, which corresponds to the first natural frequency for the flat element ω = 2.62 (Fig. 3b). Due to the damping properties of the elastic layer, the amplitude of oscillations decreases according to the change of b_k. At 300 mks (t=300) using $b_k = 0.01$ oscillations completely disappear, at $b_k = 0.05$ - decreased by 96%, at $b_k = 0.1$ - decreased by 82% relatively to the maximum absolute amplitude of 77 mkm. It should be noted that the oscillation amplitude of a single-layer element is 16-20% of the amplitude of oscillations of a five-layer element, i.e. the conversion of electrical energy into mechanical energy in multilayer elements is much more efficient.

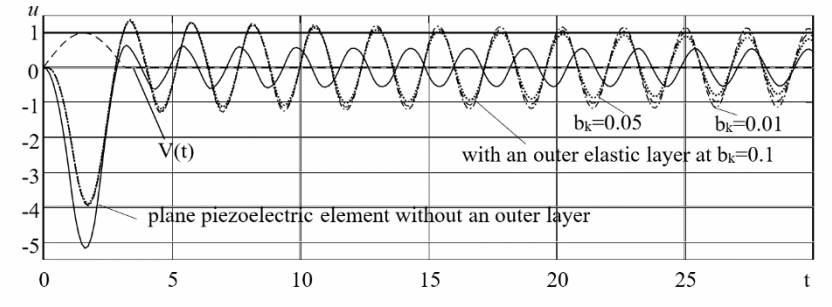

Fig. 4. Oscillations of the outer surface of a plane piezoelectric element (N = 0) without an outer layer and with an outer elastic layer with different damping coefficients

The oscillations of the cylindrical element are shown on Fig. 5. The presence of an elastic layer reduces the maximum amplitude and frequency of oscillations, as the stiffness of the element has increased. The oscillation period changed from 19 to 17 mks. The oscillations are a combination of thickness and radial oscillations, as a result of which the amplitude has increased 8 times compared to a flat element. We see that for $b_k = 0.01$ at 300 mks the amplitude decreased by 30%, at $b_k = 0.05$ - by 73%, at $b_k = 0.1$ - by 92%. The maximum amplitude of oscillations was 0.55 mm. As the ratio of radius to cylinder thickness increases, the amplitude and period of oscillations also increase.

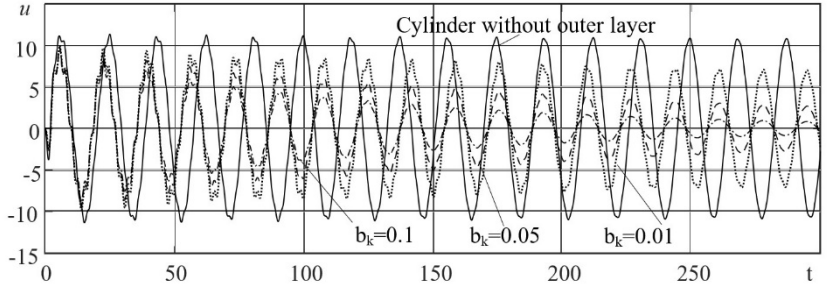

Fig. 5. Oscillations of the outer surface of a cylindrical piezoelectric element (N = 1) without an outer layer and with an outer elastic layer at different damping coefficients

Consider the oscillations of a multilayer piezoceramic sphere (Fig. 6). The period of oscillations, taking into account the elastic layer, changed from 11.1 to 10.5mks. The maximum amplitude of oscillations was 0.5mm. For 300mks at $b_k = 0.01$ amplitude decreased by 22%, at $b_k = 0.05$ - by 59%, at $b_k = 0.1$ - by 89%.

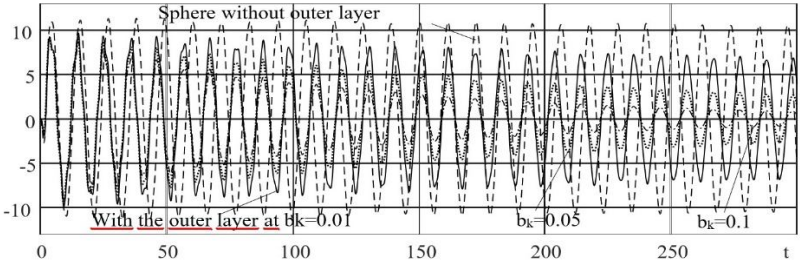

Fig. 6. Oscillations of the outer surface of a spherical piezoelectric element ($N = 2$) without an outer layer and with an outer elastic layer with different damping coefficients

Conclusion

Because of piezoelectric elements are often embedded in the housing and supplemented with matching layers to protect against mechanical damage, it is necessary to study their effect on the oscillations of the element. The proposed approach to the study of nonstationary oscillations of piezoceramic electromechanical converters (actuators) is easily implemented in any computer program.

The first natural frequency for cylinders and spheres corresponds to the radial mode of oscillations, while the second natural frequency for cylinders and spheres coincides with the first for flat bodies and corresponds to the thickness mode. The transient processes in the elements under impulse loads and the influence of the outer elastic layer (housing or matching layer) are studied, taking into account the Rayleigh attenuation. It is found that the presence of an elastic layer in a flat element increases the amplitude and period of natural oscillations of the piezoelectric element, and in cylindrical and spherical decreases them. An important property of the elastic layer is that its presence amplifies the third and dampens the fourth natural frequency. It should be noted that the obvious advantage in the amplitude of oscillations for the sphere and the cylinder is lost at a distance from the element, because the intensity of the emitted signal decreases inversely proportional to the distance. But due to the comprehensive direction of the signal, the probability of finding defects or other obstacles increases significantly.

Thus, the influence of the outer elastic layer with viscoelastic properties on the oscillations of the multilayer element is significant and should not be neglected. To reduce the impact, we need to reduce the thickness of the housing compared to the thickness of the element. The use of multilayer elements with electroded interface surfaces and variable direction of polarization of the layers increases the conversion efficiency of electrical energy into mechanical energy almost in proportion to the number of layers.

REFERENCES

1. *Busch-Vishniac, I.J.* Electromechanical Sensors and Actuators. - Springer, New York, 1999. -359p.
2. *Sharapov V.M. i dr.* Ehlektroakusticheskie preobrazovateli // V.M. Sharapov, ZH.V. Sotula, L.G. Kunickaya. / Pod red. V.M. Sharapova. – Moskva: Tekhnosfera, 2013.- 296 s. [Sharapov V.M. and other. Electroacoustic converters // V.M. Sharapov, Zh.V. Sotula, L.G. Kunitskaya. / Ed. V.M. Sharapov. - Moscow: Technosphere, 2013.- 296 p. -in Russian].- ISBN 978-5-94836-357-8
3. *Shlyahin D.A.* Nestacionarnaya mekhanika ehlektrouprugikh polej v ehlementakh konstrukcij: monografiya / D.A. Shlyakhin. – Samara: SGASU, 2012. – 190 s. [Shlyakhin D.A. Nonstationary mechanics of electroelastic fields in structural elements. – Samara: SGASU, 2012. – 190 p. -in Russian]. - ISBN 978-5-9585-0516-6
4. *Ikeda, T.* Fundamentals of Piezoelectricity. Oxford University Press, Oxford (1996).
5. *Shulha M.O., Karlash V.L.* Rezonansni elektromekhanichni kolyvannia piezoelektry-chnykh plastyn. – K.: Naukova dumka, 2007. – 270 s. [Shul'ga M.O., Karlash V.L. Resonant electromechanical vibrations of piezoelectric plates. Naukova Dumka, Kyiv. 2008. – 270p. -in Ukrainian].
6. *Ding H.J., Wang H.M., Hou P.F.* The transient responses of piezoelectric hollow cylinders for axisymmetric plain strain problems. Int. J. of Solids and structures. 2003. Vol. 40. P. 105–123.
7. *Yu J., Ma Q., Su Sh.* Wave propagation in non-homogeneous magneto-electro-elastic hollow cylinders. Ultrasonics. 2008. Vol. 48, Issue 8, P. 664–677. doi.org/10.1016/j.ultras.2008.03.005
8. *Shulga M.O., Grigoryeva L.O.* Electromechanical unstationary thickness vibrations of piezoceramic transformers at electric excitation // Mechanical Vibrations: Types, Testing and Analysis. − Nova Science Publishers, New York. − 2010. − pp.179-204.
9. *Grigorenko A.YA., Loza I.A.* Osesimmetrichnye volny v sloistykh polykh cilindrakh s p'ezokeramicheskimi radial'no polyarizovannymi sloyami // Problemy vychislitel'noj matematiki i prochnosti konstrukcij. - Vyp.17, 2011. - S. 87−95. [A.Ya. Grigorenko, I.A. Loza. Axisymmetrical Waves in the Hollow Multilayered Cylinders with Pizoceramic Lays Polarized in Radial Direction)// Problems of Computational Mechanics and Strength of Structures. - Iss.17, 2011. P. 87−95. - in Russian].
10. *H.M. Wang, H.J. Ding, Y.M. Chen.* Transient responses of a multilayered spherically isotropic piezoelectric hollow sphere. // Arch Appl Mech (2005) 74: 581-599. DOI 10.1007/s00419-005-0374-9
11. *L. Grigoryeva.* Calculation of Cylindriclal Multilayer Electromechanical Transducer at Different Polarization Types in Non-stationary Modes // Proceedings of Odessa Polytechnic University, Issue 1(54), 2018.- P. 5-11.
12. *Hryhorieva L.O.* Nestatsionarni kolyvannia ploskoho bahatosharovoho piezoelementa z urakhuvanniam pruzhnoho pidkripliuiuchoho sharu y akustychnoho seredovyshcha // Visnyk Zaporizkoho natsionalnoho universytetu. Fizyko-matematychni nauky. - 2017. - № 1. - S. 103-109. [Grigoryeva L.O. Unsteady Vibrations of Plane Multilayered Piezoelement in View of Elastic Reinforcing Layer and an Acoustic Medium) // Visnyk of Zaporizhzhya National University. Physical and Mathematical Sciences - 2017. - № 1. - Pp. 103-109. – in Ukrainian].
13. *Dubenec V.G., Savchenko E.V., Derkach O.L.* Nestacionarnye kolebaniya balki s ehlektrovyazkouprugimi dissipativnymi nakladkami // Visnyk Chernihivskoho derzhavnoho tekhnolohichnoho universytetu № 3 (67), 2013. – S.53-61. [V.H. Dubenets, O.V. Savchenko, O.L. Derkach. Nonstationary Vibrations of a Beam with Electro-Viscoelastic Dissipative Patches // Visnyk of Chernihiv State Technological University № 3 (67), 2013. – C.53-61. - in Russian].
14. *Nasedkin A.V.* Modelirovanie piezoehlektricheskikh preobrazovatelej v Ansys. – Rostov-na-Donu: izdatel'stvo Yuzhnogo federal'nogo universiteta, 2015.- 175c. [Nasedkin A.V. Modelling Piezoelectric Transducers in Ansys. - Rostov-on-Don, 2015.- 175p.- in Russian].

Стаття надійшла 13.05.2020

Григор'єва Л.О., к.ф.-м.н.

ПЕРЕХІДНІ ПРОЦЕСИ В П'ЄЗОКЕРАМІЧНИХ БАГАТОШАРОВИХ АКТУАТОРАХ З ВРАХУВАННЯМ ЗОВНІШНЬОГО В'ЯЗКОПРУЖНОГО ШАРУ

В роботі розвивається узагальнений підхід до дослідження товщинних (радіальних) збурень, що виникають в п'єзокерамічних пластинах, циліндрах, сферах при електричних навантаженнях. Розглядаються багатошарові перетворювачі змінного напрямку поляризації з електродованими поверхнями розділу. Запропонований підхід дозволяє досліджувати коливання тіл з шарами, виконаними з різних електропружних та пружних матеріалів. Чисельна реалізація виконана за допомогою скінченних різниць. Описано коливання багатошарових пластин, циліндрів та сфер з зовнішнім пружним або в'язкопружним підкріплюючим шаром та без нього при імпульсних та гармонічних нестаціонарних навантаженнях. Встановлено, що для плоского шару зовнішній шар підвищує амплітуду та період вільних коливань після зняття навантаження, а для циліндрів та куль - понижує. Наявність пружного шару підсилює третю та гасить четверту власну частоту перетворювача, чим розширює частотний діапазон його роботи.

Ключові слова: п'єзокерамічні багатошарові перетворювачі; нестаціонарні коливання; електричне збурення; п'єзоелектричні актуатори; пружні, в'язкопружні шари; товщинні, радіальні моди коливань.

Григорьева Л.О., к.ф.-м.н.

ПЕРЕХОДНЫЕ ПРОЦЕССЫ В ПЬЕЗОКЕРАМИЧЕСКИХ МНОГОСЛОЙНЫХ АКТУАТОРАХ С УЧЕТОМ ВНЕШНЕГО ВЯЗКОУПРУГОГО СЛОЯ

В работе развивается обобщенный подход к исследованию толщинных (радиальных) возмущений, возникающих в пьезокерамических пластинах, цилиндрах, сферах при электрических нагрузках. Рассматриваются многослойные преобразователи переменного направления поляризации с электродированными поверхностями раздела. Предложенный подход позволяет исследовать колебания тел со слоями, выполненными из различных электроупругих и упругих материалов. Численная реализация выполнена с помощью конечных разностей. Описаны колебания многослойных пластин, цилиндров и сфер с внешним упругим или вязкоупругим подкрепляющим слоем и без него при импульсных и гармонических нестационарных нагрузках. Установлено, что для плоского слоя внешний слой повышает амплитуду и период свободных колебаний после снятия нагрузки, а для цилиндров и сфер - понижает. Наличие упругого слоя усиливает третью и гасит четвертую собственную частоту преобразователя, чем расширяет частотный диапазон его работы.

Ключевые слова: пьезокерамические многослойные преобразователи; нестационарные колебания; электрическое возмущение; пьезоэлектрические актуаторы; упругие, вязкоупругие слои; толщинные, радиальные колебания.

УДК 534-21:537.226.86
Григор'єва Л.О. **Перехідні процеси в п'єзокерамічних багатошарових актуаторах з врахуванням зовнішнього в'язкопружного узгоджувального шару** // Опір матеріалів і теорія споруд: наук.-тех. збірн. – К.: КНУБА, 2020. – Вип.105. – С. 255-266. – Англ.

Досліджуються коливання багатошарових п'єзокерамічних плоских, циліндричних та сферичних тіл з врахуванням зовнішнього в'язкопружного шару.
Іл. 6. Бібліогр. 14 назв.

UDC 534-21:537.226.86
Grigoryeva L.O. **Transient responses in Piezoceramic Multilayer Actuators Taking into Account External Viscoelastic Layer** // Strength of Materials and Theory of Structures: Scientific-and-technical collected articles. – K.: KNUBA, 2020. – Issue 105. – P. 255-266.

The oscillations of multilayer piezoceramic flat, cylindrical and spherical bodies taking into account the outer viscoelastic layer are investigated.
Fig. 6. Ref. 14.

УДК 534-21:537.226.86
Григорьева Л.О. **Переходные процессы в пьезокерамических многослойных актуаторах с учетом внешнего вязкоупругого слоя** // Опір матеріалів і теорія споруд: наук.-тех. збірн. – К.: КНУБА, 2019. – Вип. 103. – С. 255-266. – Англ.

Рассматривается влияние нагрева на параметры собственных колебаний параболических оболочек вращения.

Табл. 6. Іл. 10. Библиогр. 20 назв.

Автор (вчена ступень, вчене звання, посада): кандидат фізико-математичних наук, доцент кафедри опору матеріалів Григор'єва Людмила Олександрівна (Grigoryeva Ludmila)
Адреса робоча: 03680 Україна, м. Київ, Повітрофлотський проспект 31, Київський національний університет будівництва і архітектури, кафедра опору матеріалів, Григор'євій Людмилі Олександрівні
Робочий тел.: +38(044) 241-54-21;
Мобільний тел.: +38(097) 304-34-32;
Імейл: grygorieva.lo@knuba.edu.ua
ORCID ID: https://orcid.org/0000-0001-7013-0327

UDC 624.016

COMPARATIVE ANALYSIS OF STRENGTHENING OF BUILDING STRUCTURES (MASONRY, METAL STRUCTURES, REINFORCED CONCRETE) USING FRP-MATERIALS AND TRADITIONAL METHODS DURING RECONSTRUCTION

I.N. Rudnieva,
PhD, Associate Professor

Kyiv National University of Construction and Architecture,
31, Povitroflotskiy avenu, Kyiv, Ukraine

DOI: 10.32347/2410-2547.2020.105.267-291

The aim of the research is the evaluation of the structural performance of composite fibre-reinforced elements in the wider sector of the conservation of historical, architectonic and environmental heritage, as well the more contemporary buildings of the last century, which have lost of the bearing capacity focusing reliability indexes and the appearance of the structure.

In the article was described and analyzed the existing traditional methods and the alternative methods of strengthening by FRP-materials (composite materials) such building structures as masonry, metal structures, reinforced concrete, and the computation in software ABAQUS. These procedures of strengthening building structures by FRP-materials in Ukraine are not widely used due to the lack of a regulatory framework that would regulate their use, as well because these materials are relatively expensive compared to the traditional ones.

The article analyzed the existing methods of computation and design of the strengthening using FRP-materials, and the computation in software ABAQUS was performed with conclusions and recommendations based on results of the computation.

The aim of the work was to review the technology and analyze the advantages and disadvantages of each of the strengthen methods that should be used when choosing effective solutions for strengthening building structures. In conclusion, the need for further study and researches was confirmed.

Keywords: methods of strengthening, composite materials, FRP-materials, masonry, metal structures, reinforced concrete, stress-strain state, computational methods, defects, damage, reconstruction.

1. Introduction

Built mostly centuries ago, heritage buildings as well the more contemporary buildings of the last century, which have lost the bearing capacityoften need restoration and strengthening, especially in seismic regions and in regions with shrinkage phenomena (subsidence region). The need of strengthening of the building constructions during exploitation appears mostly because of their premature wear as a result of technological influences and weathering, various damage and various other factors.

Traditional methods of strengthening are effective, but in some cases not appropriate or not applicable for use. An example is the increase of the load-bearing structures of historical buildings, preserving the external appearance of which is the determining factor. In this case, the use of the discussed alternative methods can be justified alternative.

Knowledge of the causes of defects and damage of structures allows to choose the best option of repairing or strengthening. Causes of the deformation of buildings are presented in Table 1 [3].

Table 1

Causes of the buildings deformation

The type and external manifestation of the strain	Causes of the deformation
Drawdown of the middle of the building 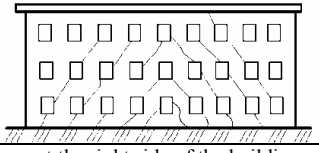	1. The weak base of the middle part of the building 2. Drawdown as a result of the soaking of the subsidence soils 3. Karst under the middle of the building.
Drawdown at the right side of the building 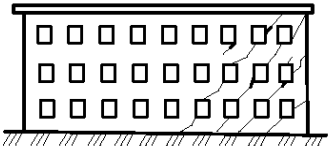	1. Weak base of the extreme part of the building 2. Drawdown as a result of the soaking of the subsidence soils 3. Karst in the extreme part of the base. 4. Location near the open pit 5. Location near the trenches and squeezing quicksand 6. Shift of the retaining wall that located near 7. Construction next to of a new building
Drawdown of two extreme parts of the building 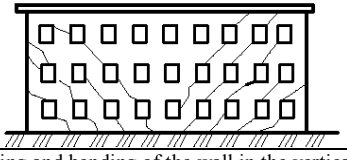	1. The same reasons as for the right of the building, acting on its two extreme parts 2. Placing under the middle of the building of a large object
Buckling and bending of the wall in the vertical and horizontal planes 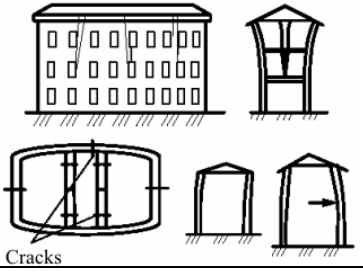 Cracks	1. Tension from the truss system 2. Horizontal force from the stretching 3. Eccentric transfer of the load from the floors 4. Vibrations from machines located in the building and seismic shifts

Cracks indicate on the poor state of the structures. They may eventually will have opened and cause the development of strains that not only change the appearance of the design, but also greatly reduce its strength and carrying capacity. In a brick and masonry buildings cracks in the walls, bridges, domes and arches are caused mostly by irregular subsidence of the bases and foundations, various deformability of the loaded or unloaded walls.

In the reinforced concrete structures cracks are caused by poor reinforcement, lack of spatial rigidity, temperature and shrinkage phenomena, violations of manufacturing technology products, their ransportation, warehousing and assembly, corrosion of the main reinforcement.

For survey and inspection of buildings, the results of laboratory tests, non-destructive and quasi-non-destructive tests and researches are usually used using **some devices and instruments for such researching parameters as:**

• Strain of the building (leveling instrument, theodolite survey, photogrammetry, 3D laser scanning),

• Deflections and displacements (leveling instrument, deflectometer, 3D laser scanning),

• Concrete strength (The method of plastic deformation - the device of the shock-impulse type, Hammer Koshkarova; the ultrasonic method),

• Solution strength (The method of plastic deformation),

• Hidden defects of the material of the design (the ultrasonic and radiometric method),

• Depth of the cracks in concrete and masonry (the ultrasonic method, a calliper),

• Width of the cracks in concrete and masonry (measuring microscope, a calliper),

• The thickness of the protective layer of the concrete (magneto-metric method),

• The density of concrete, stone and granular materials (radiometric method),

• Moisture concrete and stone (Neutron method),

• Breathability (Pneumatic method),

• Heat protection quality of the wall (Electrical methods).

Scientific Researches with using of 3D laser scanner during survey and inspection of historical buildings were represented in the articles of Naif Adel Haddad [20], Terrence F. Paret [21], Golubka Necevska -Cvetanovska [51], Vincenzo Mallardoa [52], Yusuf Arayici [53].

To carry out restoration and strengthening of building structures, it is necessary to carry out the following complex of works on the project:

1. Architectural concept of building

2. Design models of structure (using 3D laser scanning, which represents today the most advanced technology available for measuring and documenting objects and structures):

• beam (farm, frame of building) model (simplified)

• surface model (detailed, if it need)

3. Composition of loads and combinations of loads under standard operation conditions

4. analysis of stress-strain state of structures:

• analytic method

• finite element method using computer's programs for simulation the stress-strain state (SSS) of buildings structures

5. Spatial stiffening of structure (if it needs)

6. Constructional drawings of main structure and structural elements

2. Traditional methods of strengthening building structures

There are the following traditional methods to strengthen masonry: partial or total replacement of elements of masonry, installation of the core, injection of special solutions, the use of the steel cages, the steel clamps, etc. Traditional strengthening methods of building structures are shown in Fig. 1, Fig. 2.

(a) (b) (c) (d) (e) (f)

Fig. 1. Image representations traditional methods of strengthening building structures:
(a) Strengthening of reinforced concrete jumpers by metal corners;
(b) Strengthening of the floor slabs using unloading metal beams;
(c) The foundations strengthening by reinforced concrete cage;
(d) Strengthening of the supporting walls by the temporary support;
(e) Steel angles added to span across cracking in the wall;
(f) Expansion of the foundation lining of the new reinforced concrete pillow, Kiev

(a)

(b)

(c)

(d)

(e)

(f)

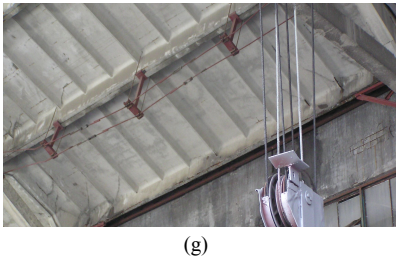

(g)

Fig. 2. Traditional methods of strengthening building structures: (a) Photo of riveted steel truss supporting roof joists and barrel vault ceiling joists; b) strengthening of brick wall by tension bars with overlays, Venice; c) installation of prestressed steel strips, Venice; d) installation of prestressed steel strips and strings with overlays, Venice; e) the strengthening of the reinforced concrete floor beam; f) strengthening of reinforced concrete beams with metal trusses; g) strengthening of the 12 meter covering slabs by consoles and by truss tightening

Using traditional methods of strengthening to increase the strength characteristics of masonry in most cases it is accompanied by a change of the external configuration of the strengthened object. When old masonry replacing

to a new the strengthening is accompanied by additional time-consuming work to install the structures of unloading. Method of injection solution is useful mostly for small damages.

Strengthening as the reinforced concrete structures as well as the metal structures by the steel panels have a lot of advantages, such as relatively low cost, sufficient fatigue strength, steel panels are universal.

Disadvantages of steel panels and rods for strengthening are possible corrosion, they have considerable weight, for installation of steel elements need high labor content of the work, and consequently the high cost of labor required, to perform the work need large area, steel elements are limited in size.

Repairing or strengthening failing structures traditionally involves using bulky and heavy external steel plates that often pose their own problems. The plates are generally prone to corrosion and overall fatigue. Therefore fibre-reinforced polymer is a great alternative for strengthening reinforced concrete and metal structures.

3. The alternative methods for strengthening building structures

Used traditional methods of amplification have a relevant and effective, but they can not always be used in case of strengthening of bearing structures of historical buildings, where it is necessary to preserve not only the building as a whole, but also external architectural appearance. Because the anchors permeate the design, and they damage the surfaces of architectural structures. In such situations, it is better to use alternative methods strengthen as the metal structures as well the masonry and reinforced concrete structures using composite materials [24].

The alternative methods for strengthening building structures are methods of reinforcement by composite materials (Fig. 3).

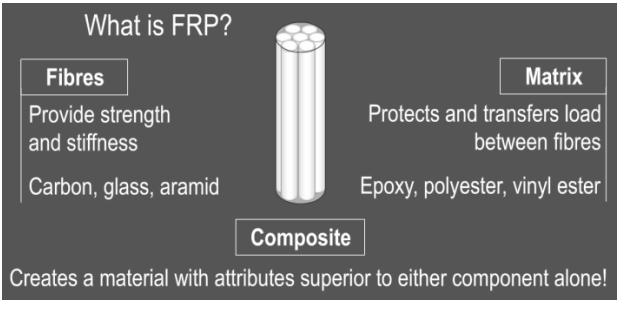

Fig. 3. Image representations composite material FRP

Composite material in the form of surface reinforcement externally bonded non-metallic strips.

FRP consists of fibers — carbon, aramid or glass — bonded together with a polymer matrix — epoxy, polyester or vinyl ester (Fig. 4).

FRP reinforcements are shaped either into composite laminates for epoxy-bonding onto the masonry surface, or into textile fabrics for laying onto the masonry surface and then impregnating the fibers with the matrix.

Fig. 4. Image representations of composite FRP materials

The main advantages of the strengthening of building constructions by composite materials are follows:

1) high durability and resistance to corrosion;

2) easy installation and low own weight;

3) high mechanical characteristics (strength and modulus of elasticity) of materials that constitute the strengthening of system;

4) a high elongation of materials strengthening;

5) possibility to joint the working element of the external reinforcement with reinforced structures at all stages of loading (such work provided by a reliable adhesive bonding).

The necessity of using FRP for strengthening building and structures is due to the internal properties of the material, such as a high strength-to-weight ratio, corrosion resistance, etc. (Tabl. 2). In addition, both the material and the geometric properties can be adapted for a specific application. Several materials are available for the fibers, e.g. glass, aramid, carbon. Therefore, a FRP with carbon fibers is abbreviated as CFRP. Properties of different fibers and typical steel are shown in Fig. 5.

Aramid fibers has good endurance and rigidity as well as low electricity and thermal conductivity. Carbon fibers are made from different starting materials. Mechanical properties of the fibers to a large extent depend on the carbonization conditions.

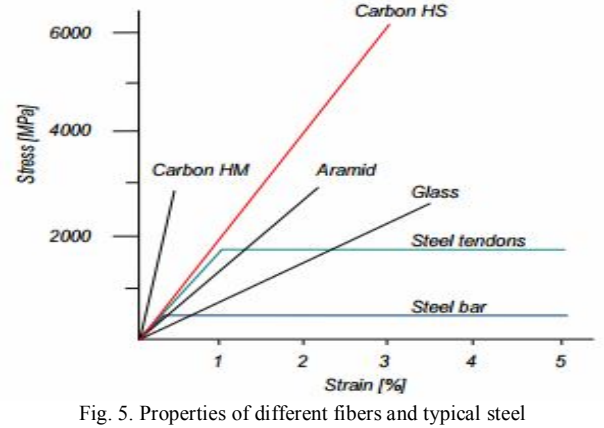

Fig. 5. Properties of different fibers and typical steel

Strengthening of building structures with elements of external reinforcement made of high-strength fibers has been used for a long time, although for Ukraine, unfortunately, it is a fairly new thing. It has been in use in Switzerland or in Italy more then 45 years. Comparison of physical and mechanical characteristics of different fibers and steel represented in Table 2.

Table 2

Fibres and steels properties

Fibres	E_{axial} / E_{radial} $[GPa]$	σ_{max} $[MPa]$	ε_{max} $[\%]$	ν	ρ $[g / cm^3]$	Price $[\in / kg]$
HM Carbon	380/12	2400	2.6	0.2	1.95	20-60
HS Carbon	230/12	3400	1.1	0.2	1.75	20-60
Glass	76/76	2000	2.6	0.22	2.6	1.5-3
Aramid	130/10	3000	2.3	0.35	1.45	20-35
Basalt	89/NA	4800	3.15	NA	2.75	NA
Steel	200-220	400			7.9	5-10

Samples of composite materials of the Italian company FIBERBUILT [17] are shown in Fig. 6.

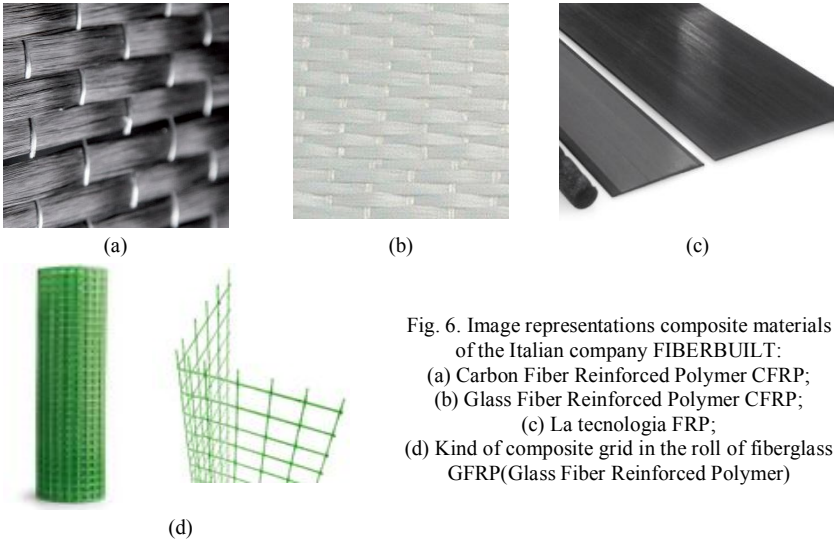

Fig. 6. Image representations composite materials of the Italian company FIBERBUILT:
(a) Carbon Fiber Reinforced Polymer CFRP;
(b) Glass Fiber Reinforced Polymer CFRP;
(c) La tecnologia FRP;
(d) Kind of composite grid in the roll of fiberglass GFRP(Glass Fiber Reinforced Polymer)

In the composite materials based on glass fiber are used quartz glass. The advantages of fiberglass are relatively low cost. Aramid fibers are used since the 70s of the last century. On chemical structure similar to nylon aramids. These fibers are anisotropic at its structure and as compared with glass have a higher strength and modulus of elasticity. They are more plastic under the

influence of tensile loads, but under compression they remain elastic before failure. Important properties of a strengthening material are the stiffness, strength, and weight.

Nevertheless, drawbacks related to brittle failure, longterm durability, sensitivity to impacts, and high cost have limited their widespread use. After the diffusion of Fibre Reinforced Polymers (FRPs), mortar-based composites have been recently developed, which make use of high performance textiles (continuum dry fibres arranged in the form of open mesh or fabric) externally bonded with either cement or lime mortars. These systems are known as either TRMs (Textile Reinforced Mortars) or FRCMs (Fibre Reinforced Cementitious Matrices). Despite their adhesion strength may be lower than FRPs in certain cases, they offer important advantages in terms of fire resistance, vapour permeability, removability, and ease, time and cost of installation, thanks to the use of inorganic matrices in place of resins.

From the viewpoint of fire resistance and safety of the works the use of microcement with addition of polymer resins as an adhesive is more effective, in contrast to the epoxy adhesive. At strengthening of structures by grids for consolidate them to the surface using adhesive mortar based on cement [37]. New reinforcing material: FRCM Components Poliparafenilen Benzobis Oxazolo (PBO), Cement-based Adhesive FRCM, C-FRCM and C-FRP are represented on Fig. 7, Fig. 8.

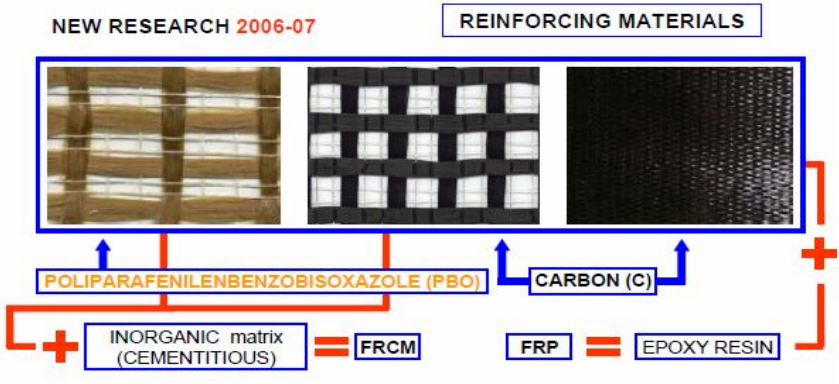

FIBERS	Tens. strength (N/mm²)	Failure strain (‰)	Young's modulus (GPa)	Nominal thickness (mm)
Carbon net	3500	15	240	0.047 (dir. 1 and 2)
PBO net	5800	21.5	270	0.046 (dir.1) 0.022 (dir. 2)
Carbon sheet	3500	15	240	0.17

Fig. 7. New FRCM

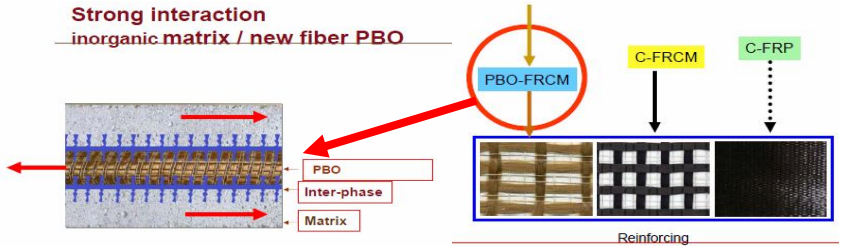

Fig. 8. Properties of new FRCM

4. The main metods for strengthening building structures using FRP-materials

4.1. Masonry. The systems for strengthening of building structures vary depending on the type of consolidation required:

• FIBREBUILD FRCM (Fiber Reinforced Cementitious Matrix) [17]: "reinforced render" method, where GFRP meshes, connections and accessories are combined with lime-based mortars to obtain collaborating reinforced renders capable of improving shear, flexural and compressive strength of masonry (Fig. 9,a).

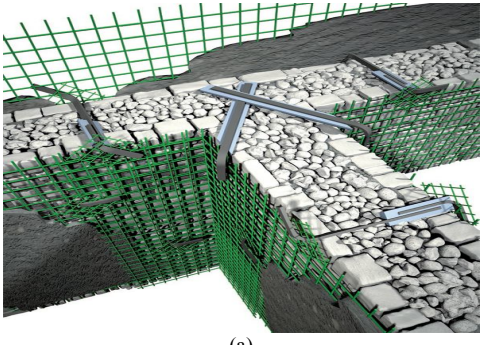

(a)

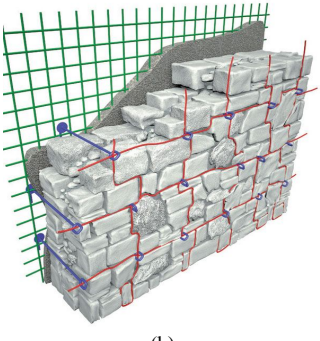

(b)

(c)

Fig. 9. Image representations the systems for strengthening of masonry walls:
(a) FIBREBUILD FRCM (Fiber Reinforced Cementitious Matrix);
(b) FIBREBUILD RETICOLA; (c) FIBREBUILD FRP

• FIBREBUILD RETICOLA: “reinforced repointing” method, where stainless steel cords and connections are used to consolidate “exposed stone” masonry. The system helps reinforce masonry diffusely and successfully, while preserving the original look (Fig. 9,b).

• FIBREBUILD FRP: fibre-reinforced sheeting method, with GFRP and CFRP weaves, sheets and bars, particularly adapted to consolidate beams, pillars and columns and any other spots where masonry requires local reinforcement (hooping) (Fig. 9,c).

Of all architectural elements, arches and vaults made of stone or brick, be they bearing or not, are the most prone to degradation and stress caused by seismic events, changes in acting loads and foundation sinking, which cause the structure to lose its original mechanical properties. Because these elements are of great historic and architectural value, they need to be consolidated in a non-invasive, compatible and consistent way with regard to their special features.

Fibre Net developed two different methods of intervention:

• FIBREBUILD FRCM (Fiber Reinforced Cementitious Matrix): the “reinforced render” method, where GFRP meshes, connections and accessories are combined with preferably lime-based mortars to obtain a thin collaborating reinforcement capable of improving mechanical strength diffusely and homogeneously (Fig. 10,a).

• FIBREBUILD FRP: fibre-reinforced sheeting method, where GFRP and CFRP weaves are used for reinforcing individual spots, ideally recommended for oddly shaped arches and vaults (Fig. 10,b).

The esthetic superiority and the general structural characteristics of FRP-systems have been recognized by Jerzy Jasienko [12,13], Angelo Di Tommaso [11] etc, as well as following international organizations: The International Federation for Structural Concrete [4] , American Concrete Institute [5], Japan Building Disaster Prevention Association [6].

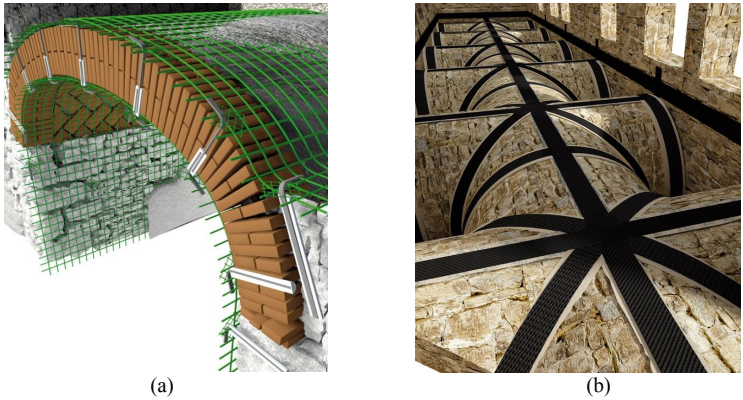

(a) (b)

Fig. 10. Image representations the systems for strengthening of arches and vaults:
(a) FIBREBUILD FRCM ; (b) FIBREBUILD FRP for arches and vaults

4.2. Reinforced concrete structures

The systems for strengthening of reinforced concrete structures by FRP-materials are represented on Fig. 11.

Fig. 11. Image representations the systems for strengthening of reinforced concrete structures by FRP-materials

4.3. Metall structures

The use of steel plates to repair and strengthen existing steel structures has been traditionally used for rehabilitation of steel girders. However, the welded detail of steel plates is sensitive to the fatigue loads.

The effectiveness of using bonded CFRP sheets or plates to improve the fatigue strength has been examined by various researchers [38, 40, 41].

Great contribution to the theory of design with using of FRP-systems was done by lot of scientists. Big contribution and good review was made by Giosuè Boscato [38].

There exists a large number of applications of the FRP-system for strengthening the metal structures for conservation of the architectural and enviromental heritage. Certainly, there are also disadvantages, such as relatively high cost and the need for protection from fire, possible delamination. This problem is studied by a number of scientists.

The study of A. Shaat and A. Fam [40] investigates the experimental behaviour of axially loaded slender steel columns composed of square Hollow Structural Section (HSS), and strengthened using high modulus-carbon fibre-reinforced polymer (HMCFRP) plates. As the slenderness ratio increases, the

HM-CFRP failure mode changes from debonding to crushing at the inner surface of the buckled column (Fig. 12, Fig. 13).

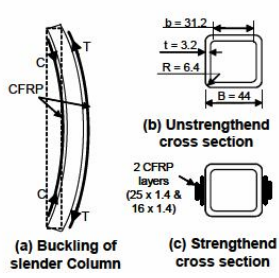

Fig. 12. Buckling and cross sectional configurations

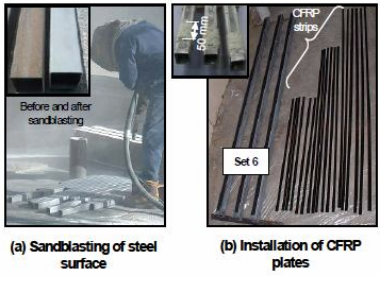

Fig. 13. Preparation of test speciments

Exploration performed during the rehabilitation of steel bridges [26] using advanced composite materials have represented many advantages of using FRP-materials for feasible and cost-effective solutions for an increasing number of deficient bridges (Fig. 14).

Load tests performed prior to and after the rehabilitation indicate a reduction in tension flange strains of 11%. The research demonstrated that this rehabilitation approach is a feasible and potentially cost-effective repair solution for deteriorated steel bridges.

Delamination of a strengthened element can take place in the reinforcement, in the reinforcement, in the substrate or at the interface. In a strengthened element with a metallic substrate, the possible delamination failure modes are listed below, as shown in Fig. 15:

a) Delamination at the substrate – adhesive or adhesive-FRP interface;

b) Cohesive failure of the adhesive;

c) Delamination in the strengthening material.

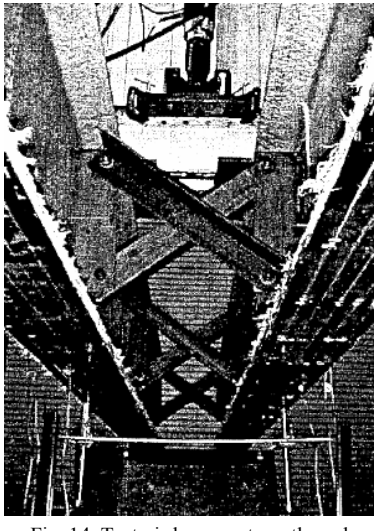

Fig. 14. Test girders are strengthened by CFRP plates

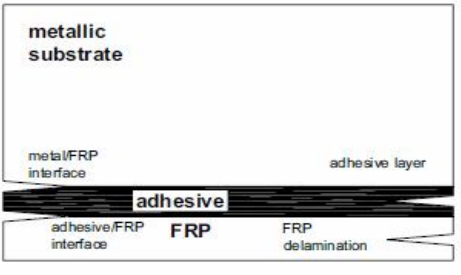

Fig. 15. Types of debonding in FRP strengthened metallic structures

5. Computation of the strengthening using FRP-system

For the calculated limit state to take the condition of achieve of the limit values of the coupling of adhesive with the reinforcing structure. Moreover, must be taken into account factors of reliability depending the used type of composite material and technology of its application.

For example, in Italy, **the main existing documents in the field of strengthening of structures by composite materials including recommendations of computation and design are:**

• Eurocode 8 - Design of structures for earthquake resistance Part 3: Assessment and retrofitting of buildings. EN 1998-3:2004. European Committee for Standardisation (November 2004) [1].

• FIB bulletin 14. Externally bonded FRP reinforcement for RC structures. July 2001 [2].

• Externally bonded FRP reinforcement for RC structures. Technical report on the Design and use of externally bonded fibre reinforced polymer reinforcement (FRP) for reinforced concrete structures. The International Federation for Structural Concrete. CEB-FIP, July, 2001 [4].

• ACI 440.2R-08. Guide for the Design and Construction of Externally Bonded FRP Systems for Strengthening Concrete Structures. ACI Committee 440, technical committee document, 2008 [5].

• CNR-DT 200/2004 Guide for the Design and Construction of Externally Bonded FRP Systems for Strengthening Existing Structures. Materials, RC and PC structures, masonry structures. ROME –CNR, 2004. 154 p. [7].

• CNR-DT 203/2006 «Guide for the Design and Construction of Concrete Structures Reinforced with Fiber-Reinforces Polymer Bars». ROME – CNR, 2007. 39 p. [8]

• CNR-DT 202/2005 «Guidelines for the Design and Construction of Externally Bonded FRP Systems for Strengthening Existing Structures». Metallic structures. Preliminary study. ROME –CNR, 2007. 57 p. [9]

CNR-DT 201/2005 «Guidelines for the Design and Construction of Externally Bonded FRP Systems for Strengthening Existing Structures». Timber structures. Preliminary study. ROME –CNR, 2007. 58 p. [10]

5.1. Design of strengthening of reinforced concrete structures by FRP-materials (Fig. 16) according with ACI (American Concrete Institute) Committee [5]:

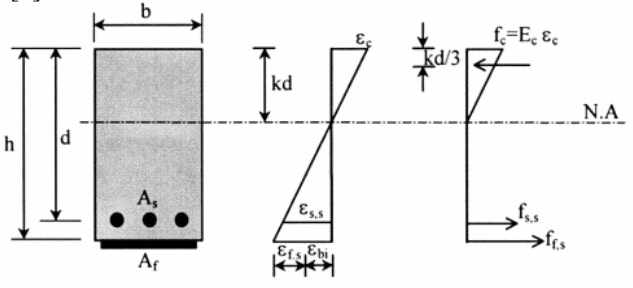

Fig. 16. Elastic strain and stress distribution

The effective stress level in the FRP reinforcement can be found from the strain level in the FRP, assuming perfectly elastic behavior $f_{fe}=E_f\cdot\varepsilon_{fe}$.

The nominal flexural strength of the section with FRP external reinforcement can be computed from

$$M_n=A_s f_s\left(d-(\beta_1 c)/2\right)+\psi_f A_f f_{fe}\left(h-(\beta_1 c)/2\right).$$

An additional reduction factor ψ_f is applied to the flexural strength contribution of the FRP reinforcement. A factor $\psi_f=0.85$ is recommended.

With the strain and stress level in the FRP and steel reinforcement determined for the assumed neutral axis depth, internal force equilibrium may be checked using

$$c=\frac{A_s f_s+A_f f_{fe}}{\gamma f_c^{'}\beta_1 b}.$$

The terms β_1 and γ - parameters defining a rectangular stress block in the concrete equivalent to the actual nonlinear distribution of stress. If concrete crushing is the controlling mode of failure (before or after steel yielding), β_1 and γ can be taken as the values associated with the Whitney stress block ($\gamma=$ 0.85 and $\beta_1=0.97-0.0025 f_c^{'}>0.67$ from Section 10.2.7.3 of ACI 318-99).

5.2. Design of strengthening of reinforced concrete structures by composite materials according with proposition from Täljsten (2006) [18]:

- the design for bending is similar for all elements the frame is performed considering the approach found in

$$A_{frp}=\frac{M/0{,}9-A_{st}f_{st}}{\varepsilon_{frp}\cdot E_{frp}},$$

where the steel area A_{st} and the yield strength of the steel, f_{st}, should not be accounted if no steel is present in the section.

- the shear contribution attributed to the strengthening material is determined as

$$t_{frp}=\frac{V_d}{0.6\cdot\varepsilon_{frp}\cdot E_{frp}\cdot b_{frp}}.$$

Guidelines for the **strengthening of tensile elements of metal structures by FRP-materials** (Fig. 17) are represented in [9].

The strengthening can be applied for the restoring of the load bearing capacity of corroded elements, as well as for the upgrading of the failure load undamaged elements.

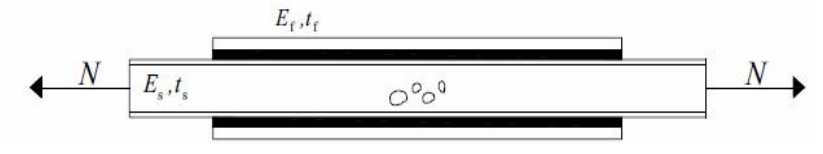

Fig. 17. Tensile element with partially corroded cross section and symmetric reinforcement.

On the conservative side, restoring of the load bearing capacity of damaged elements, not subjected to fatigue, is performed assuming that the stresses across the damaged section are bridged by the FRP materials. The Strengthening must be designed such that:

$$2A_{frp}\cdot\frac{f_{fk}}{\gamma_f}\cdot\eta\geq A_s\cdot f_{sk,\sup},$$

where: A_{frp} is the cross section area of the FRP; f_{fk} Is the lower characteristic of the composite tensile strength; γ_f is the partial factor of the reinforcement material; η Is the conversion factor; A_s Is the cross section area of the metallic substrate; $f_{sk,\sup}$ is the upper characteristic value of yielding stress (f_y) for ductile material, or failure stress (f_u) for brittle material.

Strengthening of flexural elements of metal structures by FRP-materials (Fig. 18) [9].

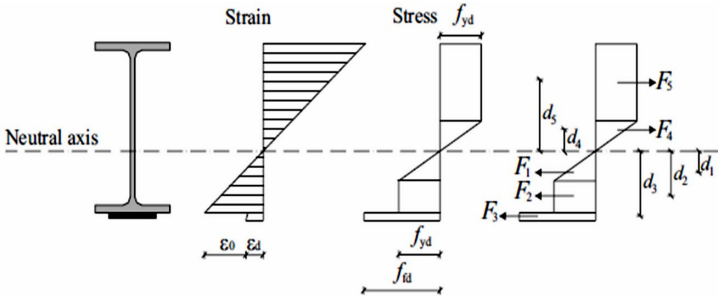

Fig. 18. Procedure for computing the flexural capacity

The ultimate limit state is checked by verifying the following Equation:

$$M_{Sd}\leq M_{Rd},$$

where M_{Sd} is the bending moment produced by the design load combination, $M_{Rd}=\sum F_i\cdot d_i$ is the design value of the flexural capacity.

The last 15 years in particular, the advent of powerful computers and the development of sophisticated nonlinear CAD software (Finite Element Analysis (FEA) Software Stand, SolidWorks, DIANA, MATLAB (finite element method FEM and discrete element method DEM), ADINA [14], ABAQUS [15], Autodesk REVIT Structure, Autodesk ROBOT Structural Analysis, ANSYS, TEKLA Structures, SCAD, LIRA and others) have enabled engineers to utilize complicated large scale structures, some of which can be classified among unique examples of engineering excellence.

6. Aanalytical modeling in ABACUS/CAE

Modeling Procedure of the steel beam. Computations of steel beam are performed in software ABAQUS.

The modeling, meshing, boundary condition and loading conditions are shown in Fig. 19.

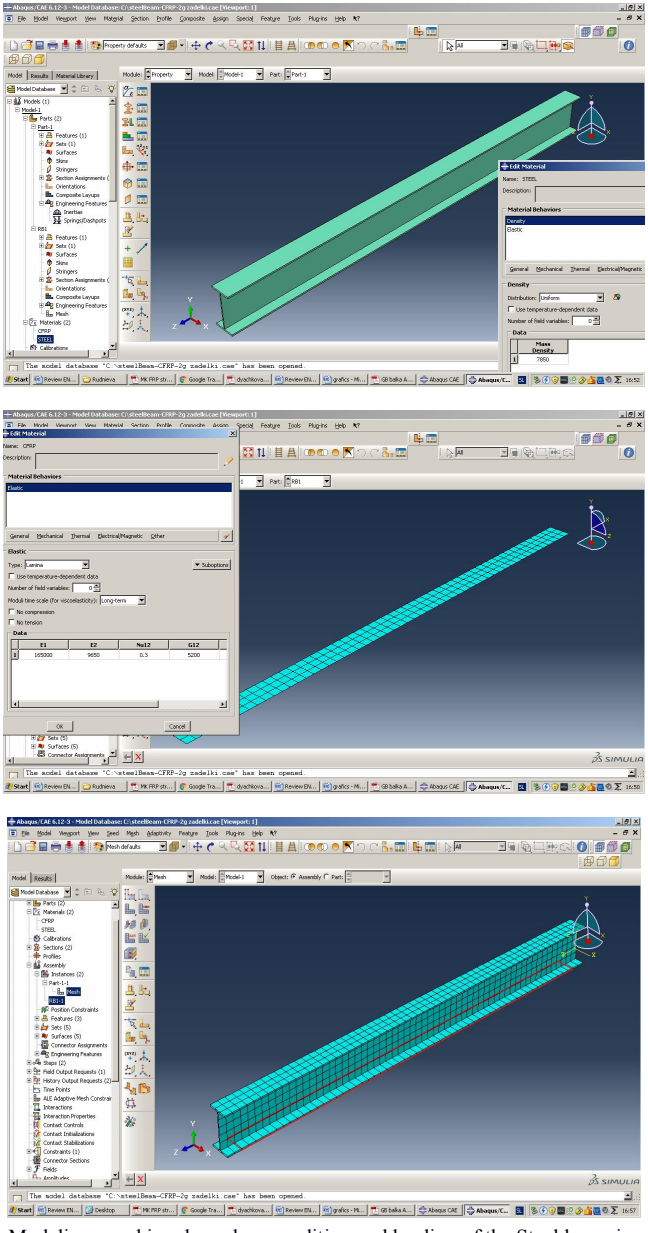

Fig. 19. Modeling, meshing, boundary condition and loading of the Steel beam in software ABAQUS (Q=15000N/m^2)

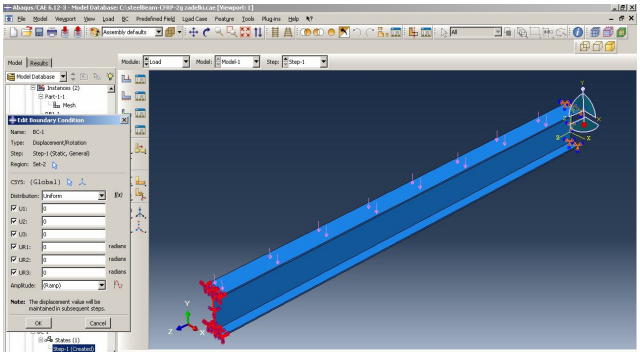

Fig. 19 (continuation). Modeling, meshing, boundary condition and loading of the Steel beam in software ABAQUS (Q=15000N/m^2)

Results of computation of the Reinforced concrete beam in software ABAQUS are represented in Fig 20.

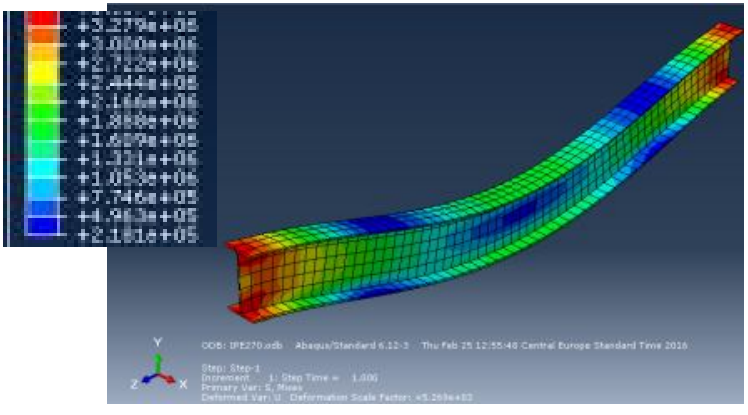

a)

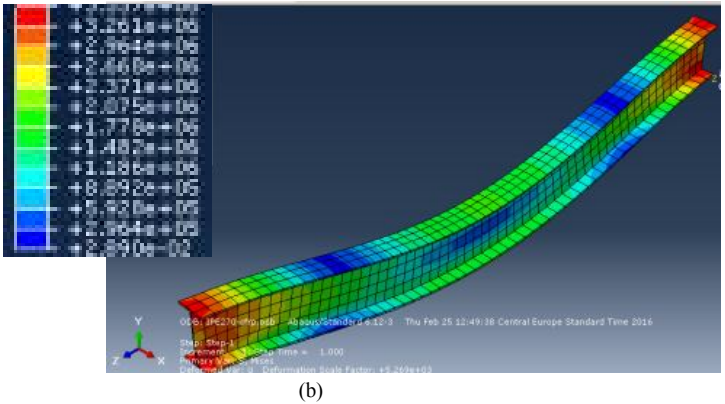

(b)

Fig. 20. Results of computation Steel beam in software ABAQUS:
(a) before strengthening by CFRP; (b) after strengthening by CFRP

Modeling of the reinforced concrete beam. Computations of reinforced concrete beam are performed in software ABAQUS.

The modeling, meshing, boundary condition and loading conditions are shown in Fig 21.

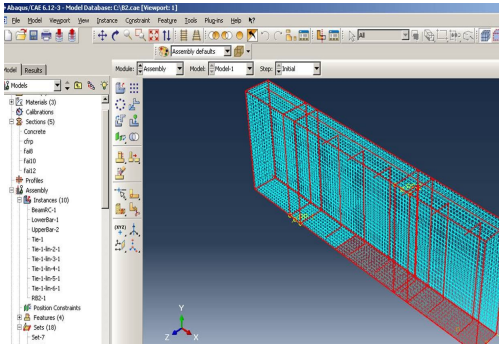

Accepted materials characteristics:

• Concrete: $f'c = 30Mpa$.

• Steel: Elastic-perfectly plastic stress-strain behavior $f_y = 507Mpa,$, $E_s = 209Gpa$ Poisson Ratio = 0.3.

• CFRP: Linear-Elastic orthotropic $E_{11} = 165Mpa, E_{22} = 9.65Gpa,$ $\mu_{12} = 0.3, G_{12} = 5.2Gpa,$ $G_{13,} = 5.2Gpa, G_{23} = 3.4Gpa.$

Thickness of CFRP sheets 1 mm.

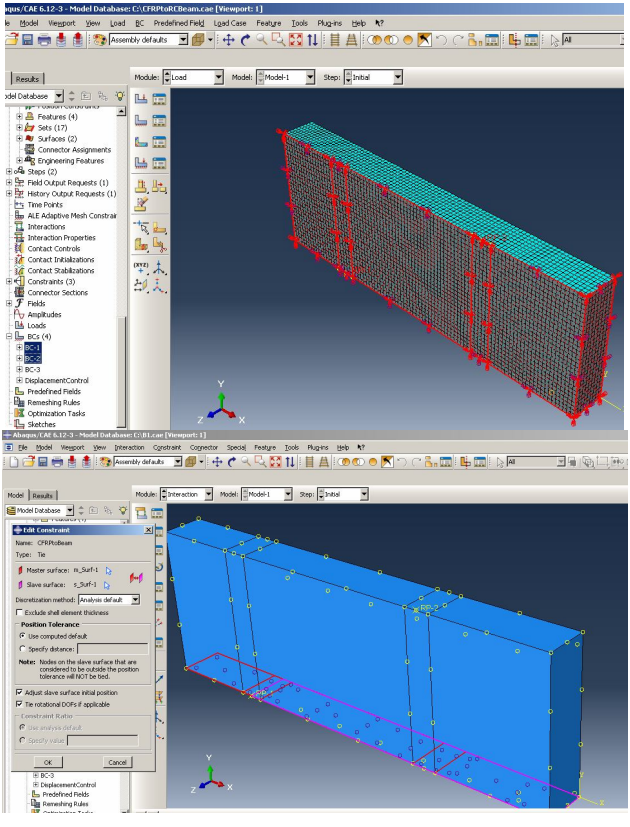

Fig. 21. Modeling, meshing, boundary condition and loading of the reinforced concrete beam in software ABAQUS (P=12MN)

Results of computation of the Reinforced concrete beam in software ABAQUS are represented in Fig. 22.

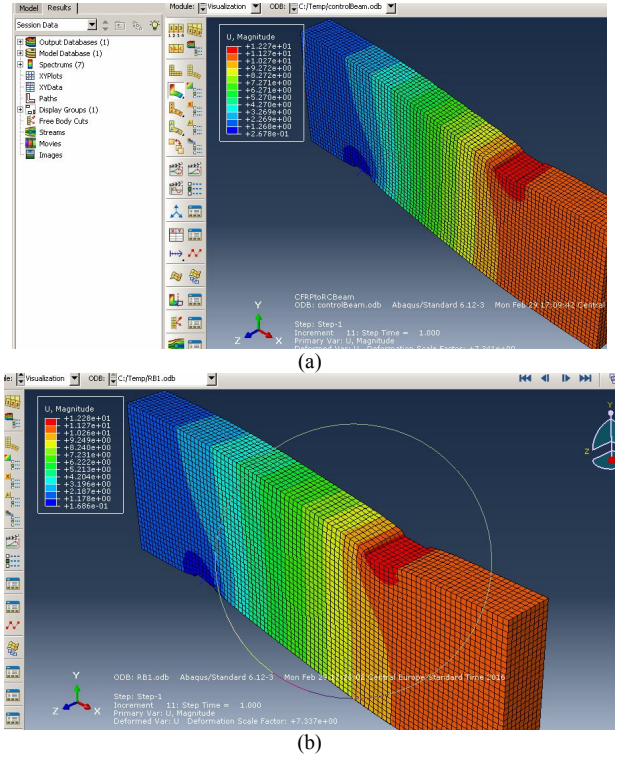

Fig. 22. Results of computation of the Reinforced concrete beam in software ABAQUS: (a) before strengthening by CFRP; (b) after strengthening by CFRP

7. CONCLUSIONS:

- This note has attempted a review of the latest issues and developments in the strengthening of building and structures, while also touching upon the historical perspective and including some information of general nature.
- The treatment is of necessity short in order to compress many issues into limited space. The paper has particularly addressed the latest trends and issues of concepts in strengthening of structures using composite materials.
- In the article it was considered variants of strengthening steel beam and reinforced concrete beam by composite materials. Computations are performed in software ABAQUS.
- CFRP strengthened steel and reinforced concrete beams resulted in reduce strain in the element and consequently to the possibility to insrease load carrying capacity.

- For example, in a metal beam after the inclusion CFRP in operation the percentage decrease of the vertical deflection was 5,6 %. The value of tensile stresses reduced by about 4,1 %.
- In a reinforced concrete beam the percentage decrease of the vertical deflection was 3,2 % for beams strengthened with CFRP laminates. The value of tensile stresses reduced by about 2,8 %.
- The beams strengthened with CFRP laminates show enhanced ductility.
- The main principle of placement of composite laminates, grids, rods consists in a parallel arrangement to tensile stresses.
- Despite the large amount of information about FRP-materials issues of reliability of alternative metods for strengthening building structures by FRP-materials have yet to be properly defined.
- In addition, durability requirements, adaptability to manufacture, economic efficiency, ecological and social factors should be fulfilled in total volume.

REFERENCES

[1] Eurocode 8 - Design of structures for earthquake resistance Part 3: Assessment and retrofitting of buildings. EN 1998-3:2004. European Committee for Standardisation (November 2004)
[2] FIB bulletin 14. Externally bonded FRP reinforcement for RC structures. July 2001.
[3] M.V. Priadko, I.M. Rudnieva, Yu.M. Priadko. Obstezhennia ta pidsylennia budivelnykh konstruktsii promyslovykh budivel: Navchalnyi posibnyk. – Kyiv: KNUBA, 2018. – 332 s.
[4] Externally bonded FRP reinforcement for RC structures. Technical report on the Design and use of externally bonded fibre reinforced polymer reinforcement (FRP) for reinforced concrete structures. The International Federation for Structural Concrete. CEB-FIP, July, 2001.
[5] ACI 440.2R-08. Guide for the Design and Construction of Externally Bonded FRP Systems for Strengthening of Concrete Structures. Michigan: American Concrete Institute, ACI Committee 440: 2008, 76 p.
[6] Design Manual «Seismic Retrofiting Design and Constraction Guidelines for Existing Reinforced Concrete (RC) Buildings with FRP Materials». Japan Building Disaster Prevention Association (JBDPA). Tokyo, Japan, (1999), 115 p.
[7] CNR-DT 200/2004 «Guide for the Design and Construction of Externally Bonded FRP Systems for Strengthening Existing Structures». Materials, RC and PC structures, masonry structures. ROME–CNR, 2004. 154p.
[8] CNR-DT 203/2006 «Guide for the Design and Construction of Concrete Structures Reinforced with Fiber-Reinforces Polymer Bars». ROME – CNR, 2007. 39 p.
[9] CNR-DT 202/2005 «Guidelines for the Design and Construction of Externally Bonded FRP Systems for Strengthening Existing Structures». Metallic structures. Preliminary study. ROME – CNR, 2007. 57 p.
[10] CNR-DT 201/2005 «Guidelines for the Design and Construction of Externally Bonded FRP Systems for Strengthening Existing Structures». Timber structures. Preliminary study. ROME – CNR, 2007. 58 p.
[11] Fiorella Facchinetti, Angelo Di Tommaso, Michele Tataseo, Giorgio Giacomin, Marzio Sartorel. La tecnologia FRP applicata agli edifice storici: rinforzo statico e sismico. Il caso di Palazzo Mozzi-Bardini a Firenze. www.aico-compositi.it
[12] Ł. Bednarz, A. Górski, J. Jasieńko, E. Rusiński. Simulations and analyses of arched brick structures. Automat Constr, 20 (7) (2011), pp. 741–754
[13] Łukasz J. Bednarz, Jerzy Jasieńkoa, Marcin Rutkowskib, Tomasz P. Nowaka. Strengthening and long-term monitoring of the structure of an historical church presbytery. Engineering Structures-2014, Volume 81. doi:10.1016/j.engstruct.2014.09.028
[14] ADINA R&D, Inc., ADINA—Theory and Modeling Guide, vol. II: ADINA, June 2012.
[15] ABAQUS, Version 6.11 Documentation, 2011. Dassault Systemes Simulia Corp. Providence,

RI, USA.
[16] Jasienko Jerzy, Dominik Logon, Witold Misztal. Trass-lime reinforced mortars in strengthening and reconstruction of historical masonry walls. Construction and Building Materials 102 (2016) 884–892]
[17]http://fibrebuild.fibrenet.it/en/historic-building/consolidating-masonry/
[18] B. Täljsten, FRP strengthening of existing concrete structures – design guidelines (fourth edition), Luleå, Sweden: Luleå University of Technology; ISBN 91-89580-03-6, (2006)
[19] Concrete Engineering Series 23 «Recommendation For Design And Construction Of Concrete Structures Using Continuous Fiber Reinforcing Materials, Research Committee on Continuous Fiber Reinforcing Materials», Tokyo, 1997. Japan Society of Civil Engineers (JSCE). 325 p.
[20] Naif Adel Haddad. From ground surveying to 3D laser scanner: A review of techniques used for spatial documentation of historic sites. Journal of King Saud University – Engineering Sciences (2011) 23, 109–11. doi:10.1016/j.jksues.2011.03.001]
[21] Terrence F. Paret, Sigmund A. Freeman, Gary R. Searer, Mahmoud Hachem, Una M. Gilmartin. Using traditional and innovative approaches in the seismic evaluation and strengthening of a historic unreinforced masonry synagogue. Engineering Structures 30 (2008) 2114–2126
[22] Al-Saidy, A.H, Klaiber, F.W. and Wipf, T.J. (2004), “Repair of Steel Composite Beams with Carbon Fiber-Reinforced Polymer Plates,” ASCE Journal of Composites for Construction, 8, pp. 163-172.
[23] SP 52-101-2003. Concrete and reinforced concrete constructions without a preliminary reinforcement stress. Moscow, 2004.
[24] I. Rudnieva, Yu. Priadko, M. Priadko, H. Tonkacheiev. Osoblyvosti ta perspektyvy vykorystannia tekhnolohii pidsylennia budivelnykh konstruktsii kompozytsiinymy materialamy pry rekonstruktsii sporud. Zbirnyk naukovykh prats "Budivelni konstruktsii. Teoriia i praktyka". № 7 (2020), c.12-22. DOI: 10.32347/2522-4182.7.2020.12-22
[25] Parkinson G., G. Shaw, J. K. Beck. (2010). Apprasial & repair of masonry. Architecture civil engineering. 2010. Issue 1. Pp. 53-62.
[26] Dennis R. Mertz, John W. Gillespie, Jr., Michael J. Chajes, and Scott A. Sabol. The Rehabilitation of Steel Bridge Girders Using Advanced Gomposite Materials. Final Report for NCHRP-IDEA Project 51. Innovations Explonatony Analysis Elesenving Pnognarns. University of Delaware, 2002.
[27] Hart-Smith, L.J. (2001), “Bolted and Bonded Joints”, in Composites, Vol. 21, ASM Handbook, American Society for Materials (ASM) International, 271-289.
[28] Hollaway L.C., Cadei J. (2002). Progress in the technique of upgrading metallic structures with advanced polymer composites. Prog. Struct. Engng. Mater., 4, 131-148.
[29] Kennedy, G.D. (1998), “Repair of Cracked Steel Elements Using Composite Fibre Patching,” M.S. Thesis, University of Alberta, Canada
[30] Lanier, B.K. (2005), “Study in the Improvement in Strength and Stiffness Capacity of Steel Multi-sided Monopole Towers Utilizing Carbon Fiber Reinforced Polymers as a Retrofitting Mechanism,” M.S. Thesis, North Carolina State University, Raleigh, NC
[31]. Liu, X., Silva, P., Nanni, A. 2001. Rehabilitation of Steel Bridge Members with FRP Composite Material. In Proc., CCC 2001, Composite in Construction, Porto, Portugal, 10-12 October, edited by J. Figueras, L. Juvandes and R. Furia. Eds.
[32]. Matta, F. (2003), “Bond between Steel and CFRP Laminates for Rehabilitation of Metallic Bridges”, Thesis, University of Padova, Padova, Italy, 171 pp.
[33]. Nozaka, K., Shield, C.K. and Hajjar, J.F. (2005), “Effective Bond Length of Carbon-Fiber-Reinforced Polymer Strips Bonded to Fatigued Steel Bridge I-Girders,” ASCE Journal of Composites for Construction, 10[2], pp. 195-205.
[34] Sebastian, W.M. (2003), “Nonlinear Influence of Contraflexure Migration on Near-curtailment Stresses in Hyperstatic FRP-Laminated Steel Members,” Computers and Structures, 81[16], pp. 1619-1632.
[35] Tavakkolizadeh, M., Saadatmanesh, H. 2002. Repair of Steel Bridges with CFRP Plates. In Proc., ACIC 2002, Southampton University, UK, 15-17 April, edited by R. A. Shenoi, S. S. J. Moy, L. C. Hollaway. Thomas Telford.-Tavakkolidazeh, M. and Saadatmanesh, H. (2003), “Strengthening of Steel-Concrete Composite Girders Using Carbon Fiber-Reinforced Polymer Sheets,” ASCE Journal of Structural Engineering, 129, pp. 30-40.

[36] Vatovec, M., Kelley, P.L., Brainerd, M.L. and Kivela, J.B. (2002), “Post Strengthening of Steel Members with CFRP”, Proceedings of the 47th International SAMPE Symposium and Exhibition, Long Beach, CA, May 12-16, 2002, Society for the Advancement of Material and Process Engineering (SAMPE), pp. 941-954.
[37] Ernest Bernat-Maso, Christian Escrig, Chrysl A. Aranda et. al. (2013). Experimental assessment of Textile Reinforced Sprayed Mortar strengthening system for brickwork wallets. Construction and Building materials. Spain, 2013. Pp 3-13.
[38] Giosuè Boscato. NUMERICAL ANALYSIS AND EXPERIMENTAL TESTS ON DYNAMIC BEHAVIOUR OF GFRP PULTRUDED ELEMENTS FOR CONSERVATION OF THE ARCHITECTURAL AND ENVIRONMENTAL HERITAGE. Dissertation, University Iuav of Venice, Venice, Italy, 2009. 215 p.
[39] Sen, R., Liby, L., Mullins, G. 2001. Strengthening Steel Bridge Sections Using CFRP Laminates, Composites: Part B, 32: from 309-322.
[40] A. Shaat and A. Fam. CONTROL OF OVERALL BUCKLING OF HSS SLENDER STEEL COLUMNS USING CFRP PLATES. Asia-Pacific Conference on FRP in Structures (APFIS 2007). International Institute for FRP in Construction.
[41] Amr Shaat, David Schnerch, Amir Fam, and Sami Rizkalla. Retrofit of Steel Structures Using Fiber Reinforced Polymers (FRP). State-of-the-Art, 2003
[42] Guide to the design of concrete and reinforced concrete structures of the heavy concrete without a preliminary reinforcement stress (to SP 52-101-2003). Moscow, 2005.
[43] CNR-DT 200 R1/2013, Guide for the Design and Construction of Externally Bonded FRP Systems for Strengthening Existing Structures, Italian National Research Council (CNR), Rome, 2013, 144 pp.
[44] Руднева И.Н., Прядко Ю.Н. Сравнительный анализ Еврокодов и национальных стандартов Украины, в том числе частных коэффициентов надежности и учета фактора времени, при проектировании конструкций. Науково-виробничий журнал «Промислове будівництво та інженерні споруди», №1, 2020, стр.39-45. http://nbuv.gov.ua/UJRN/Pbis_2020_1_10
[45] Di Tommaso Angelo, Focacci Francesco, Micelli Francesco. Strengthening Historical Masonry with FRP or FRCM: Trends in Design Approach. – Key Engineering Materials, July 2017. DOI: 10.4028/www.scientific.net/KEM.747.166
[46] I. Rudnieva, Yu. Priadko, M. Priadko. Analiz prychyn obvalennia pokrivel vyrobnychykh budivel. Zbirnyk naukovykh prats "Budivelni konstruktsii. Teoriia i praktyka". № 6 (2020), c.85-93. https://doi.org/10.32347/2522-4182.6.2020.85-93
[47] Н. Прядко, Г. Шамрина, Ю. Прядко, И. Руднева. Усиление конструкций фундаментов жилого дома // Журнал «Проблеми розвитку міського середовища». - 2014. - Вип. 2. - С. 14-22.
[48] Strengthening Historical Masonry with FRP or FRCM: Trends in Design Approach. DI TOMMASO Angelo, FOCACCI Francesco and MICELLI Francesco. – *Key Engineering Materials · July 2017* DOI: 10.4028/www.scientific.net/KEM.747.166.
[49] F. Capani, A. D'Ambrisi, M. De Stefano, R. Nudo, F. Focacci, R. Luciano, R. Penna, Experimental investigation on cyclic response of RC elements repaired by CFRP external reinforcing systems, Compos Part B 112 (2017) 290-299.
[50] American Concrete Institute, ACI 440.2R-08 Guide for the Design and Construction of Externally Bonded FRP Systems for Strengthening Concrete Structures, 2008, Farmington Hills, MI, 77 pp.
[51] Golubka Necevska-Cvetanovska1, Roberta Apostolska. Consolidation, rebuilding and strengthening of St. Clement’s church, St. Panteleymon, Plaoshnik, Ohrid. Engineering Structures 30 (2008) 2185–2193
[52] Vincenzo Mallardoa, Roberto Malvezzia, Enrico Milanib, Gabriele Milanib. Seismic vulnerability of historical masonry buildings: A case study in Ferrara. Engineering Structures 30 (2008) 2223–2241
[53] Yusuf Arayici (2010). The use of the 3D laser scanner in the built environment. 89-120. https://www.researchgate.net/publication/291308598_The_use_of_the_3D_laser_scanner_in_the_built_environment.

Стаття надійшла 20.06.2020

Руднєва І.

ПОРІВНЯЛЬНИЙ АНАЛІЗ ПІДСИЛЕННЯ БУДІВЕЛЬНИХ КОНСТРУКЦІЙ (КЛАДКИ, МЕТАЛЕВИХ КОНСТРУКЦІЙ, ЗАЛІЗОБЕТОНУ) З ВИКОРИСТАННЯМ FRP-МАТЕРІАЛІВ І ТРАДИЦІЙНИХ МЕТОДІВ ПРИ РЕКОНСТРУКЦІЇ

Побудовані в основному століття назад, історичні будівлі, а також більш сучасні будівлі минулого століття, які втратили несучу здатність, часто потребують відновлення та підсилення, особливо в сейсмічних районах і в регіонах з явищами просідання грунтів. Необхідність підсилення будівельних конструкцій в процесі експлуатації виникає головним чином через їх передчасного зносу в результаті технологічних й атмосферних впливів, різних пошкоджень та інших факторів.

Традиційні методи підсилення ефективні, але в деяких випадках не підходять або не можуть застосовуватися. Прикладом є збільшення несучих конструкцій історичних будівель, збереження зовнішнього вигляду яких є визначальним фактором. У цьому випадку використання альтернативних методів з використанням FRP-матеріалів може бути виправдане.

Знання причин дефектів і пошкоджень конструкцій дозволяє вибрати оптимальний варіант ремонту або підсилення. Метою дослідження є оцінка структурних характеристик композитних армованих елементів в більш широкому секторі збереження історичної, архітектурної та екологічної спадщини, а також в більш сучасних будівлях минулого століття, які втратили несучу здатність з фокусом на показники надійності і зовнішній вигляд конструкції.

У статті описані і проаналізовані існуючі традиційні методи і альтернативні методи підсилення FRP-матеріалами (композитними матеріалами) таких будівельних конструкцій, як кам'яна або цегляна кладка, металеві конструкції, залізобетон. Також виконано розрахунок в програмному забезпеченні ABAQUS. Ці процедури підсилення будівельних конструкцій за допомогою FRP-матеріалів в Україні широко не використовуються через відсутність нормативної бази, яка б регулювала їх використання, а також тому, що ці матеріали відносно дорогі, в порівнянні з традиційними.

У статті проаналізовані існуючі методи розрахунку і проектування підсилення конструкцій з використанням FRP-матеріалів. Розрахунок в програмному забезпеченні ABAQUS виконаний з висновками і рекомендаціями, заснованими на результатах розрахунку.

Метою роботи було розгляд технології та аналіз переваг і недоліків кожного з методів підсилення, які слід використовувати при виборі ефективних рішень для підсилення будівельних конструкцій. На завершення була підтверджена необхідність подальших досліджень на цю тему.

Ключові слова: методи підсилення, композитні матеріали, FRP-матеріали, кладка, металеві конструкції, залізобетон, напружено-деформований стан, обчислювальні методи, дефекти, пошкодження, реконструкція.

Rudnieva I.

COMPARATIVE ANALYSIS OF STRENGTHENING OF BUILDING STRUCTURES (MASONRY, METAL STRUCTURES, REINFORCED CONCRETE) USING FRP-MATERIALS AND TRADITIONAL METHODS DURING RECONSTRUCTION

Built mostly centuries ago, heritage buildings as well the more contemporary buildings of the last century, which have lost the bearing capacity often need restoration and strengthening, especially in seismic regions and in regions with shrinkage phenomena (subsidence region). The need of strengthening of the building constructions during exploitation appears mostly because of their premature wear as a result of technological influences and weathering, various damage and various other factors.

Traditional methods of strengthening are effective, but in some cases not appropriate or not applicable for use. An example is the increase of the load-bearing structures of historical buildings, preserving the external appearance of which is the determining factor. In this case, the use of the discussed alternative methods can be justified alternative.

Knowledge of the causes of defects and damage of structures allows to choose the best option of repairing or strengthening.

The aim of the research is the evaluation of the structural performance of composite fibre-reinforced elements in the wider sector of the conservation of historical, architectonic and environmental heritage, as well the more contemporary buildings of the last century, which have lost of the bearing capacity focusing reliability indexes and the appearance of the structure.

In the article was described and analyzed the existing traditional methods and the alternative methods of strengthening by FRP-materials (composite materials) such building structures as masonry, metal structures, reinforced concrete, and the computation in software ABAQUS. These procedures of strengthening building structures by FRP-materials in Ukraine are not widely used due to the lack of a regulatory framework that would regulate their use, as well because these materials are relatively expensive compared to the traditional ones.

The article analyzed the existing methods of computation and design of the strengthening using FRP-materials, and the computation in software ABAQUS was performed with conclusions and recommendations based on results of the computation.

The aim of the work was to review the technology and analyze the advantages and disadvantages of each of the strengthen methods that should be used when choosing effective solutions for strengthening building structures. In conclusion, the need for further study and researches was confirmed.

Keywords: methods of strengthening, composite materials, FRP-materials, masonry, metal structures, reinforced concrete, stress-strain state, computational methods, defects, damage, reconstruction.

УДК 624.016
Руднєва І. **Порівняльний аналіз підсилення будівельних конструкцій (кладки, металевих конструкцій, залізобетону) з використанням FRP-матеріалів і традиційних методів при реконструкції** // Опір матеріалів і теорія споруд: наук.-тех. збірн. – К.: КНУБА, 2020. – Вип. 105. – С. 267 – 291.
Табл. 2. Іл. 22. Бібліогр. 53 назв.

UDC 624.016
Rudnieva I. **Comparative analysis of strengthening of building structures (masonry, metal structures, reinforced concrete) using FRP-materials and traditional methods during reconstruction** // Strength of Materials and Theory of Structures: Scientific-and-technical collected articles – Kyiv: KNUBA, 2020. – Issue 105. – P. 267 – 291.
Tabl. 2. Fig. 22. Ref. 53.

УДК 624.016
Руднева І. **Сравнительный анализ усиления строительных конструкций (кладки, металлических конструкций, железобетона) с использованием FRP-материалов и традиционных методов при реконструкции** // Сопротивление материалов и теория сооружений: науч.- тех. сборн. – К.: КНУСА, 2020. – Вып. 105. – С. 267 – 291.
Табл. 2. Ил. 22. Библиогр. 53 назв.

Автор (науковий ступінь, вчене звання, посада)*: кандидат технічних наук, доцент кафедри опору матеріалів КНУБА РУДНЄВА Ірина Миколаївна.*
Адреса: *03680 Україна, м. Київ, Повітрофлотський проспект 31, КНУБА, кафедра опору матеріалів, Руднєва Ірина Миколаївна.*
Робочий тел.: *+38(044) 241-54-21;*
Мобільний тел.: *+38(050) 620-32-31;*
E-mail: *irene_r@ukr.net*
ORCID ID: http://orcid.org/0000-0002-9711-042X

UDC 624.012

BEARING CAPACITY OF STEEL-FIBER-CONCRETE SLABS WITH BIAXIALLY PRESTRESSED REINFORCEMENT

O.D. Zhuravskyi,
Candidate of Science (Engineering)

Kyiv National University of Construction and Architecture,
Kyiv, Povitroflotskyi ave., 31, Kyiv. 03037

DOI: 10.32347/2410-2547.2020.105.292-301

Experimental-theoretical studies of biaxially prestressed steel-fiber-concrete slabs under the action of a uniformly distributed load were performed. A method for calculating steel-fiber-concrete (SFC) slabs based on the deformation method is proposed. This takes into account stress losses in the reinforcement from creep and shrinkage deformations of reinforced concrete. The increase in compressive strength of steel-fiber-concrete under biaxial compression is also taken into account. The results of calculation of experimental samples and their comparison with the results of experimental researches are given.

Keywords: bearing capacity, steel-fiber-concrete, bending moment, curvature, prestressed reinforcement, relative deformations, stresses in reinforcement, stresses in steel-fiber-concrete.

Introduction. Modern construction is impossible without the use of reinforced concrete structures with pre-stressed reinforcement. Fiber reinforcement is used to improve the strength and deformability characteristics of concrete. Among such fibers, steel fiber is the most widely used. It significantly improves the tensile strength of steel-fiber-concrete (SFC). This makes it possible to take into account the operation of the SFC in the stretched cross-sectional area of the bending elements. The current regulations do not provide recommendations for the calculation of the SFC of flat elements that work in two directions. There are no recommendations for the calculation of SFB elements with pre-stressed reinforcement. Research of bearing capacity, crack resistance and deformations of biaxially prestressed SFC plates is practically absent. The aim of the research is to obtain new experimental data of such structures under transverse loading and to develop a method for calculating their bearing capacity.

1. Method of calculating the bearing capacity. To determine the bearing capacity of the plate, we consider a scheme in which the plate is subjected to a uniformly distributed load and pre-compression forces in two directions P_x and P_y (Fig. 1). The characteristics of reinforcement are accepted according to fig. 2.

The calculation of the carrier definition is performed in two directions, cutting strips of width $b_x = S_x$ and $b_y = S_y$. At the first stage, we determine the compressive stress of the SFC, which is transmitted by pre-stressed reinforcement, taking into account the losses from shrinkage and creep of the SFC. The stress-strain state in cross section is shown in fig. 3. When the central compression stresses and strains in cross section are the same height $\sigma_{cf(1)} = \sigma_{cf(2)}$ and $\varepsilon_{cf(1)} = \varepsilon_{cf(2)}$.

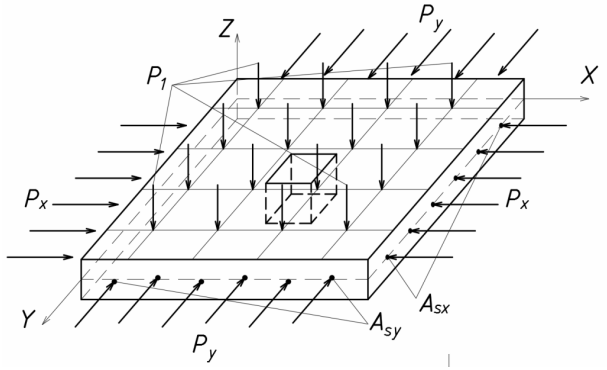

Fig. 1. The loading scheme of the experimental steel-fiber-concrete slab:
P_1 – single vertical load; P_x and P_y - pre-compression forces along the axes, respectively X and Y

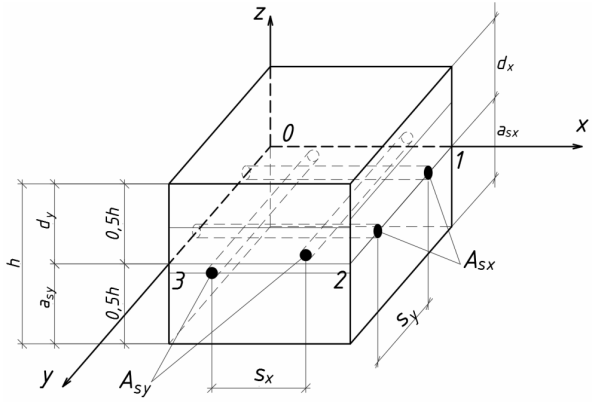

Fig. 2. Characteristics of reinforcement of a single fragment of the plate

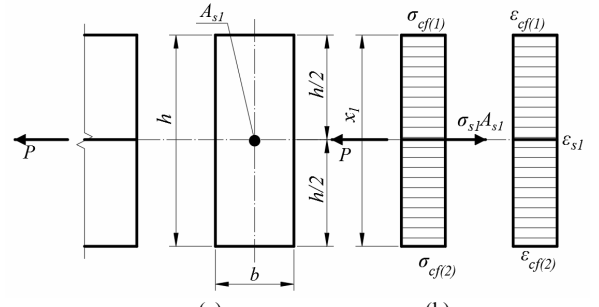

Fig. 3. Stress-strain state of a rectangular steel-fiber-concrete section with pre-stressed reinforcement in the center of the section:
(a) - cross section of the element;
(b) - diagram of stresses and strains during the transfer of forces from reinforcement to concrete

After applying a vertical load, the stress-strain state can be divided into

three stages (Fig. 4).

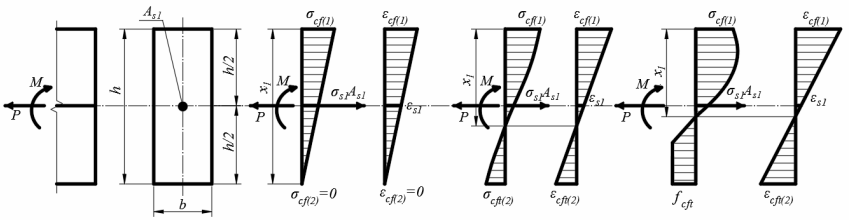

Fig. 4. Stress-strain state of a rectangular steel-fiber-concrete section with pre-stressed reinforcement in the center of the section under the action of bending moment: (a) - cross section of the element; (b) - diagram of stresses and strains under the action of bending moment and compressive force at stage I; (c) - plot of stresses and strains under the action of bending moment and compressive force at stage II (stage of crack formation); (d) - diagram of stresses and strains under the action of bending moment and compressive force at stage III (stage of destruction)

At the first stage at insignificant loading compressive stresses and deformations in the top zone of section increase, and in the bottom zone of section decrease and reach values $\sigma_{cf(2)} = 0$ and $\varepsilon_{cf(2)} = 0$ (Fig. 4b). At the same time tensile stresses in the reinforcing rod σ_{s1} will decrease

In the second stage, with a further increase in load, the compressive stresses and strains in the upper section of the section increase, and in the lower section of the section there is tension and stresses and strains change sign $-\sigma_{cf(2)} = \sigma_{cft(2)}$ and $-\varepsilon_{cf(2)} = \varepsilon_{cft(2)}$ (Fig. 4c). The tensile stresses in the reinforcing rod σ_{s1} are further reduced. At this stage, normal cracks occur and it is taken to calculate the crack resistance and crack width.

In the third stage, with a further increase in load, the compressive stresses and strains in the upper cross-sectional area reach the limit values ($\sigma_{cf(1)} = f_{cf}$ and $\varepsilon_{cf(1)} = \varepsilon_{cfu}$), and in the lower cross-sectional area, the tensile and strain stresses reach the limit values ($\sigma_{cft(1)} = f_{cft}$ and $\varepsilon_{cf(2)} = \varepsilon_{cftu}$) (Fig. 4d). The tensile stresses in the reinforcing rod σ_{s1} are further reduced. This stage is used to calculate the bearing capacity.

The value of the ultimate bending moment in the direction of one axis i=(x or y) for fiber-reinforced bending elements of rectangular cross-section with pre-stressed reinforcement is recommended to be determined by the formulas:

$$\frac{b_i f_{cf} k_{ci}}{\overline{\aleph}_i} \sum_{k=1}^{5} \frac{a_k}{k+1} \gamma^{k+1} - \frac{3}{4} b_i f_{cft} \left(h - x_{1,i}\right) + \sigma_{si} A_{si} = 0, \quad (1)$$

$$\frac{b_i f_{cf} k_{ci}}{\overline{\aleph}_i^2} \sum_{k=1}^{5} \frac{a_k}{k+2} \gamma^{k+2} - \frac{1}{6} b_i f_{cft} \left(h - x_{1i}\right)^2 + \sigma_{si} A_{si} \left(x_1 - z_{si}\right) - M_i = 0. \quad (2)$$

In formulas (4.7), (4.8) according to [7]:

$\gamma = \frac{\varepsilon_{cf(1)}}{\varepsilon_{cf1}}$; $\varepsilon_{cf(1)}$ - relative deformations of the SFC in the compressed cross-sectional area; $\varepsilon_{cf(2)}$ - relative deformations of the SFC in the stretched cross-sectional area; $\aleph_i = \left(\frac{1}{r}\right)_i = \frac{(\varepsilon_{c(1)} - \varepsilon_{c(2)})_i}{h}$ - the curvature of the curved axis in cross section; $x_{1i} = \frac{\varepsilon_{cf(1)}}{\aleph_i}$ - height of the compressed zone (m); $\overline{\aleph}_i = \frac{\aleph_i}{\varepsilon_{cf1}}$ - relative curvature; $\sigma_{spi} = E_{spi}\left(\aleph_i(x_{1i} - z_{si}) - \varepsilon_{p0i}\right)$ - stresses in reinforcing rod; ε_{p0i} - relative deformations from the prestress of the reinforcing rod, taking into account all losses; k_{ci} - coefficient that takes into account the increase in the strength of the SFC under biaxial compression and is determined by DBN [1].

The calculation of the ultimate bending moment is performed in the following sequence:

1. In the first step, we determine the relative deformations $\varepsilon_{cf(1)}$ in the most compressed face, taking $\varepsilon_{cf(2)} = 0$ (Fig. 4b). To do this, determine the values γ, $\aleph_i$, x_{1i}, $\overline{\aleph}_i$, σ_{spi} and, substituting them in equation (1), select the value $\varepsilon_{cf(1)}$ so that equation (1) is equal to 0. Next, we substitute the obtained values into equation (2) and determine the value of the moment *M*.

2. In the second step, increase the value $\varepsilon_{cf(1)}$ by $0{,}1\varepsilon_{cf(1)}$ and select the value $\varepsilon_{cf(2)}$ so that equation (1) is equal to 0 (Fig. 4c). Next, we substitute the obtained values into equation (2) and determine the value of the moment *M*. The value of the moment *M* and $\aleph_i$ plot on the graph «moment-curvature».

3. The following steps are performed by analogy with the second, gradually increasing the value $\varepsilon_{cf(1)}$ by $0{,}1\varepsilon_{cf(1)}$. The calculations are performed step by step until the value of the moment in the last step is less than in the previous step or the values of the relative deformations in the stretched zone reach the limit values.

2. Strength and deformability characteristics of SFC. The prototypes were made of SFC with a concrete matrix of the same composition. Portland cement of the M400 brand was used. Quartz sand in the ratio *C/P* = 1/3 was used as a fine aggregate. The water-cement ratio was *W/C* = 0.62.

Samples of the first series were reinforced with a mixture of steel fibers of STAFIB 50/1.0 and STAFIB 30/0.6 with anchors at the ends, the percentage of which was 0.5% by volume of each fiber. The samples of the second series contained 1.0% by volume of NOVOKON URW 50/1.0 corrugated fibers. Technical characteristics used in the study of steel fibers are given in table 1.

Determination of strength and deformation characteristics of SFC was

carried out on prisms 75x75x300 mm, 100x100x400 mm and cubes with a rib size of 75 and 100 mm at the age of 28 days. The tensile strength of the SFC was determined when testing samples of "eights" with a cross section of 40x40 mm in a rupture machine. As a result of tests, the compressive strength of SFC is $f_{cfk,prism}$=13.5 MPa (series I) and $f_{cfk,prism}$=10.3 MPa (series II). The tensile strength of SFC is f_{cftk}=1.48 MPa (series I) and f_{cftk}=1.22 MPa (series II). The initial modulus of elasticity of SFC is E_{cf}=37158 MPa (series I) and E_{cf}=18094 MPa (series II).

Table 1

Technical characteristics of steel fiber

Brand of fiber	Sketch	Diameter d_f, mm	Length l_f, mm	f_f,, MPa	l_f/d_f
STAFIB 30/0.6	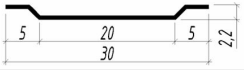	0,6	30,0	1100	50
STAFIB 50/1.0	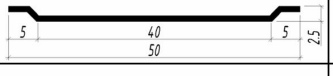	1,0	50,0	1000	50
Novocon URW 50/1.0	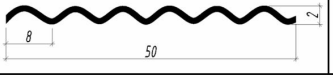	1,0	50,0	1000	50

To construct theoretical diagrams "σ-ε" during compression of SFC prisms, the dependence on DBN was used [1]:

$$\sigma_{cf} = f_{cf} \sum_{k=1}^{5} a_k \eta^k , \qquad (3)$$

where $\eta = \varepsilon_{cf} / \varepsilon_{cf1}$; ε_{cf1} - relative deformations of SFC at maximum stresses; a_k - polynomial coefficients, which are determined depending on the experimental value of the prism strength of the SFC according to the method [7] (see Table 2).

Table 2

Polynomial coefficients for SFC undercompression

	a_1	a_2	a_3	a_4	a_5
Series I	2,94069	-3,2747	1,7844	-0,50755	0,05713
Series II	3,17450	-3,8567	2,2594	-0,64700	0,06970

Diagrams of "σ-ε" at uniaxial compression of SFC prisms of the I and II series are given in fig. 5.

The relative compressive strains of the SFB were ε_{cf1}=1,78×10^{-3} (series I) and ε_{cf1}=1,6×10^{-3} (series II); ε_{cfu}=2,74×10^{-3} (series I) and ε_{cfu} =2,56×10^{-3} (series II). The relative tensile strains of the SFB were ε_{cft1}=2,1×10^{-4} (series I) and ε_{cft1}=1,8×10^{-4} (series II).

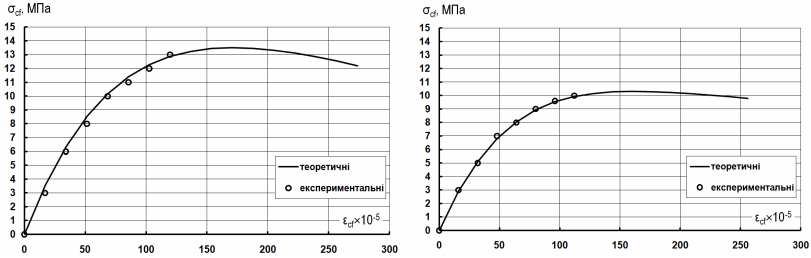

Fig. 5. Diagrams "σ-ε" at uniaxial compression of SFC prisms of the I series (a) and II series (b)

3. Experimental studies. Experimental studies were performed on plates measuring 40x800x800 mm with prestressed reinforcement Ø5Bp-II in two directions. The compression levels of the test plates are given in table 3. Made two series of plates with different levels of prestress.

Table 3

Compression levels of experimental plates

Series number	Sample name	Number of samples	Compression level along the axis				The number of reinforcing bars along the axis	
			planned		actual			
			X	Y	X	Y	X	Y
I	I–ПП–0.7/0.0	2	0.7	0.0	0.66	0	9	9
	I–ПП–0.7/0.3	2	0.7	0.3	0.66	0.29	9	6
	I–ПП–0.7/0.7	2	0.7	0.7	0.66	0.66	9	9
	I–ПП–У	2	-	-	-	-	9	9
II	II–ПП–0.7/0.0	2	0.7	0.0	0.63	0.0	9	9
	II–ПП–0.7/0.3	2	0.7	0.3	0.63	0.28	9	6
	II–ПП–0.7/0.7	2	0.7	0.7	0.63	0.63	9	9
	II–ПП–У	2	-	-	-	-	9	9

The characteristics of SFB I and II series are given in item 2. Mechanical characteristics of reinforcing steel are as follows: strength limit σ_u=1811 MPa, conditional yield strength $\sigma_{0,2}$= 1400 MPa, modulus of elasticity E_s=2,0x10^5 MPa.

The plates were loaded by 16 concentrated forces P_1 evenly over the entire area of the plate with a step of 180 mm by means of hydraulic jacks through a system of traverses with hinged units. This simulated a uniformly distributed load q (Fig. 6). The slabs were hinged on four sides. The flight along the X and Y axes was 700 mm. During the test, the deformations of the SFB on the lower and upper surfaces of the plates were measured using strain gauges. The deflections of the plates in the center of the plate and the deformation of the supports were also measured using clock-type indicators with a division price of 0.01 mm. The magnitude of the load was recorded on the manometer of the pumping station, to which the hydraulic jacks were connected.

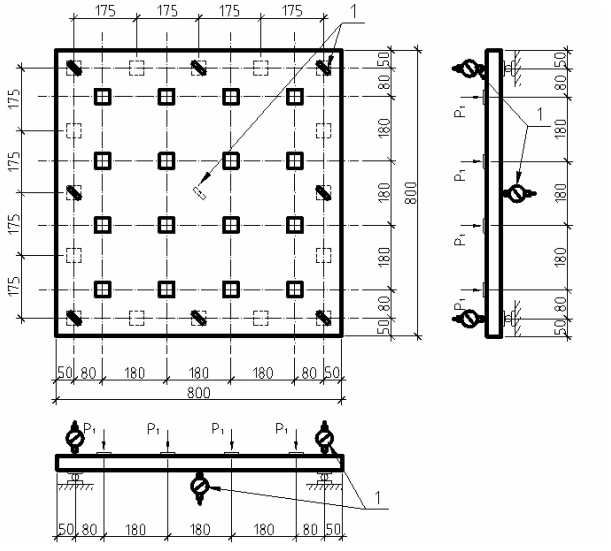

Fig. 6. The scheme of plates loading: 1 - indicators

4. Comparative analysis of experimental and theoretical studies. As a result of the tests, crack-loading loads and loads at which the plates collapsed were obtained (Table 4).

Table 4

Experimental values of loads in the formation of cracks and in the destruction of experimental plates

Sample name	Load in the formation of cracks q_{crc}, kN/m²		The load of destruction q_u, kN/m²		The moment of destruction, M_u, kNm	
	one plate	average value	one plate	average value	experi-mental	theore-tical
I–III–0.7/0.0-1	12,55	13,28	35,20	35,88	0,198	0,188
I–III–0.7/0.0-2	14,01		36,56			
I–III–0.7/0.3-1	20,86	21,20	44,00	44,46	0,245	0,251
I–III–0.7/0.3-2	21,54		44,92			
I–III–0.7/0.7-1	22,19	22,76	51,50	51,89	0,286	0,283
I–III–0.7/0.7-2	23,33		53,10			
I–III–У-1	10,70	11,04	34,14	34,45	0,190	0,186
I–III–У-2	11,38		34,76			
II–III–0.7/0.0-1	12,53	12,59	33,05	33,85	0,187	0,184
II–III–0.7/0.0-2	12,65		34,66			
II–III–0.7/0.3-1	18,77	18,90	42,29	42,63	0,235	0,233
II–III–0.7/0.3-2	19,04		42,97			
II–III–0.7/0.7-1	22,76	21,80	49,19	48,42	0,267	0,262
II–III–0.7/0.7-2	20,83		47,26			
II–III–У-1	9,45	9,79	29,14	30,29	0,167	0,163
II–III–У-2	10,13		31,43			

The following conclusions can be drawn when analyzing the experimental and theoretical values of the maximum limits. The difference in experimental and theoretical values was 1,1…2,5%. The bearing capacity of ПП-0.7/0.7 slabs was higher than ПП-0.7/0.3 slabs by 12,4…12,7%, from ПП-0.7/0.0 slabs by 42,4… 55,5%. The bearing capacity of ПП–У unstressed slabs was 1.55… 1.61 times lower than ПП–0.7/0.7 slabs, 1,35…1,43 times lower than ПП–0.7/0.3 slabs and 1,01…1,13 times from ПП-0.7/0.0 plates.

Conclusion. The proposed method of calculating the bearing capacity of SFC plates takes into account the real diagram "σ-ε" uniaxial and biaxial compression of reinforced concrete. The effect of lateral compression on the compressive strength of the SFC is also taken into account. The influence of biaxial pre-compression of SFC on the bearing capacity of slabs with pre-stressed reinforcement has been experimentally and theoretically confirmed.

REFERENCES

1. DBN V.2.6-98:2009. Konstruktsii budynkiv i sporud. Betonni ta zalizobetonni konstruktsii. Osnovni polozhennia. (DBN B.2.6-98: 2009. Constructions of houses and buildings. Concrete and reinforced concrete structures. Substantive provisions) – K.: Minrehionbud Ukrainy, 2009. -71 s.
2. DSTU B V.2.6.-156:2010. Konstruktsii budynkiv i sporud. Betonni ta zalizobetonni konstruktsii z vazhkoho betonu. Pravyla proektuvannia. (DSTU B B.2.6.-156: 2010. Constructions of houses and buildings. Concrete and reinforced concrete structures made of heavy concrete. Design rules) –K.: Minrehionbud Ukrainy, 2011. -118 s.
3. DSTU-N EN 1992-1-1:2010. Budivelni materialy i konstruktsii. Proektuvannia zalizobetonnykh konstruktsii. Osnovni polozhennia. Zahalni pravyla proektuvannia (EN 1992-1-1:2004, IDT). (DSTU-N EN 1992-1-1: 2010. Building materials and structures. Design of reinforced concrete structures. Substantive provisions. General design rules (EN 1992-1-1:2004, IDT)) – Kyiv: Minrehionbud Ukrainy, 2010. – S.341.
4. DSTU-N B V.2.6-218:2016. Nastanova z proektuvannia ta vyhotovlennia konstruktsii z dyspernoarmovanoho betonu. (DSTU-N B B.2.6-218: 2016. Guidelines for the design and manufacture of structures of dispersed reinforced concrete) – Kyiv: DP «UkrNDNTs», 2017. –S. 32.
5. *Horobets A.M.* Doslidzhennia vtrat poperednoho napruzhennia v stalefibrobetonnykh plytakh pry odnoosnomu ta dvokhosnomu obtysku (Investigation of prestress losses in SFC plates with uniaxial and biaxial compression) / Horobets A.M., Zhuravskyi O.D. // Resursoekonomni materialy, konstruktsii, budivli ta sporudy: Zbirnyk naukovykh prats. Vyp. 16, chastyna 2. - Rivne, 2008, S. 123-128.
6. *Horobets A.M.* Mitsnist ta trishchynostiikist dvokhosno poperedno-napruzhenykh stalefibrobetonnykh plyt pry poperechnomu zghyni (Strength and crack resistance of biaxially prestressed SFC plates at transverse bending) / Horobets A.M., Zhuravskyi O.D. // Budivelni konstruktsii. Teoriia i praktyka: Zbirnyk naukovykh prats. –K., KNUBA, -Vyp. 1., 2017, S. 181-186.
7. Proektuvannia zalizobetonnyz konstruktsii. Posibnyk (Design of reinforced concrete structures. Manual) / A.M.Bambura, HR.Sazonova, O.V. Dorohova, O.V.Voitsekhivskyi / Za red. A.M. Bambura. Kyiv: Maister knyh, 2018. 240 s.
8. EN 1992-1-1. Eurocode 2: Design of Concrete Structures. Part 1-1: General Rules and Rules for Buildings. [Final Draft, December, 2004]. Brussels: CEN. 2004. 225 p.
9. *Zhuravskyi O.* Experimental and theoretical studies of biaxially prestressed steel-fiber-concrete slabs / O.Zhuravskyi, A.Gorobetc // USEFUL online journal, vol. 2, no. 3, pp. 10–14, Oct. 2018. DOI: https://doi.org/10.32557/useful-2-3-2018-0003.

Стаття надійшла 25.11.2020

Журавський О.Д.

НЕСУЧА ЗДАТНІСТЬ СТАЛЕФІБРОБЕТОННИХ ПЛИТ З ДВОХОСНО ПОПЕРЕДНЬО-НАПРУЖЕНОЮ АРМАТУРОЮ

Метою досліджень є отримання нових експериментальних даних таких конструкцій при поперечному навантаженні та розробка методики розрахунку їх несучої здатності.

Виконано експериментально-теоретичні дослідження двохосно попередньо-напружених сталефібробетонних плит при дії рівномірно-розподіленого навантаження. Експериментальні дослідження виконувались на плитах розміром 40х800х800 мм з попередньо напруженою арматурою Ø5Вр-II в двох напрямках. Зразки першої серії армувались сумішшю сталевих фібр марки STAFIB 50/1.0 та STAFIB 30/0.6 із анкерами на кінцях, процентне відношення яких становило по 0,5% по об'єму кожної фібри. Зразки другої серії містили 1,0% за об'ємом хвилястих фібр марки NOVOKON URW 50/1.0.

Запропонована методика розрахунку сталефібробетонних (СФБ) плит на основі деформаційного методу. При цьому враховується реальна діаграми «σ-ε» при одноосному та двохосному стиску сталефібробетону та підвищення міцності сталефібробетону на стиск в умовах двохосного обтиску. Також враховуються втрати напружень в арматурі від деформацій повзучості та усадки сталефібробетону. Наведені результати розрахунку дослідних зразків та порівняння їх з результатами експериментальних досліджень. Вони показали достатню збіжність. Різниця становила 1,1…2,5%. Встановлено, що несуча здатність двохосно попередньо напружених плит вища від ненапружених плит в 1,55…1,61 рази та на 42,4…55,5% від одноосно напружених плит.

Ключові слова: несуча здатність, сталефібробетон, згинальний момент, кривизна, попередньо-напружена арматура, відносні деформації, напруження в арматурі, напруження в сталефібробетоні.

Zhuravskyi O.D.

BEARING CAPACITY OF STEEL-FIBER-CONCRETE SLABS WITH BIAXIALLY PRESTRESSED REINFORCEMENT

The aim of the research is to obtain new experimental data of biaxially prestressed steel-fiber-concrete slabs under transverse loading and to develop a method for calculating their bearing capacity.

Experimental-theoretical studies of biaxially prestressed steel-fiber-concrete slabs under the action of a uniformly distributed load were performed. Experimental studies were performed on plates measuring 40x800x800 mm with prestressed reinforcement Ø5Bp-II in two directions. Samples of the first series were reinforced with a mixture of steel fibers of STAFIB 50/1.0 and STAFIB 30/0.6 with anchors at the ends, the percentage of which was 0.5% by volume of each fiber. The samples of the second series contained 1.0% by volume of NOVOKON URW 50/1.0 corrugated fibers.

A method for calculating steel-fiber-concrete (SFB) slabs based on the deformation method is proposed. This takes into account the real diagram "σ-ε" for uniaxial and biaxial compression of steel-fiber-concrete and increase the compressive strength of steel-fiber-concrete under conditions of biaxial compression. Stress losses in the reinforcement from creep and shrinkage deformations of steel-fiber-concrete are also taken into account. The results of calculation of experimental samples and their comparison with the results of experimental researches are given. They showed sufficient convergence. The difference was 1.1… 2.5%. It is established that the bearing capacity of biaxially prestressed slabs is 1.55… 1.61 times higher than unstressed slabs and 42.4… 55.5% higher than uniaxially stressed slabs.

Keywords: bearing capacity, steel-fiber-concrete, bending moment, curvature, prestressed reinforcement, relative deformations, stresses in reinforcement, stresses in steel-fiber-concrete.

УДК 624.012

Журавський О.Д. **Несуча здатність сталефібробетонних плит з двохосно попередньо-напруженою арматурою //** Опір матеріалів і теорія споруд: наук.-тех. збірн. – К.: КНУБА, 2020. – Вип.105. – С. 292-301. – Англ.

Запропонована методика розрахунку сталефібробетонних плит на основі деформаційного методу. При цьому враховуються втрати напружень в арматурі від деформацій повзучості та усадки сталефібробетону. Також враховується зростання міцності сталефібробетону на стиск в умовах двохосного обтиску. Наведені результати розрахунку дослідних зразків та порівняння їх з результатами експериментальних досліджень.

Табл. 4. Іл. 6. Бібліогр. 9 назв.

UDC 624.012

Zhuravskyi O.D. **Bearing capacity of steel-fiber-concrete slabs with biaxially prestressed reinforcement** // Strength of Materials and Theory of Structures: Scientific-and-technical collected articles. – K.: KNUBA, 2020. – Issue 105. – P. 292-301.

The method of calculation of steel-fiber-concrete slabs on the basis of the deformation method is offered. This takes into account stress losses in the reinforcement from creep and shrinkage deformations of steel-fiber-concrete. The increase in compressive strength of steel-fiber-concrete under biaxial compression conditions is also taken into account. The results of calculation of experimental samples and their comparison with the results of experimental researches are given.

Tabl. 4. Fig. 6. Ref. 9.

Автор (науковий ступінь, вчене звання, посада)*: кандидат технічних наук, доцент, завідувач кафедри залізобетонних та кам'яних конструкцій КНУБА ЖУРАВСЬКИЙ Олександр Дмитрович.*
Адреса: *03037 Україна, м. Київ, Повітрофлотський проспект 31, КНУБА, кафедра залізобетонних та кам'яних конструкцій, Журавський Олександр Дмитрович.*
Робочий тел.: *+38(044) 248-48-42;*
Мобільний тел.: *+38(067) 508-60-64;*
E-mail: *zhuravskyi.od@knuba.edu.ua*
ORCID ID: https://orcid.org/0000-0001-7065-3312

UDC 539.3

MODIFIED METHOD OF LINES IN THE PROBLEMS OF THERMAL CONDUCTIVITY OF ANNULAR PLATES

Yu.V. Sovych

Kyiv National University of Construction and Architecture,
Kyiv, Povitroflotskyi ave., 31, Kyiv. 03037

DOI: 10.32347/2410-2547.2020.105.302-309

The application of the modified method of lines to reduce the dimensionality of the initial system of equations of nonstationary thermal conductivity used to determine the temperature fields of the load-bearing elements is shown in this paper. Reducing the dimensionality of the original equations by one spatial coordinate, in this case by the z coordinate, is performed using the projection method. Local basic functions are used for this purpose. To ensure the unambiguity of the solutions, the reduced equations are supplemented by initial and boundary conditions.

Keywords: thermal conductivity, dimension reduction, projection method, reduced equations, modified method of lines

Ring plates, the overall dimensions of which have the same degree under thermal influences, have spatial temperature fields. If these effects are axisymmetric relative to the vertical axis of the plate, then such fields are also axisymmetric, i.e. two-dimensional in spatial coordinates in a cylindrical coordinate system (Fig. 1). In addition, the temperature field may depend on the time coordinate, i.e. is non-stationary. The initial equation of nonstationary thermal conductivity is considered as the first order system of partial differential equations:

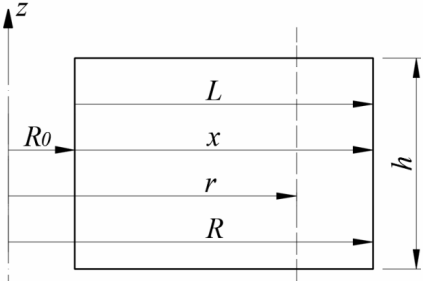

Fig. 1

- Fourier's Law:

$$q_r = -\lambda_T \cdot \frac{\partial T}{\partial x}, \qquad q_z = -\lambda_T \cdot \frac{\partial T}{\partial z}; \tag{1}$$

- heat balance equation:

$$\rho c \frac{\partial T}{\partial t} = -\frac{q_r}{x + R_0} - \frac{\partial q_r}{\partial x} - \frac{\partial q_z}{\partial z} + Q_T, \tag{2}$$

where $T(x,z,t)$ is the temperature function, $q_r(x,z,t)$, $q_z(x,z,t)$ are the components of the heat flux vector, ρ is the density of the plate material, c is the specific heat.

Since a linear substitution of the independent variable $r = R_0 + x$ is used here, the relation $\frac{\partial}{\partial r} = \frac{\partial}{\partial x}$ is obtained as a result. This was used in equation (2).

Unknown functions included in the initial equations (1), (2) must satisfy the boundary conditions, which are selected in the most general form as conditions of convective heat transfer between the boundary surfaces of the body and the environment.

In the case

when $r = R_0$:

$$q_r(0, z, t) = q^0_{r,c}(z, t) - \alpha^0[T(0, z, t) - \theta^0_c(z, t)],$$

when $x = L$: (3)

$$q_r(L, z, t) = q^L_{r,c}(z, t) - \alpha^L[T(L, z, t) - \theta^L_c(z, t)];$$

when $z = h^-$:

$$q^-_{z,c}(x, t) - \alpha^-[T(x, h^-, t) - \theta^-_c(x, t)],$$

when $z = h^+$: (4)

$$q^-_{z,c}(x, h^+, t) = q^+_{z,c}(x, t) + \alpha^+[T(x, h^-, t) - \theta^+_c(x, t)]$$

Here the symbol "c" indicates the known values of the quantities relating to the external environment; θ_c is the ambient temperature near the corresponding area of the body surface, α is the coefficient of convective heat transfer. It should be noted that when $\alpha = 0$ we have a boundary condition of the second kind, when $\alpha \to \infty$ we have a boundary condition of the first kind. As an initial condition, consider the standard ratio:

when $t = 0$:

$$T(x, z, 0) = T_0(x, z), \quad (4)$$

where $T_0(x, z)$ is the initial temperature distribution function at all points of the body.

The form of initial equations accepted in this work provides simplicity of application of dimension reduction of initial system of equations by means of the modified method of lines [6], [7]. According to the mentioned works, the dimension reduction of the initial equations by one spatial coordinate, in this case on z, it is assumed by means of the projection method [3] using as basic functions of the system the so-called functions - "caps", which are related to the lines drawn on the definition domain of the problem $z = (h^+_z - h^-_z)/(N_z - 1) \cdot i$, where $i = \overline{1, N_z}$ taking into account the edge lines $i = 1_z$, $i = N_z$.

The use of locally concentrated basis functions greatly simplifies the preliminary calculations, but requires significant explanations for the correct application of the modified method of line. The fact is that from the point of view of the vector space theory in which a scalar product is defined, the chosen system of basis functions is not orthogonal. In this case, a technique for using

oblique bases is developed in tensor algebra. n addition to the chosen covariant basis, which is considered the main one, it is necessary to consider the contravariant basis, which ensures the correct application of oblique bases. In the modified method of lines, the sequence of dimension reduction and all related mathematical operations are implemented according to standard operations of tensor algebra [4].

Using a scalar multiplication in functional space

$$(f(z), g(z)) = \int_{h_z^-}^{h_z^+} f(z), g(z) dz \tag{6}$$

we obtain:

$$\left(\frac{\partial T}{\partial x} = -\frac{1}{\lambda_T} \cdot q_r \right), \varphi_i(z) \Rightarrow \quad \frac{\partial T^i(x,t)}{\partial x} = -\frac{1}{\lambda_T} \cdot q_r^i(x,t). \tag{7}$$

Here it is taken into account that the derivative $\frac{\partial}{\partial x}$ can be moved outside the integral sign, since the integration occurs with respect to variable z, and the scalar product of any function and basis function with a superscript is the coefficient of this function with respect to the decomposition in basis functions of the basic basis. That is

$$(f(x, z, t), \varphi^i(z)) = f^i(x,t). \tag{8}$$

Here and further on the repeated indices in two-term expressions summation (Einstein summation convention) is used.

$$\begin{aligned} &\left(q_z = -\lambda_T \cdot \frac{\partial T}{\partial z} \right), \varphi^i(z) \Rightarrow q_z^i = -\lambda_T \cdot \int_{h_z^-}^{h_z^+} \frac{\partial T}{\partial z} \cdot g^{ij} \cdot \varphi_j(z) dz = \\ &= -\lambda_T \cdot g^{ij} \cdot \int_{h_z^-}^{h_z^+} \frac{\partial}{\partial z} (T^\alpha \cdot \varphi_\alpha(z)) \cdot \varphi_j(z) dz = -\lambda_T \cdot g^{ij} \cdot b_{j\alpha} \cdot T^\alpha(x,t); \end{aligned} \tag{9}$$

The tensor operation of lowering indices

$$\varphi^i(z) = g^{ij} \cdot \varphi_j(z) \tag{10}$$

using a twice contravariant metric tensor applied here

$$g^{ij} = (\varphi^i(z), \varphi^j(z)). \tag{11}$$

Marked here

$$b_{j\alpha} = \int_{h_z^-}^{h_z^+} \varphi_j(z) \cdot \varphi'_\alpha(z) dz. \tag{12}$$

Finally we get the second reduced equation:

$$q_z^i(x) = -\lambda_T \cdot g^{ij} \cdot b_{j\alpha} \cdot T^\alpha(x,t). \tag{13}$$

When reducing the heat balance equation, a distinction should be made between functions that are twice differentiated with respect to spatial coordinates - $T(x,z)$ and once differentiated - the components of the heat flux

vector $q_r(x,z,t)$ and $q_z(x,z,t)$. When calculating integrals in a sequence similar to sequence (9), it is necessary to apply the "softening" of integration [3] using integration by parts:

$$\left(\rho c\frac{\partial T}{\partial t}=-\frac{q_r}{x+R_0}-\frac{\partial q_r}{\partial x}-\frac{\partial q_z}{\partial z}+Q_T\right),\varphi^i(z)\Rightarrow$$
$$\Rightarrow \rho c\frac{\partial T^i}{\partial t}=-\frac{q_r^i}{x+R_0}-\frac{\partial q_r^i}{\partial x}-\left(\frac{\partial q_z}{\partial z},g^{ij}\cdot\varphi_j(z)\right)+Q_T^i. \tag{14}$$

Here it is necessary to calculate the component separately

$$-\left(\frac{\partial q_z}{\partial z},g^{ij}\cdot\varphi_j(z)\right)=-g^{ij}\cdot\left(\frac{\partial q_z}{\partial z},\varphi_j(z)\right)=-g^{ij}\cdot\int_{h_z^-}^{h_z^+}\frac{\partial q_z}{\partial z}\cdot\varphi_j(z)dz=$$
$$=g^{ij}\cdot\left|\begin{matrix}u=\varphi_j(z);\ du=\varphi_j'(z)dz\\ dv=\frac{\partial q_z}{\partial z}dz;\ v=q_z\end{matrix}\right|=-g^{ij}\cdot[(u\cdot v)\Big|_{h_z^-}^{h_z^+}-\int_{h_z^-}^{h_z^+}q_z\cdot\varphi_j'(z)dz]= \tag{15}$$
$$=-g^{ij}[(q_z^{N_z}\cdot\delta_j^{N_z}-q_z^{1_z}\cdot\delta_j^{1_z})-\int_{h_z^-}^{h_z^+}(q_z^\alpha\cdot\varphi^\alpha(z)\cdot\varphi_j'(z)dz)=$$
$$=-g^{iN_z}\cdot q_z^{N_z}+g^{i1_z}+g^{ij}\cdot b_{\alpha j}\cdot q_z^\alpha.$$

Here we are using the operation of index replacement $g^{ij}\cdot\delta_j^{1z}=g^{i1_z}$, $g^{ij}\cdot\delta_j^{N_z}=g^{iN_z}$, because of such interconnections $\varphi(z)\Big|^{h_z^+}=\delta_i^{N_z}$, $\varphi(z)\Big|_{h_z^-}$ - this is the value of the functions - "caps" on the edge lines $z=h_z^+$ and $z=h_z^-$ in accordance, δ_i^j - Kronecker symbol.

Einstein summation convention is not possible for fixed indices 1_z and N_z. Finally we obtain the reduced equation of heat balance:

$$\rho c\frac{\partial T^i(x,t)}{\partial t}=-\frac{q_r^i(x,t)}{x+R_0}-\frac{\partial q_r^i(x,t)}{\partial x}+g^{ij}\cdot b_{\alpha j}\cdot q_z^\alpha(x,t)-g^{iN_z}\cdot q_z^{N_z}(x,t)+$$
$$+g^{i1_z}\cdot q_z^{1_z}(x,t)+Q_T^i(x,t) \tag{16}$$

Equations (7), (13) and (16) form a complete system of reduced solving equations. But for further application of numerical methods for its solution it is more convenient to reduce it to one equation of the second order on spatial coordinates, having excluded from equations of heat balance the components of the heat flux vector , having written down their coordinates in the corresponding kind:

$$q_r^i(x,t)=-\lambda_T\cdot\frac{\partial T^i(x,t)}{\partial x},\quad q_z^\alpha(x,t)=-\lambda_T\cdot g^{\alpha\beta}\cdot b_{\beta\gamma}\cdot T^\gamma(x,t).$$

As a result we receive:

$$\rho c\frac{\partial T^i(x,t)}{\partial t}=\lambda_T[\frac{\partial^2 T^i(x,t)}{\partial x^2}+\frac{1}{x+R_0}\cdot\frac{\partial T^i(x,t)}{\partial x}\cdot g^{ij}\cdot b_{\alpha j}\cdot g^{\alpha\beta}\cdot b_{\beta\gamma}\cdot T^\gamma(x,t)]+Q_T^i. \tag{17}$$

In the case of a stationary thermal process, the initial functions are unknown and, accordingly, the reduced functions do not depend on the time variable, and then the obtained reduced equations are ordinary differential equations that depend on the x-coordinate. In this case, it is more convenient to use the system of equations (7), (3), (16) to calculate the stationary temperature field.

To ensure the unambiguity of the solutions, the reduced equations must be supplemented by initial and boundary conditions, which we obtain from the initial conditions (5) by scalarly multiplying it by the basic functions of the reciprocal basis $\varphi^i(z)$. Since the scalar product here is integration with respect to z, the result is:

when $t=0$:

$$T^i(x,z,0)=T^i(x,0). \tag{18}$$

Boundary conditions for reduced equations are also obtained from the initial boundary conditions. Since the initial equations are chosen as a system of first-order differential equations in first-order partial derivatives, the initial boundary conditions have the form of algebraic equations. In this regard, the reduced boundary conditions formally look like the initial ones, if the unknown functions included in them are replaced by the coefficients of these functions, ie:

$$\begin{aligned} T(x,z,t) &\to T^i(x,t), \\ q(x,z,t) &\to q^i(x,y). \end{aligned} \tag{19}$$

We get:

when $x=0$:

$$q_r^i(0,t)=q_{r,c}^{0,i}-\alpha^0\cdot[T^i(0,t)-\theta_c^{0,i}(t)]; \tag{20}$$

when $x=L$:

$$q_r^i(L,t)=q_{r,c}^{L,i}-\alpha^L\cdot[T^i(L,t)-\theta_c^{L,i}(t)]. \tag{21}$$

Reduced equations in the obtained form take into account only the three-dimensional effects $Q_T(x,z,t)$. But, as a rule, this is not enough. Most real thermal effects occur due to the body's contact with the environment through boundary surfaces. In this calculation model, the contact with the external environment occurs through the end surfaces $x=0$ and $x=L$ and is taken into account by boundary conditions (3) and, accordingly, reduced (20), (21).

To take into account the thermal effects from the external environment through the boundary planes $z=h_z^-, z=h_z^+$ it is necessary to include conditions (4) in the reduced equations of heat balance, excluding from these equations the components q_z^{1z} та q_z^{Nz} by means of relations (4). Thus, all possible thermal effects on the calculated object are taken into account:

$$\rho c\frac{\partial T(x,t)}{\partial t}=\lambda_T[\frac{\partial^2 T^i(x,t)}{\partial x^2}+\frac{1}{x+R_0}\cdot\frac{\partial T(x,t)}{\partial x}-g^{iNz}\cdot\alpha_T^+\cdot T^{Nz}(x,t)- \\ -g^{i1z}\cdot\alpha_T^-\cdot T^{1z}(x,t)+g^{ij}\cdot b_{\alpha j}\cdot g^{\alpha\beta}\cdot b_{\beta\gamma}\cdot T^{\gamma}(x,t)]+\overline{Q}_T^0, \quad (22)$$

where

$$\overline{Q}_T^i=Q_T^i-g^{iNz}\cdot(q_{z,c}^+(x,t)-\alpha^+\cdot\theta_c^+(x,t))+(q_z^{i1z}\cdot(x,t)+\alpha_T^-\cdot\theta_c^-(x,t)). \quad (23)$$

Conclusions. In this work, a modified method of straight lines is used to reduce the dimension of the initial system of equations of nonstationary thermal conductivity recorded in a cylindrical coordinate system. The most successful form of writing the original equations was found, which ensures ease of application of dimensionality reduction of the initial system of equations using a modified method of lines. The influence of the environment was taken into account. Initial and boundary conditions were written for this purpose. Thus, the reduced equations, boundary and initial conditions were obtained. All this makes it possible to further investigate the temperature fields of the load-bearing elements in their calculation of thermal effects.

REFERENCES

1. *Kovalenko A. D.* Vvedenie v termouprugost' (Introduction to thermoelasticity)/ *A. D. Kovalenko*. – Kiev: Naukova dumka, 1965. – 204 s.
2. *Karslou G.* Teploprovodnost' tverdyh tel (Thermal conductivity of solids)/ *G. Karslou, D. Eger*. – Moskva: Nauka, 1964. – 488 s.
3. *Marchuk G. I.* Vvedenie v proekcionno-setochnye metody (Introduction to projection-grid methods)/ *G. I. Marchuk, V. I. Agoshkov*. – Moskva: Nauka, 1981. – 416 s.
4. Modifikovanij metod pryamih, algoritm jogo zastosuvannya, mozhlivosti ta perspektivi (Modified method of direct, algorithm of its application, possibilities and prospects)/ [*V. K. Chibiryakov, A. M. Stankevich, O. P. Koshevij* ta in.]. // Mistobuduvannya ta teritorial'ne planuvannya. – 2019. – №70. – S. 595–616.
5. *Chibiryakov V.K.* Diskretno-kontinual'na model' dlya rozrahunku tovstih plastin na dinamichni vplivi (Discrete-continuous model for calculating thick plates on dynamic effects) / *V. K. Chibiryakov, A. M. Stankevich, D. V. Levkivs'kij.* // Mistobuduvannya ta teritorial'ne planuvannya. – 2014. – №51. – S. 678–687.
6. *Chibiryakov V. K.* Pro odin algoritm rozv`yazannya pochatkovo-granichnih zadach dlya rivnyannya nestacionarnoï teploprovidnosti (About one algorithm for solving initial-boundary value problems for the equation of nonstationary thermal conductivity) / *V. K. Chibiryakov, A. M. Stankevich, V. F. Mel'nichuk.* // Opir materialiv i teoriya sporud. – 2015. – №95. – S. 90–95.
7. `Application of generalized “method of lines”, for solving problems of thermoelasticity of thick plates. */ V.Chybiryakov, A. Stankevich, D. Levkivskiy, V. Melnychuk. //* “Motrol”. – 2014. – №8. – C. 11–20.

Стаття надійшла 20.09.2020

Сович Ю.В.

МОДИФІКОВАНИЙ МЕТОД ПРЯМИХ В ЗАДАЧАХ ТЕПЛОПРОВІДНОСТІ КІЛЬЦЕВИХ ПЛАСТИН

У даній роботі пропонується розв'язувати початково-граничну задачу теплопровідності за допомогою чисельно-аналітичного методу – модифікованого методу прямих. Вихідні рівняння теплопровідності визначені в циліндричній системі координат розглядаються в просторовій постановці, що значно їх ускладнює. В якості об'єкта, на якому вони визначені, розглядається кільцева пластина, габаритні розміри якої, співрозмірні. В задачах розрахунку несучих елементів на теплові впливи першим етапом є визначення температурних полів, особливо, якщо габаритні розміри конструкцій співрозмірні. До таких елементів відносяться нетонкі кільцеві пластини. Граничні умови розглядаються теж у загальному вигляді – це умови конвективного теплообміну, які за допомогою граничного переходу перетворюються в граничні умови першого та другого типів. У даній роботі показано застосування модифікованого методу прямих для зниження вимірності вихідної системи рівнянь нестаціонарної теплопровідності, що застосовуються для визначення температурних полів несучих елементів.

Застосування модифікованого методу прямих передбачає розв'язувати вказані початково-граничні задачі в два етапи. На першому етапі по одній просторовій координаті z знижується вимірність вихідних рівнянь. Для зниження вимірності використовується проекційний метод Бубнова-Гальоркіна-Петрова. В якості базисних функцій приймаються так звані функції-кришки, які пов'язані з прямими, що нанесені на область визначення даної задачі. Проекційний метод також використовується для зниження вимірності початкових та граничних умов, що дозволяє поставити редуковану початково-граничну задачу, яку зручно розв'язувати чисельним скінченно-різницевим методом, використовуючи явні або неявні різницеві схеми. Знайдено найоптимальнішу форму написання вихідних рівнянь, що забезпечує легкість зниження вимірності вихідної системи рівнянь за допомогою модифікованого методу прямих. При розрахунку було враховано вплив навколишнього середовища. В результаті, було отримано редуковані рівняння, граничні та початкові умови. Редукована задача має вигляд, зручний для застосування до її розв'язання сучасними чисельними методами.

Ключові слова: теплопровідність, зниження вимірності, проекційний метод, редуковані рівняння, модифікований метод прямих.

Sovych Yu.V.

MODIFIED METHOD OF LINES IN THE PROBLEMS OF THERMAL CONDUCTIVITY OF ANNULAR PLATES

In this paper, to solve the initial boundary value problem of thermal conductivity using a numerical-analytical method - a modified method of lines is proposed. The initial equations of thermal conductivity defined in the cylindrical coordinate system are considered in the spatial formulation, which greatly complicates them. As an object on which they are defined, an annular plate is considered, the overall dimensions of which are commensurate. In the problems of calculating of thermal effects in load-bearing elements the first step is to determine the temperature fields, especially if the overall dimensions of the structures are proportional. Such elements include non-thin annular plates. The boundary conditions are considered in a general form too - these are the conditions for convective heat transfer, which using the passage to the limit, turn into boundary conditions of the first and second types. The application of the modified method of lines to reduce the dimensionality of the initial system of equations of nonstationary thermal conductivity used to determine the temperature fields of the load-bearing elements is shown in this paper.

The application of the modified method of lines involves solving these initial boundary value problems in two stages. At the first stage, the dimensionality of the initial equations with respect to variable z is reduced. The Bubnov-Galerkin-Petrov projection method is used to reduce the dimensionality. The so-called functions-"caps" are accepted as basic functions, which are related to the lines plotted on the definition domain of the problem. The projection method is also used to reduce the dimension of the initial and boundary conditions, that allows to formulate a reduced initial-limit problem, which is convenient to solve using the numerical finite-difference method,

using explicit or implicit difference schemes. The most successful form of writing the original equations was found, which ensures ease of application of dimensionality reduction of the initial system of equations using a modified method of lines. The calculation took into account the impact of the environment. Reduced equations, boundary and initial conditions are obtained. As a result, the reduced problem has a form convenient to its solution by modern numerical methods.

Keywords: thermal conductivity, dimension reduction, projection method, reduced equations, modified method of lines.

УДК 539.3
Сович Ю.В. **Модифікований метод прямих в задачах теплопровідності кільцевих пластин** // Опір матеріалів і теорія споруд: наук.-тех. збірн. – К.: КНУБА, 2020. – Вип.105. – С. 302-309. – Англ.

У даній роботі показано застосування модифікованого методу прямих для зниження вимірності вихідної системи рівнянь нестаціонарної теплопровідності, що застосовуються для визначення температурних полів несучих елементів. Зниження вимірності вихідних рівнянь по одній просторовій координаті, в даному випадку саме по z виконується за допомогою проекційного методу. Для цього використовуються локальні базисні функції. Для забезпечення однозначності розв'язків редуковані рівняння доповнюються початковими та граничними умовами.
Іл. 1. Бібліогр. 7 назв.

UDC 539.3
Sovych Yu.V. **Modified method of direct in problems of thermal conductivity of annular plates** // Strength of Materials and Theory of Structures: Scientific-and-technical collected articles. – K.: KNUBA, 2020. – Issue 105. – P. 302-309.

The application of the modified method of lines to reduce the dimensionality of the initial system of equations of nonstationary thermal conductivity used to determine the temperature fields of the load-bearing elements is shown in this paper. Reducing the dimensionality of the original equations by one spatial coordinate, in this case by the z coordinate, is performed using the projection method. Local basic functions are used for this purpose. To ensure the uniqueness of the solutions, the reduced equations are supplemented by initial and boundary conditions.
Fig. 1. Ref. 7.

Автор (науковий ступінь, вчене звання, посада)*: аспірант кафедри опору матеріалів КНУБА СОВИЧ Юлія Вікторівна*
Адреса робоча: *03680 Україна, м. Київ, Повітрофлотський проспект 31, КНУБА, кафедра опору матеріалів, Сович Юлія Вікторівна.*
Мобільний тел.: *+38(098)981-57-31*
E-mail: *yuliiasov@bigmir.net*
ORCID ID: http://orcid.org/0000-0002-5114-6363

ЗМІСТ

Науково-технічний збірник
ОПІР МАТЕРІАЛІВ І ТЕОРІЯ СПОРУД

STRENGTH OF MATERIALS AND THEORY OF STRUCTURES
Scientific-and-technical collected articles

Випуск 105

Головний редактор В.А.Баженов

Підп. до друку 30.11.20. Формат 60x90 $^{1}/_{16}$. Папір друк №1.
Друк офсетний. Умовн. друк. арк.
Тираж 100.

КНУБА
м. Київ, Повітрофлотський пр., 31. 03037